

# Mathematical Documentation

of the objects realized in the visualization program

## 3D-XplorMath

Select the TABLE OF CONTENTS (TOC) of the desired kind of objects:

[Table Of Contents of Planar Curves](#)

[Table Of Contents of Space Curves](#)

[Surface Organisation](#)

[Go To Platonics](#)

[Table of Contents of Conformal Maps](#)

[Table Of Contents of Fractals](#)

[ODEs](#)

[Table Of Contents of Lattice Models](#)

[Table Of Contents of Soliton Traveling Waves](#)

[Shepard Tones](#)

Homepage of 3D-XPlorMath (3DXM):

<http://3d-xplormath.org/>

Tutorial movies for using 3DXM:

<http://3d-xplormath.org/Movies/index.html>

Version November 29, 2020

## The Surfaces Are Organized According To their Construction

Surfaces may appear under several headings:

The Catenoid is an explicitly parametrized, minimal surface of revolution.

[Go To Page 1](#)

[Curvature Properties of Surfaces](#)

[Surfaces of Revolution](#)

[The Unduloid, a Surface of Constant Mean Curvature](#)

[Sphere, with Stereographic and Archimedes' Projections](#)

[TOC of Explicitly Parametrized and Implicit Surfaces](#)

[Menu of Nonorientable Surfaces](#) in previous collection

[Menu of Implicit Surfaces](#) in previous collection

[TOC of Spherical Surfaces \( \$K = 1\$ \)](#)

[TOC of Pseudospherical Surfaces \( \$K = -1\$ \)](#)

[TOC of Minimal Surfaces \( \$H = 0\$ \)](#)

[Ward Solitons](#)

[Anand-Ward Solitons](#)

[Voxel Clouds of Electron Densities of Hydrogen](#)

[Go To Page 1](#)

# Planar Curves

[Go To Page 1](#)

(Click the Names)

[Circle](#)

[Ellipse](#)

[Parabola](#)

[Hyperbola](#)

[Conic Sections](#)

[Kepler Orbits, explaining  \$1/r\$ -Potential](#)

[Nephroid of Freeth](#)

[Sine Curve](#)

[Pendulum ODE Function](#)

[Lissajous Plane Curve](#)

[Catenary](#)

[Convex Curves from Support Function](#)

[Tractrix](#)

[Cisoid and Strophoid](#)

[Conchoid](#)

[Lemniscate](#)

[Clothoid](#)

[Archimedean Spiral](#)

[Logarithmic Spiral](#)

[Cycloid](#)

[Epi- and Hypocycloids](#)

[Cardioid and Limacon](#)

[Astroid](#)

[Continue TOC next page](#)

[Deltoid](#)

[Nephroid](#)

Ancient Method of Construction:

[Mechanically Generated Curves](#)

[Seven Cubic Curves](#), five with Addition:

Cubic Polynomial, Cuspidal Cubic,

Connected Rational Cubic, Rational Cubic with Poles,

Elliptic Cubic; Folium, Nodal Cubic

[Elliptic Functions](#), parametrizing Elliptic Curves

[Geometric Addition on Cubic Curves](#)

[Folium](#)

[Implicit Planar Curves](#), highly singular examples:

Tacnodal Quartic, Teissier Sextic

[Cassinian Ovals](#), an implicit family

[Userdefined Curves](#), explicitly parametrized:

User Cartesian, User Polar, User Graph

implicit: User Implicit Curves

[User Curves by Curvature](#)

[Graphs of Planar Curves](#)

[Go To Planar TOC](#)

## The Circle \*

$$x = aa \cos(t), \quad y = aa \sin(t), \quad 0 \leq t \leq 2\pi$$

3DXM - SUGGESTION: Select from the Action Menu *Show Generalized Cycloid* and vary in the Settings Menu, entry: *Set Parameters*, the (integer) ratio between the radius  $aa$  and the rolling radius  $hh$ .

The length of the drawing stick is  $ii \cdot \text{rolling radius}$ .

The circle is the simplest and best known closed curve in the plane. The default image shows the circle together with the theorem of Thales about right angled triangles. Other properties of the circle are also known since over 2000 years. In fact, many of the plane curves that have individual names were already considered (and named) by the ancient Greeks, and a large class of these can be obtained by rolling one *circle* on the inside or the outside of some other *circle*. The Greeks were interested in rolling constructions because it was their main tool for describing the motions of the planets (Ptolemy). The following curves from the Plane Curve menu can be obtained by rolling constructions:

**Cycloid, Ellipse, Astroid, Deltoid, Cardioid, Limaçon, Nephroid, Epi- and Hypocycloids.**

Not all geometric properties of these curves follow easily

---

\* This file is from the 3D-XplorMath project. Please see:

from their definition as rolling curve, but in some cases the connection with complex functions (Conformal Category) does.

**Cycloids** arise by rolling a circle on a straight line. The parametric equations code for such a cycloid is

$$\begin{aligned} P.x &:= aa \cdot t - bb \sin(t) \\ P.y &:= aa - bb \sin(t), \quad aa = bb. \end{aligned}$$

Cycloids have other cycloids of the same size as evolute (Action Menu: “Show Osculating Circles with Normals”). This fact is responsible for Huyghen’s cycloid pendulum to have a period independent of the amplitude of the oscillation.

**Ellipses** are obtained if *inside* a circle of radius  $aa$  another circle of radius  $r = hh = 0.5aa$  rolls and then traces a curve with a radial stick of length  $R = ii \cdot r$ . The parametric equations for such an ellipse is

$$\begin{aligned} P.x &:= (R + r) \cos(t) \\ P.y &:= (R - r) \sin(t). \end{aligned}$$

In the visualization of the complex map  $z \rightarrow z + 1/z$  in Polar Coordinates the image of the circle of Radius  $R$  is such an ellipse with  $r = 1/R$ .

**Astroids** are obtained if *inside* a circle of radius  $aa$  another circle of radius  $r = hh = 0.25aa$  rolls and then traces a curve with a radial stick of length  $R = ii \cdot r = r$ . Parametric equations for such Astroids are

$$P.x := (aa - r) \cos(t) + R \cos(4t)$$

$$P.y := (aa - r) \sin(t) - R \sin(4t).$$

Astroids can also be obtained by rolling the *larger* circle of radius  $r = hh = 0.75aa$  (put  $gg = 0$  in this case). Another geometric construction of the Astroids uses the fact that the length of the segment of each tangent between the x-axis and the y-axis has **constant** length. — Try  $hh := aa/3$  to obtain a **Deltoid**.

**Cardioids and Limaçons** are obtained if *outside* a circle of radius  $aa$  another circle of radius  $r = hh = -aa$  rolls and then traces a curve with a radial stick of length  $R = ii \cdot r$ ,  $ii = 1$  for the Cardioids,  $ii > 1$  for the Limaçons.

Parametric equations for Cardioids and Limaçons are

$$P.x := (aa + r) \cos(t) + R \cos(2t)$$

$$P.y := (aa + r) \sin(t) + R \sin(2t).$$

The Cardioids and Limaçons can also be obtained by rolling the larger circle of radius  $r = hh = +2aa$ ; now  $ii < 1$  for the Limaçons. Note that the fixed circle is *inside* the larger rolling circle.

The evolute of the Cardioid (Action Menu: *Show Osculating Circles with Normals*) is a smaller Cardioid. The image of the unit circle under the complex map  $z \rightarrow w = (z^2 + 2z)$  is a Cardioid; images of larger circles are Limaçons. Inverses  $z \rightarrow 1/w(z)$  of Limaçons are figure-eight shaped, one of them is a Lemniscate.

**Nephroids** are generated by rolling a circle of one ra-

dus outside of a second circle of twice the radius, as the program demonstrates. With  $R = 3r$  we thus have the parametrization

$$P.x := R \cos(t) + r \cos(3t)$$

$$P.y := R \sin(t) + r \sin(3t).$$

As with Cardioids and Limaçons one can also make the radius for the drawing stick shorter or longer: After selecting *Circle* set the parameters  $aa = 1, hh = -0.5, ii = 1$  for the Nephroid and  $ii > 1$  for its looping relatives. – Pick in the Action Menu: *Show Osculating Circles with Normals*. The Normals envelope a smaller Nephroid.

The complex map  $z \rightarrow z^3 + 3z$  maps the unit circle to such a Nephroid. To see this, in the Conformal Map Category, select  $z \rightarrow z^{ee} + ee \cdot z$  from the Conformal Map Menu, then choose Set Parameters from the Settings Menu and put  $ee = 3$ .

**Archimedes' Angle Trisection.** A demo of this construction can be selected from the Action Menu.

**Circle Involute Gear.** Another demo from the Action Menu. Involute Gear is used for heavy machinery because of the following two advantages: If one wheel rotates with constant angular velocity then so does the other, thus avoiding vibrations. If the teeth become thinner by usage, the axes can be moved closer to each other.

H.K.

[Go To Planar TOC](#)

## The Ellipse \*

$$x(t) = aa \cos(t), \quad y(t) = bb \sin(t), \quad 0 \leq t \leq 2\pi$$

3DXM-SUGGESTION:

Select in the Action Menu: *Show Osculating Circles with Normals*. In the Animate Menu try the default *Morph*.

For related curves see: Parabola, Hyperbola, Conic Sections and their ATOs.

The Ellipse is shown together with the so called *Leitkreis construction* of the curve and its tangent, see below. This construction assumes that the constants  $aa$  and  $bb$  are positive. The larger of the two is called the semi-major axis length, the smaller one is the semi-minor axis length.

The Ellipse is also the set of points satisfying the following implicit equation:  $(x/aa)^2 + (y/bb)^2 = 1$ .

A geometric definition of the Ellipse, that can be used to shape flower beds is:

An Ellipse is the set of points for which the **sum of the distances** from two focal points is a constant  $L$  equal to twice the semi-major axis length.

A gardener connects the two focal points by a cord of length  $L$ , pulls the cord tight with a stick which then draws the boundary of the flower bed with the stick. Another version of this definition is:

---

\* This file is from the 3D-XplorMath project. Please see:

An Ellipse is the set of points which have **equal distance** from a circle of radius  $L$  and a (focal) point inside the circle.

Both these definitions are illustrated in the program.

The normal to an ellipse at any point bisects the angle made by the two lines joining that point to the foci. This says that rays coming out of one focal point are reflected off the ellipse towards the other focal point. Therefore one can build elliptically shaped “whispering galleries”, where a word spoken softly at one focal point can be heard only close to the other focal point.

To add a simple proof we show that the tangent leaves the ellipse on one side; more precisely, we show that for every other point on the tangent the sum of the distances to the two focal points  $F_1, F_2$  is more than the length  $L$  of the major axis. (In the display:  $F = F_2$ .) Pick any point  $Q$  on the tangent, join it to the two focal points and reflect the segment  $QF$  in the tangent, giving another segment  $QS$ . Now  $F_1QS$  is a radial straight segment only if  $Q$  is the point of tangency—otherwise  $F_1QS$  is by the triangle inequality longer than the radius  $F_1S$  (of length  $L$ ) of the circle around  $F_1$ .

The evolute of an ellipse, i.e., the curve enveloped by the normals of the ellipse—see Action Menu: *Draw osculating circles with normals*, is a generalized Astroid, it is less symmetric than the true Astroid.

An Ellipse can also be obtained by a rolling construction:

Inside a circle of radius  $aa$  another circle of radius  $r := hh = 0.5aa$  rolls and traces the Ellipse with a stick of radius  $R := ii \cdot r$ , see Plane Curves Menu: *Circle* and select from the Action Menu: *Show Generalized Cycloids*. The parametric equation resulting from this construction is:

$$\begin{aligned}x(t) &= (R + r) \cos(t) \\y(t) &= (R - r) \sin(t)\end{aligned}$$

This is related to the visualization of the complex map  $z \rightarrow z + 1/z$  in Polar Coordinates, the image of the circle of radius  $R$  is such an ellipse with  $r = 1/R$ .

Such rolling constructions are reached with the Plane Curves Menu entry: *Circle* and then the Action Menu *Draw Generalized Cycloids* or with *Epi- and Hypocycloids*. Recall that negative values of the rolling radius  $hh$  gives curves on the outside, positive radii ( $hh < aa$ ) on the inside of the fixed circle.

Other rolling curves are:

Cycloid, Astroid, Deltoid, Cardioid, Limacon,  
Nephroid, Epi- and Hypocycloids.

H.K.

[Go To Planar TOC](#)

## Parabola \*

See also: Ellipse, Hyperbola, Conic Section and their ATOs, and in the Category Surfaces see: Conic Sections and Dandelin Spheres

The usual parametric equations for the Parabola are

$$x(t) := t^2/4p$$

$$y(t) := t,$$

where  $p = aa/4$ ,

so the Parabola visualizes the graphs of the two functions  $y(x) := \sqrt{4p \cdot x}$  and  $x(y) := y^2/4p$ .

The vertical line  $x = -p$  is called the directrix and the point  $(x, y) = (p, 0)$  is called focal point of the Parabola.

The distance from a point  $(x, y = \sqrt{4p \cdot x})$  on the Parabola to the directrix is  $(x + p)$ , and this is the same distance as from  $(x, y = \sqrt{4p \cdot x})$  to the focal point  $(p, 0)$ , because  $(x - p)^2 + y^2 = (x + p)^2$ .

The point  $(p, 0)$  is called "focal point", because light rays which come in parallel to the x-axis are reflected off the Parabola so that they continue to the focal point. This fact is illustrated in the program. It gives the following ruler construction of the Parabola:

Prepare the construction by drawing x-axis, y-axis, directrix and focal point F. Then draw any line parallel to the x-axis and intersect it with the directrix in a point S. The line orthogonal to the connection SF and through its mid-

---

\* This file is from the 3D-XplorMath project. Please see:

point is the tangent of the Parabola and intersects therefore the incoming ray in the point of the Parabola which we wanted to find.

The same construction works for Ellipse and Hyperbola, if the directrix is replaced by a circle of radius  $2*a$  around one focal point. The curve is the set of points which have the same distance from this circle and the other focal point.

The Action Menu of the Parabola has an entry “Show Normals Through Mouse Point”. This illustrates an unexpected property of the Parabola. One may already be surprised that at the intersection points of normals always **three** normals meet. We know no other curve which is accompanied by such a net of normals. The surprise should increase if one looks at the  $y$ -coordinates of the parabola points from where three such intersecting normals originate: these  $y$ -coordinates add up to 0! In other words, the intersection behaviour of the normals reflects the addition on the  $y$ -axis.

The explanation of where this intersection property comes from is quite interesting. The normals of the Parabola are the tangents to its evolute, the semi-cubical parabola, a singular cubic curve (see Cuspidal Cubic). So the intersection property of the parabola normals can be thought of as defining an addition law for the evolute, and as such it is a simpler limiting case of the addition law that exists on any cubic curve.

R.S.P.

[Go To Planar TOC](#)

## Hyperbola \*

See also Parabola, Ellipse, Conic Sections and their ATOs.

The most common parametric equations for a Hyperbola with semi-axes  $aa$  and  $bb$  are:

$$x(t) = \pm aa \cosh(t), \quad y(t) = bb \sinh(t), \quad t \in \mathbb{R};$$

and another version is:

$$x(t) = aa / \cos(t), \quad y(t) = bb \sin(t) / \cos(t), \quad t \in [0, 2\pi].$$

The corresponding implicit equation is:

$$(x/aa)^2 - (y/bb)^2 = 1.$$

The function graphs:  $\{(x, y); y = 1/x + m \cdot x\}$  are also Hyperbolae.

A geometric definition of the Hyperbola is:

A Hyperbola is the set of points for which the **difference of the distance** from two focal points is constant.

Or:

A Hyperbola is the set of points which have the **same distance** from a circle and a (focal) point **outside** that circle.

---

\* This file is from the 3D-XplorMath project. Please see:

If one applies an inversion  $(x, y) \rightarrow (x, y)/(x^2 + y^2)$  to a right Hyperbola (i.e.  $aa = bb$ ) then one obtains a Lemniscate.

In the visualization of the complex map  $z \rightarrow z + 1/z$  in Polar Coordinates, the image of the radial lines are the Hyperbolae:

$$\begin{aligned}x(R) &= (R + 1/R) \cos \phi \\y(R) &= (R - 1/R) \sin \phi, \quad R \in \mathbf{R}.\end{aligned}$$

And the image of the standard Cartesian Grid under the complex map  $z \rightarrow \sqrt{z}$  is a grid of two families of orthogonal Hyperbolae.

H.K.

[Go To Planar TOC](#)

## Conic Sections\*

See also Parabola, Ellipse, Hyperbola and their ATOs.

A cone of revolution (e.g.,  $\{(x, y, z); x^2 + y^2 = m \cdot z^2\}$ ) is one of the simplest surfaces. Its intersections with planes are called conic sections. Apart from pairs of lines these conic sections are Parabolae, Ellipses or Hyperbolae. These curves have also other geometric definitions (e.g., The locus of points having the same distance from a focal point and a circle). See their Menu entries.

On the other hand, they are also more robust than these definitions show: Photographic images of conic sections are again conic sections; or in a completely different formulation: The intersection of a plane and any “quadratic cone”, i.e.,

$$\{(x, y, z) \mid a \cdot x^2 + b \cdot y^2 + c \cdot z^2 + d \cdot xy + e \cdot yz = 0\},$$

is **not** more complicated than planar sections of circular cones but are the same old Parabolae, Ellipses or Hyperbolae as above. A special case of this robustness is the fact that orthogonal projections of conic sections in 3-space are again conic sections. This is illustrated in the program as follows:

Interpret the illustration as if it showed level lines on a hiking map. The equidist parallel lines are the level lines of a

---

\* This file is from the 3D-XplorMath project. Please see:

sloping plane; the smaller the distance between these level lines the steeper the plane. The equidistant concentric circles are the level lines of a circular cone, as for example an ant lion would dig in sandy ground; without height numbers written next to the level lines we can of course not decide whether the circular level lines represent a conical mountain or a conical hole in the ground. We suggest that the blue level line and the vertex of the cone are at height zero and the other levels are higher up so that the cone is a hole.

The intersection curve between plane and cone has then an easy pointwise construction: Simply intersect level lines of the same height on the two surfaces. (These are lines with the same color in the program illustration.) This construction reveals a new geometric property of the intersection curve on the map, of this conic section:

Take the ratio of the distances from a point on the curve, (i) to the level line at height 0 of the plane (called *directrix*) and (ii) to the vertex at height zero of the cone (called *focus*). *This ratio is the same as the ratio of adjacent level lines of plane and cone and therefore the same for all points of this conic section.*

H.K.

[Go To Planar TOC](#)

## Conic Sections, Kepler orbits \*

See also Parabola, Ellipse, Hyperbola and their ATOs.

For many properties of the conic sections a parametrization is not relevant. However, when Kepler discovered that planets and comets travel on conic sections around the sun then this discovery came with a companion: the speed on the orbit is such that angular momentum is preserved. In more elementary terms: the radial connection from the sun to the planet sweeps out equal areas in equal times. With the 3dfs demo we explain geometrically how this celestial parametrization is connected with the focal properties of conic sections. Here we give the *algebraic explanation* first.

An ellipse, parametrized as *affine image of a circle* and translated to the left is

$$P(\varphi) := (a \cos \varphi - e, b \sin \varphi).$$

If we choose  $e := \sqrt{a^2 - b^2}$  then we have  $|P(\varphi)| = (a - e \cos \varphi)$ . This gives the connection with the oldest definition of an ellipse: The sum of the distances from  $P(\varphi)$  to the two points  $(\pm e, 0)$  is  $2a$ .

Next we compute the quantity  $A$ , equal to twice the area swept out by the position vector  $P$ , and also the derivatives

---

\* This file is from the 3D-XplorMath project. Please see:

of  $P$  and  $A$ :

$$\begin{aligned}
 A(\varphi) &= \int_0^\varphi \det(P(\varphi), P'(\varphi)) d\varphi, \\
 P'(\varphi) &= (-a \sin \varphi, b \cos \varphi), \\
 A'(\varphi) &= b(a - e \cos \varphi),
 \end{aligned}$$

and we denote the function inverse to  $A(\varphi)$  by  $\Phi(A)$ , so that,

$$\Phi(A(\varphi)) = \varphi, \quad \Phi'(A) = \frac{1}{b(a - e \cos \Phi)}.$$

Let us write  $Q$  to denote the position when expressed as a function of  $A$ , i.e.,  $Q(A) := P(\Phi(A))$ . Now Kepler's Second Law says that  $A$  is proportional to time, or equivalently that  $A$  is the time in appropriate units, so the velocity is  $Q'(A) = P'(\Phi(A)) \cdot \Phi'(A)$ , and the kinetic energy is:

$$\begin{aligned}
 K.E. &= \frac{1}{2} Q'(A)^2 = \frac{a^2 \sin^2 \varphi + b^2 \sin^2 \varphi}{2b^2(a - e \cos \varphi)^2} \\
 &= \frac{a^2 - e^2 \cos^2 \varphi}{2b^2(a - e \cos \varphi)^2} \\
 &= \frac{(a + e \cos \varphi)}{2b^2(a - e \cos \varphi)} \\
 &= \frac{a}{b^2} \cdot \frac{1}{a - e \cos \varphi} - \frac{1}{2b^2}. \\
 &= \frac{a}{b^2} \cdot \frac{1}{|P(\varphi)|} - \frac{1}{2b^2}.
 \end{aligned}$$

Thus, in units where we take twice the swept out area as the time, the potential energy can be read off by using the law of energy consevation, i.e., the fact that the kinetic energy plus the potential energy is constant. In fact, it follows from this that the potential energy at orbit point  $Q(A(\varphi)) = P(\varphi)$  is equal to:

$$-\frac{a}{b^2} \cdot \frac{1}{|P(\varphi)|},$$

which is the famous  $1/r$  law for the potential energy.

Next, we present a *geometric proof*. The starting point is the determination of the correct orbital speed by the property that the product of the speed  $|v|$  with the distance  $p$  of the tangent line from the center is the constant angular momentum, Kepler's second law. Of course we can illustrate such a fact only if we also represent the size of velocities by the length of segments and we have to keep in mind that segments which illustrate a length and segments which illustrate a velocity are interpreted with different units.

Recall the following theorem about circles: if two secants of a circle intersect then the product of the subsegments of one secant ist the same as the product of the subsegments of the other secant.

This will be applied to the circle the radius of which is the length  $2a$  of the major axis. (The midpoint is the other focus, not the sun.) The two secants intersect in the focus representing the sun: one secant is an extension of the



have two similar right triangles, the small one has hypotenuse =  $r$  and one other side =  $p$ , the big one has as hypotenuse a circle diameter of length  $4a$  and the corresponding other side has length  $2p + |v|$ . Now we use the above  $const := (2a - 2e) \cdot (2a + 2e) = 2p \cdot |v|$  to eliminate  $p$  from the proportion:

$$p : r = (2p + |v|) : 4a$$

This gives

$$2a/r = 1 + |v|/2p = 1 + v^2/const.$$

Up to physical constants (units),  $v^2$  is the kinetic energy, so that (again up to units)  $-1/r$  is the potential energy – since such a potential makes kinetic plus potential energy constant.

Another simple property of Kepler ellipses and hyperbolas is: Their velocity diagram, the so called *hodograph*, is a circle. Usually one simply translates the velocity vector from the orbit point to the sun. In our picture we see the velocity vector rotated by 90 degrees; indeed, it ends on the circle. This leads to a geometric representation of the *Runge-Lenz vector*: In our picture we really see the cross product of the (tangential) velocity vector with angular momentum (a constant vector orthogonal to the orbit plane). If we add to it a vector of constant length  $2a$  and *parallel* to the position vector then we reach the midpoint of our circle, the other focal point of the orbit

ellipse. This sum vector is, up to the constant negative factor  $-(a - e)/2e$  the classical Runge-Lenz vector.

Mathematically, the *parabolic* and *hyperbolic* Kepler orbits allow similar derivations of the  $-1/r$ -potential, which we will give next. Historically this played no role since the non-repeating orbits could not be determined with enough precision at the time.

*Derivation of the  $-1/r$ -potential from a parabolic Kepler orbit.* Let in the picture (below)  $|p|$  be the distance from the sun at  $(1/4, 0)$  to a tangent of a parabolic Kepler orbit and let  $|v|$  be the orbital speed at that moment. Conservation of angular momentum says  $p \cdot |v| = \text{const}$ . Let  $\varphi$  be the angle between the segment marked  $p$  and the vertical axis; since the sun is at the focal point of the parabola we have  $p \cdot \sin \varphi = 1/4$ . This and the previous angular momentum equation say that, up to a choice of unit for velocity, we have:

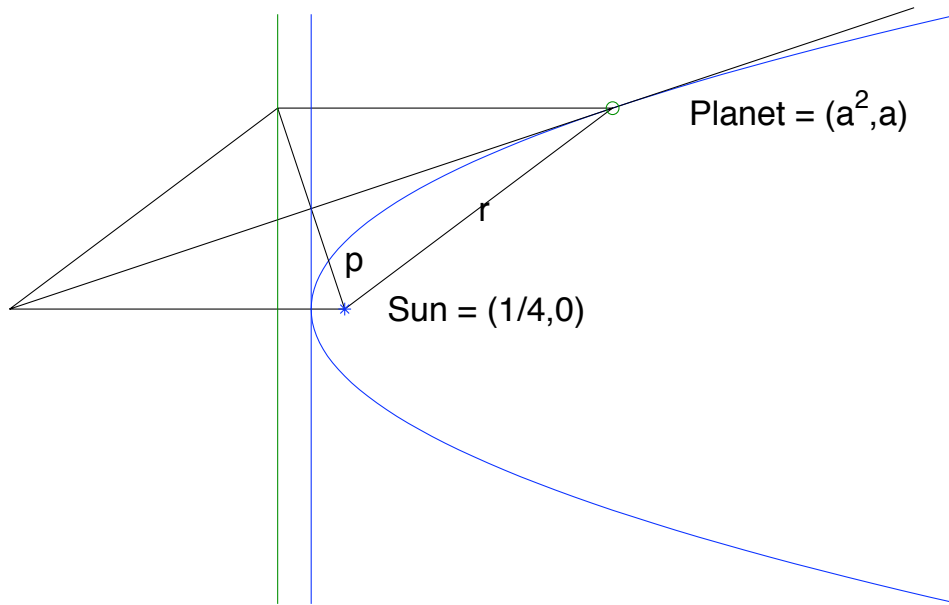
**Kepler speed:**  $|v| = \sin \varphi,$

**Angular momentum:**  $p \cdot |v| = 1/4.$

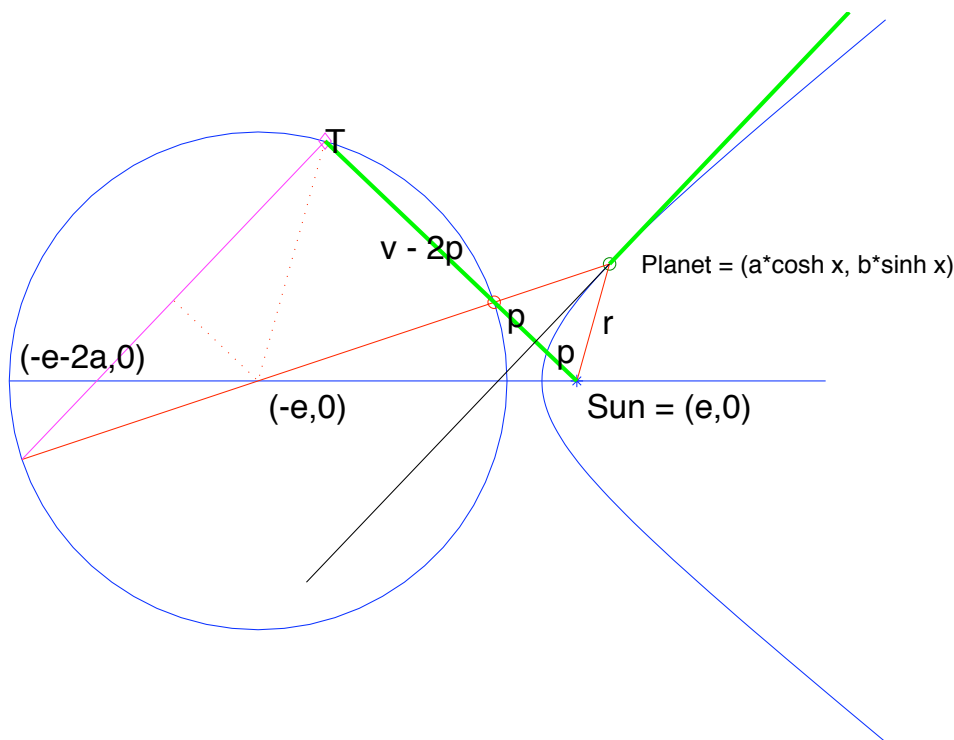
If we call  $r$  the distance to the planet, than we also have  $p/r = \sin \varphi = |v|$ . Multiplication with the angular momentum gives

**Kinetic energy:**  $\frac{1}{2}|v|^2 = \frac{1}{8r},$

**Potential energy:**  $\frac{-1}{8r}.$



*Derivation of the  $-1/r$ -potential from a hyperbolic Kepler orbit. As before we call  $p$  the distance from the sun to a tangent of the hyperbolic orbit and  $v$  the speed at that orbit point.*



Conservation of angular momentum says  $p \cdot |v| = \text{const.}$  We use the property of the circle (radius  $2a$ ) about prod-

ucts of segments on secants (which intersect at the sun  $S$ ):

$$2p \cdot |T - S| = (2e - 2a)(2e + 2a) = 4b^2.$$

Therefore, again up to the unit for velocity, we have identified the correct

$$\textbf{Kepler velocity: } v = |S - T|.$$

Finally, similar triangles give:

$$p/r = (v - 2p)/4a \quad \text{or} \quad 4a/r = v/p - 2,$$

and elimination of  $p$  with the angular momentum, i.e. with  $1/p = v/2b^2$ , shows that kinetic energy plus a radial function are constant – thus identifying the  $1/r$ -potential:

$$4ab^2/r = v^2/2 - 2b^2.$$

**Additional properties:** As in the case of elliptical orbits we see that the *hodograph* is a circle because the velocity vector, rotated by 90 degrees, ends on the circle which we used for the construction of the hyperbola. And if we add to the endpoint of this rotated velocity a vector parallel to the position vector and of constant length  $2a$  then we reach the midpoint of the circle, the other focal point of the orbit. The constant(!) difference vector between the two focal points, the geometric *Runge-Lenz vector*, differs from the common definition by the constant factor  $(e - a)/2e$ .

H.K.

[Go To Planar TOC](#)

## Nephroid of Freeth \*

This curve, first described 1879, is the member  $aa = 0$  in the following family of curves:

$$\begin{aligned}x(t) &= (1 - aa \cdot \sin(t/2)) \cos(t) \\y(t) &= (1 - aa \cdot \sin(t/2)) \sin(t)\end{aligned}$$

The default morph starts at  $aa = 0$  with a circle, traversed twice. For small  $aa > 0$  one double point develops. At  $aa = 1$  the curve reaches the origin with a cusp. This cusp deforms into a second double point. At  $aa = \sqrt{2}$  the two tangents of the double point coincide and are vertical. This point of double tangency deforms into three double points. The Nephroid of Freeth is reached at  $aa = 2$ , when two of the mentioned three double points coincide with the earliest one to form a *triple intersection*.

Apart from being in a simple family, which shows all these singularities of curves, we learnt from

<http://www.2dcurves.com/derived/strophoid.html>

that the Nephroid of Freeth has the curious property that one can construct a regular heptagon with it: The vertical tangent at the triple intersection meets the curve again in two points whose radius vectors enclose the angle  $3\pi/7$ .

H.K.

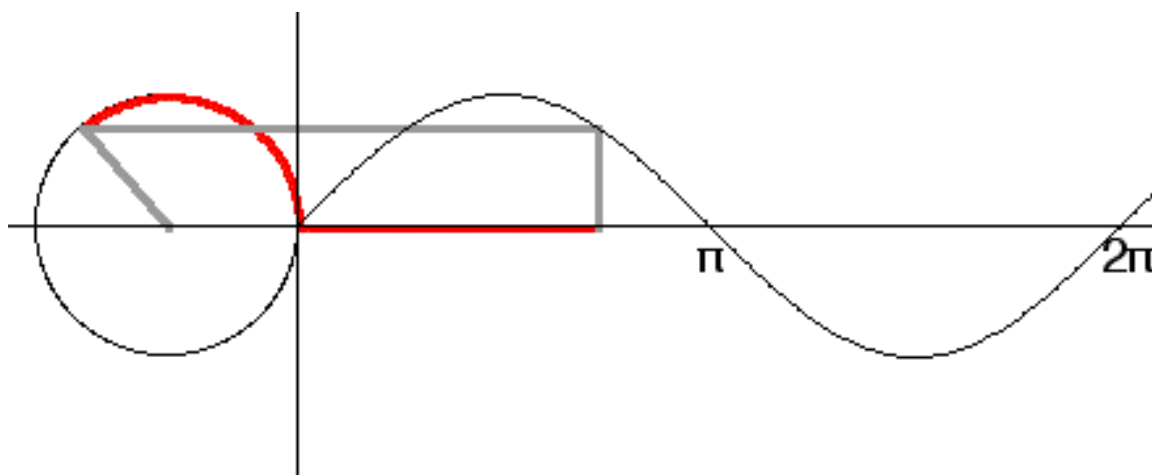
---

\* This file is from the 3D-XplorMath project. Please see:

## Sine \*

The demo in 3D-XplorMath illustrates: If a unit circle in the plane is traversed with *constant velocity* then it is parametrized with the so-called trigonometric or circular functions,

$$c(t) = (\cos t, \sin t).$$



## History

The earliest known computations with angles did not yet use degrees. In Babylonian astronomy angles were measured by their *chord*, i.e. by the base of an isoscele triangle with the vertex in the center of a unit circle and the other vertices on the circumference. Hipparchus (180 - 125 BC) is credited with the first table giving chords in terms of degrees. The table proceeded in steps of  $60^\circ/16$ . Ptolemy (ca 90 - ca 168 AD) computed more accurate tables in steps of  $1^\circ$ . With these tables trigonometric functions had come

---

\* This file is from the 3D-XplorMath project. Please see:

into existence, in modern notation the function

$$\text{chord: } \varphi \mapsto 2 \sin\left(\frac{2\pi}{360} \frac{\varphi}{2}\right).$$

Astronomy needed computations with spherical triangles. Initially these were done in geometric form, based on theorems on quadrilaterals inscribed in circles. Around 800 AD Arab astronomers developed the more streamlined computations based on properties of the functions  $\sin$  and  $\cos$ , expressed in formulas similar to the ones in use today. Since Newton's time  $\sin$  and  $\cos$  are even more conveniently defined by their linear differential equations

$$\begin{aligned}\sin'' &= -\sin, \quad \sin(0) = 0, \quad \sin'(0) = 1; \\ \cos'' &= -\cos, \quad \cos(0) = 1, \quad \cos'(0) = 0.\end{aligned}$$

The first derivatives  $\sin' = \cos$ ,  $\cos' = -\sin$  and addition theorems like

$$\begin{aligned}\sin(a + x) &= \sin(a) \cos(x) + \cos(a) \sin(x), \\ \cos(a + x) &= \cos(a) \cos(x) - \sin(a) \sin(x),\end{aligned}$$

follow from the uniqueness theorems for such differential equations (both sides satisfy the same ODE and the same initial conditions). Also the identity

$$\sin^2(x) + \cos^2(x) = \sin^2(0) + \cos^2(0) = 1$$

which is needed to show “*that  $\sin$  and  $\cos$ , defined by their differential equations, indeed parametrize the unit circle with unit velocity*”, follows directly by differentiation.

With Euler's discovery of the close connection between the exponential and the trigonometric functions computations became even more convenient, since one only needs

$$\begin{aligned} \exp' &= \exp, \quad \exp(0) = 1, \quad \exp(z + w) = \exp(z) \exp(w) \\ \exp(x + i y) &= \exp(x) \cdot (\cos(y) + i \sin(y)). \end{aligned}$$

In the 19th century approximation of functions by *Fourier polynomials*  $P_N(x) := a_0 + \sum_{n=1}^N a_n \cos(nx) + b_n \sin(nx)$  lead to unexpected difficulties and corresponding deep insights. The modern notion of a function and also the concept of continuity have their roots in these studies.

Today, when high school kids first meet sine and cosine, they do not meet them as real valued functions, but as ratios of edge lengths in rectangular triangles. There is no reference to a numerical algorithm that computes the values of sine and cosine from "angles". The above addition theorems emphasize this: if  $(c_1, s_1), (c_2, s_2) \in \mathbb{S}^1$ , then also  $(c_1 c_2 - s_1 s_2, s_1 c_2 + c_1 s_2) \in \mathbb{S}^1$ . Note that this addition of rational points gives again a rational point, and rational points on  $\mathbb{S}^1$  are the same as Pythagorean triples, namely  $(a/b)^2 + (c/d)^2 = 1$  is equivalent to  $(ad)^2 + (bc)^2 = (bd)^2$ . On this level sine and cosine belong to the geometry of similar triangles, and indeed, the addition formulas can be proved by using similarity of triangles. – So, what **is** the relation between sine, cosine and angles? One answer is to define sine, cosine in terms of their ODEs quoted above, another is, to discuss first the arc length of the circle, which means, define the inverse functions arcsine, arccosine first.

We come back to computations of sine and cosine below, but first we return to the beginning. The following formulas show (in modern notation) how the trigonometric functions enter planar and spherical geometry.

## Laws of Sines and Cosines

For any *planar triangle* with side lengths  $a$ ,  $b$  and  $c$ , whose opposite angles are  $\alpha$ ,  $\beta$  and  $\gamma$  respectively, we have:

Projection theorem:  $c = a \cdot \cos \beta + b \cdot \cos \alpha$

Sine theorem:  $b \cdot \sin \alpha = h_c = a \cdot \sin \beta$

Cosine theorem:  $c^2 = a^2 + b^2 - 2ab \cos \gamma$

In astronomy the corresponding formulas for *spherical triangles* on the unit sphere played a much more important role. They are:

Projection theorem:  $\cos a \sin c = \sin a \cos c \cos \beta + \sin b \cos \alpha$

Sine theorem:  $\sin b \cdot \sin \alpha = \sin a \cdot \sin \beta$

Cosine thm:  $\cos c = \cos a \cos b + \sin a \sin b \cos \gamma$ .

A consequence of the first two theorems is the

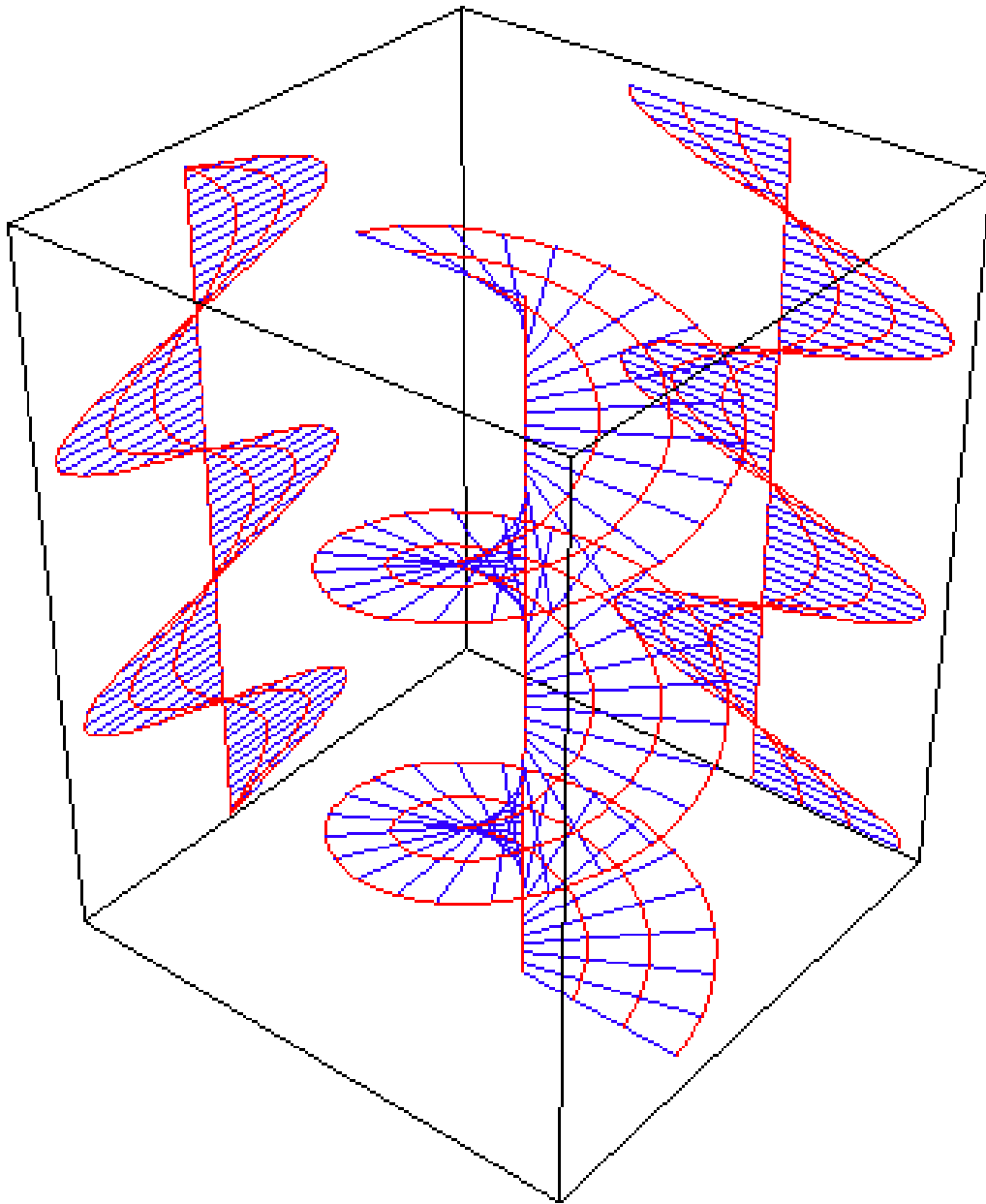
Angle Cosine thm:  $\cos \gamma = -\cos \alpha \cos \beta + \sin \alpha \sin \beta \cos c$ .

For triangles with small edge lengths  $a, b, c$  the spherical formulas become the planar ones if all terms that are at least cubic in the edge lengths are ignored, i.e.

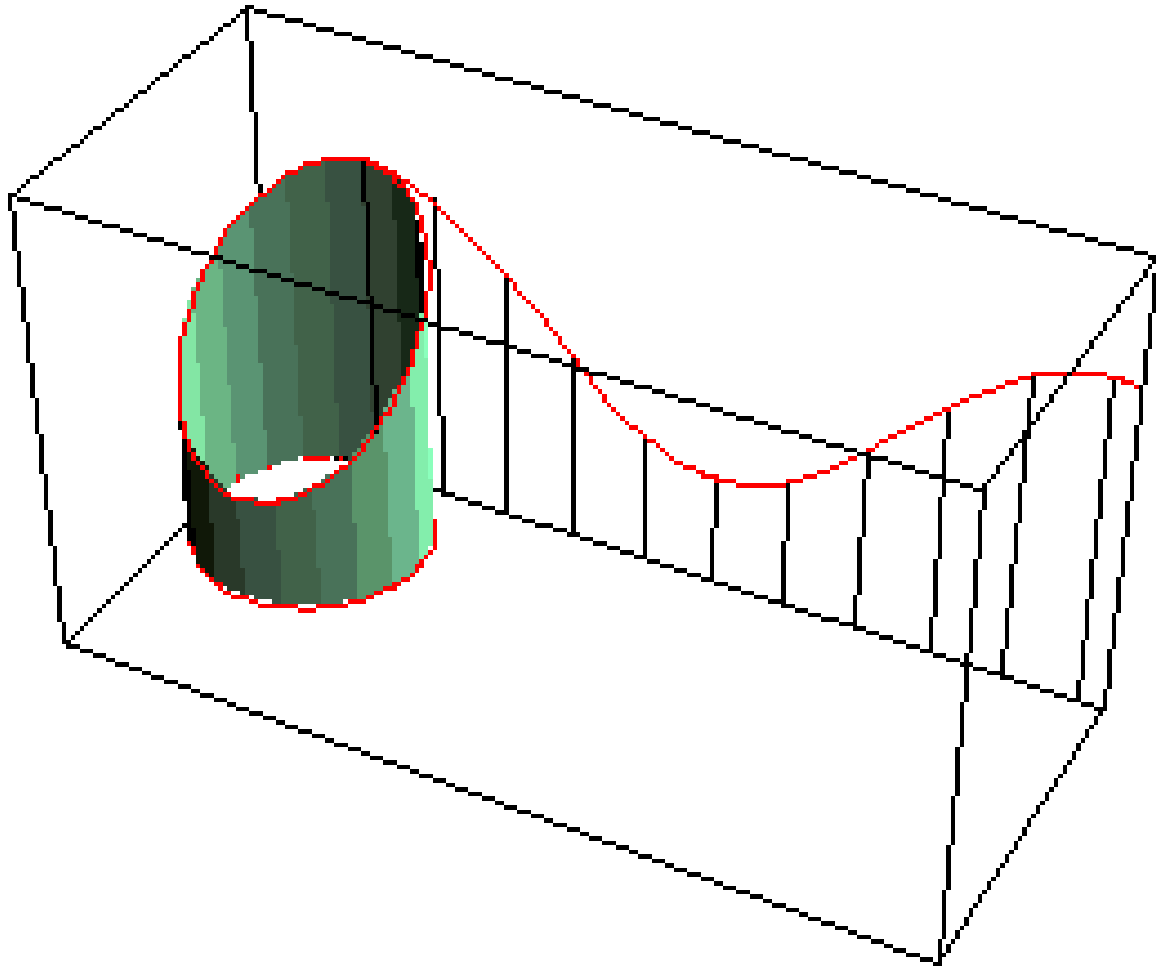
$$\sin a \approx a, \quad \cos a \approx 1 - a^2/2, \quad \sin a \cos c \approx a.$$

## Trivia

### Orthogonal Projections of the Helix



The sinusoid is an orthogonal projection of the helix space curve. In 3DXM, a helix can be seen in the Space Curves category and, independently, via the Action Menu entry Show Planar Curve As Graph, after selecting Circle.



The sinusoid is the development of an obliquely cut right circular cylinder—i.e., the edge of the cylinder rolls out to a sinusoid.

## Numerical Computations

From the ODEs one immediately gets the Taylor series ( $\lim_{N \rightarrow \infty}$  below) which are convenient to compute sine and cosine for small arguments (so that small  $N$  are sufficient):

$$\sin x \approx \sum_{k=0}^N \frac{(-1)^k}{(2k+1)!} x^{2k+1}, \quad \cos x \approx \sum_{k=0}^N \frac{(-1)^k}{(2k)!} x^{2k}.$$

Numerical efforts can be greatly reduced with the simple

angle tripling formulas

$$P_3(y) := 3y - 4y^3,$$

$$\sin(3x) = 3 \sin(x) - 4 \sin^3(x) = P_3(\sin x),$$

$$\cos(3x) = -3 \cos(x) + 4 \cos^3(x) = -P_3(\cos x).$$

Accuracy, already with  $N = 2$ , is surprising:

$$0 = \sin \pi \approx P_3(P_3(P_3(Taylor_5(\pi/27)))) \approx -1.6 \cdot 10^{-9}.$$

Since  $\sin x \approx x$  is a very good approximation for small  $x$  we get

$$\lim_{n \rightarrow \infty} P_3^{\circ n}(x/3^n) = \sin(x).$$

Or, *much faster*:  $\lim_{n \rightarrow \infty} P_3^{\circ n}(Taylor_5(x/3^n)) = \sin(x)$ .

Since  $\sin'(\pi) = -1$ , one can compute  $\pi$  with the Newton iteration

$$x_{n+1} := x_n + \sin(x_n), \quad x_0 = 3.$$

This can also be seen as a consequence of  $\arcsin(x) \approx x$  for small  $x$  and  $\pi/2 < x < \pi \Rightarrow \pi = x + \arcsin(\sin(x))$ .

Then, using the better approximation:

$$\arcsin(x) \approx x + \frac{1}{6}x^3,$$

one gets the really fast iteration

$$x_{n+1} := F(x_n) := x_n + \sin(x_n) + \frac{1}{6} \sin(x_n)^3.$$

Example:  $F(2.5) = 3.1342$ ,  $F(F(2.5)) = 3.14159265358$ .

When Archimedes estimated  $\pi$ , he used the inverse of the angle doubling formulas to compute the length of a regular inscribed  $2n$ -gon from the length of a regular  $n$ -gon, namely

$$\cos\left(\frac{x}{2}\right) = \sqrt{0.5(1 + \cos(x))}, \quad \sin\left(\frac{x}{2}\right) = 0.5 \sin(x) / \cos\left(\frac{x}{2}\right).$$

## Pendulum ODE function \*

Although one may feel that the sine function is an explicit function, it is really defined via the ODE

$$\sin''(x) = -\sin(x), \text{ with } \sin(0) = 0, \sin'(0) = 1.$$

The solutions of the ODE of the mathematical pendulum

$$f''(x) = -\sin(f(x))$$

was also studied a lot, but did not reach the popularity of the sine function. In 3D-XplorMath we use parameters as follows:

$$f''(x) = \frac{-cc}{aa} \cdot \sin(aa \cdot f(x)), \quad f(0) = hh, f'(0) = bb.$$

For better comparison with the sine function,  $aa = 0$  is allowed. The size of  $cc$  changes the frequency, as with the sine function. In addition observe that, for  $aa \neq 0$ . the period becomes longer when the amplitude grows. As with the sine function one has an “energy integral”:

$$\frac{f'(x)^2}{2} - \frac{cc}{aa^2} \cos(aa \cdot f(x)) = \frac{f'(0)^2}{2} - \frac{cc}{aa^2} \cos(aa \cdot f(0)).$$

With  $aa = 1, cc = -1$  we obtain solutions of the Sine-Gordon equation  $q_{xt} = \sin(q)$ , namely  $q(x, t) := f(x + t)$ . For  $f(0) = \pi, f'(0) = 2$  we get  $f(u) = 4 \arctan(\exp(u))$ .  
H.K. Go To Planar TOC

---

\* This file is from the 3D-XplorMath project. Please see:

## Lissajous Plane Curve \*

The Lissajous curves show the orbits of two orthogonal harmonic undamped oscillators.

$$\text{Lissajous}(t) := \begin{pmatrix} aa \cdot \sin(ee \cdot t + cc) \\ bb \cdot \sin(dd \cdot t) \end{pmatrix},$$

Default values:  $dd = 3$ ,  $ee = 5$ ,  $cc = 0$ .

If the parameters  $dd, ee$  are integers then the curves are closed. Actually, a rational ratio is sufficient.

The default morph varies the phase  $cc$ , which changes the curves a lot.

These planar curves have obvious analogues in  $\mathbb{R}^3$ .

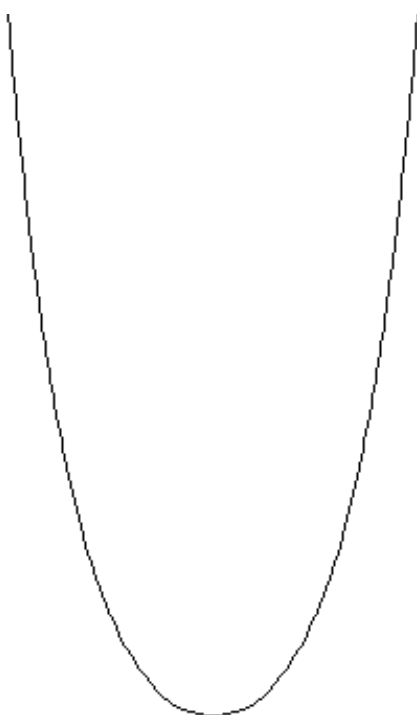
H.K.

---

\* This file is from the 3D-XplorMath project. Please see:

## Catenary \*

The catenary is also known as the chainette, alysoid, and hyperbolic cosine. It is defined as the graph of the function  $y = a \cosh(x/a)$ . (Recall  $\cosh(x) := (e^x + e^{-x})/2$ , where  $e = 2.71828\dots$  is the base of the natural logarithms.)



The Catenary

The catenary is the shape an ideal string takes when hanging between two points. By “ideal” is meant that the string is perfectly flexible and inextensible, has no thickness, is of uniform density. In other words the catenary is a mathematical abstraction of the shape of a hanging string, and it

---

\* This file is from the 3D-XplorMath project. Please see:

closely approximates the shapes of most hanging string-like objects we see, such as ropes, outdoor telecommunication wires, necklaces, chains, etc. For any particular hanging string, we will need to choose the parameter  $a$  correctly to model that string.

Notice that except for scaling there is really only a single catenary. That is, the scaling transformation  $(x, y) \mapsto (ax, ay)$  maps the graph of  $y = a \cosh(x/a)$  onto the graph of  $y = \cosh(x)$ . The scaling transformation just amounts to a change in the choice of units used to measure distances.

## History

Galileo was the first to investigate the catenary, but he mistook it for a parabola. James Bernoulli in 1691 obtained its true form and gave some of its properties. [cf., Robert C. Yates, 1952]

Galileo's suggestion that a heavy rope would hang in the shape of a parabola was disproved by Jungius in 1669, but the true shape of the catenary, was not found until 1690–91, when Huygens, Leibniz and John Bernoulli replied to a challenge by James Bernoulli. David Gregory, the Oxford professor, wrote a comprehensive treatise on the 'catenarian' in 1697. The name was first used by Huygens in a letter to Leibniz in 1690. [cf., E.H.Lockwood, 1961].

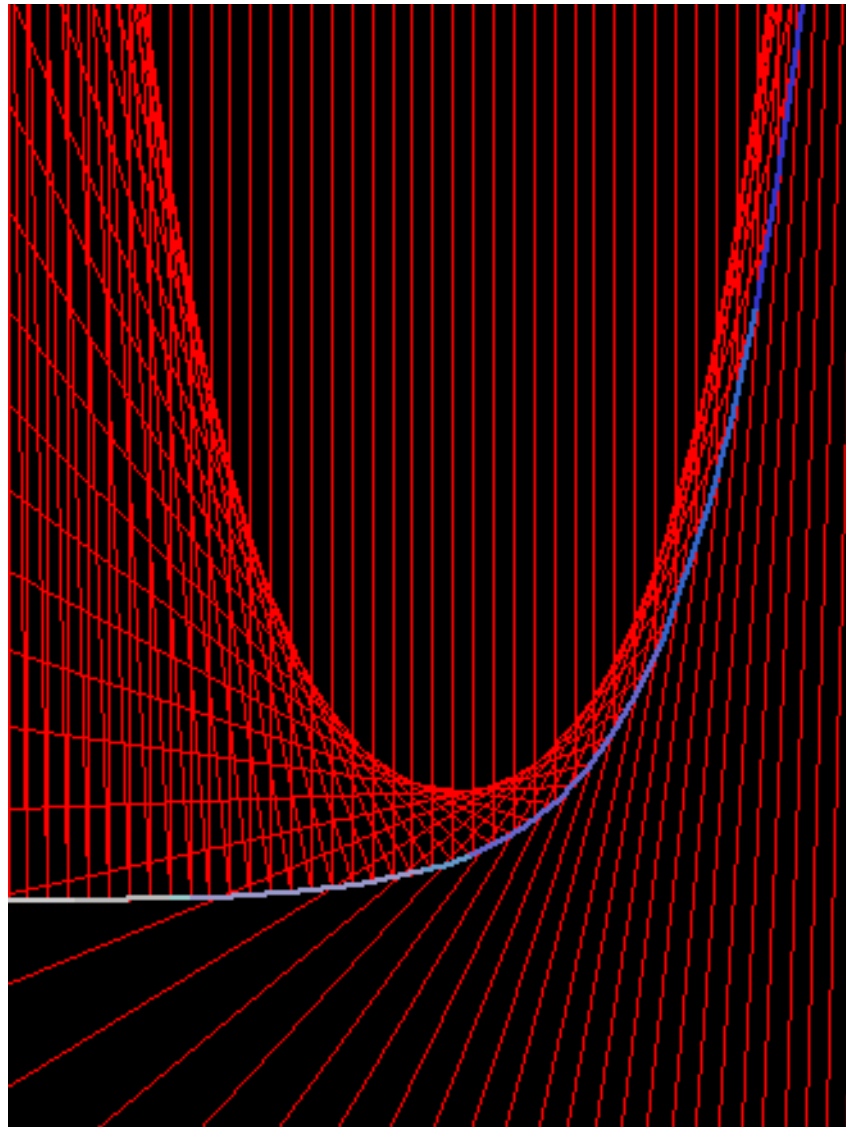
[By the way, it is true that if you carefully weight a hanging string so that their is equal weight of string per unit of horizontal distance (rather than per unit of length) then

its shape will be a parabola, so Galileo wasn't so far from the truth.]

The Catenary has numerous interesting properties.

## Properties of the Catenary

### Caustics



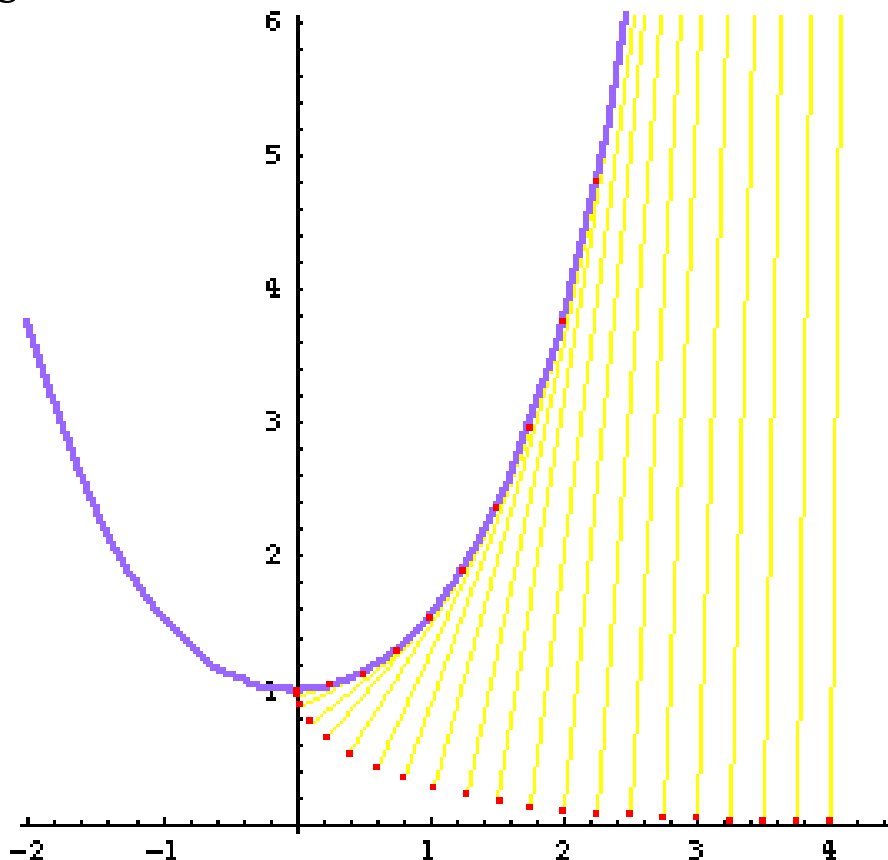
Parallel rays above the exponential curve

The Catacaustic of the exponential curve  $(x, e^x)$  with light rays from above and parallel to the y axes is the catenary.

The exponential function  $e^x$  has interesting properties it-

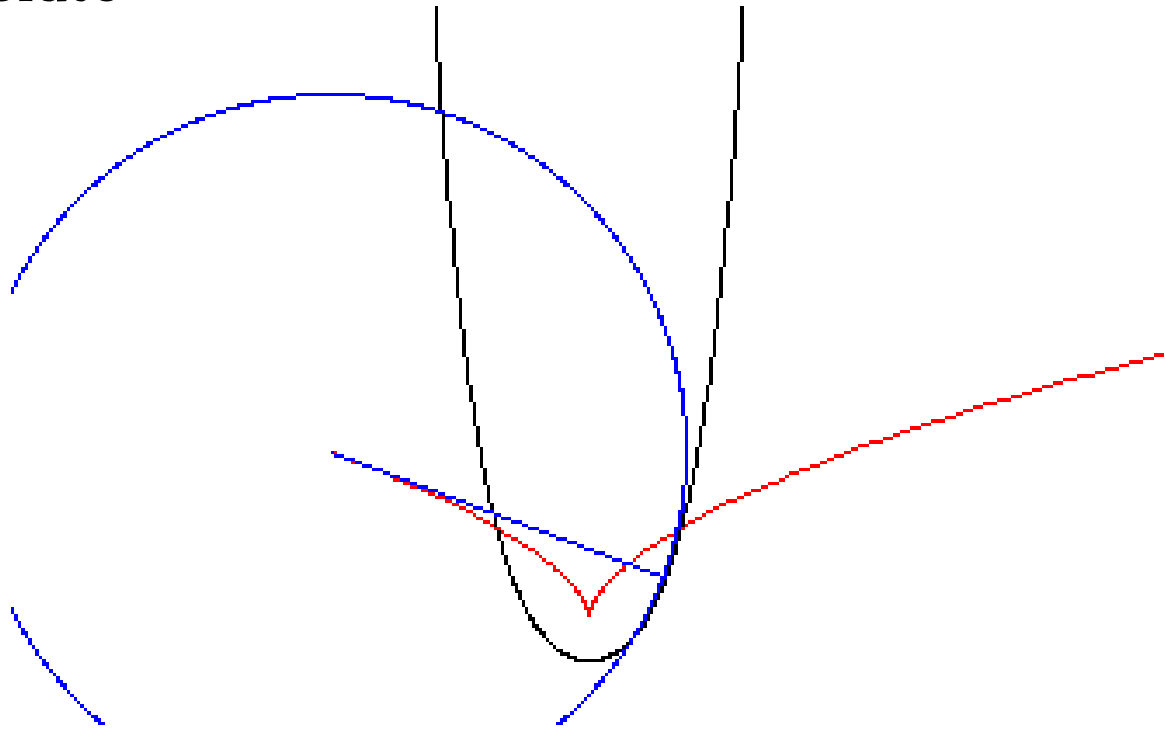
self. It is the only function who agrees with its derivative.

## Involute



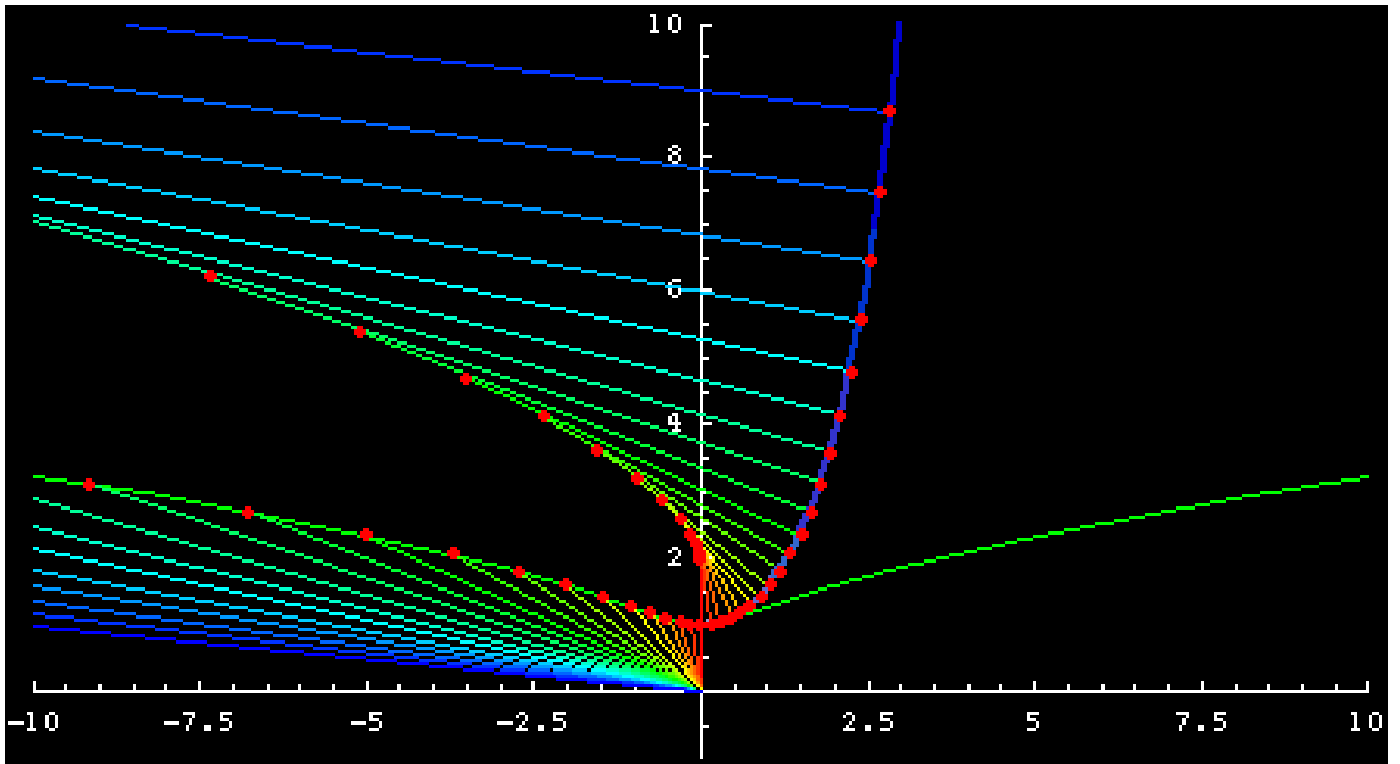
The involute of catenary starting at the vertex is the curve **Tractrix**. (In 3DXM, the involutes of a curve can be shown in the menu Action  $\rightarrow$  Show Involutives.) Note that all involutes are parallel curves of each other. This is a theorem.

## Evolute



The evolute of the catenary is also the tractrix. (In 3DXM, this can be seen from the menu Action → Show Osculating Circles.)

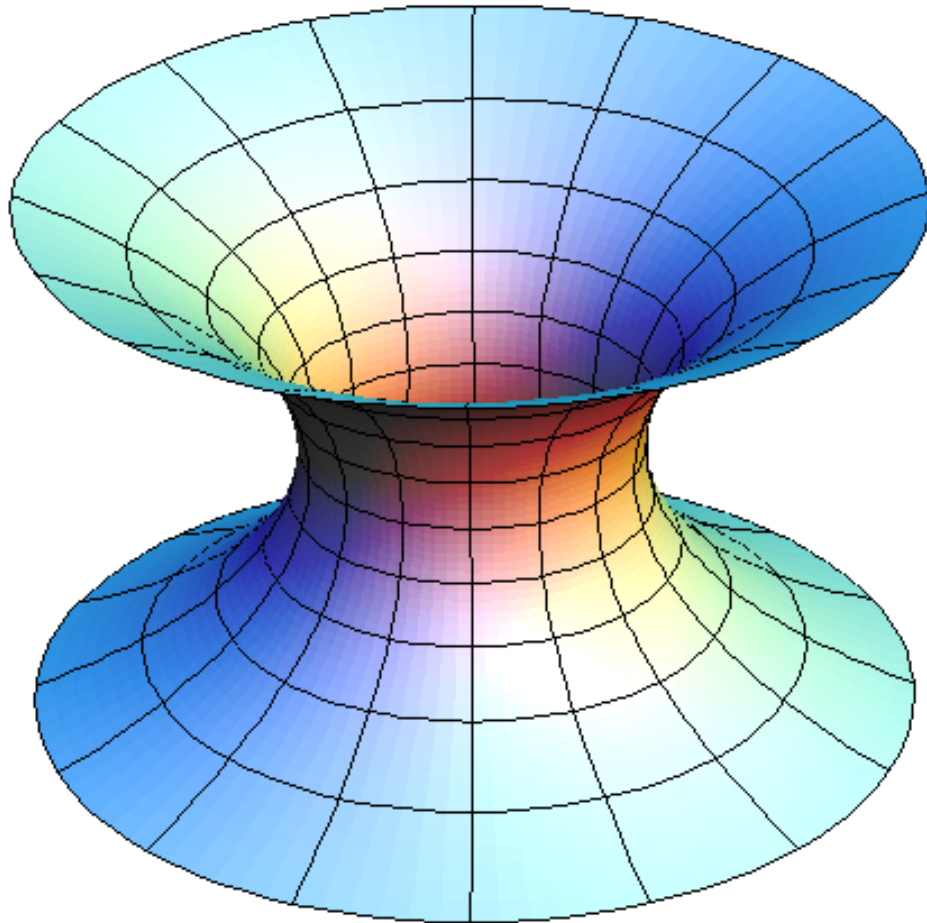
## Radial and Kampyle of Eudoxus



The radial of the catenary is the Kampyle of Eudoxus. In the figure above, the blue curve is half the catenary. The green curve is the Kampyle of Eudoxus. The rainbow lines are radii of osculating circles and their parallels through 0.

The Kampyle of Eudoxus is defined as the parametric curve  $x = -\cosh(t) \sinh(t)$ ,  $y = \cosh(t)$ .

## Catenoid



If you rotate the graph of  $x = \cosh(y)$  about the  $y$ -axis, the resulting surface of revolution is a minimal surface, called the Catenoid. It is one endpoint of an interesting morph you can see in 3DXM, by switching to the Surface category, choosing Helicoid-Catenoid from the Surface menu, and then choosing Morph from the Animate menu. If you look closely you will see that during this morph distances and angles on the surface are preserved. See About This Object... in the Documentation menu when Helicoid-Catenoid is selected for a discussion of this.

# On Curves Given By Their Support Function \*

This note is about smooth, closed, convex curves in the plane and how to define them in terms of their so-called *Minkowski support function*  $h$ . For quick reference we first show how, in 3D-XplorMath,  $h$  can be modified by specifying parameters. Then we begin with a more general class of geometric objects, namely *convex bodies*.

## 1. Parameter Dependent Formulas

In 3D-XplorMath, the support function  $h$  is given in terms of Fourier summands:

$$h(\varphi) := aa + bb \cos(\varphi) + cc \cos(2\varphi) + dd \cos(3\varphi) + ee \cos(4\varphi) + ff \cos(5\varphi).$$

In terms of this function we define the following curve:

$$c(\varphi) := h(\varphi) \cdot \begin{pmatrix} \cos(\varphi) \\ \sin(\varphi) \end{pmatrix} + h'(\varphi) \cdot \begin{pmatrix} -\sin(\varphi) \\ +\cos(\varphi) \end{pmatrix}.$$

Differentiation shows that  $c$  is given in terms of its unit normal and tangent vectors and the function  $h$ :

$$c'(\varphi) = (h + h'')(\varphi) \cdot \begin{pmatrix} -\sin(\varphi) \\ +\cos(\varphi) \end{pmatrix}.$$

---

\* This file is from the 3D-XplorMath project. Please see:

One obtains curves with nonsingular parametrization ( $|c'| > 0$ ) if  $aa$  is chosen large enough. And since  $h(\varphi)$  equals the scalar product between  $c(\varphi)$  and the unit normal  $n(\varphi) = (\cos(\varphi), \sin(\varphi))$  one has a simple geometric interpretation:  $h(\varphi)$  is the distance of the tangent at  $c(\varphi)$  from the origin.

## 2. Background And Explanations

A convex body in  $\mathbb{R}^n$  is a compact subset  $\mathbb{B}$  having non-empty interior and such that it includes the line segment joining any two of its points. A hyperplane  $H$  in  $\mathbb{R}^n$  is called a supporting hyperplane of  $\mathbb{B}$  if it contains a point of  $\mathbb{B}$  and if  $\mathbb{B}$  is included in one of the two halfspaces defined by  $H$ . It is not difficult to show that every boundary point of  $\mathbb{B}$  lies on at least one supporting hyperplane, and that  $\mathbb{B}$  is the intersection of all such halfspaces.

A smooth, closed, planar curve  $c$  is called *convex* if its tangent at each point intersects  $c$  only at that one point. The complement in  $\mathbb{R}^2$  of such a curve has a single bounded component, the *interior* of the curve, and one unbounded component, its *exterior*. The curve is the boundary of its interior, and we denote by  $\mathbb{B}$  the curve together with its interior. It is easy to see that  $\mathbb{B}$  is a convex body in  $\mathbb{R}^2$ , as defined above, and in fact the tangent line at any point of  $c$  is the unique supporting hyperplane (= line!) containing that point. (There are of course more general planar convex bodies. For example if  $P$  is a closed polygon in  $\mathbb{R}^2$  together with its interior, then  $P$  is a convex body, but there are infinitely many supporting lines through each ver-

tex, while the supporting line containing an edge contains infinitely many points.)

Now let  $O$  be some interior point of  $c$  and take  $O$  as the origin of a cartesian coordinates by fixing a ray from  $O$  as the positive  $x$ -axis. With respect to these coordinates, at each point  $p$  on  $c$  the outward directed unit normal at  $p$  will have the form  $n(\varphi) = (\cos(\varphi), \sin(\varphi))$  where  $\varphi = \varphi(p)$  satisfies  $0 \leq \varphi \leq 2\pi$ . If we as usual think of  $\mathbb{S}^1$  as the interval  $[0, 2\pi]$  with endpoints identified, then it can be shown that the map  $p \mapsto \varphi(p)$  is a smooth one-to-one map of  $c$  with  $\mathbb{S}^1$ , so that the inverse map gives a parametrization  $c(\varphi)$  of the curve by  $\mathbb{S}^1$ . (This just says that given any direction in the plane, there is a unique point  $p$  on  $c$  where the outward normal has that direction, and the point  $p$  varies smoothly with the direction.)

The Minkowski *support function* for the curve  $c$  is the function  $h$  defined on  $\mathbb{S}^1$  by letting  $h(\varphi)$  be the distance from the origin of the line of support (or tangent) through  $c(\varphi)$ , that is  $h(\varphi) := n(\varphi) \cdot c(\varphi)$ , the scalar product of  $c(\varphi)$  and  $n(\varphi)$ . From this definition it is easy to reconstruct the curve in terms of its support function as in part 1.

### 3. Things To Observe

Recall one has in any parametrization the curvature formula

$$n'(t) = \kappa(t)c'(t),$$

which in the present case reduces to:

$$1/\kappa(\varphi) = h(\varphi) + h''(\varphi) = |c'(\varphi)|.$$

Clearly  $aa$  has to be large enough to make  $\kappa$  positive and the parametrization nonsingular. Adding a linear combination of  $\cos(\varphi)$  and  $\sin(\varphi)$  to the support function corresponds to a change of only the origin, the shape of the curve stays the same. The  $bb \cos(\varphi)$ -term in the support function is therefore not really necessary, but one can use it to see how the parametrization of the curve changes.

The  $\cos$ -terms in even multiples of  $\varphi$  make up the even part  $(h(\varphi) + h(\varphi + \pi))/2$  of  $h$ . The origin is the *midpoint* of curves with even support function. If  $h$  is odd except for the constant term, i.e.,

$$h(\varphi) = aa + (h(\varphi) - h(\varphi + \pi))/2,$$

then one obtains curves of constant width  $w$  where:

$$w = h(\varphi) + h(\varphi + \pi) = 2aa.$$

The default curve in 3D-XplorMath is such a curve of constant width and the default morph shows a family of such curves. We emphasize the width of our curves by drawing them together with their pairs of parallel tangents. Since the (non-)constancy of the distance between these parallel tangents is difficult to see we have added a circle of the same width (= diameter). One cannot easily recognize how many extrema the curvature  $\kappa(\varphi)$  has. To see it clearly we recommend selecting the entry *Show Osculating Circles* from the Action Menu, since the evolute has a cusp at every extremal value of  $\kappa$ .

H.K.

[Go To Planar TOC](#)

## Tractrix \*

The Tractrix is a curve with the following nice interpretation: Suppose a dog-owner takes his pet along as he goes for a walk “down” the  $y$ -axis. He starts from the origin, with his dog initially standing on the  $x$ -axis at a distance  $aa$  away from the owner. Then the Tractrix is the path followed by the dog if he “follows his owner unwillingly”, i.e., if he constantly pulls against the leash, keeping it tight. This means mathematically that the leash is always tangent to the path of the dog, so that the length of the tangent segment from the Tractrix to the  $y$ -axis has constant length  $aa$ . Parametric equations for the Tractrix (take  $bb = 0$ ) are:

$$\begin{aligned}x(t) &= aa \cdot \sin(t)(1 + bb) \\y(t) &= aa \cdot (\cos(t)(1 + bb) + \ln(\tan(t/2))).\end{aligned}$$

The curves obtained for  $bb \neq 0$  are generated by the same kinematic motion, except that a different point of the moving plane is taken as the drawing pen. See the default Morph.

The Tractrix has a well-known surface of revolution, called the Pseudosphere, Namely, rotating it around the  $y$ -axis gives a surface with Gaussian curvature  $-1$ . This means that the Pseudosphere can be considered as a portion of

---

\* This file is from the 3D-XplorMath project. Please see:

the Hyperbolic Plane. The latter is a geometry that was discovered in the 19th century by Bolyai and Lobachevsky. It satisfies all the axioms of Euclidean Geometry except the Axiom of Parallels. In fact, through a point outside a given line (= geodesic) there are infinitely many lines that are parallel to (i.e., do not meet) the given line.

There are many connections, sometimes unexpected, between planar curves. For the Tractrix select: **Show Osculating Circles And Normals**. One observes a Catenary (see another entry in the curve menu) as the envelope of the normals.

H.K.

## Cissoid and Strophoid \*

$$\text{3DXM Family: } c(t) := 2aa \left( \frac{t(t^2 - bb)}{(1 + t^2)}, \frac{bb}{2aa} + \frac{t^2 - bb}{(1 + t^2)} \right)$$

The additive constant  $bb/2aa$  in the  $y$ -coordinate has the effect that the drawing mechanism is the same for the whole family, try the default **Morph** in the **Animate Menu**.

### History

Diocles ( 250 – ~100 BC) invented the Cissoid to solve the doubling of the cube problem (also know as the the Delian problem). The name Cissoid (ivy-shaped) derives from the shape of the curve. Later the method used to generate this curve was generalized, and we call all curves generated in a similar way Cissoids. Newton (see below) found a way to generate the Cissoid mechanically. The same kinematic motion with a different choice of the drawing pen generates the (right) Strophoid, formulas below.

From Thomas L. Heath's Euclid's Elements translation (1925) (comments on definition 2, book one):

This curve is assumed to be the same as that by means of which, according to Eutocius, Diocles in

---

\* This file is from the 3D-XplorMath project. Please see:

his book *On Burning-Glasses* solved the problem of doubling the cube.

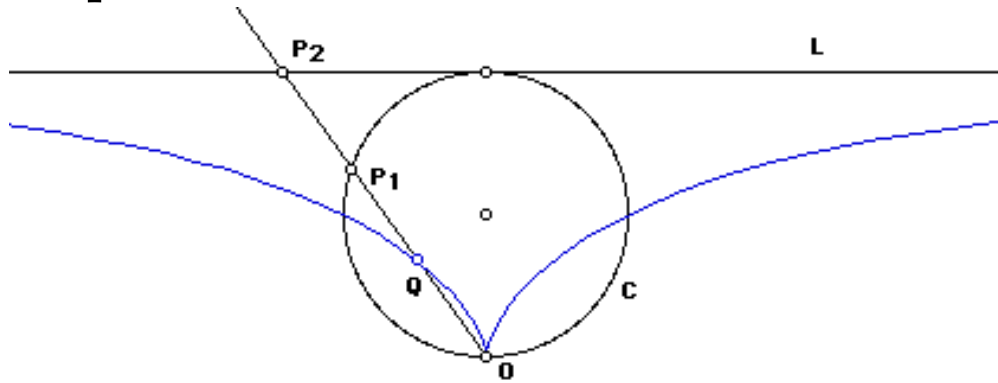
From Robert C. Yates' *Curves and their properties* (1952):

As early as 1689, J. C. Sturm, in his *Mathesis Enucleata*, gave a mechanical device for the constructions of the Cissoïd of Diocles.

From E.H.Lockwood *A book of Curves* (1961):

The name cissoïd (“Ivy-shaped”) is mentioned by Geminus in the first century B.C., that is, about a century after the death of the inventor Diocles. In the commentaries on the work by Archimedes *On the Sphere and the Cylinder*, the curve is referred to as Diocles’ contribution to the classic problem of doubling the cube. ... Fermat and Roberval constructed the tangent (1634); Huygens and Wallis found the area (1658); while Newton gives it as an example, in his *Arithmetica Universalis*, of the ancients’ attempts at solving cubic problems and again as a specimen in his *Enumeratio Linearum Tertii Ordinis*.

# 1 Description



The Cissoid of Diocles is a special case of the general cissoid. It is a cissoid of a circle and a line tangent to the circle with respect to a point on the circle opposite to the tangent point. Here is a step-by-step description of the construction:

1. Let there be given a circle  $C$  and a line  $L$  tangent to this circle.
2. Let  $O$  be the point on the circle opposite to the tangent point.
3. Let  $P_1$  be a point on the circle  $C$ .
4. Let  $P_2$  be the intersection of line  $[O, P_1]$  and  $L$ .
5. Choose  $Q$  on line  $[O, P_1]$  with  $\text{dist}[O, Q] = \text{dist}[P_1, P_2]$ .
6. The locus of  $Q$  (as  $P_1$  moves on  $C$ ) is the cissoid of Diocles.

An important property to note is that  $Q$  and  $P_1$  are symmetric with respect to the midpoint of the segment  $[O, P_2]$ . Call this midpoint  $M$ . We can reflect every element in the construction around  $M$ , which will help us visually see other properties.

## 2 Formula derivation

Let the given circle  $C$  be centered at  $(1/2, 0)$  with radius  $1/2$ . Let the given line  $L$  be  $x = 1$ , and let the given point  $O$  be the origin. Let  $P1$  be a variable point on the circle, and  $Q$  the tracing point on line  $[O, P1]$ . Let the point  $(1, 0)$  be  $A$ . We want to describe distance  $r = \text{dist}[O, Q]$  in terms of the angle  $\theta = [A, O, P1]$ . This will give us an equation for the Cissoid in polar coordinates  $(r, \theta)$ . From elementary geometry, the triangle  $[A, O, P1]$  is a right triangle, so by trigonometry, the length of  $[O, P1]$  is  $\cos(\theta)$ . Similarly, triangle  $[O, A, P2]$  is a right triangle and the length of  $[O, P2]$  is  $\frac{1}{\cos(\theta)}$ . Since  $\text{dist}[O, Q] = \text{dist}[O, P2] - \text{dist}[O, P1]$ , we have  $\text{dist}[O, Q] = \frac{1}{\cos(\theta)} - \cos(\theta)$ . Thus the polar equation is  $r = \frac{1}{\cos(\theta)} - \cos(\theta)$ . If we combine the fractions and use the identity  $\sin^2 + \cos^2 = 1$ , we arrive at an equivalent form:  $r = \sin(\theta) \tan(\theta)$ .

### 3 Formulas for the Cissoid and the Strophoid

In the following, the cusp is at the origin, and the asymptote is  $x = 1$ . (So the diameter of the circle is 1 ( $= aa$  in 3DXM).)

$$\text{Parametric: } (\sin^2(t), \sin^2(t) \tan(t)) \quad -\pi/2 < t < \pi/2.$$

$$\text{Parametric: } \left( \frac{t^2}{(1+t^2)}, \frac{t^3}{(1+t^2)} \right) \quad -\infty < t < \infty$$

$$\text{Strophoid: } \left( \frac{t^2 - 1}{(1+t^2)}, \frac{t(t^2 - 1)}{(1+t^2)} \right) \quad -\infty < t < \infty$$

$$\text{Polar: } r = \frac{1}{\cos(\theta)} - \cos(\theta) \quad -\pi/2 < t < \pi/2.$$

$$\text{Cissoid: } y^2(1-x) = x^3, \quad \text{Strophoid: } y^2(1-x) = x^2(1+x).$$

The Cissoid has numerous interesting properties.

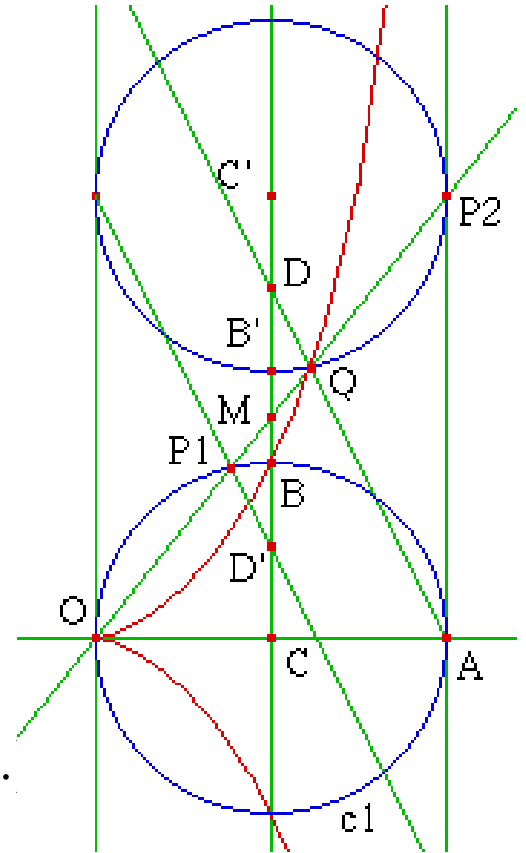
### 4 Properties

#### 4.1 Doubling the Cube

Given a segment  $[C, B]$ , with the help of the Cissoid of Diocles we can construct a segment  $[C, M]$  such that  $\text{dist}[C, M]^3 = 2 * \text{dist}[C, B]^3$ . This solves the famous doubling the cube problem.

Step-by-step description:

1. Given two points  $C$  and  $B$ .
2. Construct a circle  $c_1$ , centered on  $C$  and passing through  $B$ .
3. Construct points  $O$  and  $A$  on the circle such that line  $[O, A]$  is perpendicular to line  $[C, B]$
4. Construct a cissoid of Diocles using circle  $c_1$ , tangent at  $A$ , and pole at  $O$ .
5. Construct point  $D$  such that  $B$  is the midpoint of segment  $[C, D]$ .
6. Construct line  $[A, D]$ . Let the intersection of cissoid and line  $[A, D]$  be  $Q$ . (The intersection cannot be found with Greek Ruler and Compass. We assume it is a given.)
7. Let the intersection of line  $[C, D]$  and line  $[O, Q]$  be  $M$ .
8.  $\text{dist}[C, M]^3 = 2 \cdot \text{dist}[C, D]^3$ .

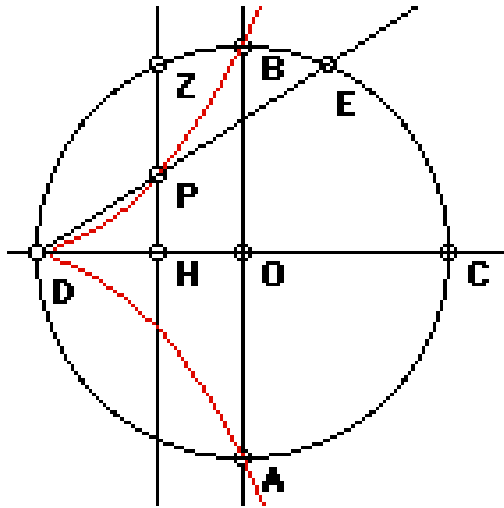


This can be proved trivially with analytic geometry.

## 4.2 Diocles' Construction

By some modern common accounts (Morris Kline, Thomas L. Heath), here's how Diocles constructed the curve in his book

*On Burning-Glasses:*

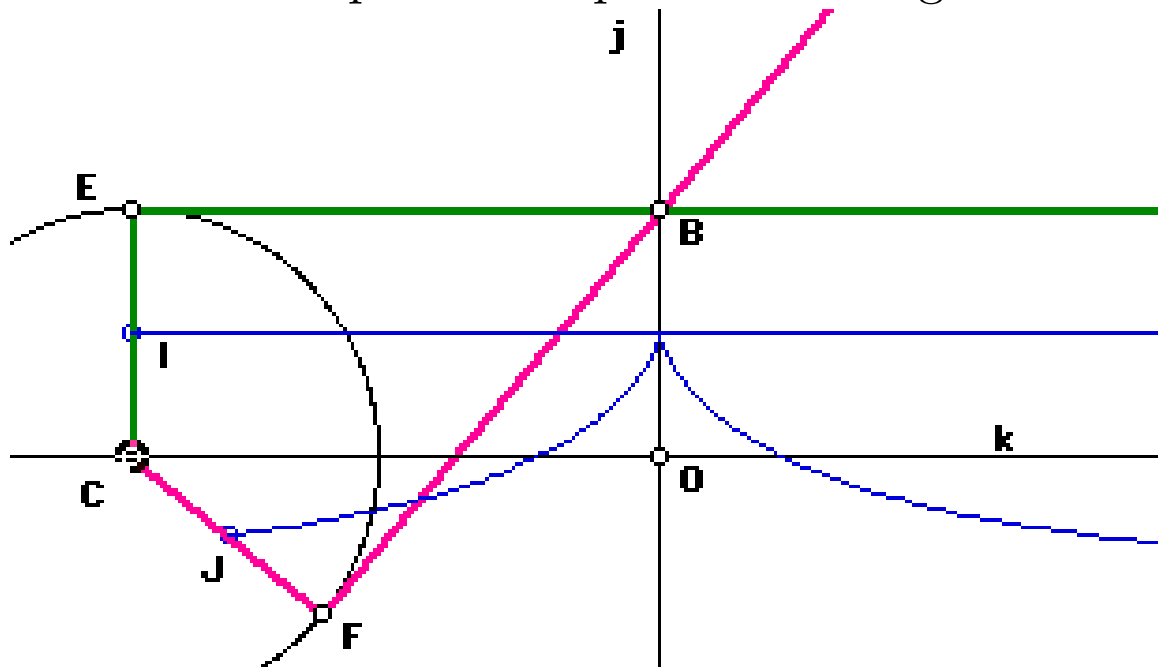


Let AB and CD be perpendicular diameters of a circle. Let E be a point on arc[B,C], and Z be a point on arc[B,D], such that BE, BZ are equal. Draw ZH perpendicular to CD. Draw ED. Let P be intersection[ZH,ED]. The cissoid is the locus of all points P determined by all positions of E on arc[B,C] and Z on arc[B,D] with  $\text{arc}[B,E] = \text{arc}[B,Z]$ . (The portion of the curve that lies outside of the circle is a later generalization).

In the curve, we have  $CH/HZ = HZ/HD = HD/HP$ . Thus HZ and HD are two mean proportionals between CH and HP. Proof: taking  $CH/HZ = HZ/HD$ , we have  $CH * HD = HZ^2$ . triangle[D,C,Z] is a right triangle since it's a triangle on a circle with one side being the diameter (elementary geometry). We know an angle[D,C,Z] and one side distance[D,C], thus by trigonometry of right angles, we can derive all lengths DZ, CZ, and HZ. Substituting the results

of computation in  $CH * HD = HZ^2$  results an identity. Similarly, we know length HP and find  $HZ/HD=HD/HP$  to be an identity.

### 4.3 Newton's Carpenter's Square and Tangent



Newton showed that Cissoid of Diocles and the right Strophoid can be generated by sliding a right triangle. The midpoint  $J$  of the edge  $CF$  draws the Cissoid, the vertex  $F$  the Strophoid. This method also easily proves the tangent construction.

Step-by-step description:

1. Let there be two distinct fixed points B and O, both on a given line  $j$ . (distance[B,O] will be the radius of the cissoid of Diocle we are about to construct.)
2. Let there be a line  $k$  passing O and perpendicular to  $j$ .
3. Let there be a circle centered on an arbitrary point C on  $k$ , with radius OB.

4. There are two tangents of this circle passing B, let the tangent points be E and F.
5. Let I be the midpoint between E and the center of the circle. Similarly, let J be the midpoint between F and the center of the circle.
6. The locus of I and J (as C moves on k) is the cissoid of Diocles and a line. Also, the locus of E and F is the right strophoid.

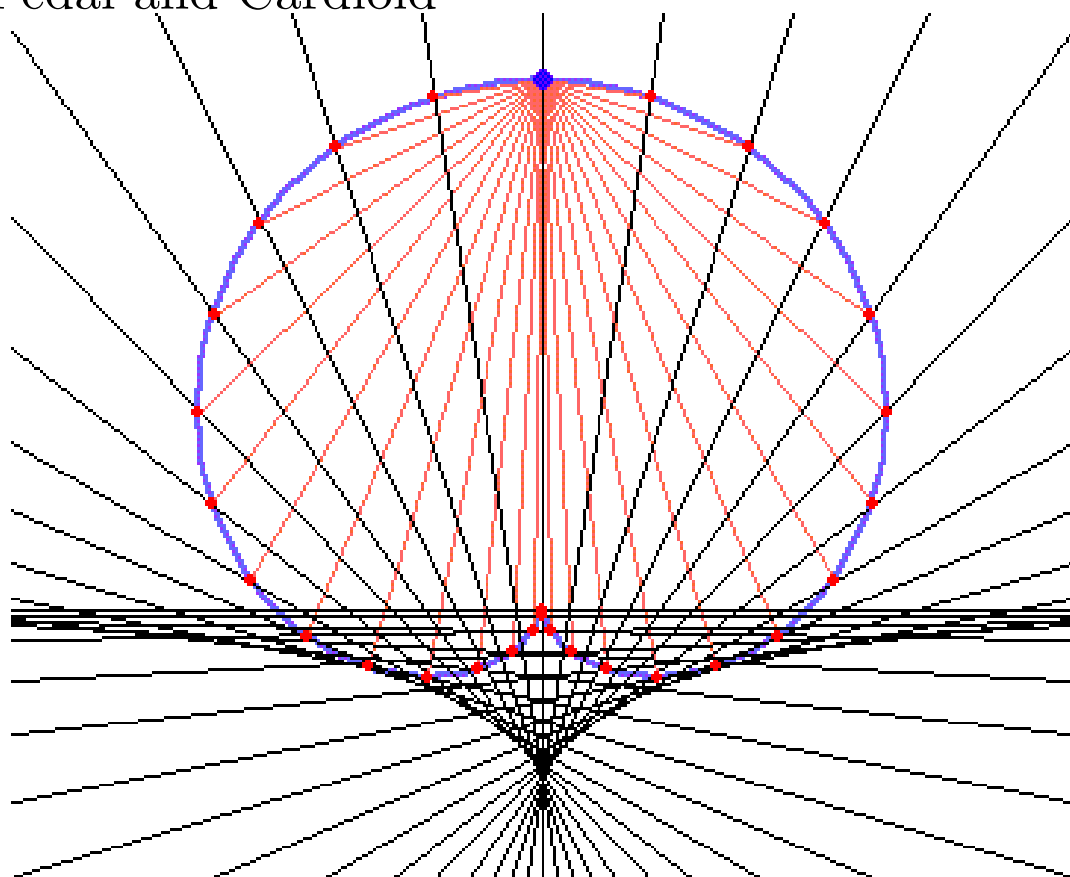
*Tangent construction for Cissoid and Strophoid:* Think of triangle[C,F,B] as a rigid moving body. The point C moves in the direction of vector[O,C], and point B moves in the direction of vector[B,F]. The intersection H (not shown) of normals of line[O,C] and line[B,F] is its center of rotation. J is the point tracing the Cissoid and is also a point on the triangle, thus HJ is normal to the Cissoid. For the Strophoid change the last sentence: Since the tracing point F is a point on the triangle, thus HF is normal to the Strophoid.

In 3D-XploreMath, this construction is shown automatically when Cissoid is chosen from the Plane Curve menu, just after the curve is drawn (or when it is redrawn by choosing Create from the Action menu or typing Command-K). In the Action Menu switch between Cissoid and Strophoid. Hold down the option key to slow the animation, hold down Control to reverse direction, and press the spacebar to pause.

In the animation, the tangent and normal are shown as

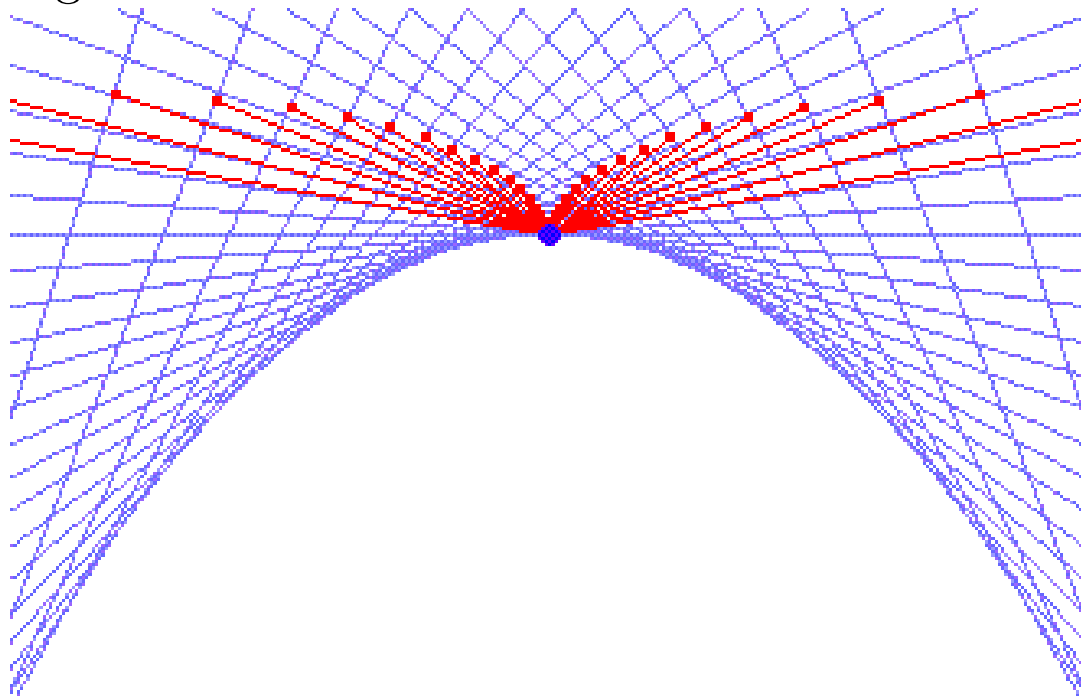
blue. The line from the critical point, from the so called momentary fixed point of the motion, is normal to the curve. This point is the intersection of the green lines; one of them is a vertical drop, the other perpendicular to the red line.

#### 4.4 Pedal and Cardioid



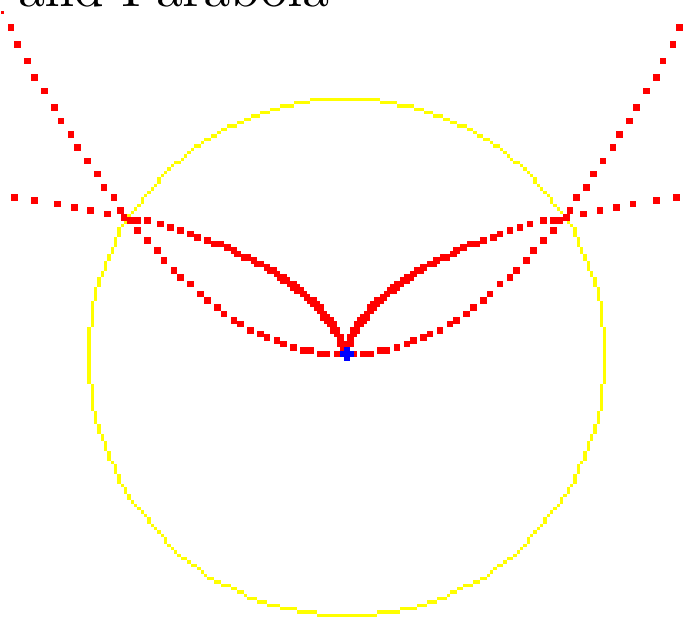
The pedal of a cissoid of Diocles with respect to a point  $P$  is the cardioid. If the cissoid's asymptote is the line  $y = 1$  and its cusp is at the origin, then  $P$  is at  $\{0, 4\}$ . It follows by definition, the negative pedal of a cardioid with respect to a point opposite its cusp is the cissoid of Diocles.

## 4.5 Negative Pedal and Parabola



The pedal of a parabola with respect to its vertex is the cissoid of Diocles. (and then by definition, the negative pedal of a cissoid of Diocles with respect to its cusp is a parabola.)

## 4.6 Inversion and Parabola



The inversion of a cissoid of Diocles at cusp is a parabola.

## 4.7 Roulette of a Parabola

Let there be a fixed parabola. Let there be an equal parabola that rolls on the given parabola in such way that the two parabolas are symmetric to the line of tangency. The vertex of the rolling parabola traces a cissoid of Diocles.

XL.

[Go To Planar TOC](#)

## Conchoid \*

3D-XplorMath parametrization:

$$r = \frac{bb}{\cos t} + aa, \quad x = r \cdot \cos t, \quad y = r \cdot \sin t.$$

### History

According to common modern accounts, the conchoid of Nicomedes was first conceived around 200 B.C by Nicomedes, to solve the angle trisection problem. The name conchoid is derived from Greek meaning “shell”, as in the word conch. The curve is also known as cochloid.

From E. H. Lockwood (1961):

The invention of the ‘mussel-shell shaped’ conchoid is ascribed to Nicomedes (second century B.C.) by Pappus and other classical authors; it was a favorite with the mathematicians of the seventeenth century as a specimen for the new method of analytical geometry and calculus. It could be used (as was the purpose of its invention) to solve the two problems of doubling the cube and of trisecting an angle; and hence for every cubic or quartic problem. For this reason, Newton suggested that it should be treated as a ‘standard’ curve.

---

\* This file is from the 3D-XplorMath project. Please see:

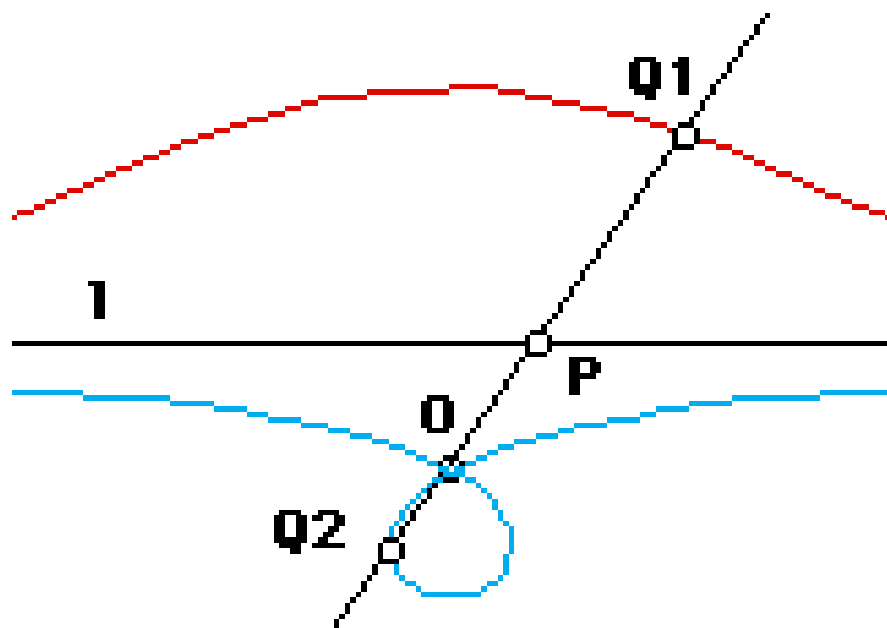
## Description

The Conchoid of Nicomedes is a one parameter family of curves. They are special cases of a more general conchoid construction, being the conchoids of a line.

Step-by-step explanation:

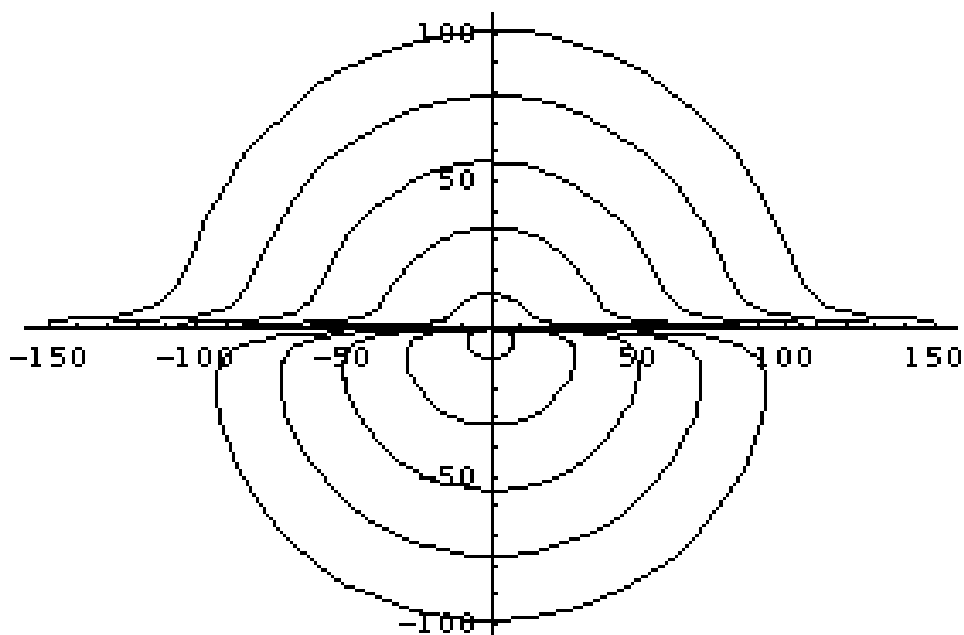
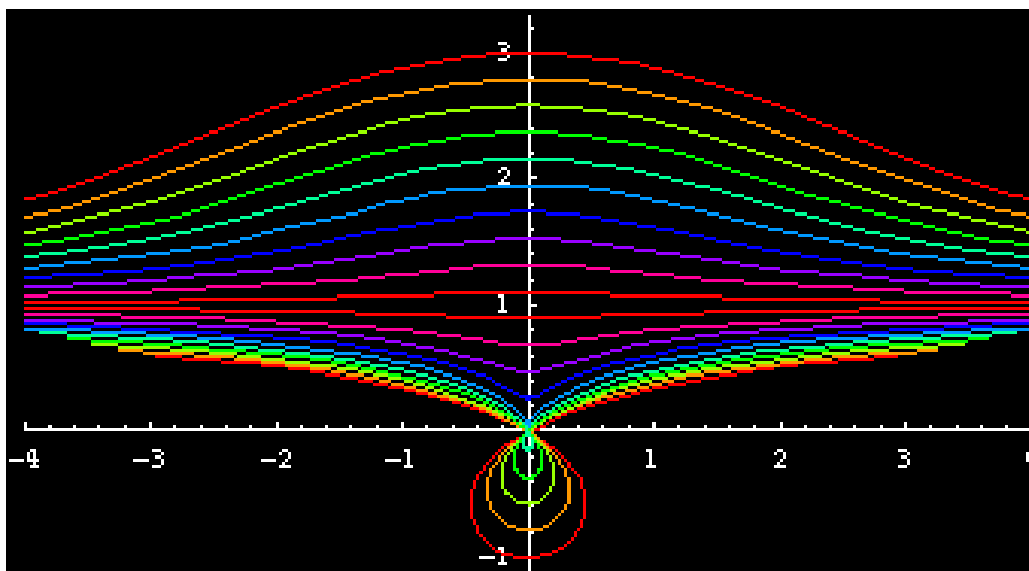
1. Given a line  $\ell$ , a point  $O$  not on  $\ell$ , and a distance  $k$ .
2. Draw a line  $m$  through  $O$  and any point  $P$  on  $\ell$ .
3. Mark points  $Q1$  and  $Q2$  on  $m$  such that  
$$\text{distance}[Q1, P] = \text{distance}[Q2, p] = k.$$
4. The locus of  $Q1$  and  $Q2$  as  $P$  varies on  $\ell$  is the conchoid of Nicomedes.

The point  $O$  is called the *pole* of the conchoid, and the line  $\ell$  is called its *directrix*. It is an asymptote of the curve.



The following figures shows the curve family. The pole is taken to be at the origin, and directrix is  $y = 1$ . The figure

on top has constants  $k$  from  $-2$  to  $2$ . The one below has constants  $k$  from  $-100$  to  $100$ .



### Formulas

Let the distance between pole and line be  $b$ , and the given constant be  $k$ . The curve has only the one parameter  $k$ , because for a given  $b$ , all families of the curve can be generated by varying  $k$  (they differ only in scale). (Similarly,

we could use  $b$  as the parameter.) In a mathematical context, we should just use  $b = 1$ , however, it is convenient to have formulas that have both  $b$  and  $k$ . Also, for a given  $k$ , the curve has two branches. In a mathematical context, it would be better to define the curve with a signed constant  $k$  corresponding to a curve of only one branch. We will be using this interpretation of  $k$ . In this respect, the conchoid of Nichomedes is then two conchoids of a line with constants  $k$  and  $-k$ .

The curve with negative offset can be classified into three types: if  $b < k$  there is a loop; if  $b = k$ , a cusp; and if  $b > k$ , it is smoothly imbedded. Curves with positive offsets are always smooth.

The following are the formulas for a conchoid of a line  $y = b$ , with pole  $O$  at the origin, and offset  $k$ .

*Polar:*  $r = b/\sin(\theta) + k$ ,  $-\pi/2 < \theta < \pi/2$ .

This equation is easily derived: the line  $x = b$  in polar equation is  $r = b/\cos\theta$ , therefore the polar equation is  $r = b/\cos(\theta) + k$  with  $-\pi/2 < \theta < \pi/2$  for a signed  $k$  (i.e., describing one branch.). Properties of cosine show that as  $\theta$  goes from 0 to  $2\pi$ , two conchoids with offset  $\pm|k|$  results from a single equation  $r = b/\cos(\theta) + k$ . To rotate the graph by  $\pi/2$ , we replace cosine by sine.

*Parametric:*

$$(t + (kt)/\sqrt{b^2 + t^2}, b + (bk)/\sqrt{b^2 + t^2}), \quad -\infty < t < \infty.$$

If we replace  $t$  in the above parametric equation by  $b \tan(t)$ ,

we get the form:

$$\left(k + \frac{b}{\cos(t)}\right) \cdot (\sin(t), \cos(t)), \quad \frac{-\pi}{2} < t < \frac{3\pi}{2}, \quad t \neq \frac{\pi}{2}.$$

For conchoids of a line with positive and negative offsets  $k$  and pole at the origin, we have the quartic

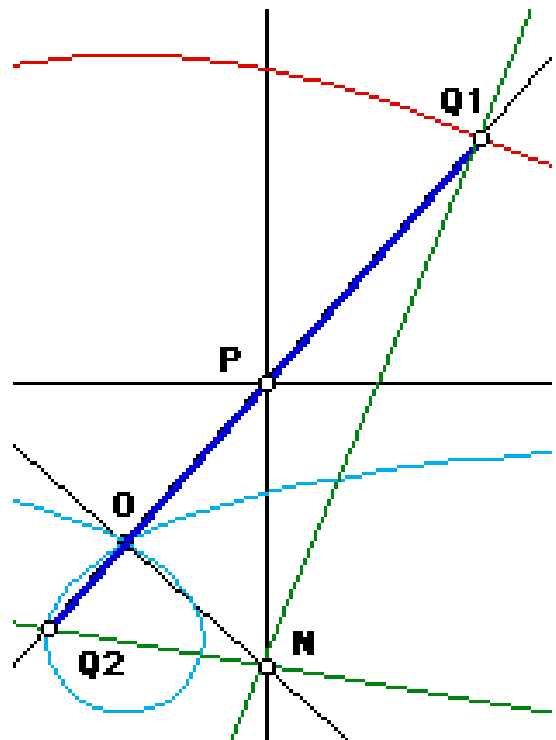
*Implicit Cartesian equation:*  $(x^2 + y^2)(y - b)^2 = k^2 y^2.$

If  $k < b$ , the point at the origin is an isolated point.

If  $k < 0$  and  $b < |k|$ , the conchoid has a loop with area  $(b\sqrt{k^2 - b^2} - 2bk \ln((k + \sqrt{k^2 - b^2})/b) + k^2 \arccos(b/k))$ . The area between any conchoid of a line and its asymptote is infinite.

## Tangent Construction

Look at the conchoid tracing as a mechanical device, where a bar line  $[O, P]$  slides on a line at  $P$  and a fixed joint  $O$ . The point  $P$  on the bar moves along the directrix, and the point at  $O$  moves in the direction of the vector  $[O, P]$ . We know the direction of motion of the bar at the points  $O$  and  $P$  at arbitrary time.



The intersection of normals to these directions form the instantaneous center of rotation  $N$ . Since the tracing points

$Q1$  and  $Q2$  are parts of the apparatus,  $N$  is also their center of rotation and therefore line  $[N, Q1]$  and line  $[N, Q2]$  are the curve's normals.

### Angle Trisection

The curve can be used to solve the Greek Angle Trisection problem. Given an acute angle  $AOB$ , we want to construct an angle that is  $1/3$  of  $AOB$ , with the help of the conchoid of Nicomedes.

Steps: Draw a line  $m$  intersecting segment  $[A, O]$  and perpendicular to it. Let  $D$  be intersection of  $m$  and the line  $[A, O]$ ,  $L$  the intersection of  $m$  and the line  $[B, O]$ . Suppose we are given a conchoid of Nicomedes, with pole at  $O$ , directrix  $m$ , and offset  $2 \cdot \text{distance}[O, L]$ . Draw a line  $\ell$  through  $L$  and perpendicular to  $m$ . Let  $C$  be the intersection of the curve and  $\ell$  on the opposite side of the pole.

**Theorem.**  $\text{angle}[A, O, B] = 3 \cdot \text{angle}[A, O, C]$ .

*Proof:*

$$\sphericalangle[A, O, C] = \sphericalangle[O, C, L]$$

because the line  $[O, C]$  cuts parallel lines. Let:

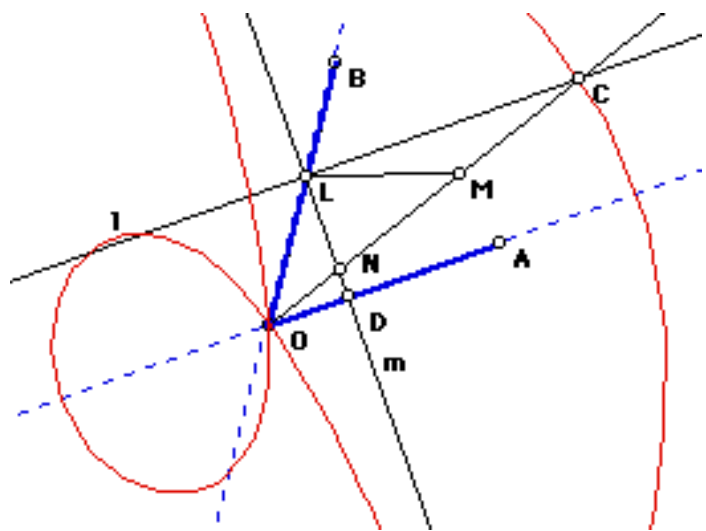
$q$  be the line  $[O, C]$ ,

$N := m \cap q$ ,

$M$  midpoint of  $[N, C]$ ,

$k := \text{distance}[O, L]$ .

By our construction,



$\text{distance}[N, M] = \text{distance}[M, C] = k$ . Since  $NLC$  is a right triangle, we see that  $MN$ ,  $ML$ ,  $MC$ , and  $OL$  all

have the same length, thus triangle  $[M, L, C]$  and triangle  $[M, L, N]$  are isosceles, and it follows that  $\sphericalangle[N, M, L] = 2 \cdot \sphericalangle[M, C, L]$ . Since  $\text{distance}[O, L] = \text{distance}[M, L]$ , triangle  $[M, L, O]$  is also isosceles, and thus its two base angles are equal. This shows that an angle equal to  $\sphericalangle[A, O, C]$  is  $1/3$  an angle equal to  $\sphericalangle[A, O, B]$ .

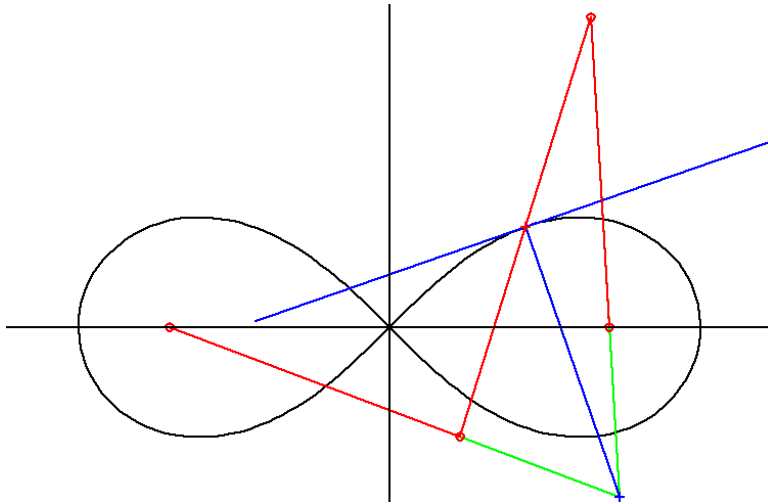
The essential point where the conchoid makes the trisection possible is in the construction of the point  $C$  on  $\ell$  such that  $\text{distance}[N, C] = 2 \text{distance}[O, L]$ , where  $N$  is the intersection of  $m$  and the line  $[O, C]$ . Note that for each new angle to trisect, a new conchoid is needed. This is in contrast to some other trisectrixes such as the quadratrix, where all angles can be trisected once the curve is given.

The conchoid can also be used to solve the classic problem of doubling the cube.

XL.

[Go To Planar TOC](#)

## Lemniscate \*



The Lemniscate is a figure-eight curve with a simple **mechanical construction** attributed to Bernoulli: Choose two 'focal' points  $F_1, F_2$  at distance  $L := 2 * dd$ , then take three rods, one of length  $L$ , two of length  $R = L/\sqrt{2}$ . The short ones can rotate around the focal points and the long one connects their free ends with rotating joints (red lines in the figure). This machine has one degree of freedom and the *midpoint* of the long rod traces out the Lemniscate while the short rods rotate (not uniformly). – This drawing mechanism will also work for arbitrary lengths  $0 < R < L, R := cc$ . The default morph in 3DXM varies  $cc$ . Another interesting morph is obtained by varying the position of the drawing pen on the long rod with  $ff \in (0, 1)$ . Click the **Init To Current Parameters** button in **Set Morphing**, then put  $f0 := 0, f1 := 1$ . Since the Bernoulli Lemniscate is much better known than

---

\* This file is from the 3D-XplorMath project. Please see:

curves drawn by mechanisms with parameters different from  $L : R = \sqrt{2} : 1$ , we will give, below, parametrizations and equations only for the Bernoulli curve.

The curves in 3DXM are obtained as follows:

The endpoint of the right rod rotates with constant speed, i.e.  $P(t) = (dd + cc \cdot \cos(t), cc \cdot \sin(t))$ . The endpoint  $Q(t)$  of the left rod is obtained by intersecting two circles (of radius  $R$  around  $F_1$  and radius  $L$  around  $P(t)$ ). One of the intersection points is  $P'(t) = (-dd + cc \cdot \cos(t), cc \cdot \sin(t))$ , since  $|F_2 - F_1| = |P(t) - P'(t)| = L = 2 \cdot dd$ . Therefore  $Q(t)$  is obtained by reflecting  $P'(t)$  in the Diagonal  $\overline{F_1 P(t)}$  of the parallelogram  $F_2, F_1, P'(t), P(t)$ .

The drawing pen is at  $ff \cdot P(t) + (1 - ff) \cdot Q(t)$ .

*Mechanical constructions* of curves give rise to simple **tangent constructions**. We imagine that a plane is attached to the long rod. Then every point of this plane traces out a curve when the rods move. The velocity vectors of these traced curves give, at each moment, a vectorfield, that has concentric circles as integral curves (or, exceptionally, parallel lines). The centers of these concentric circles are the *momentary centers of rotation* for the moving plane. If we join a point of a traced curve to the corresponding momentary center of rotation, then this *radius* (drawn blue) is orthogonal to the tangent (also blue).

How can one find the momentary center of rotation for the current drawing machine? The endpoints of the two short rods are points of the moving plane. We know that

each can only move orthogonally to its rod (namely rotate around the other endpoint, a focal point). This says that both short rods point to the momentary center of rotation, which therefore is obtained as the intersection of two lines (drawn green in the figure).

Compare the other mechanically constructed curves.

Parametrizations are not unique, here is a well known one:

$$x(t) := \cos(t)/(1 + \sin(t)^2)$$

$$y(t) := \sin(t) \cdot \cos(t)/(1 + \sin(t)^2).$$

The Bernoulli Lemniscate has this implicit equation:

$$(x^2 + y^2)^2 = x^2 - y^2.$$

Divide this by  $r^2 := x^2 + y^2$  to get the polar form:

$$r^2 = \cos(\phi)^2 - \sin(\phi)^2.$$

The points  $F_1, F_2 := \pm 1/\sqrt{2}$  are called Focal points of the Lemniscate because of the special property:

$$|P - F_1| \cdot |P - F_2| = |F_1 - F_2|^2/4.$$

If one takes the complex square root of a circle which touches the  $y$ -axis from the right at 0 then one also obtains (half of) a Lemniscate. In the Conformal Category, choose  $z \rightarrow \sqrt{z}$ , and then in the **Action Menu**, select **Choose Circle by Mouse**, and create a circle that is tangent to the  $y$ -axis at 0.

The inversion map:  $(x, y) \mapsto (x, y)/(x^2 + y^2)$  often transforms some interesting curve into another interesting curve.

And indeed, the Lemniscate, with the above parametrization, is transformed by inversion into the curve

$$x = 1/\cos(t), \quad y = \sin(t)/\cos(t).$$

Observe the implicit equation  $x^2 - y^2 = 1$ . It shows that the new curve is a hyperbola with orthogonal asymptotes. So we could have obtained the Bernoulli Lemniscate from the orthogonal hyperbola by inversion in a circle around its midpoint. – More generally, inversions of hyperbolae  $x^2/a^2 - y^2/b^2 = \text{const}$  give figure 8 curves with non-orthogonal double tangents. The angle  $2\alpha$  between the double tangents is the same as the angle between the asymptotes and satisfies  $\tan \alpha = b/a$ . The angle  $2\beta$  between the double tangents of the figure 8 curves of our drawing mechanisms satisfies  $\sin \beta = R/L$ . Set  $a := R$ ,  $b := a/\sqrt{L^2/R^2 - 1}$  to obtain  $\alpha = \beta$ . Invert, with  $\vec{x} \mapsto \vec{x} \cdot a^2/|\vec{x}|^2$ , the lemniscate and put the result into the term  $x^2/a^2 - y^2/b^2$  to find that it is **1**. This gives implicit lemniscate equations:  $x^2/a^2 - y^2/b^2 = (x^2 + y^2)^2/a^4$ .

And, invert hyperbola parametrizations, e.g.  $x = a/\cos(t)$ ,  $y = b \sin(t)/\cos(t)$ , to parametrize lemniscates.

We note that not every figure 8 curve (with orthogonal double tangents) is a Bernoulli Lemniscate. Another figure-eight is obtained by the simpler parametrization:

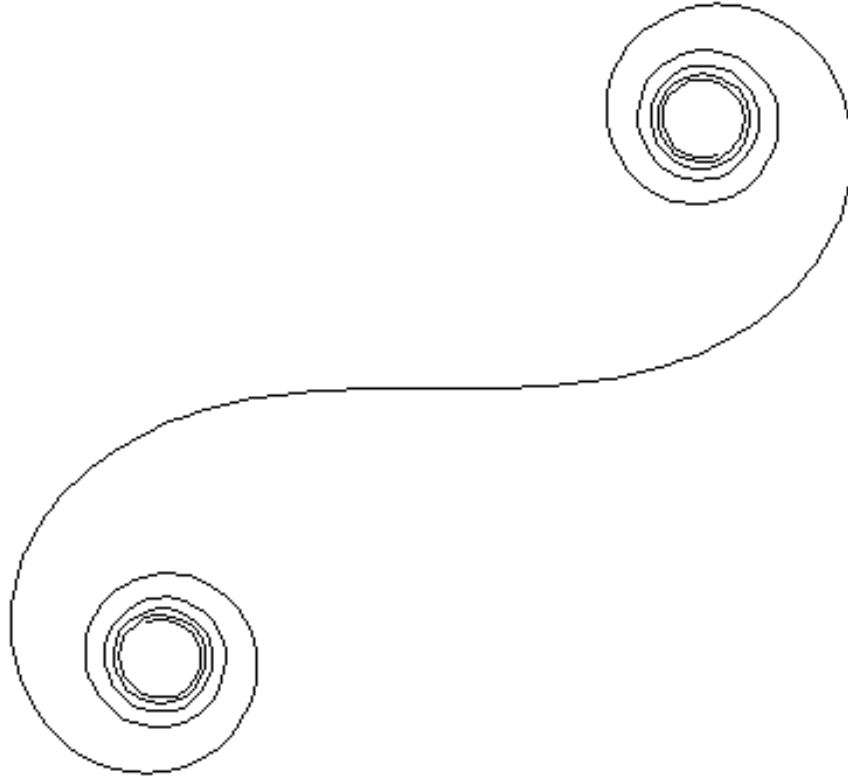
$$x(t) := \cos(t), \quad y(t) := \sin(t) \cdot \cos(t),$$

which has the implicit equation  $y^2 = x^2(1 - x^2)$ .

H.K.

[Go To Planar TOC](#)

## Clothoid \*



The Clothoid, also called Spiral of Cornu, is a curve whose curvature is equal to its arclength. It has the parametric formula:

$$\left( \int_0^t \cos(x^2/2) dx, \int_0^t \sin(x^2/2) dx \right).$$

### Discussion

If a plane curve is given by a parametric formula  $(f(t), g(t))$ , then the length of the part corresponding to a parameter

---

\* This file is from the 3D-XplorMath project. Please see:

interval  $[a, t]$  is  $s(t) = \int_a^t \sqrt{f'(\tau)^2 + g'(\tau)^2} d\tau$ . If we apply this formula to the Clothoid we see that the arclength corresponding to the interval  $[0, t]$  is  $s(t) = \int_0^t 1 dt = t$ , so that the parameter  $t$  is precisely the (signed!) arclength measured along the curve from its midpoint,  $(0, 0)$ .

Next, recall that the curvature  $\kappa$  of a plane curve is defined as the rate of change (with respect to arclength) of the angle  $\theta$  that its tangent makes with some fixed line (which we can take to be the  $x$ -axis). And since the slope  $\frac{dy}{dx}$  of the curve is  $\tan(\theta)$ , and by the chain rule  $\frac{dy}{dx} = (dy/dt)/(dx/dt) = \frac{g'}{f'}$ , we see that  $\theta(t) = \arctan(g'(t)/f'(t))$ . So if we assume that parameter  $t$  is arclength, then using the formulas for the derivative of the arctangent and of a quotient, we see that:

$$\kappa(t) = \theta'(t) = -g'(t)f''(t) + f'(t)g''(t),$$

(where we have ignored the denominator, since parameterization by arclength implies that it equals unity). Applying this to the Clothoid, we obtain  $\kappa(t) = t$ . Since the arclength function is also  $t$ , this shows that the Clothoid is indeed a curve whose curvature function is equal to its arclength function.

## The Fundamental Theorem of Plane Curves

Next let's look at this question from the other direction, and also more generally. Suppose we are given a function  $\kappa(t)$ . Can we find a plane curve parameterized by arclength  $(f(t), g(t))$  such that  $\kappa$  is its curvature function? Recall

from above that  $\frac{d\theta}{dt} = \kappa$ , and of course  $\frac{dx}{dt} = f'(t)$  and  $\frac{dy}{dt} = g'(t)$ . Now, since  $(\frac{dx}{dt})^2 + (\frac{dy}{dt})^2 = 1$ , while  $\frac{dy}{dt} / \frac{dx}{dt} = dy/dx = \tan(\theta)$ , it follows from elementary trigonometry that  $\frac{dx}{dt} = \cos(\theta)$  while  $\frac{dy}{dt} = \sin(\theta)$ . Thus we have the following system of three differential equations for the three functions  $\theta(t)$ ,  $f(t)$ , and  $g(t)$ :

$$\theta'(t) = \kappa(t), \quad f'(t) = \cos(\theta(t)), \quad g'(t) = \sin(\theta(t)).$$

The first equation is solved by  $\theta(\tau) = \theta_0 + \int_0^\tau \kappa(\sigma) d\sigma$ , and substituting this in the other two equations, we find that the general solutions for  $f$  and  $g$  are given by:

$$f(t) = x_0 + \int_0^t \cos(\theta_0 + \int_0^\tau \kappa(\sigma) d\sigma) d\tau$$

$$g(t) = y_0 + \int_0^t \sin(\theta_0 + \int_0^\tau \kappa(\sigma) d\sigma) d\tau.$$

This is an elegant explicit solution to our question! It shows that not only is there a solution to our question (say the one obtained by setting  $x_0, y_0$  and  $\theta_0$  all equal to zero), but also that the solution is unique up to a translation (by  $(x_0, y_0)$ ) and a rotation (by  $\theta_0$ ), that is unique up to a general rigid motion.

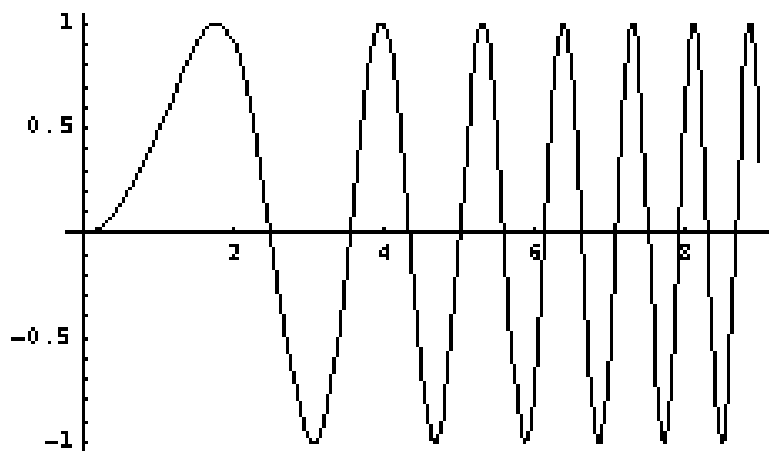
This fact has a name—it is called The Fundamental Theorem of Plane Curves. It tells us us that most geometric and most economical descriptions of plane curves is not via parametric equations, which have a lot of redundancy, but

rather by the single function  $\kappa$  that gives the curvature as a function of arclength.

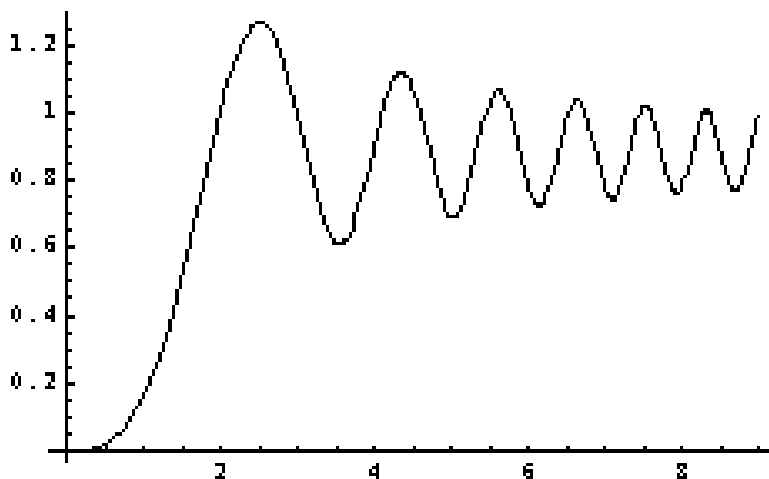
**Exercise** Take  $\kappa(t) = t$  and check that the above formulas give the parametric equations for the Clothoid in this case.

## Back to the Clothoid

We close with a few more details about the Clothoid. First, here is a plot of the integrand  $\sin(x^2/2)$ :



and next a plot of its indefinite integral,  $\int_0^t \sin(x^2/2) dx$ , the so-called Fresnel integral:



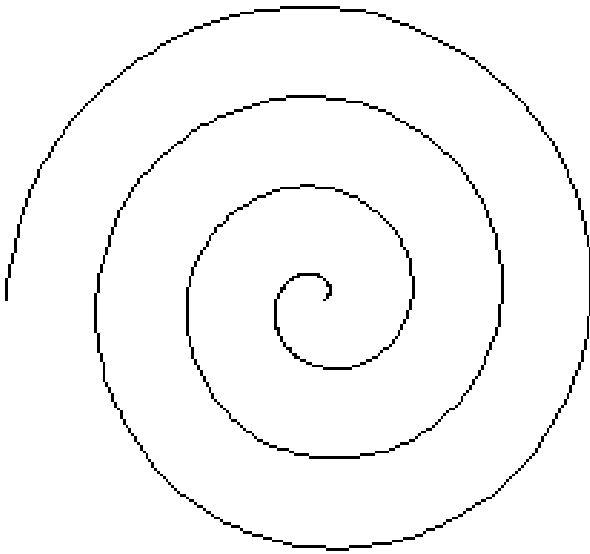
From this plot we see that the y-coordinate oscillates. Its limit as  $t$  goes to infinity is  $\sqrt{\pi}/2$ , from which we see that the centers of the two spirals of the Clothoid are at  $\pm(\sqrt{\pi}/2, \sqrt{\pi}/2)$ .

XL & RSP.

[Go To Planar TOC](#)

## Archimedean Spirals \*

An Archimedean Spiral is a curve defined by a polar equation of the form  $r = \theta^a$ . Special names are being given for certain values of  $a$ . For example if  $a = 1$ , so  $r = \theta$ , then it is called Archimedes' Spiral.



**Archimede's Spiral**

### Formulas in 3DXM:

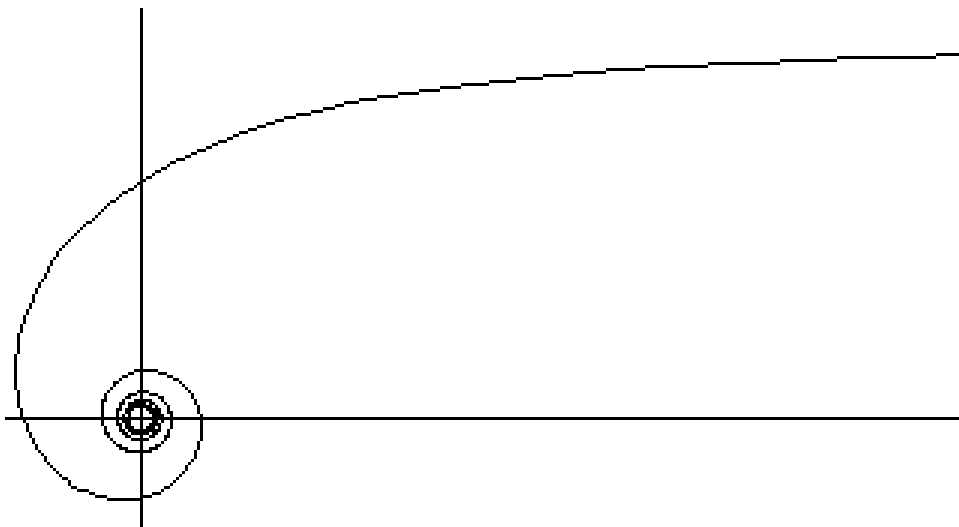
$$r(t) := cc \cdot t^{aa}, \quad \theta(t) := t,$$

Default Morph:

$$-1 \leq aa \leq 1.25.$$

$cc$  for scaling.

For  $a = -1$ , so  $r = 1/\theta$ , we get the reciprocal (or hyperbolic) spiral:

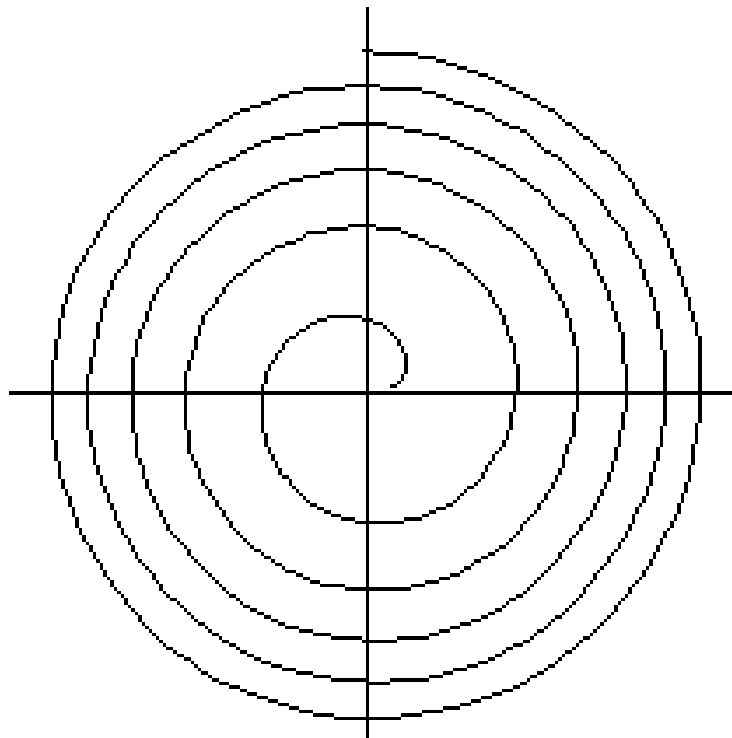


**Reciprocal Spiral**

---

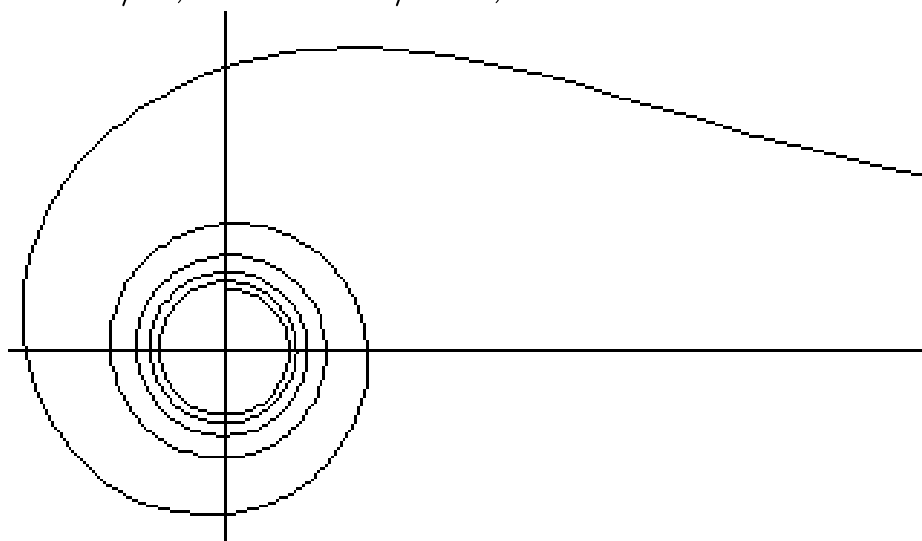
\* This file is from the 3D-XplorMath project. Please see:

The case  $a = 1/2$ , so  $r = \sqrt{\theta}$ , is called the Fermat (or hyperbolic) spiral.



**Fermat's Spiral**

While  $a = -1/2$ , or  $r = 1/\sqrt{\theta}$ , it is called the Lituus:



**Lituus**

In 3D-XplorMath, you can change the parameter  $a$  by going to the menu Settings  $\rightarrow$  Set Parameters, and change the value of  $aa$ . You can see an animation of Archimedean spirals where the exponent  $a = aa$  varies gradually, between  $-1$  and  $1.25$ . See the *Animate Menu*, entry *Morph*.

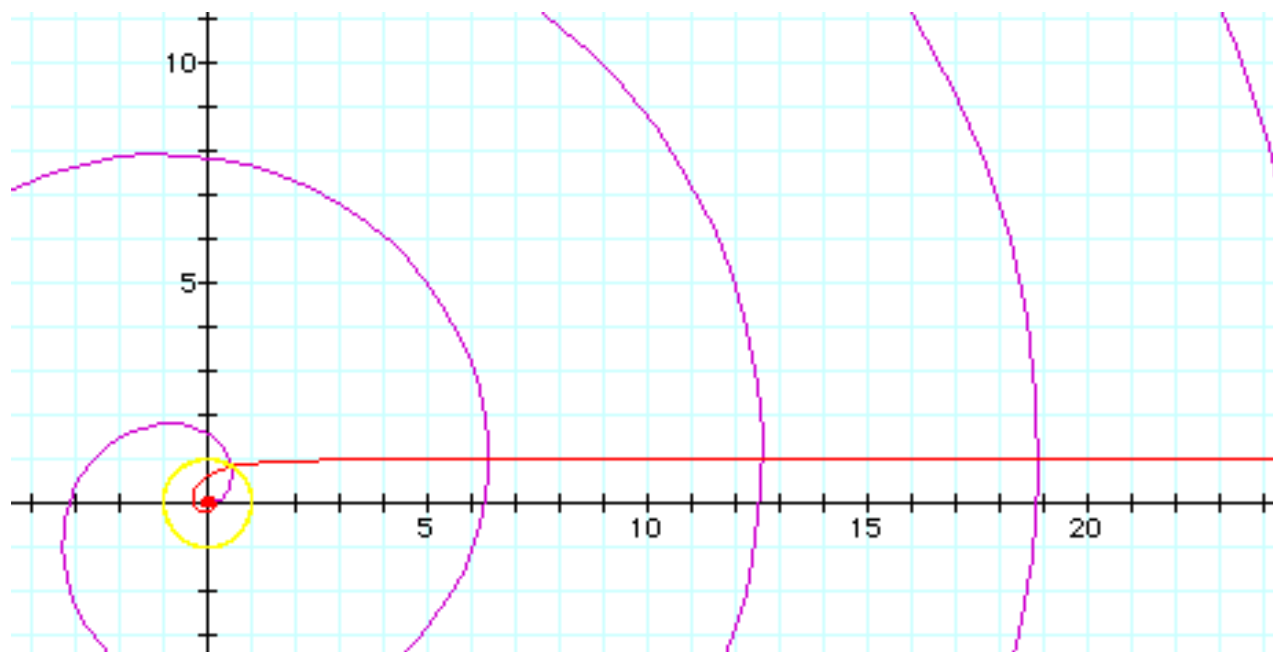
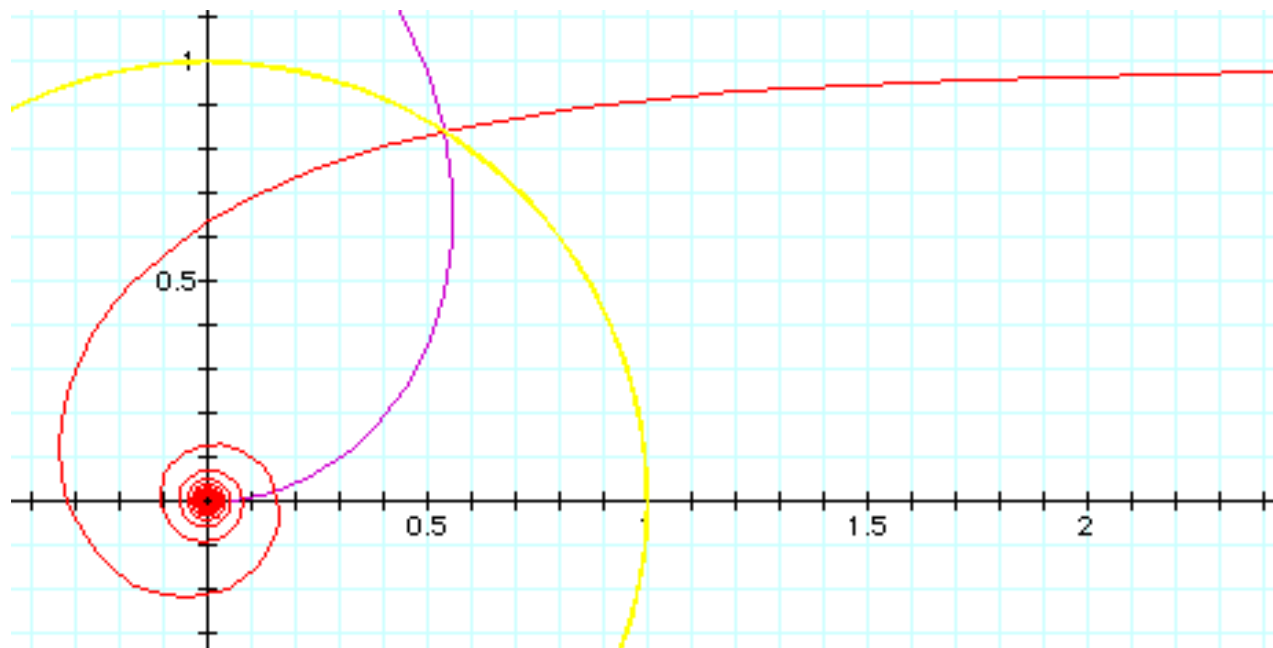
The reason that the parabolic spiral and the hyperbolic spiral are so named is that their equations in polar coordinates,  $r\theta = 1$  and  $r^2 = \theta$ , respectively resembles the equations for a hyperbola ( $xy = 1$ ) and parabola ( $x^2 = y$ ) in rectangular coordinates.

The hyperbolic spiral is also called reciprocal spiral because it is the inverse curve of Archimedes' spiral, with inversion center at the origin.

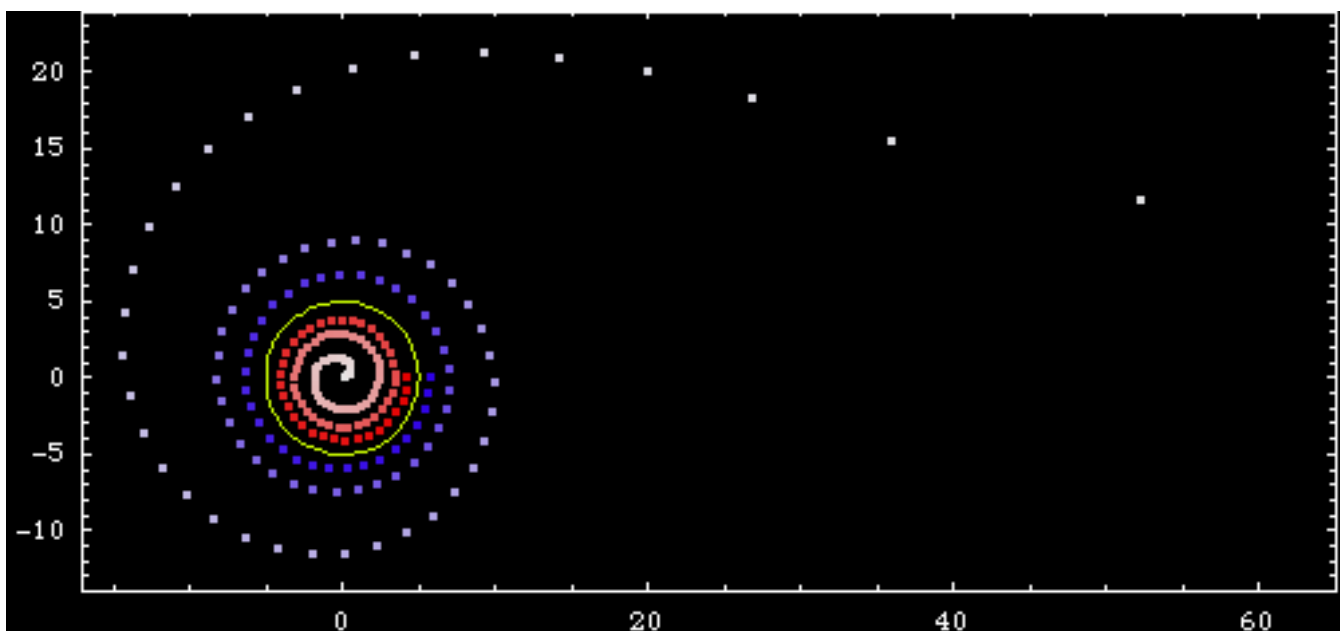
The inversion curve of any Archimedean spirals with respect to a circle as center is another Archimedean spiral, scaled by the square of the radius of the circle. This is easily seen as follows. If a point  $P$  in the plane has polar coordinates  $(r, \theta)$ , then under inversion in the circle of radius  $b$  centered at the origin, it gets mapped to the point  $P'$  with polar coordinates  $(b^2/r, \theta)$ , so that points having polar coordinates  $(t^a, \theta)$  are mapped to points having polar coordinates  $(b^2t^{-a}, \theta)$ .

From the above, we can see that the Archimedes' spiral inverts to the reciprocal spiral, and Fermat's spiral inverts to the Lituus.

The following two images illustrates Archimedes's spiral and Reciprocal spiral as mutual inverses. The red curve is the reciprocal spiral, the purple is the Archimedes' spiral. The yellow is the inversion circle.



The following image illustrates a Lituus and Fermat's spiral as mutual inverses. The red curve is the Fermat's spiral. The blue curve is its inversion, which is a lituus scaled by  $5^2$ . The yellow circle is the inversion circle with radius 5. Note that points inside the circle gets mapped to outside of the circle. The closer the point is to the origin, the farther is its corresponding point outside the circle.



XL.

[Go To Planar TOC](#)

## The Logarithmic Spiral \*

The parametric equations for the Logarithmic Spiral are:

$$\begin{aligned}x(t) &= aa \cdot \exp(bb \cdot t) \cdot \cos(t) \\y(t) &= aa \cdot \exp(bb \cdot t) \cdot \sin(t).\end{aligned}$$

This spiral is connected with the complex [Exponential Map](#) as follows:

$$x(t) + i y(t) = aa \exp((bb + i)t).$$

The animation that is automatically displayed when you select Logarithmic Spiral from the Plane Curves menu shows the osculating circles of the spiral. Their midpoints draw another curve, the *evolute* of this spiral. These osculating circles illustrate an interesting theorem, namely if the curvature is a monotone function along a segment of a plane curve, then the osculating circles are nested - because the distance of the midpoints of two osculating circles is (by definition) the length of a secant of the evolute while the difference of their radii is the arc length of the evolute between the two midpoints. (See page 31 of J.J. Stoker's "Differential Geometry", Wiley-Interscience, 1969).

For the logarithmic spiral this implies that through every point of the plane minus the origin passes exactly one osculating circle. Étienne Ghys pointed out that this leads

---

\* This file is from the 3D-XplorMath project. Please see:

to a surprise: The unit tangent vectors of the osculating circles define a vector field  $X$  on  $\mathbb{R}^2 \setminus \{0\}$  – but this vector field has more integral curves, i.e. solution curves of the ODE  $c'(t) = X(c(t))$ , than just the osculating circles, namely also the logarithmic spiral. *How is this compatible with the uniqueness results of ODE solutions?* Read words backwards for explanation:

eht dleifrotcev si ton ztihcspiL gnola eht evruc.

---

### Remarks about Spirals

All spirals with names share the following properties:

If they are left rotating their curvature is positive, and negative for right rotating ones. If they are outgoing, the absolute value of the curvature is monotone decreasing, and increasing for those which spiral inwards. Moreover, for every such curvature function  $\kappa(s)$  one can find a spiral, with  $\kappa(s)$  its curvature function, as follows:

First find an antiderivative  $T(s)$  of  $\kappa(s)$ , i.e.  $T'(s) = \kappa(s)$ .

Next define a unit field  $c'(s) := (\cos(T(s)), \sin(T(s)))$ .

Finally obtain the spiral  $c(s)$  by integrating  $c'(s)$ .

Therefore one may take the quoted curvature properties as definition of a spiral. This has the consequence that a spiral with curvature  $\kappa_1(s)$  can be deformed into a spiral with curvature  $\kappa_2(s)$  through spirals with curvature

$$\kappa_a(s) := (1 - a) \cdot \kappa_1(s) + a \cdot \kappa_2(s).$$

R.S.P., H.K.

[Go To Planar TOC](#)

## Cycloid \*

Cycloids are generated by rolling a circle on a straight line and tracing out the path of some point along the radius. The parametric equation for such a cycloid is:

$$\begin{aligned}x(t) &= aa \cdot t - bb \cdot \sin t \\y(t) &= aa - bb \cdot \cos t,\end{aligned}$$

where  $aa$  is the radius of the rolling circle and  $bb$  is the distance of the drawing point from the center of the circle.

The choice  $bb = aa$  gives the standard cycloid.

Cycloids have other cycloids of the same size as evolutes, see the Action Menu Entry *Show Osculating Circles with Normals*. This fact is responsible for Huyghen's cycloid pendulum having its period independent of the amplitude of the oscillation.

H.K.

---

\* This file is from the 3D-XplorMath project. Please see:

## About Epicycloids and Hypocycloids \*

See also the ATOs for Spherical Cycloids

### DEFINITION AND TANGENT CONSTRUCTION

Epicycloids resp. Hypocycloids are obtained if one circle of radius  $r$  rolls on the outside resp. inside of another circle of radius  $R$ .

In 3D-XplorMath:  $r = hh$ ,  $R = aa$ .

The angular velocity of the rolling circle is  $fr$  times the angular velocity of the fixed circle (negative for hypocycloids).  $fr$  has to be an integer for the hypocycloid to be closed. The formulas do not actually roll one circle around another, they represent the curve as superposition of two rotations:

$$fr := (R - r)/(-r);$$

$$c.x := (R - r) \cos(t) + r \cos(fr \cdot t);$$

$$c.y := (R - r) \sin(t) + r \sin(fr \cdot t);$$

Double generation: If one changes the radius of the rolling circle from  $r$  to  $R - r$  then these formulas are preserved, except for the parametrization speed. To view this in 3DXM replace  $hh$  by  $aa - hh$ .

---

\* This file is from the 3D-XplorMath project. Please see:

Epicycloids are obtained if one circle of radius  $r = -hh$  rolls on the outside of another circle of radius  $R = aa$ . The angular velocity of the rolling circle is  $fr > 0$  times the angular velocity of the fixed circle (again an integer for closed epicycloids).

$$\begin{aligned} fr &:= (R + r)/r; \\ c.x &:= (R + r) \cos(t) - r \cos(fr * t); \\ c.y &:= (R + r) \sin(t) - r \sin(fr * t); \end{aligned}$$

These formulas agree with those of the hypocycloids except for the sign of  $r$ . We view them in 3DXM by using negative  $hh$ .

We can also use a drawing stick of length  $ii*r$ . The default morph shows this:  $0.5 < ii < 1.5$ .

These more general ( $ii <> 1$ ) rolling curves were important for Greek astronomy because the planets orbit the sun (almost) on circles. Therefore, when one looks at other planets from earth, their orbits are (almost) such rolling curves. It is no surprise that many of these curves have individual names: Astroid, Cardioid, Limacon, Nephroid are examples in 3DXM.

Tangent construction.

Rolling curves have a very simple tangent construction. The point of the rolling circle which is in contact with the base curve has velocity zero – just watch cars going by. This means that the connecting segment from this point

of contact of the wheel to the endpoint of the drawing stick is the radius of the momentary rotation. The tangent of the curve which is drawn by the drawing stick is therefore orthogonal to this momentary radius.

The 3DXM-demo draws the rolling curve and shows its tangents.

H.K., R.S.P.

[Go To Planar TOC](#)

## Cardioids and Limaçons \*

Cardioids and Limaçons are obtained if on the outside of one fixed circle of radius  $r = aa$  another circle of the same radius rolls. These curves are traced by a radial stick of length  $R = ii * r$ ,  $ii = 1$  for Cardioids and  $ii > 1$  for Limaçons.

One choice of parametric equations for these curves is:

$$\begin{aligned}x(t) &= 2r \cos(t) + R \cos(2t) \\y(t) &= 2r \sin(t) + R \sin(2t).\end{aligned}$$

The evolute of the Cardioid is a smaller Cardioid, see in the Action Menu the entry **Show Osculating Circles with Normals**. In the entry **Add Caustics** one can rotate all normals by a fixed amount and these rotated lines always envelope a Cardioid.

To see the Cardioid generated by rolling a larger circle around a smaller one choose in the exhibit *Epi- and Hypocycloids* parameters  $hh = 2 * aa$ ,  $ii = 1$ .

The image of the unit circle under the complex map

$$z \mapsto w(z) = z^2 + 2z$$

is a Cardioid; images of larger circles (around 0) are Limaçons. Inverses  $z \mapsto 1/w(z)$  of Limaçons are figure-eight shaped, including a Lemniscate.

H.K.

---

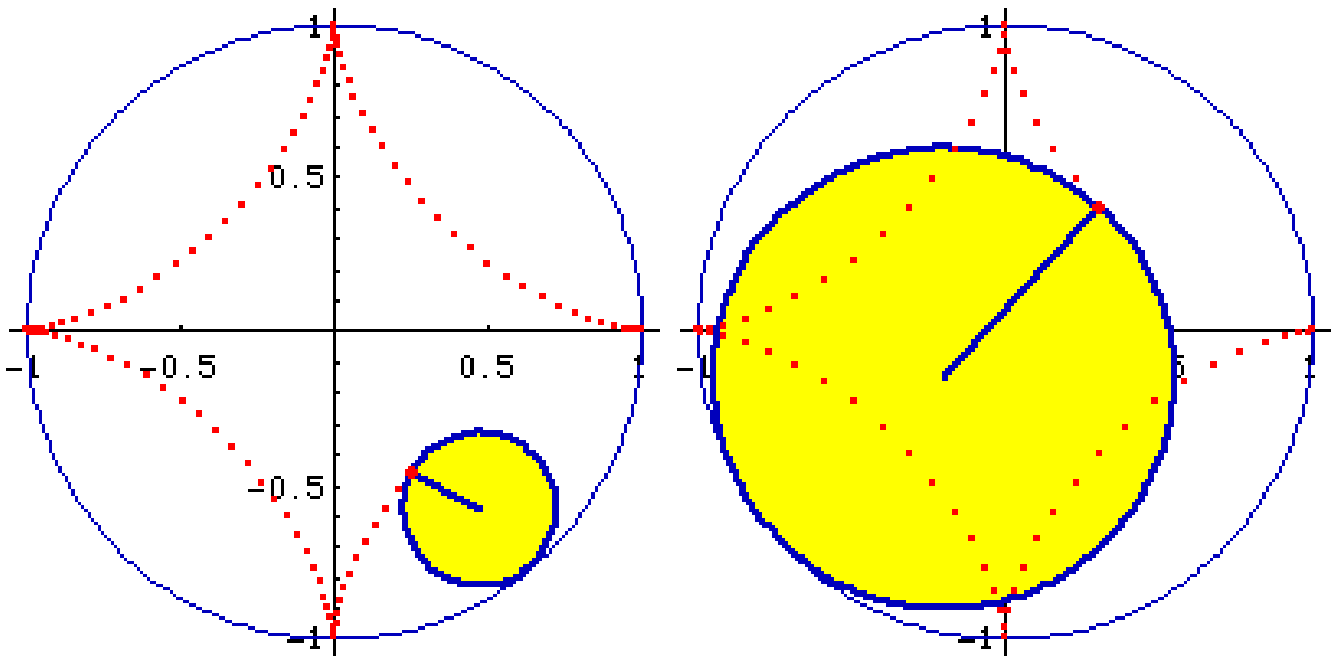
\* This file is from the 3D-XplorMath project. Please see:

## Astroid\*

Parametrization in 3DXM:  $c(t) := aa \cdot (\cos^3(t), \sin^3(t))$ .

Implicit equation:  $x^{2/3} + y^{2/3} = aa^{2/3}$ .

### Description



An Astroid is a curve traced out by a point on the circumference of one circle (of radius  $r$ ) as that circle rolls without slipping on the inside of a second circle having four times or four-thirds times the radius of the first. The latter is known as *double generation*. The Astroid is thus a special kind of a hypocycloid—the family of analogous curves one gets if one allows the ratios of the radii to be arbitrary.

---

\* This file is from the 3D-XplorMath project. Please see:

In 3D-XplorMath, the radius  $r$  is represented by the parameter  $aa$ . A nice geometric property of the Astroid is that its tangents, when extended until they cut the x-axis and the y-axis, all have the same length. This means, if one leans a ladder (say of length  $L$ ) against a wall at all possible angles, then the envelope of the ladder's positions is part of an Astroid. Since (by symmetry) the tangent to the Astroid at a point  $p$  closest to the origin has a slope of plus or minus one, it follows that the distance of  $p$  from the origin is  $L/2$ , and so  $L$  is the “waist-diameter” of the Astroid, i.e., the distance from  $p$  to  $-p$ . Since the diagonal of the Astroid clearly has length  $2L$ , it is twice as long as the waist-diameter.

It can be shown that the normals of an Astroid envelope an Astroid of twice the size. (To see a visual demonstration of this fact, in 3D-XplorMath, select Show Osculating Circles and Normals from the Action Menu.) If you think about what this means, you should see that it gives a ruler construction for the Astroid: Intersect each ladder (between the x-axis and the y-axis) for the smaller Astroid with the orthogonal and twice as long ladder (between the 45-degree lines) for the larger Astroid.

## More Formulas

The initial formulas give an astroid centered at the origin with its four cusps lying on the axes at distance  $aa$  from

the origin. To derive a polynomial equation first cube both sides of the above implicit equation (with  $aa = 1$ ), factorize and simplify:

$$1 = x^2 + y^2 + 3x^{4/3}y^{2/3} + 3x^{2/3}y^{4/3}$$
$$1 - x^2 - y^2 = 3x^{2/3}y^{2/3}(x^{2/3} + y^{2/3}) = 3x^{2/3}y^{2/3}.$$

Then cube again:

$$(1 - x^2 - y^2)^3 = 27x^2y^2.$$

## History

Quote from Robert C. Yates, 1952:

The cycloidal curves, including the astroid, were discovered by Roemer (1674) in his search for the best form for gear teeth. Double generation was first noticed by Daniel Bernoulli in 1725.

Quote from E. H. Lockwood, 1961:

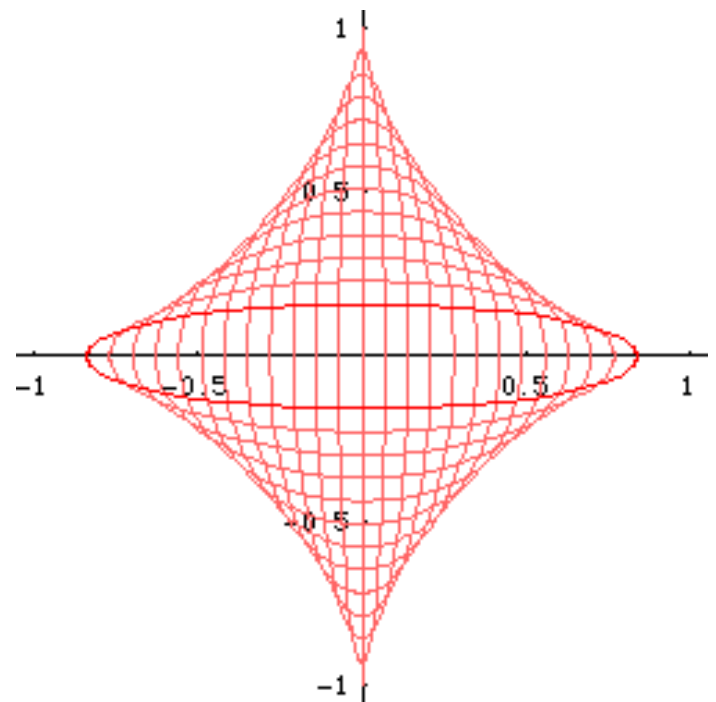
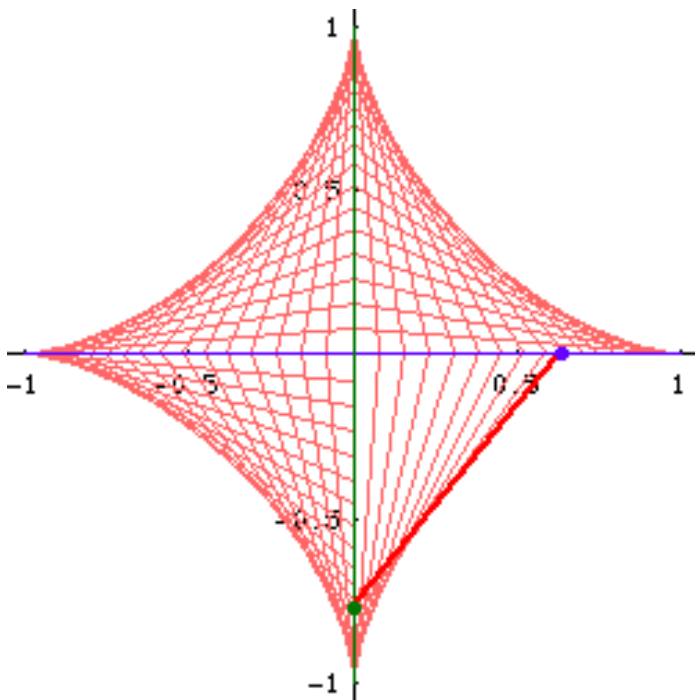
The astroid seems to have acquired its present name only in 1838, in a book published in Vienna; it went, even after that time, under various other names, such as cubocycloid, paracycle, four-cusp-curve, and so on. The equation  $x^{2/3} + y^{2/3} = a^{2/3}$  can, however, be found in Leibniz's correspondence as early as 1715.

## Properties

### *Trammel of Archimedes and Envelope of Ellipses*

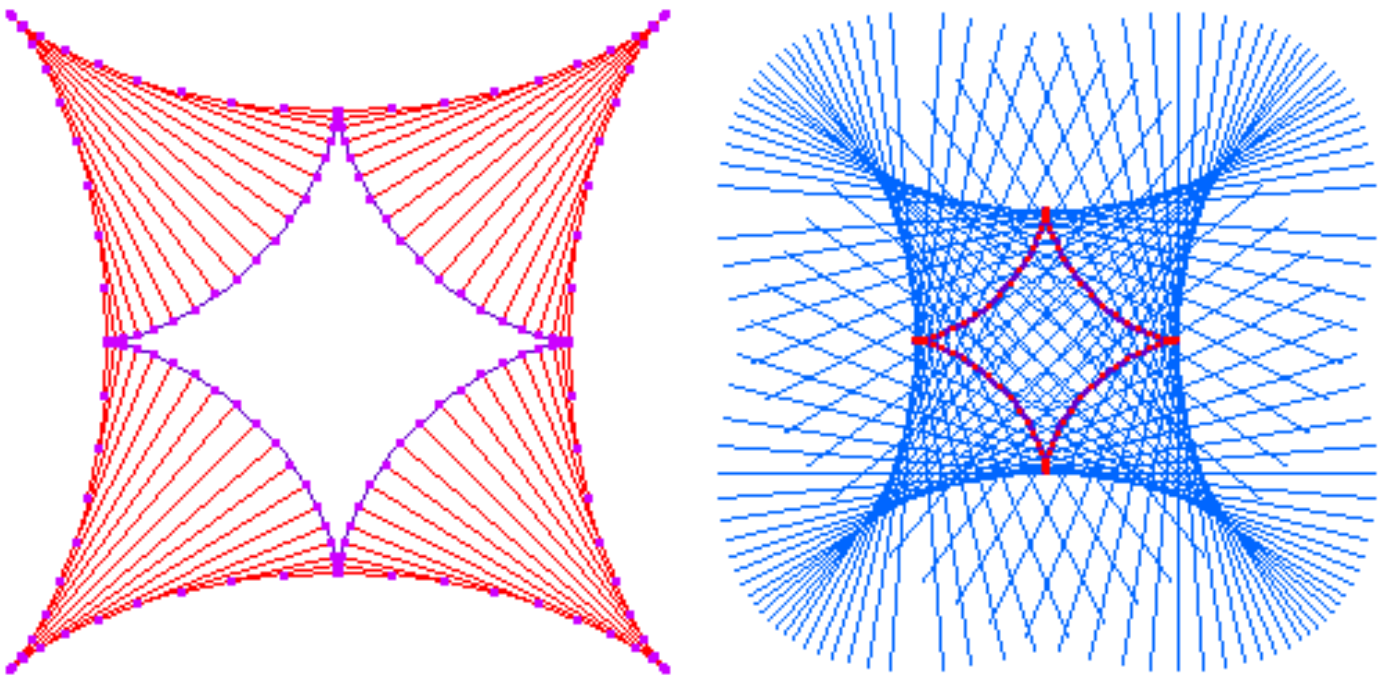
Define the *axes* of the astroid to be the two perpendicular lines passing through the pairs of alternate cusps. A fundamental property of the Astroid is that the length of the segment of a tangent between these two axes is a constant. The Trammel of Archimedes is a mechanical device that is based on this property: it has a fixed bar whose ends slide on two perpendicular tracks. The envelope of the moving bar is then the Astroid, while any particular point on the bar is then the Astroid, while any particular point on the bar will trace out an ellipse.

The Astroid is also the envelope of co-axial ellipses whose sum of major and minor axes is constant.



## The Evolute of the Astroid

The evolute of an astroid is another astroid. (In fact, the evolute of any epi- or hypo- cycloid is a scaled version of itself.) In the first figure below, each point on the curve is connected to the center of its osculating circle, while in the second, the evolute is seen as the envelope of normals.



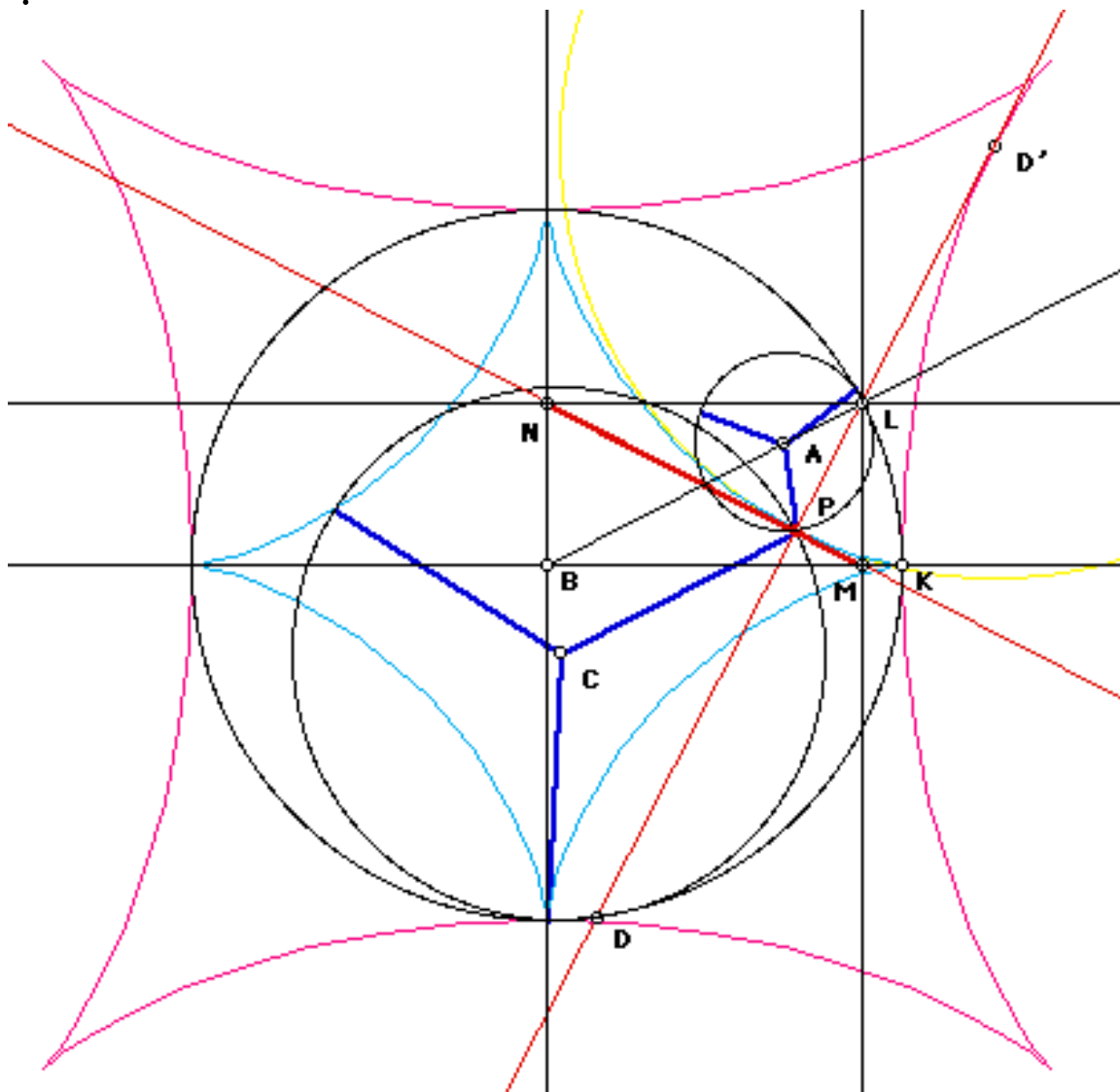
### Curve Construction

The Astroid is rich in properties that can be used to devise other mechanical means to generate the curve and to construct its tangents, and the centers of its osculating circles.

Suppose we have a circle  $C$  centered at  $B$  and passing through some point  $K$ . We will construct an Astroid that is also centered at  $B$  and that has one of its cusps at  $K$ .

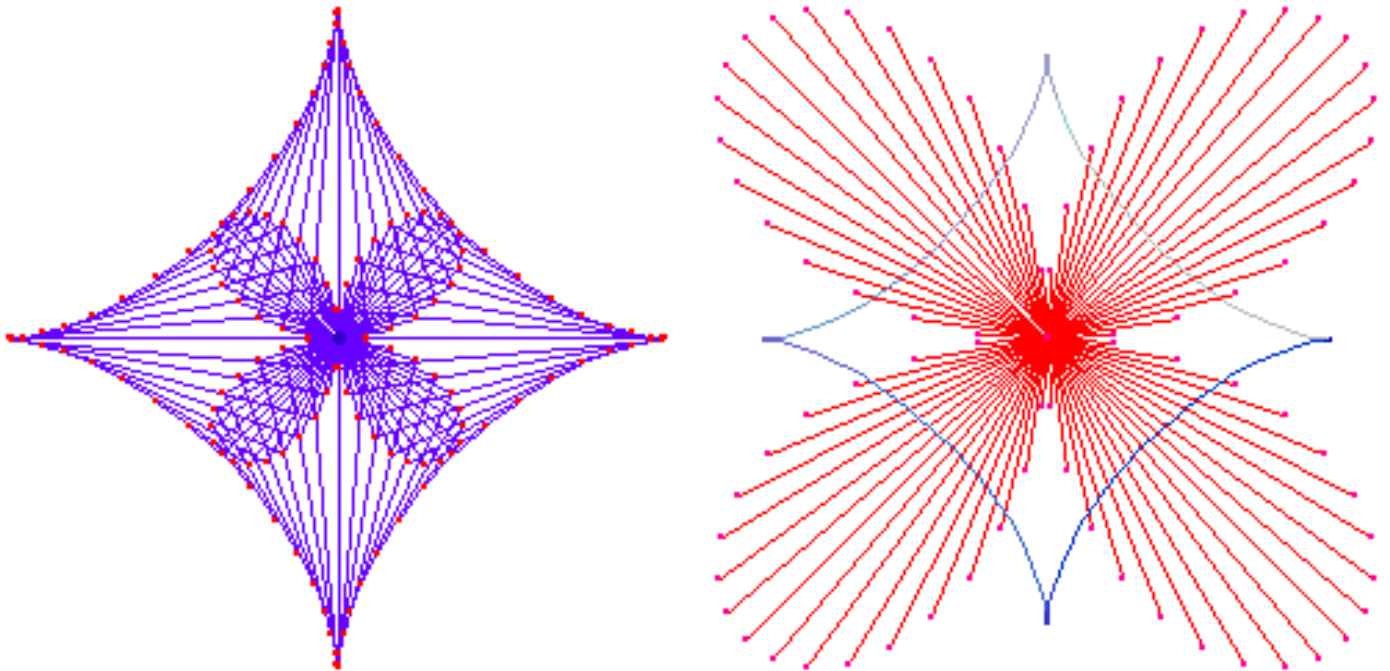
Choose the origin of a cartesian coordinate system at  $B$ ,

and take the point  $(1, 0)$  at  $K$ . Given a point  $L$  on the circle  $C$ , drop a perpendicular from  $L$  to the  $x$ -axis, and let  $M$  be their intersection. Similarly drop a perpendicular from  $L$  to the  $y$ -axis and call the intersection  $N$ . Let  $P$  be the point on  $MN$  such that  $LP$  and  $MN$  are perpendicular. Then  $P$  is a point of the Astroid,  $MN$  is the tangent to the Astroid at  $P$ , and  $LP$  the normal at  $P$ . If  $D$  is the intersection of  $LP$  and the circle  $C$ , and  $D'$  is the reflection of  $D$  thru  $MN$ , then  $D'$  is the center of osculating circle at  $P$ .



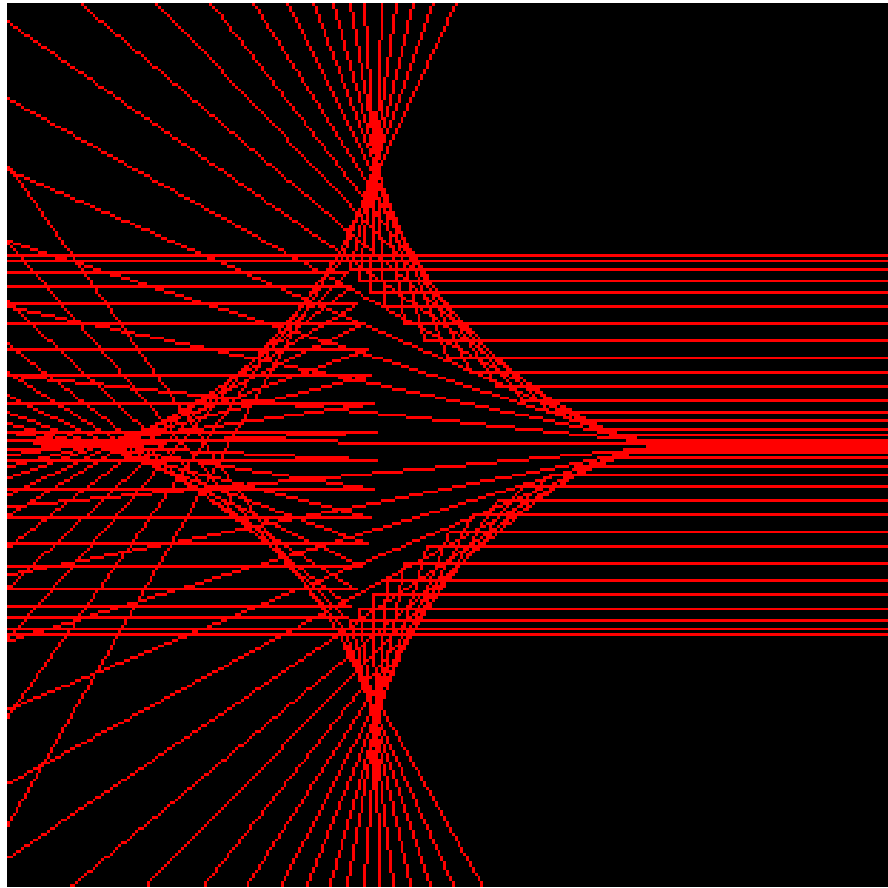
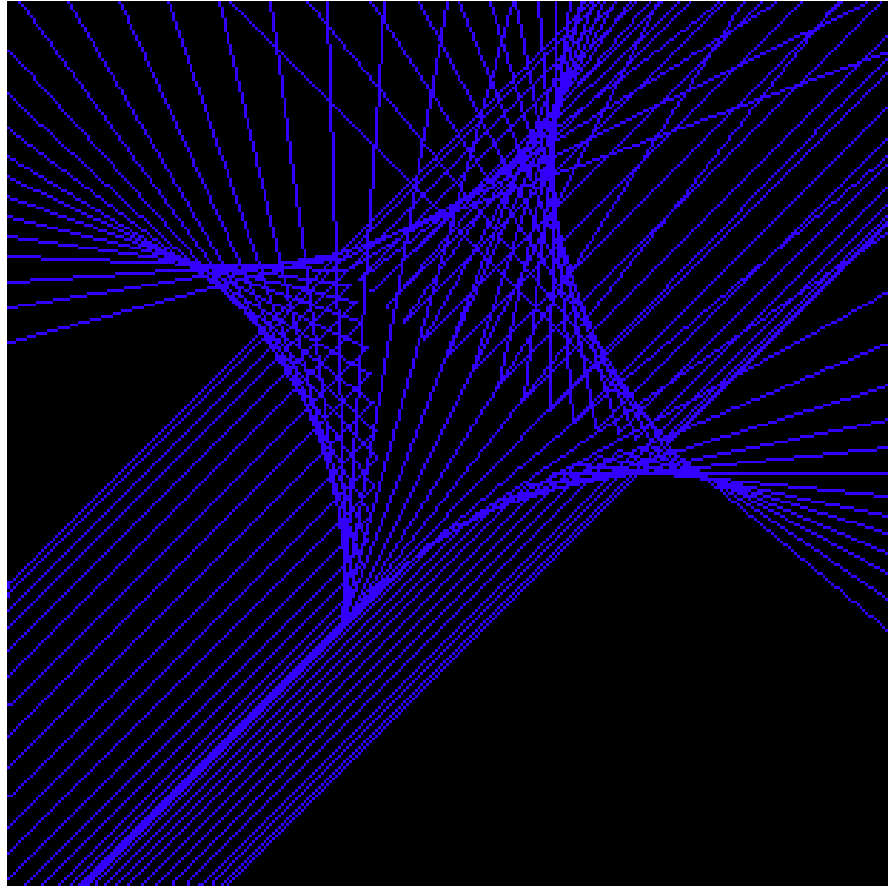
## Pedal, Radial, and Rose

The pedal of an Astroid with respect to its center is a 4-petaled rose, called a quadrifolium. The Astroid's radial is also a quadrifolium. (For any epi- or hypo- cycloid, the pedal and radial are equal, and is a rose.)



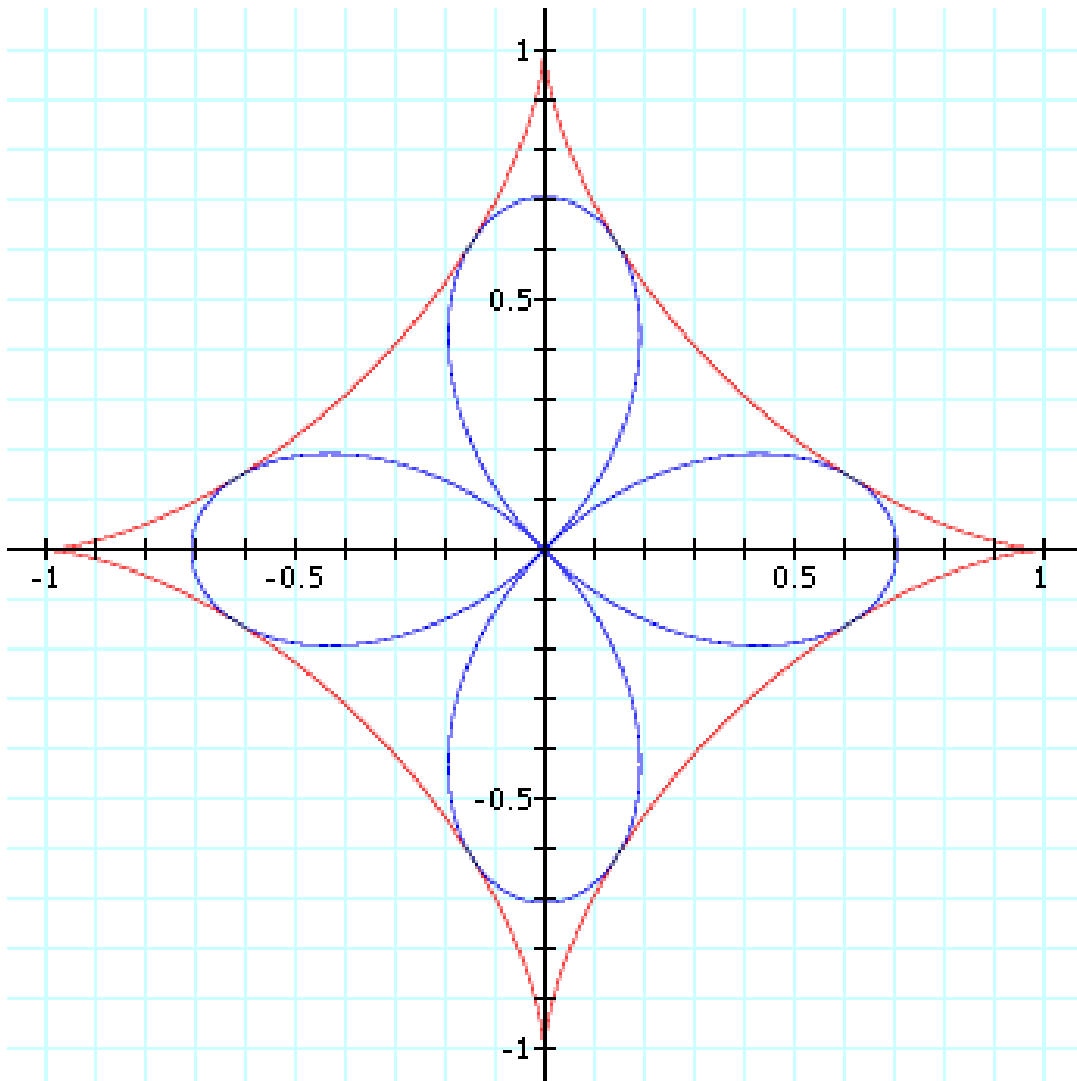
## Catacaustic and Deltoid

The catacaustic of a Deltoid with respect to parallel rays in any direction is an Astroid.



## Orthoptic

We recall that the *orthoptic* of a curve  $C$  is the locus of points  $P$  where two tangents to  $C$  meet at right angles. The orthoptic of the Astroid is the quadrifolium  $r^2 = (1/2) \cos(2\theta)^2$ . [Robert C. Yates.]



XL.

[Go To Planar TOC](#)

## Deltoid \*

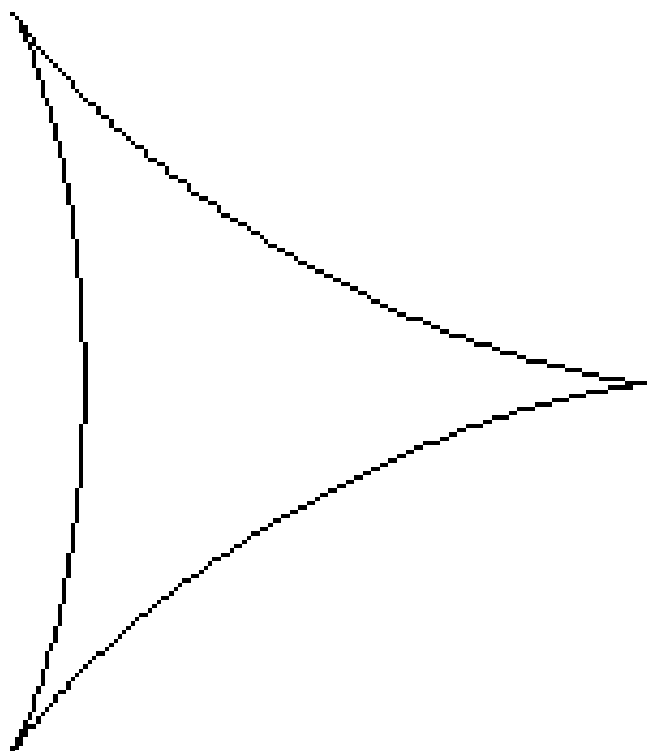
The Deltoid curve was conceived by Euler in 1745 in connection with his study of caustics.

Formulas in 3D-XplorMath:

$$x = 2 \cos(t) + \cos(2t), \quad y = 2 \sin(t) - \sin(2t), \quad 0 < t \leq 2\pi,$$

and its implicit equation is:

$$(x^2 + y^2)^2 - 8x(x^2 - 3y^2) + 18(x^2 + y^2) - 27 = 0.$$



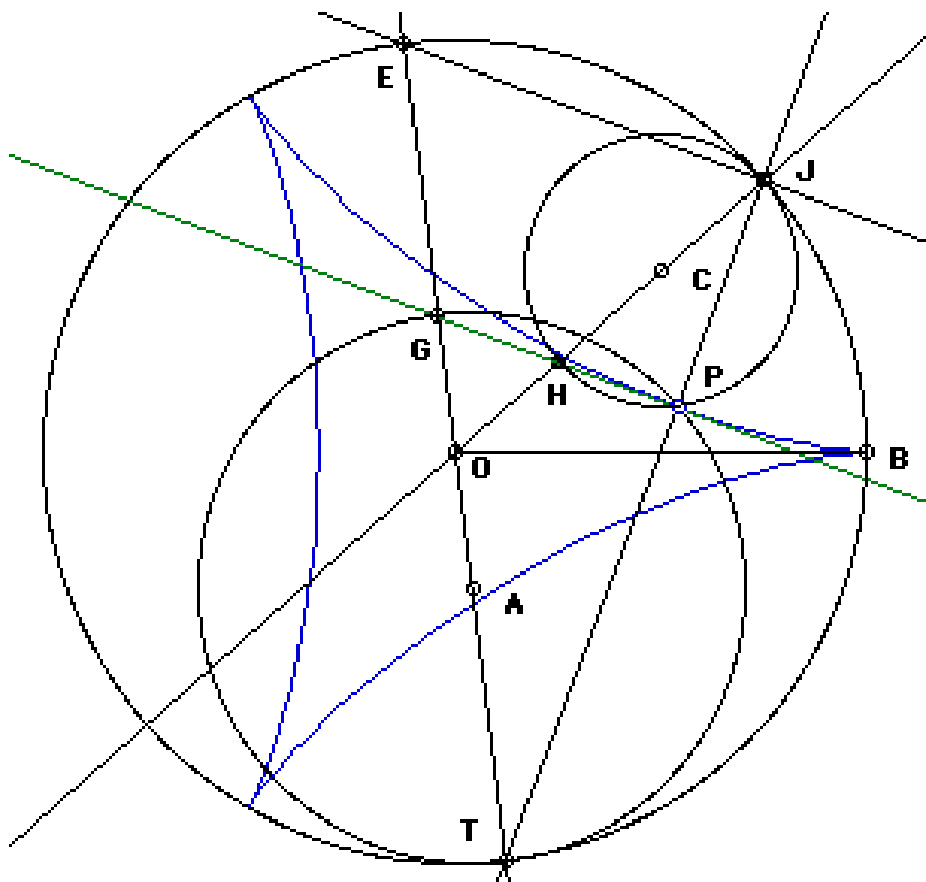
The Deltoid or Tricuspid

The Deltoid is also known as the Tricuspid, and can be defined as the trace of a point on one circle that rolls inside

---

\* This file is from the 3D-XplorMath project. Please see:

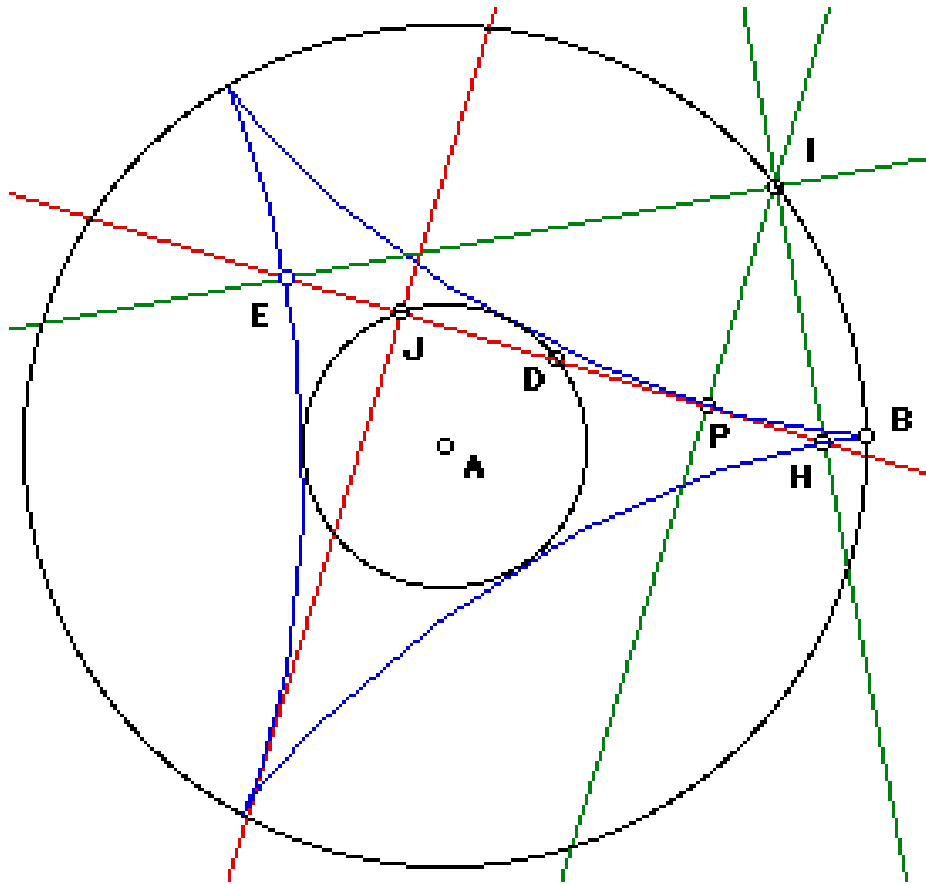
another circle of 3 or  $3/2$  times as large a radius. The latter is called double generation. The figure below shows both of these methods. O is the center of the fixed circle of radius  $a$ , C the center of the rolling circle of radius  $a/3$ , and P the tracing point. OHCJ, JPT and TAOGE are colinear, where G and A are distant  $a/3$  from O, and A is the center of the rolling circle with radius  $2a/3$ . PHG is colinear and gives the tangent at P. Triangles TEJ, TGP, and JHP are all similar and  $TP/JP = 2$ . Angle JCP =  $3 \times$  Angle BOJ. Let the point Q (not shown) be the intersection of JE and the circle centered on C. Points Q, P are symmetric with respect to point C. The intersection of OQ, PJ forms the center of osculating circle at P.



The Deltoid has numerous interesting properties.

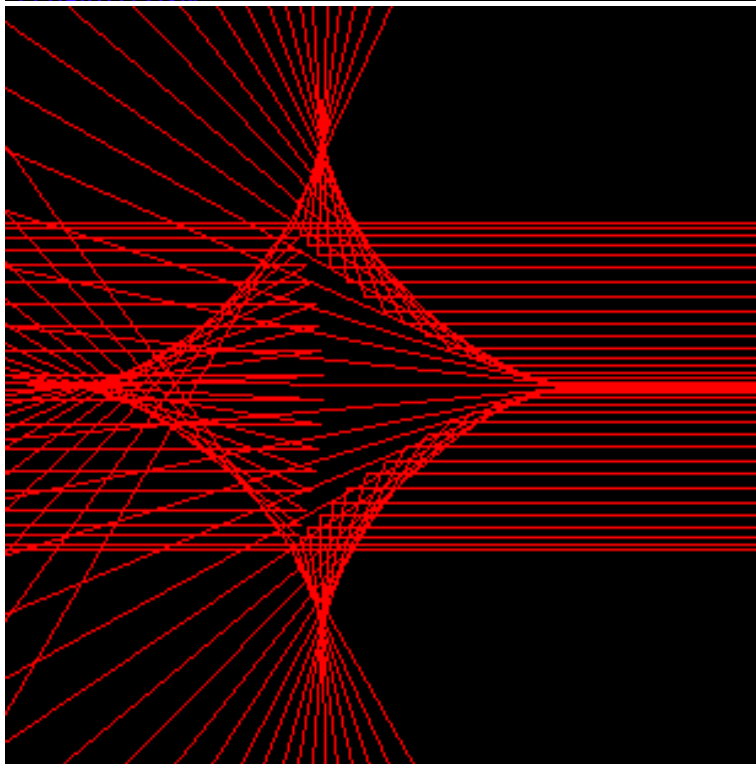
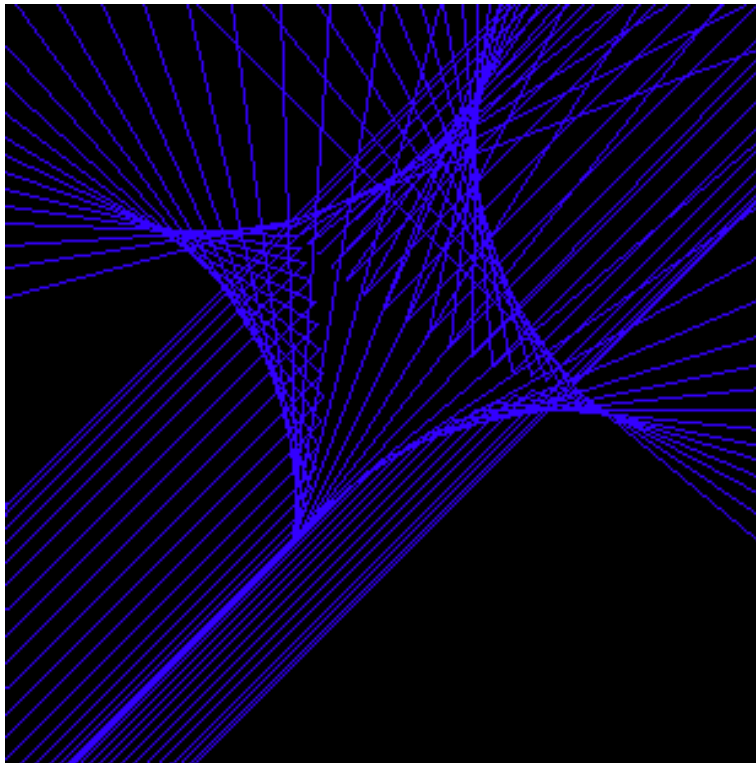
## Properties

### Tangent



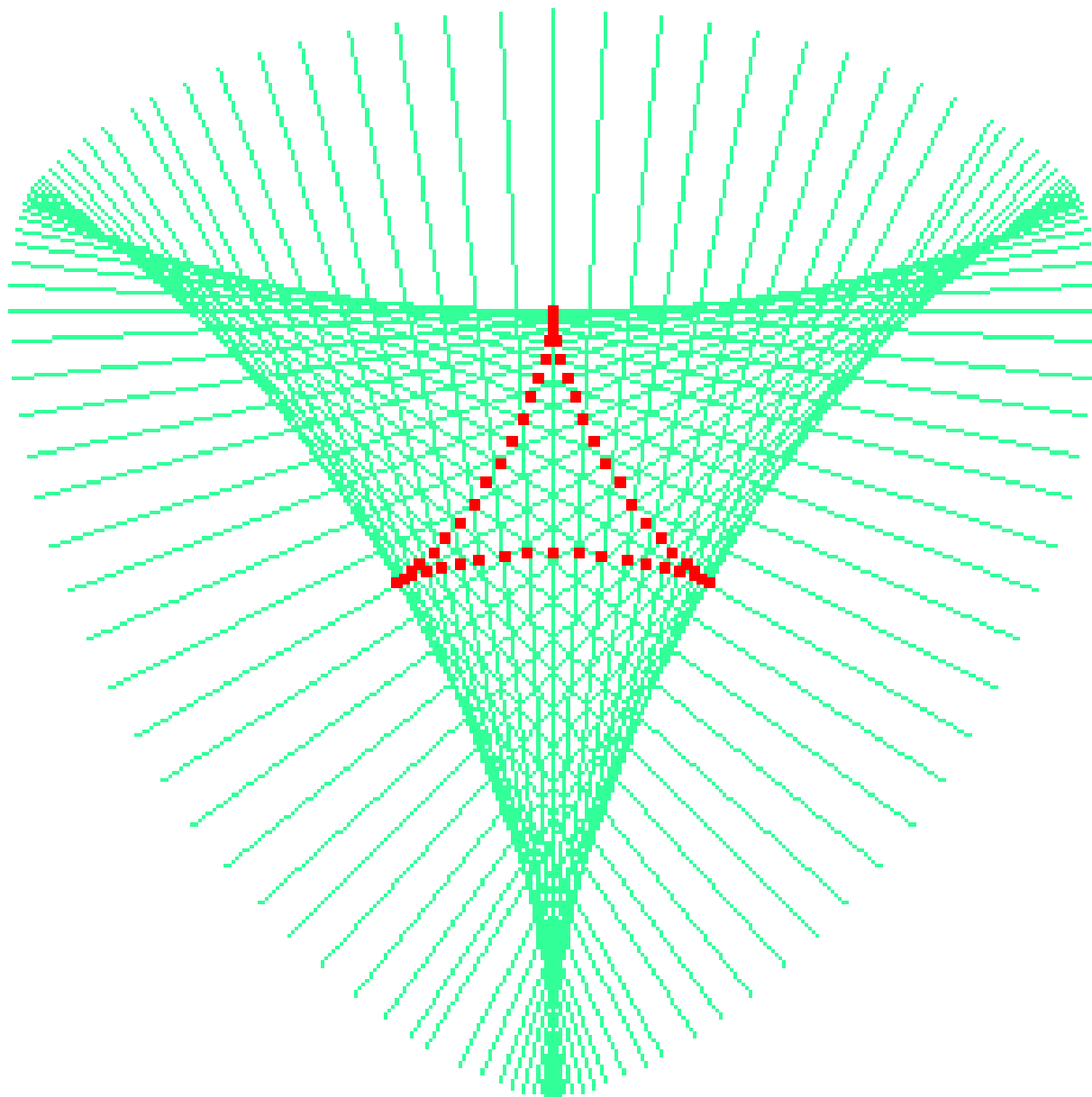
Let A be the center of the curve, B be one of the cusp points, and P be any point on the curve. Let E, H be the intersections of the curve and the tangent at P. The segment EH has constant length  $\text{distance}[E,H] = \frac{4}{3} \cdot \text{distance}[A,B]$ . The locus of midpoint D of the tangent segment EH is the inscribed circle. The normals at E, P, H are concurrent, and the locus of these intersections is the circumscribed circle. If J is the intersection of another tangent, cutting EH at right angle, then the locus traced by J (the Deltoid's orthoptic) is the inscribed circle.

## The Deltoid and the Astroid



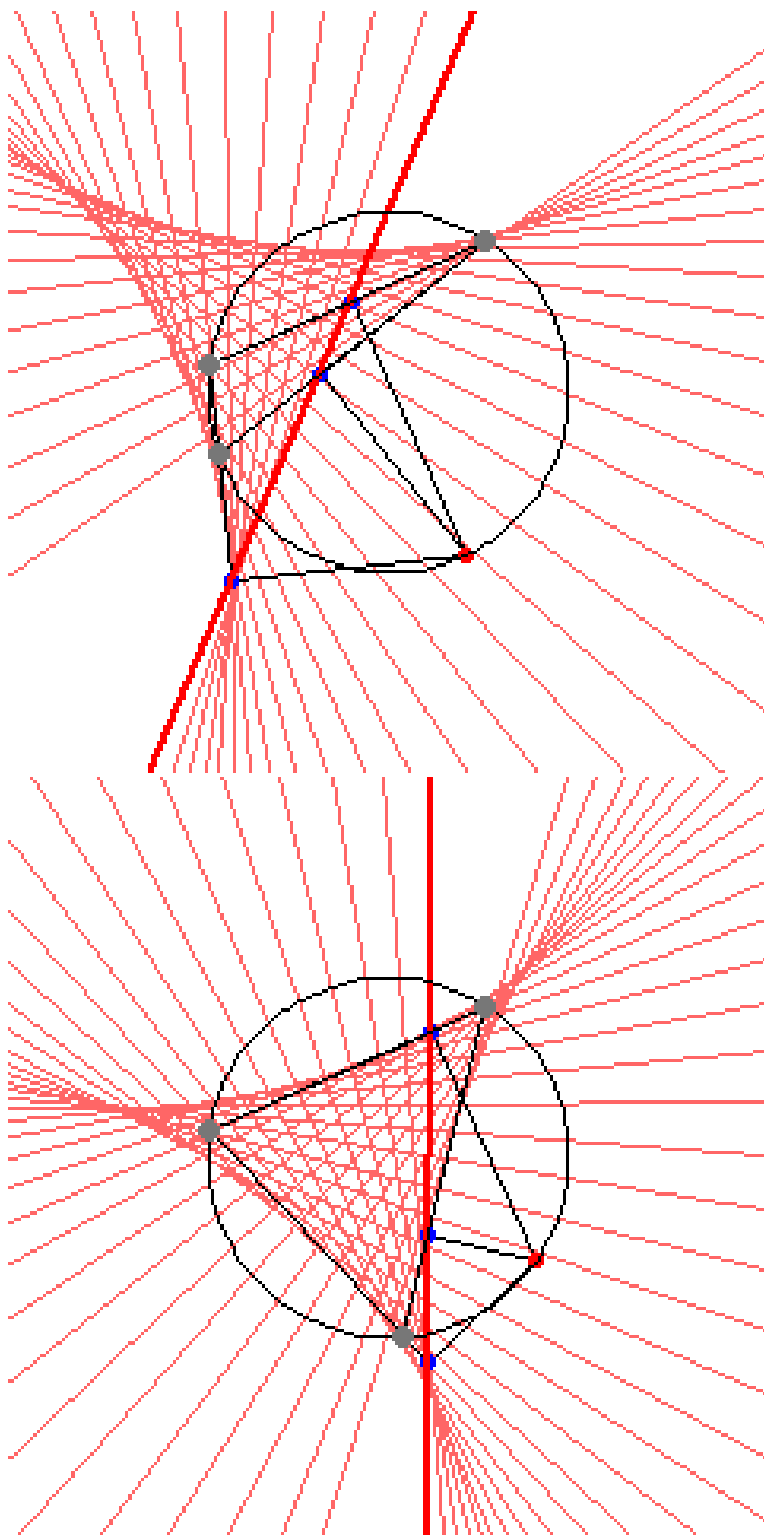
The caustic of the Deltoid with respect to parallel rays in any direction is an Astroid.

## Evolute



The evolute of Deltoid is another Deltoid. (In fact, the evolutes of all epicycloids and hypocycloids are scaled version of themselves.) In the above figure, the evolute is shown as the envelope of its normals.

# Simson Lines

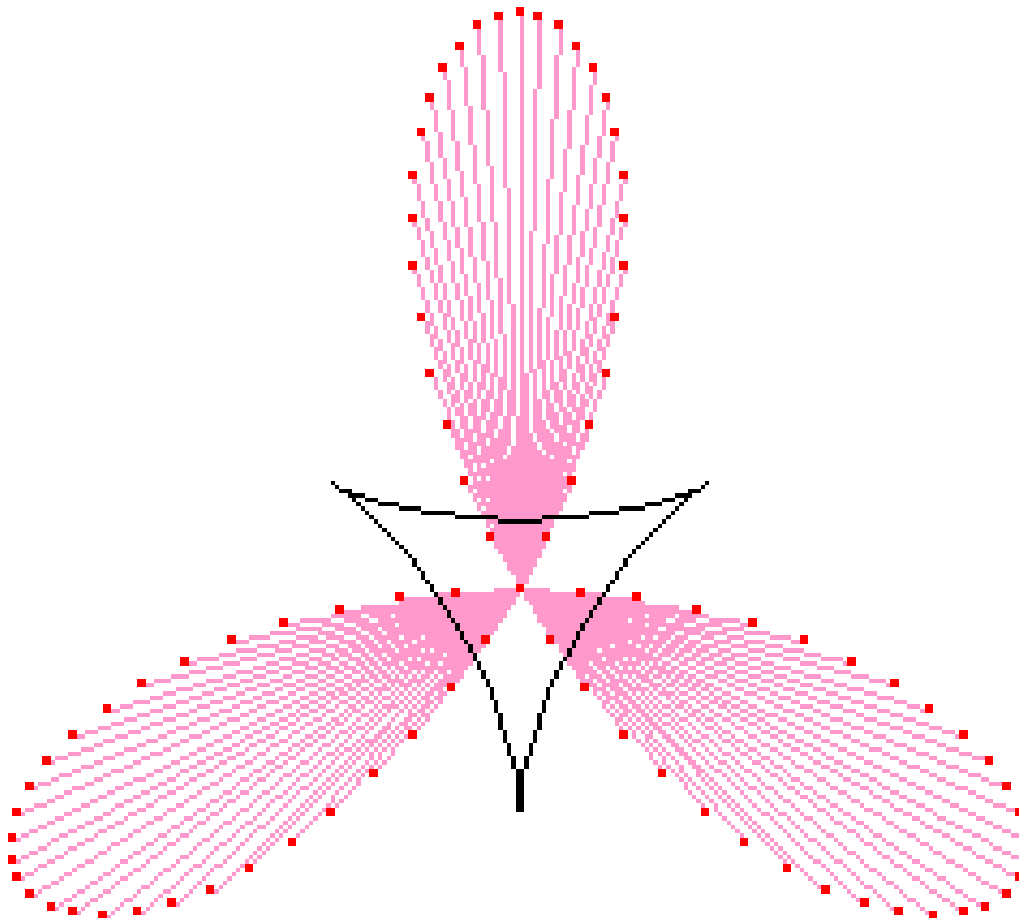


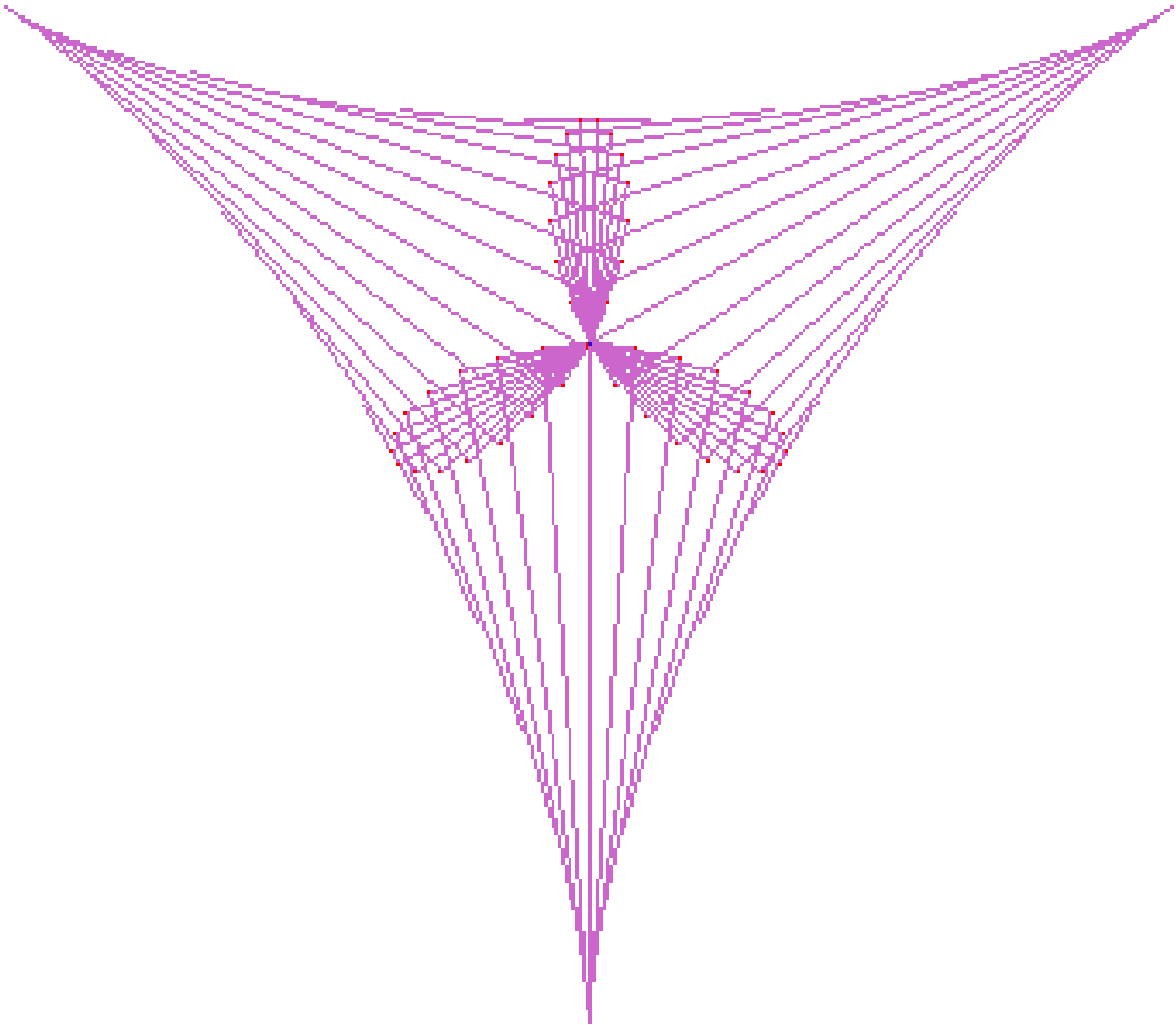
The Deltoid is the envelope of the Simson lines of any triangle. (Robert Simson, 1687–1768)

Step by step description:

1. Let a triangle be inscribed in a circle. 2. Pick any point  $P$  on the circle. 3. Mark a point  $Q_1$  on any side of the triangle such that line  $[P, Q_1]$  is perpendicular to it, extending the side if necessary. 4. Similarly, find points  $Q_2$  and  $Q_3$  with respect to  $P$  for the other two sides. 5. The points  $Q_1$ ,  $Q_2$ , and  $Q_3$  are colinear, and the line passing through them is called the Simson line of the triangle with respect to  $P$ . 6. Find Simson lines for the other points  $P$  on the circle. Their envelope is the deltoid. Amazingly, this is true for any triangle.

### **Pedal, Radial, and Rose**





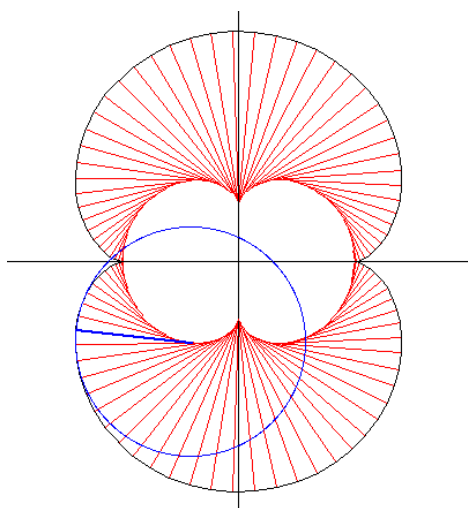
The pedal curve of a Deltoid with respect to a cusp, vertex, or center is a folium curve with one, two, or three loops respectively. The last one is called the trifoilium, a three petalled rose. The Deltoid's radial is a trifoilium too.

XL.

[Go To Planar TOC](#)

## The Nephroid \*

The Nephroid is generated by rolling a circle of one radius on the outside of a second circle of twice the radius. In 3D-XplorMath, either choose Nephroid from the Plane Curve menu, or choose Circle, then select Set Parameters... from the Settings menu and set  $hh = -0.5 \cdot aa$ ,  $ii = 1$ . With  $R = 3r$  we thus have the parametrization for Nephroids:



$$\begin{aligned}x(t) &= R \cdot \sin(t) + r \cdot \sin(3t) \\y(t) &= R \cdot \cos(t) + r \cdot \cos(3t)\end{aligned}$$

As with Cardioids and Limaçons, one can also make the radius for the drawing stick shorter or longer: Set  $ii > 1$  for the looping relatives of the Nephroid or see the default Morph in the Animation menu.

The complex map  $z \mapsto z^3 + 3z$  maps the unit circle to such a Nephroid. To see this, in the Conformal Map Category,

---

\* This file is from the 3D-XplorMath project. Please see:

select  $z \mapsto z^e e + ee z$  from the Conformal Map menu, and then choose Set Parameters from the Settings menu and set  $ee$  to 3.

The normals of one Nephroid have as envelope another, smaller Nephroid—the same phenomenon as for the Cardioid and the Cycloid. (To see this select **Show Osculating Circles With Normals** from the Action menu). In technical jargon, the caustics for each of these curves is a similar curve.

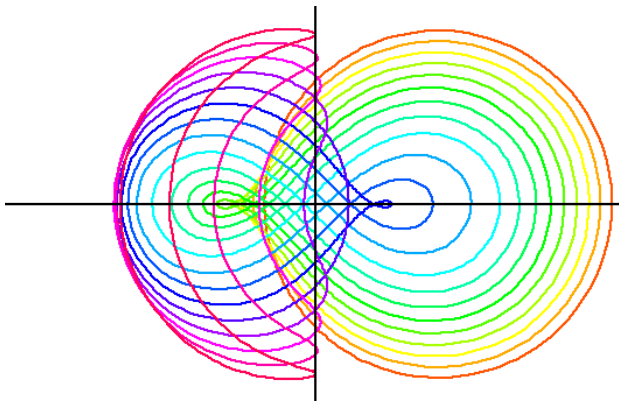
H.K.

[Go To Planar TOC](#)

# About Mechanically Generated Curves \*

## Examples

Presently we have the following mechanically generated plane curves programmed together with a decoration which shows this generation and the corresponding construction of the tangents of the curve:



Epi- and Hypocycloids,  
all other rolling curves.  
Also: Tractrix, Cissoid,  
Conchoid, Lemniscate.

This image is obtained with **Color Morph** in the Animation menu, it shows the family obtained from the current drawing mechanism (here Lemniscate).

## Moving Planes

It is often convenient to discuss such mechanical generations in terms of two planes, a fixed plane on which the drawing is done (paper plane) and a second plane which is attached to that piece of the mechanical contraption that holds the drawing pen (drawing plane). In the case of rolling curves we have the drawing plane attached to the

---

\* This file is from the 3D-XplorMath project. Please see:

rolling wheel, in the case of the Lemniscate the drawing plane is attached to the middle one of the three connected moving segments.

*We think of the orbits of the points of the drawing plane as curves that are mechanically generated by the apparatus under consideration.*

The velocity vectors of these orbits clearly give a time dependent vector field. Since this vector field is obtained by differentiating the orbits of a family of **isometries** we obtain at each time  $t$  the vector field of a Euclidean **group of motions**, in other words: for most  $t$  the vector field consists of the velocity vectors of a rotation, a rotation around the so called momentary center of rotation. This way of looking at the generation gives immediately tangent constructions for all orbits: join the momentary center of rotation to the moving point, the perpendicular line through the point is tangent to its orbit.

It is therefore useful to visualize the movement of the drawing plane together with the time dependent velocity field of its points. We have done this by decorating the drawing plane with not too many but enough random points so that the movement of the drawing plane becomes visible, but the curve under consideration is not obscured. Moreover, to make the vector field visible at each moment  $t$ , we have drawn the random points not once, but at two subsequent positions. This picture is interpreted by the brain correctly.

Finally, one has to determine the momentary center of ro-

tation. This is different for each construction. For rolling curves the definition of “rolling” is such that that point, where the rolling wheel touches the fixed curve (“street”), is the momentary center of rotation. In general one has to look for points of the mechanical apparatus for which the direction of the momentary movement (“orbit tangent”) can be decided. The momentary center is then on the line (“radius”) perpendicular to the tangent, so that two such lines are needed. The 3DXM demos use green lines to determine the momentary center.

H.K.

[Go To Planar TOC](#)

## Cubic Curves \*

Real Cubic Curves in  $\mathbb{R}^2$  were studied extensively by Newton. Later these curves were considered as the real points of complex curves in  $\mathbb{C}^2$ . If they do not have double points they can be parametrized by additive groups. This means that the points on these curves can be added. Surprisingly this addition is a *geometric addition*, i.e. the sum  $P + Q$  can be geometrically constructed from  $P, Q$  and the curve. In the case of cubic curves we have:

$$P + Q + R = 0 \Leftrightarrow$$

A straight line intersects the curve in  $P, Q, R$  .

**In 3D-XplorMath are the following examples:**

Cubic Polynomial Graph,  $x(t) = t, y(t) = x(t)^3 + aa \cdot x(t)$ ,

Cuspidal Cubic,  $x(t) = 3t^2/(4aa), y(t) = t(t^2 + bb)/(4aa^2)$ ,

Cubic Rational Graph I,  $x(t) = \tan(t/2)/aa, y(t) = \sin(t)$ ,

Cubic Rat'l Graph II,  $x(t) = \tanh(t/2)/aa, y(t) = \sinh(t)$ ,

Elliptic Cubic,  $x + 1/x - aa \cdot (y - 1/y) = ff$  (implicit),

Folium,  $[x, y] = aa[(t^2 - t^3), (t - 2t^2 + t^3)]/(1 - 3t - 3t^2)$ ,

Nodal Cubic,  $x = 1 - t^2, y = ((1 - t^2) + bb) \cdot t$ .

---

\* This file is from the 3D-XplorMath project. Please see:

The last two of these are cubics with one double point. Their points do not form a group, therefore their Action Menu has only the Standard Actions for plane curves.

All the others are parametrized by a 1-dim. Abelian group and the curves are shown with a default demo explaining the geometric addition.

If we intersect a Cubic Polynomial Graph without quadratic term with a line, then the x-coordinates of the intersection points are always roots of a polynomial without quadratic term. In other words: these three x-coordinates add up to 0., the *geometric addition* is the standard addition on the x-axis.

The Cuspidal Cubic is also parametrized by  $\mathbb{R}$  (or  $\mathbb{C}$ ) and a simple computation shows: if  $1/t_1 + 1/t_2 + 1/t_3 = 0$  then the three points  $[x(t_i), y(t_i)]$  lie on a straight line. And dually, if  $t_1 + t_2 + t_3 = 0$  then the tangents at the three points  $[x(t_i), y(t_i)]$  pass through one point. Again, the addition has a simple geometric interpretation that allows to construct, if two points and the curve are given, their sum.

The first Rational Cubic Graph is parametrized by a circle  $\mathbb{S}^1$  (we have to add the infinite point  $(\infty, 0)$ ). The demo that comes with the curve shows how the sum point can be constructed by intersecting lines. The Action Menu offers a second demo that shows how addition on the parametrizing circle and on the curve are the same.

The second Rational Cubic Graph would not be here if we could visualize these curves over the complex Numbers. Over  $\mathbb{C}$  one can think of this curve as the group  $\mathbb{S}^1 \oplus \mathbb{R}$ ,

a cylinder. The first rational graph visualizes the equator circle, the second one visualizes the generator through the neutral element plus the opposite generator: two copies of  $\mathbb{R}$  (and a double point at  $\infty$ ).

The Elliptic Cubic is parametrized by a pair of so called *Elliptic Functions*. Such functions can be viewed either as doubly periodic functions from  $\mathbb{C}$  to  $\mathbb{S}^1$  or as functions defined on some torus. For more details see the text *Elliptic Functions*.

The addition on elliptic curves can be compared with addition on the circle. The formulas for trigonometric functions

$$\begin{aligned}\cos(\alpha + \beta) &= \cos(\alpha) \cos(\beta) - \sin(\alpha) \sin(\beta) \\ \sin(\alpha + \beta) &= \sin(\alpha) \cos(\beta) + \cos(\alpha) \sin(\beta)\end{aligned}$$

show that

$$(x_1, y_1) \oplus (x_2, y_2) := (x_1 x_2 - y_1 y_2, x_1 y_2 + y_1 x_2)$$

gives the addition of points  $(x_1, y_1), (x_2, y_2) \in \mathbb{S}^1$ . Notice that the rational points (i.e. the pythagorean triples) are a subgroup. The elliptic functions have analogous functional equations which are similarly the basis for addition formulas for points on elliptic cubics. This is explained in the text [Addition on Cubic Curves](#).

H.K.

[Go To Planar TOC](#)

## Symmetries Of Elliptic Functions \*

[The approach below to elliptic functions follows that given in section 3 of "The Genus One Helicoid and the Minimal Surfaces that led to its Discovery", by David Hoffman, Hermann Karcher, and Fusheng Wei, published in Global Analysis and Modern Mathematics, Publish or Perish Press, 1993. For convenience, the full text of section 3 (without diagrams) has been made an appendix to the chapter on the Conformal Map Category in the documentation of 3D-XplorMath.]

An elliptic function is a doubly periodic meromorphic function,  $F(z)$ , on the complex plane  $\mathbb{C}$ . The subgroup  $\mathbb{L}$  of  $\mathbb{C}$  consisting of the periods of  $F$  (the period lattice) is isomorphic to the direct sum of two copies of  $\mathbb{Z}$ , so that the quotient,  $T = \mathbb{C}/\mathbb{L}$ , is a torus with a conformal structure, i.e., a Riemann surface of genus one. Since  $F$  is well-defined on  $\mathbb{C}/\mathbb{L}$ , we may equally well consider it as a meromorphic function on the Riemann surface  $T$ .

It is well-known that the conformal equivalence class of such a complex torus can be described by a single complex number. If we choose two generators for  $\mathbb{L}$  then, without changing the conformal class of  $\mathbb{C}/\mathbb{L}$ , we can rotate and scale the lattice so that one generator is the complex num-

---

\* This file is from the 3D-XplorMath project. Please see:

ber 1, and the other,  $\tau$ , then determines the conformal class of  $T$ . Moreover,  $\tau_1$  and  $\tau_2$  determine the same conformal class if and only if they are conjugate under  $SL(2, Z)$ .

The simplest elliptic functions are those defining a degree two map of  $T$  to the Riemann sphere. We will be concerned with four such functions, that we call JD, JE, JF, and WP. The first three are closely related to the classical Jacobi elliptic functions, but have normalizations that are better adapted to certain geometric purposes, and similarly WP is a version of the Weierstrass  $\wp$ -function, with a geometric normalization. Any of these four functions can be considered as the projection of a branched covering over the Riemann sphere with total space  $T$ , and as such it has four branch values, i.e., points of the Riemann sphere where the ramification index is two. For JD there is a complex number  $D$  such that these four branch values are  $\{D, -D, 1/D, -1/D\}$ . Similarly for JE and JF there are complex numbers  $E$  and  $F$  so that the branch values are  $\{E, -E, 1/E, -1/E\}$  and  $\{F, -F, 1/F, -1/F\}$  respectively, while for WP there is a complex number  $P$  such that the branch values are  $\{P, -1/P, 0, \infty\}$ . The cross-ratio,  $\lambda$ , of these branch values (in proper order) determines  $\tau$  and likewise is determined by  $\tau$ .

The branch values  $E$ ,  $F$ , and  $P$  of JE, JF, and WP can be easily computed from the branch value  $D$  of JD (and hence from  $\tau$ ) using the following formulas:

$$E = (D - 1)/(D + 1), \quad F = -i(D - i)/(D + i),$$

$$P = i(D^2 + 1)/(D^2 - 1),$$

and we will use  $D$  as our preferred parameter for describing the conformal class of  $T$ . In 3D-XplorMath,  $D$  is related to the parameter  $dd$  (of the Set Parameter... dialog) by  $D = \exp(dd)$ , i.e., if  $dd = a + ib$ , the  $D = \exp(a) \exp(ib)$ . This is convenient, since if  $D$  lies on the unit circle (i.e., if  $dd$  is imaginary) then the torus is rectilinear, while if  $D$  has equal real and imaginary parts (i.e., if  $b = \pi/4$ ) then the torus is rhombic. (The square torus being both rectilinear and rhombic, corresponds to  $dd = i \cdot \pi/4$ ).

To completely specify an elliptic function in 3D-XplorMath, choose one of JD, JE, JF, or WP from the Conformal Map menu, and specify  $dd$  in the Set Parameter... dialog. (Choosing Elliptic Function from the Conformal map menu will give the default choices of JD and a square torus.)

When elliptic functions were first constructed by Jacobi and by Weierstrass these authors assumed that the lattice of the torus was given. On the other hand, in Algebraic Geometry, tori appeared as elliptic curves. In this representation the branch values of functions on the torus are given with the equation, while an integration of a holomorphic form (unique up to a multiplicative constant) is required to find the lattice. Therefore the relation between the period quotient  $\tau$  (or rather its  $SL(2, Z)$ -orbit) and the cross ratio  $\lambda$  of the four branch values has been well-studied. More recently, in Minimal Surface Theory, it was

also more convenient to assume that the branch values of a degree two elliptic functions were given and that the periods had to be computed. Moreover, symmetries became more important than in the earlier studies.

Note that the four branch points of a degree two elliptic function (also called "two-division points", or *Zweitteilungspunkte*) form a half-period lattice. There are three involutions of the torus which permute these branch points; each of these involutions has again four fixed-points and these are all midpoints between the four branch points. Since each of the involutions permutes the branch points, it transforms the elliptic function by a Moebius transformation. In Minimal Surface Theory, period conditions could be solved without computations if those Moebius transformations were not arbitrary, but rather were isometric rotations of the Riemann sphere—see in the Surface Category the minimal surfaces by Riemann and those named *Jd* and *Je*. This suggested the following construction: As degree two MAPS from a torus ( $T = \mathbb{C}/\mathbb{L}$ ) to a sphere, we have the natural quotient maps  $T/-id$ ; these maps have four branch points, since the 180 degree rotations have four fixed points. To get well defined FUNCTIONS we have to choose three points and send them to  $\{0, 1, \infty\}$ . We choose these points from the midpoints between the branch points, and the different choices lead to different functions. The symmetries also determine the points that are sent to  $\{-1, +i, -i\}$ . In this way we get the most symmetric elliptic functions, and they are denoted *JD*, *JE*, *JF*.

The program allows one to compare them with Jacobi's elliptic functions. The function  $WP = JE * JF$  has a double zero, a double pole and the values  $\{+i, -i\}$  on certain midpoints (diagonal ones in the case of rectangular tori). Up to an additive and a multiplicative constant it agrees with the Weierstrass  $\wp$ -function, but in our normalization it is the Gauss map of Riemann's minimal surface on each rectangular torus.

We compute the J-functions as follows. If one branch value is called  $+B$ , then the others are  $\{-B, +1/B, -1/B\}$ . Therefore the function satisfies the *differential equations*

$$(J')^2 = (J'(0))^2(J^4 + 1 - (B^2 + 1/B^2)J^2) = F(J),$$

$$J'' = (J'(0))^2(2J^3 - (B^2 + 1/B^2)J = F'(J)/2).$$

*Numerically* we solve this with a fourth order scheme that has the analytic continuation of the square root  $J' = \sqrt{J'^2}$  built into it:

Let  $J(0), J'(0)$  be given. Compute  $J''(0) := F'(J(0))/2$  and, for small  $z$ ,

$$J_m := J(0) + J'(0) \cdot z/2 + J''(0) \cdot z^2/8, \quad J''_m := F'(J_m)/2,$$

$$J(z) := J(0) + J'(0) \cdot z + (J''(0) + 2 \cdot J''_m) \cdot z^2/6.$$

Finally let  $J'(z)$  be that square root of  $F(J(z))$  that is closer to  $J'(0) + J''_m \cdot z$  (analytic continuation!). Repeat.

H.K.

[Go To Planar TOC](#)

## Addition on Cubic Curves \*

See also the Action Menu of the Parabola “Show Normals through Mouse Point” and the comments in the ATO.

As an introductory example view the unit circle as a group. Then the addition of angles  $\phi \in (\mathbb{R} \bmod 2\pi)$  gets translated via the parametrization

$$x = \cos(\phi), y = \sin(\phi)$$

into

$$(x_1, y_1) \oplus (x_2, y_2) := (x_1x_2 - y_1y_2, x_1y_2 + x_2y_1).$$

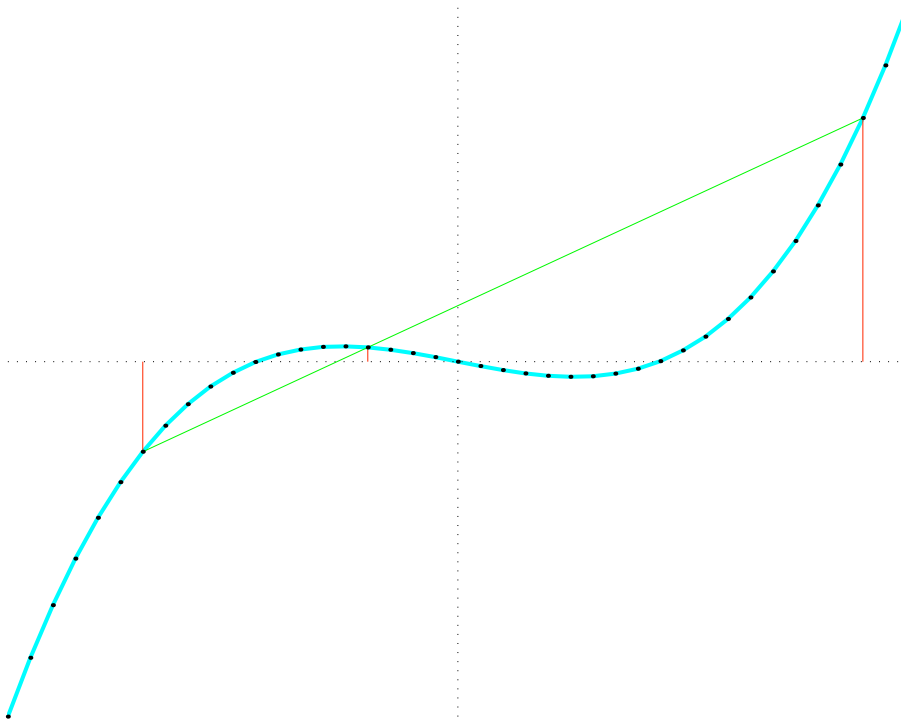
Once this addition law is known one does not need the transcendental functions  $\sin$  and  $\cos$  to “add” points on the circle. Even to do this addition with ruler and compass is easy. And it is amusing to note that the Pythagorean (or rational) points of the circle are a subgroup, e.g.  $(3/5, 4/5) \oplus (12/13, 5/13) = ((36 - 20)/65, (15 + 48)/65)$ .

In a similar way there exists a geometric addition on cubic curves, and if the cubic is parametrized with appropriate functions (defined either on  $\mathbb{C}$ , or on  $\mathbb{C}/2\pi\mathbb{Z}$ , or on  $\mathbb{C}/\Gamma$ ,  $\Gamma$  a lattice in  $\mathbb{C}$ ) then the well known addition in the domain is, under the special parametrization, the same as the geometric addition on the cubic. The simplest instance is when the cubic is the graph of a cubic polynomial without

---

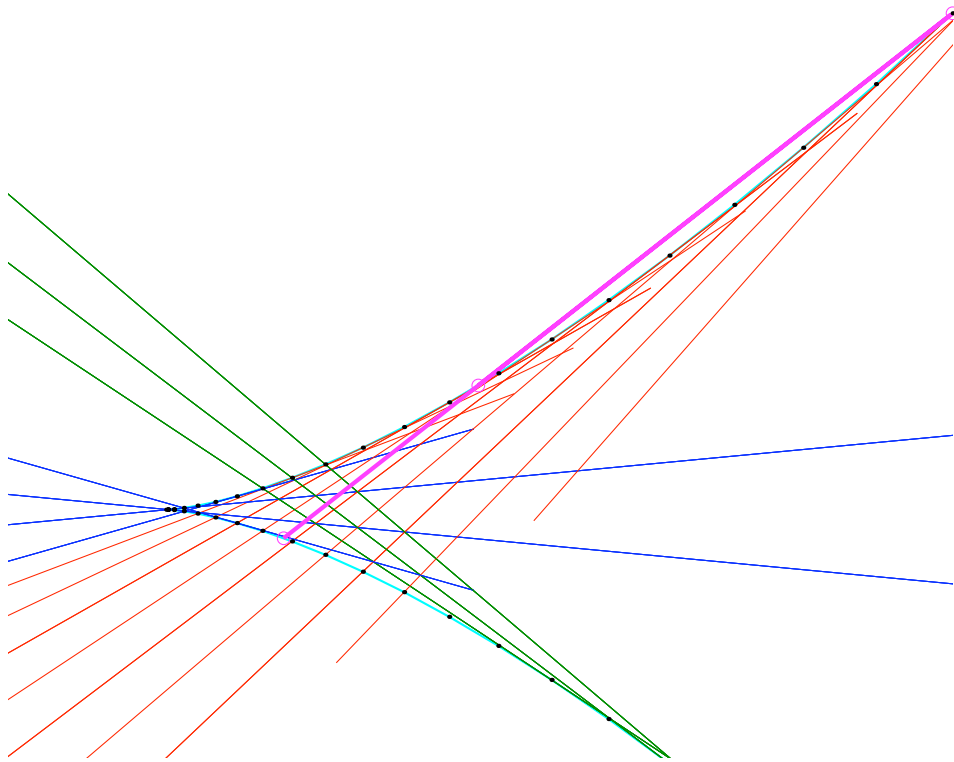
\* This file is from the 3D-XplorMath project. Please see:

quadratic term:  $y = x^3 + mz + c$ . Then, if we have two points  $(x_1, y_1), (x_2, y_2)$  on this cubic and join them by a line, this line intersects the graph in a third point  $(x_3, y_3)$  such that  $x_1 + x_2 + x_3 = 0$ . This gives a geometric definition of addition on this cubic graph.



Addition on a polynomial cubic graph without quadratic term. Every line intersects so that  $x_1 + x_2 + x_3 = 0$ . Note discrete subgroup.

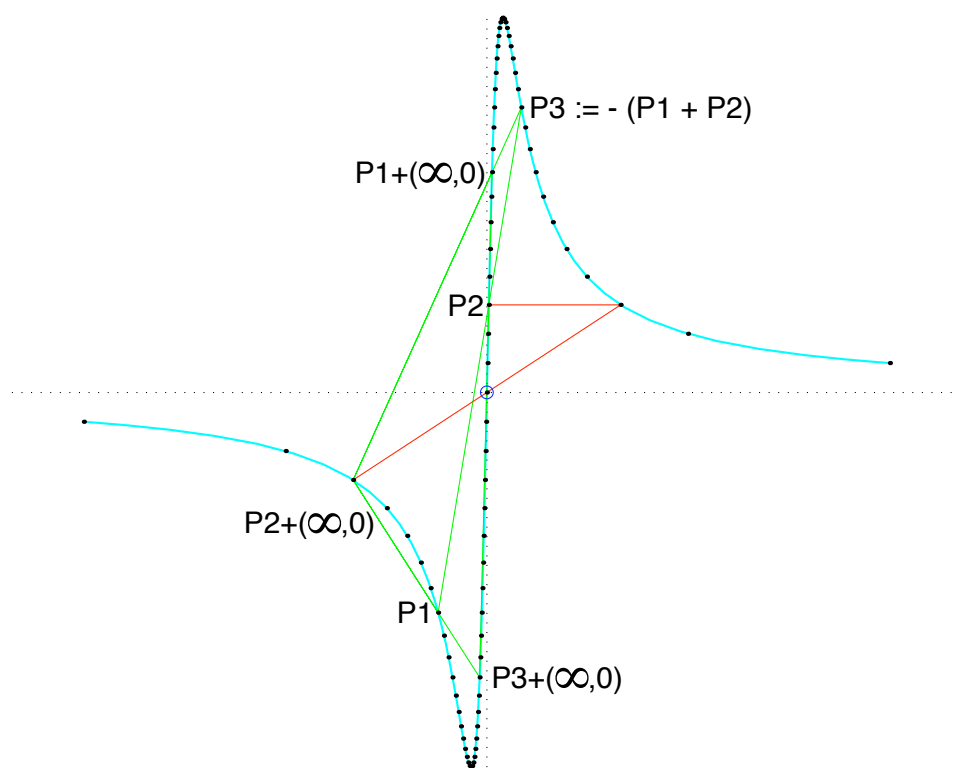
Similarly, let us map  $\mathbb{C}$  bijectively onto the Cuspidal Cubic by  $z \mapsto (z^2, z^3)$ . In this case, if we have  $z_1 + z_2 + z_3 = 0$ , then the tangents at the three points  $(z_j^2, z_j^3)$  are concurrent—we have seen this as a property of the Parabola, because the Cuspidal Cubic is the evolute of the Parabola. One can also see the previous colinearity as reflecting addition, because the three points  $(z_j^2, z_j^3), j = 1, 2, 3$ , of this cubic lie on a line if  $1/z_1 + 1/z_2 + 1/z_3 = 0$ .



Addition on the cuspidal cubic  $z \mapsto (z^2, z^3)$ . Note the discrete subgroup. If  $z_1 + z_2 + z_3 = 0$ , then the tangents at these three points are concurrent. If  $1/z_1 + 1/z_2 + 1/z_3 = 0$ , then these three points lie on a straight line.

The next case is the group  $\mathbb{C}/2\pi\mathbb{Z}$ . The trigonometric functions identify points in  $\mathbb{C} \bmod 2\pi$ . We map this group to a cubic curve by  $x := \tan(z/2)$ ,  $y := \sin(z)$ , so that  $y = 2x/(x^2 + 1)$  and this cubic is again a graph. The addition theorems  $\tan(z + w) = (\tan(z) + \tan(w))/(1 - \tan(z)\tan(w))$  and  $\sin(z+w) = \sin(z)\cos(w) + \cos(z)\sin(w)$  with  $\cos(z) = 1 - 2\sin(z/2)^2 = 1 - \sin(z) \cdot \tan(z/2)$  again give an addition on this cubic graph: it is a geometric addition because the three points  $(x_j, y_j)$  lie on one line iff  $z_1 + z_2 + z_3 = 0$ . The name “geometric addition” is even more justified because the third point  $(x_3, y_3)$  can be constructed

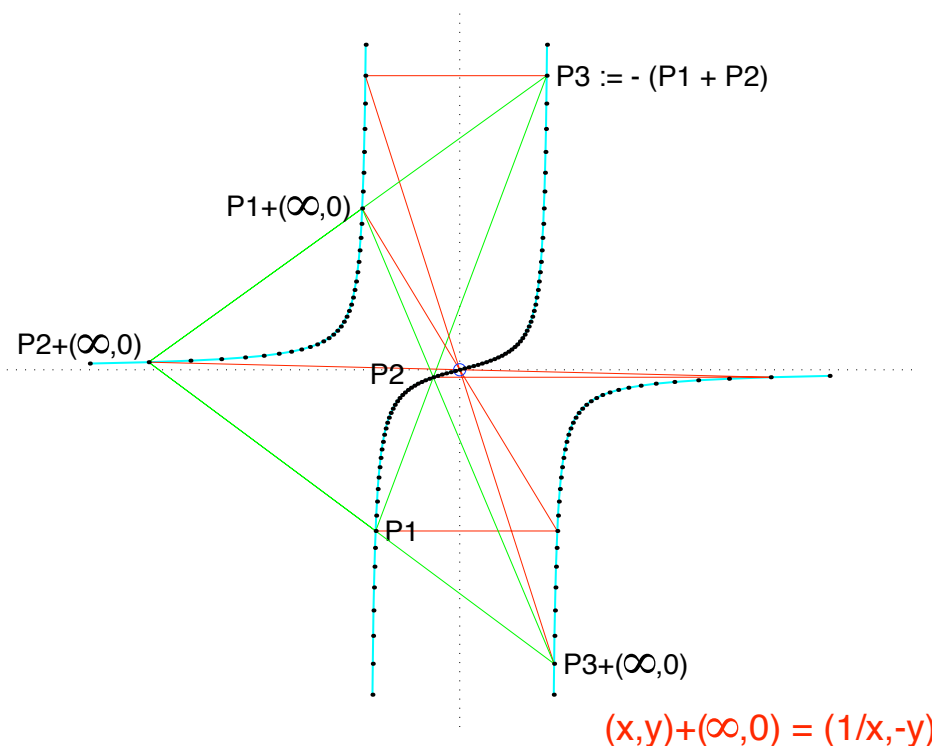
with ruler and compass from the other two. In fact, for repeated additions a ruler suffices: As a preparation we have to add to all points in sight the 2-division point  $(\infty, 0) = (\tan(\pi/2), \sin(\pi))$  as follows:  $(x, y) \oplus (\infty, 0) = (-1/x, -y)$ . One needs ruler and unit circle for this. Then the lines through  $(x_1, y_1), (x_2, y_2)$  and  $(x_1, y_1) \oplus (\infty, 0), (x_2, y_2) \oplus (\infty, 0)$  intersect in the point  $(x_3, y_3) = -(x_1, y_1) \oplus (x_2, y_2)$ .



Addition group  $\mathbb{S}^1$  on a cubic that is the graph of  $x \mapsto y = 2x/(x^2 + 1)$ , parametrized by  $x := \tan(z/2)$ ,  $y := \sin(z)$ . Note the finite discrete subgroup.  $(\infty, 0) = (\tan(\pi/2), \sin(\pi))$ , the point at infinity, is the only point of order 2.

So far we have seen the circle part of the cylinder group  $\mathbb{C}/2\pi\mathbb{Z}$ . To see a generator of the cylinder we replace  $t, x, y$  by  $it, ix, iy$ , then we obtain  $x := \tanh(z/2)$ ,  $y := \sinh(z)$ ,

so that  $y = 2x/(1 - x^2)$ . The component of the graph through 0 is a subgroup isomorphic to  $\mathbb{R}$ . It represents one generator of the cylinder. The other two components represent the opposite generator with one point missing: the 2-division point opposite 0 is the point  $(\infty, 0)$  on this cubic. This allows the same ruler construction of addition as before, except for a sign change in  $(x, y) \oplus (\infty, 0) = (+1/x, -y)$  (because  $1/i = -i$ ).



Addition group  $\mathbb{R} \cup \mathbb{R}$  on a cubic that is the graph of  $x \mapsto y = 2x/(1 - x^2)$  and is parametrized by  $x := \tanh(z/2)$ ,  $y := \sinh(z)$ .  $(\infty, 0)$  is the only point of finite order. Note the infinite discrete subgroup with one finite subgroup of order 2.

Finally we come to the group  $\mathbb{C}/\Gamma$ . The parametrizing functions of the previous example,  $\tan(z/2)$ ,  $\sin(z)$ , must

be replaced by  $\Gamma$ -invariant, “doubly periodic” functions, also called elliptic functions. The simplest of these are those of degree two, as maps from the torus  $T^2 := \mathbb{C}/\Gamma$  to the Riemann sphere  $\mathbb{S}^2 = \mathbb{C} \cup \{\infty\}$ . Two facts are important:

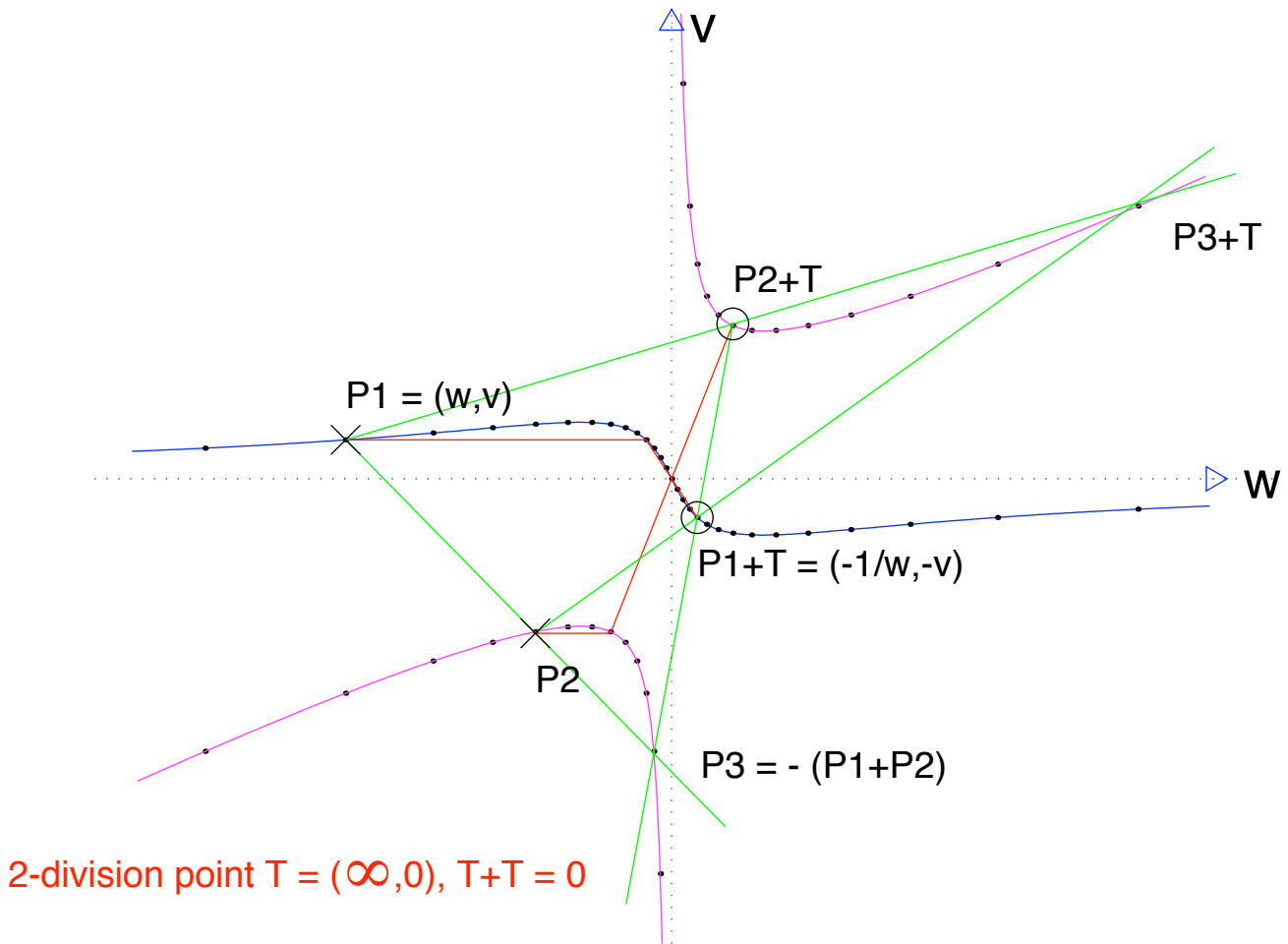
- (i) Pairs of such functions satisfy cubic equations such as  $(w^2 + 1)v = \text{const} \cdot (v^2 - 1)w$ . The solution set of any cubic equation is called a cubic curve.
- (ii) There are addition formulas, analogous to those for  $\sin$  and  $\cos$ .

They determine the pair  $(v(z_1 + z_2), w(z_1 + z_2))$  from the pairs  $(v(z_1), w(z_1))$  and  $(v(z_2), w(z_2))$ .

It turns out that these addition formulas are again “geometric” as in the previous cases, namely, the three pairs  $(v(z_1), w(z_1))$ ,  $(v(z_2), w(z_2))$ ,  $(-v(z_1 + z_2), -w(z_1 + z_2))$  lie on a line. Therefore we can again define addition on the cubic geometrically:

*Join the points to be added by a line and take the third point of intersection with the cubic as the negative of the sum.*

The addition formulas are simple enough so that the geometric addition is again a “ruler and compass construction”. The compass is only needed to add 2-division points as in the previous case, all further additions can be done by intersecting lines only.



(Notice the discrete subgroup)

Addition on a general cubic:

$$(w_1, v_1) \ominus (w_2, v_2) = \left( \frac{w_1 + w_2}{1 - w_1 w_2} \cdot \frac{v_1 - v_2}{v_1 + v_2}, \frac{1 + w_1 w_2}{1 - w_1 w_2} \cdot \frac{v_1 - v_2}{1 - v_1 v_2} \right)$$

---

The elliptic functions  $v, w$ , parametrizing the above cubic curve have numerous properties that can be used to define them. For example, they are numerically accessible, since they are solutions of the following system of differential

equations (compare  $\tan' / \tan = 1/\cot + \cot$ ):

$$\frac{v'}{v} = w'(0) \left( \frac{1}{w} - w \right),$$

$$\frac{w'}{w} = v'(0) \left( \frac{1}{v} + v \right),$$

with  $v'(0)/w'(0) = -2$  for the above cubic. These imply functional equations for  $v, w$  so that more similarities with the trigonometric case, like  $(\sin')^2 = 1 - \sin^2$ , become apparent:

$$\begin{aligned} \left( \frac{v'}{v} \right)^2 &= w'(0)^2 \left( \frac{1}{w} - w \right)^2 \\ &= w'(0)^2 \left( \left( \frac{1}{w} + w \right)^2 - 4 \right) \\ &= v'(0)^2 \left( \left( \frac{1}{v} - v \right)^2 \right) - 4w'(0)^2, \end{aligned}$$

and hence: 
$$(v')^2 = v'(0)^2 \left( (1 - v^2)^2 - 4 \frac{w'(0)^2}{v'(0)^2} \cdot v^2 \right).$$

Every differential equation

$$(f')^2 = F(f) \text{ implies } 2f'' = F'(f).$$

The first order equation determines  $f'$  only up to sign while the second order equation determines  $f''$  uniquely, in particular for trigonometric and elliptic functions.

H.K.

[Go To Planar TOC](#)

## Folium of Descartes \*

This is a famous curve with a long history (see e.g. <http://www-history.mcs.st-andrews.ac.uk/Curves/Curves.html>). The curve is the solution set of the equation

$$x^3 + y^3 = 3axy.$$

One can see that the solutions for different  $a$  differ only by scaling, namely divide the equation by  $a^3$  and replace  $x/a$ ,  $y/a$  by  $x, y$ .

The two most frequently given parametrizations are:

$$x(t) = \frac{3t}{1+t^3}, \quad y(t) = \frac{3t^2}{1+t^3},$$
$$r(\varphi) = \frac{\sin 2\varphi}{\sin^3 \varphi + \cos^3 \varphi}, \quad -\pi/4 < \varphi < 3\pi/4.$$

The first parametrization has the disadvantage that at  $t = -1$  the denominator vanishes, the curve jumps “from minus infinity to plus infinity”, while the important double point at  $0 \in \mathbb{R}^2$  is left out (or given by  $t = \infty$ ). This can be remedied by the transformation  $u = 1/(1+t)$ ,  $t =$

---

\* This file is from the 3D-XplorMath project. Please see:

$-1 + 1/u$ , which changes the parametrization to

$$x(u) = \frac{u^2 - u^3}{1 - 3u + 3u^2}, \quad y(u) = \frac{u - 2u^2 + u^3}{1 - 3u + 3u^2},$$
$$-\infty < u < \infty.$$

H.K.

[Go To Planar TOC](#)

## About Implicit Curves in the Plane \*

### Compare Implicit Surfaces in Space

There are three principal methods for describing curves in the plane:

a) As parametrized curves  $c(t) = (x(t), y(t))$  with  $x, y : (t_0, t_1) \mapsto \mathbb{R}$ . For example the unit circle can be given as

$$x(t) = R \cdot \cos(t), \quad y(t) = R \cdot \sin(t), \quad t \in [0, 2\pi].$$

b) As the graph  $y = F(x)$  of a function  $F : [x_0, x_1] \mapsto \mathbb{R}$ . For example the upper unit semi-circle can be given as the graph of the function  $F(x) = \sqrt{1 - x^2}$  for  $x \in (-1, +1)$ .

c) Implicitly as a level set  $\{f = c\}$  of a function  $f : \mathbb{R}^2 \mapsto \mathbb{R}$ . For example the unit circle is the level  $\{f = 1\}$  of the function  $f(x, y) = x^2 + y^2$ .

### Implicit Curves in 3DXM:

Cassini Ovals  $f(x, y) = ((x - aa)^2 + y^2)((x + aa)^2 + y^2) - bb^4$

Tacnodal Quartic  $f(x, y) = y^3 + y^2 - x^4$

Teissier singular Sextic  $f(x, y) = (y^2 - x^3)^2 - x^5 \cdot y$

Userdefined Implicit Curves: *available*

Parametrized Curves with Level Functions:

Cuspidal Cubic  $f(x, y) = 27aa \cdot y^2 - 4(x + bb)x^2$

Nodal Cubic  $f(x, y) = y^2 - (1 - x)x^2$

Clearly, method b) can easily be written as a special case of methods a) or c) by using for a) the “graph parametriza-

---

\* This file is from the 3D-XplorMath project. Please see:

tion”  $x(t) = t$ ,  $y(t) = F(t)$ , and by using for  $c$ ) the trivial level function  $f(x, y) = y - F(x)$  and  $\{f = 0\}$ .

However, implicit curves  $\{f(x, y) = c\}$  really give a different and somewhat richer class of objects than are given by explicit parametrization. For example, level sets may have several components; also, one is more interested in the singularities of level sets. In differential geometry one usually assumes that parametrized curves are without singularities, while in algebraic geometry the singularities of the level sets of polynomials are a major subfield of interest. The *Tacnodal Quartic* and the *Teissier Sextic* are examples in 3DXM.

Up to release 10.6 there are only a small number of implicit curves preprogrammed into 3DXM. What actually gets drawn are the solutions of the equation  $f(x, y) = ff$  with  $x_{min} \leq x \leq x_{max}$ ,  $y_{min} \leq y \leq y_{max}$  (where these limits can be set in the *Settings Menu*, dialog entry *Set t,u,v,ranges...* and, as always,  $ff$  can be set in the dialog entry *Set Parameters, Modify Object*.

Note that user-defined implicit curves can be entered.

The default morphs of the implicit curves vary the parameter  $ff$ , so that, what one sees is a family of level curves of  $f$ . It may be helpful to think of the function  $f(x, y)$  as giving the “height above sea-level” at the point  $(x, y)$ , in which case the levels  $\{f(x, y) = ff\}$  are just the level lines one is used to from topographic maps. If one chooses from the *Animation Menu* the entry *Color Morph*, the program will draw such a topographic map with each level line a

different color.

Some parametrized curves are provided with level functions. For these the *Animation Menu* has the entry *Morph Level Lines*. In the Cassini case this morph looks better with morphing parameter  $bb = ff^{1/4}$ .

Note that, while a parametrized curve depends on parameters only if the author chooses to embed it in some family, implicit curves always come naturally as 1-parameter family of curves. These families have been used to study singularities of curves via limits of nonsingular curves.

## Tangents, Normals and Curvature

The gradient of the (height) function  $f$  is a vectorfield along and normal to the level lines. Therefore we have, even without parametrizing the curve, normals and tangents:

$$n = \frac{\text{grad } f}{|\text{grad } f|}, \quad t = (-n_y, n_x).$$

Assuming we had a parametrized curve with unit normal and tangent fields  $n, t$  then the formula  $\dot{n}(s) = \kappa(s) \cdot \dot{c}(s)$  holds whether or not  $s$  is arc length parameter. This implies for our vector fields

$$\kappa = \langle \nabla_t n, t \rangle = \text{hesse } f(t, t) / |\text{grad } f|.$$

There is an Action Menu entry **Osculating Circles At Mouse Point**. It shows several level curves and the osculating circle to the level curve at the mouse point.

R.S.P.

[Go To Planar TOC](#)

## Cassinian Ovals \*

Level function in 3DXM:

$$f(x, y) := ((x - aa)^2 + y^2) \cdot ((x + aa)^2 + y^2) - bb^4$$

The default *Color Morph* varies  $bb = ff^{1/4}$  instead of  $ff$ .

The Cassinian Ovals (or Ovals of Cassini) were first studied in 1680 by Giovanni Domenico Cassini (1625–1712, aka Jean-Dominique Cassini) as a model for the orbit of the Sun around the Earth.

A Cassinian Oval is a plane curve that is the locus of all points  $P$  such that the *product of the distances* of  $P$  from two fixed points  $F_1, F_2$  has some constant value  $c$ , or  $\overline{PF_1} \overline{PF_2} = c$ . Note the analogy with the definition of an ellipse (where product is replaced by sum). As with the ellipse, the two points  $F_1$  and  $F_2$  are called *foci* of the oval. If the origin of our coordinates is the midpoint of the two foci and the  $x$ -axis the line joining them, then the foci will have the coordinates  $(a, 0)$  and  $(-a, 0)$ . Following convention,  $b := \sqrt{c}$ . Then the condition for a point  $P = (x, y)$  to lie on the oval becomes:  $((x - a)^2 + y^2)^{1/2} ((x + a)^2 + y^2)^{1/2} = b^2$ . Squaring both sides gives the following *quartic polynomial equation* for the Cassinian Oval:

$$((x - a)^2 + y^2)((x + a)^2 + y^2) = b^4.$$

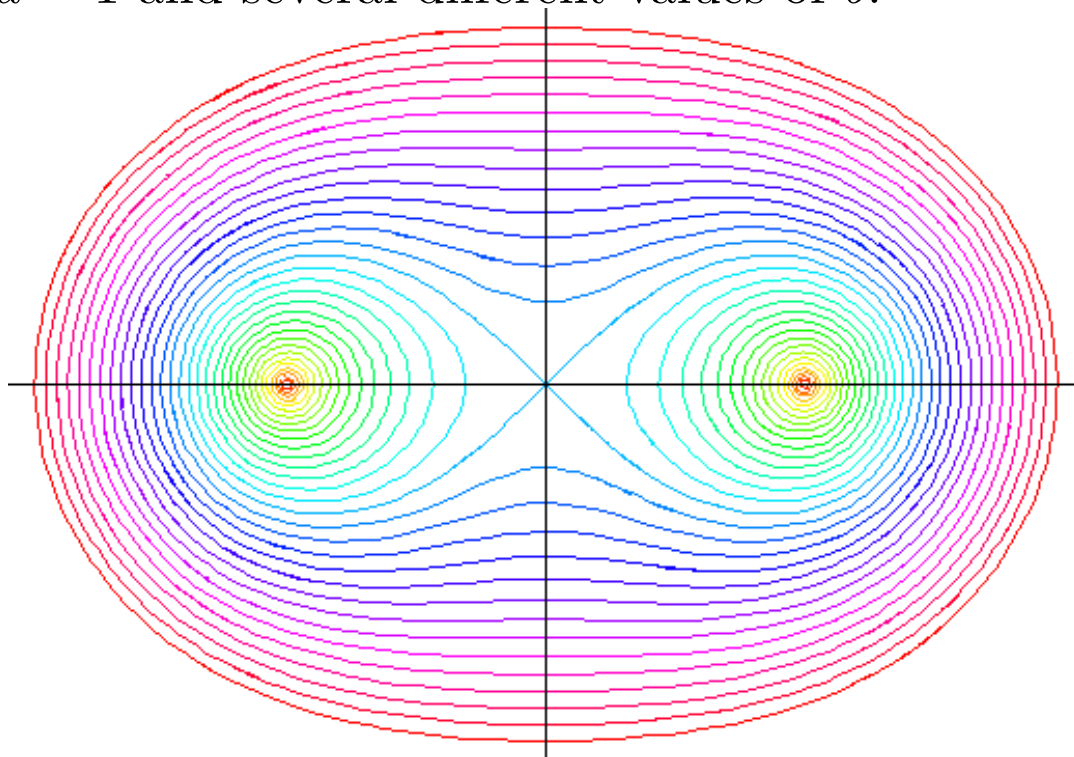
When  $b$  is less than half the distance  $2a$  between the foci, i.e.,  $b/a < 1$ , there are two branches of the curve. When

---

\* This file is from the 3D-XplorMath project. Please see:

$a = b$ , the curve has the shape of a figure eight and is known as the *Lemniscate of Bernoulli*.

The following image shows a family of Cassinian Ovals with  $a = 1$  and several different values of  $b$ .



In 3D-XplorMath, you can change the value of parameter  $b = bb$  in the Settings Menu  $\rightarrow$  SetParameters. An animation of varying values of  $b$  can be seen from the Animate Menu  $\rightarrow$  Color Morph.

Bipolar equation:  $r_1 r_2 = b^2$

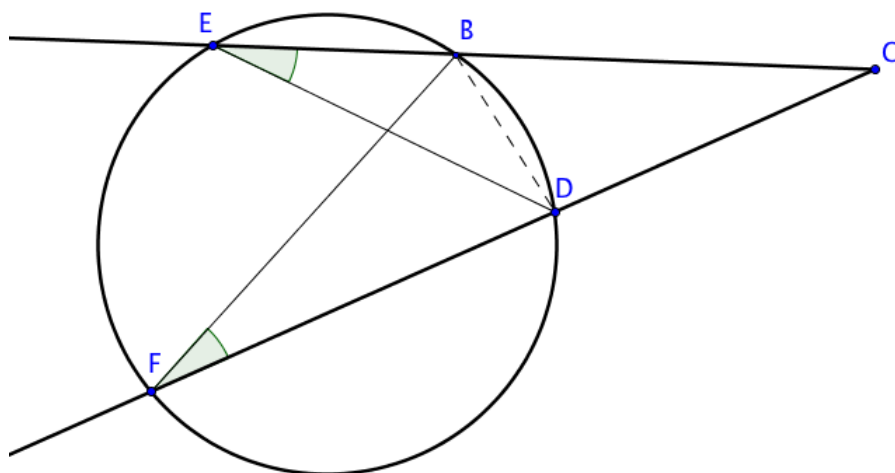
Polar equation:  $r^4 + a^4 - 2r^2 a^2 \cos(2\theta) = b^4$

A parametrization for Cassini's oval is  $r(t) \cdot (\cos(t), \sin(t))$ ,

$$r^2(t) := a^2 \cos(2t) + \sqrt{(-a^4 + b^4) + a^4(\cos(2t))^2},$$

$t \in (0, 2\pi]$ , and  $a < b$ . This parametrization only generates parts of the curve when  $a > b$ .

By default 3D-XplorMath shows how the product definition of the Cassinian ovals leads to a *ruler and circle* construction based on the following circle theorem about products of segments:



$$CD : CE = CB : CF \quad \text{-->} \quad CD * CF = CB * CE$$

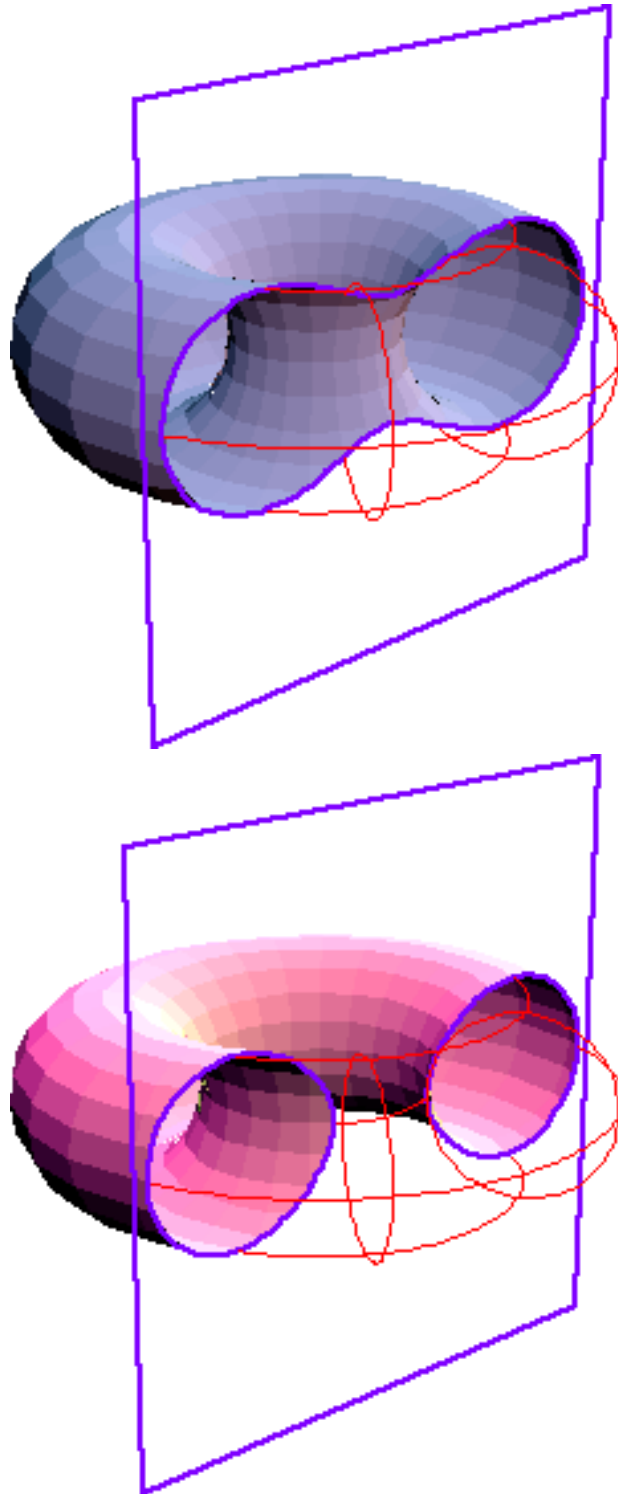
## Cassinian Ovals as sections of a Torus

Let  $c$  be the radius of the generating circle and  $d$  the distance from the center of the tube to the directrix of the torus. The intersection of a plane  $c$  distant from the torus' directrix is a Cassinian oval, with  $a = d$  and  $b^2 = \sqrt{4cd}$ , where  $a$  is half of the distance between foci, and  $b^2$  is the constant product of distances.

Cassinian ovals with a large value of  $b^2$  approach a circle, and the corresponding torus is one such that the tube radius is larger than the center to directrix, that is, a self-intersecting torus without the hole. This surface also approaches a sphere.

Note that the two tori in the figure below are not identical.

Arbitrary vertical slices of a torus are called Spiric Sections. In general they are *not* Cassinian ovals.



*Proof:* Start with the equation of a torus

$$(\sqrt{x^2 + y^2} - d)^2 + z^2 = c^2.$$

Insert  $y = c$ , rearrange and square again:

$$x^2 + z^2 + d^2 = 2d\sqrt{x^2 + c^2}, \quad (x^2 + z^2 + d^2)^2 = 4d^2(x^2 + c^2).$$

Now multiply the factors of the implicit equation of an Cassinian oval and rearrange

$$\begin{aligned} ((x - a)^2 + y^2) \cdot ((x + a)^2 + y^2) &= b^4, \\ (x^2 - a^2)^2 + y^4 + 2y^2(x^2 + a^2) &= b^4, \\ (x^2 + y^2)^2 + 2a^2(y^2 - x^2) &= b^4 - a^4. \end{aligned}$$

These two equations match because of  $a = d$ ,  $b^2 = 2dc$ , after rotation of the  $y$ -axis into the  $z$ -axis.

Curves that are the locus of points the product of whose distances from  $n$  points is constant are discussed on pages 60–63 of Visual Complex Analysis by Tristan Needham.

XL.

[Go To Planar TOC](#)

## User Defined Plane Curves in 3DXM \*

Selection of one of these entries will open a dialog to enter the data the user wishes. Default examples are provided.

*User Cartesian:* enter  $x(t) := \dots$ ,  $y(t) := \dots$

*User Polar:* enter  $r(t) := \dots$ ,  $\varphi(t) := \dots$

The curve is  $(r(t) \cos(\varphi(t)), r(t) \sin(\varphi(t)))$ .

*User Graph:* enter  $y(t) := \dots$ , implied is  $x(t) := t$ . The curve  $(t, y(t))$  is the Graph of the function  $y$ . Three approximations are shown: *Taylor, Interpolation, Fourier*.

These are the explicitly parametrized user curves. The standard decorations are available: Parallel Curves, Generalized Cycloids, Osculating Circles, Family of Normals and their Envelope, Caustics from Rotated Normals.

*User Implicit:* enter level function  $F(x, y) := \dots$

See the separate text: *Implicit Planar Curves* above, available also from the Documentation Menu (after selection of user defined implicit curve).

*User Curvature:* enter the curvature function  $\kappa(s) := \dots$

The program assumes that the parameter  $s$  is arc length. See also the text below: *User Curves By Curvature*, again available from the Documentation Menu of 3DXM.

H.K.

---

\* This file is from the 3D-XplorMath project. Please see:

## User Defined by Curvature \*

A planar curve (parametrized by arc length) can be reconstructed from its curvature function  $t \mapsto \kappa(t)$  as follows:

- (1) take the antiderivative of  $\kappa$ ,  $\alpha(t) := \int^t \kappa(\sigma) d\sigma$ ,
- (2) choose an initial point  $p$ , an initial tangent vector  $\dot{c}(0)$  and an orthonormal basis  $e_1 = \dot{c}(0)$ ,  $e_2$ ,

so the definition of curvature (namely  $\kappa := |\ddot{c}|$ , plus a sign convention) implies that,

- (3)  $\dot{c}(t) = e_1 \cdot \cos \alpha(t) + e_2 \cdot \sin \alpha(t)$ .

Then one more integration,

- (4)  $c(t) = p + \int_0^t \dot{c}(\sigma) d\sigma$ ,

determines the curve. This description explains why the curvature is also called the “rotation speed” of the tangent vector field  $\dot{c}(t)$ .

In 3D-XplorMath one can select *User Curvature*. A dialog box opens and one can enter the desired curvature function. The initial point  $p$  is taken as the origin and the initial tangent is taken as the unit vector in the positive  $x$ -direction.

The parameter  $gg$  in this case defines a “precision divisor”, that can be between 1 and 30. The size of the

---

\* This file is from the 3D-XplorMath project. Please see:

subintervals used in approximating the above integrals is  $\delta := (tMax - tMin)/(tResolution - 1)$  if  $gg = 1$ , and in general it is  $\delta/gg$ . If the curvature function  $\kappa$  becomes very large somewhere, and in particular if it is infinite at an endpoint of the interval  $[tMin, tMax]$ , it is a good idea to use a fairly large value of  $gg$  to counteract the resulting numerical inaccuracies that will occur in the evaluation of the integrals.

Note that 3D-XplorMath offers the same Action Menu Entries as for explicitly parametrized curves. For example try the caustics.

R.S.P.

[Go To Planar TOC](#)

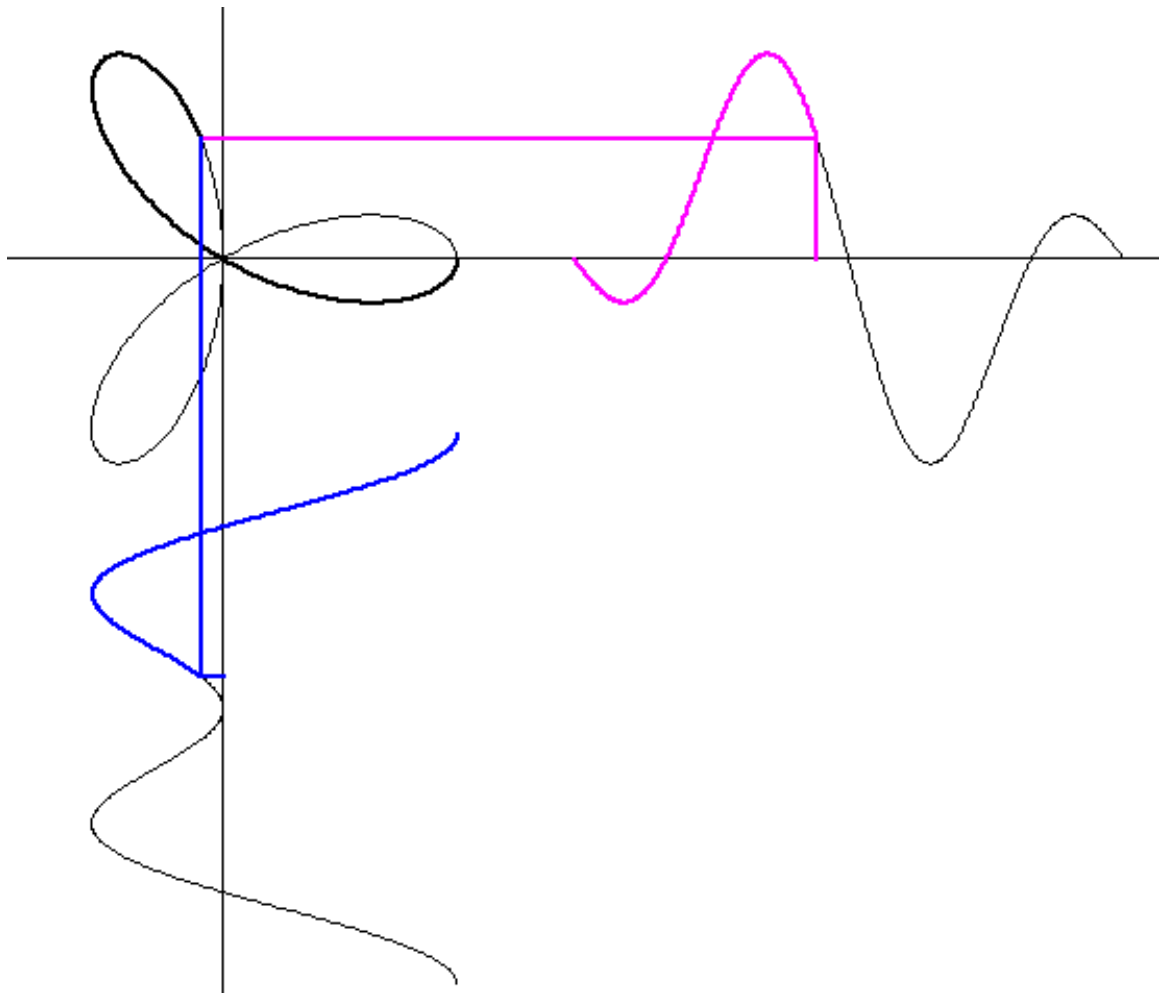
## Graphs of Functions, Graphs of Planar Curves \*

1-dimensional functions are always visualized by drawing their graphs  $\{(x, f(x))\}$ , while planar curves, although usually described as maps:  $t \in [t_0, t_1] \mapsto c(t) \in \mathbb{R}^2$ , are nevertheless visualized by their image, the set of their values:  $\{c(t) \in \mathbb{R}^2; t \in [t_0, t_1]\}$ . The graph allows to see, for each argument  $x$ , the value  $f(x)$ ; the image shows no connection between the points of the curve and the arguments  $t \in [t_0, t_1]$ . This leads to difficulties if one wants to visualize the connection between a curve and “its” component functions, because the image of a curve does not show traces of the map that was used to draw it. Therefore, strictly speaking, the image of a curve does not have “its” component functions. We need to have some specific parametrization  $t \mapsto c(t)$  of the curve in mind before we can speak of “the” component functions of the curve, or better of its representing map  $t \mapsto c(t)$ .

In 3D-XplorMath many planar curves have an Action Menu entry: **Project Curve to x-y-Axes**. The resulting demo shows the curve and the graphs of the component functions of the curve that the program uses for drawing the image of the curve. A moving point on the curve and corresponding moving points on the graphs are shown. The moving point on the curve demonstrates the parametrization that is employed by the program.

---

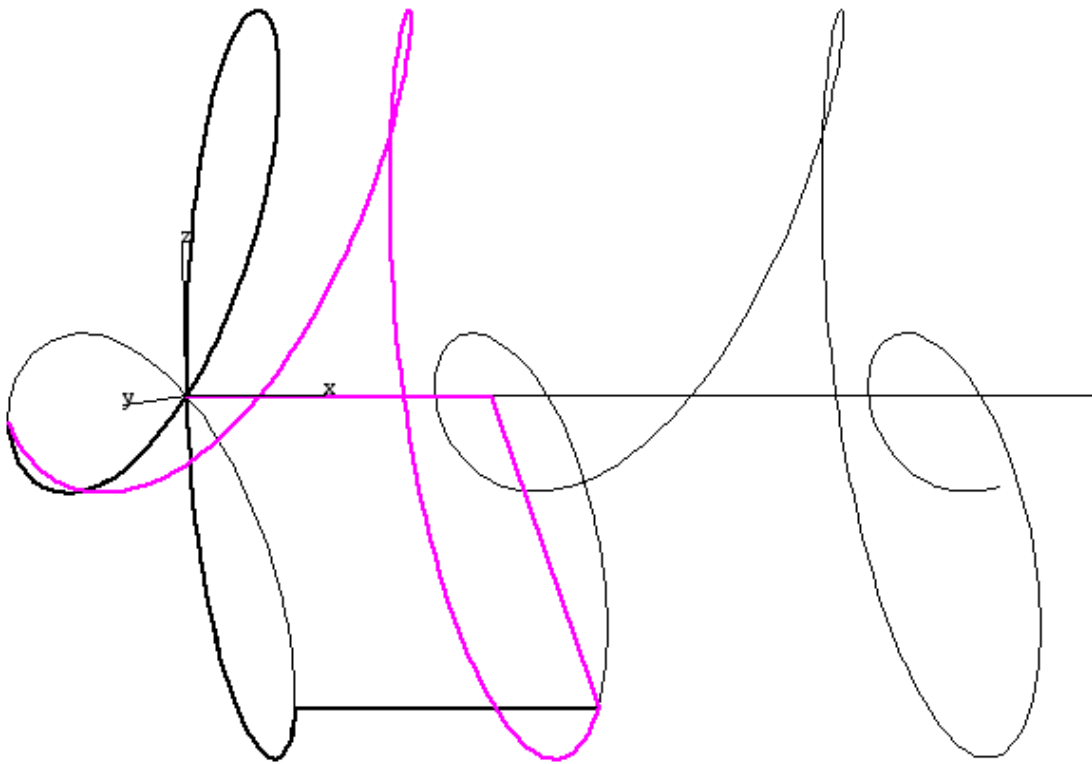
\* This file is from the 3D-XplorMath project. Please see:



Epicycloid with graphs of component functions.

We have enough dimensions to also show the graph of a parametrized planar curve,  $\{(t, c(t)); t \in [t_0, t_1]\} \subset \mathbb{R}^3$ . This is not used much, except for world lines in Relativity Theory. However, the graphs of the component functions of the curve are just orthogonal projections of the graph of the curve! So, after getting used to the unusual sight of the graph of a curve, see in **3D-XplorMath** the Action Menu entry **Show Planar Curve as Graph**, such a demo may help to bridge the gap between the graph representation of 1-dim functions and the image representation of higher dimensional maps. Actually, in  $\mathbb{R}^3$

there are only two more cases for which the dimensions fit, the frequently used graphs of real valued “height” functions  $h$  from  $\mathbb{R}^2$ :  $\{(x, y, h(x, y)); (x, y) \in \mathbb{R}^2, h(x, y) \in \mathbb{R}\}$  (think of “mountains”) and the mentioned graphs of planar curves:  $\{(t, c(t)) \in \mathbb{R}^3; t \in [t_0, t_1]\}$ , which are curves in  $\mathbb{R}^3$  that frequently look like deformed helices.



Epicycloid in y-z-plane and its graph in  $\mathbb{R}^3$ .

This image is easier to interpret when the point of the curve moves and when the visualization is in stereo.

H.K.

[Go To Planar TOC](#)

# Space Curves

[Go To Page 1](#)

## **Explicitly Parametrized Curves** (Click the Names)

[The Helix](#)

[Torus Knots](#)

[Genus Two Knots](#)

[Cinquefoil Knot](#)

[Trefoil Knot](#)

[Figure 8 -, Square - and Granny Knots](#)

[Morph Through Prime Knots  \$3\_1, 4\_1, 5\_2, 6\_1, 7\_2\$](#)

[Lissajous Curves, e.g. Prime Knot  \$7\_4\$](#)

[V. Jones' Braid List of all Knots up to 10 Crossings](#)

## **Implicitly Defined Curves**

[Intersection of Two Cylinders](#)

[Userdefined Implicit Space Curves](#)

## **Spherical Curves**

[About Spherical Curves](#)

[Loxodromes \(Constant Angle with Meridians\)](#)

[Viviani Curve \(Intersect Sphere and Cylinder\)](#)

[Spherical Cycloids](#)

[Spherical Lemniscates](#)

[Spherical Ellipses](#)

## **Curves Defined By ODEs**

[Space Curves of Constant Curvature On Cylinders](#)

[Space Curves of Constant Curvature on Tori](#)

[Continue TOC next page](#)

Closed Space Curves of Constant Curvature

Autoevolutes

Closed Space Curves of Constant Torsion

From Angular Velocity to Rigid Motion

Solid Body Motion: Euler's Polhode

Userdefined by Curvature and Torsion

Other Userdefined Parametrized Space Curves

Space Curve TOC

## The Helix \*

The helix is the simplest nonplanar space curve. It can be translated along itself by a group of isometries (called *screw motions*) and therefore has its geometric invariants – the curvature and the torsion – constant.

Our (circular) helix as a parametrized curve  $c$  is given (with defaults  $aa = bb = 1.5$ ,  $cc = 0.25$ ) as

$$c(t) = (aa \cos(t), bb \sin(t), cc(t - tmin) - 3).$$

In the default Morph we extend the helix like pulling a bed spring and therefore want to keep its length constant. To do this we compute  $f := (aa^2 + cc^2)^{-1/2}$  and show the reparametrized curve  $c(f \cdot t)$ .

Before we do the morph we select from the Action Menu **Show As Tube**. These tubes are either made with the 'Frenet Frame' or with a 'Parallel Frame'. The tube behaves like an elastic rod if we choose in the Action Menu **Parallel Frame**. The default morph now shows (at the right end, the left is kept fixed) that the tube also twists around itself while it is extended. When this occurs with electrical wires or water hoses that are pulled sideways from their coil, it is a well known and annoying phenomenon.  
H.K.

---

\* This file is from the 3D-XplorMath project. Please see:

## Torus Knots \*

Torus knots are quite popular space curves because they represent the simplest way to write down knotted curves in  $\mathbb{R}^3$ . Our knots are parametrized as

$$c(t) := \begin{pmatrix} aa + bb \cdot \cos(dd \cdot t) \cdot \cos(ee \cdot t) \\ aa + bb \cdot \cos(dd \cdot t) \cdot \sin(ee \cdot t) \\ cc \cdot \sin(dd \cdot t) \end{pmatrix}$$

with defaults  $aa = 3$ ,  $bb = 1.5$ ,  $cc = 1.5$ ,  $dd = 5$ ,  $ee = 2$ .

The default **Morph** changes the torus size. If, before the morph, one chooses in the Action Menu **Show As Tube** and **Parallel Frame** then one notices that the twisting of the tube (see the ATO of the helix for more details) is clearly visible already for rather small changes of the shape of the torus.

The Action Menu has also the entry **Show Dotted Torus**. Selecting it adds the torus to the picture. This is more spectacular when viewing in **Anaglyph Stereo Vision**, through red/green filter glasses. Observe that our brain gets these several thousand dots sorted out into corresponding pairs of red and green dots that then form the torus surface in  $\mathbb{R}^3$  - and this seems to happen instantly.

---

\* This file is from the 3D-XplorMath project. Please see:

The best method to get a feeling for the curvature of a space curve is to select in the Action Menu **Show Osculating Circles & Evolute**. The Radius  $r$  of the circle is the *radius of curvature* of the curve at the current point and  $\kappa := 1/r$  is called the *curvature* (at that point). The direction from  $c(t)$  to the midpoint of the osculating circle determines always the direction of the second basis vector of the Frenet frame.

If one uses the Parallel Frame, then one has to represent the curvature by a vector of length  $\kappa$  in the plane spanned by the two normal vectors of the Parallel frame. If one has selected, in the Action Menu, **Parallel Frame** and clicks **Show Repère Mobile** then this curvature vector is drawn, together with its past history, in each normal plane. – The last entry in the Action Menu, **Show Frenet Integration** does the opposite: if the curvature vector function is given in the initial normal plane then the demo reconstructs the curve by integrating the Frenet equation.

H.K.

[Space Curve TOC](#)

## Genus Two Knots \*

**Torus Knots**, see the previous entry, are the most easily described knots and, in particular when viewed on a torus, they are also very easy to visualize.

If one wants to visualize other knots on some surface, one needs more complicated surfaces than tori. From this point of view the next simplest knots can be put on a genus 2 surface. The surface we chose looks like two tori which are joined by a small handle. (The size of these tori is controlled by the parameters *aa* and *bb* as for torus knots.) The surface is implicitly described by an equation (see implicit surfaces in the surface category) and can be made fatter by increasing *ff*. As examples of genus 2 knots we chose the connected sums of two (*dd*, *ee*) - torus knots. The sign of *hh* controls whether the two torus knots are connected with reflectional symmetry or with 180° rotational symmetry. The two simplest examples are the *Square Knot* and the *Granny Knot* where two (3, 2) - torus knots (=Trefoil Knots) are connected with the two types of symmetry, see **Figure 8 - , Square - and Granny Knots**.

The sum of the two torus knots is first constructed outside the surface, then projected onto the surface and finally smoothed with a length minimizing algorithm. The result is good enough for tubes made with a Parallel frame, but the tube from the Frenet frame is not smooth. – H.K.

---

\* This file is from the 3D-XplorMath project. Please see:

## Cinquefoil Knot \*

Parametric Formulas for the Cinquefoil Knot:

$$P.x := (2 - \cos(2 t / (2 aa + 1))) \cdot \cos(t);$$

$$P.y := (2 - \cos(2 t / (2 aa + 1))) \cdot \sin(t);$$

$$P.z := -\sin(2 t / (2 aa + 1));$$

The choice  $aa = 1$  gives a Trefoil knot,  $aa = 2$  the Cinquefoil, and in general  $aa = k$  gives the  $(2k+1)$ -foil knot (the program rounds  $aa$  before using it). The parameter range for  $t$  should be 0 to  $(4k+2)\pi$ . If you change  $aa$  in the Set Parameters... dialog, then these values of  $tMin$  and  $tMax$  are set also, but you can change them later in the Set  $t,u,v$  Ranges... dialog.

A nice animation of the Cinquefoil knot can be obtained by first choosing **Show As Tube** from the Action menu, **Anaglyph Stereo Vision** from the View menu, and then **Rotate** from the Animation menu.

R.S.P.

---

\* This file is from the 3D-XplorMath project. Please see:

## Trefoil Knot \*

Parametric formulas for the Trefoil Knot:

$$\begin{aligned}x &= 0.01 (41 \cos(t) - 18 \sin(t) - 83 \cos(2 t) - \\ & 83 \sin(2 t) - 11 \cos(3 t) + 27 \sin(3 t)) \cdot hh \\ y &= 0.01 (36 \cos(t) + 27 \sin(t) - 113 \cos(2 t) + \\ & 30 \sin(2 t) + 11 \cos(3 t) - 27 \sin(3 t)) \cdot hh \\ z &= 0.01 (45 \sin(t) - 30 \cos(2 t) + 113 \sin(2 t) - \\ & 11 \cos(3 t) + 27 \sin(3 t)) \cdot hh\end{aligned}$$

The Trefoil knot, [Figure 8 -](#), [Square -](#) and [Granny Knots](#) displayed by 3D-XplorMath are all harmonic or Fourier knots. That is they are parametrized using finite Fourier series for all three coordinates. The particular parametrizations are taken from the 1995 PhD thesis of Aaron Trautwein at The University of Iowa.

Compare the rotation of the Frenet frame along this trefoil knot (defined with harmonic polynomials) and along the trefoil that results when you select **Torus Knot** with the parameters ( $dd=3$ ,  $ee=2$ ): Near the points on the torus knot where the curvature is very small, the rotation speed of the Frenet frame is large. - The Trefoil Knot can be shown with a Satellite Knot, default  $dd = 55$ ,  $ee = 2$ .

In stereo mode a Möbius band bounded by the Trefoil Knot is added. Their handedness depends on the sign of  $hh$ . R.S.P.

---

\* This file is from the 3D-XplorMath project. Please see:

## Figure 8 Knot, Granny Knot, Square Knot \*

The Trefoil knot, Figure 8 Knot, Granny Knot, Square Knot, displayed by 3D-XplorMath are all harmonic or Fourier knots. That is they are parametrized using finite Fourier series for all three coordinates. The particular parametrizations are taken from the 1995 PhD thesis of Aaron Trautwein at The University of Iowa.

Satellite Knots can be added in the Action Menu to these four knots.

The Figure 8 Knot is an alternating prime knot with minimal crossing number 4. It is the next simplest knot after the Trefoil Knot (see [Morph Through Prime Knots 3<sub>1</sub>, 4<sub>1</sub>, 5<sub>2</sub>, 6<sub>1</sub> 7<sub>2</sub>](#) ).

Parametric formulas for the Figure 8 Knot:

$$x = (32 \cos(t) - 51 \sin(t) - 104 \cos(2t) - 34 \sin(2t) + 104 \cos(3t) - 91 \sin(3t)) / 100$$

$$y = (94 \cos(t) + 41 \sin(t) + 113 \cos(2t) - 68 \cos(3t) - 124 \sin(3t)) / 140$$

$$z = (16 \sin(t) - 138 \cos(2t) - 39 \sin(2t) - 99 \cos(3t) - 21 \sin(3t)) / 70$$

The Granny Knot and the Square Knot are not prime, both are sums of two Trefoil Knots. The Square Knot has

---

\* This file is from the 3D-XplorMath project. Please see:

a mirror symmetry so that one Trefoil is left handed the other right handed. The Granny Knot is the sum of two same-handed Trefoil Knots.

Parametric formulas for the Granny Knot:

$$\begin{aligned}x &= (-22 \cos(t) - 128 \sin(t) - 44 \cos(3t) - 78 \sin(3t))/80 \\y &= (-10 \cos(2t) - 27 \sin(2t) + 38 \cos(4t) + 46 \sin(4t))/80 \\z &= (70 \cos(3t) - 40 \sin(3t))/100\end{aligned}$$

Parametric formulas for the Square Knot:

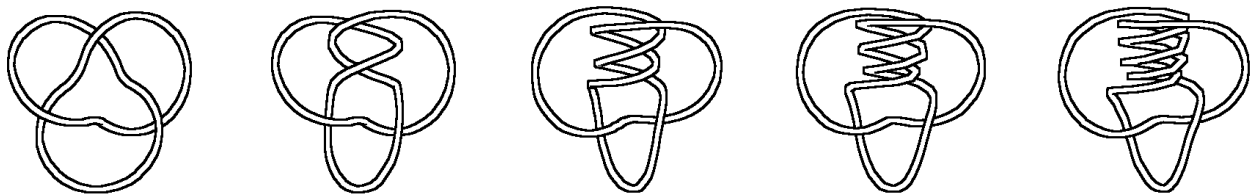
$$\begin{aligned}x &= (-22 \cos(t) - 128 \sin(t) - 44 \cos(3t) - 78 \sin(3t))/100 \\y &= (11 \cos(t) - 43 \sin(3t) + 34 \cos(5t) - 39 \sin(5t))/100 \\z &= (70 \cos(3t) - 40 \sin(3t) + 18 \cos(5t) - 9 \sin(5t))/100\end{aligned}$$

R.S.P.

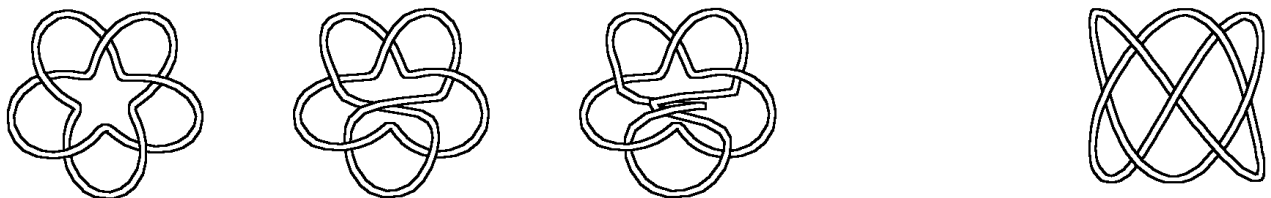
Space Curve TOC

## Morph Through Five Prime Knots \*

A prime knot is a knot that cannot be written as the knot sum of smaller knots. For example, the Square Knot and the Granny Knot are not prime since each is a sum of two Trefoil Knots. There are 14 prime knots with at most 7 minimal number of crossings. They have been hand drawn so often that they have assumed an esthetically defined standard shape. Of these first 14 prime knots the following ones are in a morphing family, the prime knots  $3_1, 4_1, 5_2, 6_1, 7_2$ . Choose  $dd = 3$  and  $0 \leq ff \leq 4.3$  in Set Morphing and the program will deform the Trefoil Knot through the following images:



If one chooses  $dd = 5$  and  $0 \leq ff \leq 2.3$  in Set Morphing then the program will deform the (5,2)-Torus Knot through the following images of the prime knots  $5_1, 6_2, 7_5$



The prime knot  $7_4$  is the default Lissajous space curve.

There are 249 prime knots with at most 10 minimal num-

---

\* This file is from the 3D-XplorMath project. Please see:

ber of crossings. One can visualize those via the Space Curves Menu entry: **V.Jones Braid List**.

The notion of prime knot is important because Horst Schubert proved that the decomposition of a knot as knot sum (= connected sum) of prime knots is unique. The knot invariants are a good way to check whether a given knot is a prime knot.

There is an easy sufficient criterion that guarantees that the knot under consideration cannot be drawn with fewer crossings. First we define *alternating* and *reduced alternating* knots: if the thread of the knot passes alternatingly through overcrossings and undercrossings then the knot is called **alternating**. For example, if we twist a circle into a figure 8 we obtain an alternating trivial knot. In this case we observe an easily recognizable property of the crossing in the knot diagram: if the crossing is removed the knot diagram decomposes into two components. A crossing with this property is called an *isthmus*. Clearly, one can rotate one component of the knot diagram through 180 degrees, i.e. untwist and thereby remove the isthmus to obtain a representation with fewer crossings. An alternating knot without an isthmus is called a *reduced alternating knot*.

*Theorem* : Reduced alternating knots cannot be represented with fewer crossings, they are always non-trivial.

All prime knots with at most 7 crossings are reduced alternating knots.

H.K.

Space Curve TOC

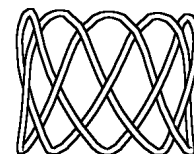
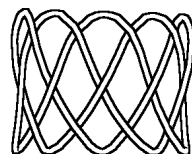
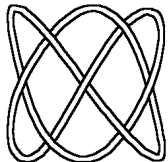
## Lissajous Curves, e.g. the Prime Knot $7_4$ \*

Lissajous curves are a popular family of planar curves, resp. space curves. They are complicated enough to be interesting, but regular enough to be esthetically pleasing. They are described by simple formulas:

$$\begin{aligned}x(t) &:= aa \cdot \sin(2\pi \cdot dd \cdot t) \\y(t) &:= bb \cdot \sin(2\pi \cdot ee \cdot t + gg) \\z(t) &:= aa \cdot \sin(2\pi \cdot ff \cdot t + cc)\end{aligned}$$

In 3DXM the parameters  $dd, ee, ff$  are rounded to integers so that the curves are closed on the interval  $[0, 1]$ . The default morph varies the phase  $gg$  from 0 to  $\pi/2$ . – The Lissajous curves are also physically interesting, they describe the joint motion of orthogonal uncoupled oscillators  $(x(t), y(t), z(t))$  with different frequencies.

A **prime knot** is not a knot sum of smaller knots. E.g. Square Knot and Granny Knot are not prime: each is a sum of two Trefoil Knots. There are 14 prime knots with the minimal number of crossings  $\leq 7$ , see the documentation **About This Object** for **V.Jones Braid List**. The 4th 7-crossings-knot, the prime knot  $7_4$ , is our default Lissajous space curve,  $(dd, ee, ff, gg) = (2, 3, 7, \pi/2)$ . – Other alternating examples are:  $(dd, ee, ff) = (2, 5, 13), (4, 3, 23)$ :



---

\* This file is from the 3D-XplorMath project. Please see:

There are 249 prime knots with at most 10 minimal number of crossings. One can visualize those via the Space Curves Menu entry: **V.Jones Braid List**.

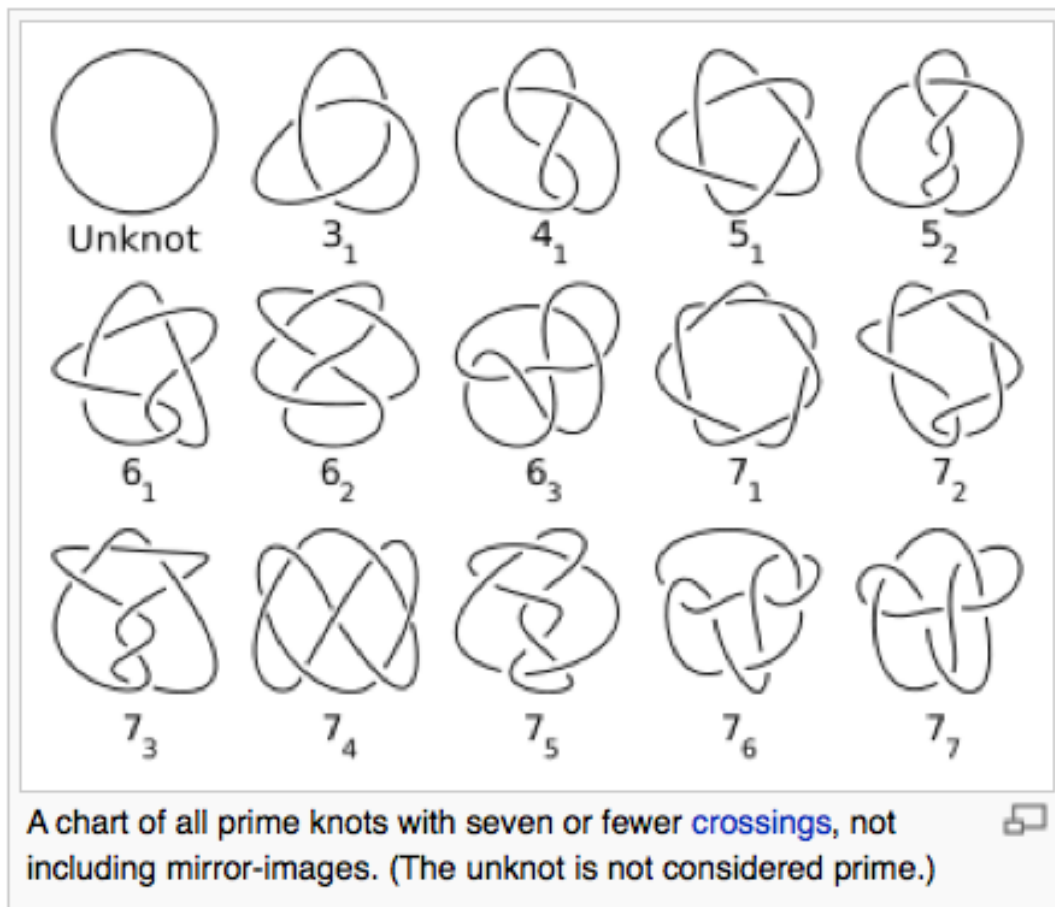
The notion of prime knot is important because Horst Schubert proved that the decomposition of a knot as knot sum (= connected sum) of prime knots is unique. The knot invariants are a good way to check whether a given knot is a prime knot. There is no more elementary criterion to recognize a knot as prime.

There is an easy sufficient criterion that guarantees that the knot under consideration cannot be drawn with fewer crossings. First we define *alternating* and *reduced alternating* knots: if the thread of the knot passes alternately through overcrossings and undercrossings then the knot is called **alternating**. For example, if we twist a circle into a figure 8 we obtain an alternating trivial knot. In this case we observe an easily recognizable property of the crossing in the knot diagram: if the crossing is removed the knot diagram decomposes into two components. A crossing with this property is called an *isthmus*. Clearly, one can always rotate one component of the knot diagram through 180 degrees, untwist and thereby remove the isthmus to obtain a representation with one less crossings. An alternating knot without an isthmus is called a *reduced alternating knot*.

*Theorem* : Reduced alternating knots cannot be represented with fewer crossings, they are always non-trivial.

## Braid List Of Prime Knots \*

A prime knot is a knot that cannot be written as the knot sum of smaller knots. For example, the Square Knot and the Granny Knot are not prime since each is a sum of two Trefoil Knots. There are 249 prime knots with at most 10 minimal number of crossings. In 3DXM we use the braid representation of knots. Vaughn Jones gave this list to one of us in the 80s. The usual hand drawn versions are prettier than the braids:



Copied from the article 'Prime Knot' in Wikipedia.

---

\* This file is from the 3D-XplorMath project. Please see:

The above first 14 prime knots are all so called *alternating knots*: if one follows the thread of the knot then one passes – alternatingly(!) – overcrossings and undercrossings. A knot that is represented as a “reduced” alternating knot cannot be drawn with fewer crossings, in particular: a reduced alternating knot is always non-trivial. If one twists a circle to a figure 8 then one obtains a non-reduced alternating knot that is clearly trivial. Similarly, one can take the alternating **Granny Knot** in 3DXM and turn one of the Trefoil parts 180 degrees around the horizontal axis. One obtains an alternating knot with an additional crossing in the middle. Again, this knot is not reduced because by cutting out the new crossing the knot diagram decomposes into two components. Such an easily recognizable crossing is called an *isthmus*. One can always untwist an isthmus and obtain a knot with one less crossing. A knot diagram without an isthmus is called *reduced*.

The notion of prime knot is important because Horst Schubert proved that the decomposition of a knot as knot sum (= connected sum) of prime knots is unique.

All torus knots are prime knots. The genus 2 knots in 3DXM are sums of two torus knots.

The space curve ”Morph Prime Knots 5 4 3” has a default morph that runs through the prime knots 3.1, 4.1, 5.2, 6.1, 7.2. If one changes dd from 3 to 5 then the ff-morph runs through 5.1, 6.2, 7.5. The prime knot 7.4 is shown as a Lissajous knot.

## The Intersection of Two Cylinders \*

The image shows the space curve defined implicitly as the intersection of the two cylinders:

$$y^2 + z^2 = ff$$

and

$$(\cos(aa)x + \sin(aa)y)^2 + (z - cc)^2 = gg.$$

These two cylinders are made visible by displaying a random set of dots on each of them. In the Action Menu one can choose to put more random dots on the boundary of the intersection of the two solid cylinders.

In the default settings the two cylinders touch and the default morph rotates one of them by changing  $aa$ .

We find it interesting to change the radius of the smaller cylinder while the cylinders keep touching: morph  $gg$  up to  $ff$  while keeping  $dd = 0$ , since we compute (behind the user)

$$cc = \sqrt{ff} - \sqrt{gg} + dd.$$

At  $gg = ff$  the intersection curve degenerates into two ellipses (for each  $aa$ ).

The distance between the tangent planes of the two cylinders (at their common normal) is  $dd$ .

H.K.

---

\* This file is from the 3D-XplorMath project. Please see:

## Userdefined Implicit Space Curves \*

The exhibit shows the intersection curve of two surfaces, given by equations  $F1(x, y, z) = ff$ ,  $F2(x, y, z) = gg$ .

To see also the surfaces (as dotted point clouds) choose the corresponding entry in the Action Menu.

The initial dialogue offers three different defaults for the surfaces given by  $F1$ ,  $F2$ :

- 1.) A conic and a plane with the default morph tilting the plane.
- 2.) The graph of a function  $\mathbb{R}^3 \mapsto \mathbb{R}$  and a cylinder. This exhibit can be used to explain extrema under side conditions.
- 3.) A torus and a tangent plane. This is an example where the intersection has double point singularities at those points where the intersection of the surfaces is not transversal.

By varying these defaults one can create a rich collection of space curves. (The number of points in the point clouds cannot be changed in this exhibit.)

Note that the surfaces are only computed inside a sphere of radius ORB around the origin. This parameter can be set in the first entry of the Settings Menu.

H.K.

---

\* This file is from the 3D-XplorMath project. Please see:

## About Spherical Curves \*

In many ways there is a close analogy between planar Euclidean geometry and two-dimensional spherical geometry. In the ATO for [Spherical Ellipses](#) we translate the sum-of-distances definition from the plane to the sphere and use the same arguments as in the plane to construct points and tangents of the curve. Similarly, in the ATOs about [Spherical Cycloids](#), we roll spherical circles along spherical circles. See also [Spherical Lemniscates](#). Such analogies of course require basic notions which correspond to each other.

### Lines and Triangles

Straight lines in the plane are the shortest connections between their points. On the sphere the shortest connections are great circle arcs that are not longer than half way around. A line cuts the plane into two congruent half-planes that are interchanged by the reflection in the line. Similarly, the sphere is cut by the plane of a great circle into two congruent half-spheres, and the reflection in the plane interchanges these two half-spheres. Therefore we speak of the reflection (of the sphere) in a great circle. These analogies are enough to translate the planar notion *straight line* to the spherical notion *great circle*. Three points  $A, B, C$  and three shortest connections of lengths

---

\* This file is from the 3D-XplorMath project. Please see:

$a, b, c$  make a triangle — in the plane or on the sphere. The angles at the points (or vertices) are denoted  $\alpha, \beta, \gamma$ . For the plane, the basic triangle formulas are close to the definition of sine and cosine:

Projection theorem:  $c = a \cdot \cos \beta + b \cdot \cos \alpha$

Sine theorem:  $b \cdot \sin \alpha = h_c = a \cdot \sin \beta$

Cosine theorem:  $c^2 = a^2 + b^2 - 2ab \cos \gamma$

Note that the more complicated third formula follows from the first two: Use the Sine theorem in the form  $0 = b \cdot \sin \alpha - a \cdot \sin \beta$  and add the square of this to the square of the Projection theorem. Simplify with  $\cos^2 + \sin^2 = 1$  and use the trigonometric identity  $\cos \alpha \cos \beta - \sin \alpha \sin \beta = \cos(\alpha + \beta) = \cos(\pi - \gamma) = -\cos(\gamma)$  to obtain the Cosine theorem.

To derive similar formulas for spherical triangles, use geographic coordinates on the standard unit sphere, with the polar center at the north pole  $C := (0, 0, 1)$ . A point  $A$  at spherical distance  $b$  from  $C$  satisfies  $\langle A, C \rangle = \cos b$ . Thus, after rotation into the x-z-plane, it has coordinates  $A := (\sin b, 0, \cos b)$ . A third point  $B$  at distance  $a$  from the pole  $C$  and such that the angle  $\angle ACB$  equals  $\gamma$  has spherical polar coordinates  $B := (\sin a \cos \gamma, \sin a \sin \gamma, \cos a)$ . The spherical cosine formula follows by taking a scalar product:

$$\langle A, B \rangle = \cos c = \cos a \cos b + \sin a \sin b \cos \gamma.$$

The name is justified since a Taylor approximation up to second order gives the corresponding formula for the plane.

*For more details: note that the graph of the function  $x \rightarrow \cos x$  lies above the graph of the quadratic function  $x \rightarrow 1 - x^2/2$  and not above any wider parabola  $x \rightarrow 1 - x^2/(2 + \epsilon)$ . Therefore  $1 - x^2/2$  is called the quadratic Taylor approximation of  $\cos$  near  $x = 0$ . We substitute this approximation for  $x = a, x = b, x = c$ , and similarly  $\sin x \approx x$ , in the spherical cosine formula and obtain:*

*$\cos c \approx 1 - c^2/2 \approx (1 - a^2/2)(1 - b^2/2) + ab \cos \gamma$ , or  $c^2 \approx a^2 + b^2 - 2ab \cos \gamma$ , which is the planar formula.*

For a more systematic derivation we use the reflection  $R$  which interchanges  $C, A$  and observe that  $R(B)$  has the coordinates  $R(B) := (\sin c \cos \alpha, \sin c \sin \alpha, \cos c)$ . But  $R(B)$  can also be computed from the reflection matrix and the coordinates of  $B$ . Equating the two expressions gives three formulas between  $a, b, \gamma$  on one side and  $c, \alpha$  on the other side. Of course these formulas hold for any permutation of  $A, B, C$ :

$$\begin{pmatrix} -\cos b & 0 & \sin b \\ 0 & 1 & 0 \\ \sin b & 0 & \cos b \end{pmatrix} \cdot \begin{pmatrix} \sin a \cos \gamma \\ \sin a \sin \gamma \\ \cos a \end{pmatrix} = \begin{pmatrix} -\sin a \cos b \cos \gamma + \cos a \sin b \\ \sin a \sin \gamma \\ \cos a \cos b + \sin a \sin b \cos \gamma \end{pmatrix} = \begin{pmatrix} \sin c \cos \alpha \\ \sin c \sin \alpha \\ \cos c \end{pmatrix}.$$

We use for these formulas the same names as in the planar

case since an even simpler Taylor approximation simplifies also the first two equations to their planar counterparts:

**Projection theorem:**  $\sin c \cos \alpha =$   
 $- \sin a \cos b \cos \gamma + \cos a \sin b$

**Sine theorem:**  $\sin c \cdot \sin \alpha = \sin a \cdot \sin \gamma$

**Cosine thm:**  $\cos c = \cos a \cos b + \sin a \sin b \cos \gamma.$

A consequence of the first two theorems is the

**Angle cosine:**  $\cos \gamma = - \cos \alpha \cos \beta + \sin \alpha \sin \beta \cos c.$

Application: [Go To Platonics](#)

Two-dimensional spherical geometry captures certain aspects of three-dimensional Euclidean geometry. For example, if we project an *icosahedron* from its center to its circumsphere then the 20 triangular faces of the icosahedron are mapped to a tessellation of  $\mathbb{S}^2$  by 20 equilateral triangles *whose angles are  $72^\circ$  because five triangles meet at every vertex.* From the angle cosine theorem we read off the edge-length  $\sigma$  of these triangles, with  $\alpha = 2\pi/5$  we have for the

Icosahedron:  $(\cos \alpha + \cos^2 \alpha) / \sin^2 \alpha = \cos \sigma.$

Given the above spherical tools this is a conceptually very simple construction.

### Osculating Circles

At every point of a twice differentiable curve  $c$  on  $\mathbb{S}^2$  one can determine its osculating circle: the parametrized circle that agrees with  $c$  up to the second derivative at that

point. While it is easy to place a ruler next to a curve so that the ruler approximates a tangent line, one cannot so easily guess these best approximating circles. For all planar curves and space curves in 3DXM one can choose Osculating Circles from the Action Menu and one can believe that the resulting images show best approximating circles. In the case of spherical curves one observes that these osculating circles actually lie on the sphere. To understand this, consider the usual osculating circle in  $\mathbb{R}^3$  and intersect its plane, the *osculating plane* of the curve  $c$ , with  $\mathbb{S}^2$ ; this intersection circle is clearly a better approximation of the curve than any other circle in this plane and therefore it is the osculating circle. Although we cannot yet describe the *curvature* of a curve by a real valued function, we can already agree that, at each point, a space curve is curved as strongly as its osculating circle. We call the spherical radii of these circles the spherical curvature radii and we are ready to translate geometric constructions (with curves) from the plane to the sphere.

*Parallel curves* of a spherical curve  $c$  on  $\mathbb{S}^2$ . We define  $\eta(t) := \dot{c}(t) \times c(t) / |\dot{c}(t)|$  as the oriented spherical unit normal of  $c$ . The parallel curve at spherical distance  $\epsilon$  is then in complete analogy with the plane given as

$$\text{Parallel Curves on } \mathbb{S}^2 : c_\epsilon(t) := \cos \epsilon \cdot c(t) + \sin \epsilon \cdot \eta(t).$$

It is easy to check that the curvature radii of  $c_\epsilon$  are obtained by adding  $\epsilon$  to the curvature radii of  $c$  — which is what our intuition expects of parallel curves.

*Spherical Evolvents* (also called involutes). For a physical realization of an evolvent attach a string segment to the curve and move the end point so that the string is always tangent to the curve, in the forward or in the backward direction. The Euclidean formula for the backwards evolvent is (assuming  $|\dot{c}(t)| = 1$ )

$$e(t) := c(t) - (t - t_0) \cdot \dot{c}(t), \quad t \geq t_0.$$

A remarkable property of the evolvent is that  $t - t_0$  is its curvature radius at  $e(t)$ .

We translate this construction to the sphere. The formula for the spherical evolvent is (assume again  $|\dot{c}(t)| = 1$ )

$$e(t) := \cos(t - t_0) \cdot c(t) - \sin(t - t_0) \cdot \dot{c}(t).$$

A short computation shows that the spherical curvature radius at  $e(t)$  is  $t - t_0$ , as in the plane. Also, it is true for the plane and for the sphere that the segment from  $c(t)$  to  $e(t)$  is orthogonal to  $\dot{c}(t)$ , i.e., this segment is the curvature radius of the evolvent at  $e(t)$ .

*Spherical Evolutes.* For any given (planar or) spherical curve  $c$  we call the curve of the (planar or) spherical midpoints of the osculating circles of  $c$  the (*planar or*) *spherical evolute* of  $c$ . In 3DXM this can best be seen in the demo for *Spherical Ellipses*. In the previous paragraph we have seen that, in the plane and on the sphere, the evolvent of the evolute of  $c$  is this given curve  $c$ . Thus, the natural translations of notions from the plane to the sphere continue to have natural properties.

## What is Curvature?

More precisely, what real number should measure the size

of the curvature at one point of the curve  $c$ , and which real valued function should describe the curvatures of  $c$ ? For the plane, differential geometers have agreed to take the rotation speed of a unit normal of  $c$  as the quantitative size of its curvature. For example, the rotation speed of the unit normal  $n$  of a circle of radius  $r$  (use arc length parametrization) is  $1/r$ , since  $c(t) = r \cdot (\cos(t/r), \sin(t/r))$ ,  $|\dot{c}(t)| = 1$  and  $n(t) = (\cos(t/r), \sin(t/r))$ , hence  $\dot{n}(t) = (1/r) \cdot \dot{c}(t)$ . Although this is a good reason for taking  $1/r$  as the curvature of a circle of radius  $r$  in the plane, the argument does not carry over to  $\mathbb{S}^2$ , since: *What is the spherical rotation speed of the spherical normal?* Of course we could also call on the sphere  $1/\text{curvature radius}$  the curvature of the curve. This is not a good idea on  $\mathbb{S}^2$  since circles of radius  $\pi/2$  are great circles, i.e., shortest connections, and we would expect them to have curvature 0. Fortunately, there is for the plane another good reason for taking  $1/r$  as “the” curvature, and this time the corresponding computation can be repeated on  $\mathbb{S}^2$ . If we imagine a family of parallel curves then it looks as if the length grows faster if the curvature is larger.

We can make this intuition more precise with a computation. First, in the plane:

$$c_\epsilon(t) := c(t) + \epsilon \cdot n(t), \quad \{\dot{c}(t), n(t)\} \text{ orthonormal}$$

$$\dot{c}_\epsilon(t) = \dot{c}(t) + \epsilon \cdot \dot{n}(t), \quad \dot{n}(t) = \kappa(t) \cdot \dot{c}(t)$$

$$\frac{d}{d\epsilon} |\dot{c}_\epsilon(t)|_{\epsilon=0} / |\dot{c}(t)| = \kappa(t).$$

Here, the second line defines the curvature as the rotation speed of the normal and the third line says *that this curvature function can also be computed as the change of length of tangent vectors in a parallel family of curves*. Of course we can do the same computation as in line three for spherical curves:

$$\begin{aligned}
c_\epsilon(t) &:= \cos \epsilon \cdot c(t) + \sin \epsilon \cdot \eta(t) \\
\dot{c}_\epsilon(t) &= \cos \epsilon \cdot \dot{c}(t) + \sin \epsilon \cdot \dot{\eta}(t) \\
\dot{\eta}(t) &= \ddot{c}(t) \times c(t) \\
|\dot{c}_\epsilon(t)|/|\dot{c}(t)| &= \langle \dot{c}_\epsilon(t), \dot{c}(t) \rangle / \langle \dot{c}(t), \dot{c}(t) \rangle = \\
&\cos \epsilon + \sin \epsilon \langle \dot{\eta}(t), \dot{c}(t) \rangle / \langle \dot{c}(t), \dot{c}(t) \rangle \\
\frac{d}{d\epsilon} |\dot{c}_\epsilon(t)|_{\epsilon=0} / |\dot{c}(t)| &= -\langle \eta(t), \ddot{c}(t) \rangle / \langle \dot{c}(t), \dot{c}(t) \rangle.
\end{aligned}$$

Before we take this as the definition of spherical curvature for spherical curves we check which function of the radius we get for circles of spherical radius  $r$ :

$$\begin{aligned}
c_r(t) &= (\sin r \cos t, \sin r \sin t, \cos r) \\
\eta(t) &= \frac{d}{dr} c_r(t) = (\cos r \cos t, \cos r \sin t, -\sin r) \\
\ddot{c}_r(t) &= -(\sin r \cos t, \sin r \sin t, 0), \quad \text{finally:} \\
-\langle \eta(t), \ddot{c}(t) \rangle / \langle \dot{c}(t), \dot{c}(t) \rangle &= \frac{\sin r \cos r}{\sin^2 r} = \cot r.
\end{aligned}$$

This is a satisfying answer, since  $\cot r$  behaves like  $1/r$  for small  $r$  and  $\cot(r = \pi/2) = 0$  as we expect for great circles.

Now we are ready for the definition and we remark that the historical name is *geodesic curvature*, not the more naive spherical curvature which we used above.

*Definition.* The geodesic curvature  $\kappa_g(t)$  of a spherical curve  $c(t)$  with spherical unit normal  $\eta(t)$  is

$$\kappa_g(t) := -\langle \eta(t), \ddot{c}(t) \rangle / \langle \dot{c}(t), \dot{c}(t) \rangle.$$

### The Spherical Frenet Equation

Finally we observe that for a unit speed spherical curve  $c$  we have the following natural orthonormal frame along the curve:

$$(e_1(t), e_2(t), e_3(t)) := (\dot{c}(t), c(t), \eta(t)),$$

and the geodesic curvature controls the derivative of this frame via the following *spherical Frenet equation*:

$$\frac{d}{dt} \dot{c}(t) = -1 \cdot c(t) - \kappa_g(t) \cdot \eta(t)$$

$$\frac{d}{dt} c(t) = +1 \cdot \dot{c}(t)$$

$$\frac{d}{dt} \eta(t) = +\kappa_g(t) \cdot \dot{c}(t)$$

Observe that the coefficient matrix

$$\begin{pmatrix} 0 & -1 & -\kappa_g \\ 1 & 0 & 0 \\ \kappa_g & 0 & 0 \end{pmatrix}$$

is skew symmetric. This fact implies that any solution  $(e(t), f(t), g(t))$  with *orthonormal* initial conditions stays orthonormal. This says that  $t \rightarrow f(t)$  is a spherical curve parametrized by arclength (namely:  $|\dot{f}(t)| = |e(t)| = 1$ ). Moreover  $g(t)$  is orthogonal to  $f(t), \dot{f}(t)$  and therefore the spherical unit normal of  $f$ . The third Frenet equation says that the given function  $\kappa_g(t)$  (because of  $\dot{g}(t) = \kappa_g(t) \cdot e(t)$ ) is indeed the geodesic curvature of the curve  $t \rightarrow f(t)$ : to any given  $\kappa_g(t)$  we have found a curve with that geodesic curvature.

We repeat: from elementary distance and triangle geometry to the differential geometry of curves we have explained a very close analogy between the Euclidean plane and the sphere. The 3DXM demos try to emphasize this, in particular [Spherical Ellipses](#), [Spherical Cycloids](#), [Spherical Lemniscates](#).

HK.

[Space Curve TOC](#)

## Loxodrome \*

A Loxodrome (or “rhumb line”) is a route that a boat would take if it kept a constant compass heading (so that on a Mercator projection it is simply a straight line). To be more formal, a loxodrome is a path on the unit sphere  $\mathbb{S}^2 \subset \mathbb{R}^3$  that makes a constant angle with the great circles of longitude (“meridians”). Recall that a **Logarithmic Spiral** in the (complex) plane  $\mathbb{C}$  makes a constant angle with the rays through the origin. *Stereographic Projection*  $\text{St}: \mathbb{C} \mapsto \mathbb{S}^2$  unites these two facts: It maps the radial lines in  $\mathbb{C}$  to the meridians on  $\mathbb{S}^2$  and it is also angle preserving (“conformal”). The logarithmic spirals - which meet the radial lines in  $\mathbb{C}$  under constant angles - are therefore mapped by stereographic projection to the loxodromes on  $\mathbb{S}^2$  - which meet the meridians under constant angles.

On the other hand, the complex **Exponential Map**  $\exp: \mathbb{C} \mapsto \mathbb{C}$  is also conformal and it maps the lines parallel to the real axis to the radial lines in  $\mathbb{C}$  and all other straight lines to curves which meet the radial lines under constant angles, i.e. the logarithmic spirals. These are therefore parametrized as  $c(t) = \exp((1 + i \cdot aa) \cdot t + \text{const})$  and the loxodromes on the sphere are given parametrically as

$$t \mapsto \text{St}(\exp((1 + i \cdot aa) \cdot t + \text{const})).$$

1: Their osculating circles all lie on the sphere. And 2: the Mercator map from the sphere is:  $\exp^{-1} \circ \text{St}^{-1}: \mathbb{S}^2 \mapsto \mathbb{C}$ .

R.S.P.

---

\* This file is from the 3D-XplorMath project. Please see:

## The Viviani Curve \*

The Viviani curve is the intersection of a sphere of radius  $2 \cdot aa$  and a cylinder of radius  $aa$  that touch at a single point, the double point of the curve. Parametric formulas for it are:

$$z = aa (1 + \cos(t)) = aa 2 \cos(t/2)^2,$$

$$y = aa \sin(t) = aa 2 \sin(t/2) \cos(t/2), \text{ and}$$

$$x = aa 2 \sin(t/2)$$

Implicit equations for the two intersecting surfaces are:

$$x^2 + y^2 + z^2 = 4 aa^2, \quad \text{a sphere of radius } 2 aa,$$

$$(z - aa - bb)^2 + y^2 = aa^2, \quad \text{a cylinder of radius } aa.$$

The planar projections of this curve are therefore in general curves of degree 4, but because of its symmetries the Viviani curve has two orthogonal two-to-one projections that are simpler; namely curves of degree 2. Indeed projecting it to the y-z-plane we get a twice covered circle (use Settings Menu: Set Viewpoint and Up Direction 200,0,0), projecting to the x-z-plane gives a twice covered parabolic piece,  $(1 - z/(2aa)) = (x/(2aa))^2$ , while the projection to the x-y-plane is the degree 4 figure 8 with the equation (for  $aa = 1/2$ ):  $x^2 - y^2 = x^4$ .

Note that the osculating circles lie on the sphere.

R.S.P.

---

\* This file is from the 3D-XplorMath project. Please see:

## About Spherical Cycloids \*

See also the ATOs for Spherical Ellipses and for Planar Rolling Curves, e.g. Astroid, Cardioid

### Spherical Definition ( in analogy to planar case)

The spherical ellipses demonstrated already how definitions from planar Euclidean geometry can be repeated on the sphere; the demo illustrates that also spherical evolutes are analogous to the planar ones. Rolling curves, spherical cycloids, provide more such examples: simply let one spherical circle *roll* (on the inside or the outside) along another spherical circle. Here *roll* means that the arclengths (= angle at the center times sine of the spherical radius) of corresponding arcs of the two circles agree. The true rolling curves are obtained by looking at the curve traced out by one point of the rolling circle, but, just as in the plane, one may also look at the traces of other points on a fixed radius, inside or outside the rolling circle — choose *bb* different from 1 in the Settings Menu, Set Parameters Dialog.

The rolling construction is illustrated by choosing *Show Rolling Circle* in the Action Menu.

---

\* This file is from the 3D-XplorMath project. Please see:

Rolling curves have a very simple tangent construction. The point of the rolling circle which is in contact with the base curve has velocity zero – just watch cars going by. This means that the connecting segment (which is a piece of a great circle of the sphere) from this point of contact of the wheel to the endpoint of the (great circle) drawing stick is the (great circle) radius of the momentary rotation. The tangent of the curve drawn by the drawing stick is therefore orthogonal to this momentary radius. The 3DXM-demo draws the rolling curve and shows its tangents.

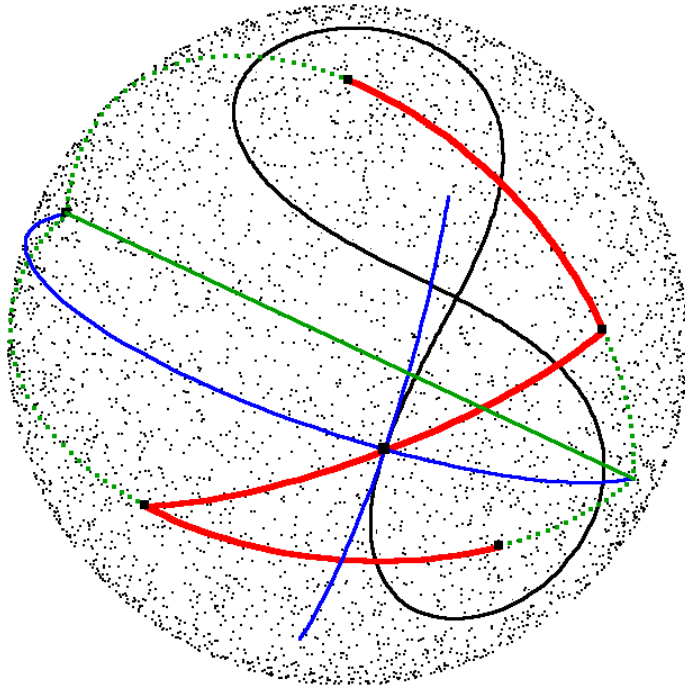
One can observe, for all spherical curves (in 3DXM: [Viviani Curve \(Intersect Sphere and Cylinder\)](#), [Loxodromes \(Constant Angle with Meridians\)](#), [Spherical Ellipses](#), [Spherical Cycloids](#), [Spherical Lemniscates](#)), that the osculating circles lie on the sphere of the spherical curve by choosing *Show Osculating Circle* in the Action Menu. To understand this, note, that the osculating circle lies in the osculating plane (Action Menu!) and, of course, no circle in a given osculating plane can be a better approximation of the curve than the intersection of this plane with the sphere on which the curve lies.

H.K.

[Space Curve TOC](#)

## About Spherical Lemniscates\*

See ATOs for [Spherical Ellipses](#), [Planar Lemniscate](#)



The spherical definition is completely analogous to the planar case. The curves are traced by a mechanical drawing mechanism. It consists of three great circle rods, two shorter ones of (spherical) length  $\rho = cc$  and a longer one of length  $\lambda = 2 \cdot dd$  (drawn red in the figure). The shorter ones have one endpoint each at ‘focal’ points  $F_1, F_2$ , around which they can rotate. The longer great circle rod connects the two shorter ones, thus creating a mechanism with one degree of freedom: If one of the short rods rotates with constant angular velocity, then the connecting long rod forces the other short rod to rotate with non-constant angular

---

\* This file is from the 3D-XplorMath project. Please see:

velocity. – The parameter  $ff \in [0, 1]$  chooses the drawing pen on the middle rod and this pen draws the curve.

This demo should be seen as another example of how constructions from Euclidean geometry can be repeated in spherical geometry. See also [About Mechanically Generated Curves](#) from the Documentation Menu of Planar Curves.

Mechanically generated curves come together with a *construction of their tangents!* Our drawing mechanism is anchored with its focal points on a fixed sphere. On this fixed sphere the drawing takes place. A second *moving sphere* (same radius and midpoint as the fixed sphere) is attached to the drawing part of the mechanical apparatus, in the present case attached to the middle rod. One can imagine that *any point of the moving sphere traces a curve on the fixed sphere!* The velocity vectors of these traced curves give a time-dependent vector field on the fixed sphere. It is a marvellous theorem that *for each fixed time  $t$  the vectors of the time-dependent field are the velocity vectors of a standard rotation of the sphere.* In other words: For each fixed time  $t$  are the integral curves of this momentary velocity field *concentric circles*, the orbits of a standard rotation. The antipodal centers of these circles are therefore called momentary centers of rotation. Any point  $c(t)$  on one of the traced curves can be connected (by a great circle) to the antipodal momentary centers of rotation (drawn blue) and the tangent of the traced curve at  $c(t)$  (also blue) is orthogonal to this momentary radius.

How can one find, for a specific drawing mechanism, these momentary centers of rotation? Consider the endpoints of the middle rod of the present mechanism. They are points of the moving sphere. Since they are also the endpoints of the two rotating rods, they can only move orthogonally to their rods. The two rotating rods are therefore always pointing to the momentary center of rotation. We can find these centers by intersecting the two great circles on which the short rods lie (drawn dotted green).

H.K.

Space Curve TOC

## About Spherical Ellipses \*

See ATO for Planar [Ellipses](#)

In 3DXPLORMATH the *Default Morph* shows a family of ellipses with fixed focal points  $F_1, F_2$  as the larger axis  $aa$  varies from its allowed minimum  $e = bb/2$  to its allowed maximum  $\pi - e = \pi - bb/2$ . Another interesting morph is  $0.11 \leq aa \leq 1.43$ ,  $0.2 \leq bb \leq \pi - 0.2$ : the distance of the focal points increases until they are almost antipodal and the major axis is only slightly longer than the distance of the focal points.

---

**ELEMENTARY DEFINITION.** Many elementary constructions from planar Euclidean geometry have natural analogues on the twodimensional sphere  $\mathbb{S}^2$ . For example, we can take the definition of planar ellipses and use it on the sphere as follows: Pick two points  $F_1, F_2 \in \mathbb{S}^2$  of spherical distance  $2e := \text{dist}(F_1, F_2) < \pi$  and **define** the set of points  $P \in \mathbb{S}^2$  for which the sum of the distances to the two points  $F_1, F_2$  equals a constant  $=: 2a$ , i.e. the set:

$$P \in \mathbb{S}^2; \text{dist}(P, F_1) + \text{dist}(P, F_2) = 2a,$$

to be a **Spherical Ellipse**.

In the Euclidean plane there is only one restriction between the parameters of an ellipse:  $2e < 2a$ . Since distances on

---

\* This file is from the 3D-XplorMath project. Please see:

$\mathbb{S}^2$  cannot be larger than  $\pi$  we have two restrictions in spherical geometry:  $2e < 2a < 2\pi - 2e$ .

For fixed focal points, i.e. for fixed  $e$ , these curves cover the sphere (we allow that the smallest and the largest ellipse degenerate to great circle segments). One observes that the ellipse with  $2a = \pi$  is a great circle and that ellipses with  $2a > \pi$  are congruent to ellipses with  $2a < \pi$  and focal points  $-F_1, -F_2$ .

This is because  $dist(P, F) = \pi - dist(P, -F)$  implies

$$\begin{aligned} \pi < 2a = dist(P, F_1) + dist(P, F_2) &\Rightarrow \\ dist(P, -F_1) + dist(P, -F_2) = 2\pi - 2a < \pi. \end{aligned}$$

Similarly, on the sphere one does not need to distinguish between ellipses and hyperbolas:

$$\begin{aligned} \{P \in \mathbb{S}^2; dist(P, F_1) + dist(P, F_2) = 2a\} = \\ \{P \in \mathbb{S}^2; dist(P, F_1) - dist(P, -F_2) = 2a - \pi\}. \end{aligned}$$

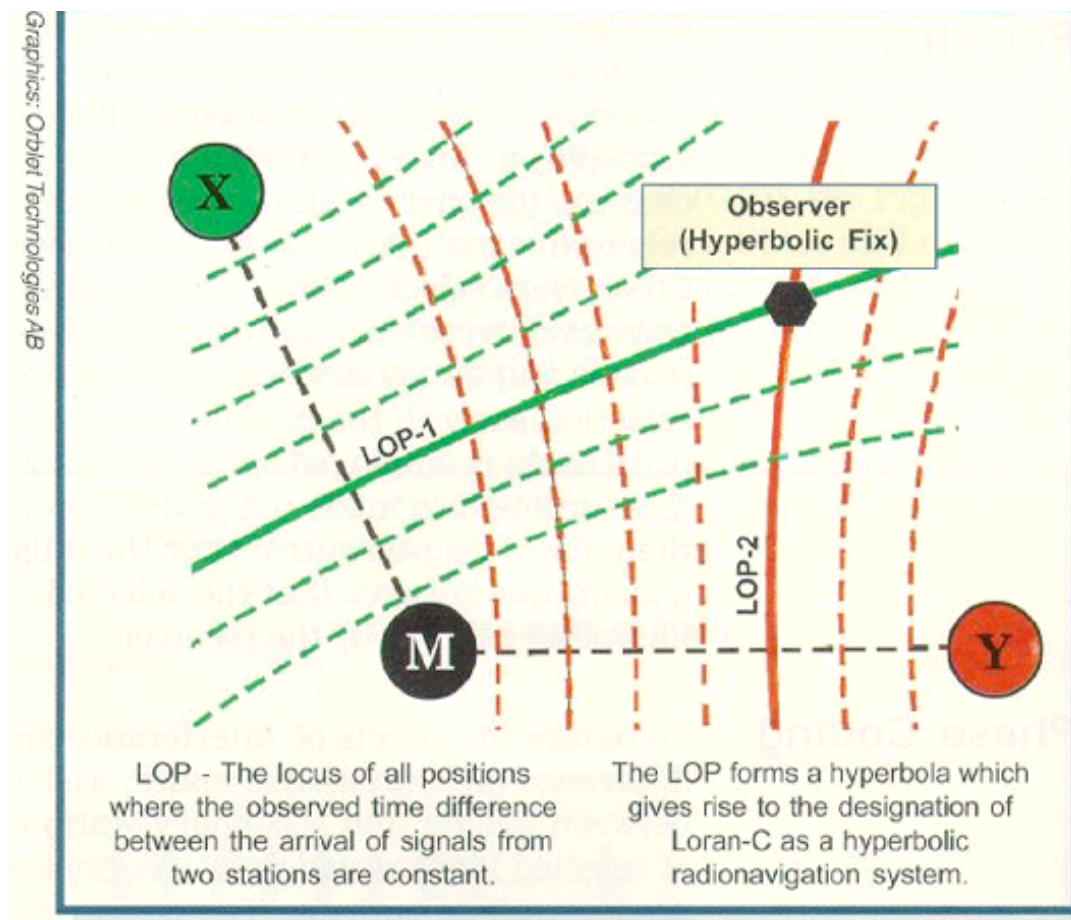
**PRACTICAL APPLICATION.** These curves are used since more than 50 years in the LORAN System to determine the position of a ship on the ocean as follows. Consider a pair of radio stations which broadcast synchronized signals. If one measures at any point  $P$  on the earth the time difference with which a pair of signals from the two stations arrives, then one knows the difference of the two distances from  $P$  to the radio stations. Therefore sea charts were prepared which show the curves of constant difference of

the distances to the two radio stations. This has to be done for several pairs of radio stations. In areas of the ocean where the families of curves (for at least two pairs of radio stations) intersect reasonably transversal it is sufficient to measure two time differences, then a look on the sea chart will show the ship's position as the intersection point of two curves, two sperical hyperbolas. On the site [http://webhome.idirect.com/...](http://webhome.idirect.com/)

~ [jproc/hyperbolic/index.html](http://webhome.idirect.com/~jproc/hyperbolic/index.html) or

~ [jproc/hyperbolic/lorc\\_hyperbola.jpg](http://webhome.idirect.com/~jproc/hyperbolic/lorc_hyperbola.jpg)

this is explained by the following map:



## ELEMENTARY CONSTRUCTION, 3DXM-DEMO

Begin by drawing a circle of radius  $2a$  around  $F_1$  (called *Leitkreis* in German). Next, for every point  $C$  on this circle we find a point  $X$  on the spherical ellipse as follows: Let  $M$  be the midpoint of the great circle segment from  $C$  to  $F_2$  and let  $T$  be the great circle through  $M$  and perpendicular to that segment. In other words,  $T$  is the symmetry line between  $C$  and  $F_2$ . Finally we intersect  $T$  with the *Leitkreis* radius from  $F_1$  to  $C$  in  $X$ . — Because we used the symmetry line  $T$  we have  $\text{dist}(X, C) = \text{dist}(X, F_2)$  and therefore:

$$\begin{aligned} \text{dist}(X, F_1) + \text{dist}(X, F_2) &= \text{dist}(X, F_1) + \text{dist}(X, C) \\ &= \text{dist}(C, F_1) = 2a. \end{aligned}$$

It is easy to prove that the great circle  $T$  is tangent to the ellipse at the point  $X$ .

## CONNECTION WITH ELLIPTIC FUNCTIONS

We met a family of ellipses all having the same focal points ('confocal') and also the orthogonal family of confocal hyperbolas in the visualization of the complex function  $z \rightarrow z + 1/z$ . In the same way two orthogonal families of confocal spherical ellipses show up in the visualization of [Elliptic Functions](#) from *rectangular tori* to the Riemann sphere (choose in the Action Menu: *Show Image on Riemann Sphere* and in the View Menu: *Anaglyph Stereo Vision*). — Note that in the plane all such families of confocal ellipses and hyperbolas are essentially the same, they differ

only in scale. On the sphere we get different families for different rectangular tori, i.e. for different quadrupels of focal points  $\{F_1, F_2, -F_1, -F_2\}$ .

## AN EQUATION FOR THE SPHERICAL ELLIPSE

Abbreviate  $\alpha := \text{dist}(X, F_1)$ ,  $\beta := \text{dist}(X, F_2)$ . The definition of a spherical ellipse says:

$$\begin{aligned} \cos(2a) &= \cos(\alpha + \beta) = \cos \alpha \cos \beta - \sin \alpha \sin \beta. \\ \text{with } \cos \alpha &= \langle X, F_1 \rangle, \quad \cos \beta = \langle X, F_2 \rangle. \end{aligned}$$

We want to write the equation in terms of the scalar products which are linear in  $X$ . Therefore we replace  $\sin^2 = 1 - \cos^2$  to get:

$$(1 - \cos^2 \alpha)(1 - \cos^2 \beta) = (\cos \alpha \cos \beta - \cos(2a))^2$$

or

$$1 - \cos^2 \alpha - \cos^2 \beta = -2 \cos(2a) \cos \alpha \cos \beta + \cos^2(2a)$$

or, by replacing the cosines by the scalar products:

$$\begin{aligned} \sin^2(2a) \langle X, X \rangle - \langle X, F_1 \rangle^2 - \langle X, F_2 \rangle^2 = \\ - 2 \cos(2a) \cdot \langle X, F_1 \rangle \cdot \langle X, F_2 \rangle. \end{aligned}$$

Observe that this is a homogenous quadratic equation in  $X = (x, y, z)$ . In other words: Our spherical ellipse is the intersection of the unit sphere with a quadratic cone whose vertex is at the midpoint of the sphere. So we get the surprisingly simple result: If one projects a spherical

ellipse from the midpoint of the sphere onto some plane then one obtains a (planar) conic section.

H.K.

Space Curve TOC

## Space Curves of Constant Curvature on Cylinders\*

These Curves are special cases of the ones described in [Space Curves of Constant Curvature on Tori](#), but the situation simplifies so much that they deserve special attention.

First we roll the plane onto a cylinder of radius  $R = 1/bb$ :

$$F : \begin{pmatrix} x \\ y \end{pmatrix} \mapsto \begin{pmatrix} x \\ R \cos(y/R) \\ R \sin(y/R) \end{pmatrix}.$$

In the plane we describe a curve by its rotation angle against the x-axis,  $\alpha(s) = \int_0^s \kappa_g(\sigma) d\sigma$ , where  $\kappa_g$  is the curvature of the plane curve, or its geodesic curvature when rolled onto the cylinder:

$$c'(s) := \begin{pmatrix} \cos(\alpha(s)) \\ \sin(\alpha(s)) \end{pmatrix}, \quad c(s) := \int_0^s c'(\sigma) d\sigma.$$

The cylinder has normal curvature 0 in the x-direction and  $1/R$  in the y-direction. The space curvature  $\kappa$  of  $F \circ c$  is therefore given by

$$\kappa^2 = \sin^4(\alpha(s))/R^2 + \kappa_g^2(s) = \sin^4(\alpha(s))/R^2 + (\alpha'(s))^2.$$

This is a first order ODE for  $\alpha(s)$ , if we want  $\kappa = \text{const} = dd$ . The default morph of 3D-XplorMath varies  $dd$ .

---

\* This file is from the 3D-XplorMath project. Please see:

This ODE is harmless, if we look for curves with  $\kappa > 1/R$ :

$$\alpha'(s) = +\sqrt{\kappa^2 - \sin^4(\alpha(s))/R^2} > 0.$$

The solution curves are, in the plane, convex curves. They reach  $\alpha = \pi/2$  in finite time. They are closed because the normals at  $\alpha = 0$  and at  $\alpha = \pi/2$  are lines of reflectional symmetry.

To discuss curves with  $\kappa \leq 1/R$ , we differentiate the square of the ODE and cancel  $2\alpha'(s)$ :

$$\alpha''(s) = -2 \sin^3(\alpha(s)) \cos(\alpha(s))/R^2.$$

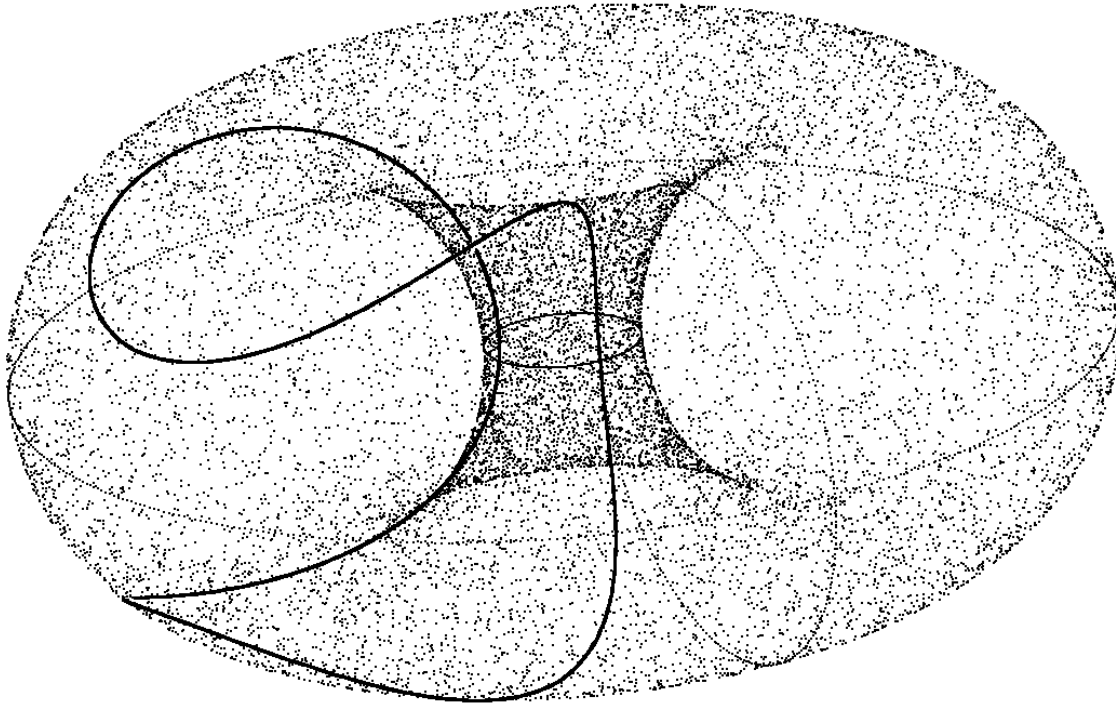
This is a Lipschitz-ODE with unique solutions for any given initial data.

If we choose  $\kappa < 1/R$ , then the second order ODE forces  $\alpha'(s)$  to change sign when  $\alpha(s)$  reaches  $\alpha_{\max}$  given by  $\sin^2(\alpha_{\max}) = \kappa/R < 1$ . The solution curves oscillate around a parallel to the x-axis and look a bit like sin-curves.

If we choose  $\kappa = 1/R$ , then  $\alpha_{\max} = \pi/2$ . We see that  $\alpha(s) := \pi/2$  is a solution of the second order ODE. Hence, any solution which starts with  $\alpha(0) < \pi/2$  cannot reach  $\pi/2$  in finite time, but converges to  $\pi/2$  asymptotically. The corresponding curve  $F \circ c$  therefore spirals towards one of the circle-latitudes of the cylinder - unexpectedly?

## Space Curves of Constant Curvature on Tori\*

These are the simplest non-planar closed constant curvature space curves that we have so far met. Their existence proof depends only on symmetry arguments. Example:



The program 3D-XplorMath allows to switch (in the Action Menu) between such curves on three surface families with rotation symmetry and equator mirror symmetry: namely on tori, ellipsoids and cylinders. The meridian curves of the tori and ellipsoids and the cross sections of the horizontal cylinders are ellipses with vertical axis  $cc$  and horizontal axis  $bb$ . The midpoints of these ellipses, in the torus case, lie on a circle of radius  $aa$  ( $> bb$ ). The

---

\* This file is from the 3D-XplorMath project. Please see:

cylinders, viewed as limits of the tori, have their lengths controlled by  $aa$  and the rotation symmetry degenerated to translation symmetry. The ellipsoids are described as tori with  $aa = 0$ .

Space curves of constant curvature  $k = dd$ , which lie on a given surface, can easily be computed via the ODE below, if the desired space curvature is chosen *larger* than all the normal curvatures of the surface. (In fact, only those normal curvatures which the curve meets, do matter.) We are interested in curves which are symmetric with respect to the equator plane and with respect to some meridian plane - such curves are made up of four congruent arcs and are automatically closed. The initial point is therefore chosen on the equator and the initial direction is vertical. The ODE is such that the angle, with which the meridians are intersected, increases until  $90^\circ$  is reached and we have obtained the quarter piece which gives our closed curve. One can have the initial point on the inner or the outer equator of the torus by switching the sign of the parameter  $bb$ .

The angle between the initial direction and the vertical meridian can be set. It is  $\pi * ee$ . All these curves have selfintersections, but they give some feeling, how constant curvature space curves wind around on the given surface. With more care we can allow constant space curvature which is *smaller* than the maximum of the normal curvatures of the surface. Below we will find closed ones also among these. – First we turn to the ODE.

## The ODE for Constant Space Curvature

For every tangential unit vector  $\vec{v}$  surfaces have a normal curvature  $b(\vec{v}, \vec{v})$ , where  $b(\cdot, \cdot)$  is the second fundamental form of the surface. Here we describe surfaces as the levels of a function  $f : \mathbb{R}^3 \mapsto \mathbb{R}$ , where the ‘level’ is the set of points where the function  $f$  has the value 0. (This constant can be changed with the parameter  $ff$ .) This description as a level of  $f$  allows to compute the *normal curvature* as

$$\kappa_n(\vec{v}) = \langle d_{\vec{v}} \text{grad } f, \vec{v} \rangle / |\text{grad } f|.$$

A curve on the surface with tangent vector  $\vec{v}$  will have space curvature  $dd$  at that point if the *tangential curvature* (also called *geodesic curvature*) is

$$\kappa_g(\vec{v}) = \sqrt{dd^2 - \kappa_n(\vec{v})^2}.$$

Note that  $N := \text{grad } f / |\text{grad } f|$  is the preferred unit normal field of the torus. The desired curve on the surface is therefore determined by the ODE:

$$c''(s) = \kappa_n(c'(s)) \cdot N(c(s)) + \kappa_g(c'(s)) \cdot c'(s) \times N(c(s)).$$

Any solution of this ODE with

$$f(c(0)) = 0 \text{ and } c'(0) \perp \text{grad } f(c(0))$$

stays on the level  $\{f = 0\}$ , i.e. on the given surface, and  
*is a space curve of constant curvature  $k = dd$ .*

To force such curves, with simple arguments, to close up we need to employ symmetries of the surface. Therefore we use this ODE on surfaces of revolution which, in addition, have a reflection symmetry orthogonal to the axis of rotation. The previous argument works on such surfaces.

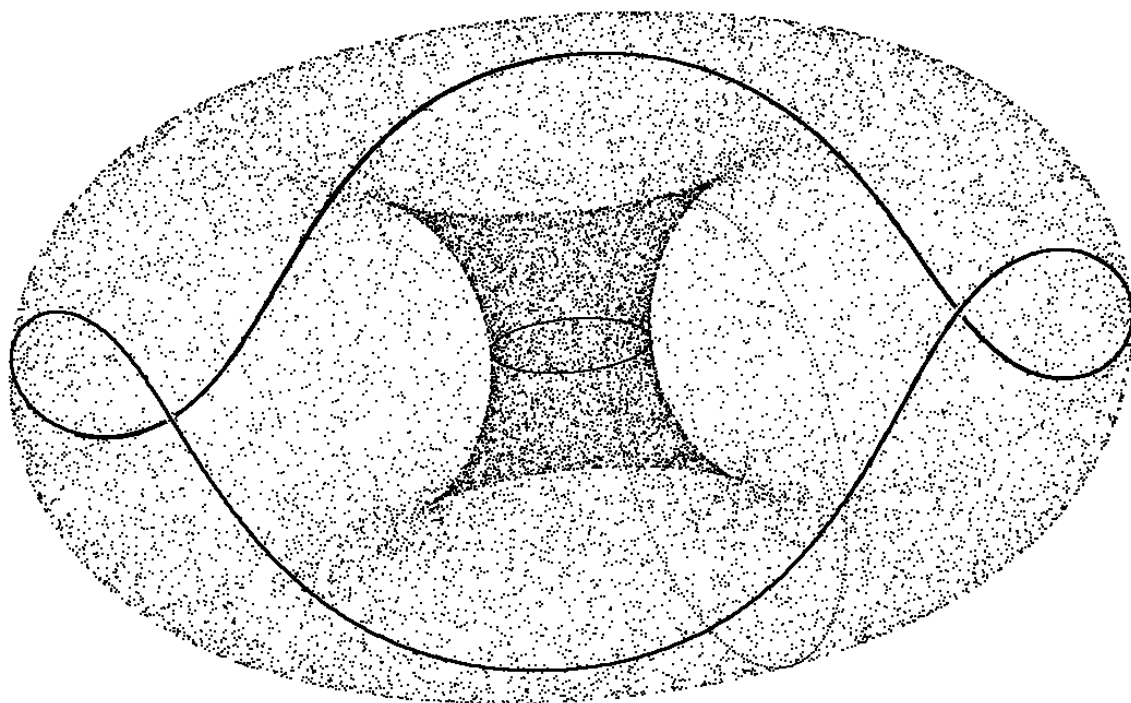
## More Closed Constant Curvature Curves.

The idea is to look for other symmetries of the curves. Our surfaces allow  $180^\circ$  rotations around normals at any equator point. Such symmetries rotate an arc of positive geodesic curvature  $\kappa_g$  into an arc with  $\kappa_g < 0$ , i.e. we need  $\kappa_g = 0$  where the curve crosses the equator. The only choice for the space curvature therefore is:

$$k = dd := \pm \kappa_n(c'(0)), \text{ hence } \kappa_g := \pm \sqrt{dd^2 - \kappa_n^2}.$$

We choose  $\kappa_g > 0$  above the equator,  $\kappa_g < 0$  below it. Note that on the cylinder there are helices with these initial conditions. They solve our ODE. On the other hand, on the torus and on the ellipsoid of revolution the latitudes have smaller radius than the equator. Angular momentum conservation therefore requires that the solution curves increase their angle against the meridians. Exactly as in the simpler case above they turn until they intersect a meridian orthogonally and then continue reflection symmetric (with respect to the plane of the meridian). This symmetry implies that they reach the equator again when their geodesic curvature is zero. Therefore they can cross the equator as smooth curves and the continuation agrees with the  $180^\circ$  normal rotation symmetry! And so on at all further crossings until the solution comes around the surface and to the vicinity of the initial point. In general it will not close. We can vary the size of the equator ( $aa$  for the torus,  $bb$  for the ellipsoid) until the solution hits the initial point. There, it is either half a period off or, because of the angular momentum, it reaches the initial point with the same tangent,

as a smoothly closed curve! This constructs many closed constant curvature space curves, because we have the parameters  $aa, bb, cc, ee$  to play with. – Numerically we can use the morphing feature of 3D-XplorMath and appeal to the intermediate value theorem to find solutions.



Surprisingly, we can find these oscillating curves also on circular cylinders. We start the integration where we expect the reflection symmetry: tangential to a straight line and with geodesic curvature  $\kappa_g(c(0)) \in (0, \max \kappa_n)$ . For the solution the angle against the straight lines will increase and the geodesic curvature decrease until it becomes zero. If we call the straight line through that point *equator of the cylinder*, then we have on the cylinder the same kind of curve that we obtained before on tori and ellipsoids. In the Action Menu of 3D-XplorMath one can switch between the described two kinds of symmetries of the curves.

## Some Numerical Remarks

The helices on the cylinders show that we should expect trouble when we try to solve our ODE numerically with initial value  $\kappa_g(c(0)) = 0$ . Recall that the Runge-Kutta method needs to make *four first order trial steps* before the high accuracy Runge-Kutta step is obtained as an average of those four trial steps. These trial steps cannot always be computed because  $dd^2 - \kappa_n^2 < 0$  at the endpoint of some trial step. Currently I do not know  $c'''(0)$  for the theoretically constructed curves (the even derivatives vanish because of the  $180^\circ$  symmetry). Therefore I cannot construct a numerical method which avoids the above problem.

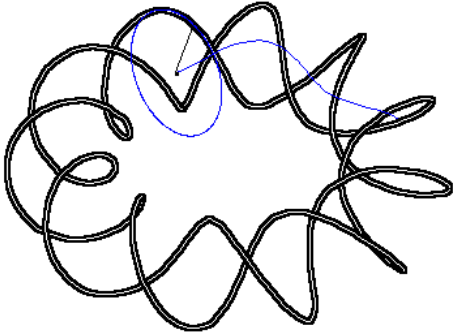
Instead I solve a slightly wrong equation by defining a slightly too large space curvature:

$$k = dd := |\kappa_n(c(0), c'(0))| + 0.00001.$$

This error is big enough for Runge-Kutta to proceed and small enough so that the osculating circles, while drawing the evolute, show no discontinuity. (The evolute increases errors of the curve very much.)

*Warning:* If the selection in the Action Menu is such that the curves with two orthogonal reflection symmetries are computed then the user may set the space curvature  $k = dd$  *arbitrarily*. To avoid crashes caused by square roots of negative numbers the program computes  $\sqrt{\max(0, dd^2 - \kappa_n^2)}$ . The computed curves in such situations are geodesics, not curves with constant space curvature.

## Space Curves of Constant Curvature \*



2 - 11 Torus Knot of constant curvature.

See also:

[About Spherical Curves](#)

*Definition via Differential Equations.* Space Curves that 3DXM can exhibit are mostly given in terms of explicit formulas or explicit geometric constructions. The differential geometric treatment of curves starts from such examples and defines geometric properties, i.e., properties which do not change when the curve is transformed by an isometry (= distance preserving map, also called a rigid motion) of Euclidean space  $\mathbb{R}^3$ . The most important such properties are the curvature function  $\kappa$  and the torsion function  $\tau$ . Once they have been defined one proves the *Fundamental Theorem of Space Curves*, which states that for any given continuous functions  $\kappa, \tau$  there is a space curve with these curvature and torsion functions, and, that this curve is uniquely determined up to a rigid motion. In 3DXM we obtain closed constant curvature space curves from:

$$\kappa(t) := aa,$$

$$\tau(t) := bb + cc \cdot \sin(t) + dd \cdot \sin(2t) + ee \cdot \sin(3t).$$

---

\* This file is from the 3D-XplorMath project. Please see:

We recall the definition of curvature and how the ODE shows up. At each point of a parametrized space curve  $c(t)$  there is a parametrized circle  $\gamma(t)$  with

$$c(t_0) = \gamma(t_0), \quad \dot{c}(t_0) = \dot{\gamma}(t_0), \quad \ddot{c}(t_0) = \ddot{\gamma}(t_0).$$

This circle – which may degenerate to a straight line – is called the *osculating circle at  $t_0$* , its radius is called *curvature radius at  $t_0$*  and the inverse of the radius is called *the curvature at  $t_0$* ,  $\kappa(t_0)$ . The computation of curvature is simpler if the curve is parametrized by arc length, i.e. if the length of all tangent vectors is one,  $|\dot{c}(t)| = 1$ . One gets  $\kappa(t) = |\ddot{c}(t)|$ . Check this for the circle (arclength parametrization)  $c(t) := r \cdot (\cos(t/r), \sin(t/r))$ . The most common way to proceed is to assume that  $\kappa(t) > 0$ . This allows to define the *Frenet basis* along the curve:

$$\begin{aligned} e_1(t) &:= \dot{c}(t), \\ e_2(t) &:= \ddot{c}(t)/\kappa(t), \\ e_3(t) &:= e_1(t) \times e_2(t). \end{aligned}$$

The Frenet basis defines three curves  $t \mapsto e_j(t)$  on the unit sphere. To emphasize the fact that  $e_j(t)$  are to be considered as vectors, not as points, one calls the length of their derivative,  $|\dot{e}_j(t)|$ , *angular velocity* or *rotation speed* and not just velocity. For example, the formula  $\ddot{c}(t) = \kappa(t)e_2(t)$  says that  $\kappa(t)$  is the rotation speed of  $\dot{c}(t)$ . We get from  $\dot{e}_1(t) \sim e_2(t)$  that the derivative  $\dot{e}_3(t) = e_1(t) \times \dot{e}_2(t)$  is proportional to  $e_2(t)$ . The proportionality factor, the rotation speed of  $e_3(t)$ , is called the torsion function  $\tau(t)$  of the curve  $c(t)$ . In formulas:  $\tau(t) := \langle \dot{e}_3(t), e_2(t) \rangle$ .

Having made these definitions, one can change the point

of view and consider the two functions  $\kappa, \tau$  as given. This turns the equations that were originally *definitions* of  $\kappa$  and  $\tau$  into *differential equations* for the curve, the famous

*Frenet-Serret Equations:*

$$\begin{aligned}\dot{e}_1(t) &= \kappa(t) \cdot e_2(t), \\ \dot{e}_2(t) &= -\kappa(t) \cdot e_1(t) - \tau(t) \cdot e_3(t), \\ \dot{e}_3(t) &= \tau(t) \cdot e_2(t),\end{aligned}$$

or, more compactly with the angular velocity vector

$$\begin{aligned}\vec{\omega}(t) &:= -\tau(t) \cdot e_1(t) + \kappa(t) \cdot e_3(t), \\ \dot{e}_j(t) &= \vec{\omega}(t) \times e_j(t), \quad j = 1, 2, 3.\end{aligned}$$

Finally  $\dot{c}(t) := e_1(t)$ .

For given continuous functions  $\kappa, \tau$  these differential equations have — for given orthonormal initial values — unique orthonormal solutions  $\{e_1(t), e_2(t), e_3(t)\}$ .

The curve  $c(t) := \int^t e_1(s) ds$  is then parametrized by arc length and has the given curvature functions  $\kappa, \tau$ .

To find *closed curves of constant curvature*, we employ symmetries. The simplest case is reflection symmetry in normal planes of the curve. When crossing such symmetry planes the torsion, in our case

$$\tau(t) := bb + cc \cdot \sin(t) + dd \cdot \sin(2t) + ee \cdot \sin(3t),$$

changes sign and is skew symmetric w.r.t. those points. Therefore we need  $bb = 0$ . The symmetry points then are at  $t = n \cdot \pi$ ,  $n \in \mathbb{Z}$  and all symmetry planes pass through the intersection line of two neighboring ones. If and only if the planes intersect in rational angles do the curves close.

Therefore we find many closed curves in any 1-parameter family (if  $bb = 0$ ), see e.g. the **default morph**.

With the  $\tau$ -function that we chose, there is another type of symmetry: If we set  $dd = 0$  then  $\tau$  is even w.r.t. the parameters  $t = \pi/2 + n \cdot \pi$ ,  $n \in \mathbb{Z}$  and this implies that  $180^\circ$  rotation around  $e_2(t)$  is a symmetry of the curve. Closed curves with this symmetry can be obtained from the Action Menu in the Submenu **Other Closed Curves**. If one chooses in the Action Menu **Add Symmetry Elements** then these normal rotation axes are added to the picture. The closing condition is easy to see:

- (i) The symmetry normals have all to be in the same plane and therefore all will intersect in one point.
- (ii) The intersection angle between two adjacent normals has to be rational.

For curves with this normal symmetry the parameter  $bb$ , the mean value of the torsion  $\tau$ , has a very nice property. To see it, select one of the curves with normal symmetry, then **Add Symmetry Elements**. Next go to **Set Morphing**, the 2nd entry of the Settings Menu, click the button **Init to Current Parameters** and finally increase the upper morphing bound  $b1$  by about 0.2. Preferably choose one of the stereo options and start morphing: The symmetry normals will move apart but remain orthogonal to a common, helicoidal, symmetry axis.

This regular behavior allowed us to program the morph  **$bb$  Keeps SymLines Colinear**, the last entry in the Animate Menu. Start with a closed curve with normal symme-

tries (from the submenu of the Action Menu). In **Set Morphing** click again the button **Init to Current Parameters**, but this time increase the upper bound  $c1$  by about 0.2. Click **OK** and click the last entry in the **Animate Menu**. *In the resulting deformation the program adjusts the mean value  $bb$  of the torsion in such a way that the symmetry normals remain collinear!!*

This feature allows the user to find other closed curves: Watch the morph until the symmetry normals appear to form again a rational angle, stop the morph by clicking the mouse. The parameters at which you stopped are now the current parameters. Click **Init to Current Parameters** in **Set Morphing** and now increase or decrease  $c1$  by about 0.02, do **OK** and run the last-entry-morph again. With few such steps the new curve can be visibly closed. One last time **Init to Current Parameters** and now do in the **Animate Menu**  *$aa, bb$  Keep Curves closed*. This entry is there to deform closed curves as closed curves, but in the current use it will improve the visibly closed curve to being high precision closed. – Some of the closed examples which the submenu offers, have been obtained with this method. The last example, the 11-2-knot, needed such a large value of the mean value  $bb$  of  $\tau(t)$  that the torsion of this example has no sign changes! It is easier to imagine examples like **6 helices**, which look more as one would expect: being made up of left winding and right winding pieces of helices, joined by pieces of circles.

See the tutorial movie on constant curvature space curves

at <http://3d-xplormath.org/Movies/index.html>  
Do not miss to select **Show Osculating Circles & Evolute**. The constant radius of the osculating circles shows the constant curvature and the rotating motion of the radius shows size and sign of the torsion.

In 3DXM one can choose in the Action Menu **Parallel Frame**. This frame is designed to rotate as little as possible along the curve, in  $\mathbb{R}^3$ . This property is more obvious when one looks at the torus knots than at the constant curvature curves. For further details see curves of *constant torsion*. The main advantage of these parallel frames is that they neither make it necessary to assume more than continuity of the second derivative  $\ddot{c}$ , nor that  $\kappa > 0$  everywhere, even straight lines are not exceptional curves if one works with these frames. Their differential equation is also simple:

*Frenet-Serret Equations for Parallel Frames:*

$$\dot{e}_1(t) := a(t) \cdot e_2(t) + b(t) \cdot e_3(t),$$

$$\dot{e}_2(t) := -a(t) \cdot e_1(t),$$

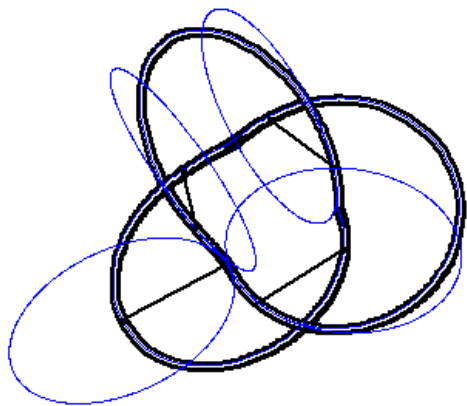
$$\dot{e}_3(t) := -b(t) \cdot e_1(t).$$

With an antiderivative  $T(t)$  of the torsion  $\tau(t) = T'(t)$  we can of course write the twodimensional curvature vector  $(a(t), b(t))$  in terms of  $\kappa(t), \tau(t)$ , namely:

$$(a(t), b(t)) := \kappa(t) \cdot (\cos(T(t)), \sin(T(t))).$$

## Autoevolutes\*

Or: Closed constant curvature space curves  
which are their own evolutes



2 - 3 - Autoevolute  
with some osculating  
circles

See also [Closed Space Curves  
of Constant Curvature](#)

The suggestion to look for these spectacular curves is from Ekkehard Tjaden, the details are joint work.

Assume that the curve  $c$  is parametrized by arc length  $s$ , has constant curvature  $\kappa$  and its Frenet frame is  $\{T(s), N(s), B(s)\}$ . Its evolute is

$$\tilde{c}(s) = c(s) + \frac{1}{\kappa} \cdot N(s), \quad \tilde{c}'(s) = \frac{\tau(s)}{\kappa} \cdot B(s).$$

The velocity of the evolute is therefore  $|\tilde{c}'(s)| = \frac{|\tau(s)|}{\kappa}$  and its Frenet frame is

$\tilde{T}(s) = \text{sign}(\tau)B(s)$ ,  $\tilde{N}(s) = -N(s)$ ,  $\tilde{B}(s) = \text{sign}(\tau)T(s)$ .  
That the evolute has the same constant curvature  $\kappa$  follows from:  $\tilde{N}'(s) = -N'(s) = \kappa \cdot T(s) - |\tau(s)| \cdot \tilde{T}(s)$ . For the torsion  $\tilde{\tau}(s)$  of the evolute differentiate  $\tilde{B}(s)$  with respect to arclength of the evolute:  $\text{sign}(\tau)\tilde{B}'(s) = T'(s) = -\kappa\tilde{N}(s)$ , hence  $\tilde{\tau}(s) = \text{sign}(\tau)\kappa/|\tilde{c}'(s)| = \kappa^2/\tau(s)$ .

---

\* This file is from the 3D-XplorMath project. Please see:

The two curves  $c, \tilde{c}$  are geodesics on the canal surface which envelops the spheres of radius  $1/2\kappa$  with midpoints on the curve  $m(s) = (c(s) + \tilde{c}(s))/2$ , because their principle normals  $N, \tilde{N}$  are orthogonal to the canal surface. This canal surface is, in the case of the example above, a wobbly torus - maybe that helps the visualization.

Constant curvature curves in general do not have congruent evolutes and even if  $c, \tilde{c}$  are congruent, this is difficult to check in case  $c$  is parametrized by arc length. One may look for curves with non-constant velocity  $v(t) = |\dot{c}(t)|$ , choose  $\tau(t)$  in terms of  $v(t)$  and try to arrange things so that the first half of the curve is congruent to the evolute of the second half and vice versa. This is achieved by the following version of the Frenet equations which Ekkehard suggested. It assumes  $t \in [0, 2\pi]$  and  $v(t + \pi) = 1/v(t)$ .

$$\begin{aligned}\dot{T}(t) &= +\kappa \cdot v(t) \cdot N(t), \\ \dot{N}(t) &= -\kappa \cdot v(t) \cdot T(t) + \kappa/v(t) \cdot B(t), \\ \dot{B}(t) &= -\kappa/v(t) \cdot N(t).\end{aligned}$$

In 3DXM we choose first  $h(t) = bb \cdot (cc \sin(t) + ee \sin(3t))$  and then  $v(t) = \sqrt{1 + h(t)^2} - h(t)$  or also  $v(t) = \exp(h(t))$ ; as with the other constant curvature curves  $\kappa = aa$ . Comparison with the standard Frenet equations shows

$$\tau(t) = \kappa/v(t)^2.$$

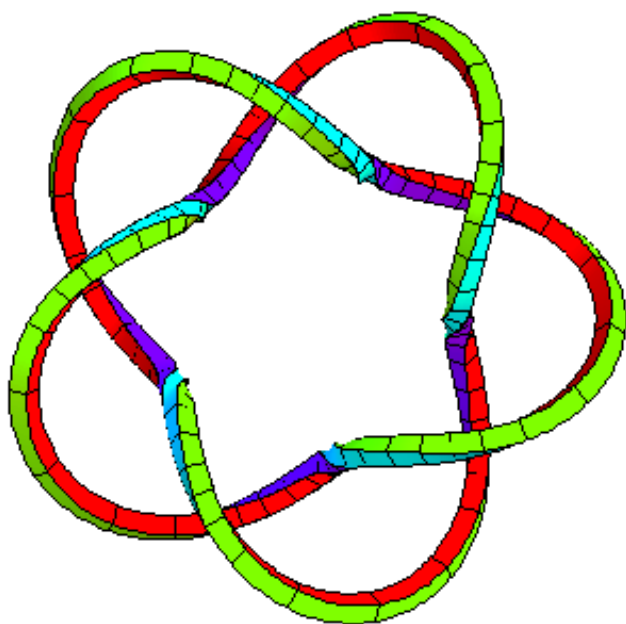
Note that  $v(t)$  and  $\tau(t)$  are, relative to  $t^* = \pi/2 + n\pi$ , even functions. This implies that the principle normals at these points are symmetry normals, saying that  $180^\circ$  rotation around these normals map the curve onto itself. Closed

examples can therefore be found by solving a 2-parameter problem:

- a) get the symmetry normals to lie in a plane – they then automatically intersect in one point.
- b) get neighbouring symmetry lines to intersect with a rational angle - preferably angles like  $\pi/2, \pi/3, 2\pi/3 \dots$

This looks similar to the case of single constant curvature curves. However in that case the constant Fourier term of the torsion is a parameter that allows to solve problem a) for all choices of other parameters. This allows to deal with problem b) assuming that a) is already solved.

For the autoevolutes we have not found such a simplifying parameter. By trial and error one has to close the curve to pixel accuracy. Only then does the automatic solution of the 2-parameter problem work and produce a high accuracy solution.



Note that the curve has large torsion – i.e. twists rapidly and moves slowly – opposite to the points with small torsion, where the curve is fairly circular and its velocity is large.

## About Space Curves of Constant Torsion \*

See: About [Closed Space Curves of Constant Curvature](#)

### DEFINITION VIA DIFFERENTIAL EQUATIONS

Most Space Curves that 3DXM can exhibit are given in terms of explicit formulas or explicit geometric constructions. In “About Space Curves of Constant Curvature” we explain how *curvature* and *torsion* of a space curve are defined. The definition immediately translates into a construction of the curve from curvature and torsion via the following *differential equations*, the famous

*Frenet-Serret Equations:*

$$\dot{e}_1(t) := \kappa(t) \cdot e_2(t),$$

$$\dot{e}_2(t) := -\kappa(t) \cdot e_1(t) - \tau(t) \cdot e_3(t),$$

$$\dot{e}_3(t) := \tau(t) \cdot e_2(t).$$

For given continuous functions  $\kappa, \tau$  these differential equations have — for given orthonormal initial values — unique orthonormal solutions  $\{e_1(t), e_2(t), e_3(t)\}$ . The curve  $c(t) := \int^t e_1(s) ds$  is then parametrized by arc length and has the given curvature functions  $\kappa, \tau$ .

The simplest curves in the plane are straight lines and circles, curves of constant curvature. It is therefore natural to discuss also space curves of constant curvature. In 3DXM we illustrate these by finding closed examples in the following family:

---

\* This file is from the 3D-XplorMath project. Please see:

$$\begin{aligned}\kappa(t) &:= aa, \\ \tau(t) &:= bb + cc \cdot \sin(t) + dd \cdot \sin(2t) + ee \cdot \sin(3t).\end{aligned}$$

To understand the Frenet-Serret equations better one can also study other special cases. Experimentation shows that the following curves of constant torsion

$$\begin{aligned}\kappa(t) &:= bb + cc \cdot \cos(ff \cdot t) + dd \cdot \cos(2ff \cdot t) + \\ &\quad ee \cdot \cos(3ff \cdot t) \\ \tau(t) &= aa\end{aligned}$$

have an amusingly strong change of shape as one changes the parameters. Again we look for closed examples with the help of symmetries. Note that  $180^\circ$  rotations around the principal normals  $e_2(t)$  at  $t/ff = k\pi, k \in \mathbb{Z}$  are isometries of the curves. At  $t/ff = \pi/2 + k\pi, k \in \mathbb{Z}$  the  $180^\circ$  rotations around the other normal vector of the frame,  $e_3(t)$ , are also isometries of the space curve. This allows us to formulate the *closing condition*:

If the normals  $e_2(0)$  at  $c(0)$ ,  $e_3(\pi \cdot ff/2)$  at  $c(\pi \cdot ff/2)$  intersect and if their angle is a rational multiple of  $\pi$  then the space curve closes up. Numerically one can use the parameter  $cc$  to keep the angle constant, e.g. at  $\pi/3, \pi/4$ , and then use  $aa$  to let the normals intersect. There are many closed solutions. Typically they look like a collection of bed springs which are joint by fairly straight pieces. If one allows these bed springs to have many turns then the closing values of  $aa$  and  $cc$  are almost equidistant. The default morph of 3DXM shows this, it contains two closed and three approximately closed curves which are made of *three* bed springs with an increasing number of turns. It is

easy to extend this family to springs with more turns, but one can also find all the small values, down to just one half turn for each spring. — We found no closed curves made of only *two springs*.

Here is a list of numerically closed curves:

Curves with 3-fold symmetry,  $ff = 0.208$ ,

$aa$ ,	0.178632213,	0.284031845,	0.417033334,
$cc$ ,	0.2874008,	0.90658882,	2.19234962,
$aa$ ,	0.513441035,	0.59263462,	0.628044,
$cc$ ,	3.489480574,	4.7901189,	5.4411264,
$aa$ ,	0.661324546,	0.69281176,	0.7227614
$cc$ ,	6.09244336,	6.7440016,	7.39575343

Curves with 4-fold symmetry,  $ff = 0.23$ ,

$aa$ ,	0.2137654757,	0.3704887,	0.479019355,
$cc$ ,	0.234123448,	0.89640923,	1.59595534,
$aa$ ,	0.56642393,	0.6414483533,	0.7081321561,
$cc$ ,	2.30473675,	3.01756515691,	3.732639742,
$aa$ ,	0.76871766,	0.8246012,	0.87671763
$cc$ ,	4.449136,	5.1666082,	5.8847911

Curve with 5-fold symmetry,  $ff = 0.2324$ ,

$$aa = 0.73855871446286, \quad cc = 2.96466$$

If one does not begin with the differential equation but starts from the curve, then one cannot define the torsion at points where the curvature vanishes. This problem is caused by the use of the Frenet frame. Another frame is suggested by a mechanical consideration: If a massive sphere would move along the space curve (imagine the

space curve as a wire and the sphere with a hole through which the wire slides without friction) then inertia would make the sphere avoid unnecessary rotations around the wire. In other words: A frame which is attached to the sphere so that it is normal to the wire remains normal and the derivatives of the normal vectors have *no normal components*. Such frames are called “parallel as normal vectors”, or simply “parallel frames”. In 3DXM one can choose **Parallel Frame** in the Action Menu . **Show Curve as Tube** illustrates the behaviour of the chosen frame. In particular the torus knots show how the parallel frames avoid “unnecessary” rotations which the Frenet frames must make.

An advantage of such parallel frames is that they neither require to assume more than *two* continuous derivatives of the curve nor that  $\kappa$  never vanishes—even straight lines are not exceptional curves if one works with these frames. Let  $\phi(t)$  be an antiderivative of the torsion function, i.e.,  $\dot{\phi}(t) = \tau(t)$ . Then the differential equation that determines this frame has the following simple form:

*Frenet-Serret Equations for Parallel Frames:*

$$\dot{e}_1(t) := \kappa(t) \cos(\phi(t)) \cdot e_2(t) + \kappa(t) \sin(\phi(t)) \cdot e_3(t)$$

$$\dot{e}_2(t) := -\kappa(t) \cos(\phi(t)) \cdot e_1(t)$$

$$\dot{e}_3(t) := -\kappa(t) \sin(\phi(t)) \cdot e_1(t).$$

# Free Rotational Motion of Rigid Bodies \*

## Part I: Angular Velocity and Rigid Motion

In this first part we will not yet consider solid objects with their inertial properties, but only so-called *rigid body kinematics*, i.e., the study of rotational motions of space. The (simpler) particle mechanics analogue of the question that we will discuss is the following: knowing the velocity curve  $v(t)$  of a point how can we reconstruct the travel path  $c(t)$ ? Since  $c'(t) = v(t)$ ,  $c(t)$  is an antiderivative of  $v(t)$  and we can find it easily by integration. (Historically  $v(t)$  was called the *hodograph* of the motion.)

### Things to try in 3D-XplorMath

The last three entries of the Action Menu of Space Curves show demos that illustrate the present discussion. The first of these Actions, *Use Curve as Hodograph*, interpretes the space curves of 3D-XplorMath as velocity curves of a particle and reconstructs the path. The demo emphasizes that the tangent vector of the constructed path is (parallel to) the position vector of the selected space curve, the hodograph.

The second of these Actions, *Use Curve as Angular Velocity*  $\vec{\omega}(t)$ , reconstructs the rotational motion which has

---

\* This file is from the 3D-XplorMath project. Please see:

the given space curve as given angular velocity function. The visualization of the motion uses a sphere with random dots and shows several consecutive points of the orbit of each random dot. One sees large orbit velocities near the equator of the rotation and small velocities near the axis of the rotation *at each moment*. – More details are explained below.

The third of these Actions, *Use Curve as Components of  $\vec{\omega}(t)$  in the Moving System*, again reconstructs that rotational motion that has its angular velocity given in the moving system by the selected space curve. The space curve therefore rotates with the motion. It leaves a trace behind which shows the corresponding angular velocity curve in the observer's space. In the second Action this curve was the given one.

Finally, there is one very special space curve, *Solid Body (Euler's Polhode)*. If this space curve is selected for the third Action above then the resulting motion is *the physical motion* around the center of mass of a rigid body, taken to be a brick with edge lengths  $aa \geq bb \geq cc$  and initial components of the angular momentum  $dd, ee, ff$ , see the ATO of Solid Body.

### Angular Velocity given in the Observer's Space

Mathematicians and Physicists have slightly different pictures of a *motion* in their minds. A physicist sees a solid object moving in space, the movement is differentiable and all points  $\vec{x}_i(t)$  of the moving object have their orbit ve-

locities  $\vec{x}_i'(t)$ . So far these functions could also describe a mass of moving air. The word *rigid motion* means that the pairwise distances  $|\vec{x}_i(t) - \vec{x}_j(t)|$  remain *constant* in time – the points  $\vec{x}_i(t)$  could be the atoms of a stone. For a mathematician on the other hand the primary concept is that of a *distance preserving map of space*, and a motion is a 1-parameter family of such maps. For physicists and mathematicians it is important to understand the velocity fields  $\vec{x}_i'(t)$  of all the particles. Physicists begin by studying rotations around *fixed* axes with *constant* angular velocities. In such a situation one can compute all the velocities  $\vec{x}_i'(t)$  from *one* vector  $\vec{\omega}$  that is parallel to the rotation axis and from the particle positions  $\vec{x}_i(t)$  as follows:

$$\vec{x}_i'(t) = \vec{\omega} \times \vec{x}_i(t).$$

It is now a mathematical fact that differentiable families of distance preserving maps have a very similar formula for the velocities of the particles: For each time  $t$  there exists a vector  $\vec{\omega}(t)$  such that we have:

$$\vec{x}_i'(t) = \vec{\omega}(t) \times \vec{x}_i(t).$$

And vice versa, if such a relation between the velocities and the positions holds then all pairwise distances between the particles are constant in time. Therefore mathematicians and physicists agree that a differentiable rigid motion is characterized by this relation between particle positions and particle velocities.

Now, a natural question is: If  $\vec{\omega}(t)$  is a given vector function in  $\mathbb{R}^3$ , how can one reconstruct the rotational motion? We answer this question by constructing a so called *moving frame*  $\{\vec{e}_x(t), \vec{e}_y(t), \vec{e}_z(t)\}$ , a time dependent orthonormal basis. To do this we have to solve the following three ODEs:

$$\begin{aligned}\vec{e}_x'(t) &= \vec{\omega}(t) \times \vec{e}_x(t), & \vec{e}_x(0) &= (1, 0, 0) \\ \vec{e}_y'(t) &= \vec{\omega}(t) \times \vec{e}_y(t), & \vec{e}_y(0) &= (0, 1, 0) \\ \vec{e}_z'(t) &= \vec{\omega}(t) \times \vec{e}_z(t), & \vec{e}_z(0) &= (0, 0, 1).\end{aligned}$$

Next we observe that *all* linear combinations with *constant* coefficients, i.e.

$\vec{x}(t) := x \cdot \vec{e}_x(t) + y \cdot \vec{e}_y(t) + z \cdot \vec{e}_z(t)$  satisfy

$\vec{x}'(t) = \vec{\omega}(t) \times \vec{x}(t)$  and are therefore orbits of the rotational motion defined by the angular velocity  $\vec{\omega}(t)$ .

To visualize this motion observe that for each *fixed*  $t$  the velocity field  $\vec{v}(\vec{x}) := \vec{\omega}(t) \times \vec{x}$  is the velocity field of the ordinary rotation around the axis  $\vec{\omega}(t)\mathbb{R}$  with constant angular velocity  $|\vec{\omega}(t)|$ .

### Angular Velocity given in the Moving Space

What could it mean *to give the angular velocity of a motion in moving space*? We saw in the previous discussion that we can describe the motion of space by giving a *moving frame*  $\{\vec{e}_x(t), \vec{e}_y(t), \vec{e}_z(t)\}$ . The particles of moving objects have position vectors that have *constant* components  $a_x, a_y, a_z$  relative to this frame:  $\vec{x}_i(t) = a_x \vec{e}_x(t) + a_y \vec{e}_y(t) + a_z \vec{e}_z(t)$ . Similarly we can prescribe  $\vec{\omega}(t)$

by giving its components relative to the moving frame:

$$\{\omega_x(t), \omega_y(t), \omega_z(t)\}.$$

There is again a natural question: can we again reconstruct a corresponding rotational motion for any vector function  $\vec{\omega}(t)$  that is given in this way?

The answer is almost the same as for the first question, except that the three ODEs are no longer separate but are coupled by the fifth line:

$$\vec{e}_x'(t) = \vec{\omega}(t) \times \vec{e}_x(t), \quad \vec{e}_x(0) = (1, 0, 0)$$

$$\vec{e}_y'(t) = \vec{\omega}(t) \times \vec{e}_y(t), \quad \vec{e}_y(0) = (0, 1, 0)$$

$$\vec{e}_z'(t) = \vec{\omega}(t) \times \vec{e}_z(t), \quad \vec{e}_z(0) = (0, 0, 1)$$

with

$$\vec{\omega}(t) = \omega_x(t) \cdot \vec{e}_x(t) + \omega_y(t) \cdot \vec{e}_y(t) + \omega_z(t) \cdot \vec{e}_z(t).$$

Historical note: The given curve  $\{\omega_x(t), \omega_y(t), \omega_z(t)\}$  in the moving system is called the *polhode* of the motion and the corresponding curve  $\vec{\omega}(t) = \omega_x(t) \cdot \vec{e}_x(t) + \omega_y(t) \cdot \vec{e}_y(t) + \omega_z(t) \cdot \vec{e}_z(t)$  in the inertial space is called the *herpolhode*. The moving polhode and the fixed herpolhode touch each other at each time  $t$  with tangents of equal length – because the points on the momentary axis of rotation,  $\vec{\omega}(t)\mathbb{R}$ , have at time  $t$  the rotational velocity field  $\vec{\omega}(t) \times \vec{\omega}(t) = \vec{0}$  in  $\mathbb{R}^3$ . A visual interpretation of this fact is that the moving polhode rolls without slipping along the fixed herpolhode. (This description actually determines the rotational motion because the origin is fixed so that the polhode has no

freedom to rotate around the common tangent with the herpolhode, there is only one way to roll along.)

H.K.

Space Curve TOC

## Free Rotational Motion of Rigid Bodies \*

What is to observe in the 3D-XplorMath exhibit

*Solid Body (Euler's Polhode) ?*

A brick – in the program of edge lengths  $aa \geq bb \geq cc \geq 0$  – is a good example of a solid (also: rigid) body. The program illustrates the free rotational movement of such a brick (i.e. gravity is ignored):

Select *Solid Body (Euler's Polhode)*, stop the alternation between two pictures by a mouse click and select *Do Poinso Construction From Polhode* at the bottom of the Action Menu. The resulting animation shows a freely tumbling brick. By changing  $aa$ ,  $bb$ , or  $cc$  one may watch other bricks tumbling.

There are three other input parameters,  $dd$ ,  $ee$ ,  $ff$ . These are initial conditions for the tumbling motion. If one uses  $(dd, ee, ff) \approx (1, 0.1, 0.1)$  or  $(dd, ee, ff) \approx (0.1, 0.1, 1)$  then there is not much tumbling. These motions are almost rotations around the longest axis ( $aa$ ) of the brick, respectively the shortest axis ( $cc$ ). The fact that these rotation axes stay close to their initial position is expressed by saying: *the rotations around the longest and the shortest axis are stable*. Now look again at the default initial conditions  $(dd, ee, ff) \approx (0.1, 1, 0.1)$ . One observes that the momen-

---

\* This file is from the 3D-XplorMath project. Please see:

tary axis of rotation moves almost to the direction opposite to the initial direction and then returns back. One says: *the rotation around the middle axis of the brick is unstable*. – By putting a tape around a book and trying to throw it so that it rotates around one of the three axes one can experimentally test these theoretical predictions.

The *explanation* of this behaviour has a mathematical part and a physical part. The physical part is contained in the initial picture, the mathematical part is the connection between the initial picture and the animation. We explain the mathematical part in

### Part I: From Angular Velocity to Rigid Motion

It is available in the *Topics* part of the *Documentation*. This mathematical part has no physical limitations, any of the space curves in the program can be used as *angular velocity curve* and in the Action Menu one can select animations that show the resulting motions.

The physical part requires in addition to *angular velocity* the physical notions *tensor of inertia* and *angular momentum*. These are explained below. What can one say before this theory about the initial picture of the program? We see two space curves. The one on the sphere is the angular momentum as a function of time *in the coordinate system of the brick*. The other one is the angular velocity curve (called *Polhode*). Both are intersections of quadratic surfaces, represented by dots in the picture. The two curves

are related by a fixed linear map – given by the tensor of inertia. To emphasize this linear map the quadratic surfaces alternate between the domain and the range of this map. Finally, these two curves together determine Euler’s differential equation for either of them. For example the derivative of the angular momentum curve is the cross product of the corresponding position vectors of the angular momentum curve and the angular velocity curve, in formulas:  $\vec{\ell}'(t) = \vec{\ell}(t) \times \vec{\omega}(t)$ . The Action Menu entry *Show Repère Mobile and ODE* illustrates this connection. The dotted curves on the sphere are solutions for other initial conditions  $dd, ee, ff$  with the same value  $dd^2 + ee^2 + ff^2$ . The default morph varies  $bb$  between  $aa$  and  $cc$ , it illustrates how the *family* of polhodes depends on the shape of the brick.

And here is the theory:

## Part II: Tensor of Inertia and Angular Momentum

The tensor of inertia is a map that transforms *angular velocity* into *angular momentum*.

Historical note: The word *tensor* is a generic word that describes objects from linear algebra that can be given by components (indices!) with respect to a base. The *tensor of inertia* is a *linear map* from the 3-dim vector space of angular velocities to the 3-dim vector space of angular momenta. What we need below is that for each solid body there exists an orthonormal frame  $\{\vec{e}_x(t), \vec{e}_y(t), \vec{e}_z(t)\}$  in the rest space of the body (i.e. moving with the body) so

that the tensor of inertia  $\Theta$  is a diagonal map:

$$\begin{aligned} \text{angular momentum} &= \Theta(\vec{\omega}(t)) = \\ &\omega_x(t) \cdot \Theta_x \vec{e}_x(t) + \omega_y(t) \cdot \Theta_y \vec{e}_y(t) + \omega_z(t) \cdot \Theta_z \vec{e}_z(t). \end{aligned}$$

$\Theta_x, \Theta_y, \Theta_z$  are called *principal moments of inertia*.

We now explain the tensor of inertia in some more detail. The result of the explanation will be the above formula for the angular momentum. We view a solid body as a collection of points of **mass**  $m_i$  and position vector  $\vec{x}_i(t)$ ; the pairwise distances between these points are constant. The origin is the center of mass of these points, i.e.  $\sum_i m_i \vec{x}_i(t) = \vec{0}$ . For each mass point we have the following definitions, the corresponding notions for the solid body are obtained by summation:

linear momentum:  $\vec{p}_i(t) := m_i \vec{x}_i'(t)$

angular momentum with respect to the origin:

$$\vec{\ell}_i(t) := \vec{x}_i(t) \times \vec{p}_i(t)$$

kinetic energy:  $E_i(t) := \frac{1}{2} m_i \langle \vec{x}_i'(t), \vec{x}_i'(t) \rangle$ .

The body is rigid, i.e. the distances between the points are constant, therefore there is an angular velocity function  $\vec{\omega}(t)$  that relates the positions and velocities:

rotational motion:  $\vec{x}_i'(t) = \vec{\omega}(t) \times \vec{x}_i(t)$ .

angular momentum:  $\vec{\ell}_i(t) = \vec{x}_i(t) \times (\vec{\omega}(t) \times \vec{x}_i(t))$   
 $=: \Theta_i(\vec{\omega}(t))$ .

This tensor of inertia is most easily understood if we use the relation between cross-product and matrix-product and

insert it into the above definitions. We obtain the expressions for angular momentum and kinetic energy in terms of the tensor of inertia and the angular velocity as follows:

$$\begin{aligned}\vec{\omega} \times \vec{x} &= \begin{pmatrix} 0 & -\omega_z & \omega_y \\ \omega_z & 0 & -\omega_x \\ -\omega_y & \omega_x & 0 \end{pmatrix} \cdot \begin{pmatrix} x \\ y \\ z \end{pmatrix} \\ &= \begin{pmatrix} 0 & z & -y \\ -z & 0 & x \\ y & -x & 0 \end{pmatrix} \cdot \begin{pmatrix} \omega_x \\ \omega_y \\ \omega_z \end{pmatrix}\end{aligned}$$

We obtain

$$\begin{aligned}\vec{\ell}_i(t) &= \\ m_i &\begin{pmatrix} 0 & z_i & -y_i \\ -z_i & 0 & x_i \\ y_i & -x_i & 0 \end{pmatrix} \begin{pmatrix} 0 & -z_i & y_i \\ z_i & 0 & -x_i \\ -y_i & x_i & 0 \end{pmatrix} \begin{pmatrix} \omega_x \\ \omega_y \\ \omega_z \end{pmatrix} \\ &= m_i \begin{pmatrix} y_i^2 + z_i^2 & -x_i y_i & -x_i z_i \\ -x_i y_i & y_i^2 + z_i^2 & -y_i z_i \\ -x_i z_i & -y_i z_i & x_i^2 + y_i^2 \end{pmatrix} \begin{pmatrix} \omega_x \\ \omega_y \\ \omega_z \end{pmatrix} \\ &= \Theta_i(\vec{\omega}) \quad (\text{Note the symmetry of the matrix of } \Theta_i).\end{aligned}$$

$$E_i(t) = \frac{1}{2} \langle \Theta_i(\vec{\omega}), \vec{\omega} \rangle.$$

The symmetry of  $\Theta := \sum_i \Theta_i$  implies that we have an orthonormal eigen basis for  $\Theta$ . The corresponding eigen values are the principal moments of inertia,  $\Theta_x, \Theta_y, \Theta_z$ .

Finally, we will derive Euler's equations, a first order ODE for  $\vec{\omega}(t)$ . Together with part I this determines the motion of a solid body that rotates without exterior forces. We will always take the eigen basis of  $\Theta$  as the moving frame of part I.

Newton's laws imply that the total angular momentum is constant in situations that are more general than the force free rotation of a solid body. We omit this general theory and show only that the conservation of angular momentum is equivalent to Euler's equations.

$$\vec{\ell}(t) := \sum_i \vec{\ell}_i(t) = \Theta(\vec{\omega}(t)) = \sum_{\xi \in \{x,y,z\}} \omega_\xi(t) \Theta_\xi \vec{e}_\xi(t)$$

implies

$$\begin{aligned} \frac{d}{dt} \vec{\ell}(t) = \\ \sum_{\xi \in \{x,y,z\}} \omega_\xi(t)' \Theta_\xi \vec{e}_\xi(t) + \sum_{\xi \in \{x,y,z\}} \omega_\xi(t) \Theta_\xi \vec{e}_\xi'(t). \end{aligned}$$

Insert  $\vec{e}_\xi'(t) = \vec{\omega}(t) \times \vec{e}_\xi(t)$  to get

$$\sum_{\xi \in \{x,y,z\}} \omega_\xi(t) \Theta_\xi \vec{e}_\xi'(t) = \vec{\omega}(t) \times \vec{\ell}(t),$$

next compute the cross product in the base given by the moving frame:

$$\vec{\omega}(t) \times \vec{\ell}(t) = \sum_{\xi \in \{x,y,z\}} \left( \begin{pmatrix} \omega_x \\ \omega_y \\ \omega_z \end{pmatrix} \times \begin{pmatrix} l_x \\ l_y \\ l_z \end{pmatrix} \right)_\xi \cdot \vec{e}_\xi(t),$$

finally compare coefficients to get Euler's equations:

$$\begin{pmatrix} l_x \\ l_y \\ l_z \end{pmatrix}' = \begin{pmatrix} \Theta_x \omega_x \\ \Theta_y \omega_y \\ \Theta_z \omega_z \end{pmatrix}' = - \begin{pmatrix} \omega_x \\ \omega_y \\ \omega_z \end{pmatrix} \times \begin{pmatrix} l_x \\ l_y \\ l_z \end{pmatrix},$$

where the physics is contained in the relation between  $\omega$  and  $l$  :

$$l_x = \Theta_x \omega_x, \quad l_y = \Theta_y \omega_y, \quad l_z = \Theta_z \omega_z.$$

Considered as differential equation for the  $\omega$ -components these are Euler's equations. This ODE-system implies immediately that the two quadratic functions

$$|\vec{l}|^2 = l_x^2 + l_y^2 + l_z^2 = \Theta_x^2 \omega_x^2 + \Theta_y^2 \omega_y^2 + \Theta_z^2 \omega_z^2 \quad \text{and}$$

$$2E = l_x \omega_x + l_y \omega_y + l_z \omega_z = \Theta_x \omega_x^2 + \Theta_y \omega_y^2 + \Theta_z \omega_z^2$$

are constant along solution curves. The solutions are therefore intersections of two ellipsoids. If one considers the ODE-system as differential equations for the  $l$ -components then one of the ellipsoids is a sphere and the solutions  $(l_x(t), l_y(t), l_z(t))$  are spherical curves. The choice of the  $l$ -components as the functions to be determined therefore simplifies the visualization and also leads to a slightly simpler ODE-system, since the tensor of inertia enters only on the right side, linearly, into the equations.

## User Curves By Curvature And Torsion \*

The exhibit allows to create examples for the standard Frenet theory of space curves. The initial dialogue allows to input user choices for curvature and torsion as functions of arc length,  $\kappa(s), \tau(s)$ .

The solution curves are programmed as if they were explicitly parametrized. Therefore all the Action Menu entries for parametrized curves are also available for these ODE-defined curves.

The differential equations in question are the famous

*Frenet-Serret Equations:*

$$\begin{aligned}\dot{e}_1(t) &:= \kappa(t) \cdot e_2(t), \\ \dot{e}_2(t) &:= -\kappa(t) \cdot e_1(t) - \tau(t) \cdot e_3(t), \\ \dot{e}_3(t) &:= \tau(t) \cdot e_2(t).\end{aligned}$$

For given continuous functions  $\kappa, \tau$  these differential equations have — for given orthonormal initial values — unique orthonormal solutions  $\{e_1(t), e_2(t), e_3(t)\}$ .

The curve  $c(t) := \int^t e_1(s)ds$  is then parametrized by arc length and has the given curvature functions  $\kappa, \tau$ .

H.K.

---

\* This file is from the 3D-XplorMath project. Please see:

## Userdefined Parametrized Space Curves \*

These exhibits allow to input userdefined explicitly parametrized space curves in three different ways:

1.) User Cartesian: The three Cartesian coordinate functions  $x(t), y(t), z(t)$  can be entered (Of course  $t$  does not have to be arc length.)

2.) User Polar: The coordinate functions can be entered in spherical polar coordinates  $r(t), \theta(t), \varphi(t)$ . In particular, this allows to enter spherical curves. As usual:

$$x = r \cdot \sin \theta \cdot \cos \varphi, \quad y = r \cdot \sin \theta \cdot \sin \varphi, \quad z = r \cdot \cos \theta.$$

3.) User Cylindrical: The coordinate functions can be entered in cylindrical coordinates  $r(t), \theta(t), z(t)$ , with the usual convention  $x = r \cdot \cos \theta, y = r \cdot \sin \theta, z = z$ .

Since Cylinders are isometric to the plane, this allows to create space curves that are given on all the cylinders  $r = \text{const}$  by the same intrinsic geodesic curvature data  $\kappa_g(s)$ .

H.K.

---

\* This file is from the 3D-XplorMath project. Please see:

## About the Unduloid \*

What are the different shapes that a soap film can take, or to put it somewhat differently, what can we say about the differential geometry of a mathematical surface that approximates a soap film?

An important physical characteristic of the soap film is its surface tension  $T$ . This depends only on the chemical composition of the liquid from which it is made, and so it is the same at each point of the film. The difference in air pressure between the two sides of the film is an environmental variable that is also clearly the same at all points of the film. Now it follows from physical principles (that we will take for granted here) that the mean curvature  $H$  of the soap film at any point is equal to  $P/T$ , and so we see that a soap film is always represented by a surface that has constant mean curvature.

For a soap film that we get by dipping a closed loop of wire into soapy water, the air pressure on both sides is clearly the same, so such a soap film must have mean curvature zero. Such surfaces are called *minimal surfaces*, since it can be shown that if we draw any small closed curve on the surface, the area of the part of the surface inside the curve is less than or equal to the area of any other surface bounded by the curve.

---

\* This file is from the 3D-XplorMath project. Please see:

[http://3D-XplorMath.org/Surfaces of Revolution](http://3D-XplorMath.org/Surfaces_of_Revolution)

We consider minimal surfaces in considerable detail elsewhere, and here we shall be interested in the case of soap bubbles. These are soap films that (perhaps together with some other surfaces) enclose a bounded region of space (the “inside” of the bubble). For bubbles the pressure will be slightly greater on the inside than on the outside, so that the surface is what is called a *CMC surface*, that is it has **non-zero** constant mean curvature (and of course for the floating type it is often just a sphere).

If one blows a soap bubble between two parallel glass plates then one can obtain CMC surfaces that are surfaces of revolution, and such CMC surfaces are called *Unduloids*.

Consider a curve in the  $x$ - $y$ -plane, given parametrically by  $x = x(t), y = y(t)$ , or as a graph  $(x, f(x))$  of a function  $f$ . If one rotates this curve about the  $x$ -axis, it is easy to compute an expression for the mean curvature  $H$  of the resulting surface of revolution in terms of the first and second derivative of  $x(t)$  and  $y(t)$  (or, in the graph description, the derivatives of  $f$ ). If this expression is set equal to a positive constant  $H$ , one gets differential equations for the functions  $x(t)$  and  $y(t)$  (respectively for the function  $f$ ), and solving these ODE provides a method for finding all CMC surfaces of revolution. Delaunay studied this problem in 1841, and being an expert on the theory of roulettes (i.e., a locus traced out by a point attached to curve as that curve rolls on a line), he recognized that the solutions of this differential equation could be identified with the roulettes traced out by a focus of a conic section

as it rolls along the  $x$ -axis. The special case that the conic is an ellipse gives the Unduloid. In 3D-XplorMath, the Unduloid is literally constructed by this double process of first rolling an ellipse and tracking one of its foci and then rotating the resulting curve around the  $x$ -axis.

The default morph shows a family of unduloids that starts with a cylinder and deforms towards a chain of spheres. With the rolling construction of the Unduloid, we cannot reach the chain of spheres because the parameter lines become concentrated near the narrowing necks of the surfaces. However, if one resizes these necks so they have constant waist size, then the necks converge to (minimal) Catenoids. This fact was very important in the construction of very general examples by Kapouleas.

H.K.

Surfaces of Revolution

## Curvature Properties of Surfaces \*

Any curvature discussion of surfaces assumes some knowledge about curvature properties of curves.

**Planar Curves** have, at each point  $c(s)$ , only one kind of curvature. Consider a circle through  $c(s)$  that has the same first and second derivative as the curve at  $c(s)$ . Such a circle is called *osculating circle*, it approximates the curve better than any other circle and it can easily be recognized if  $c'''(s) \neq 0$  : The circle has the same tangent as the curve and is on different sides of the curve before and after  $c(s)$ . See **Osculating Circles** in the Action Menu. The radius of this circle is called *curvature radius*  $r(s)$ , and the *curvature* is defined as  $\kappa(s) := 1/r(s)$ . If  $s$  is the arclength parameter, i.e.  $|c'(s)| = 1$ , then  $\kappa(s) = \det(c'(s), c''(s))$ . The *fundamental theorem* for planar curves states:

If a continuous curvature function  $\kappa(s)$  is given then there exists, up to congruence, exactly one planar curve with this curvature function, namely:

define an antiderivative  $\alpha(s) := \alpha(0) + \int_0^s \kappa(\sigma) d\sigma$  and with it a curve  $c(s) := c(0) + \int_0^s \begin{pmatrix} \cos \alpha(\sigma) \\ \sin \alpha(\sigma) \end{pmatrix} d\sigma$ .

This curve  $c(s)$  is parametrized by arclength and has curvature function  $\kappa(s)$ .

---

\* This file is from the 3D-XplorMath project. Please see:

**Space Curves** have the same definition of *osculating circle* and of *curvature*  $\kappa(s)$  as the plane curves. If  $s$  is arc-length on  $c$  then  $c''(s)$  is called *principal curvature vector* and  $\vec{h}(s) = c''(s)/|c''(s)|$  is called *principal normal*. The *Frenet frame* along the curve is  $\{c', \vec{h}, \vec{b} = c' \times \vec{h}\}$ .

In addition, space curves have a second kind of curvature, the *rotation speed* of the *binormal*  $\vec{b}$ , also called *torsion*  $\tau(s) := -\langle \vec{b}'(s), \vec{h}(s) \rangle = +\langle \vec{h}'(s), \vec{b}(s) \rangle$ . The *fundamental theorem* for space curves (roughly) states:

If continuous curvature functions  $\kappa(s), \tau(s)$  are given then there exists, up to congruence, exactly one space curve with these curvature functions.

**Surfaces** have as their most visible curvature properties their *normal curvatures*: Consider at a surface point  $p$  the intersection of the surface with all its normal planes at  $p$ . The curvatures of these *normal sections* are the normal curvatures. They can be computed as follows: Let  $N$  be a unit normal field along the surface and  $c(s), c(0) = p$  a normal section with  $c'(0) = \vec{e}, |\vec{e}| = 1$ . Then its curvature, the normal curvature in the direction  $\vec{e}$ , is

$$\kappa_{normal}(p, \vec{e}) = \langle D_{\vec{e}}N, \vec{e} \rangle = -\langle c''(0), N \rangle.$$

These normal curvatures have a minimum and a maximum, called the *principal curvatures*  $\kappa_1, \kappa_2$  at  $p$ . The corresponding vectors  $\vec{e}$  are called the *principal directions*  $\vec{e}_1 \perp \vec{e}_2$ .  $H := \kappa_1 + \kappa_2$  and  $K := \kappa_1 \cdot \kappa_2$  are *mean curvature* and *Gauss curvature*.

If the surface is given by an *explicit parametrization*, it is straight forward to compute these data. If the surface is given by an *implicit equation*  $f(x, y, z) = 0$ , one chooses  $N(x, y, z) := \text{grad } f / |\text{grad } f|$  and computes  $\langle D_{\vec{e}}N, \vec{e} \rangle$ , as before.

For these surfaces one finds in the Action Menu the entries:  
Add Principal Curvature Fields,  
Move Principal Curvature Circles.

They allow to view and move the above curvature objects.

Surface Organisation

## Projected Sphere\*

The elementary and differential geometric properties of triangles and curves on spheres are explained in [About Spherical Curves](#) in the documentation for Space Curves.

This exhibit has two goals:

1) The mechanical constructions of *Ellipse*, *Cycloid* and *Lemniscate* in the plane are repeated on the sphere to give mechanical constructions of *Spherical Ellipses*, *Spherical Cycloids* and *Spherical Lemniscates*. In the plane and on the sphere these constructions also give the tangents of the curves. The curves are chosen in the Action Menu of the sphere exhibit. They have the same parameters as in the quoted space curve exhibits.

2) Two famous maps are explained: The angle preserving [Stereographic](#) Projection from the sphere to a tangent plane and Archimedes' area preserving projection from a circumscribed cylinder to the sphere.

The sphere can be rendered with four different grids, selectable in the Action Menu. After standard (geographical) polar coordinates have been chosen, one can add (also from the Action Menu) four different spherical curves or Archimedes' projection. The spherical ellipses can also be viewed on a grid consisting of confocal ellipses and standard longitudes. Stereographic projection is best explained on a grid whose parameter lines are two orthogonal families of circles through the projection center ("South Pole");

---

\* This file is from the 3D-XplorMath project. Please see:

<http://3D-XplorMath.org/> [Surface Organisation](#)

these circles are mapped to lines parallel to the x-axis or the y-axis. The parameter lines of the last grid are two families of **Loxodromes (Constant Angle with Meridians)**; with this grid one can see – via stereographic projection – that groups of Möbius transformations may look much simpler on the Riemann sphere than in the Gaussian plane.

Which parameters control what?

*Spherical Ellipses:*  $bb$  = distance of focal points,  $aa > bb/2$  = major axis. The default morph changes  $aa$ . For the elliptic grid also:  $bb$  = distance of the focal points. The construction demo runs automatically; if  $0 < ff < 1$  is taken as morphing parameter, the demo runs as movie.

*Spherical Cycloids:*  $aa \cdot \pi$  = radius of the fixed circle. Integer  $ee$  = order of symmetry (determines the radius of the rolling circle). Length of drawing stick =  $bb \cdot$  radius of rolling circle. Automatic demo, morphing parameter  $ff$ .

*Spherical Lemniscates:*  $cc$  = length of the middle rod,  $dd$  = length of the two outer rods.  $ff$  parameter of the drawing pen,  $ff = 0.5$  midpoint of middle rod. Automatic demo, can be saved with morphing parameter  $0 < ee < 1$ .

*Loxodromes, Loxodromic grids:*  $aa$  = slope parameter, with  $aa = 0$  giving a longitude curve resp. the standard polar grid.  $cc$  = parameter (in degrees) for rotating the sphere around the x-axis - if also stereographic projection is chosen, then its center and image plane stay fixed while the sphere rotates.

## Explanation of Archimedes' Projection

Let  $-\pi/2 \leq u \leq \pi/2$  be the latitude parameter on a unit sphere parametrized as  $(\sin(u) \cos(v), \sin(u) \sin(v), \cos(u))$ . Add the tangential cylinder around the equator ( $u = 0$ ), parametrized as  $(\cos(v), \sin(v), \cos(u))$ . Archimedes' map is horizontal radial projection, i.e. points with the same parameters  $(u, v)$  on the cylinder and the sphere correspond to each other. This map shortens latitudes of the cylinder at height  $\cos(u)$  by the factor  $\sin(u)$ . The vertical lines on the cylinder are, locally at height  $\cos(u)$ , stretched by the factor  $1/\sin(u)$ .

With formulas:

$$\text{cylinder: } \left| \frac{d}{du} (\cos(v), \sin(v), \cos(u)) \right| = \sin(u),$$

$$\text{sphere: } \left| \frac{d}{du} (\sin(u) \cos(v), \sin(u) \sin(v), \cos(u)) \right| = 1.$$

This shows that Archimedes' map is area preserving. The unit sphere has therefore the same surface area as the cylinder of height 2 and radius 1, namely  $2 \cdot 2\pi$ .

This also implies that the volume of the solid sphere is  $4\pi/3$  because we can partition the boundary sphere into very small domains and view the solid sphere as the (disjoint) union of height=1 pyramids which have as base the small domains and their vertices are at the center of the sphere.

## Explanation of Stereographic Projection

Geometrically stereographic projection is defined as the 1-1 central projection from a point on the sphere to the tangent plane at the opposite point and vice versa. The same definition works for the 2-sheeted hyperboloid, which gives a map of similar importance as in the spherical case.

Formulas are slightly simpler if one projects to the plane through the center of the sphere which is parallel to the tangent plane opposite the center. Take  $S = (0, 0, -1)$  as projection center, then:

Let  $(x, y, z) \in \mathbb{S}^2$ , i.e.  $x^2 + y^2 + z^2 = 1$ . For  $z \neq -1$  put

$$St(x, y, z) := (x, y, 0)/(1 + z).$$

The inverse map is used just as often:

Let  $(u, v, 0) \in \mathbb{R}^2 \subset \mathbb{R}^3$ , then with  $r^2 := 1 + u^2 + v^2$  put

$$St^{-1}(u, v, 0) := (2u, 2v, 2 - r^2)/r^2.$$

The most important property of stereographic projection:

*This map preserves angles or shorter: it is conformal.*

Recall: A map preserves angles if for any two intersecting curves in the domain holds: *Their intersection angle is the same as the intersection angle of their image curves.* Of course, the intersection angle of curves is defined as the intersection angle of their tangents at the intersection point. To prove that angles are preserved, it is therefore enough to take as 'curves' in the image plane just all straight lines. Their stereographic preimages on the sphere are circles through the projection center  $S$ . Any two such circles intersect at  $S$  and their other intersection point with the

*same angle.* For any such circle holds: Its tangent at  $S$  and its image line in the opposite tangent plane are *parallel*. In other words: *The image lines of two circles through  $S$  intersect with the same angle as the two circles.*

This proves that stereographic projection is conformal.

A second basic property of stereographic projection is: *Circles on the sphere which do not pass through  $S$  are mapped to circles in the image plane.* (We know already that circles through  $S$  are mapped to straight lines.)

Proof. Take a circle on the sphere and consider all tangents to the sphere which are perpendicular to the circle. They form the tangential cone which touches the sphere along the given circle. For each of these tangents consider the plane spanned by the considered tangent and the projection center  $S$ . Intersect these planes with the sphere to get circles through  $S$  which all intersect the given circle orthogonally and all pass through one point, namely the intersection of the line through  $S$  and the vertex of the tangential cone with the sphere. The stereographic images of these circles are all straight lines which all pass through one point and meet the image curve orthogonally, i.e. they are like radii. The image curve is therefore a circle – either by the uniqueness theorem for ODEs or because the cone with vertex  $S$  through the given circle is a quadratic cone so that the image curve is known to be an ellipse - which in turn has to be a circle because of the orthogonal radii.

(Provable also by computation)      **Surface Organisation**

## Surfaces of Revolution \*

in particular with Constant Gauß or Mean Curvature

Surfaces of revolution are the simplest family of surfaces. They are usually described by giving its meridian curve  $s \mapsto (r(s), h(s))$ , which then is rotated:

$$(x, y, z)(s, \varphi) := (r(s) \cos \varphi, r(s) \sin \varphi, h(s)).$$

The meridian curve may be given explicitly. However, any kind of curvature condition can be expressed as an ordinary differential equation for the meridian curve. Therefore ODE-determined meridians are more interesting.

Formulas are particularly simple if the meridian is parametrized by arclength, i.e.,  $r'^2 + h'^2 = 1$ . The curvature of the latitude circles is  $1/r(s)$  and the normal curvature of the surface in their direction is a principal curvature, namely  $\kappa_2(s) = 1/r \cdot h'$ . The other principal curvature is the curvature of the meridian:

$$\kappa_1(s) = \langle (r''), (h'') \rangle = -r''h' + h''r' = -r''/h'.$$

For given Gauss curvature

$$K(s) = \kappa_1(s) \cdot \kappa_2(s) = -r''(s)/r(s)$$

the meridian is determined by the simple ODE (as long as  $|r'(s)| \leq 1$ ):

$$r''(s) + K(s) \cdot r(s) = 0, \quad h(s) = \int_0^s \sqrt{1 - r'(t)^2} dt.$$

---

\* This file is from the 3D-XplorMath project. Please see:

In the case of  $K(s) := 0$  each solution  $r(s)$  is a linear function. We obtain circular cylinders and cones.

Ferdinand Minding (1806 - 1885) studied the case of constant nonzero curvature. He determined the geodesics on the Pseudosphere ( $K = -1$ ), but we could not find whether he was the first to describe this famous surface. He obtained the following formulas:

The examples for  $K = 1$ :

The Sphere:

$$r(s) = \sin(s), \quad 0 \leq s \leq \pi$$

With cone points:

$$r(s) = a \sin(s), \quad 0 \leq s \leq \pi, \quad 0 < a < 1$$

With two singularity curves:

$$r(s) = a \cos(s), \quad -b \leq s \leq b, \quad a > 1, \quad \sin(b) = 1/a.$$

---

The examples for  $K = -1$ :

The Pseudosphere (with singular curve  $\{s = 0\}$ ):

$$r(s) = \exp(-s), \quad 0 \leq s$$

With cone point and singular curve:

$$r(s) = a \sinh(s), \quad 0 \leq s \leq b, \quad 0 < a < 1, \quad \cosh(b) = 1/a$$

With two singular curves:

$$r(s) = a \cosh(s), \quad -b \leq s \leq b, \quad 0 < a, \quad \sinh(b) = 1/a.$$

The Pseudosphere cannot be extended beyond the singular curve  $\{s = 0\}$ , because  $r'(s) > 1$  for  $s < 0$ . But the metric

of the Pseudosphere,

$$ds^2 + \exp(-2s)d\varphi^2,$$

extends to a complete metric on  $\mathbb{R} \times \mathbb{R}$  with  $K = -1$  and the same is true for the metric of the last example:

$$ds^2 + a^2 \cosh^2(s)d\varphi^2.$$

The fact that such a simply connected complete Riemannian plane with  $K = -1$  is isometric to the non-Euclidean geometry of Bolyai and Lobachevsky was not yet established when Minding studied geodesic triangles on the Pseudosphere. Beltrami showed it in 1865.

Surfaces with  $K = -1$  in  $\mathbb{R}^3$  have another interesting property: If the asymptote directions are described by two vectorfields of *constant* length, then these vector fields commute. For parametrizations of  $K = -1$  surfaces with asymptote lines as parameter lines one therefore has: the edge lengths of the parameter quadrilaterals are all the same. Such nets are called Tchebycheff nets. They are determined by the angle between the asymptote lines. A quite unexpected theory developed from here. It is outlined in [Introduction to Pseudospherical Surfaces](#) (or see the Documentation Menu). The Pseudosphere turns out to be the simplest example of that theory.

These Tchebycheff nets also play a crucial role in the proof of Hilbert's theorem, stating that the hyperbolic plane cannot be smoothly immersed isometrically into  $\mathbb{R}^3$ . The proof shows that the distance to a point, where the angle between the asymptote lines is 0 or  $\pi$ , is finite.

## The Catenoid ( $H = 0$ )

For the mean curvature we have

$$H(s) = \kappa_1(s) + \kappa_2(s) = -r''/h' + h'/r$$
$$\text{with } h'(s) = \sqrt{1 - r'(s)^2}.$$

Meusnier proved in 1776 that the Catenoid and the Helicoid are solutions of the minimal surface equation which was discovered by Lagrange. The Catenoid is the surface of revolution where the meridian curve is the rotated graph  $(\cosh(x), x)$ . Reparametrization to arclength parameter gives

$$r(s) = \sqrt{1 + s^2}, \quad h(s) = \sinh^{-1}(s)$$
$$r'(s) = s/\sqrt{1 + s^2}, \quad h'(s) = 1/\sqrt{1 + s^2}$$
$$r''(s) = (\sqrt{1 + s^2})^{-3},$$

which implies indeed  $H(s) = 0$ , so that the Catenoid is a complete minimal surface of revolution, in fact the only one.

## The Unduloid ( $H = 1$ )

The Unduloid is a surface of revolution of constant mean curvature  $H = 1$ . It was a crucial example for the development of the theory of constant mean curvature surfaces. See [The Unduloid](#).

# Explicit and Implicit Surfaces

Explicit versus Implicit Surfaces

Early Minimal Surfaces

## Elementary Surfaces

Paraboloid

Ellipsoid

More About Quadratic Surfaces, includes:

1-Sheeted Hyperboloid, 2-Sheeted Hyperboloid

Hyperbolic Paraboloid, Cylinders and Cones

About Ruled Surfaces, includes:

Helicoid, Right Conoid, Whitney Umbrella

View Principal Curvature Directions on:

Monkey Saddle, Torus, Dupin Cyclides

Play With Formulas Lissajous Surface,

Double Helix, Column, Norm 1 Family

Snail Shell Surfaces are Families of Circles

Untangle Double Twist In  $SO(3)$

Dirac Belt and Feynman Plate Tricks

Surfaces of Constant Width

## Stereographic Projections from $S^3$

Clifford Tori

Hopf-fibered Linked Tori

Bianchi - Pinkall Tori

## Nonorientable Surfaces

Möbius Strip and Klein Bottle

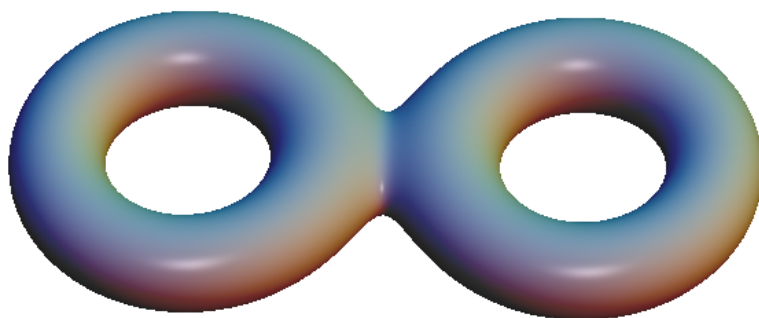
Cross-Cap and Steiner's Roman Surface

Boy Surfaces

Surface Organisation

# Explicit versus Implicit Surfaces,\*

## in particular Level Sets of Functions



Surfaces in  $\mathbb{R}^3$  are either described as *parametrized images*  $F : D^2 \rightarrow \mathbb{R}^3$  or as *implicit surfaces*, i.e., as levels of functions  $f : \mathbb{R}^3 \rightarrow \mathbb{R}$ , as the set of points where  $f$  has some given value, i.e.  $\{x \in \mathbb{R}^3; f(x) = \text{given}\}$ . *Graphs* of functions  $h : \mathbb{R}^2 \mapsto \mathbb{R}$  are both:  $F(u, v) := (u, v, h(u, v))$  is a *parametrization* and  $f(x, y, z) := h(x, y) - z$  is a level function,  $f = 0$  the *implicit equation*.

For most simple surfaces one has both representations, examples in 3DXM: *All Quadratic Surfaces, Tori, Cyclides, Cross-Cap, Steiner Surface, Algebraic Boy Surface, Whitney Umbrella*. In each case, the explicit and the implicit version open the same **Documentation**.

One can more easily make images of parametrized surfaces than of implicit surfaces, because every point  $p \in D$  can be mapped with the given function  $F$  to obtain ‘explicitly’ a point  $F(p)$  of the surface. Note however that the opposite problem: “Given a point in  $\mathbb{R}^3$ , decide whether it lies on the surface” does not have an easy answer. For an implicit

---

\* This file is from the 3D-XplorMath project. Please see:

surface, on the other hand, it is easy to decide whether a given point in  $\mathbb{R}^3$  is on the surface (simply check  $f(x)$ ), but no point is given explicitly, one has to use some algorithm to find points  $x \in \mathbb{R}^3$  which satisfy  $f(x) = \text{given value}$ .

Even after one has found many points on the surface, how does one connect them, what is a good way to represent the surface? The method of *raytracing* has been invented as one solution. Choose some center point  $C$ , think of it to be near the eyes of the viewer. Connect each pixel of the screen with  $C$  by a line and decide whether this line meets the surface. If it does then of all the intersection points on the line choose the one closest to  $C$ , compute the normal of the surface at this point  $x$  (i.e. compute  $\text{grad } f(x)$ ) and decide with this information what light (from fixed light sources) will be reflected by the surface at  $x$  towards  $C$ . Color that pixel accordingly. In this way one produces an image which presents the surface as if it were an illuminated object. The computation used to take very long, but todays computers do such pictures while you wait, but not quite fast enough for real time rotations. These pictures look very realistic, but of course they show only what is visible from the viewer, in particular: farther away parts of the surface can be hidden by nearer parts.

In 3D-XplorMath a second method is offered. Imagine that the surface is intersected with random lines until around 10 000 points have been found on the implicit surface. Then red-green stereo is used to project these points to the screen. When viewing through stereo glasses we see all these points

in the correct position in space and our brain interpolates them and lets us see a surface in space. This representation shows all parts of the surface (within some viewing sphere), not just the front most portions. Since one can achieve fairly uniform distributions of points on level surfaces, one sees many points in the direction towards *contours* of the surface. This emphasis of the contour points is so strong that one gets a fair impression of the surface even if one does not look through red-green glasses. This method is fast enough for real time rotations.

Once an implicit surface has been drawn, one has solved the problem of computing the 3D-data of surface points selected by mouse on the screen. One can therefore more easily move geometric attributes, like curvature circles, around on an implicit surface than on a parametrized surface. See in both cases the Action Menu entry **Move Principal Curvature Circles**.

What surfaces can one see?

In addition to the simple surfaces already mentioned we have two groups. *Algebraic Surfaces* which have been studied because of their *singularities*, these have established names and extensive literature. And *Compact Surfaces of higher genus*, these are added because such surfaces do not come with explicit parametrizations. (Their names are given in 3DXM and not known elsewhere.) Already fairly simple functions may have level surfaces which are more complicated than tori, they are called *bretzel surfaces* of genus  $g > 1$ .

How to find functions with compact levels of genus  $\geq 2$ . As an example, consider *two circles* of radius  $r = 1$ , in the  $x$ - $y$ -plane, with midpoints  $\pm cc$  on the  $x$ -axis. These two circles are described as the intersection of the  $x$ - $y$ -plane:  $\{g(x, y, z) := z = 0\}$  with the zero set of the function

$$h(x, y, z) := \frac{((x - cc)^2 + y^2 - 1) \cdot ((x + cc)^2 + y^2 - 1)}{1 + (1 + cc)(x^2 + y^2)}.$$

The denominator prevents the function from growing too fast, the weight factor  $1 + cc$  is experimental. Next define

$$f(x, y, z) := h(x, y, z)^2 + (1 + cc)g(x, y, z)^2.$$

Clearly, the zero set of  $f$  is the union of the two circles, which is *not* a surface, because  $\text{grad } f$  vanishes along this zero set. However, most of the levels  $\{(x, y, z); f(x, y, z) = v > 0\}$  are surfaces without singularities. If the two circles intersect ( $0 < cc < 1$ ), then for small  $v = ff$  the levels are the boundary of a thickening of the two circles, i.e., surfaces of genus 3. As  $ff$  increases either the middle hole or the two outside holes close first (depending on  $cc$ ). For large  $ff$  the level surfaces are (not completely round) spheres. Each time such a topological change occurs we observe one special surface, it is not smooth like the other levels, but has one or more cone like singularities.

If  $cc > 1$  then, for small  $ff$ , the levels are disjoint tori. As  $ff$  increases, either the tori grow together to a genus 2 surface, or the holes of the tori close first and later the two sphere-like surfaces grow together.

This family is called *Pretzel* in 3DXM.

## Functions with compact levels in 3D-XplorMath

One should always experiment with the level value  $v$  of the function  $f$ . In 3DXM:  $v = ff$ . For small values of  $ff$  one will see how the function was designed by guessing the degenerate level  $f = 0$ . The **Default Morph** often varies  $ff$ , for example showing non-singular levels converging to the singular one. In some cases other parameters are morphed, for example to get larger values of the genus  $g$ . Some cases offer: **Flow to Minimum Set**  $\{f = 0\}$  (see Action Menu). (Artificial looking denominators in the following prevent the function  $f$  from growing too fast.)

Note that the Action Menu has many decorations for implicit surfaces: Curvature line fields, net of curvature lines, normal curvature circles, geodesics with mouse chosen initial data, geodesic nets.

Pretzel: See page 5 of [Explicit versus Implicit Surfaces](#)  
The surface has genus 0,1,2 or 3, depending on parameter values.

$$f(x, y, z) := h(x, y, z)^2 + (1 + cc)z^2 \text{ with}$$
$$h(x, y, z) := \frac{((x - cc)^2 + y^2 - 1) \cdot ((x + cc)^2 + y^2 - 1))}{1 + (1 + cc)(x^2 + y^2)}$$

Bretzel2, a genus 2 tube around a figure 8, genus 0 for large  $ff$ :

$$f(x, y, z) := \frac{(((1 - x^2)x^2 - y^2)^2 + z^2/2)}{(1 + bb(x^2 + y^2 + z^2))}.$$

Bretzel5, a genus 5 tube around two intersecting ellipses:

$$f(x, y, z) := ((x^2 + y^2/4 - 1) \cdot (x^2/4 + y^2 - 1))^2 + z^2/2.$$

Pilz, a genus 3 tube around circle and orthogonal ellipse:

$$f(x, y, z) := ((x^2 + y^2 - 1)^2 + (z - 0.5)^2) \cdot (y^2/aa^2 + (z + cc)^2 - 1)^2 + x^2) - dd^2(1 + bb(z - 0.5)^2).$$

Default Morph:  $0.03 \leq cc \leq 0.83$ .

Orthocircles, a genus 5 tube around three intersecting orthogonal circles ( $aa = 1$ ,  $ff = 0.05$ ) or a tube around three Borromean ellipses ( $aa = 2.3$ ,  $ff = 0.2$ ) – choose in the Action Menu.

$$f(x, y, z) := ((x^2/aa + y^2 - 1)^2 + z^2) \cdot ((y^2/aa + z^2 - 1)^2 + x^2) \cdot ((z^2/aa + x^2 - 1)^2 + y^2).$$

Use: Flow to Minimum Set  $\{f = 0\}$  (from Action Menu).

DecoCube, tube around six circles of radius  $cc$  on the faces of a cube. Genus 5,13,17, depending on  $cc$ ,  $ff$ :

$$f(x, y, z) := ((x^2 + y^2 - cc^2)^2 + (z^2 - 1)^2) \cdot ((y^2 + z^2 - cc^2)^2 + (x^2 - 1)^2) \cdot ((z^2 + x^2 - cc^2)^2 + (y^2 - 1)^2).$$

Default Morph:  $ff = 0.02$ ,  $0.25 \leq cc \leq 1.3$ .

Use: Flow to Minimum Set  $\{f = 0\}$  (from Action Menu).

DecoTetrahedron has as its minimum set four circles on the faces of a tetrahedron. The formula is similar but more complicated than the previous one.  $cc$  changes the radius of the circles,  $bb$  changes their distance from the origin,  $ff$  selects the level. Use: Flow to Minimum Set to see the circles used for the current image.

The Default Morph changes  $cc$  and with it the genus.

JoinTwoTori is a genus 2 surface such that the connection between the two tori does not much distort them if  $ff$  is small. (It is used for genus-2-knots in Space Curves.)

$$Tor_{right} := ((x - cc)^2 + y^2 + z^2 - aa^2 - bb^2)^2 + 4aa^2(z^2 - bb^2)$$

$$Tor_{left} := ((x + cc)^2 + y^2 + z^2 - aa^2 - bb^2)^2 + 4aa^2(z^2 - bb^2)$$

$$f(x, y, z) := \frac{Tor_{right} \cdot Tor_{left}}{1 + (x - cc)^2 + (x + cc)^2 + y^2 + z^2/2}$$

The Default Morph:  $0.01 \leq ff \leq 2.5$  joins the tori.

### CubeOctahedron

The level surfaces of the function

$$f_{cube}(x, y, z) := \max(|x|, |y|, |z|) \quad \text{are cubes.}$$

The level surfaces of the function

$$f_{octa}(x, y, z) := |x| + |y| + |z| \quad \text{are octahedra.}$$

$\tilde{a} := \min(2 \cdot aa, 1)$ ,  $\tilde{b} := 2 \cdot \min(bb, 1)$ . These coefficients for the following linear combination allow an interesting morph.

$$f(x, y, z) := \max(\tilde{a} \cdot f_{octa}(x, y, z) + \tilde{b} \cdot f_{cube}(x, y, z)).$$

Default:  $aa = 0.5, bb = 1, ff = 1$ . This truncated cube is Archimedes' Cubeoctahedron.

Default Morph:  $aa = \frac{2}{3} \rightarrow \frac{1}{3}$ ,  $bb = 0.5 \rightarrow 1.5$ ,  $ff = 1$ .

This deformation from the octahedron to the cube passes through three Archimedean solids.

## Algebraic Functions with Singularities in 3DXM

CayleyCubic :

$$f(x, y, z) := 4(x^2 + y^2 + z^2) + 16xyz - 1, \quad ff = 0.$$

This cubic has 4 cone singularities at the vertices of a tetrahedron. The other surfaces in the Default *ff*-Morph are nonsingular.

ClebschCubic :

$$f(x, y, z) := 81(x^3 + y^3 + z^3) - 189(x^2(y + z) + y^2(z + x) + z^2(x + y)) + 54xyz + 126(xy + yz + zx) - 9(x^2 + x + y^2 + y + z^2 + z) + 1.$$

This cubic has no singularities but is famous for the 27 lines that lie on it. The lines are shown in 3DXM. The surface has tetrahedral symmetry.

DoublyPinchedCubic :

$$f(x, y, z) := z(x^2 + y^2) - x^2 + y^2.$$

This cubic has two pinch-point singularities at  $\pm 1$  on the *z*-axis. The segment between the singularities lies on it. The whole *z*-axis satisfies the equation; the Default Morph shows how an infinite spike converges to this line.

KummerQuartic :

$$\lambda := (3aa^2 - 1)/(3 - aa^2),$$
$$f(x, y, z) := (x^2 + y^2 + z^2 - aa^2)^2 - \lambda((1 - z)^2 - 2x^2)((1 + z)^2 - 2y^2), \quad aa = 1.3.$$

This quartic has 4+12 cone singularities and tetrahedral symmetry. Six noncompact pieces, each with two cone points, are connected by five compact pieces which look like curved tetrahedra. The singularities survive small changes, see the Default Morph :  $1.05 \leq aa \leq 1.5, ff = 0$ .

BarthSextic :

$$c_1 := (3 + \sqrt{5})/2, \quad c_2 := 2 + \sqrt{5}$$

$$f(x, y, z) :=$$

$$4(c_1x^2 - y^2)(c_1y^2 - z^2)(c_1z^2 - x^2) - c_2(x^2 + y^2 + z^2 - 1)^2.$$

Barth's Sextic has icosahedral symmetry. 20 tetrahedron-like compact pieces are placed over the vertices of a dodecahedron so that each tetrahedron has 3 of its vertices at midpoints of dodecahedron edges. This accounts for 30 of the cone singularities. Each of the 20 outward pointing vertices of the tetrahedra is connected via a cone singularity to a cone-like noncompact piece of the Sextic. The `Default Morph` embeds this singular surface in a family of nonsingular sextics. Use `Raytrace Rendering`.

D4 :

$$f(x, y, z) := 4x^3 + (aa - 3x)(x^2 + y^2) + bbz^2$$

This family of cubics has a  $D4$ -singularity. At  $bb = 0$  the family degenerates into three planes, intersecting along the  $z$ -axis.

UserDefined: Our example is the *Cayley Cubic*, see above.

H.K.

TOC

## Early Implicit Minimal Surfaces\*

See: [Helicoid-Catenoid](#) and [Scherk, Catalan, Henneberg Minimal Surfaces](#)

The early minimal surfaces have also implicit representations:

Catenoid:  $x^2 + y^2 - \cosh(z)^2 = 0$

Helicoid:  $x \cos(z) - y \sin(z) = 0$

Scherk 1-periodic:  $\sinh(x) \sinh(y) - \sin(z) = 0$

Scherk 2-periodic:  $\exp(z) \cos(x) - \cos(y) = 0$

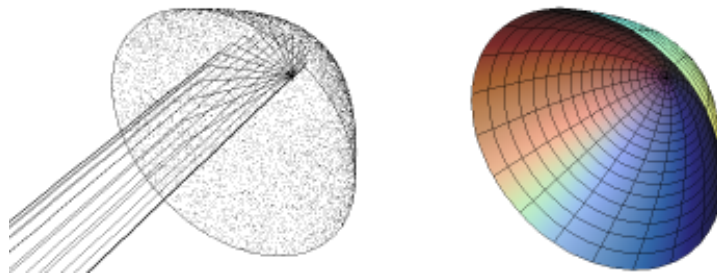
After the Weierstrass representation was discovered they were not much used – as far as we know. These implicit equations are much less close to the geometry of the surfaces than the Weierstrass representation: other levels of these functions are not minimal and the associate family cannot be obtained from this representation. Although the Gauss map at solution points of the equations is of course the gradient of the implicit function at the solution point (normalized to length 1), this does not give the Gauss map as a meromorphic function.

---

\* This file is from the 3D-XplorMath project. Please see:

## The Paraboloid \*

See in Documentation: About Quadratic Surfaces.



The Paraboloid in 3D-XplorMath is *parametrized* as

$$x = aa \cdot u \cdot \cos(v), \quad y = bb \cdot u \cdot \sin(v), \quad z = cc \cdot u^2 - dd,$$

with the default  $aa = bb = 1$ ,  $cc = 0.4$ ,  $dd = 2$ . It is given *implicitly* by  $f(x, y, z) := \frac{(z+dd)}{cc} - \left(\frac{x}{aa}\right)^2 - \left(\frac{y}{bb}\right)^2 = 0$ .

The paraboloid is shown together with a few rays parallel to the z-axis, the axis of revolution symmetry of this surface. These rays are reflected in the surface and continued until they meet in the focal point of this paraboloid. This image looks somewhat like the reflector of a car headlight together with the rays from the light bulb, reflected into parallel rays. The default Morph varies  $cc$  so that the image changes from a headlight reflector to a satellite antenna, with incoming parallel rays concentrated on the receiver at the focal point of the antenna.

The entry **Remove Focal Rays** in the Action Menu returns to the standard rendering for surfaces. Only in **Wireframe**

---

\* This file is from the 3D-XplorMath project. Please see:

Display can one switch on the focal rays in the Action Menu.

For geometric arguments concerning the focal point see: [Parabola](#) in the Plane Curve category.

H.K.

[TOC](#)

## The Ellipsoid\*

See in Documentation: About Quadratic Surfaces.

The Ellipsoid in 3D-XplorMath is *parametrized* as

$$x = aa \cdot \sin u \cdot \cos v, \quad y = bb \cdot \sin u \cdot \sin v, \quad z = cc \cdot \cos u,$$

with the default  $aa = bb = 1.5$ ,  $cc = 2.0$ . It is given by the

*Implicit Equation*

$$f(x, y, z) := (x/aa)^2 + (y/bb)^2 + (z/cc)^2 = 1.$$

In 3D-XplorMath the Ellipsoid is shown together with a few rays which leave one focal point, are reflected in the surface and come together again in the other focal point. This illustrates the use of the Ellipsoid as a *Whispering Gallery*. A whispering gallery may be realized by an Ellipsoid ceiling in a pub so that the conversations at one table can be heard at another table. Whispering galleries were also built in royal parks with some ellipsoid reflector near a table for visitors placed at one focal point and a hidden chair for the listener at the other focal point.

The first **default Morph** varies the size of the Ellipsoid. One can also select in the View Menu **Morph Light Source Of Rays** to illustrate that the rays do not come together at one point unless they start from a focal point.

---

\* This file is from the 3D-XplorMath project. Please see:

By selecting **Remove Focal Rays** in the Action Menu one returns to the standard rendering of surfaces. One may turn on the focal rays only if **Wireframe Display** is selected.

For geometric arguments concerning the focal points see: **Ellipse** in the **Plane Curve** category.

H.K.

[TOC](#)

## About Quadratic Surfaces \*

Quadratic surfaces in  $\mathbb{R}^3$  are the solution sets of quadratic equations (see: [Explicit versus Implicit Surfaces](#))

$$h(x, y, z) := Ax^2 + By^2 + Cz^2 + Dxy + Exz + Fyz \\ + Gx + Hy + Jz + K = 0.$$

*Explicit parametrizations* are given at the end.

There are poor examples, i.e.

with no solutions:  $x^2 + y^2 + z^2 + 1 = 0,$

solutions consisting of a point:  $x^2 + y^2 + z^2 = 0,$

or solution sets consisting of a line:  $x^2 + y^2 = 0,$

or solution sets like that of a linear function:  $x^2 = 0.$

But under mild assumptions, namely that the derivative of  $h$  does not vanish on (most of) the solution set, we get more interesting surfaces (possibly with singularities) as solution sets.

For products of linear functions we have intersections of (or parallel) planes:  $(x - y + a)(x \pm y + b) = 0,$  we may have cylinders over quadratic curves, e.g. if the equation does not contain  $z$ :

elliptic cylinder  $x^2 + y^2 - 1 = 0,$

hyperbolic cylinder  $x^2 - y^2 - 1 = 0,$

parabolic cylinder  $x^2 - y = 0.$

---

\* This file is from the 3D-XplorMath project. Please see:

There are various Cones, namely solution sets which contain for each solution  $(x, y, z) \neq (0, 0, 0)$  the whole line  $r \cdot (x, y, z), r \in \mathbb{R}$  through  $(0, 0, 0)$ . For example, if we intersect the previous cylinders with the plane  $z = 1$  and take the cone with vertex at  $(0, 0, 0)$  then these are described by the following (so called “homogenous”) equations.

Cones:  $x^2 + y^2 - z^2 = 0, x^2 - y^2 - z^2 = 0, x^2 - yz = 0.$

And finally we have the quadratic surfaces which have neither singular points nor are they cylinders:

Ellipsoids	$x^2/a^2 + y^2/b^2 + z^2/c^2 - 1 = 0,$
1-sheeted Hyperboloids	$x^2/a^2 + y^2/b^2 - z^2/c^2 - 1 = 0,$
2-sheeted Hyperboloids	$x^2/a^2 + y^2/b^2 - z^2/c^2 + 1 = 0,$
Elliptic Paraboloids	$x^2/a^2 + y^2/b^2 - z = 0,$
Hyperbolic Paraboloids	$x^2/a^2 - y^2/b^2 - z = 0.$

All other quadratic surfaces are obtained via coordinate transformations from these examples. Try the

**Experiment:** Select Implicit from the Surface Menu and type any quadratic equation into UserDefined. Compare the displayed surface with those described above. (Note that there may be no solutions.)

The 1-sheeted hyperboloids and the hyperbolic paraboloids have an unexpected special property, they carry two families of straight lines, see also: [About Ruled Surfaces](#).

The *hyperbolic paraboloid*:  $x^2 - y^2 - z = 0$  is cut by the parallel family  $x + y = const$  of planes in (disjoint) lines and also by the parallel planes  $x - y = const$ .

The *1-sheeted hyperboloid*:  $x^2 + y^2 - z^2 - 1 = 0$  is a surface

of revolution. Its tangent plane  $x = 1$  intersects it in the pair of orthogonal lines  $(y + z)(y - z) = 0$ ,  $x = 1$ . Rotation around the  $z$ -axis gives two families of lines on the surface. Each tangent plane cuts the surface in two lines, one from each family.

## Explicit parametrizations

Ellipsoid:

$$x = aa \cdot \sin u \cos v, \quad y = bb \cdot \sin u \sin v, \quad z = cc \cdot \cos u,$$

1-sheeted Hyperboloid:

$$x = aa \cosh u \cos v, \quad y = bb \cosh u \sin v, \quad z = cc \sinh u,$$

2-sheeted Hyperboloid (2nd sheet  $z \rightarrow -z$ ):

$$x = aa \sinh u \cos v, \quad y = bb \sinh u \sin v, \quad z = cc \cosh u,$$

Elliptic Paraboloid:

$$x = aa \cdot u \cos v, \quad y = bb \cdot u \sin v, \quad z = cc \cdot u^2,$$

Hyperbolic Paraboloid:

$$x = aa \cdot u, \quad y = bb \cdot v, \quad z = cc \cdot uv.$$

H.K.

TOC

## Ruled Surfaces \*

Cylinders, Cones, 1-sheeted Hyperboloid, Hyperbolic Paraboloid, Helicoid, Right Conoid, Whitney Umbrella.

*In other sections:* Double Helix, Möbius Strip.

Informally speaking, a **ruled surface** is one that is a union of straight lines (the rulings). To be more precise, it is a surface that can be represented parametrically in the form:

$$x(u, v) = \delta(u) + v * \lambda(u)$$

where  $\delta$  is a regular space curve (i.e.,  $\delta'$  never vanishes) called the **directrix** and  $\lambda$  is a smooth curve that does not pass through the origin. Without loss of generality, we can assume that  $|\lambda(t)| = 1$ . For each fixed  $u$  we get a line  $v \mapsto \delta(u) + v * \lambda(u)$  lying in the surface, and these are the rulings. (Some surfaces can be parameterized in the above form in two essentially different ways, and such surfaces are called **doubly-ruled surfaces**.)

A ruled surface is called a **cylinder** if the directrix lies in a plane  $P$  and  $\lambda(u)$  is a constant direction not parallel to  $P$ , and it is called a **cone** if all the rulings pass through a fixed point  $V$  (the vertex).

---

\* This file is from the 3D-XplorMath project. Please see:

Two more interesting examples are quadratic surfaces:

The **Hyperboloid of One Sheet:**

$$\frac{x^2}{a^2} + \frac{y^2}{b^2} - \frac{z^2}{c^2} = 1,$$

which is in fact doubly-ruled, since it can be given parametrically by:

$$x^+(u, v) = a(\cos(u) - v \sin(u)), b(\sin(u) + v \cos(u), cv)$$

and

$$x^-(u, v) = a(\cos(u) + v \sin(u)), b(\sin(u) - v \cos(u), -cv),$$

and the **Hyperbolic Paraboloid:**

$$(x, y, z) = (a u, b v, c u v) = a(u, 0, 0) + v(0, b, c u).$$

Another interesting ruled surface is a *minimal surface*:

the **Helicoid**,  $aa = 0$ , (Catenoid,  $aa = \pi/2$ ) in the family:

$$\begin{aligned} F(u, v) &= bb \sin(aa) (\cosh(v) \cos(u), \cosh(v) \sin(u), v) \\ &\quad + bb \cos(aa) (\sinh(v) \sin(u), -\sinh(v) \cos(u), u) \\ &= \sin(aa) ((0, 0, bb v) + bb \cosh(v) (\cos(u), \sin(u), 0)) \\ &\quad + \cos(aa) ((0, 0, bb u) + bb \sinh(v) (\sin(u), -\cos(u), 0)). \end{aligned}$$

A ruled surface is called a (generalized) **right conoid** if its rulings are parallel to some plane,  $P$ , and all pass through a line  $L$  that is orthogonal to  $P$ . *The Right Conoid* is given by taking  $P$  to be the  $xy$ -plane and  $L$  the  $z$ -axis:

*Parametrized:*  $F(u, v) = (v \cos u, v \sin u, 2 \sin u),$

*Implicitly:*  $\left(\frac{x}{y}\right)^2 - \frac{4}{z^2} = 1.$

This surface has at  $(\sin(u) = \pm 1, v = 0)$  two pinch point singularities. The **default morph** in 3DXM

deforms the **Right Conoid** to a **Helicoid**

so that the two stable pinch point singularities disappear, at the final moment, through two unstable singularities:

$F_{aa}(u, v) = (v \cos(u), v \sin(u), 2aa \sin(u) + (1 - aa)u).$

Famous for such a singularity is the **Whitney Umbrella**, another right conoid with rulings parallel to the  $x$ - $y$ -plane:

$F(u, v) = (u \cdot v, u, v \cdot v),$  *implicitly:*  $x^2 - y^2 z = 0.$

Again the **default morph** emphasizes the visualization of the singularity by embedding the **Whitney Umbrella** into a family of ruled surfaces, which develop a second pinch point singularity that closes the surface at the top:

$F_{aa}(u, v) = \begin{pmatrix} u \cdot (aa \cdot v + (1 - aa) \sin(\pi v)) \\ u \\ aa \cdot v^2 - (1 - aa) \cos(\pi v) \end{pmatrix}.$

## Monkey Saddle, Torus, Dupin Cyclide \*

The **Monkey Saddle** is a saddle shaped surface with *three* down valleys, allowing the two legs and the tail of the monkey to hang down. At its symmetry point both principal curvatures are 0, and, this umbilic point is the simplest singularity of a curvature line field. Choose in the Action Menu: Add Principal Curvature Fields; in Wireframe Display the parameter lines are omitted, the curvature line fields (or one of them) represent the surface.

Its *Parametrization* as graph of a function is

$$F_{Monkey}(u, v) = (aa \cdot v, bb \cdot u, cc \cdot (u^3 - 3uv^2)).$$

In Geometry the word **Torus** usually implies a surface of revolution; often a circle in the x-z-plane is rotated around the z-axis. In 3DXM an ellipse with axes *bb*, *cc* is rotated, its midpoint rotates in the x-y-plane on a circle of radius *aa*. The following *Parametrization* is used:

$$F_{Torus}(u, v) = \begin{pmatrix} (aa + bb \cdot \cos u) \cos v \\ (aa + bb \cdot \cos u) \sin v \\ cc \cdot \sin u \end{pmatrix}$$

Note that the parameter lines are principal curvature lines, see Action Menu: Add Principal Curvature Fields.

---

\* This file is from the 3D-XplorMath project. Please see:

The **Torus** is also visualized among the Implicit Surfaces, we derive its equation. In the x-z-plane we have two ellipses and we multiply their equations:

$$\begin{aligned} & \left( \left( \frac{x - aa}{bb} \right)^2 + \left( \frac{z}{cc} \right)^2 - 1 \right) \cdot \left( \left( \frac{x + aa}{bb} \right)^2 + \left( \frac{z}{cc} \right)^2 - 1 \right) \\ &= \left( \frac{x^2 - aa^2}{bb^2} \right)^2 + 2 \left( \frac{x^2 + aa^2}{bb^2} \right) \left( \left( \frac{z}{cc} \right)^2 - 1 \right) + \left( \left( \frac{z}{cc} \right)^2 - 1 \right)^2. \end{aligned}$$

For the rotation around the z-axis we have to replace x by  $r = \sqrt{x^2 + y^2}$ . The second expression avoids square roots.

*Implicit Equation of the **Torus**:*

$$f_{Torus}(\vec{x}) = f(r, z) = 0 \text{ with } r = \sqrt{x^2 + y^2} \quad \text{and}$$

$$f(r, z) :=$$

$$\left( \frac{r^2 - aa^2}{bb^2} \right)^2 + 2 \left( \frac{r^2 + aa^2}{bb^2} \right) \left( \left( \frac{z}{cc} \right)^2 - 1 \right) + \left( \left( \frac{z}{cc} \right)^2 - 1 \right)^2.$$

The **Cyclides of Dupin** are obtained by inverting the above torus in a sphere. The sphere of inversion has its center  $\vec{m} = (dd, 0, ee)$  in the x-z-plane and has radius  $ff$ . The **Default Morph** moves the center closer to the torus. Note that inversions map *curvature lines to curvature lines*.

$$\text{The Inversion: } \vec{x} \mapsto \text{Inv}(\vec{x}) := \frac{ff^2(\vec{x} - \vec{m})}{|\vec{x} - \vec{m}|^2} + \vec{m} + \begin{pmatrix} 0 \\ 0 \\ hh \end{pmatrix},$$

$$\text{Parametrization: } F_{Cyclide}(\vec{x}) := \text{Inv}(F_{Torus}(\vec{x})),$$

$$\text{Implicit Equation: } f_{Cyclide}(\vec{x}) := f_{Torus}(\text{Inv}^{-1}(\vec{x})) = 0.$$

## Lissajous, Double Helix, Column, Norm 1 Family \*

The French mathematician Jules Antoine Lissajous (1882-1880) studied vibrating objects by reflecting a spot of light of them, so that the various modes of vibration gave rise to *Lissajous curves*, see **Plane Curve Category**. Lissajous Space Curves and **Lissajous Surfaces** are a natural mathematical generalization. We use the *Parametrization*:

$$F_{Lissajous}(u, v) = \begin{pmatrix} \sin u \\ \sin v \\ \sin((dd - aa u - bb v)/cc) \end{pmatrix}.$$

The **Default Morph** joins a surface with tetrahedral symmetry and conical singularities and a surface with cubical symmetry and 12 pinch point singularities.

The **Double Helix** is a reminder of the famous double helix from genetics. For playing purposes there are two more parameters with default values  $dd = 0, ee = 0$ . We use the *parametrization*:

$$AA := aa + dd u, \quad \alpha := (1 - ee u)u,$$
$$F_{DblHelix}(u, v) = \begin{pmatrix} AA((1 - v) \cos \alpha + v \cos(\alpha + bb \pi)) \\ AA((1 - v) \sin \alpha + v \sin(\alpha + bb \pi)) \\ cc u - 3.5 \end{pmatrix}.$$

This is a family of *ruled surfaces*: try the **Default Morph**, it varies the limits of the parameter  $v$ . With  $bb = 1$  we get

---

\* This file is from the 3D-XplorMath project. Please see:

the Helicoid. The default parameters have been taken from Watson-Crick and give a reasonably good representation of molecular DNA. Dick Palais' biologist friend Chandler Fulton suggested the example and helped to get it right, many thanks.

We suggest to select **Move Principal Curvature Circles** from the Action Menu; this is seen best in **Point Cloud Display** from the View Menu.

**Column Surface** is used here in the sense of an architectural column, see the article by Marty Golubitzky and Ian Melbourne at

<http://www.mi.sanu.ac.rs/vismath/golub/index.html>

The order of the rotational symmetry around the z-axis is chosen with the 3DXM-parameter *ii*. Additional symmetry types can be selected with the parameter  $hh = 1, \dots, 6$ ; for other values of *hh* the unsymmetrized column shape is given by a formula that depends on the parameters  $aa, \dots, gg, ii$  and on the coordinates  $(\theta, z)$ . The formula is not determined by geometric properties, but is intended for playing.

The **Default Morph**, with  $hh = 0$ , varies the shape only mildly.

The **Norm 1 Family** is defined by the *implicit equation*:

$$f(x, y, z) = (|x|^p + |y|^p + |z|^p)^{1/p} = 1, \quad 0 < p < \infty.$$

We get at  $p = 1$  an *Octahedron*, at  $p = 2$  a *Sphere* and at  $p = \infty$  a *Cube*. For  $1 \leq p \leq \infty$  these surfaces can be

viewed as the unit sphere in  $\mathbb{R}^3$  for a Banach metric determined by  $p$ .

We *parametrize* these surfaces by spherical polar coordinates:

$$\begin{aligned}xp &:= \sin v \cos u, & yp &:= \sin v \sin u, & zp &:= \cos v, \\x &:= \text{sign}(xp)|xp|^e, & y &:= \text{sign}(yp)|yp|^e, & z &:= \text{sign}(zp)|zp|^e.\end{aligned}$$

To obtain a reasonable family we set the exponent  $e$  in terms of the `default morphing` parameter  $ee$  as follows:

$$e := 1 + \tan(ee), \quad -\pi/4 < ee < \pi/2.$$

We obtain the Sphere at  $ee = 0$ ,  
the Octahedron at  $ee = \pi/4$ .

Numerical reasons prevent computation at  $ee = -\pi/4$  (anyway a degenerate surface) and at  $ee = \pi/2$ , the Cube. Already where we stop the computation the Pascal-values of  $\sin$  near  $\pi$  had to be improved.

H.K.

TOC

## Snail Shell Surface \*

These snail-like surfaces are included for their entertaining shapes. Try making one of your own. In spite of their complicated appearance, the snail surfaces are constructed as *one-parameter families of circles*  $u \mapsto C_v(u)$ . First we introduce two auxiliary variables. The surface parameter  $v$  is changed by a quadratic term that permits closing the snails at the top. The parameter  $ee$  controls the size of the opening of the snail (default  $ee = -2$ ):

$$vv := v + (v + ee)^2/16.$$

The second variable controls the radius of the circles:

$$s := \exp(-cc \cdot vv). \quad (\text{Note that } s \text{ is a function of } v.)$$

The circles  $u \mapsto C_v(u)$  of radius  $s \cdot bb$  lie in an  $r$ - $y$ -plane:

$$r := s \cdot aa + s \cdot bb \cdot \cos(u),$$

$$y := dd(1 - s) + s \cdot bb \cdot \sin(u).$$

The parameter  $dd$  controls the length of the snail from top to bottom. And the other two coordinates in  $\mathbb{R}^3$  are

$$x := r \cos(vv),$$

$$z := r \sin(vv),$$

so that the plane of the circle  $C_v$  also rotates with  $v$ .

*Advice:* Make only **small** changes to  $cc$  and keep  $bb \geq aa$ .

The **Default Morph** varies  $dd$  and adjusts  $bb$  a little.

T.K.

TOC

---

\* This file is from the 3D-XplorMath project. Please see:

## Untangle Double Twist In $SO(3)$ \*

The goal of this animation is first to visualize closed curves in  $SO(3)$  and then morph these closed curves to visualize homotopies. While a full rotation around a fixed axis is a nontrivial loop in  $SO(3)$ , doing it twice is a nullhomotopic loop. It was made famous outside mathematics by Dirac's belt trick and Feynman's plate trick.

Bob Palais has two descriptions of the homotopy in  $SO(3)$  which are much simpler than to look at a 2-parameter family of orthogonal matrices:

(a) A rotation with axis vector  $\vec{a}$  and rotation angle  $\varphi$  can be obtained as composition of two  $180^\circ$  rotations around axes  $\vec{b}, \vec{c} \perp \vec{a}$  with  $\text{angle}(\vec{b}, \vec{c}) = \varphi/2$ . To get the double twist around the z-axis (the loop of the above tricks) choose

$$\vec{b} := (1, 0, 0), \quad \vec{c}(s) := (\sin(s), \cos(s), 0), \quad 0 \leq s \leq 2\pi.$$

It is obvious how to homotop the equator  $s \mapsto \vec{c}(s)$  into the point loop  $\vec{b}$ , hence homotop the double twist into id.

(b) A homotopy from one full twist to its inverse is given by rotating the axis vector to its negative - simple enough. Composition of this homotopy with the chosen full twist is a homotopy from a double twist to the id-loop.

In other words, the challenge is not to formulate such a homotopy, but to visualize it. And, again, the challenge is to visualize a loop in  $SO(3)$ , because a homotopy is simply a time dependent morph of a loop.

---

\* This file is from the 3D-XplorMath project. Please see:

Let  $A(s) \in SO(3)$  be a loop of rotations with  $A(0) = \text{id} = A(1)$ . Consider a family of concentric spheres. They should really be all the same spheres, but we use the radius parameter similar to the graph representation of a 1-dimensional function. Draw a spherical polygon  $P$  on the innermost sphere of radius 1. Then draw the spherical polygons  $A(s)P$  on the spheres of radius  $1 + s$ . By following the position of the moving spherical polygon as  $s$  increases, one gets a good impression of the family  $A(s)$  of rotations.

We use two opposite spherical polygons instead of one, to emphasize the fixed innermost sphere.

The default morph  $0 \leq aa \leq 1$  unwraps the double twist, of course keeping the endpoints fixed.

The morph  $0 \leq bb \leq 1$  with  $aa = 0$  creates the double twist around the z-axis (a loop only if  $bb = 1$ ).

The circum radius of the spherical polygons is  $cc$ .

One can choose with  $dd \in \{3, 4, 5, 6\}$  the number of vertices of the spherical polygon ( $dd = 5.2$  is a pentagon star).

In the Action Menu is an entry intended for this demo:

**Reflect tube in ImagePlaneYdirection**

This allows to change the position of the spherical polygon. The default position is around the z-axis. Moving it away from the axis towards the equator creates rather different images of the same family  $A(s)$  of rotations. Clicking this entry a second time returns to the original position - unless one has rotated the object with the mouse.

H.K.

**TOC**

## Dirac Belt and Feynman Plate Tricks \*

Dirac invented the famous belt trick to demonstrate a property of the motions of Euclidean Space that is indeed difficult to imagine without visual help.

The trick is performed with a strip, or belt, that is initially parallel to the screen. The orthogonal projection of the performance looks as follows: The left end of the belt stays fixed, the right end moves around the left end in a circular motion. It is important that the moving end **stays parallel** to the fixed end through the whole trick (parallel means: the final edge and the final normal each stay parallel to the initial edge and initial normal). One observes with surprise:

*After moving the right end once around the circle the belt is twisted twice. After the second circular move the belt is untwisted (as it was initially).*

The trick is shown in stereo because it is impossible that the belt stays in its initial plane when the ends are moved as described. It is important to visualize how the different parts of the belt move **vertically** to the screen.

It will be no surprise to observe that the first circular movement – when looked at in 3D – is different from the second circular movement. During the first circular movement the

---

\* This file is from the 3D-XplorMath project. Please see:

middle part of the belt moves vertically to be **in front** of the screen while the two ends stay on the screen. During the second circular movement it is the other way round: the middle part of the belt moves vertically to be **behind** the screen while the ends continue to be at their fixed vertical position. As soon as one can fix this image in one's mind it is obvious how the circular motion with parallel ends produces the twist of the belt.

Another instance of the same property of the Group of Euclidean motions is the **Feynman Plate Trick** or *Waiter's Cup Trick* : It is possible to continuously rotate a cup on ones horizontal hand in the **same** direction if during the first rotation the hand is above elbow height, during the second rotation below elbow height and so on, alternatingly above and below elbow height. Namely, imagine that the shoulder is the fixed end of the belt and the always horizontal – but continuously rotating – middle part of the belt is the hand. Choose **Do Plate Trick** from the Animation Menu to see half the belt performing the trick.

Some people cannot believe what they see. In such a case one can switch to **Monocular Vision** and **Orthographic Projection** in the View Menu to watch the belt – without at all observing the motion vertical to the screen. Or try **Patch Display** for a solid belt.

B.P.

TOC

## Surfaces of Constant Width\*

The name of these surfaces derives from the fact that the distance between opposite parallel tangent planes is constant. See first: **Convex Curve** in the planar curve category. There the default curve and the default morph show curves of constant width and the **ATO: On Curves Given By Their Support Function** explains how they are made. Our surfaces of constant width are also described via their

Support Function  $h : \mathbb{S}^2 \mapsto \mathbb{R}$  as:

$$F(x, y, z) := h(x, y, z) \cdot \begin{pmatrix} x \\ y \\ z \end{pmatrix} + \text{grad}_{\mathbb{S}^2} h(x, y, z),$$
$$h(x, y, z) := aa + bb z^3 + cc xy^2 + dd yz^2 + ee xz^2 + ff xyz + gg xy^2 z^2 > 0,$$

where  $x^2 + y^2 + z^2 = 1$ .

The constant  $aa$  has to be chosen large enough so that  $h(x, y, z) > 0$ . The default values are  $aa = 1$ ,  $ff = 0.66$ , all others = 0, for tetrahedral symmetry. With just  $aa, bb > 0$  one gets surfaces of revolution, with  $aa, cc \neq 0$  the surfaces have  $120^\circ$  dihedral symmetry. Note that  $gg$  is the only coefficient of a polynomial of degree 5.

Let  $c(t) = (x, y, z)(t)$  be a curve on  $\mathbb{S}^2$ . One computes with

---

\* This file is from the 3D-XplorMath project. Please see:

$\vec{n} := (x, y, z)^t$  that  $\frac{d}{dt}F(x, y, z)(t) \perp \vec{n}$ , so that  $\vec{n}(x, y, z)$  is the normal of the surface parametrized by  $F$ . Therefore  $h(x, y, z)$  is indeed the distance of the tangent plane at  $F(x, y, z)$  from the origin. The origin is inside the surface because  $h > 0$ . All terms defining  $h$ , except the constant  $aa$ , are odd. This gives  $h(x, y, z) + h(-x, -y, -z) = 2 \cdot aa$  and this is the distance between opposite tangent planes, i.e. the constant width.

Finally we compute the normal curvature, more precisely the Weingarten map  $S$ .

$$\begin{aligned} \frac{d}{dt}\vec{n}(t) &= \dot{c}(t) =: S \cdot \frac{d}{dt}F(c(t)) \\ \frac{d}{dt}F(x, y, z)(t) &= \langle \text{grad}_{\mathbb{S}^2} h, \dot{c}(t) \rangle c(t) + h \cdot \dot{c}(t) \\ &\quad + d_{\dot{c}(t)} \text{grad}_{\mathbb{S}^2} h \\ &= h \cdot \dot{c}(t) + (d_{\dot{c}(t)} \text{grad}_{\mathbb{S}^2} h)^{\text{tangential}} \\ &= h \cdot \dot{c}(t) + D_{\dot{c}(t)} \text{grad}_{\mathbb{S}^2} h, \end{aligned}$$

where  $D_{\dot{c}}$ , the tangential component of the Euclidean derivative  $d_{\dot{c}(t)}$ , is the covariant derivative of  $\mathbb{S}^2$ . We thus obtain the Weingarten map  $S$  of the surface, computed in the domain  $\mathbb{S}^2$  of  $F$ :

$$\frac{d}{dt}\vec{n}(t) = (h \cdot \text{id} + D \text{grad}_{\mathbb{S}^2} h)^{-1} \cdot \frac{d}{dt}F(c(t)) = S \cdot \frac{d}{dt}F(c(t)).$$

## Clifford Tori \*

a) *Parametrized by Curvature Lines*, b) *Hopf-fibered*

**Clifford Tori** are embeddings of the torus into the unit sphere  $\mathbb{S}^3$  of  $\mathbb{R}^4$ , by  $(u, v) \rightarrow F(u, v) := (w, x, y, z)$ , where

$$F_{\text{Clifford}}(u, v) = \begin{pmatrix} w \\ x \\ y \\ z \end{pmatrix}(u, v) = \begin{pmatrix} \cos \alpha \cos u \\ \cos \alpha \sin u \\ \sin \alpha \cos v \\ \sin \alpha \sin v \end{pmatrix}$$

$\alpha := aa + bb \sin(ee \cdot 2v)$ ,  $bb \neq 0$  for Bianchi-Pinkall Tori.

(Note that this is, for  $bb = 0$ , the product of a circle in the  $(w, x)$  plane with a second circle in the  $(y, z)$  plane, and so is clearly flat.) To get something that we can see in  $\mathbb{R}^3$ , we stereographically project  $\mathbb{S}^3 \mapsto \mathbb{R}^3$ ; i.e., the Clifford tori in  $\mathbb{R}^3$  are the embeddings  $(u, v) \rightarrow P(F(u, v))$ , where  $P: \mathbb{S}^3 \rightarrow \mathbb{R}^3$  is **Stereographic** projection.

We take as the center of the stereographic projection map the point  $(\cos(cc\pi), 0, \sin(cc\pi), 0)$ . Varying  $cc$  deforms a torus of revolution through cyclides. The **Default Morph** varies  $aa$ , hence changes the ratio of the two circles.

Another morph, **Conformal Inside-Out Morph** (also in the Animation Menu), is in  $\mathbb{R}^4$  a rotation (parametrized by  $0 \leq ff \leq 2\pi$ ), that moves the torus through the center of the stereographic projection. The image in  $\mathbb{R}^3$  therefore passes through infinity: we see a torus with one puncture that has a flat end. It looks like a plane with a handle.

---

\* This file is from the 3D-XplorMath project. Please see:

The Clifford tori (in  $\mathbb{S}^3$ ) are fibered by *Great Circles*, the Hopf fibers,  $u + v = \text{const}$ . These Great Circles are of course the *asymptote lines* on the tori. We show two versions of the stereographically projected Clifford tori: a) parameterized by curvature lines and b) by Hopf fibers. (To get the explicit parametrization of the latter, take  $F(u + v, u - v)$  in the above formulae.)

The classical Clifford Torus corresponds to  $\alpha = aa = \pi/4$ . It has maximal area among the family and divides  $\mathbb{S}^3$  into two congruent solid tori. But the other torus-leaves of the foliation, obtained by varying  $aa$ , are also interesting. All of them are foliated by *Clifford-parallel* great circles and hence flat. They are special cases of the flat Bianchi-Pinkall Tori in  $\mathbb{S}^3$  (visible after stereographic projection) and discussed in more detail in their ATO (“About This Object...”), see the Documentation Menu.

Why is the  $ff$ -morph a **Conformal Inside-Out Morph**? A compact surface divides  $\mathbb{R}^3$  in two components and the bounded component is called the inside. One surface of the family, the once punctured torus that passes through infinity, divides  $\mathbb{R}^3$  into two congruent unbounded components. This surface has no inside and at this moment in the deformation inside and outside are interchanged. The 180 degree rotation in the rotation family is, on the  $\pi/4$ -torus, a conformal anti-involution. It has a Hopf fiber as connected fixed point set. Use in the Action Menu **Surface Coloration** and choose the default **two-sided user coloration** which emphasizes the fixed fiber.

# Hopf Fibration and Clifford Translation \*

## of the 3-sphere

See [Clifford Tori](#)

Most rotations of the 3-dimensional sphere  $\mathbb{S}^3$  are quite different from what we might expect from familiarity with 2-sphere rotations. To begin with, most of them have no fixed points, and in fact, certain 1-parameter subgroups of rotations of  $\mathbb{S}^3$  resemble *translations* so much, that they are referred to as *Clifford translations*. The description by formulas looks nicer in complex notation. For this we identify  $\mathbb{R}^2$  with  $\mathbb{C}$ , as usual, and multiplication by  $\mathbf{i}$  in  $\mathbb{C}$  represented in  $\mathbb{R}^2$  by matrix multiplication by  $\begin{pmatrix} 0 & -1 \\ 1 & 0 \end{pmatrix}$ .

Then the unit sphere  $\mathbb{S}^3$  in  $\mathbb{R}^4$  is given by:

$$\begin{aligned} \mathbb{S}^3 &:= \{p = (z_1, z_2) \in \mathbb{C}^2; |z_1|^2 + |z_2|^2 = 1\} \\ &\sim \{(x_1, x_2, x_3, x_4) \in \mathbb{R}^4; \sum (x_k)^2 = 1\}. \end{aligned}$$

And for  $\varphi \in \mathbb{R}$  we define the Clifford Translation  $C_\varphi : \mathbb{S}^3 \rightarrow \mathbb{S}^3$  by  $C_\varphi(z_1, z_2) := (e^{\mathbf{i}\varphi} z_1, e^{\mathbf{i}\varphi} z_2)$ .

The orbits of the one-parameter group  $C_\varphi$  are all great circles, and they are equidistant from each other in analogy

---

\* This file is from the 3D-XplorMath project. Please see:

to a family of parallel lines; it is because of this behaviour that the  $C_\varphi$  are called Clifford translations.

But in another respect the behaviour of the  $C_\varphi$  is quite different from a translation – so different that it is difficult to imagine in  $\mathbb{R}^3$ . At each point  $p \in \mathbb{S}^3$  we have one 2-dimensional subspace of the tangent space of  $\mathbb{S}^3$  which is orthogonal to the great circle orbit through  $p$ . A Euclidean translation would simply translate these normal spaces into each other, but a Clifford translation rotates them so that the velocity of the translation along the orbit is equal to the angular velocity of the rotation of the normal spaces. This normal rotation is responsible for a very curious fact which is illustrated by the image in 3DXM:

*Any two orbits are linked !*

The fact that any two orbits are equidistant permits us to make the set of orbits into a metric space., and one can check that this space is isometric to the sphere of radius one-half in  $\mathbb{R}^3$ . Therefore one can map  $h : \mathbb{S}^3 \rightarrow \mathbb{S}^2$  by mapping  $p \in \mathbb{S}^3$  to its orbit, identified as a point of  $\mathbb{S}^2$ , and one can write this mapping in coordinates as:

$$h(z_1, z_2) = (|z_1|^2 - |z_2|^2, \operatorname{Re}(z_1 z_2), \operatorname{Im}(z_1 z_2))$$

This map  $h$  is called the *Hopf map* (or Hopf Fibration), and the orbits, the fibres of this map, are called *Hopf fibres*. It is named for Heinz Hopf, who studied it in detail, and

found the completely unexpected fact that this map could not be deformed to a constant map.

The visualization in 3D-XplorMath shows *four tori each of which is made up of Hopf fibres*. We emphasize this with the coloration: each fibre has a constant colour and the colour varies with the distance of the fibres. One can see that any two of the four tori are linked, and one can also see that any two fibres on any one such torus are linked. Since 3D-XplorMath visualizes objects in  $\mathbb{R}^3$ , not in  $\mathbb{S}^3$ , before rendering the tori, we first map them into  $\mathbb{R}^3$  using the following stereographic projection  $\mathbb{S}^3 \rightarrow \mathbb{R}^3$

‘T13’:

$$(x_1, x_2, x_3, x_4) \rightarrow (x_1, x_2, x_3)/(1 + x_4).$$

The use of morphing parameters:

The three cyclide-tori are made from the torus of revolution by *quaternion multiplication* in  $\mathbb{S}^3$  with

$$Qt2 = (\cos ee, 0, \sin ee \sin bb, \sin ee \cos bb),$$

$$Qt3 = (\cos ff \cos cc, \sin ff, 0, \cos ff \sin cc),$$

$$Qt4 = (\cos gg, 0, \sin gg \cos dd, \sin gg \sin dd).$$

One can therefore morph the first cyclide with the parameters  $bb, ee$ , the second with  $cc, ff$  and the third with  $dd, gg$ . The **Default Morph** changes the first two cyclides slightly while the third one performs a full rotation in  $\mathbb{S}^3$  which moves it in  $\mathbb{R}^3$  from its initial position through the torus of revolution and continues back to the initial position.

## Bianchi-Pinkall Flat Tori in $\mathbb{S}^3$ \*

See ‘[Clifford](#)’ and [Hopf-fibered Linked Tori](#) first.

### 1. Parameter Dependent Formulas in 3DXM

We can parametrize  $\mathbb{S}^3$ , considered as a submanifold of  $\mathbb{C}^2$ , by:

$$F(u, \alpha, v) = (\cos(\alpha)e^{iu}e^{iv}, \sin(\alpha)e^{iu}e^{-iv}),$$

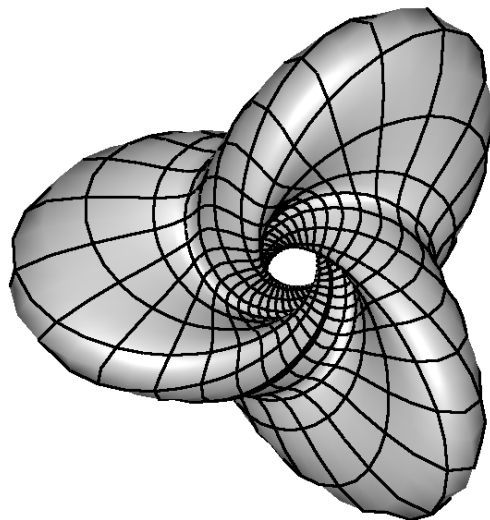
where  $u \in [0, 2\pi)$ ,  $\alpha \in [0, \pi/2]$ , and  $v \in [0, \pi]$ . We will get the **Bianchi-Pinkall Tori** first as *flat tori* in  $\mathbb{S}^3$  by taking  $\alpha$  to be a function of  $v$ ,

$$\alpha := aa + bb \sin(ee \cdot 2v)$$

(although the theory allows more general choices.) Next we *stereographically project*  $\mathbb{S}^3$  from

$$p = (\cos(cc \cdot \pi), 0, \sin(cc \cdot \pi), 0)$$

to get **conformal** images of the flat tori in  $\mathbb{S}^3$ . The lines  $v = \text{const}$  are circles, the stereographic images of the Hopf circles  $u \mapsto F(u, \alpha, v)$ .



---

\* This file is from the 3D-XplorMath project. Please see:

The `Default Morph` chooses  $ee = 5$  and changes the amplitude  $bb$  thus increasing the five 'ears' of the torus. The `Range Morph` starts with a narrow band between two Hopf circles and widenes this band to the complete surface. Finally, the `Conformal Inside-Out Morph`,  $0 \leq ff \leq 2\pi$ , isometrically rotates  $\mathbb{S}^3$  so that the Hopf circle  $v = 0$  is the rotation axis. The stereographic image of this rotation is a conformal transformation of  $\mathbb{R}^3 \cup \{\infty\}$  which "rotates"  $\mathbb{R}^3$  around a circle on the pictured torus. In the case  $aa = \pi/4$  we obtain for  $ff = 0$  and  $ff = \pi$  the same torus, but inside and outside interchanged. This is best viewed with the default `Two Sided User Coloration`, selectable from the `Surface Coloration` Submenu of the Action Menu.

## 2. Background and Explanations

The tori that we usually see are, from the point of view of complex analysis, rectangular tori, meaning that they have an orientation reversing symmetry and the set of fixed points of this symmetry has two components. (The better known tori of revolution have isometric reflections with **two** circles as fixed point sets.) Of course one tries to deform these tori to obtain non-rectangular ones. Obviously one can destroy the mirror symmetry, but this does not imply that one gets tori with a non-rectangular complex structure. The first proof, by Garcia, that one can embed all tori in  $\mathbb{R}^3$  was non-constructive and difficult.

A simpler and constructive way to get tori with arbitrary

conformal type was found by Pinkall, whose idea was to construct tori that are flat in  $\mathbb{S}^3$  (and hence have an easy way to compute their conformal type from their flat geometry), and then stereographically project them to  $\mathbb{R}^3$ . While the resulting tori are no longer flat, this does preserve their conformal type.

The construction of flat surfaces in  $\mathbb{S}^3$  goes back to 1894, when Bianchi classified all flat immersions in  $\mathbb{S}^3$ . In particular, he realized that the two families of asymptotic lines of a flat surface in  $\mathbb{S}^3$  are left translations of a pair of curves that are either great circles or have constant torsion  $+1$  and  $-1$ , respectively. The left translations arise by viewing  $\mathbb{S}^3$  as the group of unit quaternions. An open problem for Bianchi was to determine when his flat surfaces were closed.

The first case when one of the curves is a great circle is of special interest for this problem. To explain why, we will need the Hopf fibration. Thinking of  $\mathbb{S}^3$  as being part of  $\mathbb{C}^2$ , we can multiply points of  $\mathbb{S}^3$  by  $e^{iu}$ , thus fibering  $\mathbb{S}^3$  with circles, the Hopf circles, and the set of all such circles forms a metric space with distance being the distance between the Hopf circles in  $\mathbb{S}^3$ . As such it is isometric to a 2-dimensional sphere of radius  $1/2$ . We thus obtain a natural projection  $\mathbb{S}^3 \rightarrow \mathbb{S}^2$ , the Hopf map. It can be written as  $(z_1, z_2) \mapsto z_1/z_2$ , where we interpret the range as the Riemann sphere  $\hat{\mathbb{C}}$ . Moreover, Hopf circles are mapped to Hopf circles by left translations.

Now suppose we have a flat surface in  $\mathbb{S}^3$  where one of the generating curves is a great circle. We can arrange  $\mathbb{S}^3$  so that this great circle is part of the Hopf fibration, and thus all curves of the same family of asymptotic lines are Hopf circles. The surface in  $\mathbb{S}^3$  is thus invariant under the Hopf action and projects to a curve in  $\mathbb{S}^2$  under the Hopf map. Vice versa, the preimage of a curve in  $\mathbb{S}^2$  under the Hopf map yields a flat surface in  $\mathbb{S}^3$ . In case the curve in  $\mathbb{S}^2$  is closed, the surface in  $\mathbb{S}^3$  is a flat torus. (The explanation so far is described in more detail in Spivak IV, p. 139ff.)

Pinkall found a simple way to determine the conformal type of the flat torus in terms of the geometry of the curve in  $\mathbb{S}^2$  — in particular it was then easy to see that **all** possible conformal types can occur.

### 3. Visualizing Parts of the Theoretic Description

We cannot visualize  $\mathbb{S}^3$  in such a way that all distances are preserved. We will use stereographic projection from  $p = (\cos(cc \cdot \pi), 0, \sin(cc \cdot \pi), 0)$  to map  $\mathbb{S}^3 - \{p\}$  one-to-one onto  $\mathbb{R}^3$ . Recall that: angles are not changed by stereographic projection, circles are mapped to circles or straight lines, and the images of great circles meet the equator sphere in antipodal points, so many properties of  $\mathbb{S}^3$  get represented in geometrically comprehensible ways.

Our parametrization  $F$  of  $\mathbb{S}^3$  emphasizes the Hopf fibration since the great circles  $u \mapsto F(u, \alpha, v)$  are indeed the orbits of the Hopf-action of  $\mathbb{S}^1$  on  $\mathbb{S}^3$ , given by  $(u, p) \mapsto e^{iu}p$ . Each such “Hopf Fiber” lies in one of the parallel tori  $\alpha =$

constant, and the great circles  $\alpha \mapsto F(u, \alpha, v)$ , meet these ( $\alpha = \text{constant}$ )-tori orthogonally, so that  $\alpha$  measures the distance between them.

We get all the Hopf circles on each  $\alpha$ -torus for  $0 \leq v \leq \pi$ , except that those tori degenerate to just one Hopf circle if  $\alpha = 0$  or  $\alpha = \pi$ . This makes it plausible that  $(\alpha, 2v)$  are polar coordinates on the metric space of Hopf circles, on the image  $\mathbb{S}^2$  of the Hopf map.

Pinkall has observed that the closed curves on this image sphere, in polar coordinates given as:  $(\alpha(s), 2v(s))$ , (with  $\alpha(s)$  never equal to 0 or  $\pi/2$ ) allow one to write down immersed tori in  $\mathbb{S}^3$  as:

$$(u, s) \mapsto (F(u, \alpha(s), v(s))).$$

For example taking  $\alpha(s) = \pi/4$  gives the “Clifford Torus” in  $\mathbb{S}^3$ , a minimal embedding of the square torus. For other constant  $\alpha(s)$  in  $(0, \pi/2)$  one gets the above parallel family of  $\alpha$ -tori, the lengths of their two orthogonal generators are  $2\pi \cos(\alpha)$  and  $2\pi \sin(\alpha)$ .

On all of these tori we still have that the parameter lines  $s = \text{constant}$  are Hopf-Fibers, and since these are equidistant (as orbits of an isometric action) it follows that the metric is flat. Pinkall proved that length and area of the curve in  $\mathbb{S}^2$  determine the conformal structure of the torus in  $\mathbb{S}^3$ , hence in  $\mathbb{R}^3$ , and that all conformal structures occur.

Observe that the usual tori of revolution in  $\mathbb{R}^3$  are all rectangular, and most of the Bianchi-Pinkall tori shown by 3D-XplorMath are very different from these. The tori

with  $aa = \pi/4$  are all rhombic, because they can be rotated into themselves by  $180^\circ$  rotations (in  $\mathbb{S}^3$ , not in  $\mathbb{R}^3$ ) around any of the Hopf-Fibers on them. A cyclic morph with  $0 \leq ff \leq 2\pi$  rotates around the circle  $v = 0$  (we see of course the stereographic image of that rotation). For  $ff = \pi$  we get an anti-involution of the torus with the circle as the (connected) fixed point set—only rhombic tori have such anti-involutions. (The square torus is rectangular and rhombic.) In the rhombic case  $aa = \pi/4$  we get for  $ff = \pi/2$  and  $ff = 3\pi/2$  surfaces in  $\mathbb{S}^3$  that pass through  $p$  so that the stereographic images in  $\mathbb{R}^3$  pass through  $\infty$ —otherwise we could not turn the torus inside out continuously.

The program takes  $\alpha(v) := aa + bb \sin(ee 2v)$  (with  $ee = 3$  for the default image and  $ee = 5$  for the default morph), allowing rather different examples.

Again, these tori are shown in  $\mathbb{R}^3$  by using the (conformal) stereographic projection of  $\mathbb{S}^3 \setminus \{p\} \rightarrow \mathbb{R}^3$ , where  $p = (\cos(cc \cdot \pi), 0, \sin(cc \cdot \pi), 0)$ . Morphing  $cc$  therefore gives other images of  $\mathbb{S}^3$ , in particular other conformal images of these tori.

H.K.

TOC

## Möbius Strip and Klein Bottle \*

Other non-orientable surfaces in 3DXM:

Cross-Cap, Steiner Surface, Boy Surfaces.

The **Möbius Strip** is the simplest of the non-orientable surfaces. On all others one can find Möbius Strips. In 3DXM we show a family with  $ff$  halftwists (non-orientable for odd  $ff$ ,  $ff = 1$  the standard strip). All of them are *ruled surfaces*, their lines rotate around a central circle.

Möbius Strip *Parametrization*:

$$F_{Möbius}(u, v) = \begin{pmatrix} aa(\cos(v) + u \cos(ff \cdot v/2) \cos(v)) \\ aa(\sin(v) + u \cos(ff \cdot v/2) \sin(v)) \\ aa u \sin(ff \cdot v/2) \end{pmatrix}.$$

Try from the View Menu: **Distinguish Sides By Color**. You will see that the sides are not distinguished—because there is only one: follow the band around.

We construct a **Klein Bottle** by curving the rulings of the Möbius Strip into figure eight curves, see the Klein Bottle *Parametrization* below and its **Range Morph** in 3DXM.

$$w = ff \cdot v/2$$

$$F_{Klein}(u, v) = \begin{pmatrix} (aa + \cos w \sin u - \sin w \sin 2u) \cos v \\ (aa + \cos w \sin u - \sin w \sin 2u) \sin v \\ \sin w \sin u + \cos w \sin 2u \end{pmatrix}.$$

---

\* This file is from the 3D-XplorMath project. Please see:

There are *three different Klein Bottles* which cannot be deformed into each other through immersions. The best known one has a reflectional symmetry and looks like a weird bottle. See formulas at the end. The other two are mirror images of each other. Along the central circle one of them is left-rotating the other right-rotating. See the **Default Morph** of the *Möbius Strip* or of the *Klein Bottle*: both morphs connect a left-rotating to a right-rotating surface.

On the *Boy Surface* one can see different Möbius Strips. The **Default Morph** begins with an equator band which is a Möbius Strip with *three halftwists*. As the strip widens during the deformation it first passes through the triple intersection point and at the end closes the surfaces with a disk around the center of the polar coordinates.

Moreover, each meridian is the centerline of an *ordinary Möbius Strip*. Our second morph, the **Range Morph**, rotates a meridian band around the polar center and covers the surface with embedded Möbius Strips. - We suggest to also view these morphs using **Distinguish Sides By Color** from the View Menu.

On the *Steiner Surface* and the *Cross-Cap* the Möbius Strips have self-intersections and are therefore more difficult to see. The **Default Morph** for the *Steiner Surface* emphasizes this unusual Möbius Strip. - The **Range Morph** of the *Cross-Cap* shows a family of embedded disks, except at the last moment, when opposite points of the boundary are identified, covering the self-intersection segment twice.

The construction of the mirror symmetric Klein bottle starts from a planar loop with parallel, touching ends and zero velocity at the ends (see the default morph):

$$\begin{aligned}
 cx(u) &= -cc \cdot \cos(u), & 0 \leq u \leq 2\pi \\
 cy(u) &= ee \cdot \sin(u^3/\pi^2), & 0 \leq u \leq \pi \\
 cy(u) &= ee \cdot \sin((2\pi - u)^3/\pi^2), & \pi \leq u \leq 2\pi \\
 (nx, ny)(u) & \text{ is the unit normal,} & 0 < u \leq 2\pi
 \end{aligned}$$

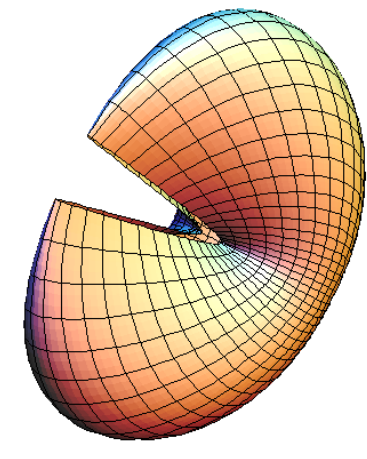
The Klein bottle is a tube of varying radius  $\text{rad}(u)$  around this curve. The function  $\text{rad}(u)$  is experimental:

$$\text{rad}(u) = bb \cdot (dd + \sin(1.5\pi \cdot (1 - \cos^3((u + 0.5)/2.85))));$$

The parameters  $cc, ee, bb$  just control the amplitudes of the functions;  $dd > 1$  allows to vary the ratio between maximum and minimum of  $\text{rad}(u)$ .

$$F_{symKlein}(u, v) = aa \cdot \begin{pmatrix} cx(u) + \text{rad}(u) \cdot nx(u) \cos(v) \\ cy(u) + \text{rad}(u) \cdot ny(u) \cos(v) \\ \text{rad}(u) \cdot \sin(v) \end{pmatrix}.$$

## The Cross-Cap and Steiner's Roman Surface \*



Opposite boundary points of this embedded disk are identified along a segment of double points when the surface is closed to make the Cross-Cap. Pinchpoint singularities form at the endpoints of the selfintersection segment.

In the 19th century images of the projective plane were found by restricting quadratic maps  $f : \mathbb{R}^3 \mapsto \mathbb{R}^3$  to the unit sphere. For example a **Cross-Cap** is obtained with  $f(x, y, z) = (xz, yz, (z^2 - x^2)/2)$ , and **Steiner's Roman Surface** with  $f(x, y, z) = (xy, yz, zx)$ .

Parametrizations follow by restricting to a parametrized sphere  $F_{Sphere}(u, v) = (\sin u \cos v, \sin u \sin v, \cos u)$ .

Steiner's surface has three self-intersection segments and six pinchpoint singularities. The **Default Morph** emphasizes a (self-intersecting) Möbius Band on this surface.

Cross-caps occur naturally as a family by a differential geometric construction. Consider at a point  $p$  of positive curvature of some surface the family of all the normal curvature circles at  $p$ . They form a cross-cap and the two

---

\* This file is from the 3D-XplorMath project. Please see:

pinchpoint singularities are the points opposite to  $p$  on the two principal curvature circles. The parameters  $aa, bb$  in 3DXM are the two principal curvature radii. The **Default Morph** varies  $bb$  from  $bb = 0.4aa$  to  $bb = aa$ , a sphere. A **Range Morph** starts by taking half of each normal curvature circle and slowly extends them to full circles.

To derive a parametrization of this family of cross-caps let  $e_1, e_2$  be a principal curvature frame at  $p$ , let  $\kappa_1, \kappa_2$  be the principal curvatures and  $r_1 := 1/\kappa_1, r_2 := 1/\kappa_2$  the principal curvature radii at  $p$ . The normal curvature in the direction  $e(\varphi) := e_1 \cos \varphi + e_2 \sin \varphi$  is

$$\kappa(\varphi) := \kappa_1 \cos^2 \varphi + \kappa_2 \sin^2 \varphi \quad \text{with} \quad r(\varphi) := 1/\kappa(\varphi).$$

In 3DXM we parametrize the circles by  $u \in [-\pi, \pi]$  and use  $v = \varphi$ . Denoting the surface normal by  $n$  we get the family of normal circles as

$$r(v) \cdot (-n + n \cdot \cos u + e(v) \cdot \sin u), \quad u \in [0, \pi], \quad v \in [0, 2\pi].$$

Finally we take  $\{e_1, e_2, n\}$  as the  $(x, y, z)$  coordinate frame and allow translation by  $cc$  along the  $z$ -axis to get our

### *Parametrization of the normal curvature Cross-cap*

$$r(v) = r_1 r_2 / (r_2 \cos^2 v + r_1 \sin^2 v),$$

$$x = r(v) \cos v \sin u,$$

$$y = r(v) \sin v \sin u,$$

$$z - cc = r(v)(-1 + \cos u) = 2r(v) \sin^2(u/2),$$

$$u \in [0, \pi], \quad v \in [0, 2\pi].$$

To also get an *implicit equation* we observe  $y/x = \tan v$  and  $z^2/(x^2 + y^2) = \tan^2(u/2)$ .

This leads to

$$\begin{aligned}x^2/(x^2 + y^2) &= \cos^2 v, \\y^2/(x^2 + y^2) &= \sin^2 v, \\z^2/(x^2 + y^2 + z^2) &= \sin^2 u/2, \\(x^2 + y^2)/(x^2 + y^2 + z^2) &= \cos^2 u/2.\end{aligned}$$

The first two of these equations eliminate  $v$  from  $r(v)$ . The third one eliminates  $u$  from  $z/r(v) = 2 \sin^2(u/2)$  and gives (with  $r_1 = aa$ ,  $r_2 = bb$ ) an

*Implicit equation of the normal curvature Cross-cap*

$$\left(\frac{x^2}{aa} + \frac{y^2}{bb}\right)(x^2 + y^2 + z^2) + 2z(x^2 + y^2) = 0.$$

Finally, replacing  $z$  by  $z - cc$  will translate the cross-cap, e.g.  $cc = 2bb$  puts the pinchpoint of the smaller curvature circle to the origin of  $\mathbb{R}^3$ .

H.K.

TOC

## Boy Surfaces,\*

following **Apery** and **Bryant-Kusner**

See [Möbius Strip](#) and [Cross-Cap](#) first.

All the early images of the projective plane in  $\mathbb{R}^3$  had singularities, the **Boy Surface** was the first *immersion*. Since the projective plane is *non-orientable*, no embedding into  $\mathbb{R}^3$  exists and *self-intersection curves* have to occur on the image. In fact, the self-intersection curve of the Boy surface is also *not* embedded, the surface has a *triple point*. Boy discovered the surface while working for his PhD under Hilbert. Boy's construction was differential topology work, his surface has no special local geometry.

**Apery** found an **Algebraic Boy Surface**. Moreover, his surface is covered by a 1-parameter family of ellipses. This is his *Parametrization*:

$$F_{Apery}(u, v) = \begin{pmatrix} \frac{\cos^2(u) \cos(2v) + \sin(2u) \cos(v) / \sqrt{2}}{\sqrt{2} - \sin(2u) \sin(3v)} \\ \frac{\cos^2(u) \sin(2v) - \sin(2u) \sin(v) / \sqrt{2}}{\sqrt{2} - \sin(2u) \sin(3v)} \\ \frac{\sqrt{2} \cos^2(u)}{(\sqrt{2} - \sin(2u) \sin(3v))} \end{pmatrix}.$$

This parametrization is obtained by restricting the following *even* map from  $\mathbb{R}^3$  to  $\mathbb{R}^3$  to the unit sphere:

---

\* This file is from the 3D-XplorMath project. Please see:

$$\begin{aligned}
denom &:= (\sqrt{2} - 6xz)(x^2 + y^2) + 8x^3z \\
F_x &:= ((x^2 - y^2)z^2 + \sqrt{2}xz(x^2 + y^2))/denom \\
F_y &:= (2xyz^2 - \sqrt{2}yz(x^2 + y^2))/denom \\
F_z &:= z^2(x^2 + y^2)/denom
\end{aligned}$$

The image of the unit sphere is also an *image of the projective plane* since  $(F_x, F_y, F_z)(-p) = (F_x, F_y, F_z)(p)$ .

The **Default Morph** starts with a band around the equator, which is a Möbius Strip with *three* halftwists. The complete surface is obtained by attaching a disk (centered at the polar center). **3DXM** supplies a second morph, **Range Morph** in the Animation Menu. It starts with a band around a meridian, which is another Möbius Strip with *one* halftwist. This Möbius Strip is moved over all the meridians, covering the surface with embedded Möbius Strips.

**Bryant-Kusner Boy Surfaces** are obtained by an inversion from a minimal surface in  $\mathbb{R}^3$ . The minimal surface is an immersion of  $\mathbb{S}^2 - \{6 \text{ points}\}$  such that antipodal points have the same image in  $\mathbb{R}^3$ , so that the minimal surface is an image of the projective plane minus three points. The six punctures are three antipodal pairs, and the minimal surface has so called *planar ends* at these punctures. This is the same as saying that the Weierstrass-integrand has no residues, hence can be explicitly integrated. In this context it is important that the inversion of a planar end has a puncture that can be *smoothly* closed by adding one point.

The closing of the three pairs of antipodal ends thus gives a triple point on the smoothly immersed surface which is obtained by inverting the minimal surface.

As `Default Morph` and as `Range Morph` we took the same deformations as in the algebraic case. The first emphasizes the equator Möbius Strip with *three* halftwists, the second covers the surface with embedded Möbius Strips that have meridians as center lines.

A *Parametrization* is obtained by first describing the minimal surface as an image of the Gaussian plane, then invert it in the unit sphere. Parameter lines come by taking polar coordinates in the unit disk.

$MinSurf(z) := \text{Re}(V(z)/a(z)) + (0, 0, 1/2)$ , where

$a(z) := (z^3 - z^{-3} + \sqrt{5})$  and

$V(z) := (i(z^2 + z^{-2}), z^2 + z^{-2}, \frac{2i}{3}(z^3 + z^{-3}))$ .

Finally the inversion:

$$Boy(z) := \frac{MinSurf(z)}{\|MinSurf(z)\|^2}.$$

We add the description of an ODE which allows to compute the self-intersection curve as long as the two normals along the self-intersection are not parallel – in other words, as long as the self-intersection is transversal.

Let  $F : D^2 \mapsto \mathbb{R}^3$  be a parametrized surface with unit normal field  $N : D^2 \mapsto \mathbb{R}^3$ . Let  $p, q \in D^2$  be any two points with  $N(p) \neq \pm N(q)$ .

The vector  $T := N(p) \times N(q)$  is then tangent to the surface at  $F(p)$  and  $F(q)$ .

Therefore we have unique vectors  $\dot{p} \in T_p D^2, \dot{q} \in T_q D^2$  such that  $T = dF_p \cdot \dot{p} = dF_q \cdot \dot{q}$ .

This defines an ODE on  $D^2 \times D^2$  with singularities where  $N(p) = \pm N(q)$ .

CLAIM: Along the pair of solution curves we have

$$F(p(t)) - F(q(t)) = \text{const.}$$

Clearly:

$$(F(p(t)) - F(q(t)))' = dF_p \cdot \dot{p} - dF_q \cdot \dot{q} = T - T = 0.$$

In particular, if we start at a self-intersection point

$$F(p(0)) = F(q(0)),$$

then the solution curve runs along the self-intersection,

$$F(p(t)) = F(q(t)).$$

In case one does not have an explicit self-intersection point one can start from nearby points, meaning the distance between  $F(p)$  and  $F(q)$  is small. On the intersection of the tangent planes at these points find the point  $C$  which is closest to the segment  $\overline{F(p)F(q)}$ . Use  $C - F(p) = dF_p \cdot \Delta p$  and  $C - F(q) = dF_q \cdot \Delta q$  to get points  $p + \Delta p, q + \Delta q$  which are much closer to a self-intersection point,

$$F(p + \Delta p) \approx F(q + \Delta q).$$

Iteration of this procedure converges rapidly.

H.K.

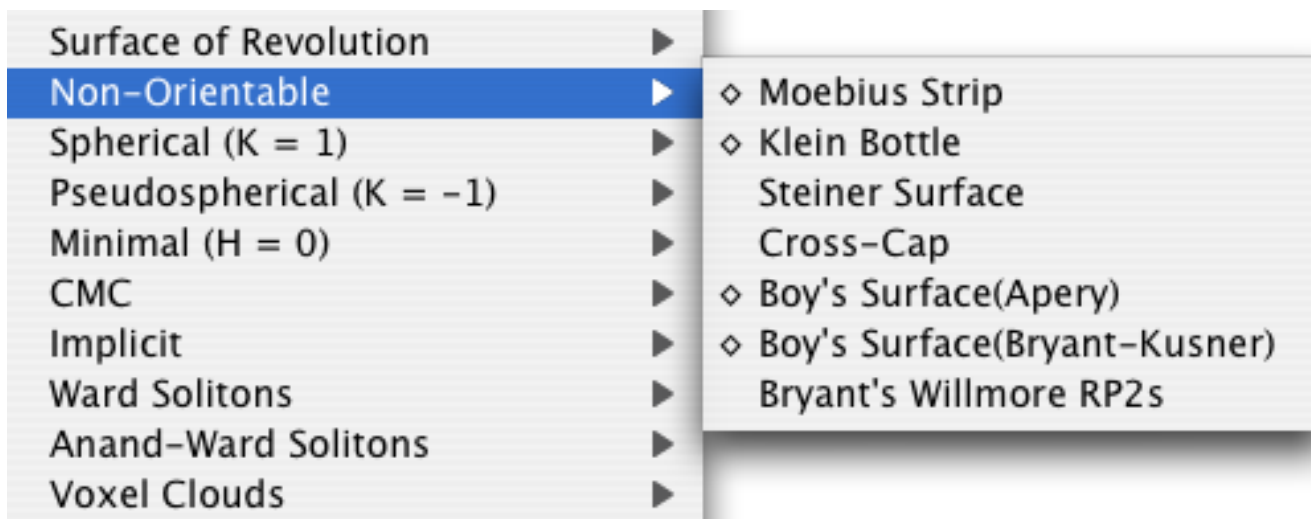
TOC

## Nonorientable Surfaces \*

All nonorientable surfaces in 3DXM are explained as subset of the explicitly parametrized surfaces.

See [TOC](#) of explicitly parametrized or implicit surfaces.

Currently the menu offers seven examples:



Check the **Animate** Menu for special morphs, designed to explain less obvious features of these surfaces.

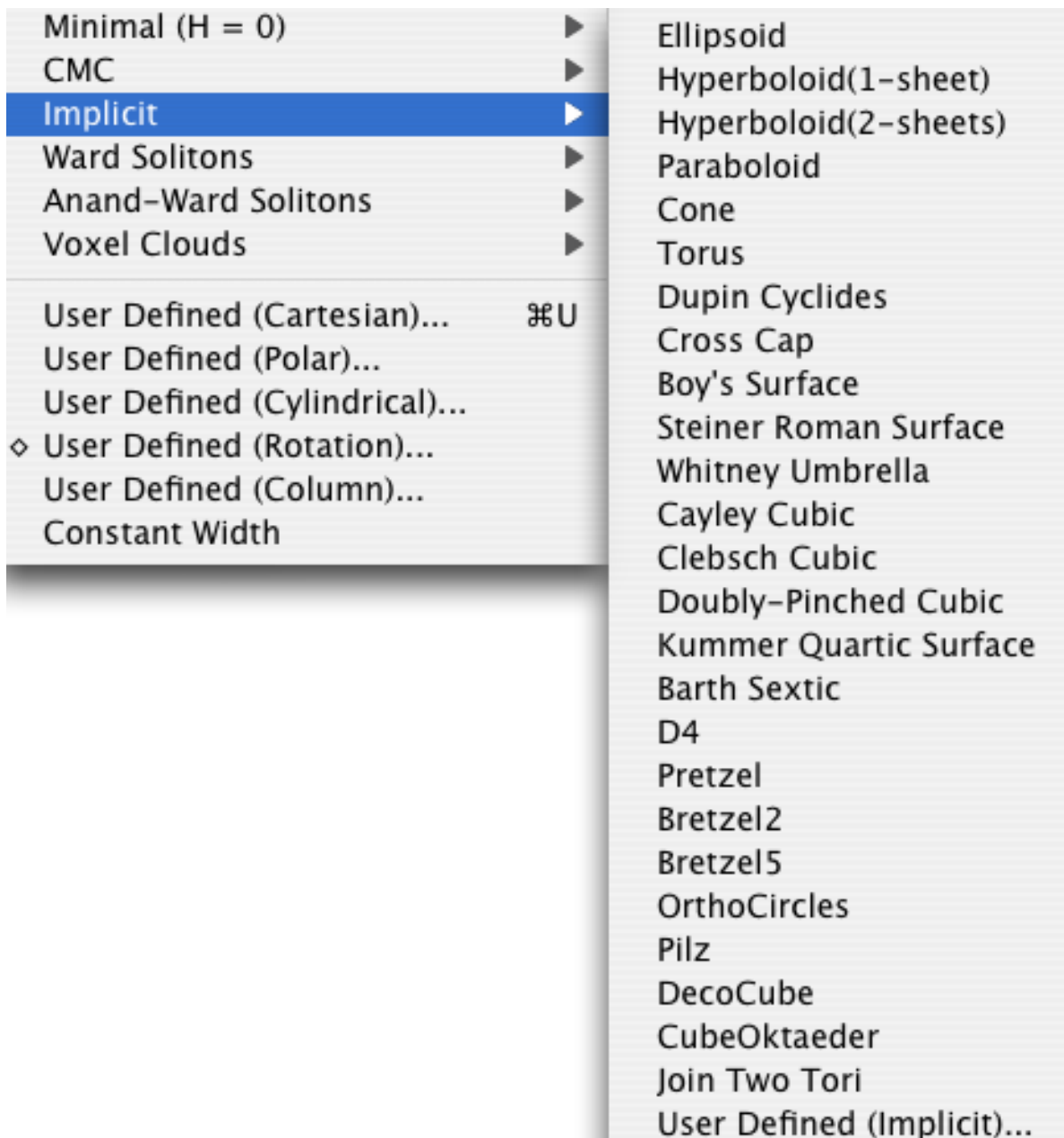
---

\* This file is from the 3D-XplorMath project. Please see:

<http://3D-XplorMath.org/> [Surface Organisation](#)

## Implicit Surfaces \*

All implicit surfaces in 3DXM are explained as subset of the collection *Explicitly parametrized or Implicit Surfaces*.



---

\* This file is from the 3D-XplorMath project. Please see:

## The Spherical Helicoids\*

See also:  $K=1$  Surfaces of Revolution

A general helicoid can be obtained by applying a screw motion to a planar curve. Suppose the curve is given as  $s \mapsto (f(s), g(s))$ , then the helicoid can be written as

$$F(s, t) = (f(s) \cos t, f(s) \sin t, g(s) + ht)$$

with a non-zero constant  $h$ . The surface which is generally called *the* helicoid arises as the special case  $f(s) = s$  and  $g(s) = 0$ . Our more general class of helicoids is useful because it allows to construct concrete examples of surfaces that are otherwise elusive.

For example, let us specialize a little by taking  $f(s) = s$  (so that the curve is a graph over the  $t$ -axis). Then the Gauss curvature of these helicoids is

$$K = \frac{-h^2 + s^3 g'(s) g''(s)}{\left(h^2 + s^2 + s^2 g'(s)^2\right)^2}$$

This is just a first order ODE for  $g'(s)$ , and it is easy to check that

$$g'(s) = \sqrt{-1 - \frac{h^2}{s^2} + \frac{1}{a - \sqrt{K} s^2}}$$

---

\* This file is from the 3D-XplorMath project. Please see:

is a 1-parameter family of solutions in the case that  $K$  is a (positive) constant. The family parameter is  $a$ . Observe that the additional integration constant we get by integrating  $g'$  only amounts to a vertical translation of the surface.

As all *complete* surfaces of positive constant curvatures are round spheres, any other example must necessarily develop singularities. This was for a long time a perfectly good reason to ignore them, and now it has been for a while a perfectly good reason to find them interesting.

For our spherical helicoids, the singularity arises as the curve  $s = s_0$  for the value of  $s_0$  where the integrand  $g'(s)$  becomes 0, and is thus a horizontal circle.

The surface appears as an exercise in Eisenhart's *A Treatise On The Differential Geometry of Curves And Surfaces*. It was certainly well known much earlier.

M.W.

TOC

Alternative description: next page.

## An alternative description

### TOC

The velocity vector field  $X$  of a screw motion in  $\mathbb{R}^3$  is  $X(x, y, z) = (-y, x, h)$ . On a surface that is screw motion invariant one finds that the unit speed curves  $\gamma$  orthogonal to  $X$  are geodesics: The covariant derivative  $\frac{D}{ds}\gamma'$  is zero because it is orthogonal to  $\gamma'$  and to  $X \circ \gamma$ , namely:

$$0 = \langle \gamma', \gamma' \rangle' = 2 \langle \gamma', \frac{D}{ds} \gamma' \rangle$$

$$0 = \langle \gamma', X \circ \gamma \rangle \implies 0 = \langle \frac{D}{ds} \gamma', X \circ \gamma \rangle + 0.$$

A Killing field restricts along a geodesic to a Jacobi field  $J = X \circ \gamma$ , and on a 2-dim surface we have (because of  $\gamma' \perp J$ ) that  $J/|J|$  is a parallel field. Therefore we get from the Jacobi equation

$$|J|'' = -K \cdot |J|, \text{ i.e., if } K = 1 \text{ then } |J(s)| = a \cdot \cos(s).$$

We write  $\gamma(s) = (\gamma_1(s), \gamma_2(s), \gamma_3(s))$  and abbreviate  $r^2 = x^2 + y^2$ ,  $r(s) := \sqrt{\gamma_1^2(s) + \gamma_2^2(s)}$ . This gives:

$$|J(s)| = \sqrt{r^2(s) + h^2} = a \cdot \cos(s).$$

What remains is a first order ODE for  $\gamma(s)$ .

We abbreviate the radial horizontal vector field as  $n_r$ , i.e.,  $n_r \circ \gamma = (\gamma_1, \gamma_2, 0)/r$ , and we extend the orthonormal vectors  $\{n_r, X/|X|\}$  to an orthonormal basis with  $n_z(x, y, z) := (y \cdot h/r, -x \cdot h/r, r)/\sqrt{r^2 + h^2}$ . Then

$$\gamma'(s) = r'(s) \cdot n_r \circ \gamma(s) + \sqrt{1 - r'(s)^2} \cdot n_z \circ \gamma(s).$$

One needs  $|r'(s)| \leq 1$  and this condition gives

$$s_{max} := \sqrt{\frac{h^2}{a^4} + \left(\frac{1-a^2}{2a^2}\right)^2} + \frac{a^2-1}{2a^2}.$$

One can check that this condition implies

$$r^2(s) = a^2 \cos^2(s) - h^2 \geq 0.$$

The final family, with parameters  $a$  and  $h$ , is

$$F(s, t) = \begin{pmatrix} \gamma_1(s) \cos t - \gamma_2(s) \sin t \\ \gamma_1(s) \sin t + \gamma_2(s) \cos t \\ \gamma_3(s) + h \cdot t \end{pmatrix}.$$

If  $h = 0$  one obtains surfaces of revolution with meridian  $\gamma(s)$ , and  $a = 1$  is the sphere.

H.K.

TOC



the latter case large portions of the surface are already very spherically shaped, but the holes are always there. So one may wonder why one does not extend Sievert's surface beyond its boundary. A similar phenomenon can more easily be explained for those  $K = 1$  surfaces of revolution which have their equator longer than that of the unit sphere (and which are obtained in 3DXM by setting  $cc > 1$  in the Set Parameters Dialog). They, too, have holes instead of polar regions. In this case one can see from the formulas that the meridians are more and more strongly curved as their distance from the equator increases; the holes cannot be closed because the curvature of the meridians becomes  $\infty$  at the rim of each hole.

The Sievert-Enneper Surface has even more in common with these  $K = 1$  surfaces of revolution. As with them the parameter lines are principal curvature directions. This means that the surface is least strongly, respectively most strongly, curved in the directions of the two parameter lines through any point. On a surface of revolution these principal curvature lines are planar curves, the meridians and the latitudes. The infinitely long parameter lines of the Sievert-Enneper surface are also *planar curves*, and these planes all contain the y-axis, the line which is tangent to the two tails at infinity. (This is clear from the formulas below because the function  $\Phi$  depends only on  $u$  and not on  $v$ .) The second family of parameter lines on the Sievert-Enneper Surface ( $v = const$ ) looks planar also, but this is not the case. However, as  $aa$  becomes very large so

that the surface looks very spherical, one observes that the two families of parameter lines converge to two orthogonal families of circles on the sphere. This explains why they look almost planar.

The formulas for the Sievert-Enneper Surface do not look very appealing. We write them with the help of three auxiliary functions:

$$\begin{aligned}\Phi(u) &:= -u/\sqrt{aa + 1} + \arctan(\sqrt{aa + 1} \cdot \tan u), \\ a(u, v) &:= 2/(aa + 1 - aa \sin^2 v \cos^2 u), \\ r(u, v) &:= a(u, v) \sqrt{(1 + 1/aa)(1 + aa \sin^2 u)} \sin v.\end{aligned}$$

The Sievert-Enneper Surfaces:

$$\begin{aligned}x(u, v) &:= r(u, v) \cos \Phi(u), \\ y(u, v) &:= r(u, v) \sin \Phi(u), \\ z(u, v) &:= \frac{\log(\tan(v/2)) + (aa + 1)a(u, v) \cos v}{\sqrt{aa}}.\end{aligned}$$

## Surfaces of Gauss Curvature $K = 1$ \*

The 3DXM submenu of the Surface menu contains these examples:



See first the second page of [Surfaces of Revolution](#)  
[Enneper-Sievert Surface](#)  
[Spherical Helicoids](#)

It is interesting to deform these surfaces by using the default morph in each case.

---

\* This file is from the 3D-XplorMath project. Please see:

# Pseudospherical Surfaces

## Surface Organisation

( Click the Names )

- 1.) [Introduction to Pseudospherical Surfaces](#)
- 2.) [Dini, Kuen and Breather Surfaces](#)
- 3.) [Surfaces of Revolution](#)
- 4.) [The Pseudosphere from SGE](#)
- 5.) [Surfaces from SGE solutions](#)

## About Pseudospherical Surfaces\*

If  $X : M \subset \mathbf{R}^3$  is a surface with Gaussian curvature  $K = -1$ , then it is known that there exists a local asymptotic coordinate system  $(x, t)$  on  $M$  such that the first and second fundamental forms are

$$I = dx^2 + dt^2 + 2 \cos q \, dx \, dt, \quad II = 2 \sin q \, dx \, dt,$$

where  $q$  is the angle between asymptotic lines (the  $x$ -curves and  $t$ -curves). Such coordinates are called Tchebyshef coordinates. The Gauss-Codazzi equations for  $M$  in these coordinates become a single equation, the sine-Gordon equation (SGE)

$$q_{xt} = \sin q. \quad (SGE)$$

Surfaces in  $\mathbf{R}^3$  having constant Gaussian curvature  $K$  equal minus one are usually called *pseudospherical surfaces* (after the most well-known example, the pseudosphere) and the so-called Fundamental Theorem of Surfaces gives us a local correspondence between pseudospherical surfaces (up to rigid motion) and solutions of SGE. A general pseudospherical surface shares with the pseudosphere the fact that its intrinsic geometry is a portion of the hyperbolic geometry of Lobachevsky.

Now classical results of Bäcklund and of Bianchi concerning pseudospherical surfaces provide methods to find many

---

\* This file is from the 3D-XplorMath project. Please see:

explicit solutions of the SGE and construct the corresponding pseudospherical surfaces. In fact, the SGE is one of the model soliton equations, and these classical methods give rise to all of the soliton solutions of SGE. We will describe next a little of this very classical differential geometry.

For surfaces  $M, M^*$  in  $\mathbf{R}^3$ , a diffeomorphism  $\ell : M \rightarrow M^*$  is called a *pseudospherical congruence* with constant  $\theta$  if:

- (i) the line joining  $p$  and  $p^* = \ell(p)$  is tangent to both  $M$  and  $M^*$ ,
- (ii) the angle between the normal of  $M$  at  $p$  and the normal of  $M^*$  at  $p^* = \ell(p)$  is  $\theta$ , and
- (iii) the distance from  $p$  to  $p^*$  is  $\sin \theta$  for all  $p \in M$ .

The following result of Bäcklund is fundamental to the study of pseudospherical surfaces.

**Bäcklund Theorem.** *Let  $M, M^*$  be two surfaces in  $\mathbf{R}^3$ , and  $\ell : M \rightarrow M^*$  a pseudospherical congruence with constant  $\theta$ . Then*

- (a) *both  $M$  and  $M^*$  are pseudospherical surfaces,*
- (b) *the Tchebyshef coordinates  $x, t$  on  $M$  maps to the Tchebyshef coordinates on  $M^*$  under  $\ell$ ,*
- (c) *if  $q$  and  $q^*$  are the solutions of SGE corresponding to  $M$  and  $M^*$  respectively, then  $q, q^*$  satisfies*

$$\begin{cases} q_x^* = q_x + 2s \sin\left(\frac{q^* + q}{2}\right), \\ q_t^* = -q_t + \frac{2}{s} \sin\left(\frac{q^* - q}{2}\right), \end{cases} \quad (\text{BT}_\theta)$$

where  $s = \tan \frac{\theta}{2}$ .

Moreover, given  $q$ , system  $(\text{BT}_\theta)$  is solvable for  $q^*$  if and only if  $q$  is a solution of the SGE, and the solution  $q^*$  is again a solution of the SGE.

We will call both  $\ell$  and the transform from  $q$  to  $q^*$  a Bäcklund transformation. This description of Bäcklund transformations gives us an algorithm for generating families of solutions of the PDE by solving a pair of ordinary differential equations. The procedure can be repeated, but the miracle is that after the first step, the procedure can be carried out algebraically. This is the Bianchi Permutability Theorem. Given two pseudospherical congruences  $\ell_i : M_0 \rightarrow M_i$  with angles  $\theta_i$  respectively and  $\sin \theta_1^2 \neq \sin \theta_2^2$ , then there exist an algebraic construction of a unique surface  $M_3$ , and pseudospherical congruences  $\tilde{\ell}_1 : M_2 \rightarrow M_3$  and  $\tilde{\ell}_2 : M_1 \rightarrow M_3$  with angles  $\theta_1$  and  $\theta_2$  respectively such that  $\tilde{\ell}_2 \ell_1 = \tilde{\ell}_1 \ell_2$ . The analytic reformulation of this theorem is the following: Suppose  $q$  is a solution of the SGE and  $q_1, q_2$  are two solutions of system  $(\text{BT}_\theta)$  with angles  $\theta = \theta_1, \theta_2$  respectively. The Bianchi permutability theorem gives a third local solution  $q_3$  to the SGE

$$\tan \frac{q_3 - q}{4} = \frac{s_1 + s_2}{s_1 - s_2} \tan \frac{q_1 - q_2}{4},$$

where  $s_1 = \tan \frac{\theta_1}{2}$  and  $s_2 = \tan \frac{\theta_2}{2}$ .

To see how the scheme works, we start with the trivial solution  $q = 0$  of SGE, then  $(\text{BT}_\theta)$  can be solved explicitly to get

$$q^*(x, t) = 4 \tan^{-1}(e^{sx + \frac{t}{s}}), \quad (1)$$

the 1-soliton solutions of SGE. (Here  $s = \tan \frac{\theta}{2}$ . ) An application of the Permutability theorem then give the 2-soliton solutions

$$q(x, t) = 4 \tan^{-1} \left( \frac{s_1 + s_2}{s_1 - s_2} \frac{e^{s_1 x + \frac{1}{s_1} t} - e^{s_2 x + \frac{1}{s_2} t}}{1 + e^{(s_1 + s_2)x + (\frac{1}{s_1} + \frac{1}{s_2})t}} \right). \quad (2)$$

Repeated applications of the Permutability theorem give complicated but nevertheless explicit  $n$ -soliton solutions. Note that the parameters  $s_1, s_2$  in the above formula for 2-solitons are real. But for  $s_1 = ie^{i\theta}$  and  $s_2 = -ie^{-i\theta}$ , even though  $q_1, q_2$  are not real-valued, nevertheless

$$q_3(x, t) = 4 \tan^{-1} \left( \frac{\sin \theta \sin(T \cos \theta)}{\cos \theta \cosh(X \sin \theta)} \right) \quad (3)$$

is real and a solution of SGE, where  $X = x - t$ , and  $T = x + t$  are space-time coordinates. This solution is periodic in  $T$  and is called a *Breather*.

The “surface” corresponding to  $q = 0$  is degenerate and in fact is a straight line. The surfaces corresponding to

- (i) 1-soliton ( formula (1)) with  $s = 1$  is the Pseudo-sphere,
- (ii) 1-soliton (formula (1)) with  $s \neq 1$  is a Dini Surface,
- (iii) 2-soliton (formula (2)) contains the Kuen Surface.
- (iv) Breather solution (formula (3)) with  $\cos \theta$  a rational number is a pseudospherical surface periodic in the  $T$  direction.

Even though the breather solution  $q$  is periodic in  $T$ , the corresponding pseudospherical surface may not be periodic in  $T$ . This is because when we use the Fundamental Theorem of Surfaces to construct the surface from solution  $q$  of the SGE, we need to solve two compatible ODEs whose coefficients are given by functions of  $q$  and  $q_x$ . For Breathers, the solutions of these ODEs are periodic in  $T$  if  $\cos \theta$  is rational.

You will notice that all of the pseudospherical surfaces shown in the program have obvious singularities. In fact, a theorem of Hilbert says that the hyperbolic plane can not be isometrically immersed in  $\mathbf{R}^3$ , and this implies that all complete pseudospherical surfaces must have singularities. Although soliton solutions are smooth on the entire  $(x, t)$ -plane, the corresponding pseudospherical surfaces have singularities where the induced metric becomes degenerate, i.e., where

$$\det \begin{pmatrix} 1 & \cos q \\ \cos q & 1 \end{pmatrix} = 0.$$

In other words, a surface corresponding to a global solution  $q$  of SGE will have a singularities along the curves where  $q$  is a multiple of  $\pi$ . Moreover, since the metric has rank 1 there, these surfaces have cusp singularities.

For an elementary and short introduction to soliton theory and its relation to SGE, see the article by C. L. Terng and K. Uhlenbeck: *Geometry of Solitons*, Notices of AMS, 47(2000), 17-25. One may also download the pdf file of

this paper from

<http://www.math.neu.edu/~ternng/MyPapers.html>

CLT

TOC

## Three Pseudospherical Surfaces,\*

### Dini Family, Kuen, Breather

The theory to obtain these surfaces of Gauss curvature  $K = -1$  is explained in

#### About Pseudospherical Surfaces.

The construction begins with explicit solutions of the Sine-Gordon-Equation (SGE). A first and a second fundamental form are written down in terms of an SGE solution. These surface data satisfy the Gauss-Codazzi integrability conditions, hence determine immersed surfaces. For the earliest examples this integration of the surface data could be carried out explicitly. See the quoted text above for more details.

Parametrization of the Dini surfaces:

$$\begin{pmatrix} x \\ y \\ z \end{pmatrix} (u, v) := \begin{pmatrix} u - t(u, v) \\ r(u, v) \cos(v) \\ r(u, v) \sin(v) \end{pmatrix}, \text{ where}$$

$$\psi := aa \cdot \pi, \quad aa \in [0.001, 0.999],$$

$$aa = 0.5 \quad \text{gives the Pseudosphere,}$$

$$g(u, v) := (u - v \cdot \cos(\psi)) / \sin(\psi),$$

$$s(u, v) := \exp(g(u, v)),$$

$$r(u, v) := 2 \sin(\psi) / (s(u, v) + 1/s(u, v)),$$

$$t(u, v) := 0.5 \cdot r(u, v) \cdot (s(u, v) - 1/s(u, v)).$$

---

\* This file is from the 3D-XplorMath project. Please see:

Parametrization of the Kuen Surface:

$$\begin{pmatrix} x \\ y \\ z \end{pmatrix} (u, v) := \begin{pmatrix} \frac{2 \cosh(v)(\cos(u) + u \cdot \sin(u))}{\cosh(v) \cdot \cosh(v) + u \cdot u} \\ \frac{2 \cosh(v)(-u \cdot \cos(u) + \sin(u))}{\cosh(v) \cdot \cosh(v) + u \cdot u} \\ v - \frac{2 \sinh(v) \cosh(v)}{\cosh(v) \cdot \cosh(v) + u \cdot u} \end{pmatrix}$$

Parametrization of the Breather surfaces:

Parameter of the family is  $aa \in (0, 1)$ .

If  $w := \sqrt{1 - aa^2}$  is rational then the surfaces are periodic.

$$denom := aa \cdot ((w \cosh(aa \cdot u))^2 + (aa \sin(w \cdot v))^2)$$

$$x(u, v) := -u + \frac{2(1 - aa^2)}{denom} \cosh(aa \cdot u) \sin(aa \cdot u)$$

$$y(u, v) := \frac{2w \cosh(aa u)}{denom} (-w \cos(v) \cos(w v) - \sin(v) \sin(w v))$$

$$z(u, v) := \frac{2w \cosh(aa u)}{denom} (-w \sin(v) \cos(w v) + \cos(v) \sin(w v))$$

## The Pseudosphere\*

### from a Sine-Gordon solution

The Pseudosphere was first found as a surface of revolution, with the Tractrix as meridian (see Planar Curves). It has Gauss curvature  $K = -1$ . See:

**Constant Curvature Surfaces of Revolution.**

Later in the 19th century it was discovered that surfaces with  $K = -1$  can be constructed from soliton solutions of the Sine-Gordon Equation (SGE). This is explained in:

**About Pseudospherical Surfaces,**

which can be obtained from the Documentation Menu.

At about the same time, in 1868, Beltrami proved that the axiomatically constructed non-Euclidean geometry of Bolyai and Lobachevsky was the same as the simply connected 2-dimensional Riemannian geometry of Gauss curvature  $K = -1$ ; for example the Riemannian metric of the Pseudosphere, extended to the plane:  $du^2 + \exp(-2u)dv^2$ . Their common name today is *Hyperbolic Geometry*.

The meridians are examples of *asymptotic geodesics*, a key notion in hyperbolic geometry. Curves, orthogonal to a family of asymptotic geodesics are called *horocycles* in hyperbolic geometry. They have infinite length in the simply connected case, on the Pseudosphere one sees finite por-

---

\* This file is from the 3D-XplorMath project. Please see:

tions as the latitude circles.

In the theory which relates SGE solutions to surface in  $\mathbb{R}^3$  of Gauss curvature  $K = -1$ , one first writes down the first and second fundamental forms in terms of such a solution  $q(x, t)$  of SGE:

$$I = dx^2 + dt^2 + 2 \cos q \, dx \, dt, \quad II = 2 \sin q \, dx \, dt,$$

The Gauss-Codazzi integrability conditions are satisfied, because  $q$  is an SGE solution. The Gauss curvature is the quotient of the determinants of the two forms, i.e.  $K = -\sin^2(q)/\sin^2(q) = -1$ . One then obtains the first parameter line of the surface by integrating an ODE and the transversal other family by integrating a second ODE. The first and second fundamental forms above are written in asymptote coordinates, which means: the normal curvature of the surface in the direction of the parameter lines is 0. (Note that  $x$  and  $t$  are arc length parameters on the parameter lines. This leads to the Tchebycheff net mentioned in “About Pseudospherical Curves”.) Such parametrizations do not offer a good view of the surface. In 3DXM, therefore, the integration first creates one curvature line of the surface and secondly the orthogonal family of curvature lines with  $u = x + t, v = x - t$ . One can view the integration before the surface is shown, with these parameter lines.

The SGE solution for the Pseudosphere is:

$$q(x, t) := 4 \arctan(\exp(x+t)), \quad qc(u, v) = 4 \arctan(\exp(u)).$$

## $(K = -1)$ - Surfaces from SGE solitons \*

In 3DXM there are several explicit solutions  $q(u, v)$  of the Sine-Gordon Equation (SGE:  $q_{uu} - q_{vv} = \sin(q(u, v))$ ). They use Parameters as follows:

Pseudosphere: No parameters,  $q(u, v) = 4 \arctan(\exp(u))$

One-Soliton (or Dini family or Kink solutions):

$0 < aa < 1$ , used for the so called Dini deformation:

$$q(u, v) = 4 \arctan(\exp(u / \sin(\pi aa) + v / \tan(\pi aa)))$$

Two-Soliton:  $0 < aa, bb < 1$ . The limit  $aa = bb$  is included, because it is a deformation of the Kuen surface.

Three-Soliton:  $0 < aa, bb, cc < 1$ , no equal parameters.

Four-Soliton:  $0 < aa, \dots, dd < 1$ , no equal parameters.

Periodic SGE solutions:  $f''(u) = -\frac{cc}{aa} * \sin(aa \cdot f(u))$ ,  
 $aa = 1, cc = -1, f(0) = hh, f'(0) = bb, 0 < dd < \infty$ .

(Either  $bb = 0$  for even, or  $hh = 0$  for odd solutions.)

$$q(u, v) = f\left(\frac{(dd+1/dd)}{2} \cdot u + \frac{(dd-1/dd)}{2} \cdot v\right),$$

$dd = 1$  for rotational symmetry, try:  $hh = 1, dd = 1.35$ .

Breather:  $0 < aa \leq 1, bb = cc = 0$ , ( $aa = 1$  allowed)

$$q(u, v) = 4 \arctan\left(\frac{aa}{\cosh(aa \cdot u)} \cdot \frac{\sin(\sqrt{(1-aa^2)} \cdot v)}{\sqrt{(1-aa^2)}}\right)$$

If  $cc = 0$  and  $bb > 0$  integer, then 3DXM chooses  $aa$  so that the breather closes up with order  $bb$  rotation symmetry.

Finally  $cc > 0$  applies the Dini deformation to this breather.

Double Breather:  $aa, cc \neq 0$ . Coded to do the complex 2-Soliton. Currently:  $z = aa + i \cdot cc, \bar{z} = aa - i \cdot cc$ .

---

\* This file is from the 3D-XplorMath project. Please see:

Each  $q(u, v)$  determines a pair of first and second fundamental forms, in asymptote parameters  $x = \frac{u+v}{2}, t = \frac{u-v}{2}$ :

$$I = dx^2 + dt^2 + 2 \cos q \, dx \, dt, \quad II = 2 \sin q \, dx \, dt,$$

for which the Gauss-Codazzi integrability conditions are satisfied (because they simplify to  $q$  being an SGE solution  $q_{xt} = \sin(q(x, t))$ ). This says:

There are parametrized surfaces in  $\mathbb{R}^3$  with these first and second fundamental forms. They have Gauss curvature  $K = -1 = \det(II) / \det(I)$ . The parameter lines are asymptote lines on these surfaces and  $x, t$  are arclengths on the parameter lines. For more details see:

**About Pseudospherical Surfaces**

available from the Documentation Menu.

Since pictures of surfaces, drawn with asymptote line parametrization, do not give a good 3D-impression of the surface, 3DXM uses instead curvature line parametrizations, i.e.  $u = x + t, v = x - t$  with the corresponding SGE solution  $qc(u, v) := q((u + v)/2, (u - v)/2)$ . 3DXM first computes one curvature line as solution of an ODE. Next the family of orthogonal curvature lines is drawn. This determines the parametrized surface. It is then rendered according to the viewer's choice.

Recall the definition  $\operatorname{cosec} := 1 / \sin$ .

The **One-Soliton** solution of SGE ( $s + \frac{1}{s} = 2 \operatorname{cosec}(aa\pi)$ ):  
 $q(x, t) = 4 \arctan(\exp( s \cdot x + 1/s \cdot t ))$ , in curvature lines:  
 $qc(u, v) = 4 \arctan(\exp( \operatorname{cosec}(aa \cdot \pi) \cdot u + \cotan(aa \cdot \pi) \cdot v ))$ .  
 The first drawn curvature line is a planar curve.

For  $s = 1$ ,  $aa = 1/2$  the solution  $qc$  depends only on  $u$ , the corresponding surface is the Pseudosphere. Vice versa, for every surface of revolution the function  $qc$  depends only on  $u$  and the SGE reduces to the ODE  $f''(u) = +\sin(f(u))$ . The even solutions of this ODE correspond to the hyperbolic ( $K = -1$ ) surfaces and the odd solutions give the surfaces of revolution with finite cone singularities. The only elementary solution is  $f(u) = 4 \arctan(\exp(u))$  with  $f(0) = \pi$ ,  $f'(0) = 2$  and the cone singularity at infinity.

While this first step is obtained as explicit integration of the ODE  $f''(u) = \sin(f(u))$ , the next steps follow from a result of Bianchi, reformulated for SGE solutions:

If a pair of functions  $q(x, t), Q(x, t)$  satisfy the pair of ODEs:

$$\begin{aligned} Q_x(x, t) &= +q_x(x, t) + 2s \cdot \sin\left(\frac{Q+q}{2}(x, t)\right) \\ Q_t(x, t) &= -q_t(x, t) + 2/s \cdot \sin\left(\frac{Q-q}{2}(x, t)\right) \end{aligned}$$

then, for given  $q(x, t)$ , the system is solvable for  $Q(x, t)$  iff  $q(x, t)$  is an SGE solution. And then  $Q(x, t)$  is also SGE solution and the two functions are called Bäcklund transformations of each other. Moreover, if, for  $s_1 \neq s_2$  two such solutions  $Q1(x, t), Q2(x, t)$  are given, then a third solution  $Qq(x, t)$  is marvelously obtained from

$$\tan\left(\frac{Qq-q}{4}(x, t)\right) = \frac{s_1+s_2}{s_1-s_2} \cdot \tan\left(\frac{Q1-Q2}{4}(x, t)\right).$$

The 1-Soliton solution gives two such functions  $Q1, Q2$  which are Bäcklund transformations of the trivial SGE solution  $q(x, t) = 0$  and  $Qq(x, t)$  is the following 2-Soliton solution

(recall  $\tan(\alpha - \beta) = (\tan(\alpha) - \tan(\beta)) / (1 + \tan(\alpha) \cdot \tan(\beta))$ ):  

$$Qq(x, t) = 4 \arctan\left(\frac{s_1 + s_2}{s_1 - s_2} \cdot \frac{\exp(s_1 \cdot x + 1/s_1 \cdot t) - \exp(s_2 \cdot x + 1/s_2 \cdot t)}{1 + \exp(s_1 \cdot x + 1/s_1 \cdot t) \cdot \exp(s_2 \cdot x + 1/s_2 \cdot t)}\right)$$

This Bianchi generalization also works for complex parameters and one can see directly that for  $s_1 = z, s_2 = \bar{z} \neq 0$  the new solution  $Qq(x, t)$  is again real. If  $|z| = 1$ , it is the breather solution below. In 3DXM we use  $z = aa + i \cdot cc$ . The other (periodic) solutions of  $q_{uu} = \sin(q(u))$  are not Bäcklund transformations of known solutions.

The curvature line version, which is needed for visualization, looks more complicated:

The **Two-Soliton** solution of SGE (parameters  $aa, bb$ ):

Define a constant  $B$  and functions  $A1, A2$  first.

$$B := (\cos(bb \pi) - \cos(aa \pi)) / (\cos((aa - bb)\pi) - 1),$$

$$A1(u, v) := \operatorname{cosec}(aa \pi)u + \operatorname{cotan}(aa \pi)v,$$

$$A2(u, v) := \operatorname{cosec}(bb \pi)u + \operatorname{cotan}(bb \pi)v, \quad \text{then put:}$$

$$qc(u, v) := 4 \arctan\left( B \cdot \frac{\exp(A1(u, v)) - \exp(A2(u, v))}{1 + \exp(A1(u, v) + A2(u, v))} \right).$$

Now observe that the 2-Soliton solutions are Bäcklund transformations of the two 1-Soliton solutions which were used in the Bianchi construction!! Therefore the Bianchi construction can be repeated to give the following:

**Three-Soliton** solution of SGE (params  $aa, bb, cc$ ):

Define three auxiliary functions  $E, F, H$  first.

$$E(\xi, u, v) := \exp(\operatorname{cosec}(\xi \pi)u + \operatorname{cotan}(\xi \pi)v),$$

$$F(\xi_1, \xi_2, u, v) := \frac{\cos(\xi_2 \pi) - \cos(\xi_1 \pi)}{\cos((\xi_2 - \xi_1)\pi) - 1} \cdot \frac{E(\xi_1, u, v) - E(\xi_2, u, v)}{1 + E(\xi_1, u, v) \cdot E(\xi_2, u, v)},$$

$$H(\xi_1, \xi_2, \xi_3, u, v) := \frac{\cos(\xi_3 \pi) - \cos(\xi_2 \pi)}{\cos((\xi_3 - \xi_2)\pi) - 1} \cdot \frac{F(\xi_1, \xi_2, u, v) - F(\xi_1, \xi_3, u, v)}{1 + F(\xi_1, \xi_2, u, v) \cdot F(\xi_1, \xi_3, u, v)},$$

$$qc(aa, bb, cc, u, v) := 4 \arctan(E(aa, u, v)) \\ + 4 \arctan(H(aa, bb, cc, u, v)).$$

The **Four-Soliton** solution of SGE (params  $aa, bb, cc, dd$ ) we give in asymptote coordinates:

Define functions  $E, F, H$  (as before) and  $K$  first.

$$E(s, x, t) := \exp( s \cdot x + 1/s \cdot t),$$

$$F(s_1, s_2, x, t) := \frac{s_1+s_2}{s_1-s_2} \cdot \frac{E(s_1, x, t) - E(s_2, x, t)}{1 + E(s_1, x, t) \cdot E(s_2, x, t)},$$

Recall that  $4 \arctan(F(s_1, s_2, x, t))$  are 2-Soliton solutions.

$$H((s_1, s_2, s_3, x, t) := \frac{s_2+s_3}{s_s-s_3} \cdot \frac{F(s_1, s_2, x, t) - F(s_1, s_3, x, t)}{1 + F(s_1, s_2, x, t) \cdot F(s_1, s_3, x, t)},$$

$$K(s_1, s_2, s_3, s_4, x, t) := \\ \frac{s_3+s_4}{s_3-s_4} \cdot \frac{H((s_1, s_2, s_3, x, t) - H((s_1, s_2, s_4, x, t)}{1 + H((s_1, s_2, s_3, x, t) \cdot H((s_1, s_2, s_4, x, t)},$$

Finally

$$q(s_1, s_2, s_3, s_4, x, t) := \\ 4 \arctan(F(s_1, s_2, x, t)) + 4 \arctan(K(s_1, s_2, s_3, s_4, x, t)).$$

Recall as before  $qc(u, v) = q((u+v)/2, (u-v)/2)$ .

The **Breather** (soliton) solution of SGE (parameter  $aa$ ):  
Abbreviate  $bb := \sqrt{1 - aa^2}$ , then

$$qc(bb, aa, u, v) := 4 \arctan\left( \frac{\sin(bb v)}{bb} \cdot \frac{aa}{\cosh(aa u)} \right).$$

Recall from above that each of these solutions determines a first and a second fundamental form which satisfy the Gauss-Codazzi integrability conditions. Each parameter line gives a space curve via an ODE which is determined by these fundamental forms. Because of the integrability

conditions these space curves fit together to form a surface of Gauss curvature  $K = -1$ .

H.K.

TOC

# Minimal Surfaces

Surface Organisation

About Minimal Surfaces

## Explicitly Parametrized Minimal Surfaces

Helicoid-Catenoid (1776)

Scherk, Catalan, Henneberg Surfaces (1835-1865)

Enneper Surfaces

Minimal Inverted Boy Surface

5.) Kusner (Dihedral Symmetric)

## Weierstrass' Minimal Surface Representation

*Surfaces parametrized by punctured spheres:*

*ff*-wavy k-fold Enneper Surface

Catenoid - k-fold Enneper

Planar k-fold Enneper

Double k-fold Enneper

Scherk Saddle Towers

Twisted Saddle Towers

Symmetric and Skew k-Noids

The Lopez-Ros No-Go-Theorem

Two Planar And Two Catenoid Ends

Half-Catenoids and Weierstrass Representation

*Surfaces parametrized by punctured tori:*

Chain of Half-Catenoids and Field of Half-Catenoids

Karcher  $j_d$  Saddle Towers

Karcher  $j_e$  Saddle Towers

Riemann's Minimal Surfaces

Continue next page

The Chen-Gackstatter Minimal Surface  
Costa's Minimal Surface  
The Costa-Hoffman-Meeks Minimal Surfaces  
Fence of Catenoids  
Scherk's Surface with a Handle  
R. Schoen's No-Go-Theorem

*Embedded Triply Periodic Minimal Surfaces (genus  $\geq 3$ ):*  
The Conjugate Plateau Construction  
Schwarz' P-D-Families, with A. Schoen's Gyroid  
Schwarz' H-Family, with Lidin's Lidinoid  
Four Triply Periodic Minimal Surfaces  
The Fujimori-Weber Surfaces  
Userdefined Minimal Surfaces

## Bibliography

In most cases the program code follows the formulas in:

[Ka1] H. Karcher, Embedded minimal surfaces derived from Scherk's examples, *Manuscripta Math.* 62 (1988) pp. 83–114.

or with more details in

[Ka2] H. Karcher, Construction of minimal surfaces, in "Surveys in Geometry", Univ. of Tokyo, 1989, and Lecture Notes No.12, SFB 256, Bonn, 1989, pp. 1–96.

For a discussion of techniques for creating minimal surfaces with various qualitative features by appropriate choices of

Weierstrass data, see either:

- [KWH] H. Karcher, F. Wei, and D. Hoffman, The genus one helicoid, and the minimal surfaces that led to its discovery, in “Global Analysis in Modern Mathematics, A Symposium in Honor of Richard Palais’ Sixtieth Birthday”, K. Uhlenbeck Editor, Publish or Perish Press, 1993.

or pages 192 – 217 of:

- [DHKW] U. Dierkes, S. Hildebrand, A. Küster, and O. Wohlrab, Minimal Surfaces I, Grundlehren der Math. Wiss. vol 295, Springer-Verlag, 1991.

A survey with emphasis on theoretical advances is

- [HK] [Hoffman, Karcher] Complete embedded minimal surfaces of finite total curvature. Encyclopaedia of Mathematical Sciences, vol. 90. Geometry V (Ed. R. Osserman), pp. 5-93

The last two references have an extensive bibliography.

Minimal [TOC](#)

[Surface Organisation](#)

## About Minimal Surfaces \*

### DISCOVERY AND PHYSICAL INTERPRETATION.

The question *which surfaces locally minimize area* led Lagrange in 1760 to the minimal surface equation for graphs. By 1765 Meusnier had found that a geometric interpretation of this equation is: *the mean curvature of the surface vanishes*. He discovered that the catenoid and the helicoid are nonplanar examples. It took until 1835 for the next examples to appear, discovered by Scherk; his doubly periodic surface is a graph over the black squares of a checkerboard tessellation of the plane and his singly periodic surface is nowadays viewed as a desingularization of two orthogonally intersecting planes. In the following years complex analysis developed and by 1865 many examples were known through the efforts of Riemann, Weierstraß, Enneper and in particular Schwarz.

Also in that period Plateau had made careful experiments with soap films. He convinced people that soap films were a perfect physical realization of minimal surfaces, and he convinced mathematicians that they should solve *Plateau's Problem*, i.e. prove that every continuous injective closed curve in  $\mathbb{R}^3$  spans a minimal surface. This problem was solved in 1932 by Douglas and independently by Rado.

---

\* This file is from the 3D-XplorMath project. Please see:

On the way to this solution mathematicians had learnt a lot about nonlinear elliptic partial differential equations. In particular the importance of the *maximum principle* had become clear, it implies for example that every compact minimal surface is contained in the convex hull of its boundary and that boundary value problems are well posed for the minimal surface equation.

On the other hand, although the Cauchy-Kowalewski theorem allows to solve locally initial value problems with analytic data, there is no continuous dependence on the data and no hope to obtain complete immersed examples with this method. — But, already Weierstraß had established the close connection of minimal surfaces with complex analysis. In particular: the spherical Gauss map composed with stereographic projection is locally a holomorphic function  $G : M^2 \rightarrow \mathbb{C}$ . In terms of the  $90^\circ$  rotation of each tangent space of the minimal surface  $M^2$  holomorphicity has the following intuitive interpretation: for each  $v \in TM^2$  we have the following version of the Cauchy-Riemann equations

$$dG(\mathbf{R}90 \circ v) = i \cdot dG(v).$$

Moreover, the three component functions of the immersion  $(F^1, F^2, F^3) : M^2 \rightarrow \mathbb{R}^3$  are, locally, the real parts of holomorphic functions, because the differential forms

$$\omega^j := -dF^j \circ \mathbf{R}90$$

are closed for surfaces with mean curvature zero (Meusnier's above interpretation of “minimal”). This fact establishes

the Weierstraß representation:

Let  $G$  be the holomorphic Gauss map and

$$dh := dF^3 - i \cdot dF^3 \circ \mathbf{R90}$$

the (holomorphic) complexification of the differential of the height function  $F^3$  then

$$(F^1, F^2, F^3) = \operatorname{Re} \int \left( \frac{1}{2} \left( \frac{1}{G} - G \right), \frac{i}{2} \left( \frac{1}{G} + G \right), 1 \right) dh.$$

The examples of the second half of the 19<sup>th</sup> century were made with this representation. But results, achieved by 1960 by Huber and Osserman show, that *all* minimal surfaces of a certain kind can be obtained by a global application of this representation, namely:

Complete, immersed minimal surfaces of finite total curvature can be conformally compactified by closing finitely many punctures; moreover, the Weierstraß data  $G, dh$  extend *meromorphically* to this *compact Riemann surface*.

The wealth of examples, discovered since about 1980, rely on this theorem. To understand these examples better we note the first and second fundamental forms (Riemannian metric and, if  $|v| = 1$ , normal curvature)

$$I(v, v) = \frac{1}{4} \left( \frac{1}{|G|} + |G| \right)^2 |dh(v)|^2$$

$$II(v, v) = \operatorname{Re} \frac{dG(v)}{G} dh(v).$$

The points  $p$  on the Riemann surface which are poles of  $dh$  do not correspond to points on the minimal surface. Every (differentiable) curve which runs into such a *puncture*  $p$  has infinite length on the minimal surface. The same is true if  $G$  has a zero or pole of higher order than the vanishing order of  $dh$ . If these orders are the same then we simply have a point with vertical normal on the minimal surface. And at points where the vanishing order of  $dh$  is larger, the metric becomes singular and the minimal surface has a so called *branch point*, it is no longer an immersion.

#### VISUALIZATION OF MINIMAL SURFACES.

The Weierstraß representation allows to write down a number of simple minimal surfaces which can be visualized like any other surface for which an explicit parametrization is given. Our parameter lines come from polar coordinates with centers  $\{0, \infty\}$  or  $\{1, +1\}$ . Note that the zeros and poles of  $G, dh$  fit together so that no branch points occur and so that the minimal surfaces are complete on the punctured spheres mentioned in each case. The surfaces are of finite total curvature, since the Gauss map is meromorphic, i.e., its image covers the Riemann sphere a finite number of times.

FIRST EXAMPLES,

defined on  $\mathbb{C}$  or  $\mathbb{C} \setminus \{0\}$  or  $\mathbb{S}^2 \setminus \{1, -1\}$ :

Enneper Surface:

$$z \in \mathbb{C}, G(z) := z, dh := z dz$$

Polynomial Enneper:

$$z \in \mathbb{C}, G(z) := P(z), dh := P(z) dz$$

Rational Enneper:

$$z \in \mathbb{C}, G(z) := P(z)/Q(z), dh := P(z)Q(z) dz$$

$P$  and  $Q$  are polynomials without common zeros.

Vertical Catenoid:

$$z \in \mathbb{C} \setminus \{0\}, G(z) := z, dh := dz/z,$$

or  $G(z) := 1/z$

Helicoid:

$$z \in \mathbb{C}, G(z) := \exp(z), dh := \mathbf{i} dz = \mathbf{i} \frac{dG}{G}$$

Helicoid:

$$z \in \mathbb{C} \setminus \{0\}, G(z) := z, dh := \mathbf{i} dz/z$$

Planar to Enneper:

$$z \in \mathbb{C} \setminus \{0\}, G(z) := z^{k+1}, dh := z^{k-1} dz$$

Wavy Catenoid:

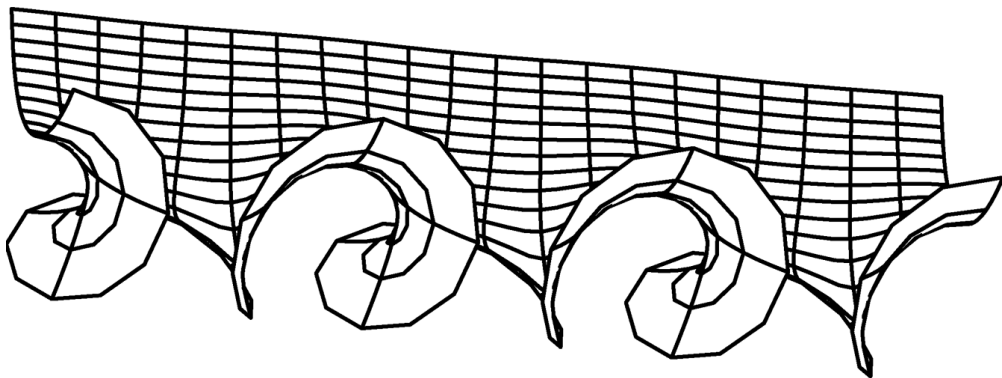
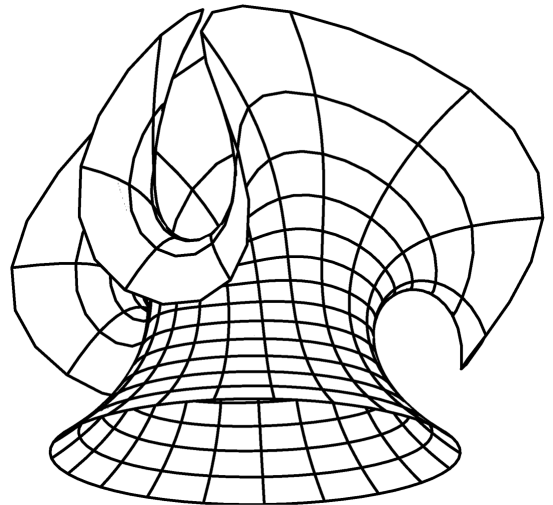
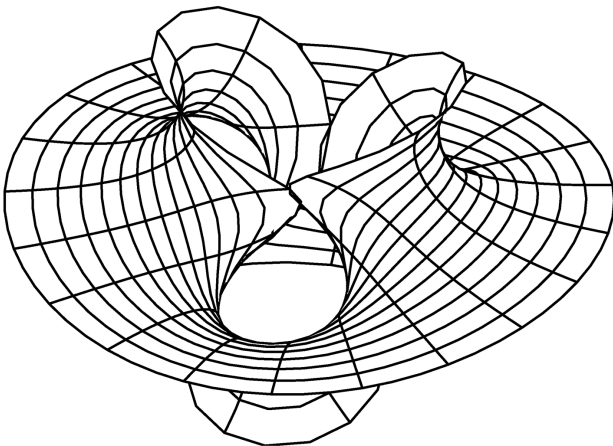
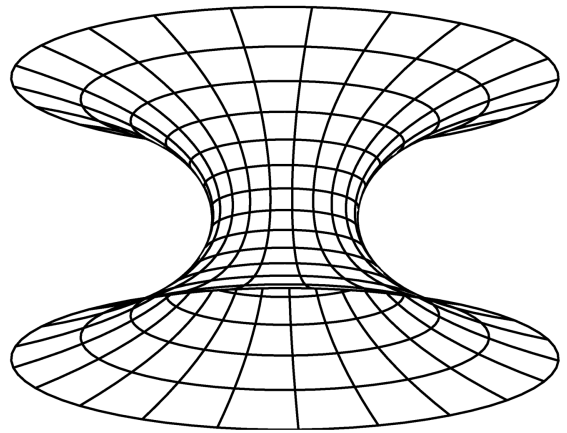
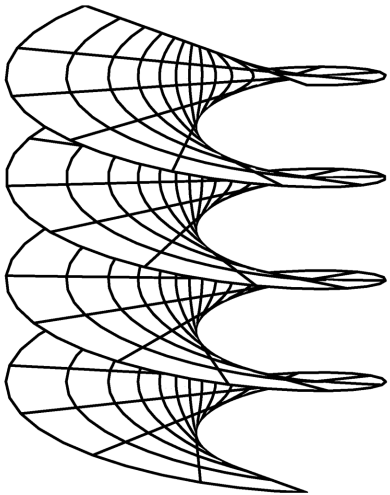
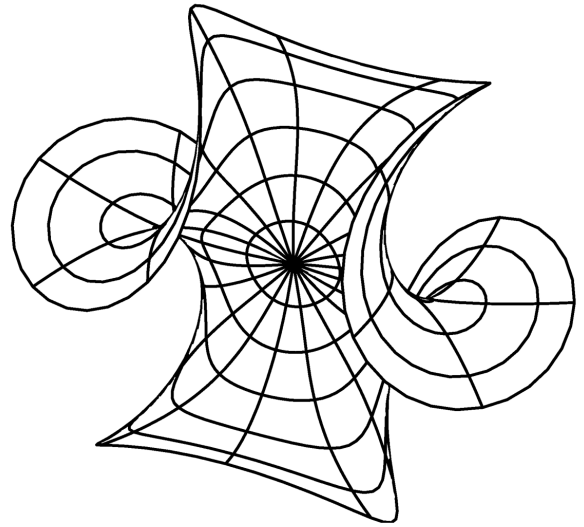
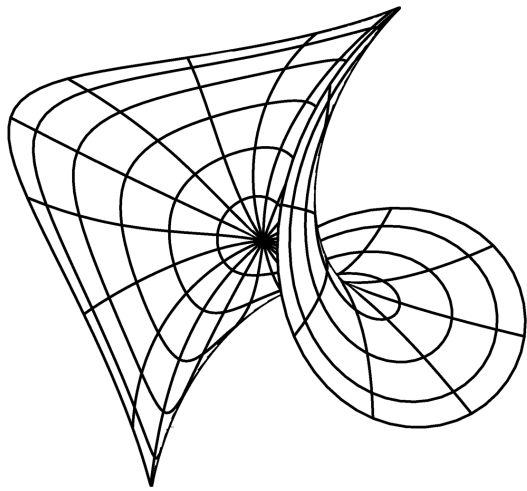
$$z \in \mathbb{C} \setminus \{0\}, G(z) := (1 + \epsilon \cdot z^k)/z, dh := G(z) dz$$

Wavy Plane:

$$z \in \mathbb{C} \setminus \{0\}, G(z) := z, dh := dz$$

Horizontal Catenoid:

$$z \in \mathbb{S}^2 \setminus \{1, -1\}, G(z) := z, dh := \frac{dz/z}{(z - 1/z)^2}.$$



All of these simple minimal surfaces have *symmetries*: (i) straight lines on a minimal surface allow  $180^\circ$  rotations of the minimal surface into itself, and (ii) planar geodesics on a minimal surface allow reflection (in the plane of the geodesic) of the minimal surface into itself. Since these symmetries become more important for understanding more complicated surfaces one should learn how to recognize them. The straight lines are geodesics with normal curvature  $II(c', c') = 0$  or  $dG(c')/G \cdot dh(c') \in \mathbf{i} \cdot \mathbb{R}$ . In the present context we recognize geodesics as fixed point sets of isometric involutions. The formula for the first fundamental form is so simple that one can easily see in all of these examples that the expected symmetry indeed does not change the Riemannian arc length of curves. To recognize the planar geodesics note that a geodesic on a surface is planar if it is also a principal curvature line; in addition to seeing it as the fixed point set of a length preserving involution we therefore only need to check  $dG(c')/G \cdot dh(c') \in \mathbb{R}$ , which is also easy in these examples.

In 3D-XplorMath one can easily change (in the Settings Menu) the range of the parametrization and also the symmetry of the surface. We recommend that the surfaces are looked at from far away when a large range for the parametrization is chosen. We also recommend to look at the default morphs of WavyEnneper and WavyCatenoid since it is quite surprising how suddenly the perturbation becomes visible. This should be taken as an illustration that the initial value problem for minimal surfaces is highly

unstable, it is *ill posed* and no numerical solution is possible.

#### MORE COMPLICATED SPHERICAL EXAMPLES.

The sudden increase of the interest in minimal surfaces after 1980 was largely caused by the discovery of a quite unexpected embedded finite total curvature minimal surface by Costa with embeddedness discovered and proved by Hoffman-Meeks. We are not yet close to such an example because of the following

*Theorem of Lopez-Ros.* An embedded, minimal, finite total curvature punctured sphere is a plane or a catenoid.

To practise using the Weierstraß representation we therefore have to be content with a few immersed punctured spheres. We want to learn *how to see the Gauss map* when one looks at the picture of such a minimal surface. The main fact to use is: a meromorphic function on a compact Riemann surface is determined up to a constant factor by its zeros and poles. In the case of the Jorge-Meeks  $k$ -noids one clearly sees a  $k$ -punctured sphere with a horizontal symmetry plane. One observes only two points with vertical normal, one up, one down. The qualitative behaviour of the Gauss map along the horizontal symmetry line suggests a mapping degree  $k - 1$ . This leaves no choice but  $G(z) = z^{k-1}$ . If we look back at the very simple examples then we can observe that, at a catenoid like puncture, either  $Gdh$  or  $dh/G$  has precisely a double pole. This determines the  $dh$  below up to a constant factor.

The next two examples, the 4-noid with orthogonal ends of different size, and the double Enneper, have a quite different appearance, but they have the same Gauss map. The vertical points are symmetric with respect to the origin and symmetric with respect to the unit circle, and the degree of the Gauss map is three; this determines the Blaschke product expression below. In the case of the 4-noid we need to create the four catenoid ends with double poles of  $dh$  and we need to compensate the simple zeros and poles of  $G$  by simple zeros of  $dh$ ; then, if we also treat zero and infinity symmetrically, the expression below is forced. In the case of the double Enneper surface we just need to compensate the simple zeros and poles of  $G$  (outside  $0, \infty$ ); symmetric treatment of  $0, \infty$  gives the  $dh$  below (except for a constant factor).

The last example illustrates in which way attempted counter examples to the Lopez-Ros theorem fail. A residue computation for the Weierstraß integrands shows that closed curves around the punctures  $\pm 1$  on the sphere are *not* closed curves on the minimal surface, if we want all limit normals to be vertical. It is easy to close this so called *period* when one allows tilted catenoid ends, but, as one decreases the tilt, the distance between the half catenoids increases, and they intersect the planar middle end if one computes the surface far enough towards the punctures.

The  $k$ -noids of Jorge-Meeks:

$$z \in \mathbb{S}^2 \setminus \{e^{2\pi \mathbf{i} \cdot l/k}; 0 \leq l < k\},$$

$$G(z) := z^{k-1}, \quad dh := (z^k + z^{-k} - 2)^{-1} \cdot dz/z.$$

4-noids with two different orthogonal ends:

$$z \in \mathbb{C} \setminus \{0, -1, +1\}, \quad G(z) := z \cdot \frac{z-r}{1-rz} \cdot \frac{z+r}{1+rz},$$

$$dh := \left(1 - \frac{z^2+z^{-2}}{r^2+r^{-2}}\right) \cdot (z^2 - z^{-2})^{-2} \cdot dz/z.$$

Two Enneper ends joined by a catenoidal neck:

$$z \in \mathbb{C} \setminus \{0\},$$

$$G(z) := z \cdot \frac{z-r}{1-rz} \cdot \frac{z+r}{1+rz}, \quad dh := \left(1 - \frac{z^2+z^{-2}}{r^2+r^{-2}}\right) \cdot dz/z.$$

Three punctures, period closes for tilted ends:

$$z \in \mathbb{C} \setminus \{-1, +1\},$$

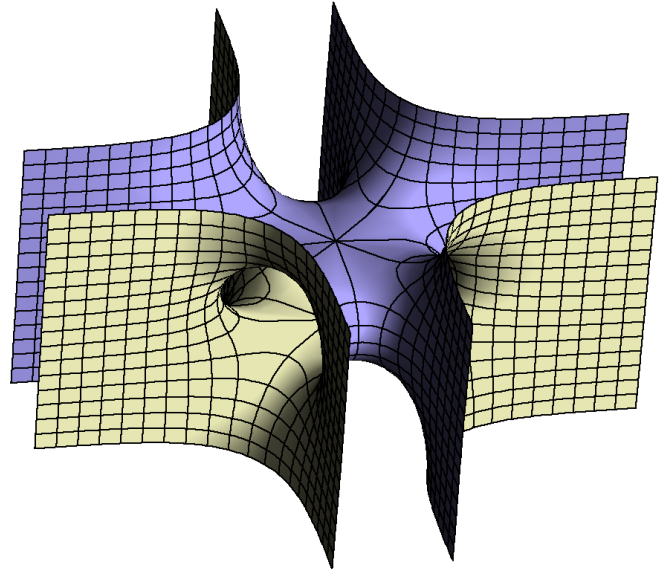
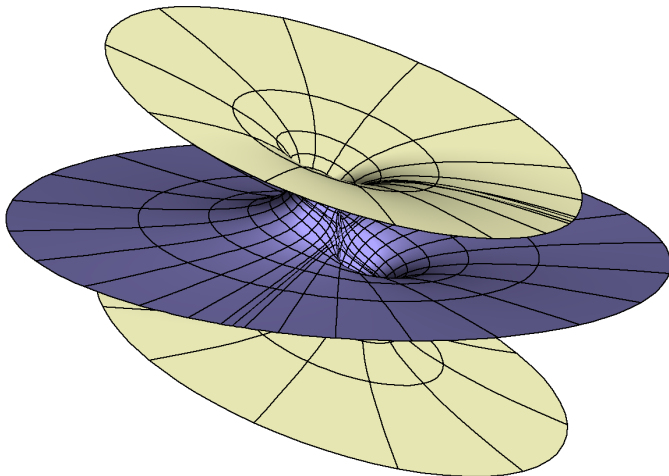
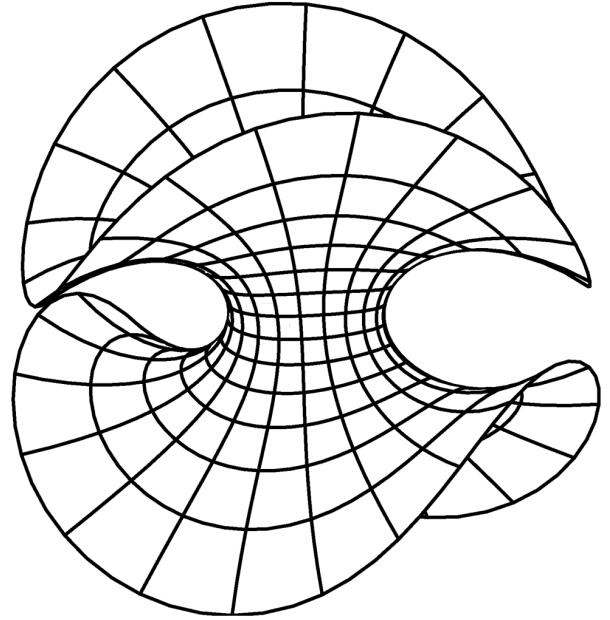
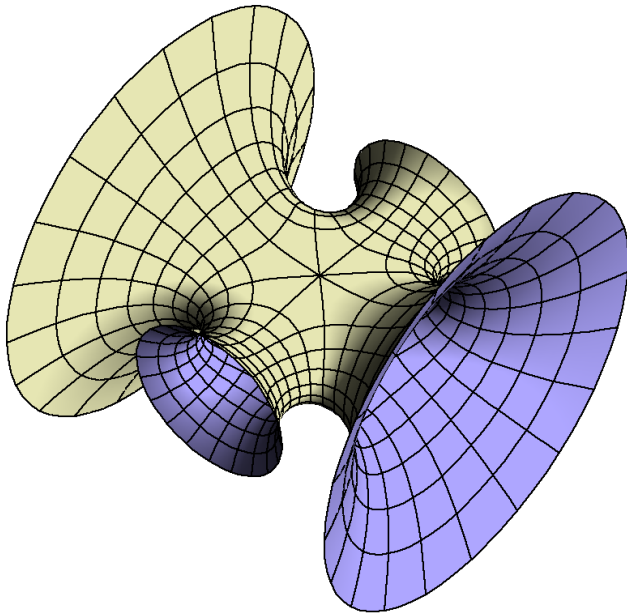
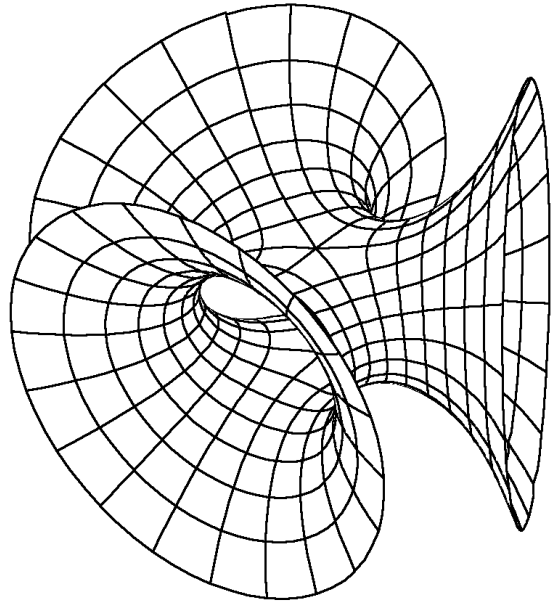
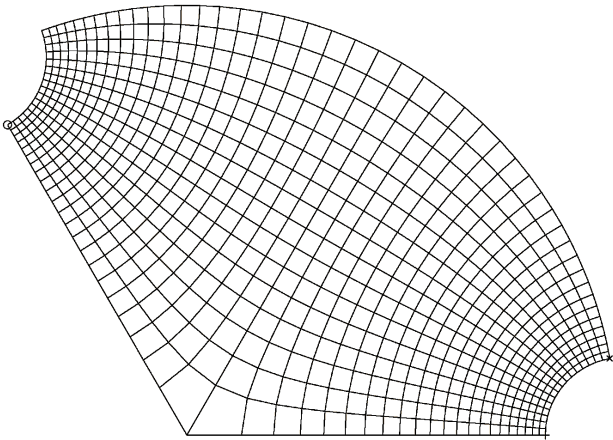
$$G(z) := \rho(z^2 - r^2), \quad dh := \frac{z^2-r^2}{(z^2-1)^2} dz.$$

Observe that the zeros and poles of the Gauss map which are not in the list of punctures are compensated by zeros of  $dh$ . At the embedded ends,  $Gdh$  or  $dh/G$  have a double pole and at the Enneper ends they have higher order poles. — In this list we do not have simple poles of  $Gdh$  and  $dh/G$ . If this happens then the Weierstraß integral behaves similar to  $\int dz/z$ : the unit disk, punctured at 0, is mapped by  $\log$  to an infinite number of half strips parallel to the negative real axis and of width  $2\pi$ . Similarly, the Weierstraß integral produces *simply periodic embedded minimal surfaces* parametrized by punctured spheres.

Generalized Scherk Saddle Towers:

$$z \in \mathbb{S}^2 \setminus \{e^{\pm\phi} \cdot e^{2\pi\mathbf{i}\cdot l/k}; 0 \leq l < k\},$$

$$G(z) := z^{k-1}, \quad dh := (z^k + z^{-k} - 2 \cos k\phi)^{-1} \cdot dz/z.$$



As in the simpler examples, observe that the symmetry lines can be seen from the Weierstraß data. We also note that at this point an important decision has to be made. If one represents the surfaces, as in all our examples, with parameter lines then each surface requires a special effort so that the parameter lines on the one hand support the complex analytic background of the minimal surface and on the other hand suggest correctly how one should imagine how the surface extends beyond what the picture shows. In 3D-XplorMath this individual approach has been taken. The other option is to spend considerably more general effort by writing software which will create a suitable triangulation of the domain. David and Jim Hoffman have such a program running. It requires much less individual work to compute another minimal surface but it is harder to illustrate the complex analysis background of the computed minimal surface.

The family of singly periodic embedded minimal surfaces which resemble the above generalized Scherk Saddle towers is much larger than the above explicit formulas suggest. So far we have only talked about the real part of the Weierstraß integral. In fact, a 1-parameter (“associate”) family of isometric (and in general not congruent) minimal surfaces are given by this integral because  $dh$  can be changed by the factor  $\exp(-2\pi i\varphi)$ . In particular, the imaginary part of the Weierstraß integral is the “conjugate” minimal surface. In the case of the generalized Scherk saddle towers we have that the conjugate minimal immersion maps the

unit disk (with the punctures on the boundary) to a graph over a convex polygon; its edge lengths all agree. The minimal graph has over each edge the boundary value  $+\infty$  or  $-\infty$ , alternatingly. — Jenkins-Serrin proved the converse: every such infinite boundary value problem has a graph solution, a minimal disk whose conjugate minimal surface is the fundamental piece of an embedded singly periodic saddle tower.

Having seen a good collection of minimal surfaces parametrized by punctured spheres we now turn to minimal surfaces parametrized by other Riemann surfaces. (To be written)

H.K.

TOC

## The Helicoid - Catenoid Family\*

Lagrange found in 1762 the minimal surface equation as Euler-Lagrange equation for the area minimization problem. Geometrically, this equation means that the mean curvature is 0. He found no other solution than the plane. In 1776 Meusnier discovered that the Helicoid and the Catenoid are also solutions. The next solutions were found 60 years later by Scherk.

The **Helicoid** ( $aa = 0$ ) – **Catenoid** ( $aa = 1$ ) **Family**:

$$x(u, v) := \cos(aa \cdot \pi/2) \sin(u) \sinh(v) + \sin(aa \cdot \pi/2) \cos(u) \cosh(v)$$

$$y(u, v) := \cos(aa \cdot \pi/2) \cos(u) \sinh(v) + \sin(aa \cdot \pi/2) \sin(u) \cosh(v)$$

$$z(u, v) := \cos(aa \cdot \pi/2) \cdot u + \sin(aa \cdot \pi/2) \cdot v$$

These formulas describe, for each  $aa$ , a minimal surface. Moreover, these surfaces are all isometric to each other; their Riemannian metrics, in the given parametrization, all have the same expression. The parameter lines  $u = \text{const}$  on the Helicoid ( $aa = 0$ ) are straight lines and no other minimal surface is such a *ruled* surface. The Catenoid ( $aa = 1$ ) is the only minimal surface of revolution. These two are the only embedded surfaces in the  $aa$ -family.

---

\* This file is from the 3D-XplorMath project. Please see:

The isometric  $aa$ -deformation is very fascinating, use **Cyclic Morph** in the Animation Menu. The small parameter squares do not change size or shape during the deformation, they just get bent a little. If the two sides of the surfaces are colored differently and  $aa$  varies from  $aa = 1$  to  $aa = 3$ , one can observe that the Catenoid is turned inside out. The deformation period is 4 and really amazing to watch.

H.K.

TOC

## Minimal Surfaces of Catalan, Henneberg, Scherk\*

These surfaces are early discovered minimal surfaces. They were found as explicitly parametrized surfaces, while soon afterwards variations of the Weierstrass representation became the main tool of description. This changed again in the early 1930s when Douglas and Rado solved the Plateau Problem with Functional Analysis methods. The Weierstrass representation had, after the work of Ossermann, a comeback in the 1980s.

Scherk's doubly periodic minimal surface (1835):

$$x(u, v) := \frac{u}{bb}, \quad y(u, v) := \frac{v}{bb}, \quad z(u, v) := \frac{1}{bb} \ln\left(\frac{\cos(v)}{\cos(u)}\right).$$

Catalan's minimal surface (1855), associate family:

$$x(u, v) := \frac{1}{bb} (\cos(aa \cdot \pi)(u - \sin(u) \cosh(v)) + \sin(aa \cdot \pi)(v - \cos(u) \sinh(v)) - 4)$$

$$y(u, v) := \frac{1}{bb} (\cos(aa \cdot \pi)(1 - \cos(u) \cosh(v)) + \sin(aa \cdot \pi) \sin(u) \sinh(v))$$

$$z(u, v) := \frac{1}{bb} (\cos(aa \cdot \pi)4 \sin(u/2) \sinh(v/2) + \sin(aa \cdot \pi)4 \cos(u/2) \cosh(v/2)).$$

---

\* This file is from the 3D-XplorMath project. Please see:

Henneberg's minimal surface (1875), associate family:

$$caa := \frac{2 \cos(aa \cdot \pi)}{0.01 + |bb|}, \quad saa := \frac{2 \sin(aa \cdot \pi)}{0.01 + |bb|}$$

$$x(u, v) := caa \cdot (\sinh(u) \cos(v) - \frac{1}{3} \sinh(3u) \cos(3v))$$

$$+ saa \cdot (\cosh(u) \sin(v) - \frac{1}{3} \cosh(3u) \sin(3v))$$

$$y(u, v) := caa \cdot (\sinh(u) \sin(v) + \frac{1}{3} \sinh(3u) \sin(3v))$$

$$+ saa \cdot (-\cosh(u) \cos(v) - \frac{1}{3} \cosh(3u) \cos(3v) + \frac{4cc}{3})$$

$$z(u, v) := caa \cdot (\cosh(2u) \cos(2v) - cc)$$

$$+ saa \cdot \sinh(2u) \sin(2v)$$

$$u \in \mathbb{R}, v \in [-\pi, \pi], \text{ a cylinder domain.}$$

The default value of the translation parameter,  $cc = 0$ , puts the symmetry point of Henneberg's surface at the origin. If one wants to scale up a neighborhood of the branch point at  $u = 0, v = 0$ , use  $cc = 1$  to put that branch point at the origin and make use of the scaling parameter  $bb$  in the denominator.

Scherk's discovery of the above doubly periodic surface, of its singly periodic conjugate surface and of three less spectacular ones was a sensation since the only other known minimal surfaces, the catenoid and the helicoid, were already 50 years old. Scherk's surfaces were destined to play a major role in the discovery period after 1980.

Catalan's surface was next, 20 years later. This slow progress reflects the fact that no methods for the construction of minimal surfaces were known. This changed with Riemann, Weierstrass, Enneper and finally Schwarz. Their methods built on complex analysis and allowed to write down arbitrarily many examples. Therefore the emphasis shifted to examples that had additional properties. In particular complete, embedded minimal surfaces were sought. Quite a few triply periodic embedded ones were found, but it took another 100 years before the next embedded finite total curvature example after the catenoid was constructed: Costa's example, a minimal embedding of the thrice punctured square torus.

Henneberg's minimal surface was studied a lot because of its two branch point singularities (on the  $z$ -axis). Such singularities are difficult to imagine and Henneberg's surface is a simple example to exhibit them. The default image in 3DXM shows a small neighborhood of the two branch points. The segment between them is a selfintersection line of the surface. The lines  $\{x = \pm y, z = 0\}$  lie also on the surface.  $180^\circ$  rotation around any of these straight lines is a symmetry of the surface and the conjugate surface has, correspondingly, the three planes which pass through the origin and are orthogonal to one of these three lines, as symmetry planes. - Note: The conjugate surface has twice the area of Henneberg's surface. This is because Henneberg's surface is covered twice. For about 100 years it was the only known non-orientable minimal surface.

The last entry in the Action Menu emphasizes a Möbius band on Henneberg's surface. The default morph is the associate family morph.

The Range Morph (from the Animate Menu) shows larger and larger pieces of the surface - scaled down to fit on the screen. One can see still larger portions by increasing `uMax` beyond 0.95. (Choose  $b1 > 1$  to compensate for the growing size.)

A third morph expands a band around the two branch points and moves it over the surface.

The parameter line  $u = 0, v \in [-\pi, \pi]$  is a symmetry line of the domain cylinder. It is mapped to the segment between the branch points on the  $z$ -axis and  $180^\circ$  rotation around it is a symmetry of the surface. The two lines  $v = 0$  and  $v = \pi$  are also symmetry lines of the domain cylinder. They are mapped to curves of reflectional symmetry, reflection in the  $x$ - $z$ -plane. They end in the branch points like a Neil parabola,  $\{x^3 = z^2\}$ .

H.K.

TOC

# About the Classical Enneper Surface \*

## and some Polynomial Relatives

See also: [About Minimal Surfaces](#)

### DEFINITION WITH EXPLICIT FORMULAS

The *classical Enneper Surface* is a minimal immersion of the complex plane,  $\mathbb{C}$ , into Euclidean space  $\mathbb{R}^3$ . It is given by the formula

$$F(z) := \text{real}(\{z^3/3 - z, i \cdot (z^3/3 + z), z^2\}).$$

If one wants to see coordinate lines on the image one can use Cartesian coordinates for the complex plane,  $z := x + i \cdot y$ , or polar coordinates  $z := r \cdot (\cos \varphi + i \cdot \sin \varphi)$ , and map those grids with  $F$ . The Cartesian choice is natural here since its parameter lines are principal curvature lines. However the polar choice also has merits—namely, rotations around the origin are isometries and the coordinate lines are orbits. Moreover all symmetry lines of the surface are radial parameter lines. The Action Menu of 3DXM allows to switch between these parametrizations. In 3DXM one can also deform this classical surface, but we need to explain the significance of what one sees. See the last page of this text.

---

\* This file is from the 3D-XplorMath project. Please see:

Early in the second half of the nineteenth century the *Enneper-Weierstraß representation* of minimal surfaces was discovered. Its main advantage is that it permits one to write a formula for a minimal surface in terms of important geometric quantities. Every surface in  $\mathbb{R}^3$  can be mapped to the 2-sphere  $\mathbb{S}^2$  by sending each point on the surface to the unit normal at this point; this map is called the geometric Gauß map  $N$ . For minimal surfaces this map is angle preserving, but orientation reversing. Composition of  $N$  with the orientation reversing stereographic projection therefore gives a map  $g$  from the surface into  $\mathbb{C}$  which is both *and* orientation preserving. Finally, if we interpret  $90^\circ$  rotation on each tangent space of a surface in  $\mathbb{R}^3$  as multiplication of tangent vectors by  $i$ , then with this convention  $g$  becomes a meromorphic function, the meromorphic Gauß map of the minimal surface. This meromorphic Gauß map is one-half of the *Weierstraß data* which are needed to write down the Enneper-Weierstraß representation. The remaining part of these data is the differential  $dF^3$  of the third component of  $F$ , i.e., of the height function on the minimal surface. It might seem at first that we must know a minimal surface rather well before we have its Weierstraß data. However, on a large class of geometrically important minimal surfaces the situation is simple indeed. If a minimal surface is complete and has finite total curvature then the Gauß map  $g$  is determined—up to a constant factor—by its zeros and poles, in other words by its vertical normals. This important result extends to differentials, in

particular to the differential of the height function, after we perform a small trick, namely extend the real valued differential  $dF^3$  to a complex valued one by putting for every tangent vector  $v$  of the surface

$$\begin{aligned} dh(v) &:= dF^3(v) - i \cdot dF^3(i \cdot v) \\ &:= dF^3(v) - i \cdot dF^3(\text{Rot}^{90}(v)). \end{aligned}$$

To make matters even simpler, observe that the points on the surface, where the normal is vertical, are the same points where the differential of the height function is zero. More precisely, the zeros and poles of  $g$  on the minimal surface are precisely the zeros of  $dh$ , even with the same multiplicity. (To complete this discussion we would have to study the situation at infinity, but we will omit this.) The main point is to point out that very few, *finitely many*, data about such minimal surfaces suffice to find their Weierstraß data and therefore explicitly parametrize them. Here is this famous formula:

Weierstraß Representation in terms of  $g$ ,  $dh$ :

$$F(z) := \text{Re} \left( \int_*^z \left\{ \frac{1}{2} \left( g - \frac{1}{g} \right) dh, \frac{i}{2} \left( g + \frac{1}{g} \right) dh, dh \right\} \right)$$

The classical Enneper surface is obtained if we put  $g(z) = z$ ,  $dh = z dz$ .

This generalizes to polynomials  $P(z)$ , put:

$$g(z) = P(z), \quad dh = P(z) dz.$$


---

3DXM allows  $P(z) := aa \cdot z + bb \cdot z^2 + cc \cdot z^3$ .

---

The pure powers have again the rotations around the origin as metric isometry group and *polar coordinates* provide a much better view of these surfaces and are recommended. All surfaces of the associate family are, for  $g(z) = z^k$ , congruent. There are straight lines on the surface, and if one looks in the direction of the z-axis onto the surface, then the portion below these lines is drawn first. The default morph deforms two such surfaces into each other.

H.K.

TOC

## A Minimally Immersed Projective Plane \*

See first: [About Minimal Surfaces](#)

This minimal surface is remarkable because its associate family contains an immersion of the triply punctured projective plane. It was discovered independently by Rob Kusner and Robert Bryant. It is also an example where the Weierstraß data can be explicitly integrated to a rational parametrization of the surface:

$$\begin{aligned}W_1(z) &= \frac{i(z^2 - z^{-2})}{z^3 - z^{-3} + \sqrt{5}} = \frac{i(z^5 - z)}{z^6 - 1 + \sqrt{5}z^3} \\W_2(z) &= \frac{z^2 + z^{-2}}{z^3 - z^{-3} + \sqrt{5}} = \frac{z^5 + z}{z^6 - 1 + \sqrt{5}z^3} \\W_3(z) &= \frac{\frac{2i}{3}(z^3 + z^{-3})}{z^3 - z^{-3} + \sqrt{5}} - \frac{2i}{3} = \frac{2i}{3} \left( \frac{z^6 + 1}{z^6 - 1 + \sqrt{5}z^3} - 1 \right)\end{aligned}$$

The associate family is  $F_\varphi(z) := \operatorname{Re}(e^{i\varphi}W(z))$ .

Note the antipodal symmetry  $W(-1/\bar{z}) = \overline{W(z)}$ , which says that  $F_0 = \operatorname{Re}(W) = -F_\pi$  is an immersion of the punctured projective plane. The poles of  $W$  are at the six zeros of the denominator, with  $a^3 = \frac{3-\sqrt{5}}{2}$ ,  $a \approx 0.72556$  they are  $(a, -1/a) \cdot (1, e^{2\pi i/3}, e^{-2\pi i/3})$ , three antipodal pairs.

The above formulas indeed represent minimal surfaces since

$$W_1'(z) + W_2'(z) + W_3'(z) = 0.$$

This is expressed as:  $z \mapsto W(z)$  is a holomorphic null curve.

---

\* This file is from the 3D-XplorMath project. Please see:

We also give the Weierstrass data:

$$g(z) = \frac{z^2(z^3 - \sqrt{5})}{\sqrt{5}z^3 + 1}, \text{ with } g(-1/z) = -1/g(z),$$
$$dh_z = \frac{2iz^2(z^3 - \sqrt{5})(\sqrt{5}z^3 + 1)}{(z^6 - 1 + \sqrt{5}z^3)^2} dz$$

For parameter lines we use conformal polar coordinates  $z = \exp(u + iv)$ . A band  $-0.2 < u < 0$ ,  $0 \leq v \leq 2\pi$  is mapped to a minimal Möbius band, see the Action Menu. Near the punctures the minimal surfaces  $F_\varphi$  are asymptotic to planes. One says: these minimal surfaces have planar ends. At such planar ends  $g \cdot dh$  or  $1/g \cdot dh$  must have a double pole and  $g$  must have a branch point, i.e.  $g'(z) = 0$  for finite  $z$ . Indeed, one can check that  $g'(z_0) = 0$  at the zeros  $z_0$  of the denominator of  $dh$ .

Planar ends have the following nice property: Invert the minimal surface in some sphere. Its planar ends invert to surface pieces with one-point holes. *These holes can be smoothly closed.* This gives immersions of the complete projective plane by inverting the minimal surface  $F_0$  and closing the holes of its three inverted ends. The point at infinity inverts to a triple point of such immersions. These immersions are called **Boy Surfaces** since a topological version was constructed in Boy's PhD thesis under Hilbert. It was the first immersion of the projective plane into  $\mathbb{R}^3$ . A model stands in front of the Oberwolfach Institute.

## About Wavy Enneper \*

The surfaces Wavy Enneper, Catenoid Enneper, Planar Enneper, and Double Enneper are finite total curvature minimal immersions of the once or twice punctured sphere—shown with standard polar coordinates. These surfaces illustrate how the different types of ends can be combined in a simple way.

Morphing ( $0 \leq bb \leq 2$ ) Wavy Enneper rotates a high order Enneper perturbation (amplitude =  $aa$ , frequency= $ff$ ) over the  $ee$  tongues of a lower order Enneper surface. Note how the perturbation decreases quickly with the distance from the boundary.

$aa=0$ ,  $ee=2$  gives the standard Enneper surface.

Gauss map :

$$Gauss(z) = z^{ee-1}(1 + aa \exp(i\pi bb)z^{ff})/(1 + aa)$$

Differential:

$$dh = scaling \cdot Gauss(z) dz$$

The pure Enneper surfaces ( $aa = 0$ ) and the Planar Enneper surfaces have been re-discovered many times, because the members of the associate family are *congruent*

---

\* This file is from the 3D-XplorMath project. Please see:

surfaces (as can be seen in an associate family morphing) and the Weierstrass integrals integrate to polynomial (respectively) rational immersions. Double Enneper was one of the early examples in which I joined two classical surfaces by a handle; we suggest to morph the size of the handle or the rotational position of the top Enneper surface against the bottom Enneper surface.

H.K.

TOC

## About Catenoid Enneper \*

The surfaces Wavy Enneper, Catenoid Enneper, Planar Enneper, and Double Enneper are finite total curvature minimal immersions of the once or twice punctured sphere—shown with standard polar coordinates. These surfaces illustrate how the different types of ends can be combined in a simple way.

Here an Enneper perturbation with  $ee$  tongues (size adjusted with  $aa$ ) crumples one rim of a catenoid in the suggested morphing. It is also interesting to choose  $aa=0.65$ ,  $ee=13$ , or so. The catenoid is  $aa=0$ .

Gauss map :  $Gauss(z) = (4 - aa(1 + z^{ee}))/z$

Differential:  $dh = (1 + aa^2/2) \cdot Gauss(z) dz$ .

The pure Enneper surfaces ( $Gauss(z) = z^k$ ) and the Planar Enneper surfaces have been re-discovered many times, because the members of the associate family are *congruent* surfaces (as can be seen in an associate family morphing) and the Weierstrass integrals integrate to polynomial (respectively) rational immersions. Double Enneper was one of the early examples in which I joined two classical surfaces by a handle; we suggest to morph the size of the handle or the rotational position of the top Enneper surface against the bottom Enneper surface.

H.K.

TOC

---

\* This file is from the 3D-XplorMath project. Please see:

## About Planar Enneper \*

The surfaces Wavy Enneper, Catenoid Enneper, Planar Enneper, and Double Enneper are finite total curvature minimal immersions of the once or twice punctured sphere—shown with standard polar coordinates. These surfaces illustrate how the different types of ends can be combined in a simple way.

The pure Enneper surfaces ( $aa = 0, dd = 0$ ) and the Planar Enneper surfaces ( $aa = 0, dd = 2$ ) with Weierstrass data:

Gauss map :  $Gauss(z) = z^{ee+1}(1 + aa z^{ff})$

Differential:  $dh = scaling \cdot Gauss(z)/z^{dd} dz$

have been re-discovered many times, because the members of the associate family are *congruent* surfaces (as can be seen in the interesting associate family morphing!!) and the Weierstrass integrals integrate to polynomial (respectively rational) immersions. For  $aa = 0, dd = 1$  one does not obtain a finite total curvature surface, but a periodic surface that looks like a halfplane with periodically attached Enneper pieces. One obtains larger pieces of this *Wavy Plane* if one either increases  $ee$  or the range of  $v$ . The members of the associate family are also congruent, try *Cyclic Associate Family Morph*.

For small  $aa \neq 0$  one has wavy perturbations of the Enneper end.

---

\* This file is from the 3D-XplorMath project. Please see:

For the ( $aa = 0$ )-examples  $ee$  is an integer valued parameter that determines the degree of dihedral symmetry of the surfaces. Morphing the range of  $u$  helps to imagine these surfaces by starting with a plane minus a disk and then observe how an Enneper end is attached. In the Set Morphing Dialog first press *Initiate to current parameters*, then choose  $umax0 = -0.5$ ,  $umax1 = 0.6$ .

H.K.

TOC

## About Double Enneper \*

The surfaces Wavy Enneper, Catenoid Enneper, Planar Enneper and Double Enneper are finite total curvature minimal immersions of the once or twice punctured sphere—shown with standard polar coordinates. These surfaces illustrate how the different types of ends can be combined in a simple way.

The pure Enneper surfaces ( $\text{Gauss}(z) = z^k$ ,  $dh = \text{Gauss}(z) dz$ ) and the Planar Enneper surfaces

$$(\text{Gauss}(z) = z^k, dh = \text{Gauss}(z)/z^2 dz)$$

have been re-discovered many times, because the members of the associate family are *congruent* surfaces (as can be seen in an associate family morphing) and the Weierstrass integrals integrate to polynomial (respectively) rational immersions. Double Enneper was one of the early examples in which I joined two classical surfaces by a handle. The Weierstrass data are:

Gauss map :

$$\text{Gauss}(z) = z^{ee-1}(z^{ee} - A^{ee})/(A^{ee}z^{ee} - 1)$$

Differential:

$$dh = e^{i\varphi}(1 - (z^{ee} - z^{-ee})/(A^{ee} - A^{-ee})) dz/z.$$

with  $A = \sqrt{aa} \cdot \exp(i\alpha)$ ,  $\alpha = \pi bb/ee$

and  $(A^{ee} + A^{-ee}) \tan \varphi = -(A^{ee} - A^{-ee}) \tan 2\alpha$ . The last

---

\* This file is from the 3D-XplorMath project. Please see:

equality is needed to avoid periods of the Weierstrass integral.

In this example the parameter  $aa$  controls the size of the neck between the top and bottom Enneper ends (it should be kept in the range  $3 < aa < 7$ ). The parameter  $bb$  rotates the top and the bottom ends relative to each other, The integer parameter  $ee = 2, 3, \dots$  determines the winding number of the Enneper ends and also the rotational symmetry of the surface—the default is  $ee = 2$ . And  $umin$  and  $umax$  control how far into the ends one computes.

Try a *Cyclic Morph* with the default parameters (this rotates the upper and lower ends in opposite directions). We also suggest morphing the size ( $aa$ ) of the handles. If the ends intersect too much (e.g. for too large  $u$ -range or too large  $ee$ ) one has to reduce the  $u$ -range. The Cyclic Morph is also interesting for large  $ee$ , for example  $ee = 12$ ,  $umin = -1.45$ ,  $umax = 1.5$  and reduced scaling.

H.K.

TOC

## About the Saddle Tower Surface \*

These examples generalize Scherk's conjugate pair of singly-periodic/doubly-periodic minimal surfaces. The singly-periodic examples stay embedded if the dihedral symmetry (and with it the number of punctures) is increased ( $\text{Gauss}(z) = z^k, k = ee - 1$ ). The most symmetric ones ( $bb=0.5/ee$ ) can be deformed by decreasing  $bb$ . See [K1], [K2] for more details.

These surfaces are parametrized by punctured spheres, but the Weierstrass integrals have periods, a vertical one in the singly periodic case, two horizontal ones for doubly periodic surfaces. The parameter lines extend polar coordinates around the punctures to the whole sphere—in these cases giving level lines on the surfaces.

The degree of dihedral symmetry is, of course, a discrete property, and it is controlled by the parameter  $ee$ . Thus,  $ee$  should be set to an integer (the default is 2). For each choice of  $ee$ , changing  $bb$  gives a one-parameter family of surfaces, of which the most symmetric member is obtained by setting  $bb = 0.5/ee$ . Try setting  $ee$  to 3 and 4, and  $bb$  to 0.333 and 0.25 respectively. The wings of the singly periodic saddle tower surfaces become parallel in pairs if (for  $ee > 2$ ) one sets  $bb = 0.0825$ . These stay embedded

---

\* This file is from the 3D-XplorMath project. Please see:

for  $ee=3$  and  $ee=4$ .

We also recommend viewing the associate family morphing.

[K1] H. Karcher, Embedded minimal surfaces derived from Scherk's examples, *Manuscripta Math.* 62 (1988) pp. 83–114.

H.K.

TOC

## The Twisted Saddle Towers \*

The *Twisted Scherk Saddle Towers* are minimal surfaces that were found in 1988 as deformations of the Scherk Saddle Towers. Therefore one should first look at these latter simpler surfaces. One can imagine that one grips such a saddle tower at the top and the bottom and deforms the surface by twisting it. Of course it is not clear whether this can be done in such a way that the deformations stay minimal.

Fortunately, the most symmetric Scherk Saddle Towers carry straight lines through their saddles, and it is easy to imagine these lines staying on the twisted surface and remaining as lines of symmetry. Using these lines we can obtain the existence of the desired surfaces by solving the following Plateau Problem.

Consider a pair of adjacent half-lines through one saddle and another pair of half-lines, starting from the saddle above the first and with one of its half-lines vertically above the sector between the first two. These two “broken lines” cut a simply connected strip out of the surface. (One can see it by selecting “Don’t Show Reflections” from the Action Menu).

---

\* This file is from the 3D-XplorMath project. Please see:

Now, vice versa, start with the two broken-lines and solve the Plateau problem for this infinite boundary to find a minimal strip they bound. Finally use  $180^\circ$  rotations around the half-lines to extend the Plateau strip to a complete minimal surface, a Twisted Scherk Saddle Tower. These surfaces played an important role in the development of the theory of minimal surfaces since—except for the Helicoid itself—they were the first examples having helicoidal ends,

The integer parameter  $ee$  controls the dihedral rotational symmetry of the surface: the angle of each pair of half lines above is  $\pi/ee$ . The parameter  $aa$  controls the amount of twist, with  $aa = 0$  giving the straight Scherk Saddle Towers. We must keep  $aa < \pi/ee$ , since otherwise the existence construction fails. Of course the default morph varies  $aa$ .

In 3D-XplorMath minimal surfaces are computed via their Weierstraß representation. The Scherk Saddle Towers are parametrized by punctured spheres and our twist deformation does not change this conformal type. However, due to this twist, the Gauß map of the surface is not single-valued: it is rather a multivalued function on the punctured sphere, and this makes the computation more difficult than for the other spherical minimal surfaces, since during the integration of the multivalued Weierstraß integrand, it is necessary to use analytic continuation in order to guarantee that we always have the correct value of the

Gauß map.

The Weierstraß representation is given in:

Karcher, H., Embedded Minimal Surfaces derived from Scherk's Examples, *Manuscripta math.* 62 (1988), pp. 83 - 114.

Recently Traizet and Weber have found a new construction of embedded singly periodic minimal surfaces that can be illustrated with the twisted Scherk saddle towers. Choose  $aa$  close to its theoretical limit  $1/ee$  and try to see the resulting surfaces as made out of  $ee$  ordinary helicoids. Obviously one has to allow modifications of the helicoids in the middle, but away from the middle one can see these helicoids well. Traizet and Weber were able to turn this observation around. They found conditions how to place a collection of helicoids so that they could prove the existence of a family of singly periodic embedded minimal surfaces which converged to the given helicoids in the same sense as the twisted Scherk saddle towers converge as  $aa \rightarrow \pm 1/ee$ .

H.K.

TOC

## Symmetric and Skew-symmetric k-Noids \*

The symmetric and skew k-noids are parametrized by k-punctured spheres. The number  $k$  of ends is selected with the 3DXM parameter  $ee$ . We use parameter lines that extend polar coordinates around the punctures. Formulas are taken from [K2]. These formulas easily allow to change the relative size of neighboring catenoid ends for the **symmetric 2k-noids**, try the *default morph* which varies the 3DXM parameter  $aa$  in  $[0, 1]$ . The symmetric k-noids, where the number  $k$  of ends is odd, cannot be deformed in 3DXM.

The ends of the **skew-symmetric k-noids** in 3DXM are all of the same size. The *default morph* varies the angle between neighboring ends, again by changing the 3DXM parameter  $aa$  in  $[0, 1]$ .

The size of the ends is always controlled using  $bb$ .

The intersection of the two families are the symmetric k-noids with all ends of the same size, a family found by Jorge and Meeks. Their k-noids are the first finite total curvature immersions for which the Weierstrass data were manufactured to fit a previously conceived qualitative global picture of the surfaces.

---

\* This file is from the 3D-XplorMath project. Please see:

The default morph of the symmetric  $2k$ -noids ends at symmetric  $k$ -noids with  $k$  punctures as  $aa$  goes to zero.

In the default morph of the skew-symmetric  $k$ -noids the angle between neighboring pairs of ends goes to zero. Near the limit the 4-noid looks like a pair of parallel catenoids that are joined by a very thin “catenoidal” handle. In fact the picture looked so suggestive that it convinced David Hoffman immediately that the idea of adding handles might be promising in a wide range of situations. *Try this default morph!*

H.K.

TOC

## About the Lopez-Ros No-Go Theorem \*

The Lopez-Ros Theorem [LR] says that a complete, minimal embedding of a punctured sphere is either a Catenoid or a plane. Our example is parametrized by a 3-punctured sphere. Its Gauss map is  $\text{Gauss}(z) := cc(z-1)(z+1)$ . The differential  $dh = (z^2 - 1)/(z^2 - ee)^2$  puts the punctures at  $+ee$ ,  $-ee$  and  $\infty$ . Parameter lines on the sphere extend polar coordinates around the punctures at  $z = +ee$ ,  $z = -ee$ ,  $z = \infty$  in order to make the ends look nice.

A necessary condition for embeddedness is that the normals of all ends are parallel, i.e.,  $ee = 1$ . In this case a residue computation shows that the period cannot be closed, in agreement with the theorem of Lopez-Ros. If  $ee > 1$ , then  $cc$  can be chosen to close the period, but then the catenoid ends are tilted so that they intersect the third (planar) end. The default morph in 3DXM shows what happens when  $ee$  approaches 1 while the periods are always closed (with a closing value of  $cc$  that grows to infinity). In a properly scaled picture the surface looks more and more like two catenoids at larger and larger distance. Since we also want to show morphs were the period opens up, the program uses  $cc$  as follows: If the user sets  $cc = 0$

---

\* This file is from the 3D-XplorMath project. Please see:

then the program recomputes  $cc$  to the period-closing value  $cc_{close}$ . Otherwise we only restrict  $cc$  by resetting it as

$$cc = \max(0.5 \cdot cc_{close}, \min(cc, 2 \cdot cc_{close})).$$

To choose one's own morph, note that the surface has a gap if  $cc$  is larger than  $cc_{close}$ , and that it intersects itself if  $cc$  is smaller than  $cc_{close}$ . As an example, compute first with  $ee = 1.01, cc = 0$ ; then, in the Set Morphing Dialog, click the button *Initialize to current parameters*, and finally morph  $ee$  from the current value  $ee0 = 1.01$  to some larger value, e.g.  $ee1 = 1.08$ .

[LR] F.J. Lopez and A. Ros, On embedded complete minimal surfaces of genus zero, *Journal of Differential Geometry* 33 (1), 1991, pp 293–300.

H.K.

TOC

## Two Planar And Two Catenoid Ends \*

This Minimal surface is parametrized by a sphere with four punctures. In the complex plane its Weierstrass data are

$$\text{gaus}(z) := \frac{z - a}{az + 1} \cdot z^2, \quad dh := \frac{z - 1/z - a + 1/a}{(z - 1/z - c + 1/c)^2} \cdot \frac{dz}{z}.$$

The Gauss map has a simple zero and pole at  $a$  and  $-1/a$ . These are finite points on the minimal surface since they are cancelled by the simple zeros of  $dh$  at  $a, -1/a$ . And the Gauss map has a double zero and pole at  $0, \infty$ . These give planar ends because  $dh$  is neither  $0$  nor  $\infty$  there. The double poles of  $dh$  at  $c, -1/c$  give catenoid ends because the Gauss map has simple finite values there - see **About Minimal Surfaces** in the Documentation Menu.

Catenoid ends usually come with a period. A residue computation shows that the choice  $a := c - 1/c$  makes the period of the real part of the Weierstrass integral zero.

Note that the Weierstrass data are symmetric with respect to  $180^\circ$  rotation around  $i, -i$ . This corresponds to a  $180^\circ$  rotation of the minimal surface around the  $y$ -axis in  $\mathbb{R}^3$ .

Recall that the *Lopez-Ros theorem* states that the only complete *embedded* minimal surfaces that are parametrized by punctured spheres (and have finite total curvature) are *the plane and the catenoid*.

One can view the shape of the current surface as made from two copies of our Lopez-Ros-No-Go example by stacking these above each other and deforming the two half

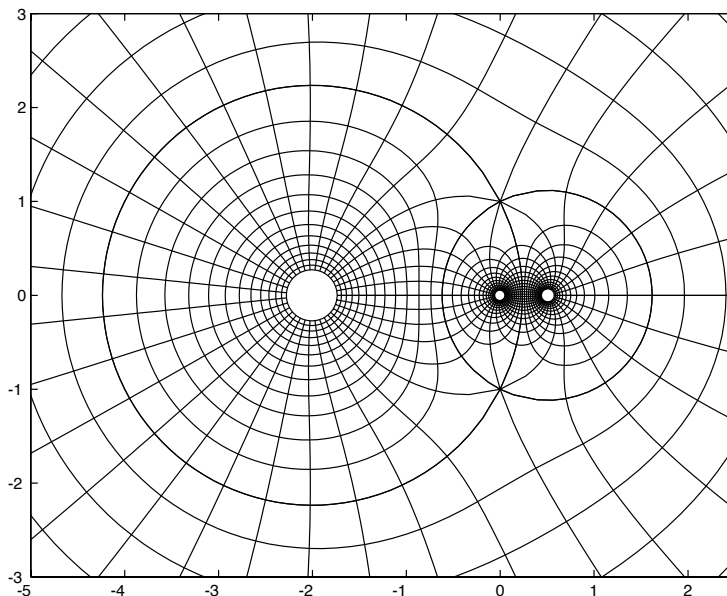
---

\* This file is from the 3D-XplorMath project. Please see:

catenoids between them into the handle of the current surface between its two planes. The new surface is therefore another failing attempt of a counter example to the Lopez-Ros theorem. View in the Animate Menu the morph: **Watch The closed Catenoids Tilt**. It shows: The two catenoid ends get more vertical as  $c$  approaches 0, but in the limit the whole surface degenerates to a doubly covered plane.

Compare the current surface also to the *Riemann minimal surface*. Its shape can be viewed as an infinite stack of copies of the current surface – again, of course, with the half-catenoids between adjacent copies deformed into handles which join the copies.

Minimal surfaces look much better when the grid lines in the parameter domain behave like polar centers around the punctures. With this in mind, the current surface was parametrize by the following grid in  $\mathbb{C}$ :



## Half-Catenoids and Weierstrass Representation \*

In this text we try to explain, starting from scratch, minimal surfaces parametrized by tori.

We assume from complex analysis roughly the following: The complex logarithm,  $\log(z)$ , is a multivalued function with derivative  $\log'(z) = 1/z$ . One can compute the logarithm by integrating the differential form  $dz/z$  along a curve  $c : [0, 1] \mapsto \mathbb{C}$  with  $c(0) = 1$ ,  $c(1) = z$ :

$$\log(z) := \int_c \frac{1}{\zeta} d\zeta := \int_0^1 \frac{c'(t)}{c(t)} dt$$

Of course, the integration path  $c$  has to avoid 0. Therefore one can reach  $z$  from 1 in many ways. A basic property of such complex line integrals is that their value does not change if the path is deformed, but with fixed endpoints. Two paths which wind around 0 a different number of times cannot be deformed into each other and, indeed, the values of the integrals along the two paths differ by an integer multiple of  $2\pi i$ . This number, the value of the integral from 1 once around 0 and back to 1, is called *the period of the differential form  $dz/z$  at its singularity 0*. The real part of this integral has no period, we have:  $\operatorname{Re}(\log(z)) = \log|z|$  for all paths from 1 to  $z$ .

Instead of integrating one differential form we can integrate three, so that the real part of such an integral maps (a piece of) the complex plane into  $\mathbb{R}^3$ . The image is a surface

---

\* This file is from the 3D-XplorMath project. Please see:

without singularities if the integrand is never  $(0, 0, 0)$ . If the integrand has singularities, the integration path has to avoid them and there may be periods. This means that the integral gives us not just one image of its domain, but a periodic repetition of one image. The obtained surfaces are in general not minimal surfaces, but one is close to them.

Weierstrass derived the following representation:

Let  $D \subset \mathbb{C}$  be some domain,  $g : D \mapsto \mathbb{C}$  a holomorphic function and  $dh$  a holomorphic 1-form on  $D$ . Then:

$$F_\varphi(z) := \operatorname{Re} \left( e^{i\varphi} \cdot \int_*^z \left( \frac{1}{2}(1/g - g), \frac{i}{2}(1/g + g), 1 \right) dh \right)$$

maps, for each  $\varphi$ ,  $D$  to a minimal surface piece in  $\mathbb{R}^3$ .

The length of the image of curves  $c$  in  $D$  can be computed with the Riemannian metric:

$$ds = \frac{1}{2} \left( |g(c(t))| + \frac{1}{|g(c(t))|} \right) |dh(c'(t))dt|.$$

Beyond the metric we do not discuss the differential geometry here. See [About Minimal Surfaces](#) for a derivation of the above Weierstrass representation that starts from the minimal surface definition. Instead we discuss Weierstrass' formula.

Since the Riemannian metric does not depend on the parameter  $\varphi$  the above surface pieces are all isometric to each other (almost never congruent). This is a rare phenomenon

in surface theory. – Zeros of the differential form  $dh$  lead to zeros of  $dF_\varphi$ . Such singularities are called *branch points* of the minimal surface. The Riemannian metric shows that they can be avoided if the function  $g$  has a zero or a pole of the same order as the zero of  $dh$ . View branch points on the Henneberg surface ( [Scherk, Catalan, Henneberg](#) ).

[Stereographic](#) projection between the Gaussian plane  $\mathbb{C}$  and the Riemann sphere  $\mathbb{S}^2$  is an important tool in complex analysis. Composition of the function  $g$  with stereographic projection is

$$\vec{N}(z) := (2\operatorname{Re}(g), 2\operatorname{Im}(g), |g|^2 - 1) / (|g|^2 + 1) \in \mathbb{S}^2.$$

This vector is orthogonal to the integrand of the Weierstrass formula and therefore a unit normal vector field of the surface. The Weierstrass representation is therefore built from a unit normal field and the differential of the height function. The functions  $g, \vec{N}$  are both called *Gauss map* of the surface. – We mention that a surface is minimal if its Gauss map  $\vec{N}$  is anti-conformal. The 'anti' comes in because a minimal surface has Gauss curvature  $K \leq 0$ . Of the two choices for stereographic projection we used the anticonformal one.

One of the simplest examples, the catenoid and its conjugate, the helicoid, are obtained from the following Weierstrass data (see [Helicoid-Catenoid](#) ):

$$D := \mathbb{C} \setminus \{0\}, \quad g(z) = z, \quad dh = \frac{dz}{z}.$$

The 3rd component of the Weierstrass integrand has the

imaginary period of  $dz/z$  which we discussed. The first and second components have no periods because the singular terms  $dz/z^2$  have the antiderivative  $-1/z$  (so that the period integrals around the singularity vanish). If we set the *associate family* parameter  $\varphi = 0$  we get a surface without period, a conformal immersion of  $\mathbb{C} \setminus \{0\}$ , the catenoid. If we set  $\varphi = \pi/2$  we obtain a surface with vertical translation period, an immersion of the universal covering of  $\mathbb{C} \setminus \{0\}$ , the helicoid.

Remark. If one wants to visualize a surface one usually needs to choose parameter lines. In case of the catenoid: Only if one chooses polar coordinates around  $\{0, \infty\}$ , does the catenoid look familiar. For all other choices one can hardly recognize it. With the good choice, the parameter lines are the principal curvature lines. I believe these lines give the eye the best clues to imagine the surface correctly in space.

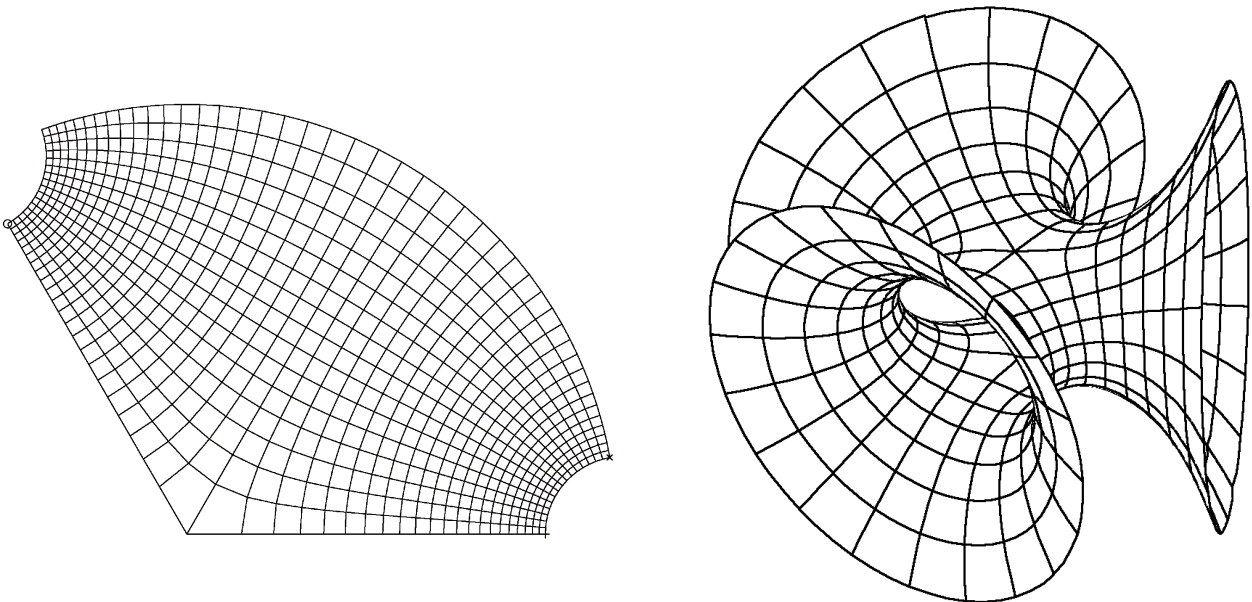
As in the case of the catenoid: Interesting Weierstrass data have isolated singularities, usually zeros or poles. The following summary helps to find interesting examples:

Poles of  $dh$  are never on the surface and lines into the puncture are infinitely long on the surface.

Zeros of  $dh$  have to be canceled by either a zero or else a pole of  $g$  which have the same orders as the zeros of  $dh$ .

If a puncture is to be a half-catenoid, then the Gauss map  $g$  must be single valued at the puncture. Furthermore, either  $g \cdot dh$  or else  $dh/g$  must have a double pole (as in the case of the catenoid).

Let us try to find the Weierstrass data for the Trinoid of Jorge-Meeks (see [Symmetric and Skew k-Noids](#)):



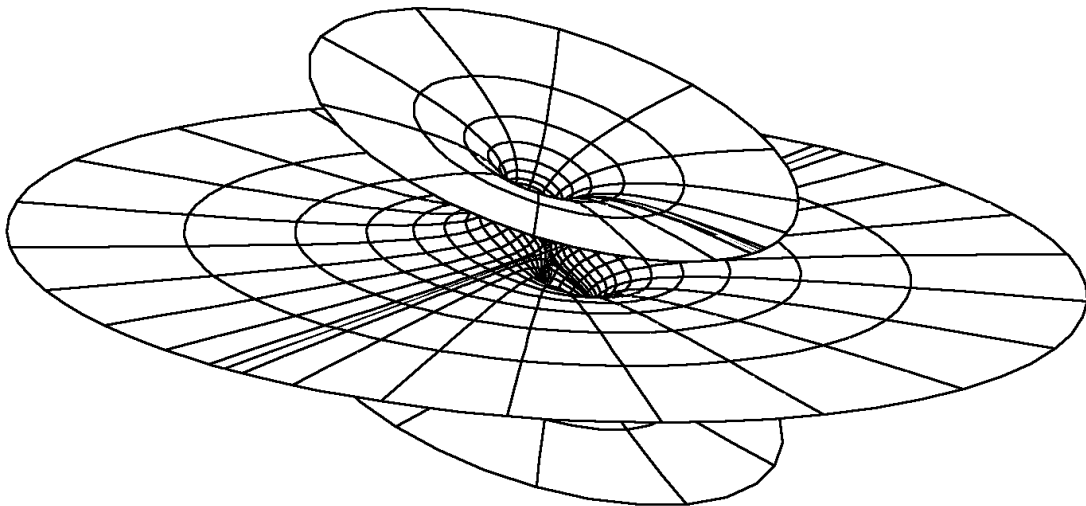
We have learnt from the catenoid that the huge opening of a catenoid is conformally only a puncture, just one *point* missing. The picture therefore shows a sphere with three punctures, say on the equator. With this orientation there are just two points with vertical normals, one pointing up, the other down. This implies that the Gauss map is some power of  $z$ . Along the equator we find, for each half-catenoid, one more normal which points in the same direction as its limiting normal. The degree of  $g$  is therefore 2, hence  $g(z) = \text{const} \cdot z^2$ , and  $|\text{const}| = 1$  to have horizontal normals along the equator. Next  $dh$ . It needs double zeros at  $0, \infty$  to cancel the double zero and pole of  $g$  and it needs double poles at the third roots of unity to create the half-catenoids. Since  $dz/z$  is, up to sign, invariant under inversion  $z \mapsto 1/z$ , we write  $dh$  as a multiple of  $dz/z$  (which has simple poles at  $0, \infty$ ).

This gives the Weierstrass data of the trinoid:

$$g(z) := z^2, \quad dh = \frac{z^3}{(z^3 - 1)^2} \cdot \frac{dz}{z}$$

To get good parameter lines, i.e. polar coordinates near the punctures, we use for one third of the unit disk the grid shown to the left of the trinoid. Closed parameter lines ('circles') in the domain around a puncture are mapped to closed curves in space since two orthogonal planes of symmetry cut the space curves into four congruent arcs.

Next let us grow two half-catenoids out of the plane as follows (see also [The Lopez-Ros No-Go-Theorem](#)):



Observe that the limiting normals of the two half-catenoids point in the same direction, but not quite opposite to the normal of the plane. On each half-catenoid one can locate a finite point where the normal is opposite to the normal of the plane. The Gauss map has two simple zeros at these points, say at  $\pm 1$ , and a double pole at  $\infty$ . Therefore we found  $g(z) = c \cdot (z - 1)(z + 1)$ . The zeros of  $g$  have to be

canceled by simple zeros of  $dh$  and  $dh$  needs double poles at points  $\pm r$  to create half-catenoids there.

This gives us a 2-parameter family of Weierstrass data:

$$g(z) := c \cdot (z - 1)(z + 1), \quad dh := \frac{z^2 - 1}{(z^2 - r^2)^2} \cdot dz.$$

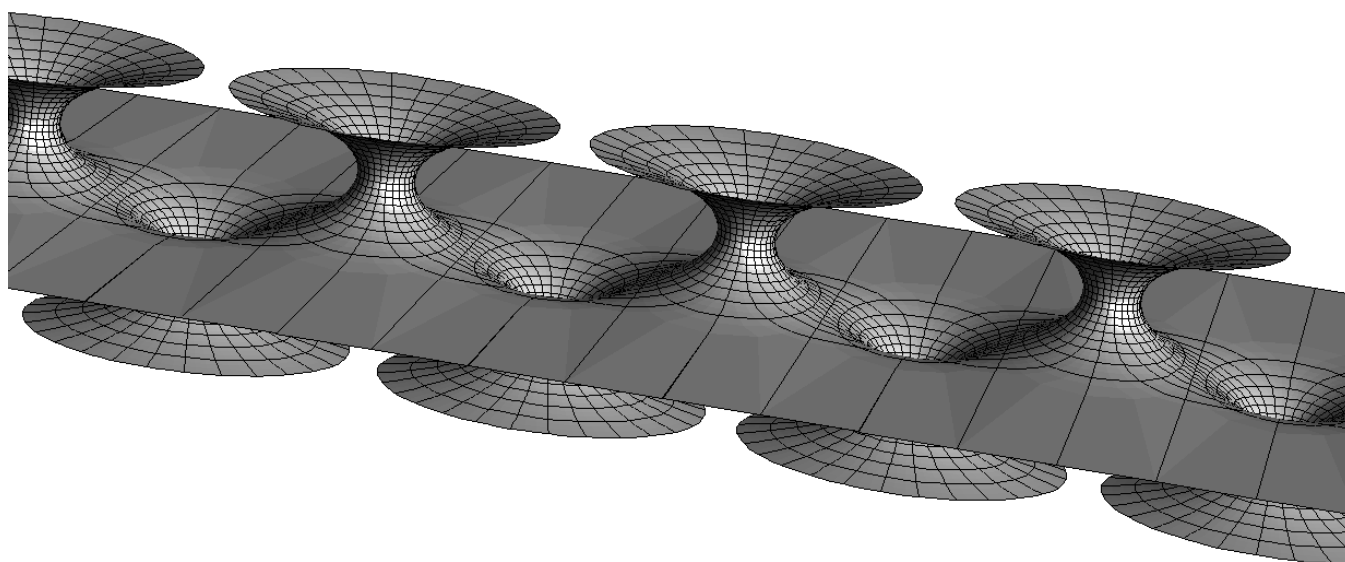
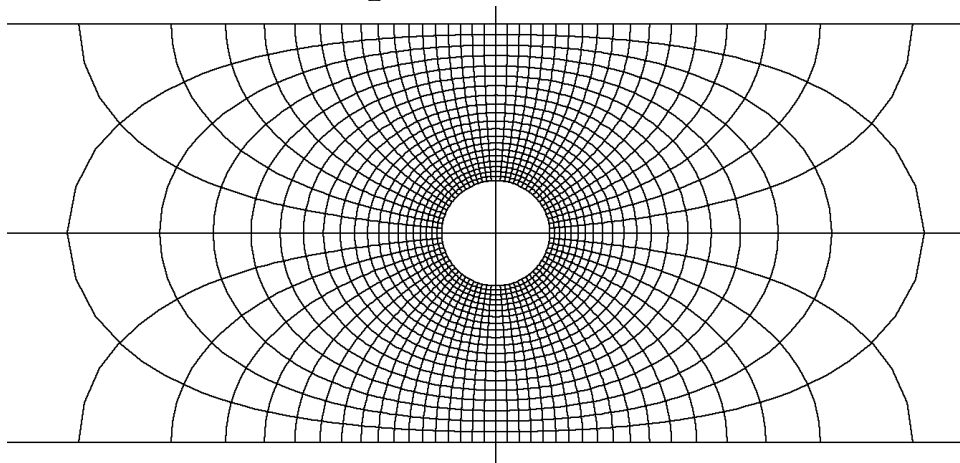
In this case there is only one vertical symmetry plane cutting the half-catenoids. Therefore closed curves around the punctures are not by symmetry mapped to closed curves in space, a period orthogonal to this plane can occur. The parameter  $c$  can be used to make this period vanish, for each  $r > 1$ . As  $r$  approaches 1 the two half-catenoids move further and further apart. In other words: one cannot grow two half-catenoids with limiting normals orthogonal to the plane. The half-catenoids will therefore always intersect the plane so that all these surfaces are only immersed, none is embedded.

It is however possible to grow infinitely many equidistant half catenoids out of the plane such that all these half-catenoids have the same limiting normal and this normal is opposite to the normal of the plane. The straight symmetry line between neighboring half-catenoids – which was present in the previous example – continues to exist. Therefore one needs to compute the surface only in a strip between neighboring symmetry lines.

The Weierstrass data of this *Catenoid Chain* are easy to guess:

$$g(z) := c \cdot \sin(z), \quad dh := \frac{dz}{\sin(z)},$$

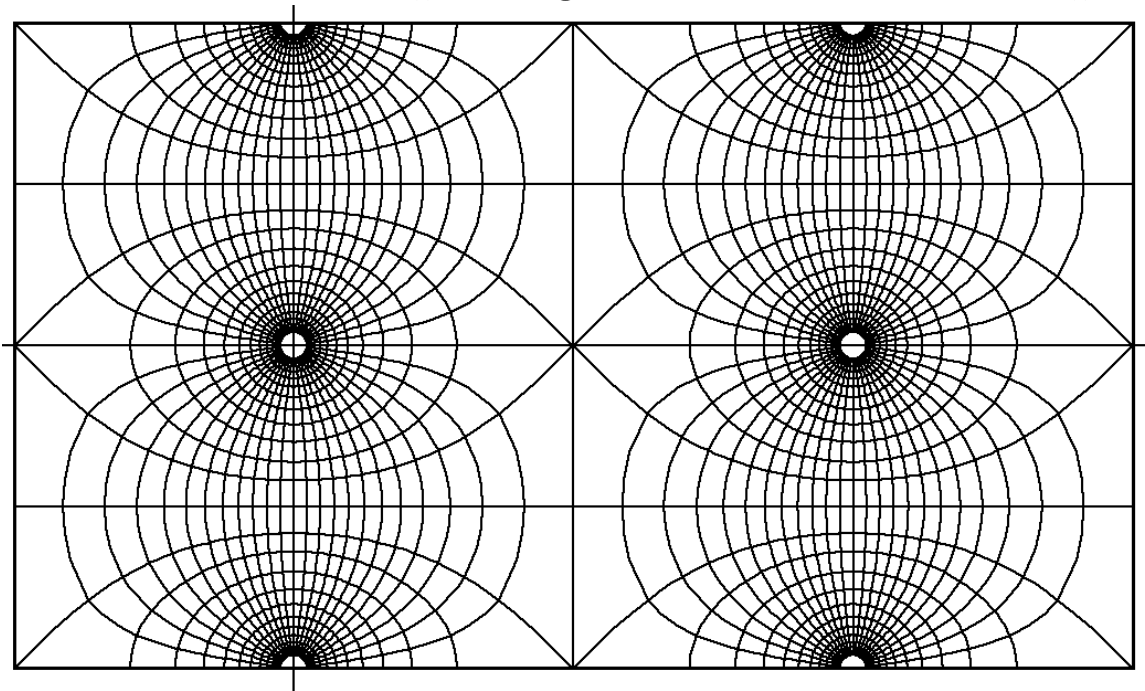
where  $c \in \mathbb{R}$  controls the size of the half-catenoids relative to their distance. It is more complicated to get polar coordinates in a strip. Here is the result:



While  $\sin$  has in the plane an essential singularity at  $\infty$ , in the strip there is convergence. The strip with edges identified is a cylinder with two half-catenoid punctures – or a sphere with four punctures, the two half-catenoids and the two ends of the flat strip. This last point of view suggests rational Weierstrass data:

$$g(z) := c \cdot (z - 1/z), \quad dh := \frac{1}{z - 1/z} \cdot \frac{dz}{z}, \quad c \in \mathbb{R}.$$

Beyond the singly periodic trigonometric functions one has the doubly periodic meromorphic elliptic functions. *Doubly periodic* means that we have two independent translational symmetries. The group of translational symmetries is called a lattice  $\Gamma$  in  $\mathbb{C}$ . Each lattice has a parallelogram as fundamental domain and identification of opposite edges makes the parallelogram into a torus. Meromorphic elliptic functions can therefore be viewed as maps from tori to the Riemann sphere. We visualize an elliptic function (denoted  $J_F$  in 3D-XplorMath) by drawing the preimage on the torus of the usual polar grid on the Riemann sphere:



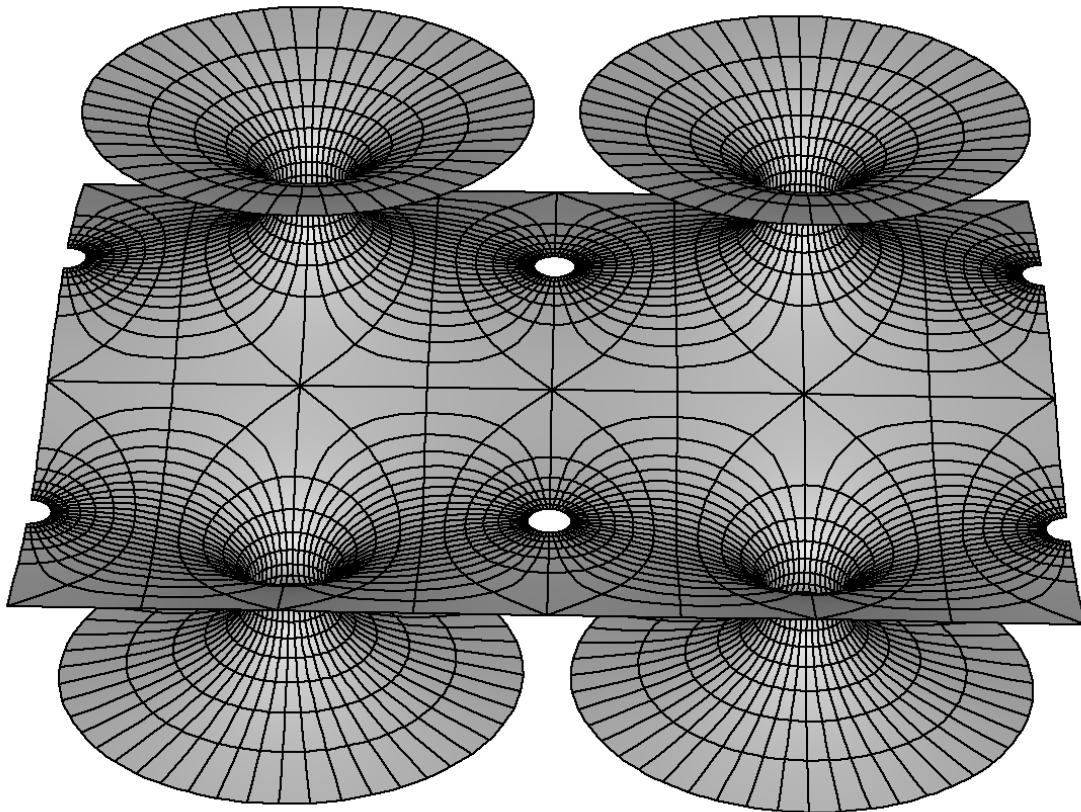
The two coordinate centers in the middle are zeros of the function, the two centers on the (identified) boundary are poles. The rectangles around the polar centers (made of symmetry lines of the picture) are preimages of the unit circle.

If we use this elliptic function in the same way as we used

the sin-function before:

$$g(z) := c \cdot J_{-F}(z), \quad dh := \frac{dz}{J_{-F}(z)},$$

then we obtain the following doubly periodic minimal surface:



The picture shows two copies of a fundamental domain for the translational symmetries. The half-catenoids are at the zeros of the function  $J_{-F}$ . At its poles are the zeros of  $dh$  and these cancel the poles of the Gauss map  $g$ . In other words: the poles of  $J_{-F}$  are points on the surface with vertical normal. – The parameter lines on the surface clearly are the image under the Weierstrass integral of the grid on the torus shown before.

## The Coordinate Viewpoint

The minimal surface just discussed could have been computed in the described way, but it was not. So far we looked at the torus as a quotient  $\mathbb{C}/\Gamma$  and meromorphic functions on a torus therefore were the same as meromorphic functions in  $\mathbb{C}$  which had the translations  $\tau \in \Gamma$  as periods, meaning  $f(z + \tau) = f(z)$ . And the Weierstrass integral was evaluated on a fundamental parallelogram for the lattice  $\Gamma$ .

Elliptic functions  $J : \mathbb{C}/\Gamma \mapsto \mathbb{C}$  are, away from their branch points, locally invertible. They can therefore be viewed as coordinate functions on the torus. The Weierstrass data of our doubly periodic surface are given in terms of such a function  $J$ . We also need to express  $dz$  in terms of  $J$ , namely:  $dz = dJ/J'$ . This is almost all what we need, to perform the Weierstrass integration not on the torus, but in the range of the coordinate function  $J$ , i.e. in  $\mathbb{C}$ . We still need to express  $J'$  in terms of  $J$ . The Jacobi-type elliptic functions which we constructed in 'Symmetries of [Elliptic Functions](#)' all had four branch values:  $\pm B, \pm 1/B$ . The two functions  $(J')^2$  and  $(J^2 - B^2) \cdot (J^2 - 1/B^2)$  have the same four double zeros and the same two fourth order poles. Since the domain torus is compact this implies that these two functions are proportional. We ignore this multiplicative constant because it only determines the scaling-size of the fundamental domain. Thus we derived the ...

Differential Equation for Jacobi-type Elliptic Functions:

$$\begin{aligned} J'(z)^2 &= P(J) = J^4 - (B^2 + B^{-2}) \cdot J^2 + 1, \\ J''(z) &= P'(J)/2 = 2J^3 - (B^2 + B^{-2}) \cdot J. \end{aligned}$$

And the above Weierstrass data take this form:

$$g(J) = c \cdot J, \quad dh = \frac{1}{J} \cdot \frac{dJ}{\sqrt{(P(J))}}, \quad J \in \mathbb{C}.$$

This looks much simpler than before and can be directly integrated on a standard polar coordinate grid in  $\mathbb{C}$ . The remaining problem is the square root. It is a multivalued function and we have to choose the correct branch. Since we are doing path integrals along curves which avoid the branch values (i.e. the zeros of the polynomial  $P$ ), such an analytic continuation of the square root can be built into the integration routine.

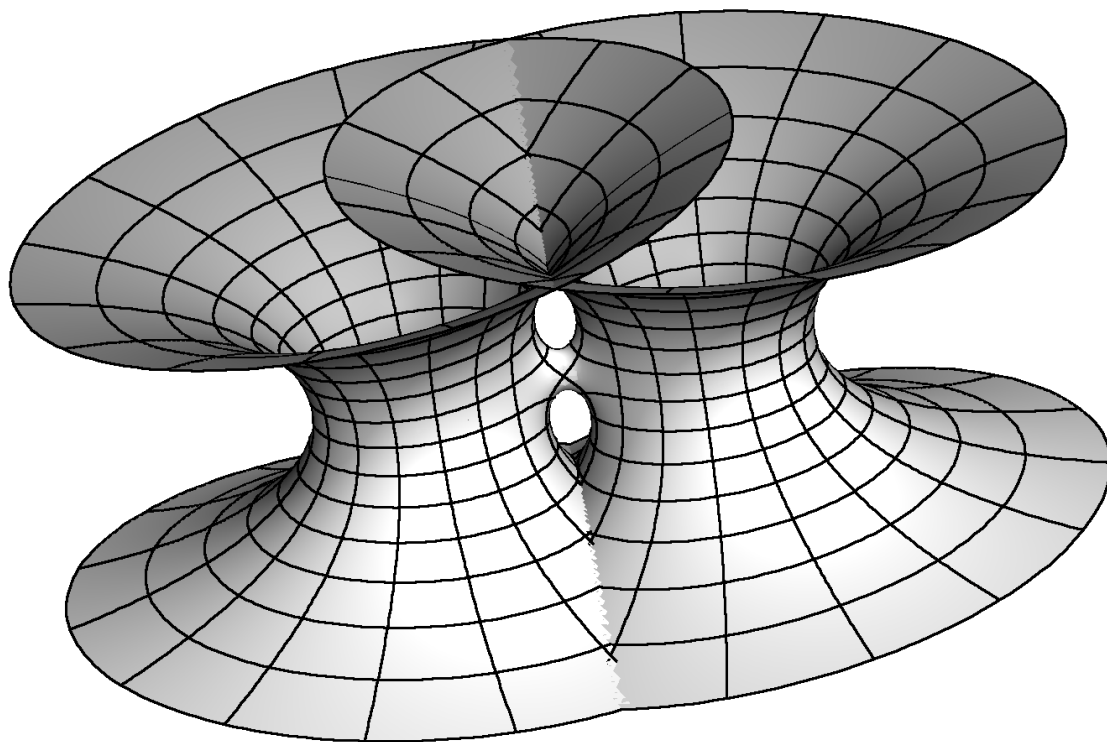
REMARK 1. This coordinate view point is a first important step towards the theory of Riemann surfaces. While for tori this view point is only a simplification, it becomes essential for minimal surfaces parametrized by higher genus surfaces.

REMARK 2. The above differential equation is an example where the dominating Runge-Kutta method fails: If one starts the integration at a zero of  $P$  then Runge-Kutta produces a constant solution. There are 4th order methods which use  $J''$  and work fine.

The same is already true for the ODE  $(\sin')^2 = 1 - \sin^2$ .

## Half-Catenoids with opposite normals

How can one find a Weierstrass representation for this surface? (See also [Symmetric and Skew k-Noids.](#))



The surface looks like two catenoids joined by a handle, in other words: a sphere with four half-catenoid punctures. We place the surface so that the four limiting normals of the half-catenoids lie in the horizontal plane and form small angles  $\pm\varphi$  with the  $y$ -axis. On the handle, and also on the waist of each catenoid, one sees one point with the normal pointing vertically up, one point with the normal down. The gauss map therefore has three zeros and three poles on the real axis:  $g(z) = z(z^2 - r^2)/(1 - r^2z^2)$ . They are positioned symmetric to the  $y$ -axis and to the unit circle. The differential  $dh$  must have 6 zeros at these points to make them into finite points on the surface, and it must

have four double poles on the unit circle to create the horizontal half-catenoids. This gives a 2-parameter family of Weierstrass data:

$$g(z) := z \frac{z^2 - r^2}{1 - r^2 z^2},$$

$$dh := \left(1 - \frac{z^2 + z^{-2}}{r^2 + r^{-2}}\right) \left(\frac{z^2 + z^{-2}}{e^{2\varphi} + e^{-2\varphi}} - 1\right)^{-2} \frac{dz}{z}.$$

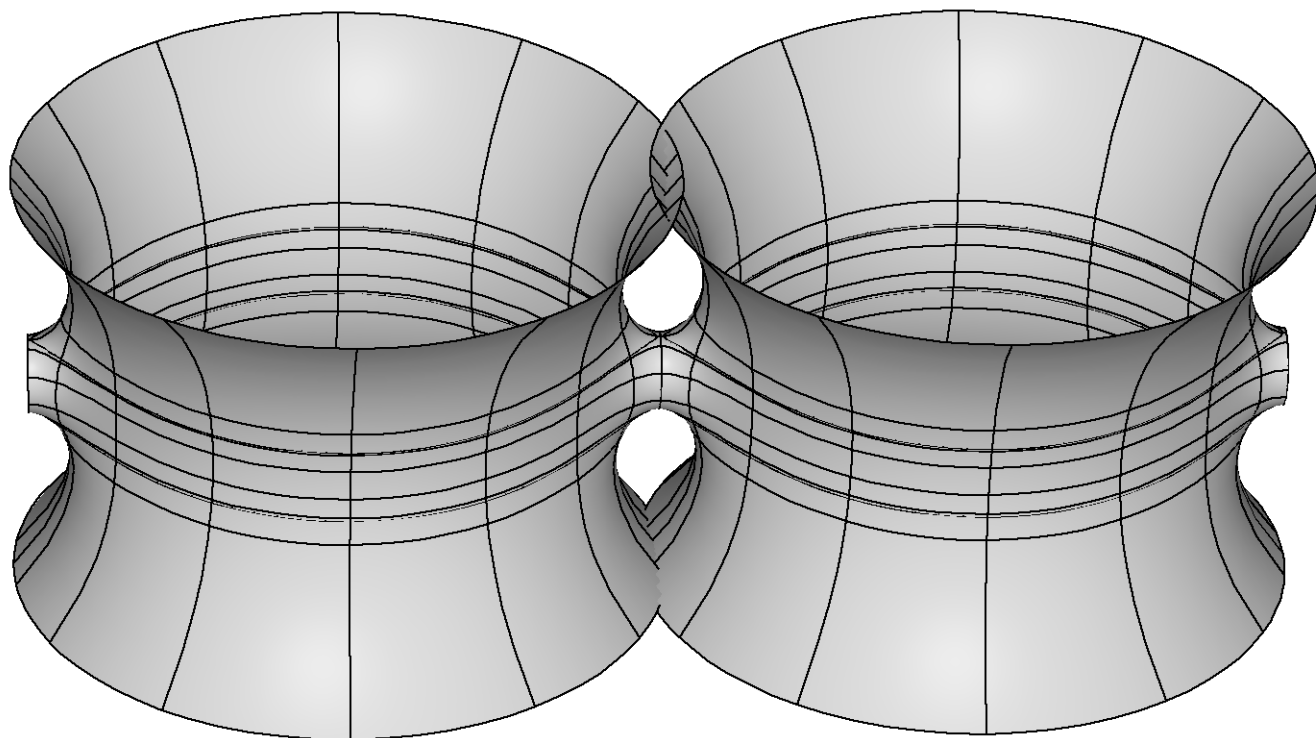
For most choices of parameters the half-catenoid punctures have vertical periods. A residue computation shows that these periods vanish if

$$e^{2\varphi} + e^{-2\varphi} = 2 \cos 2\varphi = 4r^2 / (1 + r^4).$$

Historically this is the first surface that showed David Hoffman and me a *handle which connected two minimal surfaces*, deforming them slightly.

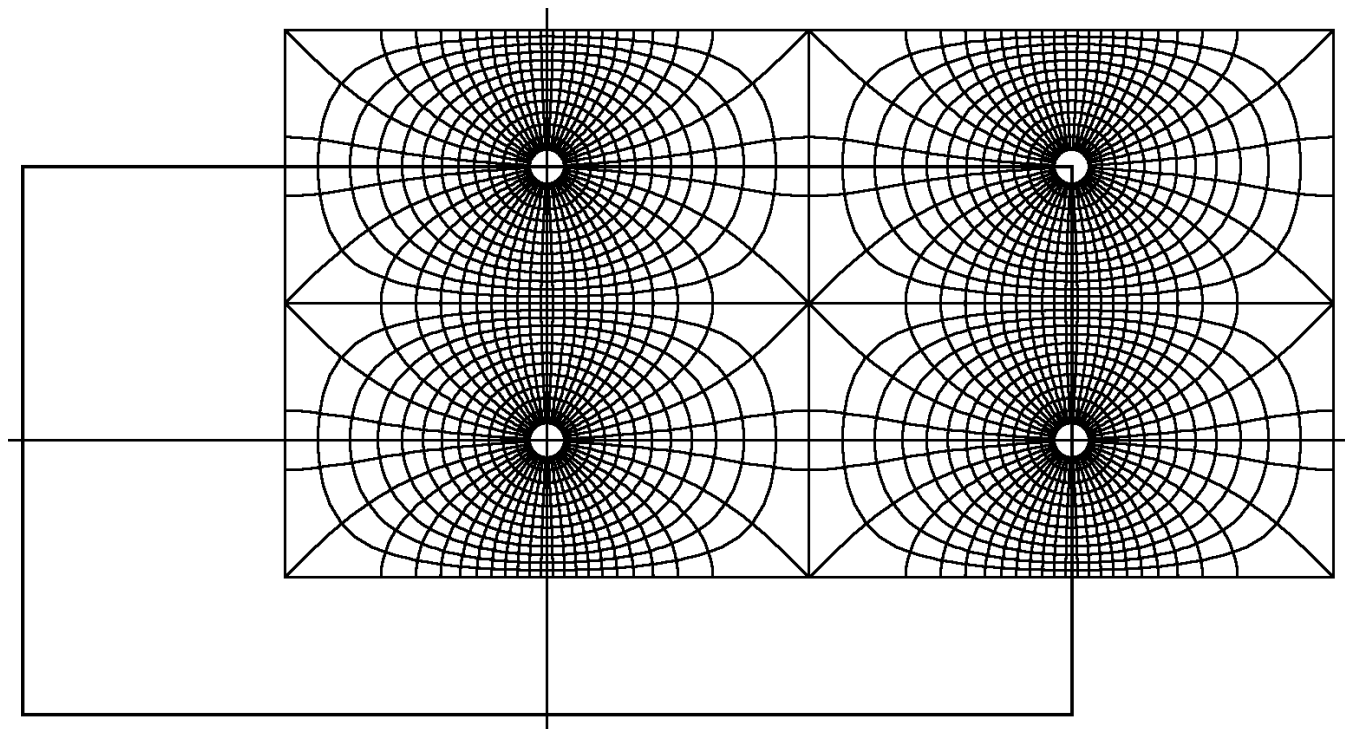
If we imagine such handles to grow in two opposite directions out of the waist of the catenoid, then symmetry would allow the catenoid to stay straight. Therefore we can think of making a *fence of parallel catenoids*, see [Fence of Catenoids](#). Parallel translation from the symmetry plane of one handle to the symmetry plane of the next handle would be a congruence map of this surface. The quotient by this translation group is a torus with two half-catenoid punctures whose limiting normals point in opposite directions. The handle has two points with normals parallel to the limiting normals of the half-catenoids. The surface in the following picture therefore has a Gauss map with

two zeros and two poles. One zero and one pole are half-catenoid punctures, the other two are finite points on the handle.



So first, what kind of a torus is this? There are two types of tori which have involutive symmetries, the rectangular tori and the rhombic tori. They are easy to distinguish: the fixed point set of such an involution of a rectangular torus has two components, while such involutions of rhombic tori have fixed point sets with only one component. (Note that the interruption of a fixed point set by a puncture is ignored in this count because the puncture is a point on the torus, it is only missing on the image minimal surface.) There are symmetry lines going from the handle into each puncture: They lie in the same plane and are two components of the fixed point set of the surface reflection

in this plane. The parametrizing torus is therefore rectangular. Each of the two symmetry arcs joins points with vertical normals in opposite directions. The following picture allows to visualize this elliptic function, it is again the preimage of a standard polar grid on the Riemann sphere.



The left bottom and right top polar centers are zeros of the function, the other two polar centers are first order poles. Because of this diagonal arrangement this function is called  $J_D$  in 'Symmetries of [Elliptic Functions](#)'. The rectangles which are filled with a polar grid are preimages of the unit circle. The branch points are the points where more than 2 parameter lines cross. For rectangular tori, the branch values are all on the unit circle.

We will make the two top polar centers the punctures, the two bottom polar centers the finite points with vertical normals (on the handle). Then the function  $J_F$ , repre-

sented by the earlier grid, gives us the second part of the Weierstrass data:

$$g(z) := J_{-D}(z), \quad dh := J_{-F}(z)dz.$$

As before we can integrate in the range of an elliptic function of our choice. The functions  $J_{-D}$ ,  $J_{-F}$  can be computed from each other by solving quadratic equations ( $D$  is the branch value of  $J_{-D}$  in the first quadrant):

$$\begin{aligned} J_{-D} + \frac{1}{J_{-D}} &= \frac{D + 1/D}{2} \left( J_{-F} + \frac{1}{J_{-F}} \right), \\ (J_{-F})' &= J_{-F} \cdot (J_{-D})'(0) \cdot \left( \frac{1}{J_{-D}} - J_{-D} \right), \\ dz &= d(J_{-F}) / (J_{-F})'. \end{aligned}$$

(Recall:  $(J_{-D})'(0)$  controls the size of the fundamental domain.) Again square roots appear and the correct branch has to be chosen. (For the last surface a more complicated grid than the standard polar grid on the sphere was used.)

---

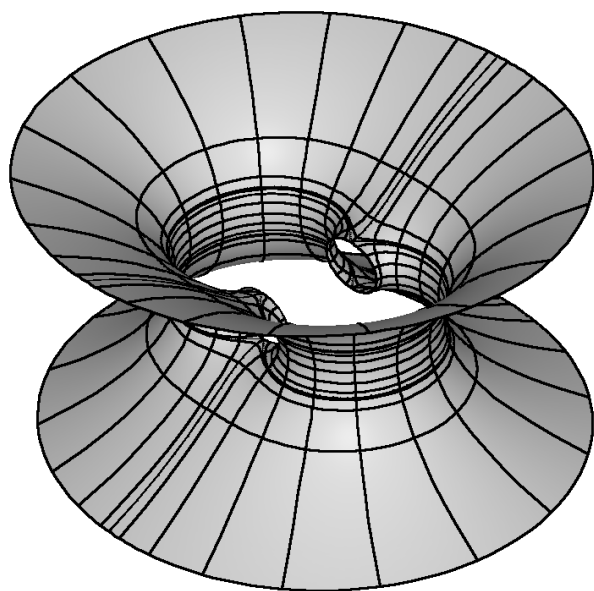
So far we have explained how the Weierstrass representation works for minimal surfaces which are punctured tori. But we have not touched an important question. The Weierstrass representation is well suited to create immersions, and rather many easily. But it requires separate considerations to decide whether the immersed surface is without selfintersections, whether it is *embedded*. For 300 years the plane and the catenoid were the only complete embedded minimal surfaces (CEMS) which have finite to-

tal curvature. Finite total curvature means that the normal Gauss map from the surface to the unit sphere has finite degree, i.e. there is a number  $d$  such that almost all points of the sphere are hit  $d$  times by the gauss map. Or put differently: that the Gauss map is a meromorphic function.

Lopez-Ros have proved: The only CEMS of finite total curvature *which are conformally punctured spheres*, are the plane and the catenoid. **The Lopez-Ros No-Go-Theorem.**

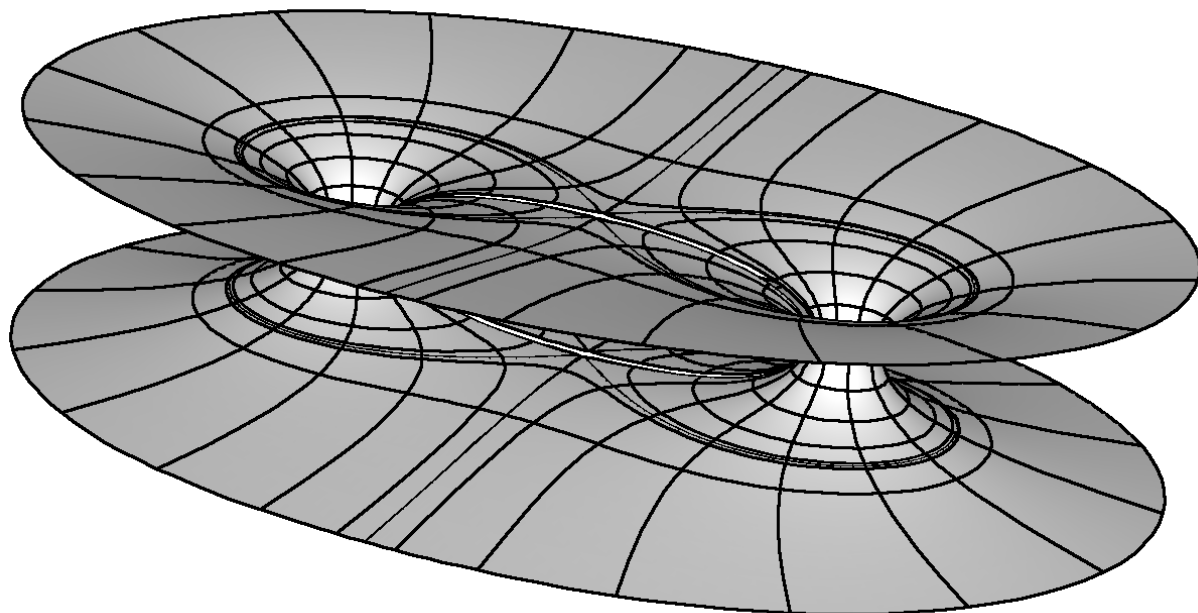
R. Schoen has proved: The only CEMS which have no more infinities than *two catenoid punctures* are the catenoids themselves. **R. Schoen's No-Go-Theorem.**

There is an obvious attempt to make a torus with two catenoid ends: Instead of growing handles to the outside - which created the fence of catenoids above - one can grow the handles to the inside. It is easy to start with small handles which are too short to meet in the middle:



The handles end in planar symmetry lines which - *after translation!* - fit together perfectly. The only problem is that a curve, which is closed on the torus, has a Weierstrass image in  $\mathbb{R}^3$  that is not closed, it has a nonzero *period*. Schoen's theorem forbids that one can make the handles long enough. So, how does the example fail?

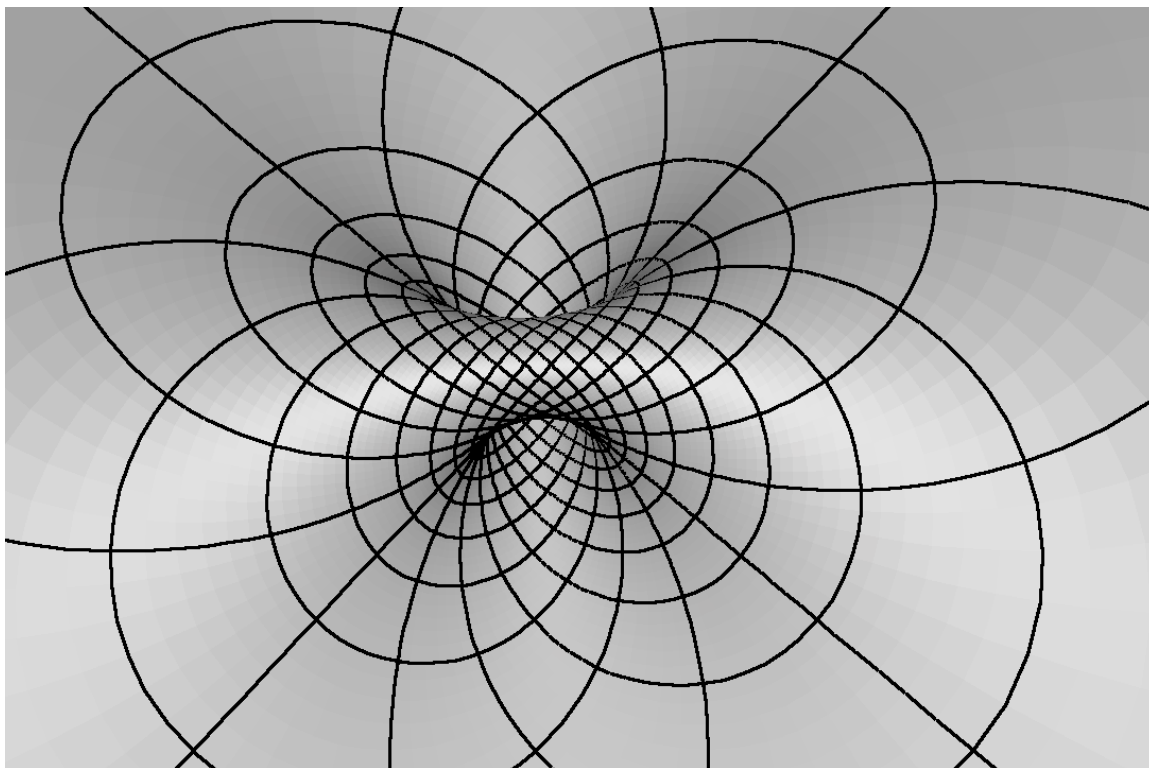
Things go well for a while: the handle grows and the gap narrows. But, as one changes the parameter further in the promising direction, the mouth of the handle becomes very elongated and the surface starts to look like *two catenoids* whose far out portions are connected. Except that the gap remains no matter how far apart the middle portions of the two catenoids are pushed. The following picture shows how close to a counterexample of Schoen's theorem one gets, or, what difficulties Schoen's proof has to overcome.



*Failing attempt to grow a handle through a catenoid.*

---

It was a big surprise when Costa found a minimally immersed punctured torus which Hoffman and Meeks proved to be embedded! The surface is a bit similar to our early example where two half-catenoids grow out of a plane. Therefore we first try to imagine a torus with a planar end. This is a difficult request until one turns it around and asks for a plane with a handle:



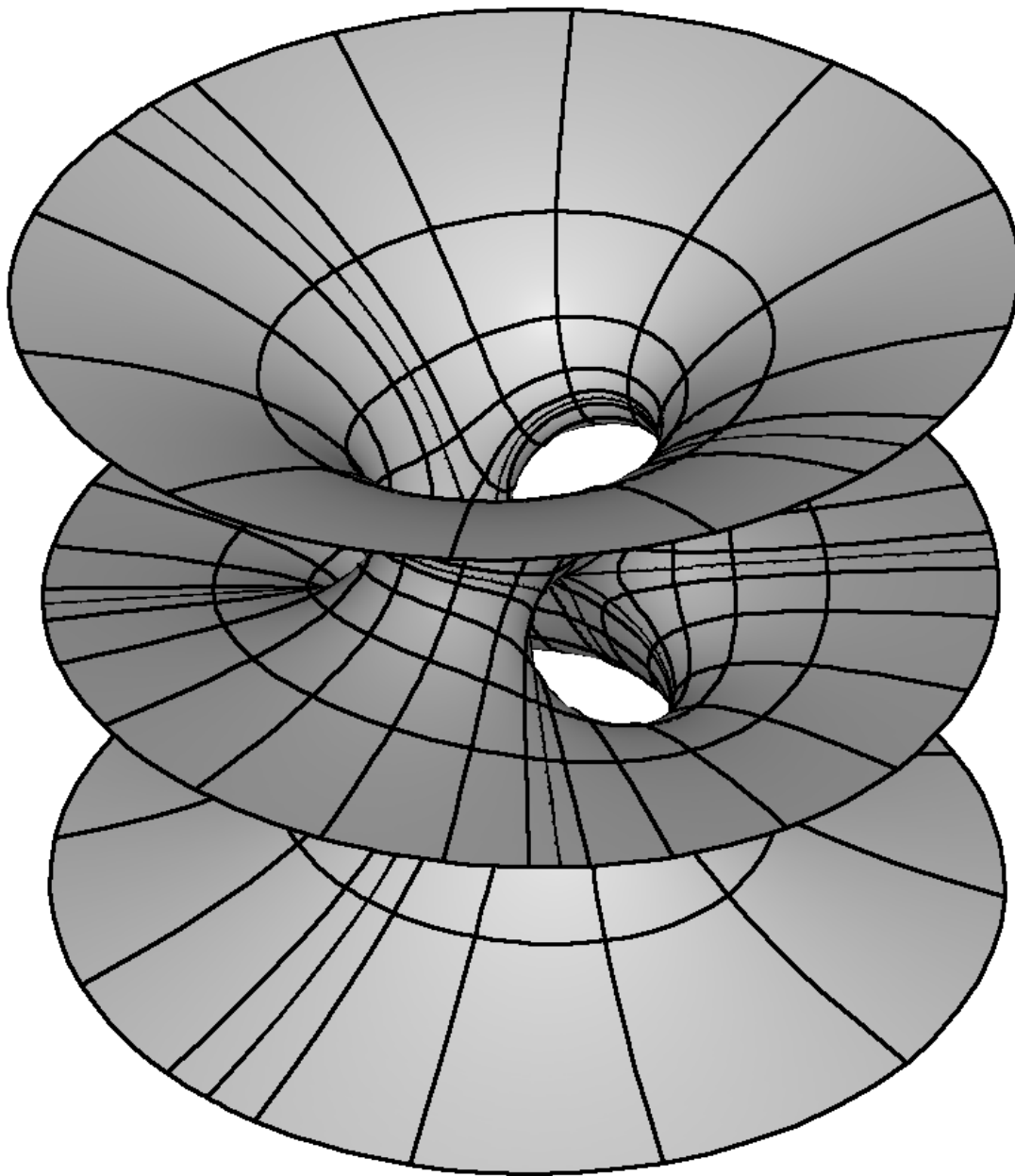
*A plane with a handle is a torus with a planar end.*

This surface is a stereographic projection of one of the **Clifford Tori**, the projection center is on the surface. All its parameter lines are circles, except for the two straight lines which pass through the midpoint of this surface. It is a torus with one puncture. The torus is the *square torus* because it is a) rectangular since the fixed point sets (on the surface) of the reflections in two vertical planes have *two components* and it is b) rhombic because  $180^\circ$  rotation about the straight lines are symmetries whose fixed point sets have only *one component*.

The strategy is: puncture the torus in the two points where the normal to the two straight lines (= the intersection of the symmetry planes) intersect the surface again and grow half-catenoids at these points towards the outside (or away

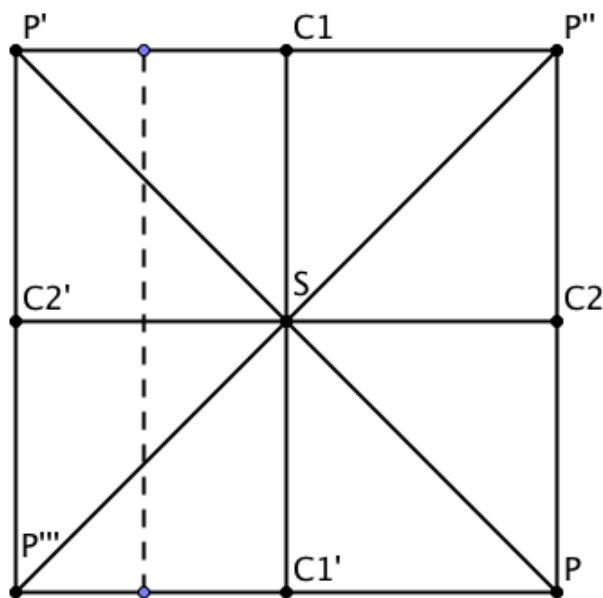
from the straight lines).

This plan contains enough information to write down the Weierstrass data of



Costa's Minimal Surface:

We draw the quadratic fundamental domain of our square torus such that the straight lines on the cyclide surface become the diagonals. Note that they are also one component fixed point sets of orientation reversing involutions. The pair of horizontal symmetry lines (the parallel boundary segments are identified) are a two component fixed point set of an involution, and the pair of vertical symmetry lines also. The points  $C1, C2$  are the punctures for the half-catenoids. The point  $P$  is the (conformal) point at infinity of our plane with handle. The center is called  $S$  (for saddle). The normals at  $S, C1, C2$  point in one direction, the normal at  $P$  in the opposite direction. We take these directions as vertical so that the Gauss map has simple zeros at  $S, C1, C2$  and therefore a triple pole at  $P$ .



This forces the height differential  $dh$  to have simple poles at  $C1, C2$  to make these points catenoid punctures. At  $S$  we need to compensate the simple pole of  $1/g$  with a simple zero. The remaining other simple zero would cause a branch point everywhere except if it

is at  $P$ . These zeros and poles determine  $g$  up to a factor  $a \exp(i \cdot \alpha)$  and  $dh$  up to a factor  $b \exp(i \cdot \beta)$ . Clearly  $b$  only scales the surface and  $\alpha$  rotates it. And  $\beta$  is the associate family parameter, it is chosen to make the pe-

riods of the catenoid punctures imaginary. Under these conditions the fixed point sets of the involutions turn out to be straight lines (the diagonals) and planar geodesics. This was not at all clear initially, but it follows immediately from the description of the functions in 'Symmetries of [Elliptic Functions](#)'. With the parameter  $a$  we have at this point the Weierstrass data of a 1-parameter family of candidates. With an intermediate value argument one can choose  $a$  so that the dotted curve - which is closed on the torus - also has a closed Weierstrass image in  $\mathbb{R}^3$ .

*Weierstrass Data for the Costa Surface:*

$$g(z) = a \cdot (J\_E \cdot J\_F)'(z), \quad dh = \frac{dz}{J\_D(z)}.$$

Up to a multiplicative constant the function  $J\_E \cdot J\_F$  is the Weierstrass  $\wp$ -function (here for the square torus).

H.K.

[TOC](#)

## Chain of Half-Catenoids and Field of Half-Catenoids \*

These surfaces played no role in the history of minimal surfaces, but they explain very nicely how the Weierstrass representation works, compare [Half-Catenoids and Weierstrass Representation](#).

Weierstrass representation of a vertical catenoid:

$$g(z) = z, \quad dh = \frac{dz}{z}.$$

Weierstrass representation of a singly periodic chain of vertical half-catenoids:

$$g(z) = bb \cdot \sin(z), \quad dh = \frac{dz}{\sin(z)}.$$

The simple zeros of the sine function create half-catenoid punctures. These punctures have no real periods since two orthogonal planes of mirror symmetry cut each half-catenoid into four congruent pieces. Neighboring half-catenoids are separated by straight lines. They are axes of  $180^\circ$  rotation symmetry. One needs to compute the surface only in a strip between two neighboring lines. The scaling

---

\* This file is from the 3D-XplorMath project. Please see:

factor  $bb$  in the Gauss map controls the size of the half-catenoids relative to the distance between them. Two such strips are a fundamental domain for the group of translation symmetries.

Weierstrass representation of a doubly periodic field of vertical half-catenoids:

$$g(z) = bb \cdot J_F(z), \quad dh = \frac{dz}{J_F(z)}.$$

The function  $J_F$  is a doubly periodic function on  $\mathbb{C}$ , in this case with a rectangular fundamental domain. In each fundamental domain  $J_F$  has two simple zeros and two simple poles, see ‘Symmetries of [Elliptic Functions](#)’. The zeros of the Gauss map  $g$  together with the poles of  $dh$  create the half-catenoid punctures. The poles of  $g$  are cancelled by the zeros of  $dh$ , they give the polar centers on the surface. As in the previous examples we have orthogonal planes of mirror symmetry cutting each half-catenoid and we have straight lines on the surface, running between the half-catenoids. These symmetries of the minimal surface are a consequence of the corresponding symmetries of the elliptic function which determines the Weierstrass data. The scaling parameter  $bb$  of the Gauss map changes the size of the half-catenoids relative to their distance.

## The Doubly Periodic JD Minimal Surfaces \*

These families are parametrized by 4-punctured rectangular tori; they and their conjugates are embedded. We therefore suggest the associate family morphing, and also morphing of the modulus,  $bb$ , ( $0 < bb < 0.5$ ) of the rectangular torus, which changes the size of the visible holes.

For the visual appearance of these surfaces it is particularly important that the punctures are centers of polar coordinate lines. Formulas are taken from [K1] or [K2]. The Gauss maps for these surfaces are degree 2 elliptic functions. The cases shown are particularly symmetric, the zeros and poles of the Gauss map are half-period points and the punctures are there. In the Jd-case the diagonal of the rectangular fundamental domain joins the two zeros, and in the Je-case it joins a zero and a pole of the Gauss map.

Under suitable choices of the modulus of the torus these surfaces look like a fence of Scherk saddle towers - with a vertical straight line (Je), respectively a planar symmetry line (Jd), separating these towers. The conjugate surfaces look qualitatively the same in the Jd-cases and like a checkerboard array of horizontal handles between vertical planes in the Je-cases.

H.K.

---

\* This file is from the 3D-XplorMath project. Please see:

## The Doubly Periodic JE Minimal Surfaces \*

These families are parametrized by 4-punctured rectangular tori; they and their conjugates are embedded. We therefore suggest the associate family morphing, and also morphing of the modulus (aa) of the rectangular torus, which changes the size of the visible holes. (The images of this deformation looked best when the u-range was modulus dependent:

$u_{\max} := (5-2*aa)+bb$ ;  $u_{\min} := -u_{\max}$ ;

The parameter bb lets the user overrule the above dependence.

For the visual appearance of these surfaces it is particularly important that the punctures are centers of polar coordinate lines. Formulas are taken from [K1] or [K2]. The Gauss maps for these surfaces are degree 2 elliptic functions. The cases shown are particularly symmetric, the zeros and poles of the Gauss map are half-period points and the punctures are there. In the Jd-case the diagonal of the rectangular fundamental domain joins the two zeros, and in the Je-case it joins a zero and a pole of the Gauss map.

Under suitable choices of the modulus of the torus these surfaces look like a fence of Scherk saddle towers - with a vertical straight line (Je), respectively a planar sym-

---

\* This file is from the 3D-XplorMath project. Please see:

metry line (Jd), separating these towers. The conjugate surfaces look qualitatively the same in the Jd-cases and like a checkerboard array of horizontal handles between vertical planes in the Je-cases.

H.K.

TOC

## Riemann's Minimal Surfaces \*

This is the family of singly-periodic embedded minimal surfaces found by Riemann. They are parametrized (aa) by rectangular tori. The Gauss map is the Weierstrass  $\wp$  function additively normalized to have a double zero at the branch point diagonally opposite the double pole and multiplicatively normalized to have the values plus or minus  $i$  at the four midpoints (on the torus) between the zero and the pole. The minimal surface has rotational symmetries around the corresponding normals. This symmetry kills the horizontal periods. The surface is parametrized by the range of the Gauss map with polar coordinates around the punctures. The surfaces look like families of parallel planes with one handle between adjacent planes. The associate family morphing joins two such embedded surfaces—they are congruent for the square torus. The standard morphing (aa) changes the branch values of the Gauss map, i.e. the tilt of the normal at the flat points ( $K = 0$ ).

H.K.

---

\* This file is from the 3D-XplorMath project. Please see:

# The Chen-Gackstatter Minimal Surface <sup>\*</sup> and Higher Dihedral Symmetry Examples

This surface is the first finite total curvature immersion of a Riemann surface of genus  $> 0$  (here the square torus). It looks like an Enneper surface with a handle added parallel to its center saddle. This description determines the Gauss map only up to a multiplicative constant (cc), which we took as the morphing parameter. If this parameter is general then we get a doubly periodic minimal immersion of the plane. The morphing indicates how the period can be closed for one value of cc with the intermediate value theorem. The resemblance with the standard Enneper surface is emphasized by using polar coordinates around the puncture. The dd=3 surface is an analogue which can be viewed as a higher order (120 degree symmetric) Enneper surface with a Y-shaped handle glued in. It was first published in a 1988 Vieweg Calendar by Polthier and Wohlgemuth.  
H.K.

---

<sup>\*</sup> This file is from the 3D-XplorMath project. Please see:

## Costa's Minimal Surface \*

This surface was responsible for the re-kindling of interest in minimal surfaces in 1982. It is a minimal **embedding** of the 3-punctured square torus. Its planar symmetry lines cut this surface into four conformal squares and the two straight lines through the saddle are the diagonals of these squares.

The Gauss map of such a surface is determined by its qualitative properties only up to a multiplicative factor  $cc$  which we suggest for the morphing (as in the Chen-Gackstatter case). It closes the period (at  $cc=0$ ) with an intermediate value argument.

After Costa's existence discovery, Hoffman-Meeks proved embeddedness; they also found a deformation family through rectangular tori, where the middle end deforms from a planar one to a catenoid end. They generalized this family to any genus by increasing the dihedral symmetry.

H.K.

---

\* This file is from the 3D-XplorMath project. Please see:

## About the Costa-Hoffman-Meeks \*

### Minimal Surfaces

The original Costa surface was responsible for the rekindling of interest in minimal surfaces in 1982. It is a minimal **embedding** of the 3-punctured square torus. Its planar symmetry lines cut this surface into four conformal squares and the two straight lines through the saddle are the diagonals of these squares. Because of the emphasis on the symmetries, our formulas are taken from [K2.] The Costa-Hoffman-Meeks surfaces are generalizations of the Costa surface; their genus grows as the dihedral symmetry (controlled by  $dd$ ) is increased. The underlying Riemann surfaces are tessellated by hyperbolic squares with angles  $\frac{\pi}{k}$ , ( $k = 2, 3, \dots$ ).

The Gauss map of such a surface is determined by its qualitative properties only up to a multiplicative factor  $cc$  which we suggest for the morphing (as in the Chen-Gackstatter case). It closes the period (at  $cc0$ ) by an intermediate value argument.

As in Costa's case, the qualitative picture determines the Gauss map only up to a multiplicative factor. The stan-

---

\* This file is from the 3D-XplorMath project. Please see:

standard morph shows the dependence of the surfaces on this factor, closing the period at  $cc_0$ .

H.K.

TOC

## The Fence of Catenoids \*

These singly periodic surfaces are parametrized (aa) by rectangular tori; our lines extend polar coordinates around the two punctures to the whole torus. The surfaces look like a fence of catenoids, joined by handles; they were made by Karcher and Hoffman, responding to the suggestive skew 4-noids. The morphing parameter aa is the modulus (a function of the length ratio) of the rectangular torus. The surface is reflection symmetric with respect to planes parallel to the coordinate planes; in each case has the fixed point set, modulo translations, *two components*. This proves that the parametrizing torus is rectangular. (The fixed point set in the rhombic case has one component and the square torus has both symmetries.)

H.K.

---

\* This file is from the 3D-XplorMath project. Please see:

## Scherk's Surface with a Handle Added \*

This surface is a genus one version of Scherk's doubly-periodic surface. Existence and embeddedness is proved in [KWH], and our formulas are from there.

The conjugate fundamental domain is bounded by straight lines. This piece can be rotated to be a graph over a convex domain, and in this position the original piece is also a graph. For this we suggest the associate family morphing.

The surface has a period problem, because the position of the punctures is not determined on the square torus by qualitative considerations. We suggest the (joint) position of the punctures as morphing parameter (ee), again to illustrate the use of intermediate value arguments for killing periods.

H.K.

---

\* This file is from the 3D-XplorMath project. Please see:

## R. Schoen's Catenoid Characterization \*

R. Schoen's theorem says:

The only finite total curvature complete, embedded minimal surface having **two** ends, is the Catenoid.

Our example shows what happens if one tries—in spite of this theorem of Schoen—to add a handle to a Catenoid.

The fundamental piece is similar to that of the catenoid fence, except that the handle does not go outward to the neighbouring catenoid but goes inward to meet its other half. However a gap remains, and as one tries to close it (by morphing with the modulus,  $aa$ , of the underlying rectangular torus) the surface degenerates to look almost like two catenoids that move farther apart as one tries to close the gap. We show this with the default morphing. The deformation goes between rather extreme surfaces where one has to adjust how far one computes into the end and then also the size. While this animation is a bit jumpy, it is instructive and therefore recommended.

H.K.

---

\* This file is from the 3D-XplorMath project. Please see:

# The Conjugate Plateau Construction Of Triply Periodic Minimal Surfaces \*

The Weierstrass representation for triply periodic minimal surfaces is more difficult than what we have explained so far. A simpler approach is the *conjugate Plateau construction* which, as we will see, can loosely be called the soap film point of view. Without further explanation we use the fact from complex analysis that the derivative of the imaginary part of a function  $z \mapsto f(z)$  can easily be computed from the derivative of the real part of  $f$ . This fact is known as the ‘Cauchy-Riemann equations’. It implies that, on a simply connected domain, the real part of  $f$  determines the imaginary part up to a constant. Of course this holds for the three components of the Weierstrass integral so that a simply connected minimal surface piece determines its conjugate surface up to an  $\mathbb{R}^3$ -constant.

The next step is the soap film part: The Plateau problem arose from the soap film experiments of the 19th century physicist Joseph A.F. Plateau. Its solution (1932) by Douglas and Rado states:

*Every closed continuous injective curve in  $\mathbb{R}^3$  is the boundary of at least one simply connected minimal surface.*

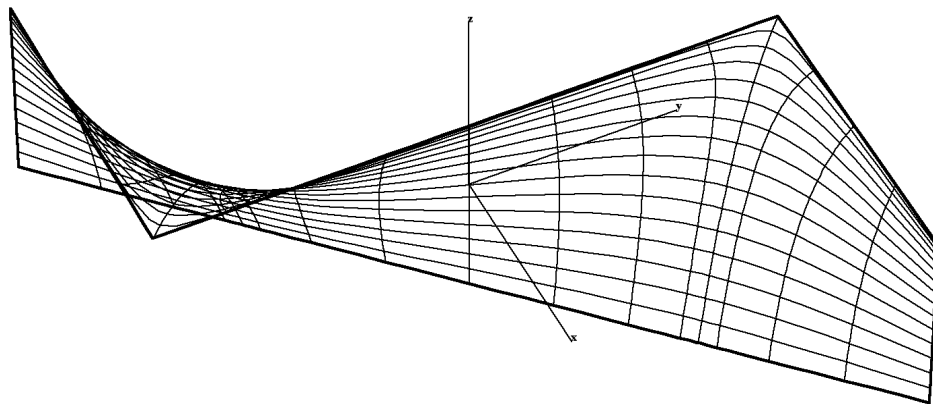
This theorem expresses a fundamental property of the minimal surface equation: It is well suited for boundary value problems. On the other hand, initial value problems usually have no solution. In particular, the minimal surface

---

\* This file is from the 3D-XplorMath project. Please see:

piece of a Plateau solution usually cannot be extended beyond its boundary curve. So, how can it help to get complete solutions without boundary?

Here symmetries come to the rescue. If the boundary curve contains a straight line segment then  $180^\circ$  rotation of a Plateau solution around this segment extends the minimal surface to twice as large a piece. If the boundary curve is a polygon then extension by  $180^\circ$  rotation works for all segments of the original polygon and all segments of the rotated polygons. The resulting surfaces usually have singularities at the vertices of these polygons. However, if all the angles of the polygon are of the form  $\pi/k$ ,  $k \in \mathbb{N}$ , then repeated rotation about the edges that start at one vertex  $p$  results in a surface for which  $p$  is an interior, regular point. Such contours therefore lead to complete minimal surfaces without boundary, but usually with lots of self-intersections. Only a few such minimal surfaces, which are embedded, are known. An example is the conjugate of the Schwarz' P-surface:



All angles of this hexagon are  $90^\circ$ , the z-axis divides it into two  $90^\circ$ -pentagons.

The next step gives us a wealth of embedded examples. We consider the conjugates of the just described Plateau solutions with polygonal boundaries. A surprise happens to the straight line segments of the boundary which are symmetry lines on the extended surface with the symmetry being  $180^\circ$ -rotation:

*The boundary of the conjugate piece consists also of symmetry arcs. These arcs are planar geodesics and the extended surface is reflection symmetric with respect to these planes.*

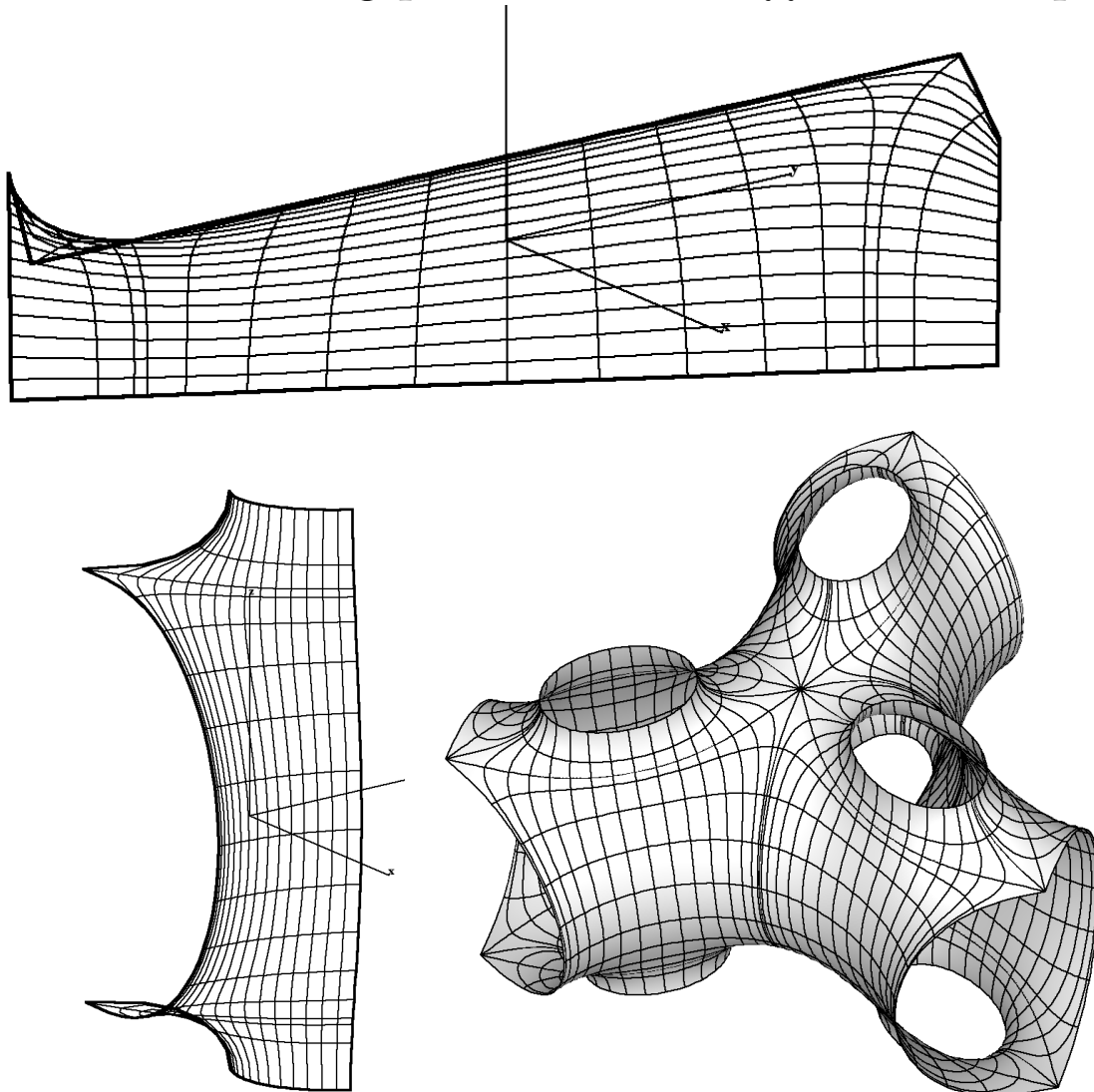
The strategy of the conjugate Plateau construction is, to choose the polygonal contour for the Plateau solution in such a way that the extension of its conjugate piece by reflection in the planes of the boundary arcs give an embedded minimal surface.

This is helped by two geometric facts:

- (i) The Plateau solution very often is a graph over a convex domain which is bounded by a suitable orthogonal projection of the boundary polygon. Therefore it is embedded. Romain Krust proved that in this situation the conjugate piece is also a graph, hence embedded.
- (ii) The boundary polygon determines the angle by which the normal of the Plateau solution rotates along each boundary segment. The Weierstrass representation shows that the normal of the conjugate piece rotates along each boundary arc by *the same angle*.

The Fujimori-Weber surfaces are very good examples for the described construction. In the Action Menu one can

select **Don't Show Reflections** to see the fundamental piece. Also in the Action Menu one can switch between a minimal surface and its conjugate. In the View Menu one can switch between **WireFrame Display**, **Patch Display**, **Point Cloud Display**. In **WireFrame** and in **Point Cloud Display** the Action Menu offers **Emphasize Boundary**, so that one can easily see the polygonal contour for the Plateau solution and its conjugate – which is the fundamental piece of a Fujimori-Weber surface, bounded by planar symmetry arcs. The following pictures are an  $ff = 4$  example:



The Plateau contour is a hexagon with four  $90^\circ$  and two  $60^\circ$  angles. The z-axis divides it into two pentagons. Observe that the conjugate piece has its normals *parallel* to the normals of the Plateau piece – at corresponding points of course. The third picture is an assembly of twelve such fundamental domains.

All of our Fujimori-Weber surfaces can be described in the above way. Note that not only the angles of the hexagon between adjacent edges are important, but also the following: Let  $a, b, c$  be three consecutive edges. The angle between a plane normal to  $a$  and a plane normal to  $c$  has to be either 0 or of the form  $\pi/k$ ,  $k = 2, 3, 4, 6$ . Otherwise the group generated by the reflections in the symmetry planes of the conjugate of the Plateau solution is not discrete and the extended surface cannot be embedded.

Several of the Fujimori-Weber surfaces agree with other examples in 3D-XplorMath:  $ff = 2$  is the Schwarz  $P$ -surface,  $ff = 5$  is the Schwarz  $H$ -surface,  $ff = 8$  is the A. Schoen  $S$ - $S$ -surface and  $ff = 7$  is the same surface 'inside-out', that is, the assembled piece has the *other side* of the surface as its outside. If a minimal surface carries a straight line, then the  $180^\circ$  symmetry rotation interchanges the two sides of the surface – therefore there is no geometric distinction between the two sides. Here this happens if the pentagon-half of the Plateau hexagon has a reflection symmetry, as in the cases  $ff = 2, 5$  above. The other cases come in such 'inside-out' pairs, which look like different surfaces but are not, because the pentagon-halves of the

Plateau hexagon are *the same* polygon. The other pairs are  $ff = 1, 3$  (A. Schoen's *H-T*-surface),  $ff = 4, 6$  (A. Schoen's *H-R*-surface) and  $ff = 9, 10$  (A. Schoen's *T-R*-surface).

Although the triply periodic surfaces in 3D-XplorMath can most easily be understood by this conjugate Plateau construction, they are not computed in this way. It is another story to explain the functions and their domains which are used in the Weierstrass representation to compute these surfaces.

In [Ka] a Weierstrass representation for several Plateau problems as above is derived. Also fifteen 1-parameter polygonal contours are discussed which give further examples because the obstructing period problem can be solved by the intermediate value theorem.

In [FW] the Fujimori-Weber surfaces are obtained with a non-standard use of the Weierstrass representation. The collection of examples described in this paper is much larger than what is shown in 3D-XplorMath.

### **Bibliography**

[Ka] Karcher, H.: The triply Periodic Minimal Surfaces of Alan Schoen And Their Constant Mean Curvature Companions. *Manuscripta Math.* 64, 291-357 (1989).

[FW] Fujimori S., Weber M.: Triply Periodic Minimal Surfaces Bounded By Vertical Symmetry Planes. *Manuscripta Math.* 129, 29 - 53 (2009).

## About the Schwarz PD Family \*

This is a 2-parameter family of triply periodic genus 3 minimal surfaces. For all parameter choices are the original surface and the conjugate surface embedded. The most symmetric example (with a cubic lattice) which is obtained when  $cc = 0$ ,  $dd = 0$ , was already constructed by H. A. Schwarz. When Alan Schoen found more triply periodic surfaces around 1970 he named the two surfaces which Schwarz found the P-surface (P for cubic primitive) and the D-surface (D for diamond). He also found a third embedded(!) surface in the associate family of these, the Gyroid (associate parameter 0.577 which is approx. 52 degrees). If  $dd=0$  then a fundamental cell for the lattice is a prism with square base. In the morphing  $cc$  changes the height of the prism.

K. Grosse-Brauckmann, M. Wohlgemuth: The Gyroid is embedded and has constant mean curvature companions. To appear Calc. Var. 1996

H.K.

---

\* This file is from the 3D-XplorMath project. Please see:

## About the Schwarz H family \*

This is a 1-parameter family of triply periodic surfaces. The surfaces are made of pieces which one could call “triangular catenoids”; annular Plateau solutions bounded by two parallel equilateral triangles. In the morphing  $aa$  changes the height-to-edge length ratio of these triangular catenoids. Observe that, as in the case of circles bounding catenoids, the distance between the triangles has to be small enough and then they bound a stable and an unstable triangular catenoid. In the PD-family with  $dd=0$  one can observe analogous “square catenoids”, except that our parametrization does not emphasize them.

When Alan Schoen found more triply periodic surfaces around 1970 he named these “Schwarz’ H surfaces”. (Maybe Schwarz constructed only one member of the family.) Later, the Swedish chemist, Lidin, found another embedded example (now called the Lidinoid) in the same associate family, when  $aa$  is approximately 0.55, and the associate family parameter is 0.7139, (about 64.25 degrees).  
H.K. TOC

---

\* This file is from the 3D-XplorMath project. Please see:

## Four Triply Periodic Minimal Surfaces \*

The four surfaces are:

- Neovius' surface inside a cube (no deformations)
- A. Schoen's S-S-surface in a quadratic prism (deforms)
- A. Schoen's H-T-surface in a hexagonal prism (deforms)
- A. Schoen's T-W-surface in a hexagonal prism (deforms)

The images in 3D-XplorMath show a fundamental domain for the group of translational symmetries. The curves on the boundary are planar symmetry arcs, reflection in their planes extends the fundamental domain to neighboring pieces. These planes, or rather their halfspaces that contain the fundamental domain, intersect in a crystallographic cell.

Neovius was a student of H. A. Schwarz. A. Schoen worked for NASA and he even made models of the surfaces he discovered. The T-W-surface is not in his list, but made in his spirit. Initially his descriptions were not accepted by mathematicians. In [Ka] it was shown that their existence follows easily with [The Conjugate Plateau Construction](#) and Schoen was finally given credit for his discoveries.

What else should one observe in these pictures?

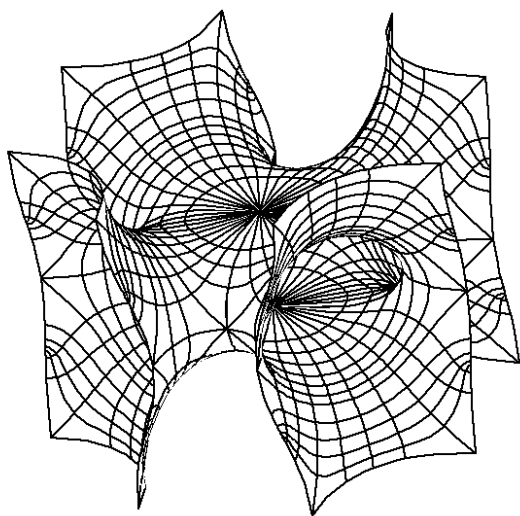
The images were not computed via the conjugate Plateau construction, but by using the Weierstrass representation. This representation requires the understanding of functions which are related to these minimal surfaces. To construct such functions is a mathematical challenge and to visualize them is not easy either. In 3D-XplorMath complex functions are (mostly) visualized by showing a grid in

---

\* This file is from the 3D-XplorMath project. Please see:

the domain and the image grid. We need functions that are well defined on the whole minimal surface. Thus visualization seems to require that we put a grid on the whole surface - which is impossible.

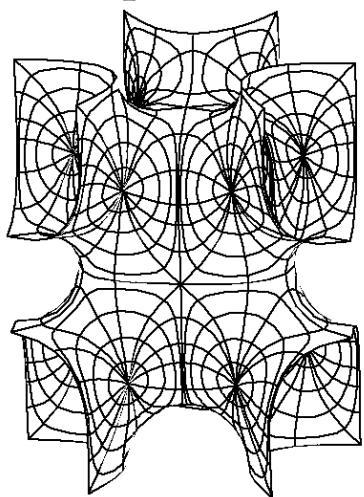
One such function is always the Gauss map which one can sort of ‘see’ by translating the normals of the surface to the origin, thus mapping the surface to the Riemann sphere. The four surface pictures are covered by patches which look like polar coordinates. This offers a different kind of visualization: The function on the surface which is responsible for these polar grids, maps the surface in such a way to the Riemann sphere that our grid becomes the *standard polar grid on the sphere*. One may compare this with the interpretation of a hiking map with level lines.



This S-S-surface shows these level lines for the Gauss map: The two big polar centers are a zero and a pole (of order 3); the preimage of a hemisphere (around 0 or  $\infty$ ) in most directions ends at a horizontal symmetry line – i.e. at the preimage of the equator; but these hori-

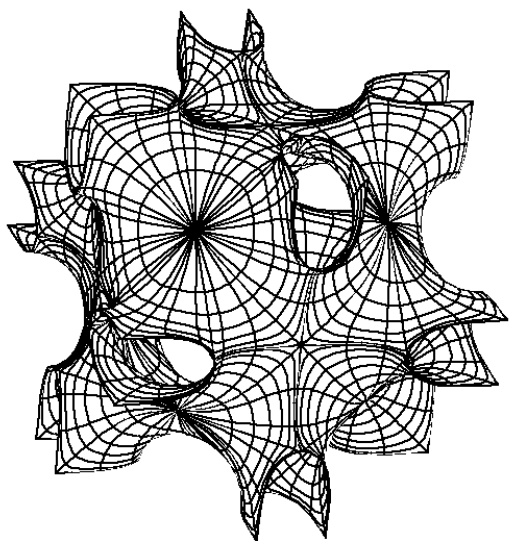
zontal arcs are connected by vertical (boundary) symmetry arcs, how is that possible? These vertical symmetry arcs have inflection points in their middle, i.e. double points of the Gauss map; the vertical symmetry arcs are therefore preimages of slits in the upper (resp. lower) hemisphere.

In the other three cases the level lines belong to functions which are obtained as quotient by a symmetry group. Although such a construction of a function is rather abstract, the grid lines at least show *how* the surface is mapped to the sphere.



Consider the T-W-surface first. Clearly there is a  $120^\circ$  rotation symmetry and orthogonal to its axis are three  $180^\circ$  rotation axes. Identification with this order 6 symmetry group makes out of the twelve polar grid patches just two, one around the northpole the other around the southpole of the quotient sphere.

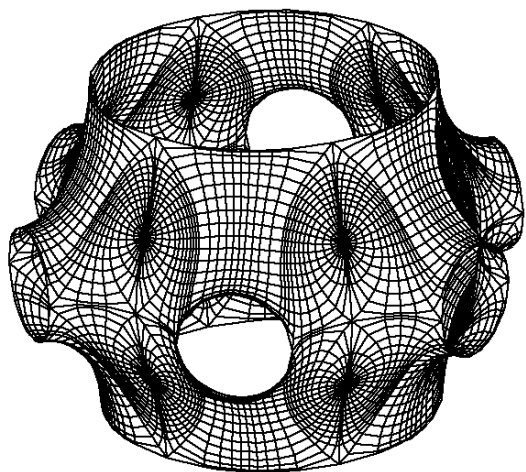
In other words: the parameter lines on this surface are the level lines of the quotient function to the sphere.



The Neovius surface has its eight polar centers on the space diagonals of its cubical crystallographic cell. The group of  $180^\circ$  rotations around the coordinate axes has order four. Identification by this symmetry group (modulo translations) makes again a sphere out of the Neovius surface and the 8 polar

patches are the preimages under the quotient map of standard polar coordinates on the quotient sphere. The preimage of the equator consists, for each polar patch, of the twelve symmetry arcs which form the boundary of these

polar patches. Our parameter lines, therefore, give an excellent impression of this quotient function.



Finally the H-T-surface. The fundamental piece itself has a  $60^\circ$  symmetry rotation group. But one can see that the neighboring polar centers along the top boundary should be preimages of a northern and a southern hemisphere, while the polar centers which lie vertically above

each other should be identified because there is a branch point of the identification map between them. We therefore take the symmetry group as for the T-W-surface: the  $120^\circ$  rotations around the vertical axis plus the three  $180^\circ$  rotations around the horizontal axes through the branch points between the polar centers. Then again our parameter lines are the preimages of standard polar coordinates on the quotient sphere.

It still takes more effort to understand the Weierstrass representation. But if these images help to see functions from these minimal surfaces to the Riemann sphere then they have prepared the ground for the final step.

### **Bibliography**

[Ka] Karcher, H.: The triply Periodic Minimal Surfaces of Alan Schoen And Their Constant Mean Curvature Companions. *Manuscripta Math.* 64, 291-357 (1989).

H.K.

TOC

## The Fujimori-Weber Surfaces\*

S. Fujimori and M. Weber derived in [FW] a Weierstrass representation for a large collection of embedded triply periodic minimal surfaces. In 3D-XplorMath ten of their families are realized, choose  $ff = 1, \dots, 10$ . For each  $ff$  we get a 1-parameter family, where the parameter  $cc$  controls the length ratio between the horizontal and vertical closed symmetry lines, see the default morph.

In the third part of **About Minimal Surfaces** (available from the Documentation Menu) we explain a construction of these surfaces with the help of minimal surface pieces which are bounded by hexagons in  $\mathbb{R}^3$ . To see these fundamental pieces, select in the Action Menu **Don't Show Reflections** and look also at the conjugate piece (which is the one bounded by a hexagon). In Wire Frame and in Point Cloud Display one can emphasize the boundary in the Action Menu.

Some of these surfaces can also be seen with a different parametrization in 3D-XplorMath. The parameter lines on the Fujimori-Weber surfaces are level lines and lines of steepest descent for the height function in z-direction. For the other triply periodic surfaces the level lines are pull backs of polar coordinates under a complex differentiable function defined on the minimal surface.

The Weber-Fujimori surfaces give for  $ff = 2$  the Schwarz P-surface,

---

\* This file is from the 3D-XplorMath project. Please see:

$ff = 5$  the Schwarz H-surface,  
 $ff = 8$  the A Schoen S-S-surface,  
 $ff = 7$  the same surface *'inside-out'*.

For minimal surfaces which carry straight lines there is no geometric distinction between the two sides, because  $180^\circ$  rotation around such a line maps the minimal surface onto itself, but interchanging the two sides. If there are no lines on the surface then the two sides may look so different that they appear to be different surfaces. But in reality the fundamental pieces are only assembled in different ways – showing mainly one side of the surface in one case and the other side in the other case (choose in the View Menu: **Distinguish Sides By Color**). The other such pairs are

$ff = 1, 3$  (A. Schoen's H-T-surface, also in 3DXM),  
 $ff = 4, 6$  (A. Schoen's H-R-surface),  
 $ff = 9, 10$  (A. Schoen's T-R-surface).

[FW] Fujimori S., Weber M.: Triply Periodic Minimal Surfaces Bounded By Vertical Symmetry Planes. *Manuscripta Math.* 129, 29 - 53 (2009).

H.K.

TOC

## User Defined Weierstrass Data \*

The close connection between minimal surfaces and complex variables was worked out in the second half of the 19th century and resulted in a flourishing of the theory of minimal surfaces. One consequence of this new insight is the so-called Weierstrass representation formula for minimal surfaces. Originally this representation was a local one that only in exceptional cases allowed the representation of a complete surface. It was not until the work of Osserman (1962) that it became clear that the Weierstrass representation was in fact global. Unfortunately it is considerably more difficult to explain the global interpretation of the Weierstrass representation than it is to write down the local formula. Moreover, the input data for global numerical computations are much more complicated than what is needed in order to draw just a local piece of a surface. For these reasons, the dialog box in 3DXplorMath for user defined Weierstrass representations only allows for the making of a local patch, and it is only the local formulation that we discuss below.

The input data for the local Weierstrass representation are two complex differentiable functions  $f, g$  defined on a region  $U$  of the complex plane. A basic fact for the repre-

---

\* This file is from the 3D-XplorMath project. Please see:

sentation formula to work is that the integral of a complex differentiable function along a curve gives a constant result if the curve is deformed keeping both end points fixed. We can therefore define a differentiable map  $F$  from the simply-connected region  $U$  into  $\mathbb{R}^3$ , by specifying a three-dimensional integrand in terms of  $f$  and  $g$ , and then integrating from a fixed base point  $* \in U$  and taking the real parts:

$$z \mapsto F(z) := \operatorname{Re} \left( \int_*^z \left( (1 - g(z)^2), i(1 + g(z)^2), 2g(z) \right) f(z) dz \right)$$

The surface piece defined by this map is always a minimal surface piece, and this formula therefore allows a user of 3DXM to view as many minimal surface pieces as desired. A short computation shows that the function  $g$  has a very nice geometric interpretation. It is customary to associate a unit vector  $u$  in  $\mathbb{R}^3$  to each complex numbers  $w$ , by considering the complex plane as the  $x$ - $y$ -plane in  $\mathbb{R}^3$  and taking  $u$  to be the inverse image of  $w$  under stereographic projection. (To see examples choose in the Conformal Category for any selected function in the Action Menu *Show Image On Riemann Sphere*.) If one associates in this way a unit vector  $u$  to  $w = g(z)$ , then one obtains for  $u$  a unit vector orthogonal to the surface at  $F(z)$ . In other words: the function  $g$  composed with stereographic projection gives the normal Gauss map of the surface. The normal Gauss map is basic in the study of surfaces, and for example the

various curvatures considered by differential geometers all have simple expressions in terms of the normal Gauss map. A geometric interpretation of the function  $f$  is much less immediate and this is perhaps one reason why it took so long for the above formula to be understood globally.

Sufficiently small pieces of any minimal surface are realistic models of soap films—provided the derivative of the parametrizing map  $F$  never vanishes. A point on a minimal surface where the derivative of  $F$  vanishes is called a *branch point*. Since soap films do not have branch points, one wants to look at minimal surfaces without branch points, and this can be decided from the Weierstrass data as follows:

If the function  $f$  has a zero at some point  $z_0$  then the derivative of  $F$  at  $z_0$  vanishes unless the other part of the integrand becomes infinite. At such points, where  $g(z_0)$  is infinite,  $f$  needs to have a zero of twice the order as the infinity (pole) of  $g$  at  $z_0$ . If the order of the zero of  $f$  is larger than this then one still has a branch point and if the order of the zero is smaller, then  $F(z_0)$  itself is infinite, so we do not get a point on the surface. The default examples allow one to contemplate these facts.

Note that we use polar conformal coordinates, that is,  $z = \exp(u + iv)$ , with  $u_{\min} \leq u \leq u_{\max}$ ,  $0 \leq v \leq 2\pi$ . The unit circle is the image of  $u = 0$ .

The **Catenoid** data have a pole at  $z = 0$ , and indeed there is no corresponding point on the catenoid. The situation

is similar at  $z = \infty$  so that the catenoid is parametrized by a sphere minus two points. – If  $f$  is changed to  $i \cdot f$  then one obtains the so called *conjugate surface*. In this case one obtains the *helicoid*, a singly periodic surface since integration of the Weierstrass integrand once around  $z = 0$  adds a period to the third coordinate function. To see larger pieces of the helicoid, increase the range of  $v$ , i.e., integrate more than once around  $z = 0$ . – The 'Cyclic Associated Family Morph' turns the Catenoid inside out.

The **Henneberg** surface is a simple surface with branch points. These are at the 4th roots of unity since  $f$  has zeros there, but  $g$  is not infinite at those points. Note that the branch points lie on the parameter line  $u = 0$ , on the F-image of the unit circle. The Henneberg surface has Enneper ends at  $z = 0$  and at  $\infty$ . – The default Cartesian grid touches only one branch point so that the image is less complicated than in the polar case.

The **Enneper** surfaces are parametrized by the full complex plane, and are therefore the simplest minimal surfaces to represent graphically. Note that a change of  $f$  by a unitary factor,  $\exp(i\varphi) \cdot f(z)$  gives in general an isometric but non-congruent surface of the *associated family*. The Enneper surfaces are exceptional since all members of the associated family are actually *congruent*. – For the classical picture choose  $aa=2$  and 'Cartesian Grid'. – For the most general Enneper surface take  $f$  constant and  $g$  a polynomial.

The **Trinoid**,  $bb = 3$ , has poles of  $f$  at the 3rd roots of unity. The Weierstrass map  $F$  is therefore not defined at those points. It is not obvious to see what happens at those points since the polar coordinates that the user defined surfaces use are not adapted to the situation. Compare the case  $ee = 3$  of the Symmetric kNoids in the list of 3DXM minimal surfaces. – Choosing the default 'Cartesian Grid' is most instructive for the Fournoid, our  $bb = 4$  default. As in all cases the 'Cyclic Associated Family Morph' is interesting.

Even the simplest surfaces can be given by Weierstrass data from which one does not immediately recognize the surface. Try:

$$g(z) = (z^k - 1)/(z^k + 1), \quad f(z) = 0.8i(z^k + 1)^2, \\ -1.8 \leq u \leq 0.2, \quad 0 \leq v \leq 2\pi, \quad (k = 0, 1, 2, 3, 4).$$

H.K.

TOC

## About Ward Solitons \*

The *Ward equation*, also called the *modified 2 + 1 chiral model* is the following equation for a map

$J : \mathbb{R}^{2,1} \rightarrow \mathbf{SU}(n)$ :

$$(J^{-1}J_t)_t - (J^{-1}J_x)_x - (J^{-1}J_y)_y - [J^{-1}J_t, J^{-1}J_y] = 0.$$

This non-linear wave equation is obtained from a dimension reduction and a gauge fixing of the self-dual Yang-Mills equation on  $\mathbb{R}^{2,2}$ . The Ward equation is an integrable system, and has a Lax pair. We explain this next.

Let

$$u = \frac{1}{2}(t + y), \quad v = \frac{1}{2}(t - y)$$

be the light-cone coordinate system for the  $yt$ -plane, and given smooth maps  $A$  and  $B$  from  $\mathbb{R}^{2,1}$  to  $su(n)$ , we consider the following linear system for a map  $\psi : \mathbb{R}^{2,1} \times \mathbb{C} \rightarrow GL(n, \mathbb{C})$ :

$$\begin{aligned} (*) \quad & (\lambda \partial_x - \partial_u)\psi = A\psi, \\ & (\lambda \partial_v - \partial_x)\psi = B\psi. \end{aligned}$$

R. Ward showed that if  $\psi(x, u, v, \lambda)$  is a solution of (\*) and satisfies the  $\mathbf{U}(n)$ -reality condition

$$\psi(x, u, v, \bar{\lambda})^* \psi(x, u, v, \lambda) = \mathbf{I},$$

---

\* This file is from the 3D-XplorMath project. Please see:

then  $J(x, u, v) = \psi(x, u, v, o)^{-1}$  is a solution of the Ward equation.

We call  $\psi$  an *extended solution* of  $J$ . The *degree* of  $\psi$  is defined to be the number of poles for  $\lambda$  counted with multiplicities. A solution  $J$  of the Ward equation is called a *Ward soliton* if  $J$  has an extended solution  $\psi(x, u, v, \lambda)$  that is rational in  $\lambda$ ,  $\psi(x, u, v, \infty) = \mathbf{I}$ , and if for each  $t$ ,  $J$  is asymptotically constant as  $(x, y)$  approaches  $\infty$ . A Ward soliton is called a *k-soliton* if the smallest degree of extended solutions of  $J$  is  $k$ .

Ward used the solution of the Riemann-Hilbert problem to write down all solitons whose extended solutions have only simple poles. He also used a limiting method to constructed 2-solitons whose extended solution have one double pole, and showed that these 2-solitons have non-trivial scattering. Anand and Ioannidou-Zakrzewski found Ward solitons whose extended solutions have only one pole of multiplicities 2 and 3 (see the Anand-Ward Solitons sub-menu of the Surfaces Catergory). Dai and Terng used Bäcklund transformations and an order  $k$  limiting method to construct all Ward solitons. Their method gives explicit formula for Ward solitons. In fact, given constant  $z_1, \dots, z_r \in \mathbb{C} \setminus \mathbb{R}$ , positive integers  $n_1, \dots, n_r$ , and rational functions  $v_0, \dots, v_k$ , they wrote down a  $k$ -soliton whose extended solution has poles at  $\lambda = z_1, \dots, z_r$  with multiplicities  $n_1, \dots, n_r$  respectively. We call

$$(z_1, \dots, z_r, n_1, \dots, n_r)$$

the *pole data* of the Ward soliton. For detail of Dai and Terng's construction, we refer the reader to their paper "Bäcklund transformations, Ward solitons, and unitons". This algorithm was used to write the code for the Ward solitons in the 3D-XplorMath. The program shows the wave profile of the energy density

$$E(x, y, t) = \|J^{-1} J_x\|^2 + \|J^{-1} J_y\|^2 + \|J^{-1} J_t\|^2.$$

The default Morph shows a sequence of these profiles for an increasing time  $t_i$  for the  $SU(2)$  Ward solitons. A Ward soliton with pole data  $(z_1, \dots, z_r, n_1, \dots, n_r)$  represents the interaction of  $r$  solitons with pole data  $(z_1, n_1), \dots, (z_r, n_r)$  respectively. The shapes of these  $r$  solitons are preserved after the interaction, but with possible phase shift. However, the solitons with pole data  $(z, k)$  do not share this common phenomenon of soliton equations. In fact, the localized lumps scatter after interaction.

To use the program to see the wave profiles of the  $SU(2)$  Ward solitons, you should be in the Surface Category and make a selection from the Ward Solitons submenu of the Surfaces menu. The submenu  $\text{MultiSoliton}_I$  means Ward  $k$ -soliton whose extended solution has a multiplicity  $k$  pole at  $\mathbf{i} = \sqrt{-1}$ ,  $\text{3-soliton}_{IIZ}$  means Ward 3-soliton whose extended solution has poles  $\mathbf{i}$ ,  $\mathbf{i}$ ,  $Z$ , and ... etc. After choosing the Ward Solitons submenu, then you can specify the pole locations and rational maps from the submenu Ward Soliton Settings to construct the corresponding Ward solitons. For simplicity of writing the codes, we

only wrote code for  $k$ -solitons with  $1 \leq k \leq 4$  and the rational maps from  $\mathbb{C}$  to  $\mathbb{C}^2$  are of the form  $(1, a_i(w))$ , where  $a_i(w)$  is a polynomial in  $w$  of degree less than 5. You may specify the coefficients of these  $a_i$ 's in the Ward Soliton Settings. Since the maximum of the energy density of these solitons is often large, you may choose a scaling factor in the Settings menu. If you choose Energy Scale Factor  $:= 0.05$ , this means the wave profile you see from the program is for  $0.05E(x, y, t)$ . If you want to see some Quicktime movies made from this program, you may go to [www.math.neu.edu/~terng/WardSolitonMovies.html](http://www.math.neu.edu/~terng/WardSolitonMovies.html).

CLT

Surface Organisation

## About Anand-Ward Solitons\*

Christopher Anand

Generally speaking, solitons are solutions to nonlinear wave equations that exhibit particle-like behaviour, but the term is frequently retracted further by demanding that the wave equation be “integrable” in one of several technical senses of that term. The earliest known soliton equations (Korteweg-DeVries, Sine-Gordon, Cubic Schroedinger, ...) were all in one space dimension, and for a time it was even suspected that soliton-like behavior could not occur in higher dimensions.

The solutions in this subcategory are all pure soliton solutions of a modified Chiral Model introduced by Richard Ward. One ‘reason’ that this model is integrable is that it is a reduction of the Yang-Mills equations, or the Bogomolny equations in an indefinite signature. It is this relationship which allows the solutions to be constructed using twistor or inverse-scattering methods.

Twistor theory works by setting up a correspondence between analytic objects (e.g. solutions of differential equations) and certain geometric objects (e.g., complex analytic functions with prescribed poles, holomorphic vector bun-

---

\* This file is from the 3D-XplorMath project. Please see:

<http://3D-XplorMath.org/> Surface Organisation

dles). In our case, the correspondence is between those solutions of Ward’s model that extend analytically to the compactification of space-time (a highly restrictive ’boundary condition at infinity’) and holomorphic bundles on a two-dimensional, compact, complex manifold. In analogy with Liouville’s theorem, stating that a bounded, holomorphic function on the complex plane is constant, Serre’s GAGA principle states that certain objects on compact, complex spaces, known a priori only to be complex analytic, are necessarily algebraic. Think of this as an existence theory. The next step is to find an efficient way to represent the associated vector bundles. It turns out that there is a nice representation in terms of “monads” (which are matrices satisfying certain relations), and one can even write the solutions and energy density down explicitly—without any integrals or derivatives, in terms of the monad data. This is how the pre-programmed solutions here have been created, and it is how you can construct further solutions by entering monad data using the Setup AW solitons... dialogue.

To get solutions of Ward’s equations, the matrices must satisfy the relation

$$\alpha_1 \cdot \gamma - \gamma \cdot \alpha_1 + b \cdot a = 0.$$

You are responsible for checking this equation yourself. There is also an additional nondegeneracy condition to insure that the associated solution is not singular, and a condition that corresponds to the solution being static,

but the description of these conditions is too complicated to include here.

Under the Set Parameters... menu, you can also change the way the energy density is displayed. The parameters  $bb$  and  $cc$  scale distance and energy respectively;  $aa$  is time; and  $dd$  is a cut-off value for the energy above which the value  $ee$  will be plotted (this is because some solutions can have very tall "spikes" at certain times).

The full story, including the derivation of all these conditions and the geometry behind the construction can be found in my preprints at:

<http://www.maths.warwick.ac.uk/~anand/preprints.html>

Please address any questions to me at:

[sendmail://anand@maths.warwick.ac.uk](mailto:anand@maths.warwick.ac.uk).

Surface Organisation

## Hydrogen Probability Densities\*

for  $(n, l, m) = (1, 0, 0)$  to  $(n, l, m) = (3, 2, 2)$

Point clouds, preferably in stereo, are used to visualize the electron probability densities in a Hydrogen atom. Since these densities are rotationally symmetric around the  $z$ -axis, only a wedge of the density cloud is shown.

The Action Menu offers several viewing options:

The entry **Show Coordinate Slices** plays a sequence of coordinate slices, first in polar coordinates, then in Cartesian coordinates.

The entry

**Show Constant Density Surface as Point Cloud**

shows that surface along which the density has its mean value. One can morph the constant density surfaces with the parameter  $ff$ . In some cases these surfaces have several components inside each other. Therefore a stereo point cloud gives a better impression than the raytrace version.

The entry **Show Voxel Raytrace** is the slowest option. It is visually more impressive than the point cloud, but less informative.

The entry **Create** returns to the default volume cloud.

The electron densities are of course listed in Physics texts. For comparison with our visualizations we repeat them here:

---

\* This file is from the 3D-XplorMath project. Please see:

<http://3D-XplorMath.org/> **Surface Organisation**

In 3DXM we use the parameter  $ii$  for the Bohr radius  $a_0$ .

$$(n,l,m)=(1,0,0):$$

$$\text{density} := \left( \exp\left(-\frac{r}{a_0}\right) \right)^2,$$

$$(n,l,m)=(2,0,0):$$

$$\text{density} := \left( \left(2 - \frac{r}{a_0}\right) \cdot \exp\left(\frac{-r}{2a_0}\right) \right)^2,$$

$$(n,l,m)=(2,1,0):$$

$$\text{density} := \left( \frac{r}{a_0} \cdot \exp\left(\frac{-r}{2a_0}\right) \cdot \cos \theta \right)^2,$$

$$(n,l,m)=(2,1,1):$$

$$\text{density} := \left( \frac{r}{a_0} \cdot \exp\left(\frac{-r}{2a_0}\right) \cdot \sin \theta \right)^2,$$

$$(n,l,m)=(3,0,0):$$

$$\text{density} := \left( \left(27 - 18\frac{r}{a_0} + 2\left(\frac{r}{a_0}\right)^2\right) \cdot \exp\left(\frac{-r}{3a_0}\right) \right)^2,$$

$$(n,l,m)=(3,1,0):$$

$$\text{density} := \left( \left(6 - \frac{r}{a_0}\right) \cdot \frac{r}{a_0} \cdot \exp\left(\frac{-r}{3a_0}\right) \cdot \cos \theta \right)^2,$$

$$(n,l,m)=(3,1,1):$$

$$\text{density} := \left( \left(6 - \frac{r}{a_0}\right) \cdot \frac{r}{a_0} \cdot \exp\left(\frac{-r}{3a_0}\right) \cdot \sin \theta \right)^2,$$

$$(n,l,m)=(3,2,0):$$

$$\text{density} := \left( \left(\frac{r}{a_0}\right)^2 \cdot \exp\left(\frac{-r}{3a_0}\right) \cdot (3 \cos^2 \theta - 1) \right)^2,$$

$$(n,l,m)=(3,2,1):$$

$$\text{density} := \left( \left(\frac{r}{a_0}\right)^2 \cdot \exp\left(\frac{-r}{3a_0}\right) \cdot \cos \theta \cdot \sin \theta \right)^2,$$

$$(n,l,m)=(3,2,2):$$

$$\text{density} := \left( \left(\frac{r}{a_0}\right)^2 \cdot \exp\left(\frac{-r}{3a_0}\right) \cdot \sin^2 \theta \right)^2,$$

## Part I: Platonic Solids\*

### Relations among them, Simple Truncations

Go To Page 1

Part II below: **Archimedean Solids**

includes: Cubeoctahedron, Icosidodecahedron, Buckyball

Part III below: **DualPolyhedra**

There are five (and only five) Platonic solids. Three of them are easy to imagine — Cube, Octahedron and Tetrahedron — while the remaining two are more difficult: Icosahedron and Dodecahedron. The earliest known models date from the Stone Age.

#### WHAT TO DO IN 3D-XPLORMATH?

First, the program shows how the other four Platonic solids are obtained from the Cube: Select first one of the other polyhedra, then in the Action Menu:

**Show Relation with Cube.**

For the Octahedron one sees that its six vertices are the midpoints of the faces of a cube; the Octahedron faces are equilateral triangles. The Tetrahedron sits in the cube so that its four vertices are vertices of the Cube, and the six Tetrahedron edges are face diagonals of the Cube. The Icosahedron can be placed inside a Cube so that its twelve vertices lie on the six faces of the Cube: see the default morph in 3DXM, preferably when **Show Relation with Cube** is chosen. The Dodecahedron can be placed around

---

\* This file is from the 3D-XplorMath project. Please see:

a Cube so that its twelve pentagon faces rest on the twelve edges of the cube. See again the default morph going from the Rhombic Dodecahedron via the Platonic Dodecahedron to a cube with subdivided faces.

Second, by cutting off appropriately the vertices or the edges of a Platonic solid one obtains the simpler ones of the **Archimedean solids**. These are polyhedra whose faces are (several kinds of) regular polygons, whose edges all have the same length and whose vertices all look the same. Select in the Action Menu any of the three **Truncations** and then do the associated default Morph. For example, the **Edge Truncations** morph from one Platonic solid to another one (which is called its dual).

Third, since our intuition handles two dimensions better than three, it is interesting to project the Platonic solids from their midpoints onto a circumscribed sphere. View in Wire Frame and select in the Action Menu:

**Show Central Projection to Sphere** .

These two-dimensional spherical views of the Platonic solids come very close to explaining why there are no other such beautiful polyhedra.

Fourth, the Icosahedron and the Dodecahedron have very beautiful **Stellations**, polyhedra that fascinated Kepler. Select (Action Menu): **Create Stellated**. Note that all the mentioned views have their own default morphs. Kepler imagined the stellated Dodecahedron as having pentagon stars as faces. One can also select it in the Polyhedra Menu

as Kepler's Great Dodecahedron. In 3DXM it is drawn as a (negative) stellation of the Icosahedron.

Fifth, for the Cube and the Icosahedron there are two special entries in the Action Menu when viewing these solids in Wire Frame. For the Cube select **Show Intersection With Plane**, preferably in one of the stereo modes. The plane is represented by random dots and the dots inside the Cube are deleted; the Cube can be rotated and moved forward and backward, always showing its polygonal intersection with the plane. For the Icosahedron select in the Action Menu **Add Borromean Link**, preferably in one of the stereo modes. Note how the boundaries of the emphasized rectangles are intertwined or linked. The edge lengths of each rectangle are equal to the lengths of an edge and a diagonal of a regular pentagon, thus showing the relation of the Icosahedron inside the Cube with the Golden Ratio. Also, the default morph of this image is worth viewing.

Finally, stone objects with Platonic Symmetry were found, mainly in Scotland. They were dated 2500 B.C. They are carved from bigger stones, but they look as if they were conceived as collections of balls. Therefore we have added the Action Menu entry: **Show As Stone Balls**. In Patch Display the balls are fine triangulations of the Bucky Ball, in Wire Frame the balls are shown with random dots. One can also view other sphere triangulations after one has selected (in Patch Display) **Create Subdivided**: another

entry appears: **Triangulate Further.**

## **Part II: Archimedean Solids**

Here is the definition again: All faces are regular polygons (of up to three different kinds). All edges have the same length. All vertices (with their outgoing edges) are congruent. In addition to the five Platonic solids there are twelve of them.

We have already seen the simplest ones: Truncate the vertices of a Platonic solid; there are two possibilities, if some portion of the edges remain this is called **Standard Truncation**, and if the truncation cuts go through the midpoints of the edges we have a **Midpoint Truncation**. One can also **truncate the edges**; this deformation leads to the same Archimedean solid if one starts from the Octahedron or the Cube, and also if one starts from the Icosahedron or the Dodecahedron. Two more are obtained if one truncates the edges and the vertices; the deformation is easier to observe if one uses the standard truncation on either the Cubeoctahedron or the Icosidodecahedron. In fact, not quite the standard truncation, because that would make rectangles instead of squares from the truncated vertices.

Finally there are the **Snub Polyhedra**. We could not find what 'snub' means in this context. We describe the construction and call it 'to snub'. Each face of a Platonic solid is scaled down from its midpoint and also rotated around the midpoint. The 'snubbed' polyhedron is the

convex hull of these deformed faces. This 2-parameter deformation can be adjusted to give a 1-parameter family of polyhedra whose faces are either regular polygons or isosceles triangles. In each family is an Archimedean solid. A snubbed Tetrahedron is an Icosahedron, snubbed Cube and Octahedron give the same Archimedean solid and also snubbed Dodecahedron and Icosahedron agree.

One can probably understand all these truncations better if one selects in the Action Menu

**Snub Or Truncate Polyhedron In Polyhedron.**

This will add the original polyhedron (as wire frame) to the truncation.

**Adapted Morphs:** Each selection in the Action Menu will cause that the default deformation, **Morph** in the Animation Menu, is adjusted to the Action Menu selection.

### **Part III: Dual Polyhedra**

Duality has the simplest definition for Platonic solids: The convex hull of the centers of the faces is the dual polyhedron. The following definition works for Platonic and Archimedean solids: Take the tangent planes to the circumscribed sphere at the vertices of the polyhedron; consider them as the boundaries of halfspaces which contain the polyhedron; the intersection of these halfspaces is the dual polyhedron. For example the rhombic dodecahedron is dual to the cubeoctahedron. Similarly, consider convex polyhedra whose inscribed sphere touches **all** faces; the

convex hull of the contact points of the faces with the inscribed sphere is the dual polyhedron.

These definitions of duality are unique up to scaling. For a general convex polyhedron definitions are no longer unique up to scaling. Choose an interior point and project the polyhedron radially onto a sphere around the chosen point; one obtains a tessalation of the sphere with the same combinatorial properties as the boundary of the polyhedron; consider on the sphere the Dirichlet or Voronoi domains of the vertices (the points which are closer to one vertex than to all others); these domains form the dual tessalation; any polyhedron whose radial projection to the sphere has the same combinatorics as this dual tessalation, is called a dual polyhedron to the given one.

In 3D-Xplormath one can view all Archimedean solids inside their dual polyhedra: First select one of the Platonic solids from the Polyhedra Menu. Then check in the Action Menu the entry:

**Show All Polyhedra Inside Their Duals** .

Now, each of the provided truncations gives an Archimedean solid, shown inside its dual polyhedron. These images can be morphed, including the surrounding dual polyhedra.

H.K.

[Go To Platonics](#)

# Complex Functions Or Conformal Maps

[Go To Page 1](#)

[Visualisation of Conformal Maps](#)

**Elementary Functions** (Click on Names)

- 1.) [Complex Square](#)  $z \mapsto z^2$
- 2.) [Exponential Map](#)  $z \mapsto \exp(z)$
- 3.) [Complex Inverse](#)  $z \mapsto 1/z$
- 4.) [Confocal Ellipses from](#)  $z \mapsto z + 1/z$
- 5.) [Rolling Curves from Polynomials](#)  $z \mapsto z^{ee} + ee \cdot z$
- 6.) [Fractional Linear Maps](#)  $z \mapsto (a \cdot z + b)/(c \cdot z + d)$
- 7.) [Hyperbolic Translations](#)  $z \mapsto \frac{(z+cc)}{(1+\overline{cc} \cdot z)}$
- 8.) [Nonconformal Complex Map](#)  $z \mapsto \text{conj}(z) + aa \cdot z^2$
- 9.) [Complex Square Root](#)  $\sqrt{(z^2)} = \pm z$
- 10.) [Complex Logarithm](#)  $\log(\exp(z)) = z + 2\pi i \cdot \mathbb{Z}$
- 11.) [Complex Sine](#)  $\sin(z) = (\exp(iz) - \exp(-iz))/2i$
- 12.) [Complex Tangent Hyperbolicus](#)
- 13.) [Stereographic Projection and its Importance](#)

**Elliptic Functions**

- 14.) [Jacobi Type Elliptic Functions](#)
- 15.) [Symmetries Of Elliptic Functions](#)

## Visualization of Conformal Maps \*

Here we deal with complex numbers,  $\mathbb{C}$ , and with complex-valued functions from domains  $D \subset \mathbb{C}$  to  $\mathbb{C}$ . The functions are assumed to be differentiable in the complex sense. This means that differences  $f(z+h) - f(z)$ ,  $z, h \in \mathbb{C}$  can be well approximated by

$$\text{complex linear maps: } l_z(h) = c(z) \cdot h, \quad c(z) \in \mathbb{C}.$$

For each  $z$  the constant  $c(z)$  is called *derivative of  $f$  at  $z$*  and written as  $c(z) = f'(z)$ .

For visualization,  $\mathbb{C}$  and  $\mathbb{R}^2$  are identified by writing the 1st basis vector  $\begin{pmatrix} 1 \\ 0 \end{pmatrix}$  of  $\mathbb{R}^2$  as  $\mathbf{1}$  and the second basis vector  $\begin{pmatrix} 0 \\ 1 \end{pmatrix}$  as  $\mathbf{i}$ . The point  $\begin{pmatrix} x \\ y \end{pmatrix} \in \mathbb{R}^2$  means the complex number  $x + \mathbf{i} \cdot y$ .

Nonzero complex numbers can be written as  $c = |c| \cdot \frac{c}{|c|}$ , where  $|c| \in \mathbb{R}$  is called the absolute value of  $c$  and  $u := \frac{c}{|c|}$  is a unitary complex number. The complex linear map  $l(z) := |c| \cdot z$  is in  $\mathbb{R}^2$  ordinary scaling by the factor  $|c|$ . The complex linear map  $l(z) := u \cdot z$ , viewed in  $\mathbb{R}^2$ , is distance preserving:  $|l(w) - l(z)| = |u \cdot (w - z)| = |u| \cdot |w - z| = |w - z|$ . For  $u \neq 1$  we have only the fixed point 0:

$$l(z) = z \Leftrightarrow (u - 1) \cdot z = 0 \Leftrightarrow z = 0.$$

Multiplication in  $\mathbb{C}$  by a unitary complex number  $u \neq 1$  is therefore a rotation around the origin. Together with the scaling by  $|c|$  we have: Complex linear maps  $l(z) := c \cdot z$  preserve angles, they are ‘*conformal*’. Multiplication by  $\mathbf{i}$ ,

---

\* This file is from the 3D-XplorMath project. Please see:

considered in  $\mathbb{R}^2$ , is counterclockwise  $90^\circ$  rotation. Evidently this is a square root of multiplication by  $-1$ . Thus the geometric interpretation removes all the mystery from a square root of  $-1$ . Computation with complex symbols started in the 16th century, but it was done reluctantly until, around 1800, the geometric interpretation was found and accepted rapidly. In the next 50 years the field of complex analysis exploded to great sophistication.

If we map two intersecting curves with a complex differentiable function  $f$  then the tangents of these curves at the intersection point  $w$  are mapped by the derivative approximation of  $f$ . If  $f'(w) \neq 0$  then the image curves intersect with the same angle as the preimage curves. We say: the function  $f$  is a conformal map.

Conformality is very important because real differentiability plus preservation of oriented angles implies complex differentiability. The words *complex function* and *conformal map* are therefore used interchangeably. Our visualizations try to emphasize conformality as clearly as possible.

A linear map (in real dimension two) is already conformal, if two non-parallel right angles are preserved, for example the angles of the edges of a square and the angle of its diagonals. Because of this fact *our visualizations decorate the domain with a square grid and we show this grid and its image*. To make the image grid as large as possible, it fills the window of 3D-XplorMath. For a comparison with the preimage one has to press the **Option** and **Command** keys and then press and release the (left) **Mouse Button**.

Showing a domain grid and its image grid visualizes complex functions as maps. This is not very common, but occurs already in Maxwell's work. The image grid shows very clearly the points where the derivative vanishes. The Action Menu entry **Show Derivative At Mouse Point** shows the linear approximation of the function at the mouse point - in other words it shows, how the derivative scales and rotates the vicinity of the preimage of the mouse point.

The conformal image of a square grid has grid meshes which are "squares" with slightly curved edges. The exponential map, for example, transforms a cartesian square grid into a "conformal polar square grid". Its grid meshes look more and more like squares the more grid lines one displays by choosing `uResolution`, `vResolution` larger. For some functions, e.g.  $z \mapsto z + 1/z$ , it is therefore better to choose such a conformal polar grid in the domain instead of a Cartesian square grid whose edges are lines parallel to the coordinate axes. - The non-conformal map  $z \mapsto \bar{z} + aa \cdot z^2$  shows that non-conformality can easily be recognized in the image grid of a cartesian grid with small square grid meshes: The grid meshes of the image are in general parallelograms.

To the domain grid one can, in the Action Menu, add lines, intervals or circles. Their images appear with the image grid. For example, if a circle passes through a point where the derivative has a simple zero, then the interior  $180^\circ$  angle of the circle at that point is doubled to a  $360^\circ$  interior angle of the image curve. Note that the image grids for all

conformal maps look very similar in the immediate vicinity of a simple zero of the derivative of the map.

Many functions show their symmetries better when their image grid is viewed (via [Stereographic Projection](#)) on the Riemann Sphere instead of the Gaussian Plane. The second entry of the Action Menu toggles between these two representations. The Riemann Sphere can also be viewed in anaglyph or in cross-eyed rendering.

For most functions one can switch between a **cartesian grid** in the domain and a **polar grid**. The different grids bring out different properties of the function. An exception are the elliptic functions: the domain is always one half fundamental parallelogram of their torus and the grid lines are parallel to the edges of the parallelogram; the image grid covers the Riemann sphere once.

The Conformal Maps Menu offers the possibility to **precompose** or **postcompose** the selected complex function with a choice of six other functions, thus increasing the collection of immediately available complex maps.

H.K.

[Conformal TOC](#)

## Complex Square $z \rightarrow z^2$ \*

We use the parameter dependent mapping  $z \mapsto aa(z - bb)^{ee} + cc$ , with the default values  $aa = 1$ ,  $bb = 0$ ,  $cc = 0$ , and  $ee = 2$ . The default Morph joins  $z^2$  to the identity, varying  $ee \in [1, 2]$ .

Look at the discussion in “About this Category” or [Visualisation of Conformal Maps](#) for what to look at, what to expect, and what to do.

Just as the appearance of the graph of a real-valued function  $x \mapsto f(x)$  is dominated by the critical points of  $f$ , it is an important fact that so also, for a conformal map,  $z \mapsto f(z)$ , the overall appearance of an image grid is very much dominated by those points  $z$  where the derivative  $f'$  vanishes. Most obviously, near points  $a$  with  $f'(a) = 0$  the grid meshes get very small and, as a consequence, the grid lines usually are strongly curved. If one looks more closely then one notices that the angle between curves through  $a$  is **not** the same as the angle between the image curves through  $f(a)$  (recall:  $f'(a) = 0$ ). We will find this general description applicable to many examples.

One should first look at the behaviour of the simple quadratic function  $z \rightarrow z^2$  near  $z = 0$ , both in Cartesian and in Polar coordinates. One sees that a rectangle, which

---

\* This file is from the 3D-XplorMath project. Please see:

touches  $z = 0$  from one side is folded around 0 with strongly curved parameter lines, and one also sees in Polar coordinates that the angle between rays from 0 gets **doubled**. The image grid in the Cartesian case consists of two families of orthogonally intersecting parabolas.

One should return to this prototype picture after one has seen others like  $z \rightarrow z + 1/z$ ,  $z \rightarrow z^2 + 2z$  and even the Elliptic functions and looked at the behaviour near their critical points.

The first examples to look at, (using Cartesian **and** Polar Grids) are  $z \rightarrow z^2$ ,  $z \rightarrow 1/z$ ,  $z \rightarrow \sqrt{z}$ ,  $z \rightarrow e^z$ .

H.K.

Conformal TOC

## The Complex Exponential Map $z \mapsto e^z$ \*

Our example is  $z \mapsto \exp(aa(z - bb)) + cc$ , its parameters are set to  $aa = 1$ ,  $bb = 0$ ,  $cc = 0$ ;  $aa$  gets morphed in  $\mathbb{C}$ . See the functions  $z \mapsto z^2$ ,  $z \mapsto 1/z$  and their ATOs first.

The complex exponential function  $z \mapsto e^z$  is one of the most marvellous functions around. It shares with the real function  $x \mapsto \exp(x)$  the differential equation  $\exp' = \exp$  and the functional equation  $\exp(z + w) = \exp(z) \cdot \exp(w)$ . This latter identity implies that one can understand the complex Exponential in terms of real functions, for if we put  $z = x + i \cdot y$  then we have

$$\begin{aligned}\exp(x + i \cdot y) &= \exp(x) \cdot \exp(i \cdot y) = \\ &\exp(x) \cdot \cos(y) + i \cdot \exp(x) \cdot \sin(y).\end{aligned}$$

This says that a Cartesian Grid is mapped “conformally” (i.e., preserving angles) to a Polar Grid: the parallels to the real axis are mapped to radial lines, and segments of length  $2\pi$  that are parallel to the imaginary axis are mapped to circles around 0. This function is therefore used to make, in the Action Menu, the Conformal Polar Grid. Observe how justified it is to describe the image grid as “made out of curved small squares”.

If you have seen  $z \mapsto e^z$  and  $z \mapsto z + 1/z$  then now look at  $z \mapsto \sin(z)$ . H.K.

---

\* This file is from the 3D-XplorMath project. Please see:

## The Complex Map $z \mapsto 1/z$ \*

The actual mapping for this example is  $z \mapsto aa/(z-bb)+cc$ , with the default values  $aa = 1$ ,  $bb = 0$ , and  $cc = 0$ .

Look at function and ATO **Complex Square**  $z \mapsto z^2$  first.

The function  $z \mapsto 1/z$  should be looked at both in Cartesian and Polar Grids. The default Morph varies  $bb \in [0, 1]$ .

Notice first:

- 1) The real axis, imaginary axis and unit circle are mapped into themselves,
- 2) the upper half plane and the lower half plane are interchanged, and
- 3) the inside of the unit circle and its outside are also interchanged.

This is best seen in the (default) Conformal Polar Grid. In the Cartesian Grid one should in particular observe that all straight parameter lines (in the domain) are mapped to circles (some exceptions, like the real axis, remain lines). The behaviour of these circles near zero can be looked at as an image of the behaviour of the standard Cartesian Grid near infinity. In fact **all** circles are mapped to circles or lines.

Examples to look at after this are

---

\* This file is from the 3D-XplorMath project. Please see:

$$z \mapsto (az + b)/(cz + d) \text{ and } z \mapsto (z + cc)/(1 + \bar{c}cz),$$

both of which can be obtained from  $z \rightarrow 1/z$  by composition with translations  $z \rightarrow z+a$  or scaled rotations  $z \rightarrow a \cdot z$ . Therefore all of these so-called “Möbius transformations” map circles and lines to circles and lines.

H.K.

Conformal TOC

## Complex Map $z \mapsto z + aa/z$ \*

See the functions  $z \rightarrow z^2$ ,  $z \rightarrow 1/z$ ,  $z \rightarrow z^2 + 2z$ ,  $z \rightarrow e^z$  and their ATOs first. Use the default Morph,  $aa \in [0, 1]$ .

This function is best applied to a Conformal Polar Grid. The image of the outside of the unit circle is the same as the image of the inside of the unit circle, namely the full plane minus the segment  $[-2, 2]$ . The unit circle is mapped to this interval, each interior point  $w = 2 \cdot \cos(\phi) \in [-2, 2]$  appears twice as image point, namely of  $z = \exp(\pm i\phi)$ .

The default choice shows how the outside of the unit disk is mapped to the outside of the interval  $[-2, 2]$ . If we note that  $f'(\pm 1) = 0$  then we understand this behaviour: the interior  $180^\circ$  angle at these critical points  $\pm 1$  of the outside domain is again **doubled** to become the angle of the image domain (outside  $[-2, 2]$ ) at  $\pm 2$ .

A domain circle  $z_R(\phi) = R \exp(i\phi)$  is mapped to the image ellipse  $(R + 1/R) \cos(\phi) + i(R - 1/R) \sin(\phi)$ , and a domain radius  $z_\phi(R) = R \exp(i\phi)$  is mapped to the Hyperbola  $(R + 1/R) \cos(\phi) + i(R - 1/R) \sin(\phi)$ . The image grid therefore consists of a *family of ellipses* that intersect orthogonally a *family of hyperbolae*, and all these Conic Sections (see the Plane Curves Category) are “confocal”, i.e., they have the **same Focal Points**, namely at  $+2$  and  $-2$ .

H.K.

---

\* This file is from the 3D-XplorMath project. Please see:

**Complex Map**  $z \mapsto aa \cdot z^{ee} + ee \cdot z^*$

(Default:  $z \rightarrow z^2 + 2z$ )

Look at the functions  $z \rightarrow z^2$ ,  $z \rightarrow 1/z$  and their ATOs first. The default Morph varies  $aa \in [0, 1.2]$  for  $ee = 4$ .

Of course, since  $z^2 + 2z + 1 = (z + 1)^2$ , this function is not very different from the first example  $z \rightarrow z^2$ . But the change puts the critical point to  $-1$  on the unit circle ( $f'(-1) = 0$ ). Therefore, if one looks what this map does to a Polar Grid, one can study the behaviour near the critical point  $z = -1$  with a different grid picture than in the first example. Circles outside the unit circle are mapped to Limaçons (Plane Curves Category, [Cardioid and Limacon](#)) which wind around  $-1$  twice. The unit circle is mapped to a Cardioid and one can see the interior angle of  $180^\circ$  of the unit circle at  $-1$  mapped to the interior angle of  $360^\circ$  of the Cardioid at  $-1$ . Also one can see that a neighbourhood of  $-1$  is strongly contracted by this function.

See the function  $z \rightarrow z + 1/z$  next.

H.K.

---

\* This file is from the 3D-XplorMath project. Please see:

## Fractional Linear Maps <sup>\*</sup> or Möbius Transformations

$$z \mapsto (a \cdot z + b)/(c \cdot z + d)$$

See the functions  $z \mapsto z^2$ ,  $z \mapsto 1/z$  and their ATOs first. The default Morph uses a conformal polar grid and varies  $a \in [1, 2]$ ,  $c \in [0, 1]$ .

These functions are called fractional linear maps or **Möbius transformations**. They differ from the map  $z \mapsto 1/z$  by composition with a translation  $z \mapsto z + a$  or scaled rotations  $z \mapsto a \cdot z$ . As discussed for  $z \mapsto 1/z$  they transform lines and circles to lines and circles.

The default special case is  $z \mapsto (z - 1)/(z + 1)$ . It is best understood in the (default) Conformal Polar Grid. Since it maps 0 to  $-1$  and  $\infty$  to  $+1$ , one can see the Polar coordinate centers moved from  $0, \infty$  to  $-1, +1$ . This picture is the first step towards understanding the complex (or “Gaussian”) plane plus the point at infinity as the “Riemann Sphere”. Use the 2nd entry in the Action Menu: **Show Image On Riemann Sphere**.

See also the other Möbius transformations from the Conformal Maps menu.

H.K.

---

\* This file is from the 3D-XplorMath project. Please see:

## The Möbius Transformation \*

$$z \rightarrow \frac{(z + cc)}{(1 + \overline{cc} \cdot z)} \quad \text{of the unit disk.}$$

Look at the Möbius transformation  $z \rightarrow \frac{(a \cdot z + b)}{(c \cdot z + d)}$  and its ATO first. The default Morph varies  $cc \in [-0.9, 0.9]$ .

This function maps the interior of the unit disk bijectively to itself, for every choice of  $cc$  with  $|cc| < 1$ . The behaviour outside of the unit disk is obtained by reflection in the unit circle, i.e.,  $z \rightarrow 1/\bar{z}$ .

These maps have an interesting geometric interpretation: they are isometries for the “hyperbolic metric” on the unit disk. To understand this further, imagine that the unit disk is a map of this two-dimensional hyperbolic world and that the scale of this map is not a constant but equals  $1/(1 - z\bar{z})$ . This means that we do not obtain the length of a curve  $t \rightarrow z(t)$  as in the Euclidean plane by the integral  $\int |z'(t)| dt$ —we have to take the scale into account and define its hyperbolic length by  $\int |z'(t)| / (1 - |z(t)|^2) dt$ . It is this hyperbolic length of curves that is left invariant by the “hyperbolic translations”  $z \rightarrow (z + cc) / (1 + \overline{cc} \cdot z)$ .

Locally the Pseudosphere (see: [Surfaces of Revolution](#)) has the same hyperbolic geometry.

H.K.

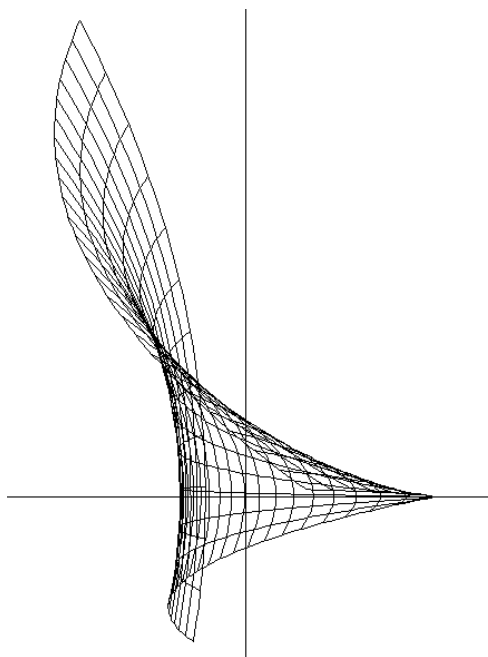
---

\* This file is from the 3D-XplorMath project. Please see:

## Nonconformal Complex Map $z \mapsto \text{conj}(z) + aa \cdot z^2$ \*

Look first at other functions and their ATOs, for example  $z \rightarrow z^2$  and  $\exp$ . The default Morph varies  $aa \in [0, 1]$ .

The map  $z \mapsto \text{conj}(z) + aa \cdot z^2$  is a map from the complex plane to itself. The harmless looking “conj” is responsible for the fact that this map is not complex differentiable and therefore not a “conformal” map, that is, a map for which the angles between any two curves and their images are the same. It is clearly visible in the image that the squares of the domain grid are mapped to rectangles and even to parallelograms in the range.



The image also shows two “fold lines”. We observe that interior points of the domain are mapped so that they lie on the boundary of the image. For a complex differentiable function this can never happen as is asserted by the *Open Mapping Theorem*. See the default morph.

H. K.

---

\* This file is from the 3D-XplorMath project. Please see:

## The Complex Map $z \mapsto \sqrt{z}$ \*

See the functions  $z \mapsto z^2$ ,  $z \mapsto 1/z$  and their ATOs first. The map  $z \mapsto \sqrt{z}$  should be looked at both in Cartesian and Polar Grids and in the default morph  $z^{ee}$ ,  $ee \in [\frac{1}{2}, 1]$ . Note that since this function is the inverse of  $z \rightarrow z^2$ , we expect to see related phenomena: circles around 0 go to circles around 0, radial lines from 0 go to radial lines from 0, but now with **half** the angle between them (since we look at the inverse map). A neighbourhood of 0 was very much contracted by  $z \rightarrow z^2$ , now we see the opposite, the distance of points from zero is increased very much (beyond any Lipschitz bound).

A more complicated aspect is the fact that the function  $z \mapsto \sqrt{z}$  is not really a well defined map until we make some choices. Namely observe: all  $z \neq 0$  have **two** distinct square roots, differing by a factor of  $-1$ .

The function  $\sqrt{z}$  used by 3D-XplorMath maps the upper half plane to the first quadrant, the (strict) lower half plane to the fourth quadrant, and the negative real axis to the positive imaginary axis—so there is no continuity from above to below the negative real axis (which is therefore called a “branch cut”).

The Cartesian grid lines are mapped to two families of **hyperbolae** which intersect each other orthogonally.

H.K.

---

\* This file is from the 3D-XplorMath project. Please see:

## The Complex Logarithm \*

$$z \mapsto \log z$$

Look at the function  $z \rightarrow e^z$  and its ATO first. The default Morph shows  $a \cdot \log(z) + (1 - a) \cdot z$  for  $a \in [0, 1]$ .

The complex Logarithm tries to be the inverse function of the complex Exponential. However,  $\exp$  is  $2\pi i$ -periodic, so such an inverse can only exist as a multivalued function.

From the differential equation  $\exp' = \exp$  follows that the derivative of the inverse is not multivalued and in fact very simple:

$$\log'(z) = 1/z.$$

Integration of the geometric series

$$\begin{aligned} 1/z &= 1/(1 - (1 - z)) = \sum_k (1 - z)^k \\ &= \left( \sum_k -(1 - z)^{k+1}/(k + 1) \right)' \end{aligned}$$

gives the Taylor expansion around 1 of  $\log$ . The so called “principal value” of the complex Logarithm is defined in the whole plane, but slit along the negative real axis, for example by integrating the derivative  $\log'(z) = 1/z$  in that simply connected domain along any path starting at 1.

Different values of  $\log z$  differ by integer multiples of  $2\pi i$ , e.g.  $i = \exp(\pi i/2)$  implies  $\log i = \pi i/2 + 2\pi i \cdot \mathbb{Z}$ .

H.K.

---

\* This file is from the 3D-XplorMath project. Please see:

## The Complex Sine $z \rightarrow \sin(z)$ \*

Look at the functions  $z \rightarrow z^2$ ,  $z \rightarrow 1/z$ ,  $z \rightarrow z^2 + 2z$ ,  $z \rightarrow e^z$  and their ATOs first. The default Morph varies the family  $f_a(z) = a \cdot \sin(z) + (1 - a) \cdot z$  for  $a \in [0, 1]$ .

While the behaviour of the one-dimensional real functions  $x \mapsto \exp(x)$  and  $x \mapsto \sin(x)$  are quite dissimilar ( $\exp$  is convex and positive, while  $\sin$  is periodic and bounded), as complex functions they are very closely related:

$$\sin(z) = \frac{\exp(iz) - \exp(-iz)}{2i},$$

an identity that explains why the image grid under  $\sin$  of the default Cartesian grid looks exactly like the image grid under  $z \rightarrow z + 1/z$  applied to a Conformal Polar Grid outside the unit circle. For if we put  $w(z) := \exp(iz)/i$ , then  $\sin(z) = (w(z) + 1/w(z))/2$ , and: recall that  $\exp$  maps the standard Cartesian Grid to the Conformal Polar Grid around 0. The parameter curves in the image grid of  $\sin$  are therefore the same orthogonal and confocal ellipses and hyperbolas as in the image of  $z \mapsto z + 1/z$ .

H.K.

---

\* This file is from the 3D-XplorMath project. Please see:

## Hyperbolic Tangent\*

Definition:

$$\begin{aligned}\tanh(z) &:= \frac{\exp(z) - \exp(-z)}{\exp(z) + \exp(-z)} \\ &= \frac{w - 1}{w + 1} \text{ with } w = \exp(z)^2\end{aligned}$$

$$\tan(z) := -i \cdot \tanh(iz) = \frac{\sin(z)}{\cos(z)}$$

In 3DXM:  $\tanh(aa \cdot z/2) + bb \cdot z/2$ ,  $bb = 1 - aa$

default:  $aa = 1$ ,  $bb = 0$ , morph:  $0 \leq aa \leq 1$ .

The default visualization of this function is on the standard Cartesian Grid. The exponential map transforms this grid into a polar grid. The rational map  $w \mapsto (w - 1)/(w + 1)$  sends the polar centers at  $0, \infty$  to polar centers at  $-1, 1$ . The default morph connects  $z/2 \mapsto \tanh(z/2)$  to the identity.

Recall that all real functions that have power series representations can be extended to be functions over part of the complex plane. Of course this includes all functions that have simple definitions in terms of the exponential map.

H.K.

---

\* This file is from the 3D-XplorMath project. Please see:

## Stereographic Projection and its Importance \*

Stereographic projection was invented for making maps of the earth and the celestial sphere. It is an angle preserving map of the sphere minus one point onto the Euclidean plane.

Complex differentiability (of maps from the plane to the plane) is the same as real differentiability plus preservation of oriented angles (except where the derivative vanishes). Angle preserving differentiable maps are therefore important for the theory of complex functions. The stereographic projection can be interpreted as mapping the 2-sphere to the Euclidean plane, compactified by a *point at infinity*. All the complex rational functions can be extended to *infinity*, i.e. they can be considered as differentiable, angle preserving maps from the 2-sphere to the 2-sphere. The stereographic projection turns this “can be considered as” into a simple explicit relation. The 2-sphere, in this context, is called the *Riemann Sphere* and the image plane is called the *Gaussian Plane*.

In 3D-XPLORMATH a 3D image of the stereographic projection can be reached via the last entry of the Action Menu in the Conformal Map Category. *Stereographic projection is defined as the central projection from one point on the sphere onto the opposite tangent plane.*

---

\* This file is from the 3D-XplorMath project. Please see:

## Formulas for the Stereographic Projection

Algebraically it is slightly more convenient to map the sphere not to the opposite tangent plane but to the parallel plane through the midpoint. More explicitly, the unit sphere  $\mathbb{S}^2 \subset \mathbb{R}^3$  is projected from  $(0, 0, -1)$  to the plane  $\{z = 0\}$  (and similar formulas work in all dimensions):

$$St(x, y, z) := \frac{1}{1+z} \cdot (x, y, 0), \text{ where } x^2 + y^2 + z^2 = 1.$$

because the three points involved lie on a line:

$$\frac{1}{1+z} \cdot \begin{pmatrix} x \\ y \\ z \end{pmatrix} + \frac{z}{1+z} \cdot \begin{pmatrix} 0 \\ 0 \\ -1 \end{pmatrix} = \begin{pmatrix} \frac{x}{(1+z)} \\ \frac{y}{(1+z)} \\ 0 \end{pmatrix} =: \begin{pmatrix} \xi \\ \eta \\ 0 \end{pmatrix}.$$

The inverse map is given by:

$$St^{-1}(\xi, \eta) := \frac{1}{1+\xi^2+\eta^2} \cdot \begin{pmatrix} 2\xi \\ 2\eta \\ 1 - \xi^2 - \eta^2 \end{pmatrix} \in \mathbb{S}^2,$$

because, again, the three points lie on a line:

$$\frac{2}{1+\xi^2+\eta^2} \cdot \begin{pmatrix} \xi \\ \eta \\ 0 \end{pmatrix} + \frac{-1+\xi^2+\eta^2}{+1+\xi^2+\eta^2} \cdot \begin{pmatrix} 0 \\ 0 \\ -1 \end{pmatrix} = St^{-1}(\xi, \eta) =$$

$$\frac{1}{1+\xi^2+\eta^2} \cdot \begin{pmatrix} 2\xi \\ 2\eta \\ 1 - \xi^2 - \eta^2 \end{pmatrix}.$$

### Claim: Stereographic Projection

maps circles on  $\mathbb{S}^2$  to circles and lines in the plane.

The case of lines is easier: The line in the image plane and the projection center define a plane. This plane intersects the sphere in the preimage circle of the line. – In other words: all circles on the sphere which pass through the projection center are mapped to lines.

For every circle  $\{(\xi, \eta); (\xi - m)^2 + (\eta - n)^2 = r^2\}$  in the image plane one can easily compute the plane of the preimage circle, while the other direction needs a case distinction because of the lines.

We put  $\xi^2 + \eta^2 := 2m\xi + 2n\eta + r^2 - m^2 - n^2$  into the third component of the preimage formula. Then clearly

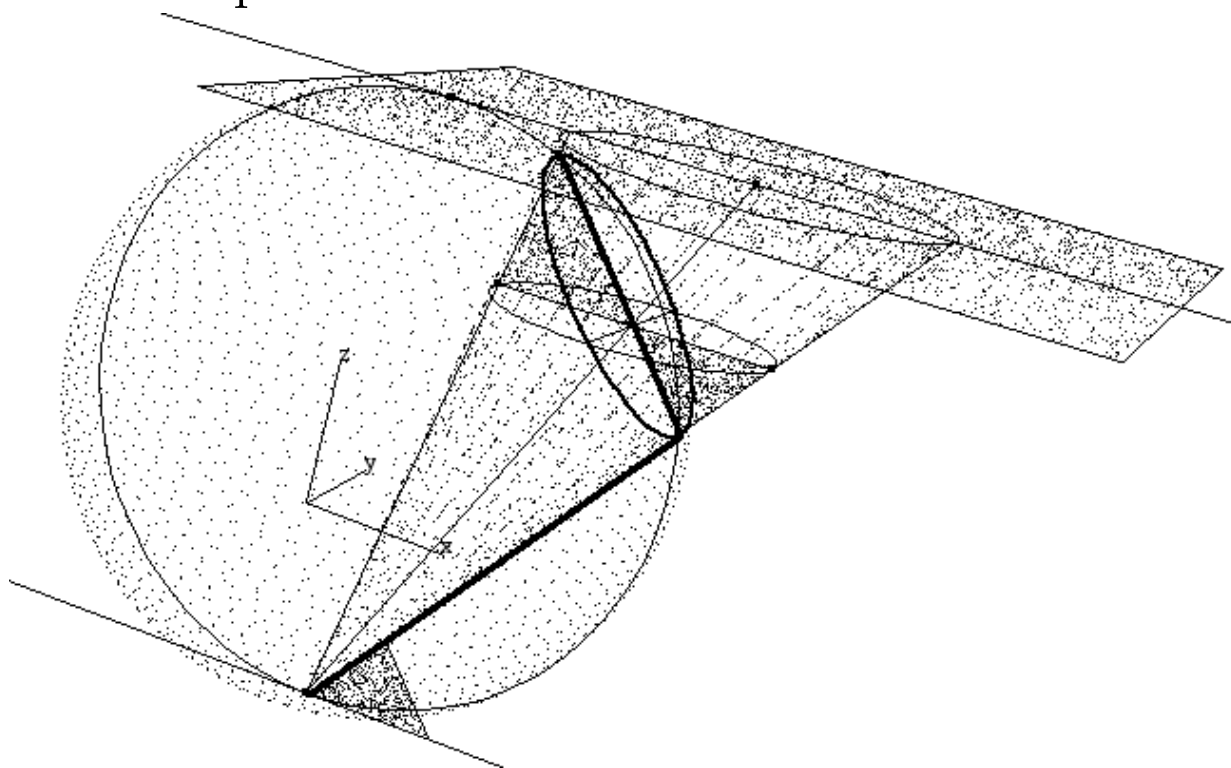
$$(1 + \xi^2 + \eta^2) \cdot (z + mx + ny + r^2 - m^2 - n^2 - 1) = 0,$$

which shows the equation for the plane of the preimage.

Claim: Stereographic Projection preserves angles.

Through every point  $p \in \mathbb{S}^2$  and tangential direction  $v$  there exists a circle on the sphere which passes through the projection center and through  $p$  and is tangential to  $v$ . Every such circle is mapped to a line which is **parallel** to the tangent of that circle at the projection center. The image lines of two such circles therefore intersect with the same angle as the two preimage circles, and the two preimage circles were chosen to represent an arbitrary angle on the sphere. – One can also prove this by computing with the derivative of the stereographic projection.

The image in 3D-XplorMath shows a nice proof of why circles are mapped to circles. A circle on the sphere and the projection center define a quadratic cone (unless the circle passes through the center and the image is a line). In general, therefore, the image of the circle is an ellipse. And all planes parallel to the image plane cut this cone in similar ellipses.



To prove that they are circles we show that their axes are equal. We add the line which joins the projection center and the midpoint of the image ellipse and we intersect it, at  $m$ , with the diameter of the circle (on the sphere) that is in the symmetry plane of the figure. Now consider the ellipse which intersects the cone in the parallel plane through  $m$ . Its axis orthogonal to the symmetry plane and the mentioned diameter of the circle are two intersecting secants of the circle. For their two subsegments holds:

$\text{axisA}^2 = D1 \cdot D2$ . The other,  $\text{axisB}$ , has its two halves as edges of similar triangles which also have the edges  $D1, D2$ . So we conclude  $D1 \cdot D2 = \text{axisB}^2$ , hence  $\text{axisA} = \text{axisB}$ . – Note that the three shaded triangles are similar: two of them are bounded by parallel segments and the bottom triangle has the angle at the cone vertex equal to the angle of the top triangle opposite  $\text{axisB}$ .

A remarkable property of the formulas for stereographic projection and its inverse is: *They map points with rational coordinates to points with rational coordinates!* For example, if we stereographically project a tangent line to the unit circle, then the rational points on the line give us all rational points on the circle! Multiply  $(p/q)^2 + (s/t)^2 = 1$  by the denominators to get all Pythagorean triples.

A differential geometric result in Dimension 3 and higher says: Any angle preserving map between spaces of constant curvature maps planes and spheres to planes and spheres. For people with that background it is therefore obvious that stereographic projection maps circles to circles.

In 3D-XplorMath one has stereo vision available so that one can see visualizations of images on the Riemann sphere in 3D. This shows the symmetries, for example, of the doubly periodic functions much more clearly than their images in the Gaussian plane do.

H.K.

Conformal TOC

## Elliptic Functions of Jacobi Type \*

What to do in 3D-XplorMath at the end of this text.

Elliptic functions are doubly periodic functions in the complex plane. A period of a function  $f$  is a number  $\omega \in \mathbb{C}$  such that  $f(z) = f(z + \omega)$  for all  $z \in \mathbb{C}$ . *Doubly periodic* means that the function has two periods  $\omega_1, \omega_2$  with  $\omega_1/\omega_2 \notin \mathbb{R}$ . The set of all period translations is a lattice  $\Gamma$ , and  $\Gamma$  has some parallelogram as fundamental domain. Period translations identify parallel edges of this parallelogram to a torus and elliptic functions can therefore be viewed as functions on such a torus or equivalently as conformal maps from the torus to the Riemann sphere.

The simplest such functions are two-to-one maps from the torus to the sphere. They have either *one double pole* and are not very different from the Weierstrass  $\wp$ -function:  $f(z) = a \cdot \wp(z) + b$ , or they have *two simple poles*; the oldest of these are Jacobi's functions  $\text{sn}$ ,  $\text{cn}$ ,  $\text{dn}$ , more below.

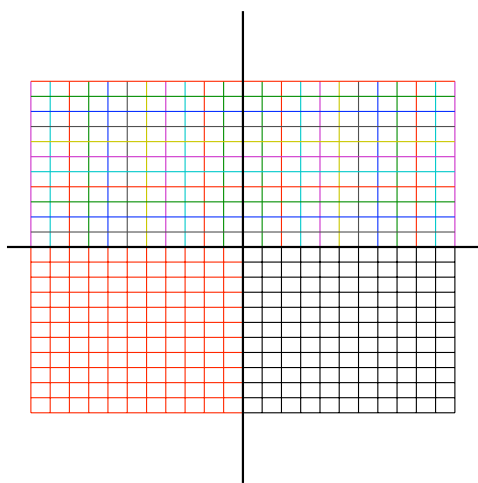
These doubly periodic functions have various properties in common with the singly periodic trigonometric functions. They are inverse functions of certain integrals and therefore are solutions of first order ODEs, just like the inverse function of  $\int_0^z 1/\sqrt{1-\zeta^2} d\zeta$  is a solution of the non-Lipschitz ODE  $f'(z)^2 = 1 - f(z)^2$ . And, as in this trigonometric case, differentiation of the first order ODE gives a second order ODE which is Lipschitz, here  $f''(z) = -f(z)$ . The trigonometric functions have more symmetries than

---

\* This file is from the 3D-XplorMath project. Please see:

their translations. These symmetries give all values from the values on  $[0, \pi/2] \times \mathbf{i} \cdot \mathbb{R}$ . For the two-to-one elliptic functions all values occur already on half a torus and the further symmetries compute all these values from the values on one eighth of the torus. If the torus happens to be rectangular, it has further symmetries: reflections which are anticonformal. In this case, from the values on one sixteenth of the torus, one can obtain all other values via Möbius transformations. And, one can define interesting elliptic functions with the Riemann mapping theorem:

The rectangle in the first quadrant of the picture below is one sixteenth of a rectangular torus. The Riemann mapping theorem is used to map this rectangle to the quarter unit circle in the first quadrant of the second picture. Riemann's theorem allows to specify that three corners of the rectangle go to  $1, 0, \mathbf{i}$  and at the 4th corner the derivative vanishes and two edges are mapped to the quarter circle:



Torus  $\frac{1}{4}$ -fundamental domain

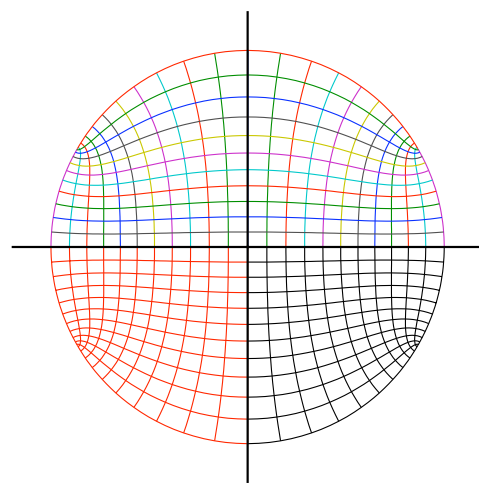


Image of  $J_D$ -function

The extension of this definition to a two-to-one map from

the torus to the (Riemann) sphere is made possible by *Schwarz Reflection*. Its simplest version, for complex power series  $f(z) = \sum_{k=0}^{\infty} a_k z^k$  with  $a_k \in \mathbb{R}$ , says  $f(\bar{z}) = \overline{f(z)}$ . We use the next step: Instead of reflection in  $\mathbb{R}$ , reflection in any straight or circular boundary arc (in domain and range) extends the definition of the function.

While all rational functions can be obtained by rational operations from the **single** polynomial  $P(z) = z$ , one needs **two** elliptic functions on a given torus to obtain all others by rational operations from these. Two choices for such a second function are obtained if one maps three other vertices of the rectangle in the first quadrant to  $0, 1, \mathbf{i}$  on the quarter circle in the first quadrant (but always origin to origin). In each case the derivative of the map vanishes at the last corner and the  $90^\circ$  angle between adjacent edges is opened to the  $180^\circ$  angle between the image arcs:

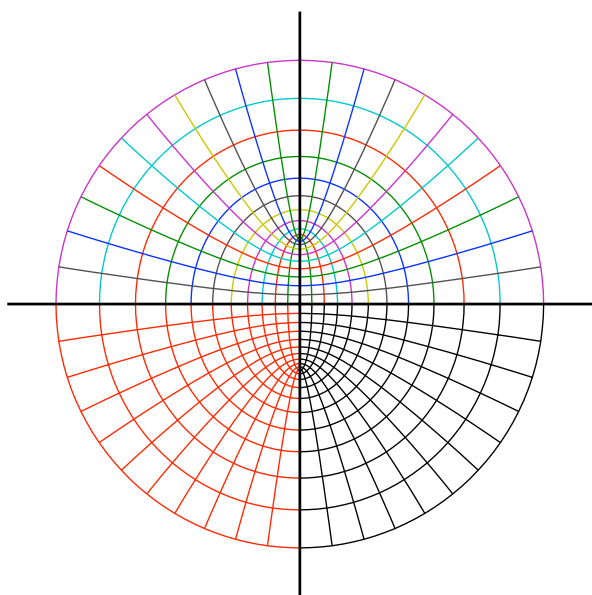


Image of  $J_E$ -function

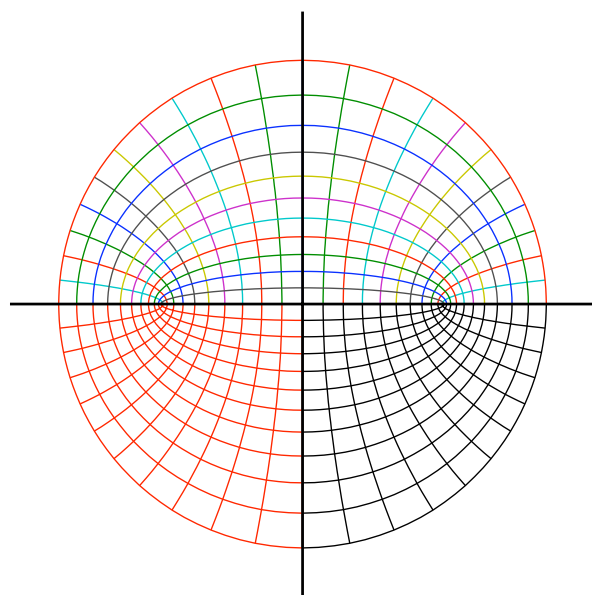


Image of  $J_F$ - or sn-function

The three functions  $J_D, J_E, J_F$  were developed in work on

minimal surfaces. In this context they have two advantages over Jacobi's sn,cn,dn:

a)  $J_D, J_E, J_F$  are defined on the same torus while sn,cn,dn are defined on three different tori, which are closely related, namely doubly covered by a common rectangular torus. On this larger rectangular torus Jacobi's functions are of degree 4.

b) At points  $z_1, z_2$  of the torus which are related by a symmetry of the four branch points of  $J_D, J_E$  or  $J_F$ , the **values**  $J(z_1), J(z_2)$  are related by **isometries** of the Riemann sphere, while for sn, cn, dn the relations between the values are by more general Möbius transformations. In applications to minimal surfaces such isometric relations translate into symmetries of the minimal surface, while Möbius relations do not.

Example: On each rectangular torus we have Riemann's embedded minimal surface and its conjugate; the Gauss map of these surfaces is the geometrically normalized Weierstrass  $\wp$ -function (denoted  $\wp_g$ ), not the original  $\wp$ -function. We have  $\wp_g = J_E \cdot J_F$ . If  $\sigma$  is a  $180^\circ$  rotation around a midpoint between the double zero and double pole of  $\wp_g$ , then  $\wp_g(\sigma(z)) = -1/\wp_g(z)$ .

Jacobi's sn-function and our  $J_F$ -function (on rectangular tori) are very closely related:

The branch values of sn are  $\{\pm 1, \pm k\}$ , modul  $m = k^2$ .

The branch values of  $J_F$  are  $\{\pm F, \pm F^{-1}\}$ ,  $F := \sqrt{k}$ .

The fundamental domain of sn is such that  $\text{sn}'(0) = 1$ .

The fundamental domain of  $J_F$  is such that  $J_F'(0) = \frac{2}{F+1/F}$ .

The function  $\text{dn}$  is also defined on a rectangular torus and has real branch values  $\{\pm 1, \pm\sqrt{1-k^2}\}$ .

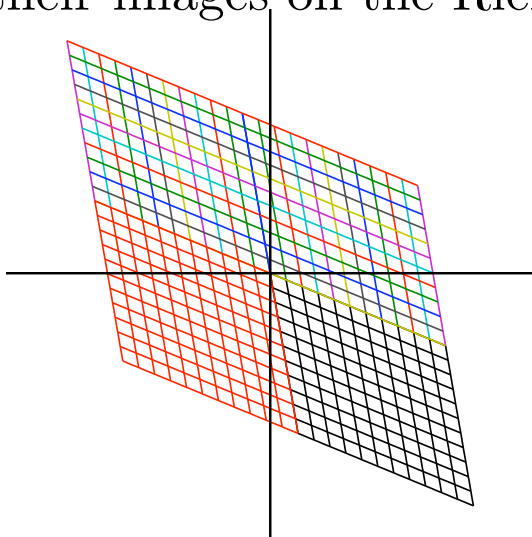
The function  $\text{cn}$  is not defined on a rectangular torus.

$\text{cn}(0), \text{dn}(0) \neq 0, \text{cn}'(0) = 0, \text{dn}'(0) = 0$ .

On non-rectangular tori we cannot define Jacobi type elliptic functions by the Riemann mapping theorem.

In [Symmetries of Elliptic Functions](#) we construct them with a more abstract tool: One can rotate any parallelogram torus by  $180^\circ$  around any of its points. This symmetry has four fixed points which are the vertices of a parallelogram with half the edgelength as the fundamental domain of the torus.

*The quotient by such a symmetry is a conformal sphere!* The uniformization theorem of complex analysis states that every conformal sphere is biholomorphic to the Riemann sphere. Therefore we can make the quotient map into a function by specifying three points on the torus and call their images on the Riemann sphere  $0, 1, \infty$ . Example:



Torus  $\frac{1}{4}$ -fundamental domain

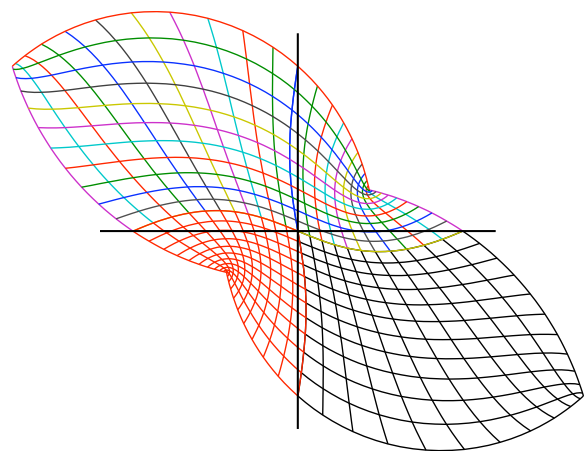


Image of  $J_D$ -function

180° rotation of the torus around the edge midpoints of the quarter domain and the corresponding 180° Möbius rotations extend the shown portion to a two-to-one conformal map from the torus to the sphere.

Our computation of these images uses the ODE. We scaled the function so that its branch values are  $\{\pm B, \pm B^{-1}\}$ . Our three Jacobi type functions  $J_D, J_E, J_F$  satisfy the ODE:

$$(J')^2 = J'(0)^2 \cdot (J^4 - (B^2 + B^{-2}) \cdot J^2 + 1).$$

The two functions on both sides of the equality sign agree because they have the same zeros and poles, hence are proportional, and  $J'(0)^2$  is the correct proportionality factor. Differentiation of this ODE and cancellation of  $2J'$  give the more harmless 2nd order nonlinear ODE (which is needed because Runge-Kutta cannot integrate the 1st order ODE in the vicinity of the zeros of the right side, called the branch values of  $J$ ):

$$J'' = J'(0)^2 \cdot (2J^2 - (B^2 + B^{-2})) \cdot J.$$

These equations can be used for  $J_D, J_E, J_F$ . To be on the same torus one has to transform the branch values as:

$$E = \frac{D-1}{D+1}, \quad F = \mathbf{i} \cdot \frac{D-\mathbf{i}}{D+\mathbf{i}}, \quad F = -\frac{E-\mathbf{i}}{E+\mathbf{i}},$$

and to use the same scale for the fundamental domain:

$$J'_D(0) = 1, \quad J'_E(0) = \frac{D-1/D}{2\mathbf{i}}, \quad J'_F(0) = \frac{D+1/D}{2}.$$

In 3D-XplorMath the **morphing parameter** for Jacobi's sn is the modul  $m$  and for  $J_D, J_E, J_F$  it is the branch value  $D$  of  $J_D$  in the 1st quadrant. Note that  $|D| = 1$  for rectangular tori and  $\operatorname{Re}(D) = \operatorname{Im}(D) > 0$  for rhombic tori.

Users cannot change the size of the domain of elliptic functions, it is always one half of the torus, chosen so that the values cover the Riemann Sphere once. In the domain we use a grid made up of eight copies of one sixteenth of the torus. The number of grid lines is the same in both directions so that the grid meshes are proportional to the fundamental domain of the torus. The default picture is, as always for our conformal maps, the image grid and the grid meshes show approximately the conformal type of the torus.

If one selects in the Action Menu **Show Image on Riemann Sphere** one can see the symmetries of these elliptic functions more clearly.

The entry **Show Inverse Function** in the Action Menu offers a second visualization. It assumes that standard polar coordinates on the Riemann Sphere are well known. The preimage of this polar grid is shown. Note that the preimages of all latitudes – except the equator – are pairs of congruent smooth closed curves. The preimage of the equator consists of four squares. The preimages of the northern and southern hemisphere are therefore easily recognized parts of the torus. – This visualization is completed only for rectangular tori.

H.K.

Conformal TOC

## Symmetries Of Elliptic Functions \*

[The approach below to elliptic functions follows that given in section 3 of "The Genus One Helicoid and the Minimal Surfaces that led to its Discovery", by David Hoffman, Hermann Karcher, and Fusheng Wei, published in Global Analysis and Modern Mathematics, Publish or Perish Press, 1993. For convenience, the full text of section 3 (without diagrams) has been made an appendix to the chapter on the Conformal Map Category in the documentation of 3D-XplorMath.]

An elliptic function is a doubly periodic meromorphic function,  $F(z)$ , on the complex plane  $\mathbb{C}$ . The subgroup  $\mathbb{L}$  of  $\mathbb{C}$  consisting of the periods of  $F$  (the period lattice) is isomorphic to the direct sum of two copies of  $\mathbb{Z}$ , so that the quotient,  $T = \mathbb{C}/\mathbb{L}$ , is a torus with a conformal structure, i.e., a Riemann surface of genus one. Since  $F$  is well-defined on  $\mathbb{C}/\mathbb{L}$ , we may equally well consider it as a meromorphic function on the Riemann surface  $T$ .

It is well-known that the conformal equivalence class of such a complex torus can be described by a single complex number. If we choose two generators for  $\mathbb{L}$  then, without changing the conformal class of  $\mathbb{C}/\mathbb{L}$ , we can rotate and

---

\* This file is from the 3D-XplorMath project. Please see:

scale the lattice so that one generator is the complex number 1, and the other,  $\tau$ , then determines the conformal class of  $T$ . Moreover,  $\tau_1$  and  $\tau_2$  determine the same conformal class if and only if they are conjugate under  $SL(2, Z)$ .

The simplest elliptic functions are those defining a degree two map of  $T$  to the Riemann sphere. We will be concerned with four such functions, that we call JD, JE, JF, and WP. The first three are closely related to the classical Jacobi elliptic functions, but have normalizations that are better adapted to certain geometric purposes, and similarly WP is a version of the Weierstrass  $\wp$ -function, with a geometric normalization. Any of these four functions can be considered as the projection of a branched covering over the Riemann sphere with total space  $T$ , and as such it has four branch values, i.e., points of the Riemann sphere where the ramification index is two. For JD there is a complex number  $D$  such that these four branch values are  $\{D, -D, 1/D, -1/D\}$ . Similarly for JE and JF there are complex numbers  $E$  and  $F$  so that the branch values are  $\{E, -E, 1/E, -1/E\}$  and  $\{F, -F, 1/F, -1/F\}$  respectively, while for WP there is a complex number  $P$  such that the branch values are  $\{P, -1/P, 0, \infty\}$ . The cross-ratio,  $\lambda$ , of these branch values (in proper order) determines  $\tau$  and likewise is determined by  $\tau$ .

The branch values  $E$ ,  $F$ , and  $P$  of JE, JF, and WP can be easily computed from the branch value  $D$  of JD (and hence

from  $dd$ ) using the following formulas:

$$E = (D - 1)/(D + 1), \quad F = -i(D - i)/(D + i),$$
$$P = i(D^2 + 1)/(D^2 - 1),$$

and we will use  $D$  as our preferred parameter for describing the conformal class of  $T$ . In 3D-XplorMath,  $D$  is related to the parameter  $dd$  (of the Set Parameter... dialog) by  $D = \exp(dd)$ , i.e., if  $dd = a + ib$ , then  $D = \exp(a) \exp(ib)$ . This is convenient, since if  $D$  lies on the unit circle (i.e., if  $dd$  is imaginary) then the torus is rectilinear, while if  $D$  has equal real and imaginary parts (i.e., if  $b = \pi/4$ ) then the torus is rhombic. (The square torus being both rectilinear and rhombic, corresponds to  $dd = i \cdot \pi/4$ ).

To specify an elliptic function in 3D-XplorMath, choose one of JD, JE, JF, or WP from the Conformal Map menu, and specify  $dd$  in the Set Parameter... dialog. (Choosing Elliptic Function from the Conformal map menu will give the default choices of JD on square torus.)

When elliptic functions were first constructed by Jacobi and by Weierstrass these authors assumed that the lattice of the torus was given. On the other hand, in Algebraic Geometry, tori appeared as elliptic curves. In this representation the branch values of functions on the torus are given with the equation, while an integration of a holomorphic form (unique up to a multiplicative constant) is required to find the lattice. Therefore the relation between the period quotient  $\tau$  (or rather its  $SL(2, Z)$ -orbit) and the

cross ratio  $\lambda$  of the four branch values has been well-studied. More recently, in Minimal Surface Theory, it was also more convenient to assume that the branch values of a degree two elliptic function were given and that the periods had to be computed. Moreover, symmetries became more important than in the earlier studies.

Note that the four branch points of a degree two elliptic function (also called "two-division points", or *Zweitteilungspunkte*) form a half-period lattice. There are three involutions of the torus which permute these branch points; each of these involutions has again four fixed-points and these are all midpoints between the four branch points. Since each of the involutions permutes the branch points, it transforms the elliptic function by a Moebius transformation. In Minimal Surface Theory, period conditions could be solved without computations if those Moebius transformations were not arbitrary, but rather were isometric rotations of the Riemann sphere—see in the Surface Category the minimal surfaces by Riemann and those named *Jd* and *Je*. This suggested the following construction: As degree two MAPS from a torus ( $T = \mathbb{C}/\mathbb{L}$ ) to a sphere, we have the natural quotient maps  $T/-id$ ; these maps have four branch points, since the 180 degree rotations have four fixed points. To get well defined FUNCTIONS we have to choose three points and send them to  $\{0, 1, \infty\}$ . We choose these points from the midpoints between the branch points, and the different choices lead to different functions. The symmetries also determine the points that

are sent to  $\{-1, +i, -i\}$ . In this way we get the most symmetric elliptic functions, and they are denoted JD, JE, JF. The program allows one to compare them with Jacobi's elliptic functions. The function  $WP = JE \cdot JF$  has a double zero, a double pole and the values  $\{+i, -i\}$  on certain midpoints (diagonal ones in the case of rectangular tori). Up to an additive and a multiplicative constant it agrees with the Weierstrass  $\wp$ -function, but in our normalization it is the Gauss map of Riemann's minimal surface on each rectangular torus.

We compute the J-functions as follows. If one branch value is called  $+B$ , then the others are  $\{-B, +1/B, -1/B\}$ . Therefore the function satisfies the *differential equations*

$$(J')^2 = (J'(0))^2(J^4 + 1 - (B^2 + 1/B^2)J^2) = F(J),$$

$$J'' = (J'(0))^2(2J^3 - (B^2 + 1/B^2)J = F'(J)/2).$$

*Numerically* we solve this with a fourth order scheme that has the analytic continuation of the square root  $J' = \sqrt{J'^2}$  built into it:

Let  $J(0), J'(0)$  be given. Compute  $J''(0) := F'(J(0))/2$  and, for small  $z$ ,

$$J_m := J(0) + J'(0) \cdot z/2 + J''(0) \cdot z^2/8, J''_m := F'(J_m)/2,$$

$$J(z) := J(0) + J'(0) \cdot z + (J''(0) + 2 \cdot J''_m) \cdot z^2/6.$$

Finally let  $J'(z)$  be that square root of  $F(J(z))$  that is closer to  $J'(0) + J''_m \cdot z$  (analytic continuation!). Repeat.

# Fractal Curves And Dynamical Systems

[Go To Page 1](#)

**Fractal Curves**      (Click the Names)

- 1.) [Dragon Curve](#)
- 2.) [Koch Snowflake](#)
- 3.) [Hilbert Square Filling Curve](#)
- 4.) [Sierpinski Curve](#)
- 5.) [Hilbert Cube Filling Curve](#)

**Dynamical Systems**

- 6.) [Henon Attractor](#)
- 7.) [Feigenbaum Tree](#)
- 8.) [Userdefined Feigenbaum Iteration](#)
- 9.) [Userdefined x y Iteration](#)
- 10.) [Mandelbrot Set And Its Julia Sets](#)

## About The Dragon Curve \*

see also: Koch Snowflake, Hilbert SquareFillCurve

To speed up demos, press DELETE

The Dragon is constructed as a limit of polygonal approximations  $D_n$ . These are emphasized in the 3DXM default demo and can be described as follows:

- 1)  $D_1$  is just a horizontal line segment.
- 2)  $D_{n+1}$  is obtained from  $D_n$  as follows:
  - a) Translate  $D_n$ , moving its end point to the origin.
  - b) Multiply the translated copy by  $\sqrt{1/2}$ .
  - c) Rotate the result of b) by  $-45^\circ$  degrees and call the result  $C_n$ .
  - d) Rotate  $C_n$  by  $-90^\circ$  degrees and join this rotated copy to the end of  $C_n$  to get  $D_{n+1}$ .

The fact that the **limit points** of a sequence of longer and longer polygons can form a two-dimensional set is not surprising. What makes the Dragon spectacular is that it is a **continuous curve** whose image has positive area—properties that it shares with Hilbert's square filling curve.

There is a second construction of the Dragon that makes it easier to view the limit as a continuous curve and is also similar to the constructions of the following curves. Select in the Action Menu: **Show With Previous Iteration**.

---

\* This file is from the 3D-XplorMath project. Please see:

This demo shows a local construction of the Dragon: We obtain the next iteration  $D_{n+1}$  if we modify each segment of  $D_n$  by replacing it by an isoscele  $90^\circ$  triangle, alternatingly one to the left of the segment, and the next to the right of the next segment. This description has two advantages:

(i) Every vertex of  $D_n$  is already a point on the limit curve. Therefore one gets a dense set of points,  $c(j/2^n)$ , on the limit curve  $c$ .

(ii) One can modify the construction by decreasing the height of the modifying triangles from  $aa = 0.5$  to  $aa = 0$ . The polygonal curves are, for  $aa < 0.5$ , polygons without self-intersections. This makes it easier to imagine the limit as a curve. In fact, the *Default Morph* shows a deformation from a segment through continuous curves to the Dragon—more precisely, it shows the results of the ( $ee = 11$ )th iterations towards those continuous limit curves.

The Dragon is a fractal tile for the plane., see several versions at [http://en.wikipedia.org/wiki/Dragon\\_curve](http://en.wikipedia.org/wiki/Dragon_curve). For two beautiful possibilities select from the Action Menu **Tile Plane With Dragon Pairs**, or: **Tile Plane With Dragon Quartetts**.

Finally, one can choose in the Action Menu to map any selected Fractal curve by either the complex map  $z \rightarrow z^2$  or by the complex exponential. The program waits for a mouse click and then chooses the mouse point as origin.

## About the Koch Snowflake (or Island) \*

The Koch Snowflake Curve (aka the Koch Island) is a fractal planar curve of infinite length and dimension approximately 1.262. It is defined as the limit of a sequence of polygonal curves defined recursively as follows:

- 1) The first polygon is an equilateral triangle.
- 2) The  $(n+1)$ -st polygon is created from the  $n$ -th polygon by applying the following rule to each edge: construct an equilateral triangle with base the middle third of the edge and pointing towards the outside of the polygon, then remove the base of this new triangle.

Note that at each step the number of segments increases by a factor 4 with the new segments being one third the length of the old ones. Since all end points of segments are already points on the limit curve we see that no part of the limit curve has finite length.

Actually this is true for a 1-parameter family of similar constructions: Vary the parameter  $aa$  (**Set Parameters** in the Settings Menu) in the interval  $[0.25, 0.5]$  and watch how the iterations evolve or choose **Morph** in the Animation Menu and observe the deformation of the limit curves.

**Hausdorff Dimension:** Consider the union of those disks which have a segment of one polygonal approximation as a diameter, then this union covers all the further approximations. From one step to the next the diameter of the

---

\* This file is from the 3D-XplorMath project. Please see:

disks shrinks to one third while the number of disks is multiplied by 4—so that the area of these covering disk unions converges to zero. The fractal Hausdorff d-measure is defined as the infimum (as the diameter goes to zero) of the quantity  $(\text{diameter})^d \times (\text{number-of-disks})$ , and the fractal Hausdorff dimension is the infimum of those  $d$  for which the d-measure is 0. This shows that the Hausdorff dimension of the Koch curve is less than or equal to  $\log(4)/\log(3)$ , and since the union of the disks of every second segment does not cover the limit curve one can conclude that the Hausdorff dimension is precisely  $\log(4)/\log(3)$ .

The artist Escher has made rather complicated fundamental domains for tilings of the plane by modifying the boundary between neighboring tiles. This idea can be used to illustrate the flexibility of fractal constructions: Select from the Action Menu of the Koch Snowflake **Choose Escher Version** and observe:

*The new polygonal curves remain boundaries of tiles of the plane under the iteration steps that make them more and more complicated.*

Finally, one can choose in the Action Menu to map any selected Fractal curve by either the complex map  $z \rightarrow z^2$  or by the complex exponential. The program waits for a mouse click and then chooses the mouse point as origin.

Note that one gets the graph of a continuous function if one plots the x-coordinate of a continuous curve against the curve parameter. This can be viewed with the last Action Menu entry. – H.K.

## About Hilbert's Square Filling Curve \*

See also: Koch Snowflake, Dragon Curve  
Speed up demos by pressing DELETE

In 1890—the year the German Mathematical Society was founded, David Hilbert published a construction of a continuous curve whose image completely fills a square. At the time, this was a contribution to the understanding of continuity, a notion that had become important for Analysis in the second half of the 19th century. Today, Hilbert's curve has become well-known for a very different reason—every computer science student learns about it because the algorithm has proved useful in image compression. In this application one has to enumerate a first square, its four half size subsquares, their sixteen quarter-size subsquares and so on, in such a way that squares whose numbers are close are also close to each other geometrically. In other words, the continuity of this space filling curve is now important, in contrast to the fact that the curve was considered a pathological example of continuity for many years after Hilbert's discovery.

It was known in 1890 that such a curve, i.e., a continuous map  $c$  of  $[0, 1]$  onto  $[0, 1] \times [0, 1]$ , could not be one-to-one, i.e., *Certain pairs of points  $t_1, t_2$  of the interval  $[0, 1]$  must have the same image  $c(t_1) = c(t_2) \in [0, 1] \times [0, 1]$ .* This

---

\* This file is from the 3D-XplorMath project. Please see:

led Hilbert to give a special twist to his construction: He gave a sequence of polygon approximations of the strange limit curve that, surprisingly, were all one-to-one! In retrospect it seems almost as if Hilbert foresaw what would be needed a century later in image compression; when people say that they are using Hilbert's square-filling curve, they mean more precisely that they are using Hilbert's approximations to that curve!

The basis of Hilbert's construction is a single step that is repeated over and over again. We first explain a simplified version, although this does not exactly give Hilbert's one-to-one approximations that made the construction so famous. Assume that we already have a curve inside the square and joining the left bottom corner to the right bottom corner. 3DXM offers four different initial such curves, leading to quite different pictures. The basic construction step is to scale the square and its curve by  $\frac{1}{2}$  and put **four** copies of this smaller square side by side in the original square, in such a way that these four smaller copies of the curve fit together to form a new curve from the left bottom corner to the right bottom corner of the original square. But instead of reading more words, we suggest that you view the default approximations of the Hilbert curve in 3DXM. We use a rainbow coloration to emphasize the continuous parametrization, and we repeat the colors **four** times to emphasize that four copies of the previous approximation make up the new one.

The two end points of the curve (to which this basic iter-

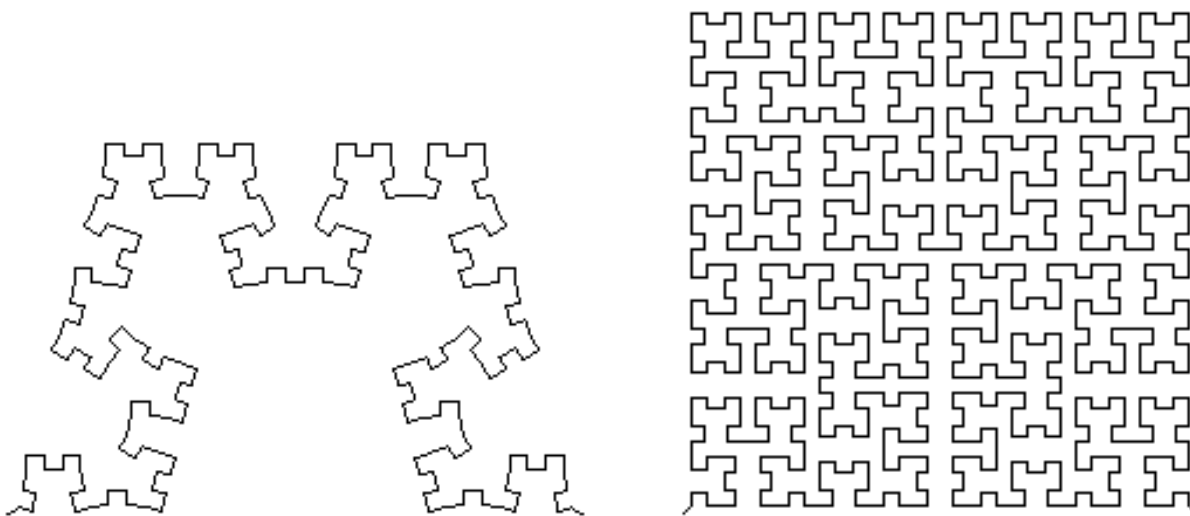
ation step is applied) play a special role, on the one hand they lead at each iteration step to more points that are already points on the limit curve, on the other hand exactly these easy points lead to double points on the approximations! Hilbert therefore removed small portions of the curve near its two end points before he applied the above iteration step. One can see how these Hilbert approximations manage to stay one-to-one and how they wander through all the little squares of the current subdivision of the original square—and these are just the properties used in image compression.

In 3DXM one can choose with the parameter  $cc$  between several initial curves. An even number and the following odd number choose the same curve, but for even  $cc$  the Hilbert iteration is done *without* the endpoints and for odd  $cc$  *including* the endpoints. In the Action Menu one can switch between Hilbert's approximation ( $cc=0$ ) and one that emphasizes the iteration of the endpoints ( $cc=5$ ).

Finally we add to the above descriptive part some more technical explanations, namely how to understand the limit as a continuous curve. Select the Action Menu entry “Emphasize Limit Points”. The first shown step (for our default value  $cc = 5$ ) is a curve that is mostly a straight segment, but has also two little wiggles, that emphasize the initial point  $c(0)$  and the end point  $c(1)$ . The second step is a curve with four straight segments that join five wiggles, the points  $c(j/4)$ ,  $j := 0, \dots, 4$ . These points are really points on the limit curve because they remain fixed

under all further applications of Hilbert's basic construction step. In the third step we get 17 wiggles, the points  $c(j/16)$ ,  $j := 0, \dots, 16$  of the limit curve, and so on. The 3DXM demo shows six such iterations. One can deduce from this the continuity of the limit curve if one proves for these approximations:

$$|t_2 - t_1| \leq \frac{1}{4^n} \Rightarrow |c(t_2) - c(t_1)| \leq \frac{1}{2^n}.$$



Early iterations for  $bb = 0.4$  (left), for  $bb = 0.5$  (right, the Hilbert case).

H.K.

Fractal TOC

## The Sierpinski Triangle, The Sierpinski Curve \*

The Sierpinski Triangle is a well known example of a “large” compact *set* without interior points. It is defined by the following construction:

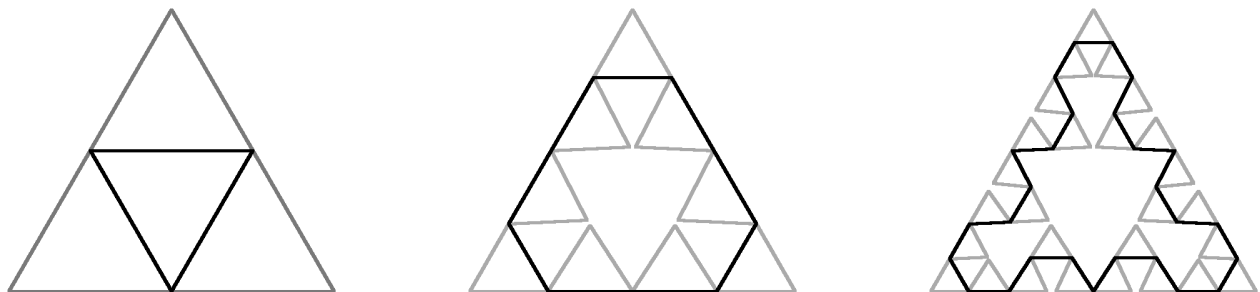
Start with an equilateral triangle and subdivide it into four congruent equilateral triangles. Remove the middle one. Subdivide the remaining triangles again and remove in each the middle one. Repeat this procedure. Each step reduces the area by a factor  $3/4$ . – But more is true:

---

Sierpinski’s Triangle is the image of a continuous curve.

---

As in the other fractal curves in 3DXM we have to define an iteratively defined and uniformly convergent sequence of polygonal curves. As in the case of the Hilbert square filling curve there is an easier construction by *non-injective* curves which, however, can be modified to give better looking *injective* approximations. In the following illustration we have chosen the 3DXM parameter  $bb = 0.49$ , because for  $bb < 0.5$  the easier construction also gives injective approximations. ( $bb = 0.5$  gives Sierpinski’s curve.)



---

\* This file is from the 3D-XplorMath project. Please see:

The starting polygonal curve has the vertices and the edge midpoints of an equilateral triangle as its vertices. The initial point is the midpoint of the bottom edge. The curve that joins every second vertex of the starting curve is the triangle in the middle. We view the starting curve as passing through two edges of each of the three outer triangles. We only have to describe for one of these triangles how the next iteration is obtained. We will obtain curves that always run through two edges of each triangle, and the basic iteration can always be applied. If we join every second vertex of the resulting curves then we obtain the injective approximations of the Sierpinski Curve.

The basic iteration step, for one triangle:

First add the two midpoints of the traversed edges of the triangle. Two more points are added, one over the first and one over the last of the four subsegments. The points lie in the inside of the traversed triangle and they are the tips of isosceles triangles whose base is the first, resp. the last, of the four subsegments. In the case of the Sierpinski Curve these isosceles triangles are in fact equilateral. If the parameter  $bb$  is smaller than 0.5 then the height of the isosceles triangle is by the factor  $bb/0.5$  smaller than the height of the equilateral triangle – thus avoiding the creation of double points of the approximation.

The iterated polygonal curve joins the initial point of the first edge to the first tip, continues to the first edge-midpoint, passes through the vertex of the original triangle to the

second edge-midpoint, continues through the second tip and ends at the final point of the last segment. The iterated polygonal curve traverses three triangles, two edges in each. Therefore the iteration step can be repeated.

The default **Morph** from the Animation Menu of 3DXM varies  $bb$  from  $1/3$  to  $1/2$  thus joining the first triangle contour by a family of continuous (and injective) curves to the Sierpinski Curve.

Finally, one can choose in the Action Menu to map any selected Fractal curve by either the complex map  $z \rightarrow z^2$  or by the complex exponential. The program waits for a mouse click and then chooses the mouse point as origin.

H.K.

Fractal TOC

## About Hilbert's Cube Filling Curve \*

See also: The more famous Hilbert SquareFillCurve.

Hilbert's cube filling curve is a continuous curve whose image fills a cube. It is a straight forward generalization of the continuous square filling curve. It is shown in anaglyph stereo via a sequence of polygonal approximations. Each approximation is a polygon that joins two neighboring vertices of the cube.

The iteration step goes as follows:

The cube with the given (initial or a later) approximation is scaled with the factor  $1/2$ . Eight of these smaller copies are put together so that they again make up the original cube, and this is done in such a way that the endpoint of the curve in the first cube and the initial point of the curve in the second cube fit together, and so on with all eight cubes. The result of one iteration therefore is a curve that is four times as long as the previous curve and that runs more densely through the cube. In 3DXM, if one rotates the cube with the mouse then the cube and its first subdividing eight cubes are shown together with one iteration of the initial curve.

To achieve a better feeling for the iteration step, one can

---

\* This file is from the 3D-XplorMath project. Please see:

set the parameter  $cc$  to integer values between 0 and 5. This will select different initial curves. An even value of  $cc$  and the following odd value give the same initial curve, but for even  $cc$  the Hilbert iteration is done *without* the endpoints, while for odd  $cc$  the endpoints are *included* in the iteration. (Using the Action Menu, one can switch between Hilbert's default ( $cc=0$ ) and a case that emphasizes the iteration of the endpoints,  $cc=5$ .)

We have the same situation as in the two-dimensional case: The endpoints and their iterates are points that already lie on the limit curve because they are not changed under further iterations. One can say that the endpoints and their iterates are related to the limit curve in a very simple way. On the other hand, the approximating polygons develop double points at these iterates and the result is that the approximations look much more confusing if the endpoints and their iterates are included in the iteration. This is why we offer the choice between iterating with and without the endpoints.

H.K.

Fractal TOC

## The Quadratic Henon Map and its Attractor \*

The Henon Map visualization gives the orbit under iteration of the map  $(x, y) \rightarrow (y + 1 - aa x^2, bb x)$ .

The default values are  $aa = 1.4$  and  $bb = 0.3$ . The initial point is  $(x, y) = (cc, dd)$ , defaults  $cc = 1.0, dd = 1.0$ . The number of iterations plotted is  $ee$ , but the first  $ff$  iterates are omitted. The defaults are  $ee = 3000$  and  $ff = 20$ . The map has two fixed points, they are obtained by solving a quadratic equation and they are marked by small circles. Also from a quadratic equation one obtains an orbit of period 2, marked by small spades. Numerically we found no indication of an orbit of period 3. We found one orbit of period 4 numerically and marked it by small squares. — The derivative of the Henon map has determinant  $-bb$ , i.e. the Henon map reduces area with a uniform rate. One can view the eigen directions of the derivative via an Action Menu entry. — The inverse of the Henon map is the quadratic map  $(X, Y) \rightarrow (\frac{1}{bb}Y, X - 1 + \frac{aa}{bb^2}Y^2)$ .

In 3DXM, to move the finished image, drag the image with the mouse. To zoom in our out, drag vertically with the Shift key pressed. (If you zoom in, you might want to increase parameter  $ee$  using Settings > Set Parameters.) To zoom into a particular region, hold down Command and then drag a rectangle in the window, then the program will

---

\* This file is from the 3D-XplorMath project. Please see:

zoom into that region of the Henon attractor, allowing you to see it in greater detail.

Are there more periodic points on the Henon attractor? An Action Menu entry allows to search for orbits of period  $ii$ . Since numerical inaccuracies, e.g. of the period 2 orbit, build up after about 60 iterations to visibly leave the orbit, we restricted to:  $ii < 80$ . Each numerically found orbit is iterated until the user stops the iteration. If this stop is by mouse button, the orbit is saved and the last orbit of these is added to the visually indicated periodic points.

The Henon map depends strongly on the parameters. For example, we can obtain an attracting orbit of period 6 with  $aa = 1.45$ . To see it, change  $aa$ , stop the iteration and click in the Action Menu: **Do 500 Iterations**.

(Morphing  $aa$  and  $bb$  works, but there is no default morph, so first select **Set Morphing...** from the Settings menu to set up the morph—be sure to click the **Init To Current Values** button, then change  $aa0$   $aa1$ ,  $bb0$  and  $bb1$ .)

Finally, we added to the Action Menu: **Use Hit Count Coloration**. This changes the representation by adding vertical bars over the points of the Henon attractor. The length of these bars shows how often that - pixelized - point of the attractor is visited during the iteration. The graphic therefore illustrates the iteration-invariant measure on the attractor. For a 1-dimensional such hit count see the Feigenbaum Tree.

## About The Feigenbaum Tree \*

See also: Julia Set of  $z \rightarrow (z^2 - c)$

The Feigenbaum Tree is one of the earliest examples of parameter dependent behavior of a dynamical system. The dynamical system in question is called the *Logistic Map*:

$$f_{\mu}(y) := 4\mu \cdot y(1 - y), \quad y \in [0, 1], \quad \mu \in [1/4, 1].$$

Since both the parameter space,  $[1/4, 1]$ , and the dynamical space,  $[0, 1]$ , are 1-dimensional, one can illustrate in a  $(\mu, y)$ -plane how the dynamical behavior changes as the parameter  $\mu$  varies. The usual experiment (and the one used in 3DXM) goes as follows: Starting with a set of initial values  $\{y_k; y_k \in [0, 1], k = 1, \dots, K\}$  (and with as many parameter values  $\mu$  as one wants to handle) one computes many iterations  $f_{\mu}^{\circ n}(y_k), n = 1, \dots, N$  with  $N$  large.

If one plots only the iterations with say  $n \geq 1000$ , then one observes in the  $(\mu, y)$ -plane the *Feigenbaum Tree*: for small  $\mu$  the iterated points  $f_{\mu}^{\circ n}(y_k)$  converge to a stable fixed point of the map  $f_{\mu}, y_f = f_{\mu}(y_f), y_f := 1 - 1/4\mu$ . Observe that the derivative  $f'$  at the fixed point is  $2 - 4\mu \leq 0$ . At  $\mu = 3/4$  the derivative at the fixed point is  $-1$ , so that the fixed point stops being attractive. It turns out that

---

\* This file is from the 3D-XplorMath project. Please see:

for larger  $\mu$  the orbit of period 2 is attractive for a while – until  $\mu$  reaches another bifurcation point after which an orbit of period 4 becomes attractive.

This period doubling “cascade” continues up to a certain  $\mu$ -value, past which there is for a while no longer an attractive orbit. All this is clearly visible in the 3DXM demo. One should use the Action Menu entry: **Iterate Mouse Point Forward** to watch how arbitrary initial points are iterated and how these iterations converge to the attracting orbits of period  $2^d$  in the left, period doubling, part of the Feigenbaum Tree. —*Speed-Up Note:* If one presses DELETE either during the default iterations or during the iteration of a point chosen by mouse, then all delays are skipped and the result of the iteration is reached quickly.

After the period doubling in the left part has been observed one wants to look at the right part of the Feigenbaum Tree more closely. The  $\mu$ -interval which the illustration uses is the interval  $[bb, cc]$ . It can be changed in the Parameter entry of the Settings Menu. Since the attractive orbit of period 2 appears after  $\mu = 0.75$ , one loses only the simple attractors if one increases  $bb$  from 0.25 to 0.75, and one gains that the remaining part of the Tree is stretched by a factor of 3. In the same way one can magnify any part of the parameter space. Of course the dynamical space is always fully shown—unless one decides to use SHIFT+MOUSE to scale the image to see part of the dynamical space magnified. In this case translation using CONTROL+MOUSE-DRAG may be useful.

The most obvious feature in the right part of the Feigenbaum Tree are gaps, three fairly large ones and any number of thinner ones. The three large ones belong to parameter intervals where the map  $f_\mu$  has attractive orbits of period 6, period 5, resp. period 3. If one magnifies a gap enough, one can experimentally check that the gaps belong to attractive orbits (use in the Action Menu **Iterate Mouse Point Forward**). One also observes that at the right end of these intervals the periods double again, and again. In other words, the Feigenbaum Tree illuminates, almost at the first glimpse, many properties of this 1-parameter family of iterated maps.

The Action Menu has been expanded by four entries **Iteration Invariant Density** (either with mouse choice of  $aa = \mu$  or previous  $aa$ ) and **Density Function** (again with mouse choice of  $aa$  or previous value). Before one chooses any of these one should look at **Iterate Mouse Point Forward**, where one sees how the iterated point, given by the vertical coordinate  $y$ , jumps around with fixed  $\mu$ . The **Iteration Invariant Density** expands this: 1000 different  $y$ -values are chosen and represented in the left-most column on the screen. These points are iterated and shown in the second column, iterated again and shown in the third column, and so on, 400 times. Except for the first few columns one clearly sees a density pattern develop: all the vertical columns look essentially alike. This can be studied further with the entry **Density Function**: Here we count how often each pixel-sized interval of the dynamical (=ver-

tical) interval is visited during the iterations and we plot the counting result (normalized to fit on the screen). We observe a function that describes the probability density with which each pixel interval is visited. – These demos explain why the curves that represent attractors do extend into the chaotic regions.

Finally we remark that the Feigenbaum Tree is related to the real part of the Mandelbrot set because the Mandelbrot set also parametrizes quadratic maps  $z \rightarrow f_c(z) := (z^2 - c)$  according to their dynamical properties. If  $c$  is chosen from the big bottom apple then  $f_c$  has an attractive fixed point. As one passes on the real axis from the apple to the disk above it, the fixed point changes from attractive through indifferent to unstable and the orbit of period 2 becomes attractive. As one moves (always along the real axis) towards the top of the Mandelbrot set one continues to meet exactly the same kind of dynamical behavior as one sees in the Feigenbaum Tree. For more details see the documentation for *Julia Set of  $z \rightarrow (z^2 - c)$* .

H.K.

Fractal TOC

## User Defined Feigenbaum Iteration \*

Please see first: About The Feigenbaum Tree

The question “*How can one find periodic attractors of, say, a family of Newton Iterations?*” led to the development of this exhibit. The user can input an iteration function that depends on one parameter  $aa$  (which is, as in the Feigenbaum case, represented horizontally). The dynamical space consists of some interval of arguments  $y$  of the function. We can view them as starting values of the iteration. The default iteration in 3DXM is the Newton iteration for the zeros of the polynomial  $y \rightarrow (y^2 - 3)^2 + 3aa$ .

The Feigenbaum picture is ideally suited to watch how the  $aa$ -family of iterations behaves: One quickly spots attractive fixed points or attractive orbits with small period; but one also observes the density curves in a seemingly chaotic region. If one expands the scale, i.e. stretches a very small  $aa$ -interval over the whole screen, then one sees easily whether there are in this interval periodic attractors, or whether still only chaos is visible (then choose a different  $aa$ -interval or expand the current interval further).

The remaining details are the same as for the classical Feigenbaum Tree and are explained in detail in the documentation for that exhibit.

H.K.

---

\* This file is from the 3D-XplorMath project. Please see:

# The Area Preserving Henon Twist Map \*

## User Defined Example

The User Defined entry is designed to study the behaviour of 2-dimensional maps under forward iteration near an isolated, neutral fixed point. (We want a fixed point inside the window since otherwise most of the iterated points will move out of sight.) Our example is Henon's quadratic, area preserving twist map  $F$ :

$$F(x, y) := \begin{pmatrix} \cos(aa) \cdot x - \sin(aa) \cdot (y - e^{bb} \cdot x|x|) \\ \sin(aa) \cdot x + \cos(aa) \cdot (y - e^{bb} \cdot x|x|) \end{pmatrix}.$$

Henon used  $x^2$  instead of  $x|x|$  for the perturbation term. See below.

The main parameter  $aa$  controls the derivative of  $F$  at the fixed point  $(0, 0)$ ;  $dF|_{(0,0)}$  is the rotation matrix with angle  $aa$ . The behaviour of the iterations changes strongly with  $aa$ . Try also  $-aa$ .  $F$  is area preserving since the Jacobian determinant  $\det(dF) = 1$  everywhere.

By default  $e^{bb} = 1$ . This parameter serves to choose the size of the neighborhood of the fixed point, because of the scaling property

$$F(\vec{x}; e^{bb}) = e^{-bb} \cdot F(e^{bb} \cdot \vec{x}; 1).$$

We use  $\exp(bb)$  instead of  $bb$ , because the scaling parameter is a multiplicative rather than an additive parameter.

---

\* This file is from the 3D-XplorMath project. Please see:

The iteration is applied to the segment  $[0, 1] \cdot (cc, dd)$ . The number of points on this segment is  $tResolution$ . The default number of iterations is  $ee = 2000$ . The next 2000 iterations are obtained from the Action Menu Entry: **Continue Curve Iteration**.

Since the graphic rendering is much slower than the the computation of iterations one can increase the parameter  $hh$  from its default value  $hh = 1$  and then only one out of  $hh$  iterations is shown on the screen. This is useful if one needs to see the result of a large number of iterations. (For example  $hh = 4 \cdot n$  in the case  $aa = \pi/2$ .)

The Action Menu Entry **Iterate Mouse Point Forward** allows to iterate a single point. During the selection the point coordinates appear on the screen. If DELETE is pressed during the iteration then the waiting time at each step is cancelled so that the point races through its orbit.

The Action Menu Entry **Choose Iteration Segment By Mouse** allows to Mouse-select initial and final point of a segment on which  $ff$  points will be distributed and iterated (by default  $ff = 16$ ). The parameter  $hh$  speeds up the iteration as above. After the first  $ee$  iterations an Action Menu Entry is activated and allows to iterate further.

As usual one can **translate** the image by dragging or one can **scale** it by depressing SHIFT and dragging vertically.

One can also **morph** the images. They change rather drasti-

cally with  $aa$ . As default morph  $bb$  is decreased so that the neighborhood of the fixed point gets expanded. One observes that most of the iterated points travel on *invariant curves* around the fixed point. Occasional periodic points clearly show up in the image. If  $aa$  is an irrational multiple of  $\pi$  then the visible periods do increase as the neighborhood of the fixed point expands with decreasing  $bb$ . (For the default morph the number  $ee$  of iterations is restricted to 500 to reduce waiting times.)

The Henon twist map can be written as a rotation plus a quadratic perturbation:

$$F(x, y) := \begin{pmatrix} \cos(aa) - \sin(aa) \\ \sin(aa) + \cos(aa) \end{pmatrix} \cdot \begin{pmatrix} x \\ y \end{pmatrix} + \text{perturb},$$

$$\text{perturb} := e^{bb} \cdot x|x| \cdot \begin{pmatrix} + \sin(aa) \\ - \cos(aa) \end{pmatrix}.$$

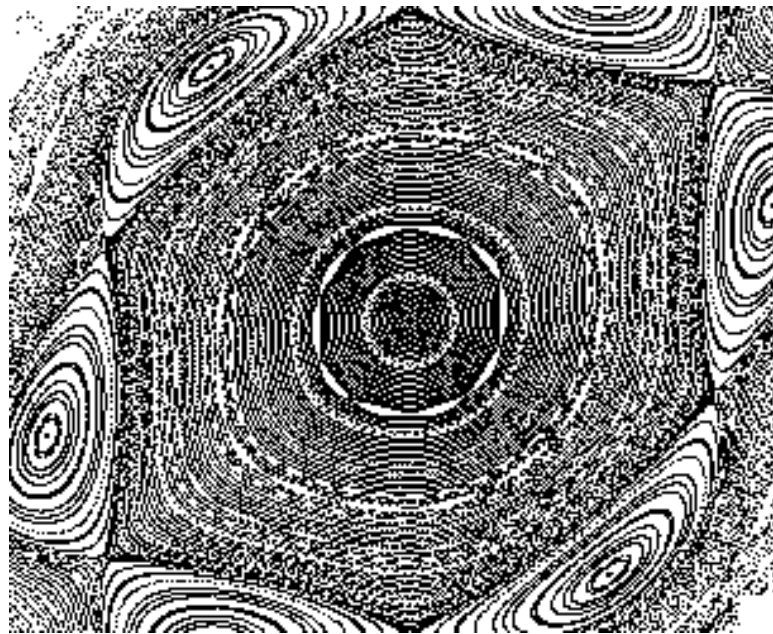
The scalar product between the perturbation and the tangent to the rotation circles is the

$$\text{Forward Perturbation} = -e^{bb}|x|^3 \cdot (\sin^2(aa) + \cos^2(aa)).$$

This explains why we changed the Henon map. Our negative forward perturbation means that the images under  $F$  stay behind the rotation image, and more so the larger  $|x|$ . This is the usual behavior of a monotone twist map. Henon's perturbation has the factor  $x^3$  instead of  $|x|^3$ , so

that the twist in the left half plane partially cancels the twist in the right half plane. In our definition do the elliptical islands around periodic points appear more easily, while with Henon's definition the behaviour near the fixed point, in the case when  $aa$  is a rational multiple of  $\pi$  (e.g.  $aa = \pi/2$ ), is much more complicated.

We recommend that users try out also Henon's definition and definitions of their own.



## The Mandelbrot Set And Its Julia Sets \*

If one wants to study iterations of functions or mappings,  $f^{\circ n} = f \circ \dots \circ f$ , as  $n$  becomes arbitrarily large then *Julia sets* are an important tool. They show up as the boundaries of those sets of points  $p$  whose iteration sequences  $f^{\circ n}(p)$  converge to a selected *fixed point*  $p_f = f(p_f)$ . One of the best studied cases is the study of iterations in the complex plane given by the family of quadratic maps

$$z \rightarrow f_c(z) := z^2 - c.$$

The *Mandelbrot set* will be defined as a set of parameter values  $c$ . It provides us with some classification of the different ‘dynamical’ behaviour of the functions  $f_c$  in the following sense: If one chooses a  $c$ -value from some specific part of the Mandelbrot set then one can predict rather well how the iteration sequences  $z_{n+1} := f_c(z_n)$  behave.

**1) Infinity is always an attractor.** Or, more precisely, for each parameter value  $c$  we can define a Radius  $R_c \geq 1$  such that for  $|z| > R_c$  the iteration sequences  $f^{\circ n}(z)$  converge to infinity. Proof: The triangle inequality shows that  $|f_c(z)| \geq |z|^2 - |c|$  and then  $|f_c(z)| > |z|$  is certainly true if  $|z|^2 - |c| > |z|$ . Therefore it is sufficient to

---

\* This file is from the 3D-XplorMath project. Please see:

define  $R_c := 1/2 + \sqrt{1/4 + |c|}$ , which is the positive solution of  $R^2 - R - |c| = 0$ .

This implies: if we start the iteration with  $z_1 > R_c$  then the absolute values  $|z_n|$  increase monotonically—and indeed faster and faster to infinity. Moreover, any starting value  $z_1$  whose iteration sequence converges to infinity will end up after *finitely many iterations* in this neighborhood of infinity,  $U_\infty := \{z \in \mathbb{C} \mid |z| > R_c\}$ . The set of all points whose iteration sequence converges to infinity is therefore an open set, called the attractor basin  $A_\infty(c)$  of infinity.

**2) Definition of the Julia set  $J_c$ .** On the other hand, the attractor basin of infinity is never all of  $\mathbb{C}$ , since  $f_c$  has fixed points  $z_f = 1/2 \pm \sqrt{1/4 + c}$  (and also points of period  $n$ , that satisfy a polynomial equation of degree  $2^n$ , namely  $f^{\circ n}(z) = z$ ).

**Definition.** The nonempty, compact boundary of the attractor basin of infinity is called the *Julia set of  $f_c$* ,

$$J_c := \partial A_\infty(c).$$

*Example.* If  $c = 0$  then the exterior of the unit circle is the attractor basin of infinity, its boundary, the unit circle, is the Julia set  $J_0$ . The open unit disk is the attractor basin of the fixed point 0 of  $f_c$ . The other fixed point 1 lies on the Julia set; 1 is an expanding fixed point since  $f'_c(1) = 2$ ; its iterated preimages  $-1, \pm i, \dots$  all lie on the Julia set.

Qualitatively this picture persists for parameter values  $c$  near 0 because the smaller fixed point remains attractive.

However, the Julia set immediately stops being a smooth curve—it becomes a continuous curve that oscillates so wildly that no segment of it has finite length. Its image is one of those sets called a *fractal* for which a fractional dimension between 1 and 2 can be defined. Our rainbow coloration is intended to show  $J_c$  as a continuously parametrized curve. We next take a more careful look at attractive fixed points.

### **3) $c$ -values for which one fixed point of $f_c$ is attractive.**

There is a simple criterion for this: if the derivative at the fixed point satisfies  $|f'_c(z_f)| = |2z_f| < 1$  then  $z_f$  is a linearly attractive fixed point; if  $|2z_f| > 1$  then  $z_f$  is an expanding fixed point; if the derivative has absolute value 1 then no general statement is true (but interesting phenomena occur for special values of the derivative).

Since the sum of the two fixed points is 1, the derivative  $f'_c$  can have absolute value  $< 1$  at most at one of them. Let  $w_c$  be that square root of  $1 + 4c$  having a positive real part. Then  $|1 - w_c|$  is the smaller of the absolute values (of the derivatives of  $f_c$  at the fixed points). The set of parameter values  $c$  with a (linearly) attractive fixed point of  $f_c$  is therefore the set  $\{c \mid |1 - w_c| < 1\}$ , or  $\{c = (w^2 - 1)/4 \mid |1 - w| < 1\}$ . In other words, the numbers  $1 + 4c$  are the squares of numbers  $w$  that lie in a disk of radius one with 0 on its boundary. The apple shaped boundary is therefore the square of a circle through 0. It is called a *cardioid*.

#### 4) The definition of the Mandelbrot set in the parameter plane.

The behavior of the iteration sequence  $z_{n+1} := f_c(z_n)$  in the  $z$ -plane depends strongly on the value of the parameter  $c$ . It turns out that for those  $c$  satisfying  $|c| > R_c$ , the set of points  $z$  whose iteration sequences do *not* converge to infinity has area = 0. Such points are too rare to be found by trial and error, but one can still compute many as iterated preimages of an unstable fixed point. It follows from  $|c| > R_c$  that only the points of the Julia set  $J_c$  do not converge to infinity. Moreover, the Julia set is no longer a curve, but is a totally disconnected set: no two points of the Julia set can be joined by a curve inside the Julia set. (In this case our coloration of  $J_c$  has no significance.)

The Mandelbrot set is defined by the opposite behaviour of the Julia sets:

Mandelbrot Set :  $\mathbf{M} := \{c \mid J_c \text{ is a connected set}\}$

There is an 80 year old theorem by Julia or Fatou that says:

$$\begin{aligned}\mathbf{M} &= \{c ; f_c^{\circ n}(0) \text{ stays bounded}\} \\ &= \{c ; |f_c^{\circ n}(0)| < R_c \text{ for all } n\}.\end{aligned}$$

This provides us with an algorithm for determining the complement of  $\mathbf{M}$ ; namely  $c \notin \mathbf{M}$  if and only if the iteration sequence  $\{f_c^{\circ n}(0)\}$  reaches an absolute value  $> R_c$  for some positive integer  $n$ . (But, the closer  $c$  is to  $\mathbf{M}$ , the larger this termination number  $n$  becomes).

On the other hand, if  $f_c$  has an attractive fixed point, then it is also known that  $\{f_c^{\circ n}(0)\}$  converges towards that fixed point. The interior of the cardioid described above is therefore part of the Mandelbrot set, and in fact it is a large part of it.

As *experiments* we suggest to choose  $c$ -values from the apple-shaped belly of the Mandelbrot set and observe how the Julia sets deform as  $c$  varies from 0 to the cardioid boundary. For an actual animation, choose the deformation interval with the mouse (Action Menu) and then select ‘Morph’ in the Animation Menu. To see how the derivative at the fixed point controls the iteration near the fixed point, choose ‘Iterate Forward’ (Action Menu) and watch how chosen points converge to the fixed point. This is very different for  $c$  from different parts of the Mandelbrot belly.

**5) Attractive periodic orbits.** As introduction let us determine the orbits of period 2, i.e., the fixed points of  $f_c \circ f_c$  that are not also fixed points of  $f_c$ . Observe that:

$$\begin{aligned} f_c \circ f_c(z) - z &= z^4 - 2cz^2 - z + c^2 - c \\ &= (z^2 - z - c)(z^2 + z - c + 1). \end{aligned}$$

The roots of the first quadratic factor are the fixed points of  $f_c$ , the roots of the other quadratic factor are a pair of points that are not fixed points of  $f_c$ , but are fixed points of  $f_c \circ f_c$ , which means, they are an orbit of period 2, clearly the only one. Such an orbit is (linearly) attractive if the product of the derivatives at the points of the orbit has absolute value  $< 1$ . The constant coefficient in the

quadratic equation is the product of its roots, i.e. the product of the points of period 2 is  $1 - c$ . Therefore:

The set of  $c$ -values for which the orbit of period 2 is attractive is the disk  $\{c ; |1 - c| < 1/4\}$ .

Again, this disk is part of the Mandelbrot set since  $\{f_c^{\circ n}(0)\}$  has the two points of period 2 as its only limit points.

The interior of the Mandelbrot set has only two components that are explicitly computable. These are the  $c$ -values giving attractive fixed points or attractive orbits of period 2. For example, the points of period 3 are the zeros of a polynomial of degree 6, namely:

$$\begin{aligned} & (f_c \circ f_c \circ f_c(z) - z)/(z^2 - z - c) \\ &= z^6 + z^5 + (1 - 3c)z^4 + (1 - 2c)z^3 + \\ & \quad + (1 - 3c + 3c^2)z^2 + (c - 1)^2z + 1 - c(c - 1)^2. \end{aligned}$$

But since this polynomial cannot be factored (with  $c$  a parameter) into two polynomials of degree 3 it does not provide us with a description of the attractive orbits of period 3. However, it does give those  $c$ -values for which the period 3 orbits are superattractive (i.e.  $(f^{\circ 3})'(orbit\ point) = 0$ ), since in this case the constant term must vanish. Approximate solutions of  $1 - c(c - 1)^2 = 0$  are  $c = 1.7549, c = 0.12256 \pm 0.74486i$ . One can navigate the Mandelbrot set and observe that the complex solutions are between the two biggest blobs that touch the primary apple from either side.

Linearly attractive orbits always have  $c$ -values which belong to open subsets of the Mandelbrot set (in particular all the blobs touching the two explicit components), but the closure of these open subsets does not exhaust the Mandelbrot set. For example for  $c = i$  the orbit of 0 is  $0 \mapsto -i \mapsto -1 - i \mapsto i \mapsto -1 - i \dots$ , i.e., after two preliminary steps it reaches an orbit of period 2. Since this orbit stays clearly bounded we have  $i \in \mathbf{M}$  (by the criterium quoted before). On the other hand, if the iteration  $z \mapsto z^2 - i$  had any attractor (besides  $\infty$ ), then the orbit of 0 would have to converge to the attracting orbit. Therefore there is no attractor and no attractor basin. In fact, the complement of the Julia set is the (simply connected) attractor basin of  $\infty$ . Because of its appearance, this Julia set is called a dendrite.

To generalize this observation, consider, for any  $c$ , the orbit of 0:  $0 \mapsto -c \mapsto c^2 - c \mapsto c^4 - 2c^3 + c^2 - c \mapsto (c^4 - 2c^3 + c^2 - c)^2 - c \mapsto \dots$ . If 0 is on a periodic orbit for some  $c$ , then this orbit is superattractive. If the periodicity starts later then this periodic orbit may not be an attractor even though the orbit of 0 reaches it in finitely many steps. For example  $c^2 - c$  is periodic of period 3, if  $c^3 \cdot (c - 2) \cdot (c^3 - 2c^2 + c - 1)^2 \cdot (c^6 - 2c^5 + 2c^4 - 2c^3 + c^2 + 1) = 0$ ;  $c = 2$  is the largest point on the Mandelbrot set, the third factor has as roots the three  $c$ -values (mentioned before) for which the iteration has superattractive orbits of period 3. The last factor has the root  $c = 1.239225555 + 0.4126021816 \cdot i$ , its Julia set is another

dendrite. A third dendrite is obtained, for example, if the 4<sup>th</sup> point  $c^4 - 2c^3 + c^2 - c$  in the orbit of 0 is a fixed point, which is the case if  $c^4(c - 2)(c^3 - 2c^2 + 2c^2 - 2) = 0$ ; here the last factor has the numerical solutions  $c = 1.543689$  and  $c = 0.2281555 \pm 1.1151425 \cdot i$ .

**6) Suggestions for experiments.** The final entry in the Action Menu for the Julia set fractal is a hierarchical menu with five submenus, each of which lists a number of related  $c$ -values that you may select. The  $c$ -values in these menus were selected because they typify either some special topological property of the associated Julia set or some dynamical property of the iteration dynamics of  $z \mapsto z^2 - c$ , and these properties are referenced by special abbreviations added to the menu item. (In addition some menu items also list a “name” that is in common use to refer to the Julia set, usually deriving from its shape). For convenience we will list in the next couple of pages all the items from these five menus, but first we explain the abbreviations used to describe them.

*Abbreviations used in the following lists of interesting  $C$ -values.* ‘FP’ means ‘fixed point’, the corresponding  $c$ -values are from the belly of the Mandelbrot set. ‘cyc  $k$ ’ means ‘cyclic of period  $k$ ’, the corresponding  $c$ -values are from the blobs directly attached to the belly; its Julia sets have a fixed point which is a common boundary point of  $k$  components of the attractor basin and the attractive orbit wanders cyclicly through these  $k$  components. ‘per  $2 \cdot 3$ ’ means: this  $c$ -value has an attractor of period 6 and the

$c$ -value is from a blob which is attached to the disk in  $\mathbf{M}$  (which gives the attractive orbits of period 2). By contrast, ‘per  $3 \cdot 2$ ’ means that the  $c$ -value is from the biggest blob which is attached to a period-3 blob (attached to the belly); its attractor has also period 6, but the open sets through which the attractive orbit travels are arranged quite differently in the two cases. One should compare both of them with the cyclic attractors of period 2 resp. 3. The abbreviation ‘tch 1-2’ means that the  $c$ -value is in the Mandelbrot set a common boundary point between the belly (i.e. the component of attractive fixed points) and the component of attractors of period 2. For the ‘Siegel disks’ see Nr. 8 of this ATO first; the column entry in the list gives the rotation number of the derivative (of the iteration map) at the fixed point. In the dendrite section of the list we mean by ‘ev per 2’ that the orbit of 0 is ‘eventually periodic with period 2’, as explained in Nr5 of this ATO. Finally, if  $c \notin \mathbf{M}$  then the Julia set is a totally disconnected Cantor set and there are no such easy distinctions between different kinds of behaviour of the iteration on the Julia set (all other points are iterated to  $\infty$ ).

# Interesting $C$ -values From the Action Submenus

## Attractors Menu

C - values				Popular Name	Behaviour
0.0	+	0.0	· i	Circle	FP
0.0	+	0.1	· i	Rough Circle	FP
0.127	+	0.6435	· i	Near-Rabbit	FP
-0.353	-	0.1025	· i	Near-Dragon	FP
0.7455	+	0.0	· i	Near San Marco	FP
1.0	+	0.0	· i		cyc 2
1.0	+	0.2	· i		cyc 2
0.1227	+	0.7545	· i	Rabbit	cyc 3
1.756	+	0.0	· i	Airplane	cyc 3
-0.2818	+	0.5341	· i		cyc 4
1.3136	+	0.0	· i		per 2·2
-0.3795	+	0.3386	· i		cyc 5
0.5045	+	0.5659	· i		cyc 5
-0.3909	+	0.2159	· i		cyc 6
0.1136	+	0.8636	· i		per 3·2
1.1409	+	0.2409	· i	Rabbit's Shadow	per 2·3
-0.3773	+	0.1455	· i		cyc 7
-0.1205	+	0.6114	· i		cyc 7
-0.36	-	0.1	· i	Dragon	cyc 8
0.3614	+	0.6182	· i		cyc 8
-0.3273	+	0.5659	· i		per 4·2
1.0	+	0.2659	· i		per 2·4
1.3795	+	0.0	· i		per 2·2·2
0.0318	+	0.7932	· i	Rabbit Triplets	per 3·3
-0.0500	+	0.6318	· i		cyc 10
-0.4068	+	0.3409	· i		per 5·2
0.5341	+	0.6023	· i		per 5·2
0.9205	+	0.2477	· i		per 2·5
1.2114	+	0.1545	· i		per 2·5
0.6977	+	0.2818	· i		cyc 11
0.4864	+	0.6023	· i	Quintuple Rabbits	per 5·3
0.65842566307252	-	0.44980525145595	· i	Super Attractor	per 21

## Interesting $C$ -values From the Action Submenus.

C - values		Popular Name	Behaviour
<b>Between Attractors Menu:</b>			
0.75	+ 0.0	• i San Marco	tch 1-2
1.25	+ 0.0	• i S.Marco's Shadow	tch 2-2•2
0.125	+ 0.64952	• i Balloon Rabbit	tch 1-3
-0.35676	+ 0.32858	• i	tch 1-5
<b>Siegel Disks Menu:</b>			
0.390540870218	+ 0.586787907347	• i	$2\pi \cdot i \cdot \text{gold}$
-0.08142637539	+ 0.61027336571	• i	$2\pi \cdot i / \sqrt{2}$
0.66973645476	- 0.316746426417	• i	$2\pi \cdot i / \sqrt{5}$
<b>One Simply Connected Open Component Menu:</b>			
0.0	+ 1.0	• i Dendrite	ev per 2
0.2281554936539	+ 1.1151425080399	• i Dendrite	FP after 3
1.2392255553895	- 0.4126021816020	• i Dendrite	ev per 3
-0.4245127190500	- 0.2075302281667	• i	FP after 7
1.1623415998840	+ 0.2923689338965	• i	per 2 after 7
<b>Outside Mandelbrot set Menu:</b>			
0.765	+ 0.12	• i Cantor set	
-0.4	- 0.25	• i Cantor set	
-0.4253	- 0.2078	• i Cantor set	

An *experiment* which one should always make after one has computed a Julia set for some  $c$  from the Mandelbrot set: Remember from which part of  $\mathbf{M}$   $c$  came and then ‘Iterate Forward’ (Action Menu) mouse selected points until they visually converge to a periodic attractor. Observe how the shape of the Julia set lets one guess the period of its attractor and how this relates to the position of  $c$  in  $\mathbf{M}$ .

**7) Computation of the Julia set.** In addition to the attractor at infinity there is at most one further attractor in the  $z \rightarrow (z^2 - c)$  systems. All preimages of non-attractive fixed points or non-attractive periodic orbits are points on the Julia set. Since  $|f'_c| > 1$  along the Julia set (with some exceptions), the preimage computation is numerically stable. This is a common method for computing Julia sets.

In our program we compute preimages starting from the circle  $\{z; |z| = R_c\}$  around the wanted Julia set. Under inverse images these curves converge from outside to the Julia set. Such an approximation by curves allows us to color the Julia set in a continuous way and thus emphasize that, despite its wild looks it is the image of a continuous curve—at least for  $c \in M$ , otherwise we recall that the Julia set is totally disconnected, so in particular is not the image of a curve. Our computation works also for  $c \notin \mathbf{M}$ , since our ‘curves’ of course consist of only finitely many points, and the inverse images of each of these points have their limit points on the Julia set.

**8) Self-similarity of a Julia set.** A well advertised property of these Julia sets is their so called ‘self-similarity’. By this one means: Take a small piece of the Julia set and enlarge it; the result looks very much like a larger piece of that same Julia set. For the Julia sets of the present quadratic iterations, this self-similarity is easily understood from the definitions: The iteration map  $f_c$  is a *conformal* map that stretches its Julia set 1:2 onto itself. In other words, the iteration map itself maps any small piece of its Julia set to roughly twice as large a piece, and it does so in an angle preserving way. From this point of view self-similarity should come as no surprise.

**9) Siegel Disks.** We next would like to explain an experimentally observable phenomenon that mathematicians find truly surprising, but this needs a little preparation.

*Simplifying Mappings.* Imagine that we want to describe something on the surface of the earth, for example a walk. For a long time, people have been more comfortable giving the description on a map of the earth rather than on the earth itself. Mathematicians view a map of the earth more precisely as a mapping  $F$  from the earth to a piece of paper and they describe (or even prove) properties of the map by properties of the mapping  $F$ . An example of a useful property is ‘conformality’: angles between curves on the earth are the same as the angles between the corresponding curves on the map.

*Conjugation by simplifying mappings.* Let us consider one of the above iteration maps  $f_c$  and assume that it has an at-

tractive fixed point  $z_f$  with derivative  $q := f'_c(z_f)$ ,  $|q| < 1$ . The simplest map with the same derivative is the linear map  $L(z) := q \cdot z$ . It is the definition of derivative that the behaviour of  $f_c$  near the fixed point looks ‘almost’ like the behaviour of  $L$  near its fixed point 0, and ‘almost’ means: the smaller the neighborhoods of the fixed points (on which the maps are compared) the more the maps look alike. But more is true for  $f_c$  because of the assumption  $|q| < 1$ , we have the *theorem*: There exists on a fixed(!) neighborhood of the fixed point  $z_f$  a simplifying map  $F$  to a neighborhood of  $0 \in \mathbb{C}$  that makes  $f_c$  look *exactly* like its linear approximation  $L$ , by which we mean:  $f_c = F^{-1} \circ L \circ F$ . In particular, this tells us everything about the iterations of  $f_c$  in terms of the iterations of  $L$  because they also look the same when compared using (‘conjugation’ by)  $F$ :  $f_c^{\circ n} = F^{-1} \circ L^{\circ n} \circ F$ .

*Siegel’s Theorem.* The previous result cannot be true in general if  $|q| = 1$ . For example if  $q = \exp(2\pi i/k)$ , then  $L^{\circ k} = \text{id}$ , but  $f_c^{\circ k} \neq \text{id}$ . Therefore they cannot look alike under a simplifying (i.e., ‘conjugating’) mapping  $F$ . But if  $z \rightarrow q \cdot z$  is an irrational rotation and if some further condition is satisfied, for example if  $q := \exp(2\pi i/\sqrt{2})$ , then there is again such a simplifying mapping  $F$  such that  $f_c$  looks near that fixed point exactly like its linearization, namely:  $f_c = F^{-1} \circ L \circ F$ .

*Experiment.* While Siegel’s proof insures only *very* small neighborhoods on which the simplifying mapping  $F$  exists, these neighborhoods are surprisingly large in the present

case. One can ‘observe’ Siegel’s theorem by first choosing  $c = ((1 - q)^2 - 1)/4$  such that  $f'_c(z_f) = q$  with  $q = \exp(2\pi i \cdot k/\sqrt{p})$ ,  $p$  prime (or square free), then one chooses points on a fairly straight radial curve from the fixed point almost out to the Julia set. Under repeated iterations these points travel on closed curves around the fixed point (‘circles’ when viewed with  $F$ ) and all of them travel with the same angular velocity, i.e., one observes that they remain on non-intersecting radial curves.

H.K.

Fractal TOC

# Ordinary Differential Equations, ODEs

[Go To Page 1](#)

(Click the Names)

- 1.) [About ODEs](#)
- 2.) [ODE Equations in 1D, 2D](#)
- 3.) [ODE Equations in 3D](#)
- 4.) [ODEs with Central Forces](#)

More Details for Selected Equations

- 5.) [The Duffing Oscillator](#)
- 6.) [Charged Particles in a Magnetic Field](#)

## Ordinary Differential Equations \*

3D-Filmstrip knows how to calculate and display solutions of the initial value problem for first and second order systems of ordinary differential equations (ODE) in one, two, or three dependent variables.

Let us recall briefly what this means. We will be dealing with vector-valued functions  $x$  of a single real variable  $t$  called the “time”. Here  $x$  can take values in  $\mathbb{R}$ ,  $\mathbb{R}^2$ , or  $\mathbb{R}^3$ . The problem is to find  $x$  from a knowledge of how  $x'$  depends on  $x$  and  $t$  (in the first order case) or a knowledge of how  $x''$  depends on  $x$ ,  $x'$ , and  $t$  (in the second order case). Thus in the first order case the ODE we are trying to solve has the form  $x' = f(x, t)$  and in the second order case it is  $x'' = f(x, x', t)$ .

In the first order case, the so-called Local Existence Theorem for First Order ODEs tells us that, provided the function  $f$  is continuously differentiable, given an “initial time”  $t_0$ , and an “initial position”  $x_0$ , then in some sufficiently small interval around  $t_0$ , there will be a unique solution  $x(t)$  to the ODE with  $x(t_0) = x_0$ .

There is a similar local existence theorem for second order ODEs (which in fact is an easy consequence of the first order theorem). It says that given an initial time  $t_0$ , an

---

\* This file is from the 3D-XplorMath project. Please see:

initial position  $x_0$ , **and** an initial velocity  $v_0$  then, in some sufficiently small interval around  $t_0$ , there will be a unique solution  $x(t)$  of the ODE with  $x(t_0) = x_0$  and  $x'(t_0) = v_0$ . Theory provides not only an abstract existence theorem, but also many explicit numerical algorithms for finding approximating solutions, in terms of the function  $f$  and the initial data. One of the all-time favorites for general purposes is the so-called Fourth Order Runge-Kutta Method, and this is the one that 3D-Filmstrip uses.

Although the overall approach to solving such ODEs is quite similar for first and second order ODEs and for the various dimensions, the details for giving initial conditions and for displaying solutions are different for each case, and for that reason instead of having a single ODE category, it turns out to be convenient to have six. The naming of these categories is fairly self-evident. For example, the ODE(1D) 1stOrder Category deals with the case that  $x$  take values in  $\mathbb{R}$ , and the equation is first order, while the ODE(3D) 2ndOrder Category deals with the case that  $x$  take values in  $\mathbb{R}^3$ , and the equation is second order.

For the ODE(1D) 2ndOrder category, the usual reduction to a first order system in two variables  $(x, u)$ , where  $u$  represents  $x'$ , is made via  $(x, u)' = (u, f(x, u, t))$ .

In the case of the ODE(2D) 1stOrder category, the orbit is drawn dotted, with a constant time interval between dots. This gives a valuable visual clue concerning the velocity at which the orbit is traced out, but if you wish to turn this

feature off, just set Dot Spacing to zero using the ODE Settings... dialog (see below).

In all the ODE categories, when you have chosen either a particular pre-programmed example (or set up your own, using the User Defined... feature) then as with the other categories you will first see a visualization of a default solution. This display will usually stop quickly on its own, but you can also click the mouse button (or type Command period) to stop it. You may then choose the item “ODE Settings...” in the Settings menu and this will allow you to set the various data the program needs to compute and display an orbit, namely:

- a) the initial time,
- b) the time-span,
- c) the step-size (used in the Runge-Kutta method),
- d) the initial value of  $x$ , and (in a second order case)
- e) the initial value of  $x'$ .

Choosing Create from the Action Menu will then display the solution for these newly selected settings.

There is an ODE control panel that opens by default just below the main display window. This has buttons to do more easily things you can also do with the menus (Create, Erase, Continue, double or half the scale, and bring up the dialog to set initial conditions, step-size, time-span, and dottedness). In addition there are buttons for single-stepping the ODE forward or backward, and there is a

read-out of the current time, position, and velocity. This control panel can be hidden using the Hide ODE Controls command of the Action menu (and then may be re-opened with the Show ODE Controls command).

The main display shows the evolution of an orbit in the phase space. By default, the program also shows projections of the orbit on the coordinate axes (using different colors to distinguish the projections). This display occurs in a second pane of the graphics window that opens automatically below the main pane. This pane can be hidden by choosing "Hide Direction Fields" from the Action menu. There is a rectangular button at the right edge of the screen where the two panes meet. If you press on this button, the button itself will disappear and be replaced by a horizontal line. Drag the horizontal line to where you would like the new boundary between panes and release the mouse. (At least twenty percent of the total screen height must be devoted to each pane.)

For first order ODE in one and two dimensions, the program by default displays the direction field defined by the current ODE. (Since second order ODEs in one variable are reduced to first order ODEs in two variables, the direction field is also shown in this case.) The direction field of a time dependent ODE is updated every few integration steps. (As far as I know, 3D-Filmstrip is the only publicly available program that shows direction fields for time-dependent ODE.) For the ODE(3D) 2ndOrder category there is also a direction field shown (when the display

is in stereo) for the special case of a charged particle in a magnetic field—but be careful, the field shown is the magnetic field, **not** the direction of the Lorentz force acting on the particle.

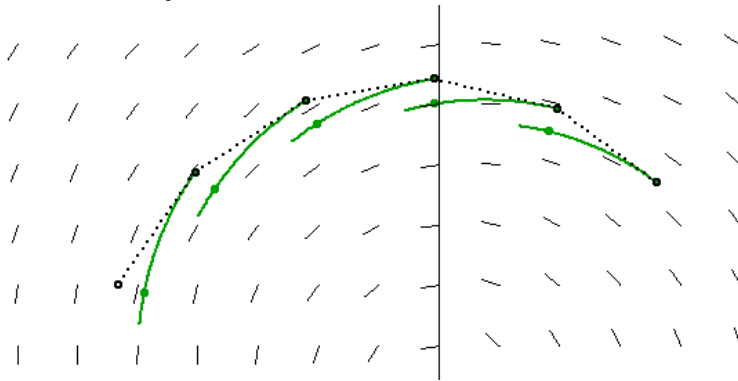
It is fairly easy to do a rough “phase space analysis” by keeping the other data fixed and varying the initial values. To make this easier, in certain categories it is possible to choose the initial conditions using the mouse. For example, in the ODE(1D) 1stOrder category, each time you click the mouse in the window, the forward and backward orbits are drawn through that initial value. Similarly, clicking the mouse in the ODE(1D) 2ndOrder category and ODE(2D) 1st Order category also creates an orbit with the mouse point as initial condition. Surprisingly, something similar even works for the ODE(2D) 2ndOrder category. Here to choose an initial condition AND velocity, either select IC By Mouse [Drag] from the Action menu or type Control I. You may then click and drag the mouse to choose the initial position (click) and velocity (drag).

## Numerical Methods for 1st Order ODEs

Numerical solutions are computed at a discrete set of time points  $t_0, t_1, \dots, t_n$  and usually one such time step of a method is described, i.e. how to get from  $x(t_0)$  to  $x(t_1)$ . One then has to repeat this step as long as one wants to. The simplest of all methods is the EULER METHOD: From the initial data  $t_0, x_0 = x(t_0)$  one computes first the INITIAL DERIVATIVE:  $x'(t_0) := f(x_0, t_0)$ , then the

EULER STEP:  $x(t_1) := x_0 + x'(t_0) \cdot (t_1 - t_0)$ .

The following picture shows five such (large) Euler steps and the corresponding exact solutions for the same time interval. Clearly, if the exact solution curves happen to be convex, the Euler Step solutions stay outside and move farther away from the exact solution with each step.



Five Euler Steps

Recall that the tangent of a parabola which is parallel to some secant touches the parabola in the middle of the secant interval. This suggests a substantial improvement over the Euler method, it is called the HALFSTEP METHOD:

STEPSIZE:  $\Delta t := t_1 - t_0$

INITIAL DERIVATIVE:  $x'_0 := f(x_0, t_0)$

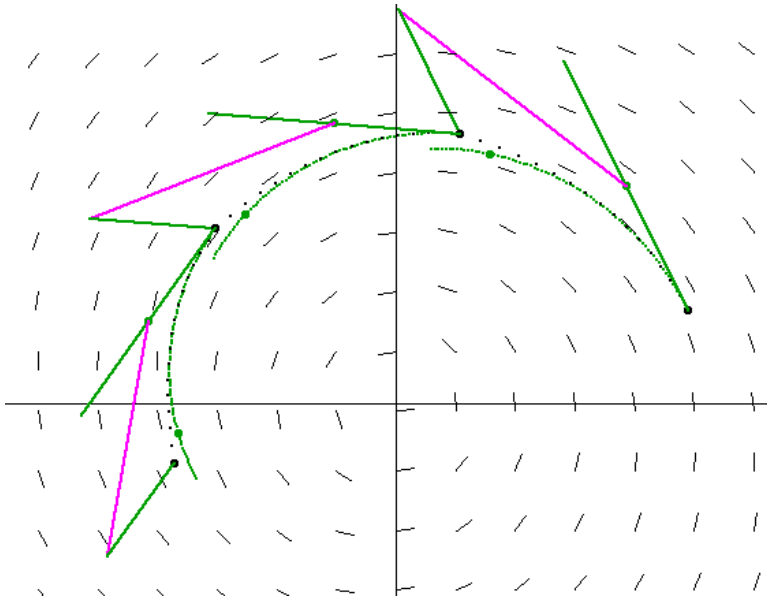
HALF STEP TOWARDS MIDDLE:  $x_m := x_0 + x'_0 \cdot \Delta t/2$

MIDDLE DERIVATIVE:  $x'_m := f(x_m, t_0 + \Delta t/2)$

FINAL STEP:  $x(t_1) := x_0 + x'_m \cdot \Delta t$ .

Again we illustrate this method with a picture, but using a larger stepsize than in the Euler case. The magenta vector is the derivative at the approximate midpoint  $x_m$  multiplied by the stepsize, i.e.  $x'_m \cdot \Delta t$ . This vector is the difference between  $x(t_1)$  and  $x(t_0)$ . One can see that this method follows the solution curve rather well, but traverses

it too fast.



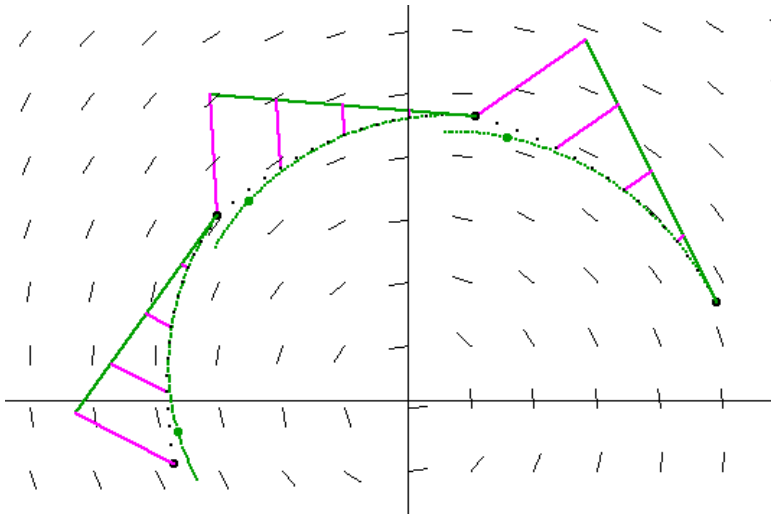
Three Halfstep Steps

Some first order ODEs have the property that the second initial derivative can be computed rather easily, more easily than differentiation of the ODE,  $x'' = \frac{\partial}{\partial x} f \cdot x' + \frac{\partial}{\partial t} f$ , suggests. In those cases one can use a second order Taylor step instead of the first order step used in Euler's method. We call this the TAYLOR-2 METHOD:

INITIAL 1ST AND 2ND DERIVATIVE:  $x'_0, x''_0$

TAYLOR STEP:  $x(t_1) := x_0 + x'_0 \cdot \Delta t + x''_0 \cdot (\Delta t)^2 / 2$ .

The endpoints of the magenta segments lie on the quadratic parabola  $p(s) := x_0 + x'_0 \cdot s + x''_0 \cdot s^2 / 2$ ,  $s \in [0, \Delta t]$  (with the same initial tangent (green) as the exact solution). The method has the same order of precision as the previous one, so that one will often prefer the Halfstep method. But in the vicinity of a point where  $f(x, t) = 0$ , the Taylor-2 method is usually better.



Three Taylor-2 Steps

Next we try to explain the famous RUNGE-KUTTA METHOD. First we need to understand what numerical analysts call an order  $k$  method. If we compute one Euler step from  $x_0$ , but with various stepsizes  $s$ , then all the computed points lie on the tangent  $x_0 + x'_0 \cdot s$ . The difference to the exact solution is controlled by a bound  $B_2$  on the second derivative of solutions near  $x_0$  as:  $\text{error}(s) \leq B_2 \cdot s^2$ . This is called a first order method.

For the Taylor-2 method these stepsize dependent numerical values lie on a parabola which was already mentioned:  $p(s) := x_0 + x'_0 \cdot s + x''_0 \cdot s^2/2$ . The difference to the exact solution  $x(s)$  is controlled in terms of a bound  $B_3$  for third derivatives as:  $\text{error}(s) \leq B_3 \cdot s^3$ . This is called a second order method.

How can one make such considerations work for the Half-step method? Clearly the approximate midpoint is a function of the stepsize:  $x_m(s) = x_0 + x'_0 \cdot s/2$  and therefore the final point also:  $x_f(s) := x_0 + f(x_m(s), t_0 + s/2) \cdot s$ . We may call this curve the method-curve. Computation shows

that the exact solution at  $t_0$  and the method-curve at  $s = 0$  have the same first and second derivative:  $x'_0(t_0) = x'_f(0)$ ,  $x''_0(t_0) = x''_f(0)$ . The error, therefore, is again  $\leq B_3 \cdot s^3$ , and the method is also called a second order method.

What we saw in these examples is true in general: Consider the initial data  $x_0, t_0$  as fixed. The numerical value of the computation of one step will then only depend on the stepsize  $s$ , giving us the method-curve  $x_f(s)$  for the considered numerical solution. If the first  $k$  initial derivatives of the exact solution agree with the first  $k$  initial derivatives of the method-curve, then we speak of an order  $k$  method.

The RUNGE-KUTTA METHOD can be seen as a generalization of the halfstep method: Instead of computing two derivatives  $x'_0, x'_m$ , Runge-Kutta computes four and averages them for the final step.

INITIAL DERIVATIVE:  $x'_0 := f(x_0, t_0)$

1ST INTERMEDIATE POINT:  $x_a(s) := x_0 + x'_0 \cdot s/2$

1ST INTERMEDIATE DERIVATIVE:  $x'_a(s) := f(x_a(s), t_0 + s/2)$

2ND INTERMEDIATE POINT:  $x_b(s) := x_0 + x'_a \cdot s/2$

2ND INTERMEDIATE DERIVATIVE:  $x'_b(s) := f(x_b(s), t_0 + s/2)$

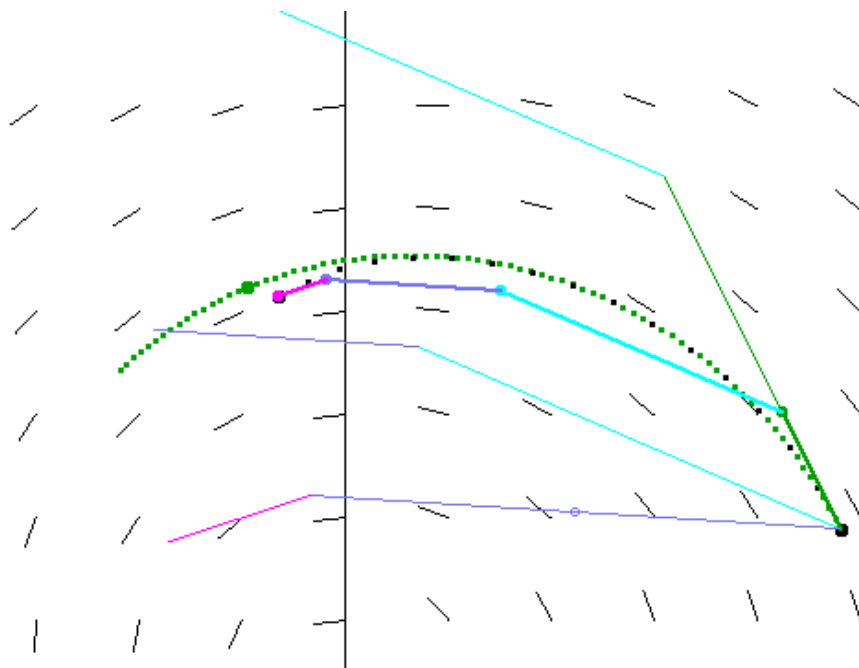
3RD INTERMEDIATE POINT:  $x_c(s) := x_0 + x'_b \cdot s$

3RD INTERMEDIATE DERIVATIVE:  $x'_c(s) := f(x_c(s), t_0 + s)$

DERIVATIVE AVERAGE:  $x'_{RK}(s) := (x'_0 + 2x'_a + 2x'_b + x'_c)/6$

FINAL STEP:  $x_f(s) := x_0 + x'_{RK}(s) \cdot s$ .

We can compute the first four derivatives of this method-curve and check that the above defines a 4th order method. It is one of the most celebrated ODE solving numerical methods. A visualisation of one Runge-Kutta step is:



The three straight segments from the initial point end at the three intermediate points  $x_a, x_b, x_c$ . Note how far they are apart from each other compared to the small error of the composite step. (The dotted green curve is the exact solution, the black dots lie on the method-curve.)

In 3D-XplorMath ODEs are not only objects of visualisations, they are an essential tool for many computations in the program. The ODE for elliptic functions  $f$ , namely:

$$f'(z)^2 = P(f(z)), \quad P \text{ a polynomial of degree 3 or 4}$$

is an example where the second derivative can be more easily computed than the first:  $f''(z) = P'(f(z))/2$ . We therefore use a different 4th order method:

INITIAL DERIVATIVES:  $x'_0, x''_0$

INTERMEDIATE POINT:  $x_m(s) := x_0 + x'_0 \cdot s/2 + x''_0 \cdot s^2/8$

INTERMEDIATE 2ND DERIVATIVE:  $x''_m(s) := P'(x_m(s))/2$

FINAL STEP:  $x_f(s) := x_0 + x'_0 \cdot s + (x''_0 + 2x''_m(s)) \cdot s^2 / 6$

Although zeros of the polynomial  $P$  are constant solutions of the first order ODE, the just described method can start to compute the non-constant function  $f$  at points  $z$  where  $f'(z) = 0$  as initial value. A Runge-Kutta solution would stay constant.

R.S.P., H.K.

ODEs

## 1D-, 2D- ODE examples in 3D-XplorMath \*

See First: About This Category (DocumentationMenu)

1D 1st Order:

logistic:  $\dot{x} = aa \cdot x(1 - x/bb)$

mass action:  $\dot{x} = aa \cdot x + bb \cdot x^2$

---

1D 2nd Order:

harmonic Osc:  $\ddot{x} = -aa^2 x - bb u$

forced Osc:  $\ddot{x} = -aa^2 x - bb u + cc \cos(dd(t - ee))$

forced Duffing:  $\ddot{x} = -hh x - ii x^3 - aa u + bb \cos(cc t)$

van der Pol:  $\ddot{x} = hh x - aa(x^2 - 1)u + bb \cos(cc t)$

Pendulum:  $\ddot{x} = -aa \sin(x) - bb u$

---

2D 1st Order:

harmonic Osc:  $\begin{pmatrix} x \\ y \end{pmatrix} \cdot = \begin{pmatrix} 0 & 1 \\ -aa & -bb \end{pmatrix} \cdot \begin{pmatrix} x \\ y \end{pmatrix}$

Pendulum:  $\begin{pmatrix} x \\ y \end{pmatrix} \cdot = \begin{pmatrix} y \\ -aa \sin(x) - bb y \end{pmatrix}$

linear 2D:  $\begin{pmatrix} x \\ y \end{pmatrix} \cdot = \begin{pmatrix} aa & bb \\ cc & dd \end{pmatrix} \cdot \begin{pmatrix} x \\ y \end{pmatrix}$

VolterraLotka:  $\begin{pmatrix} x \\ y \end{pmatrix} \cdot = \begin{pmatrix} (aa - bb y) \cdot x \\ (cc x - dd) \cdot y \end{pmatrix}$

---

2D 2nd Order:  $(\dot{x} = u, \dot{y} = v)$

coupled Osc:  $\begin{pmatrix} x \\ y \end{pmatrix} \cdot\cdot = \begin{pmatrix} -aa^2 x + dd(y - x) - gg u \\ -bb^2 y + dd(x - y) - hh v \end{pmatrix}$

forced Osc:  $\begin{pmatrix} x \\ y \end{pmatrix} \cdot\cdot = \begin{pmatrix} -aa^2 x + bb \cos(cc t) \\ -dd^2 y + ee \cos(ee t) \end{pmatrix}$

Foucault Pend:  $\begin{pmatrix} x \\ y \end{pmatrix} \cdot\cdot = \begin{pmatrix} -aa^2 x + 2 bb \sin(\pi cc/180)v \\ -aa^2 y - 2 bb \sin(\pi cc/180)u \end{pmatrix}$

bb := earth' angular velocity, cc := pendulum latitude

---

\* This file is from the 3D-XplorMath project. Please see:

## 3D-ODE examples in 3D-XplorMath \*

See First: About This Category (DocumentationMenu)

3D 1st Order:

$$\text{linear: } \begin{pmatrix} x \\ y \\ z \end{pmatrix}' = \begin{pmatrix} aa & bb & cc \\ dd & ee & ff \\ gg & hh & ii \end{pmatrix} \cdot \begin{pmatrix} x \\ y \\ z \end{pmatrix}$$

$$\text{Lorenz: } \begin{pmatrix} x \\ y \\ z \end{pmatrix}' = \begin{pmatrix} -10x + 10y \\ aa x - y - xz \\ -(8/3)z + xy \end{pmatrix}$$

$$\text{Rikitake: } \begin{pmatrix} x \\ y \\ z \end{pmatrix}' = \begin{pmatrix} -bb x + yz \\ -aa x - bb y + xz \\ 1 - xy \end{pmatrix}$$

$$\text{Rössler: } \begin{pmatrix} x \\ y \\ z \end{pmatrix}' = \begin{pmatrix} -y - z \\ x + aa y \\ bb - cc z + xz \end{pmatrix}$$

---

\* This file is from the 3D-XplorMath project. Please see:

3D 2nd Order:

$$(x' = u, y' = v, z' = w)$$

coupled Oscillator:

$$\begin{pmatrix} x \\ y \\ z \end{pmatrix}'' = \begin{pmatrix} -aa^2x + dd(y - x) + ee(z - x) - gg u \\ -bb^2y + dd(x - y) + ff(z - y) - hh v \\ -cc^2z + ee(x - z) + ff(y - z) - ii w \end{pmatrix}$$

forced Oscillator:

$$\begin{pmatrix} x \\ y \\ z \end{pmatrix}'' = \begin{pmatrix} -aa^2x + bb \cos(cc \cdot t) \\ -dd^2y + ee \cos(ff \cdot t) \\ -gg^2z + hh \cos(ii \cdot t) \end{pmatrix}$$

The ODE for a **charged particle** in a magnetic field  $M$ :

$$\vec{x}' = \vec{u}, \quad \vec{x}'' = \vec{u}' = \vec{u} \times M(x, u), \quad \text{charge and mass are 1.}$$

const Magnetic Field:  $M(\vec{x}) := (aa, bb, cc)^t$

Magnetic Field of straight wire:

$$\begin{aligned} \vec{wire} &:= (aa, bb, cc)^t / \sqrt{aa^2 + bb^2 + cc^2} \\ \vec{px} &:= \vec{x} - \langle \vec{x}, \vec{wire} \rangle \cdot \vec{wire}, \quad rr := |\vec{px}|^2 \\ M(\vec{x}) &:= dd/rr \cdot (\vec{wire} \times \vec{px}) \end{aligned}$$

Toroidal Magnetic Field:

$$M(\vec{x}) := (2y, -2x, 0)/(x^2 + y^2)$$

Magnetic Dipole Field:

$$\begin{aligned} rr &:= x^2 + y^2 + z^2 \\ eDOTp &:= aa x + bb y + cc z \end{aligned}$$

$$M(\vec{x}) := \left( \frac{3x}{rr - aa}, \frac{3y}{rr - bb}, \frac{3z}{rr - cc} \right) \frac{eDOTp}{rr^{3/2}}$$

## ODEs with Central Forces\*

This category models the motion of a particle moving according to Newton's Law " $F = ma$ ", where the force  $F$  is a "central" force, i.e., one directed towards (or away from) the origin and whose magnitude depends only on the distance of the point from the origin. (As we will recall below, this also models the motion of two particles in space when the force between them is directed along the line joining them and has a magnitude that depends only on their separation.)

By "conservation of angular momentum", the particle moves in a fixed plane, and this is taken as the plane of the screen, with the origin at the screen center. By default, the  $x$  and  $y$  axes are visible but, as usual, you can reverse this using the View Menu.

There are several pre-programmed central forces:

Coulomb:  $F(r) = -aa/r^2$  (default:  $aa = 2.5$ )

Power Law:  $F(r) = -aa r^{bb}$  (defaults:  $aa = 2.5$ ,  
 $bb = -2.01$ )

Yukawa:  $F(r) = -aa \exp(-bb r)(bb/r + 1/r^2)$   
(defaults:  $aa = 2.5$ ,  $bb = 0.25$ )

Hooke's Law :  $F(r) = -aa r$  (default:  $aa = 2.5$ )

Higgs:  $F(r) = aa r(1 - (r/cc))$  ( $aa = 3.0$ ,  $cc = 2$ ).

---

\* This file is from the 3D-XplorMath project. Please see:

(And there is also a provision for a “User Defined” central force law.)

After choosing one of the pre-programmed examples, an orbit will be displayed for a default initial position  $(x_{initial}, y_{initial})$  and initial velocity  $(\dot{x}_{initial}, \dot{y}_{initial})$ . The time evolution of the orbit will continue until the mouse is clicked. The same initial position  $(0.5, 0.5)$  and same initial velocity  $(-1.25, 2.0)$  is used for the Coulomb’s law, the Power Law, and Yukawa Law. (This, in particular, demonstrates the fact that having all bounded orbits closed is rather special to the case of a power law with exponent  $-2$ .)

To display an orbit with different initial conditions, choose “IC by mouse (Drag)” from the Central Force menu and then click to choose an initial value, and drag to choose an initial velocity—the velocity vector will be proportional to the vector difference of the MouseUp and MouseDown points. (If instead you choose “IC by mouse (Throw)” from the menu, then the initial point is again the MouseDown point, but the velocity is computed using the position of the mouse one-half second after MouseDown rather than the MouseUp position. (In either case, the new orbit will start being displayed immediately, and continue to evolve until the mouse is again clicked). There is still a third way to choose initial conditions; namely, choose “ODE Settings...” from the Settings menu. This will display a Dialog in which you can choose the initial values of  $x$  and  $y$ . In addition  $x$ - and  $y$ - components of velocity.

(In this Dialog, you can also set the value of the mass, the step-size used in the Runge-Kutta integration, and the “dotted-ness” of the orbit. You can also change the values of any parameters on which the chosen central force depends by choosing Set Parameters...from the Settings menu. (To check dependence of the current central force on the parameters  $aa, \dots, ii$ , choose either “About this Object” from the Central Force menu.) After making changes to the parameters, the mass, initial conditions, stepsize, and dotted-ness of the orbit (see below for more about the latter two) choose Create from the Central Force menu to start the display of the new orbit. (If you want the orbit drawn onto a clean screen, choose Erase before choosing Create.)

Instead of using one of the pre-programmed central forces, the user can define a central force law by choosing User Defined...in the Central Force menu and entering a function of the radius,  $r$ , and the usual usual nine parameters  $aa, \dots, ii$ . (After clicking the OK button, either choose an initial position and velocity with the mouse as described above, or use the Set Parameters...and ODE Settings...and then choose Create.)

If the Time step-size is set equal to zero in the ODE Settings Dialog, then the stepsize will be set by an adaptive algorithm that makes the stepsize (roughly) inversely proportional to the magnitude of the velocity. This has the advantage of making the stepsize very small where the velocity is large, avoiding numerical errors that are otherwise

inherent in such situations. The downside is that all timing information is lost—the orbit is traced out equal lengths in equal times rather than by Kepler’s Law of equal areas in equal times.

The Dot Spacing in the ODE Settings...Dialog sets the time between which successive dots are drawn along the orbit. If Dot Spacing is set equal to zero, then the orbit is drawn as a solid curve.

Finally, we recall that the real significance of a central force is that it models the Newtonian motion of a two-particle system (say with masses  $m_1$  and  $m_2$ ) in which the force  $F(r)$  on each particle is equal and opposite to that on the other, is along the line joining the two particles and has a magnitude depending only on their distance of separation,  $r$ . First, by conservation of linear momentum, the center of mass of the two particles moves with constant velocity in a straight line, so making a Galilean coordinate transformation we can assume the center of mass is fixed at the origin. The problem then is to find the time evolution of the vector  $\vec{r}$  joining particle one to particle two, and it is easily seen that  $\vec{r}$  satisfies Newton’s equations for a particle moving in response to the central force  $F(r)$  and with mass the harmonic mean of  $m_1$  and  $m_2$  (the so-called “reduced mass”). For details see any good text on classical mechanics, for example, Chapter 3 of Goldstein.

# Forced Duffing Oscillator \*

## What is it?

What we shall call the *Forced Duffing Oscillator Equation* is the second order ODE for a single variable  $x$ ,

$$\frac{d^2x}{dt^2} = -hhx - iix^3 - aa\frac{dx}{dt} + bb\cos(cct) \quad (1)$$

whose solutions we display via the equivalent (non-autonomous) first order system in two variables,  $x$  and  $y$ :

$$\frac{dx}{dt} = y, \quad \frac{dy}{dt} = -hhx - iix^3 - aay + bb\cos(cct) \quad (2)$$

which in turn can be made into an autonomous first order system in three variables,  $T$ ,  $x$  and  $y$ :

$$\begin{aligned} \frac{dT}{dt} &= 1, & \frac{dx}{dt} &= y, \\ \frac{dy}{dt} &= -hhx - iix^3 - aay + bb\cos(ccT). \end{aligned} \quad (3)$$

We discuss the interpretation and significance of the five parameters,  $aa, bb, cc, hh, ii$  below. Their default values are:  $aa = 0.25, bb = 0.3, cc = 1.0, hh = -1.0$ , and  $ii = 1.0$ . If  $bb \cdot cc \neq 0$  then the forcing period  $2\pi/cc$  is shown by yellow dots on the orbit.

## Why is it interesting?

Here are two of the considerations that make the oscillator equation (1) worth studying. First, with appropriate choices of parameter values it reduces to a variety of

---

\* This file is from the 3D-XplorMath project. Please see:

mathematically and physically interesting oscillator models; some classical such as the harmonic oscillator (with and without damping and forcing) and others that are more exotic, such as the classic Duffing oscillator introduced by Duffing in 1918. By putting these together in a parametric family, we can investigate how various features of these systems behave as we move around in the parameter space. Secondly—and more importantly—it was in the study of the Duffing Oscillator that symptoms of the phenomena we now call “chaos” and “strange attractor” were first glimpsed (although their significance was only appreciated later). By the Poincaré-Bendixson Theorem, three is the smallest dimension in which an autonomous system can exhibit chaotic behavior, and the Duffing system is so simple that it lends itself very easily to the study and visualization of the phenomena related to chaos.

### **The Newtonian Particle Interpretation.**

Note that (1) becomes Newton’s equation of motion for a particle of unit mass moving on the  $x$ -axis if we define the “force”,  $F(x, \frac{dx}{dt}, t)$ , acting on the particle to be the right-hand side of (1). Let’s interpret the various terms of  $F$  from this point of view.

If  $hh$  is positive then the term  $-hhx$  by itself gives Hooke’s Law for a spring, that “stress is proportional to strain” and the parameter  $hh$  has the interpretation of Hooke’s proportionality factor between the extension of the spring,  $x$ , and the restoring force. If also  $ii = 0$  then we have a

pure Hooke's Law force that gives the Harmonic Oscillator,  $\frac{d^2x}{dt^2} = -hhx$ . But a real spring only satisfies Hooke's Law approximately, and the term  $-ii x^3$  represents the next term in the Taylor expansion of the restoring force under the reasonable assumption that this force is an odd function of the spring extension,  $x$ . (If  $ii$  is positive it is called a "hardening" spring and if negative a "softening" spring.) For the classic Duffing Oscillator,  $hh$  is negative and  $ii$  is positive and there is not a good interpretation of the force in terms of a spring. Rather, the sum of the two terms  $-hhx - ii x^3$  should be interpreted as the force on a particle that is moving in a double-well potential as we will discuss in more detail below.

The term  $-aa \frac{dx}{dt}$  represents a "friction" force of the sort that would be experienced by a particle like a bullet traveling through air or a bead sliding on a wire; that is, assuming that the "damping" or "friction" coefficient  $aa$  is positive, it describes a force acting on the particle in the direction opposite to the velocity and with a magnitude that is proportional to the magnitude of the velocity.

Under the sum of the above terms of the force law  $F$ , the particle will (in general) oscillate back and forth—which of course is why it is called an oscillator—however if  $aa > 0$  these oscillations will gradually die down as the kinetic energy is absorbed by friction. The final term in the force law,  $bb \cos(cct)$  is a periodic forcing term that will act on and perturb the motion of this oscillating particle, and we

note that it is solely a function of the time and is independent of both the position and velocity of the particle. We will discuss a possible physical interpretation of this term later. The parameter  $bb$  is clearly the amplitude of this forcing term, i.e., its maximum magnitude, and the parameter  $cc$  is the angular velocity of its phase in radians per unit time, so that the period of the forcing term is  $\frac{2\pi}{cc}$  and its frequency is  $\frac{cc}{2\pi}$ . As we shall see, it is the energy that is fed into the system by this forcing term that is essential for the interesting chaos related effects to occur. In fact the most interesting behaviors of solutions of (1) are present when all the above terms are present in  $F$ , that is when the oscillator is both forced and damped, and in fact the way damping and forcing can balance each other is crucial to understanding the general behavior of solutions. However we will begin by analyzing the simpler situation when both the damping and forcing terms are missing.

### **The Undamped, Unforced Case.**

We now assume that  $aa$  and  $bb$  are both zero, so the force  $F(x) = -hhx - iix^3$  is a function of  $x$  alone. Now in one-dimension, whenever this is the case the force is *conservative*, that is, it is minus the derivative of a “potential” function,  $U(x)$ . Indeed, if we define  $U(x) := -\int_0^x F(\xi) d\xi$ , then clearly  $F(x) = -U'(x)$ . If as above we write  $y := \frac{dx}{dt}$ , define the kinetic energy by  $K(y) := \frac{1}{2}y^2$  and define the Hamiltonian or total energy function by  $H(x, y) := K(y) + U(x)$ , then  $\frac{dH}{dt} = y \frac{dy}{dt} + U'(x) \frac{dx}{dt} =$

$y(\frac{dy}{dt} + U'(x))$ . So, if Newton's Equation is satisfied,  $\frac{dy}{dt} = \frac{d^2x}{dt^2} = F(x) = -U'(x)$ , so  $\frac{dH}{dt} = 0$ . This of course is the law of conservation of energy: the total energy function  $H(x, y)$  is constant along any solution of Newton's Equations. In one-dimension this provides at least in principle a way to solve Newton's Equation for any initial conditions  $x = x_0$  and  $y = y_0$  at time  $t = t_0$ . Namely, the path or orbit of the solution is a curve in the  $x$ - $y$  plane, and by conservation of energy this curve is given by the implicit equation  $H(x, y) = H(x_0, y_0)$ . And since  $(\frac{dx}{dt})^2 = y^2 = 2K(y) = 2(H(x_0, y_0) - U(x))$ , we find:

$$\frac{dt}{dx} = \frac{1}{\sqrt{2(H(x_0, y_0) - U(x))}},$$

so we can find  $t$  as a function of  $x$  by a quadrature, and then invert this relation to find  $x$  as a function of  $t$ .

In the Harmonic Oscillator case, with  $hh = 1$  and  $ii = 0$ ,  $U(x) = \frac{1}{2}x^2$  so  $H(x, y) = \frac{1}{2}(x^2 + y^2)$ , so the orbits are circles, and it is easy to carry out the above quadrature and inversion explicitly, to obtain  $x(t) = x_0 \cos(t - t_0) + y_0 \sin(t - t_0)$ .

### **The Universal “Sliding Bead on a Wire” Model.**

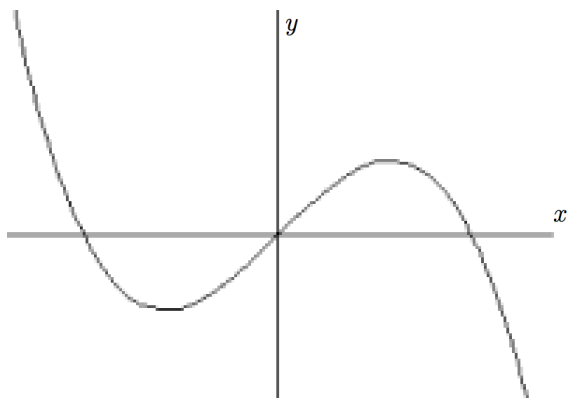
In one-dimension there is a highly intuitive physical model that makes it easy to visualize the motion of a particle under a given force. Moreover this model is “universal” in the sense that it works for all forces that are function of position only and hence, as we noted above, are of the form

$F(x) = -U'(x)$  for some potential function  $U$ . Namely, imagine that we string a bead on a frictionless piece of wire that lies along the graph of the equation  $y = U(x)$ . If the bead has mass  $m = 1$  and if we choose units so that  $g$ , the acceleration of gravity, equals one, then the gravitational potential of the bead is  $mgh = h$  where  $h$  is its height. So if as usual we interpret the ordinate of a point as its height, then the gravitational potential of the bead when it is at the point  $(x, y) = (x, U(x))$  is just  $U(x)$ , and the sliding motion of the bead along the wire under the attraction of gravity will exactly model whatever other system we started from!

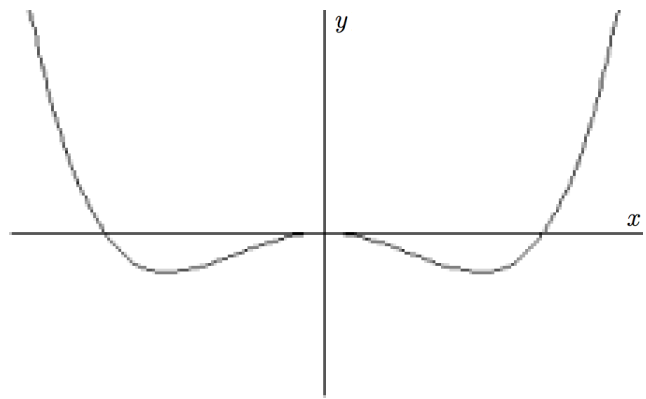
In the case of the Harmonic Oscillator, where  $F(x) = -x$  and  $U(x) = \frac{1}{2}x^2$ , the graph is the parabola,  $y = \frac{1}{2}x^2$  and it is easy to imagine the bead oscillating back and forth along this parabola.

For the unforced and undamped Duffing Oscillator the force is  $F(x) = -hhx - ii x^3$ , where for simplicity in what follows we will assume that  $ii > 0$  and  $hh < 0$ . The potential is  $U(x) = \frac{hh}{2}x^2 + \frac{ii}{4}x^4$ , which we note can be considered as the first two terms in the Taylor expansion for an arbitrary symmetric potential with local maximum at 0. It is easily checked that  $\lim_{x \rightarrow \pm\infty} U(x) = +\infty$  and in addition to the local maximum at 0, there are two other critical points of  $U$ , at  $x = \pm\sqrt{\frac{-hh}{ii}}$ , where  $U$  has local minima. For the default values,  $hh = -1$  and  $ii = 1$ , the force is  $F(x) = x(1 - x^2)$ , and the potential is  $U(x) = \frac{1}{4}x^2(x^2 - 2)$ ,

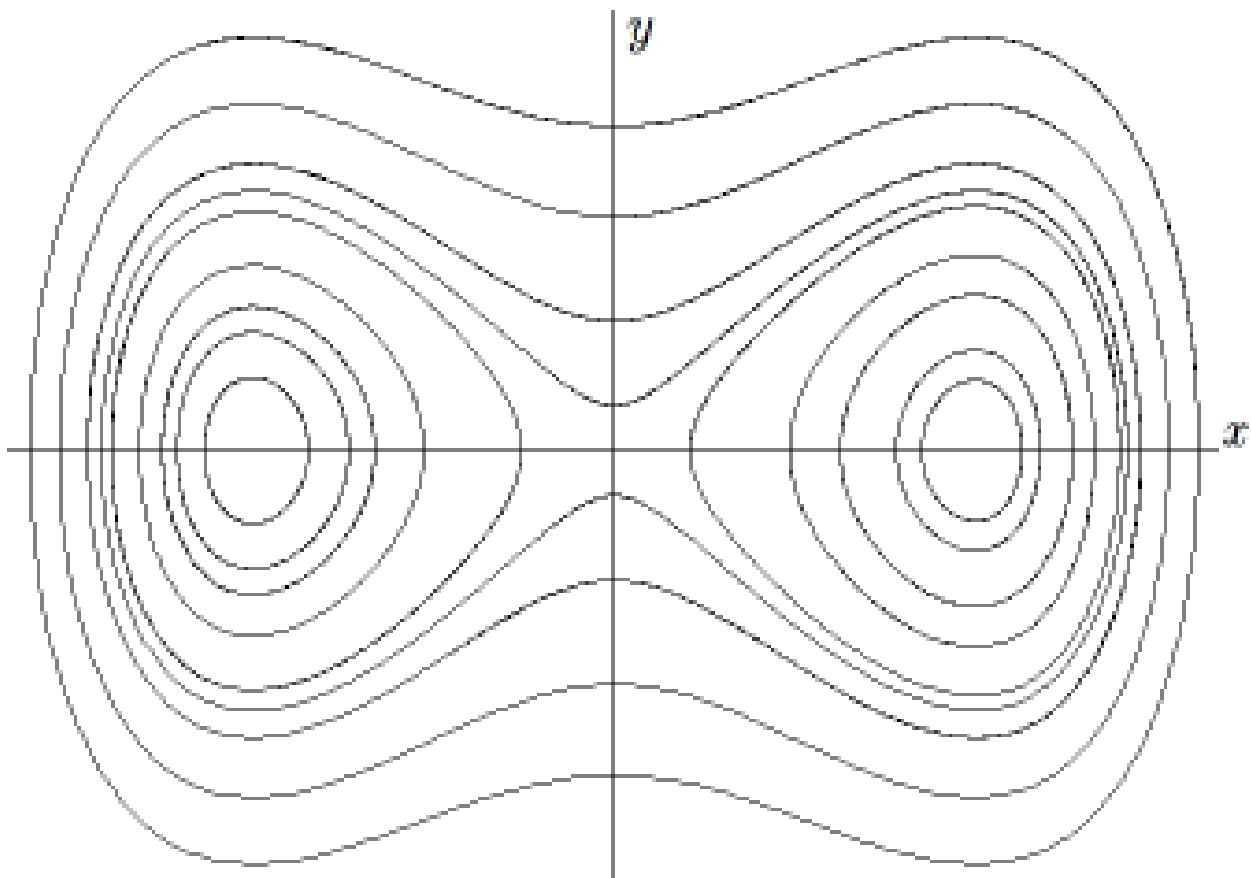
so the local minima are at  $\pm 1$ . We graph this force  $F(x)$  and potential  $U(x)$  below, and show a selection of the resulting orbits. It should be clear why  $U$  is called a double-well potential.



$F(x)$



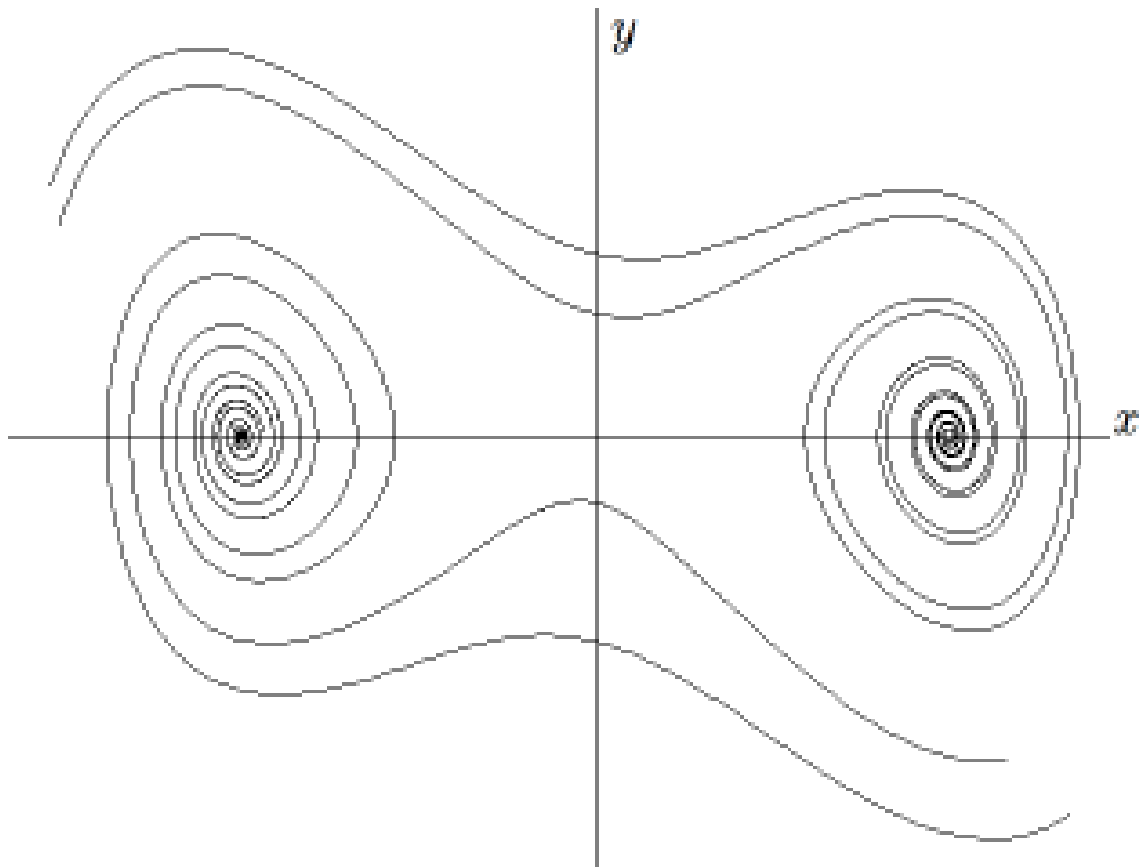
$U(x)$



Some orbits of the Unforced, Undamped Duffing Oscillator

## The Unforced, Damped Duffing Oscillator.

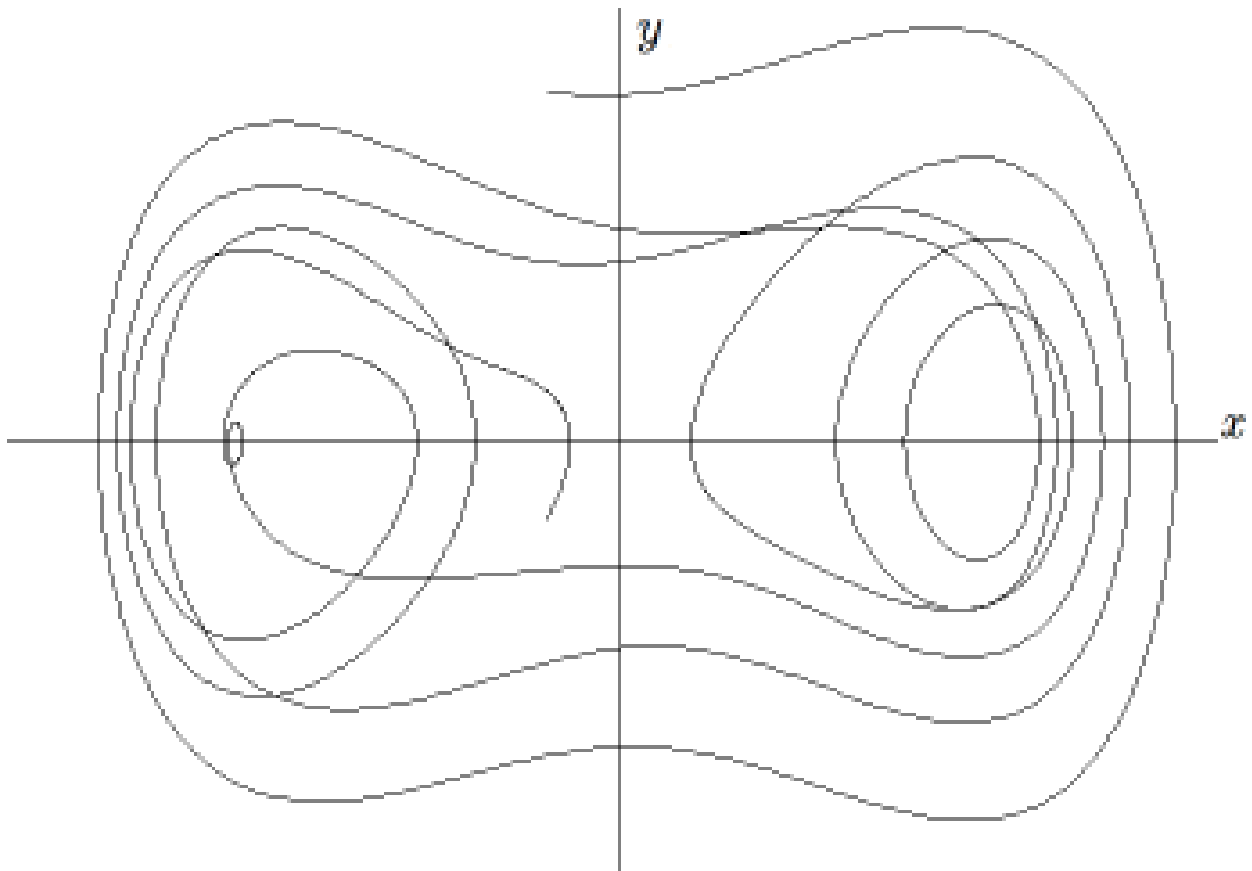
We now still assume  $bb = 0$  (so there is no forcing) but we assume that  $aa > 0$ , so there is damping. In the bead on a wire picture,  $aa \frac{dx}{dt} = aa y$  is the friction from the bead rubbing against the wire, and the force is now given by  $F(x) = -U'(x) - aa y$ . If we again calculate  $\frac{dH}{dt}$  as we did above, we now find not  $\frac{dH}{dt} = 0$  but instead  $\frac{dH}{dt} = -aa y^2$ . The result is that instead of the orbits of the bead in the  $x$ - $y$ -plane being closed curves of constant total energy  $H$ , the energy decrease along the orbits, and they cut across the  $H = \text{constant}$  curves and spiral in towards the two minima of  $H$  at the bottom of the two potential wells. We show a selection of the resulting orbits below.



Some orbits of the Unforced, Damped Duffing Oscillator

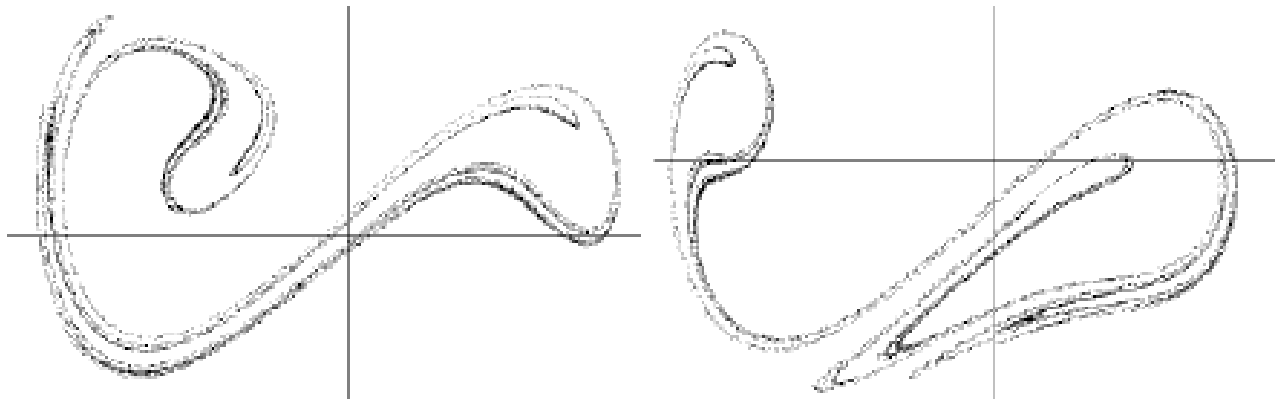
## The Forced Duffing Oscillator.

We now add back the forcing term  $bb \cos(cct)$ . First a word about how to interpret this force in the sliding bead picture. If we assume that there is an alternating electric field parallel to the  $x$  direction and with strength  $\cos(cct)$  at time  $t$ , then  $bb \cos(cct)$  will be the electric force felt by the bead if we give the bead an electric charge of magnitude  $bb$ .



Some orbits of the Forced, Damped Duffing Oscillator

# Chaos, Strange Attractors, and Poincaré Sections.



Two Time Slices of the Duffing Attractor

R.S.P.

ODEs

## 3-dim ODE of 2nd Order: Charged Particles \*

### THE MOTION OF CHARGED PARTICLES IN MAGNETIC FIELDS

The path  $p(t)$  of a particle with electric charge  $e$  and mass  $m$  in a magnetic field  $B$  is given by

$$m \cdot p''(t) = e \cdot p'(t) \times B(p).$$

(The right hand side is called the *Lorentz Force*.)

This implies that, for an arbitrary magnetic fields,  $B$ , the kinetic energy  $E(t) = \frac{m}{2} \langle p', p' \rangle(t)$  is constant in time.

One should first convince oneself in the case of a

#### *Constant Magnetic Field*

that a particle can move tangentially to the field lines, in circles around the field lines and in helices around the field lines, i.e., in any linear combination of the first two special cases.

Put in *Settings*, *ODE Settings*:

$v_x = 0.003, v_y = 0.003, v_z = 0.5$ , to obtain almost circles around the field lines.

And put  $v_x = 0.2, v_y = 0.2, v_z = 0.001$  to obtain approximate straight lines parallel to the field lines. The *Default*

---

\* This file is from the 3D-XplorMath project. Please see:

*Settings* give a general helix. We will also try to understand charged particle motions in nonlinear fields by looking at such special cases.

We consider next motion of a charged particle in the:

### *Field of an Electric Current*

along the x-axis. The field lines are circles parallel to the y-z-plane with centers on the x-axis. In this case, the *Default Settings* give initial conditions in the x-y-plane (a symmetry plane of the field) that are orthogonal to the field lines. The solution curves therefore remain in this plane, and are, for small velocities, *almost circles around the field lines*. But, because the absolute value of the field is decreasing with  $r$ , these solution curves are more strongly curved the nearer they are to the wire. They are therefore rolling curves with a translational period in the direction of the wire. (See *Plane Curves, Cycloid* and put  $aa = 1$  and  $bb = 6.5$  in the *Set Parameters* dialog.) If in *ODE Settings* one increases the velocity to  $v_y = 0.5$ , then the translational part is so large that the consecutive loops do not intersect.

We obtain solution curves which *almost follow the field lines* if we make the initial velocity tangential to the field lines and fairly small:

$$v_x = 0, v_y = 0, v_z = 0.02,$$

$$\text{Time span} = 450, \text{ Step-size} = 0.2.$$

Now slowly increase  $v_z$ , e.g., to  $v_z = 0.2$ , to obtain an-

other family of solutions *follows the field lines, but winding around them in small loops.*

Next in *Settings, ODE Settings*, put:

$$v_x = 0.02, v_y = 0.02, v_z = 0.01$$

leaving Time span = 450, Step-size = 0.2, as before.

Finally we increase the initial velocity to obtain solution curves that look fairly wild at first but can be seen to follow the pattern which we recognized for more special initial conditions, namely put

$$v_x = 0.2, v_y = 0.2, v_z = 0.1$$

to see solutions that follow helices with wide loops around them. *Try by all means to view this in stereo!*

Finally we consider the so-called *Störmer Problem*, namely the motion of charged particles in a Magnetic Dipole Field. Since the magnetic field of our Earth is a dipole field, such motions occur in the van Allan Belt when charged particles from the Sun's plasma meet the Earth. A dipole field  $B(p)$  with a magnetic moment  $mm$  is given by:

$$B(p) = 3\langle mm, p \rangle \frac{p}{|p|^5} - \frac{mm}{|p|^3}.$$

The *Default ODE Settings* give a fairly general but somewhat complicated solution curve. To see solutions that *almost follow the field lines* use ODE Settings to set a small initial velocity tangential to the field lines, say  $v_x = 0, v_y = 0, v_z = 0.05$ . To see solutions that *almost circle the field lines in the equator plane of the dipole*, in the ODE Settings dialog, choose small initial conditions in the equator

plane, e.g.,  $v_x = 0.1, v_y = 0.1, v_z = 0$ . The resulting curves are close to rolling curves. (Compare *Plane Curves, Circle* using, Parameter Settings:  $hh = -0.125, ii = 4$ , and increase t-Resolution to 200, then choose Generalized Cycloids from the Action Menu.) Since the absolute value of the field increases along the field lines from the equator towards the poles, one cannot have solutions that almost follow the field lines while circling them in narrow loops, however one can approximate such behavior with the initial condition  $v_x = 0.035, v_y = 0.035, v_z = 0.05$ .

In a Plenary address on Dynamical Systems he gave at the 1998 International Congress of Mathematicians in Berlin, Jürgen Moser had an interesting discussion of the Störmer Problem that we reproduce below from Documenta Mathematica, Extra Volume, ICM 1998, pp. 381–402. (After the lecture, one of us approached Moser and showed him the visualization of the Störmer Problem in 3D-XplorMath. He appeared to be delighted by it, but said something looked not quite right to him, a remark that helped us eliminate a small bug!)

Here is the extract from Moser’s lecture.

R.S.P. & H.K.

ODEs

### **The Störmer Problem.**

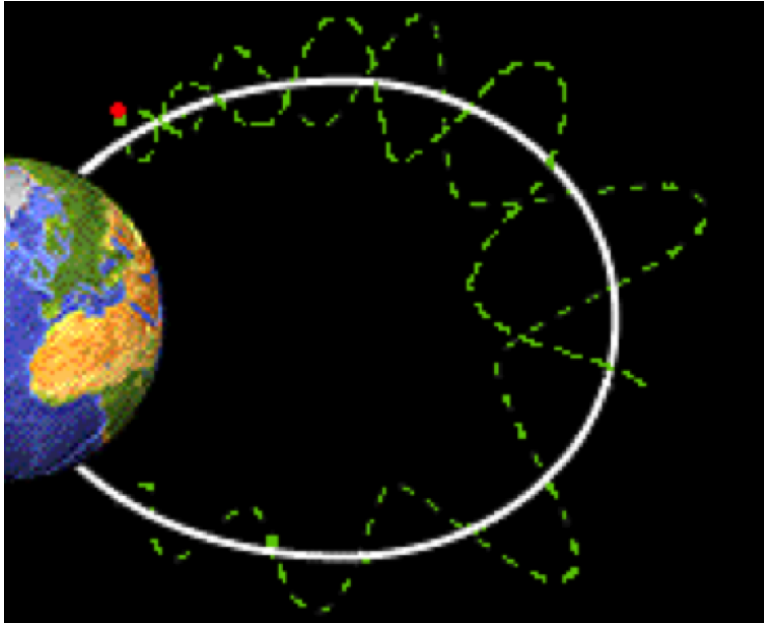
Another large scale confinement region is known in the magnetic field of the earth. With the advent in 1957 of satellites it was soon discovered that the earth was sur-

rounded by (two) belts of charged particles caused by its magnetic field. Since the beginning of the century it was known that such charged particles were present above the atmosphere and were responsible for the aurora borealis (and australis). It was Störmer (incidentally president of the ICM 1936 in Oslo) who made calculations of the orbits of these charged particles moving in the magnetic field of the earth, which he modelled as a magnetic dipole field. This is an interesting nonlinear Hamiltonian system.

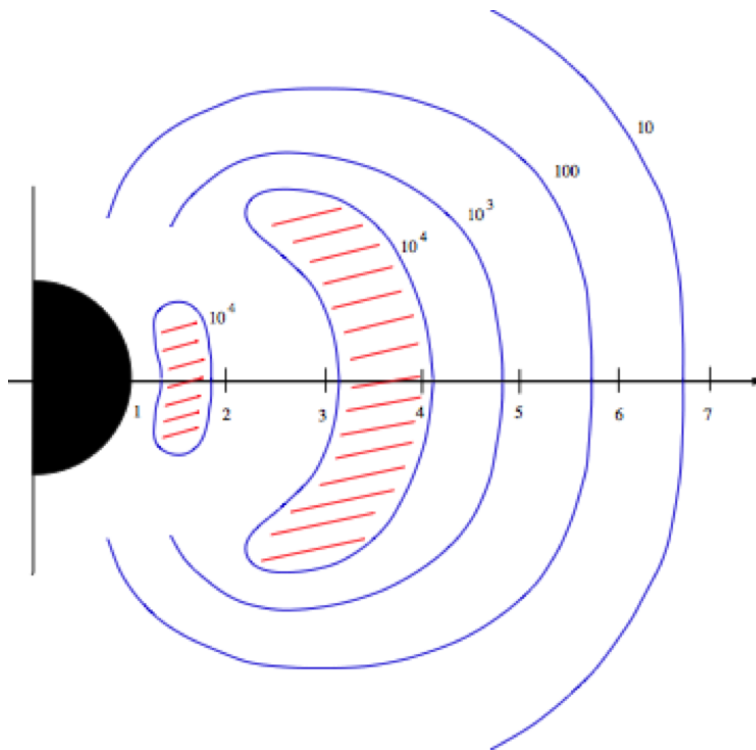
The satellite measurements led to the discovery of two regions surrounding the earth, the so-called van Allan belts, in which charged particles were trapped. It turns out that it is an example of a magnetic bottle to which the stability theory is applicable (M. Braun 1970).

It is interesting to realize the dimensions involved: For electrons, the “cyclotron radius” is of the order of a few kilometers and the corresponding periods of oscillation about one millionth of a second! The “bounce period” of travel from north pole to south pole and back is a fraction of a second.

In addition to these natural van Allan belts several artificial radiation belts have been made by the explosion of high-altitude nuclear bombs since 1958. Some of those so created belts had a lifetime up to several years—which shows the long stability of these experiments as well as the irresponsibility for carrying them out! Some 30 years ago these tests have been stopped.



**Störmer Problem**



**Van Allen Belt**

# Lattice Models

[Go To Page 1](#)

( Click the Names )

- 1.) [Summary on Lattice Models](#)
- 2.) [FERMI-PASTA-ULAM Lattice](#)
- 3.) [Toda Lattice Model](#)
- 4.) [Discrete Sine-Gordon](#)
- 5.) [Discrete Klein-Gordon](#)

## Lattice Models \*

The Lattice Model category integrates and displays the equations of motion for a one dimensional lattice of “oscillators” with nearest neighbor interactions. This is interesting for itself of course, but in addition it provides an important general method for making discrete approximations to many continuous wave equations.

An excellent introduction to lattice models can be found in Michel Remoissenet’s “Waves Called Solitons: Concepts and Experiments” (Springer-Verlag, 1994, ISBN 3-540-57000-4). Indeed, the implementation of the Lattice Model category in 3D-Filmstrip, and the choice of particular models was very strongly influenced by Remoissenet’s treatment of the subject. For this reason we will only cover below what a user of 3D-Filmstrip needs to know to use the Lattice Model category, and refer to the above text for the theoretical background.

For various reasons the number  $N$  of oscillators in the lattice is restricted to be a power of 2. Currently  $N$  can be any one of 16, 32, 64, 128, 256, or 512. (One not so obvious reason is that choice greatly speeds up the computation of the amplitudes of the normal modes for the linearized lattice.) The characteristics that determine the equations of motion of the lattice are:

---

\* This file is from the 3D-XplorMath project. Please see:

- 1) The mass of an oscillator,
- 2) The “internal” force an oscillator exerts on a neighboring oscillator,
- 3) The external force on an oscillator.

The mass of an oscillator is not set directly, but rather is derived from a parameter called the density, which has a default value of 1, but can be set to another value by the user. The mass satisfies the relation that the number  $N$  of oscillators times the mass of an oscillator is equal to the length of the lattice times its density.

The force between two neighboring oscillators is always assumed to be a function  $F(d)$  of the distance  $d$  separating them. If  $x_i$  is the displacement of the  $i$ -th oscillator from its equilibrium position, then the total force on the  $i$ -th oscillator due to its two neighbors is  $F(x_i - x_{i-1}) - F(x_{i+1} - x_i)$ . The external force on the  $i$ -th oscillator is also assumed to be some function  $G(x_i)$  of the displacement  $x_i$  from equilibrium.

There are four preprogrammed Lattices: Fermi-Pasta-Ulam, Toda, Discrete Sine-Gordon, and Discrete Klein-Gordon. The internal forces between oscillators for these four are as follows:

- 1) Fermi-Pasta-Ulam:  $F(d) = -aa d - bb d^2 - cc d^3 - dd d^4$
- 2) Toda:  $F(d) = aa(\exp(-bb d) - 1)$
- 3) Discrete Sine-Gordon:  $F(d) = (cc/aa)d$
- 4) Discrete Klein-Gordon:  $F(d) = (cc/aa)d$

and the external forces are:

- 1) Fermi-Pasta-Ulam:  $G(d) = 0$
- 2) Toda:  $G(d) = 0$
- 3) Discrete Sine-Gordon:  $G(d) = bb^2 \sin(d)$
- 4) Discrete Klein-Gordon:  $G(d) = bb^2 d$ .

In addition there is a User Defined... item in the Lattice menu that brings up a dialog that lets the user define internal and external forces.

The equations of motion can be integrated either with zero boundary conditions (i.e.,  $x_1 = x_N = 0$ ) or with periodic boundary conditions ( $x_1 = x_N$ ).

Various choices including initial conditions can be changed from their default values using the dialog brought up by the Set Lattice Parameters... menu item of the Lattice Model menu.

R.S.P.

Lattice TOC

# The FERMI-PASTA-ULAM Lattice \*

## Background

The Fermi-Pasta-Ulam lattice is named after the experiments performed by Enrico Fermi, John Pasta, and Stanislaw Ulam in 1954-5 on the Los Alamos MANIAC computer, one of the first electronic computers. As reported in Ulams autobiography [Ul], Fermi immediately suggested using the new machine for theoretical work, and it was decided to start by studying the vibrations of a string under the influence of nonlinear internal forces. Nonlinearity makes the computations very difficult and the problem could not be attacked by standard mathematical methods. However, physical intuition suggested that the motion of such a string would eventually “thermalize”. The purpose of the experiment was to investigate the rate of thermalization. For the computer calculations, the string was approximated by a finite sequence of point particles with nearest-neighbor interactions—a so-called “lattice model”. The motion of such a lattice is governed by a system of ordinary differential equations, and it is these equations that the computer solves, numerically.

The results more than justified the trouble of carefully formulating the experiment and programming it on a very primitive machine, for they went completely against all

---

\* This file is from the 3D-XplorMath project. Please see:

expectations. In fact the motion did not seem to thermalize at all! The previously accepted beliefs thus had to be re-examined, and this re-examination led eventually to the discovery of soliton theory, which became a major theme of twentieth Century mathematics.

### **How To View the Demonstration**

The Fermi-Pasta-Ulam string is the black curve. Although it appears continuous, it is in fact made up of the motion of individual points (the blue curve represents the velocities of these points). The number of points (i.e., the number of particles in the lattice) can be changed by choosing Lattice Parameters in the Action menu, and various other adjustments are possible. Fermi- Pasta-Ulam actually used a lattice with at most 64 particles.

The energies of the so-called normal modes are the red/green bars in the left hand corner. Thermalization means, roughly speaking, that the heights of the red/green bars should equalize after a sufficiently long period of time. More precisely, it is the time averages of their heights that should equalize, and these are represented by the blue bars.

The fact that this does not happen is the surprising feature of the Fermi-Pasta-Ulam experiment. What happens, and what Fermi-Pasta-Ulam observed, is first of all that only the first few normal modes are excited, and in addition that the motion is almost periodic. This can be detected by watching the motion of the red/green bars—after some time they return (apparently) to the original configuration.

Various initial shapes can be chosen from the Lattice Parameters menu, but the almost periodicity seems to occur regardless of the initial shape of the string (or the initial configuration of the red/green bars).

### Further Aspects

To put this observation into context, it is necessary to consider the effects of different internal forces in the string. As explained in the Lattice Models ATC the internal force is specified by a function  $T(y)$ . By choosing the User Lattice Model from the Lattice Models menu, the function  $T(y)$  can be specified (as well as the usual Lattice Parameters). To switch on the energies of the normal modes, select Show Normal Mode Display from the Action menu. For example,  $T(y) = ky$  (where  $k$  is a positive number) gives the motion of a “standard” string, which is exactly periodic. The red/green bars behave even more simply—they remain constant. The Fermi-Pasta-Ulam case is  $T(y) = y + \alpha y^2$ ; the default value of  $\alpha$  in 3D-XplorMath is 0.3. (Fermi-Pasta-Ulam also considered  $y + \alpha y^3$  and a piecewise linear function, with similar results.) The effect of the small nonlinear term  $\alpha y^2$  is to “perturb” the periodic behaviour of the linear case, and the red/green bars no longer remain constant. But, as we have observed, some vestiges of periodicity remain.

This is surprising because a randomly chosen nonlinear internal force  $T(y)$  generally leads to the thermalization that Fermi-Pasta-Ulam expected. For physical reasons,

$T(y)$  should be of the form  $ky + N(y)$  where  $N(y)$  is a nonlinear term which remains small during the motion, for example,  $T(y) = y + 100y^3 + 5y^4 + 5y^5$ .

Why is the Fermi-Pasta-Ulam lattice so special? This question took some time to answer, because the necessary mathematical tools were insufficiently developed at that time. In addition there were various sources of distraction: the mathematical string is only an idealized model of a real physical situation, the discrete lattice is in turn only a model of that string, and furthermore any computer calculations are subject to numerical and rounding errors. In fact the philosophical questions surrounding such “simulation” experiments, and the subject of “experimental mathematics” in general, are still being debated (see [We]).

However, it is by now generally agreed that the Fermi-Pasta-Ulam lattice is a genuine phenomenon and that it can be explained by a combination of powerful theories: the Kolmogorov-Arnold-Moser (or KAM) theory, the theory of completely integrable Hamiltonian systems, and soliton theory. The KAM theory explains, very roughly speaking, that a system which is close enough to a completely integrable Hamiltonian system retains some of the predictable behavior of such a system. The Fermi-Pasta-Ulam lattice happens to be close to the Toda lattice, which (some 20 years after the FPU experiments) was discovered to be a completely integrable Hamiltonian system. The Toda lattice is discussed further in the ATO for the Toda lattice (select Toda from the Lattice Models menu).

Soliton theory refers to the study of special solutions (solitons) of certain nonlinear wave equations such as the Korteweg-de Vries (KdV) equation. These solutions have unexpectedly persistent behavior (in contrast to randomly chosen nonlinear waves, which either disperse or break after a sufficiently long time). It turns out that the differential equations of the FPU lattice can be considered as a discrete approximation to the KdV equation; hence it is plausible that the FPU lattice admits soliton-like solutions as well.

## References

[Pa] R.S. Palais, The Symmetries of Solitons, Bull.A.M.S. 34, 1997 pp. 339-403.(See pages 355-359 for a discussion of the FPU experiments).

[To1] M. Toda, Nonlinear Waves and Solitons., Mathematics and its Applications, 5, Kluwer, 1989.

[To2] M. Toda, Theory of Nonlinear Lattices, Springer Series in Solid-State Sciences, 20, Springer-Verlag, 1989.

[Ul] S.M. Ulam, Adventures of a Mathematician, University of California Press, 1991. (See chapter 12.)

[We] T.P. Weissert, The Genesis of Simulation in Dynamics: Pursuing the Fermi-Pasta-Ulam Problem, Springer, 1997. (This recounts the history of the FPU lattice and the ensuing mathematical and philosophical fallout).

# The TODA Lattice \*

## Background

The Toda lattice is named after Morikazu Toda, who discovered in the 1960s that the differential equations for a lattice with internal force  $T(y) = \alpha(e^{\beta y} - 1)$  (with  $\alpha, \beta$  constant) admit solutions which can be written in terms of elliptic functions. This extends the fact that the standard lattice with linear internal force  $T(y) = ky$  can be solved using trigonometric functions.

Since nonlinear ODE are usually much more complicated than linear ODE, the very fact that it admits explicit solutions at all means that the Toda lattice is already a remarkable example. (The Fermi-Pasta-Ulam lattice, in contrast, has no analogous explicit solutions.) A few years later, a possible explanation of this property appeared, when it was discovered that the Toda lattice is an example of a “completely integrable Hamiltonian system”. This, in turn, led to an explanation of the unexpectedly simple behaviour of the Fermi-Pasta-Ulam lattice (see the ATO for the Fermi-Pasta-Ulam lattice): on the one hand, for a completely integrable Hamiltonian system, (almost) periodic behaviour can be predicted, and on the other hand, the Fermi-Pasta-Ulam lattice can be regarded as an approximation to the Toda lattice when the vibrations are small. We shall say

---

\* This file is from the 3D-XplorMath project. Please see:

more about completely integrable Hamiltonian systems below.

## How To View the Demonstration

It can be seen that the Toda lattice behaves in a very similar way to the Fermi-Pasta-Ulam lattice. Instead of thermalizing, the lattice motion appears to be periodic.

## Further Aspects

Mathematically, however, the Toda lattice is much easier to analyze than the Fermi-Pasta-Ulam lattice, because it is a completely integrable Hamiltonian system. This means, practically speaking, that it has the maximum possible number of conserved quantities. For a system of  $n$  ordinary differential equations of second order, this maximum number is  $n$ . For example, for the equation  $y'' = -ky^2$ , the total energy  $\frac{1}{2}y'^2 + \frac{1}{2}ky^2$  (kinetic energy plus potential energy) is a conserved quantity, i.e., it is constant when  $y$  is a solution of the differential equation, and there are no others. The standard linear lattice is of this type; each of the normal mode energies is a conserved quantity, because each represents the total energy of an uncoupled (independent) oscillator.

The fact that the Toda lattice has the maximum possible number of conserved quantities is not obvious, and certainly not on physical grounds. A mathematical explanation comes from the fact that the equations of motion may be written in the form  $L' = [L, M]$ , where  $L$  and  $M$  are

matrix functions. This type of equation is called a Lax equation (after Peter Lax), and the Lax equation for the Toda lattice was discovered by Hermann Flaschka in the 1970s. For any Lax equation, the eigenvalues of the matrix function  $L$  turn out to be conserved quantities, and this gives the required number of conserved quantities for the Toda lattice—though their physical meaning remains unclear.

The conserved quantities greatly constrain the motion of the system. In fact, the Arnold-Liouville Theorem says that the motion of an  $n$ -dimensional completely integrable Hamiltonian system must, if it is bounded (as in our case), be equivalent to linear motion on an  $n$ -dimensional torus. When  $n = 1$  this means that the motion must be periodic. When  $n = 2$  (and similarly if  $n > 2$ ) the motion must be expressible as  $(e^{2\pi iat}, e^{2\pi ibt})$  for some real numbers  $a$ ,  $b$ . If  $a/b$  is rational the motion is periodic, otherwise it is almost-periodic.

Although the Fermi-Pasta-Ulam lattice and the Toda lattice are approximately the same when the vibrations are small, it can be shown that the Fermi-Pasta-Ulam lattice is not a completely integrable Hamiltonian system. Nevertheless, the almost periodic motion of the Toda lattice is inherited by the Fermi-Pasta-Ulam lattice, at least for small vibrations, and this explains the absence of thermalization in both cases.

Completely integrable Hamiltonian systems are important, but quite special, and it is an important area of current

research to identify and study more general types of “integrable systems”.

## References

[Ar] V. Arnold, *Mathematical Methods of Classical Mechanics*, Graduate Texts in Math. 60, Springer, 1978.

[To1] M. Toda, *Nonlinear Waves and Solitons.*, Mathematics and its Applications, 5, Kluwer, 1989.

[To2] M. Toda, *Theory of Nonlinear Lattices*, Springer Series in Solid-State Sciences, 20, Springer-Verlag, 1989 .

[We] T.P. Weissert, *The Genesis of Simulation in Dynamics. Pursuing the Fermi-Pasta-Ulam Problem*, Springer, 1997.

R.S.P.

Lattice TOC

# Soliton Traveling Waves

[Go To Page 1](#)

( Click the Names )

- 1.) [The Waves Category](#)
- 2.) [The Korteweg-de Vries Equation](#)
- 3.) [The Sine-Gordon Equation](#)
- 4.) [The Nonlinear Schrödinger Equation](#)

## The Waves Category \*

The subject of wave phenomena is an exceedingly rich and varied one, playing an important rôle in everyday life, in the pure and applied sciences, and in many areas of mathematics. Water waves can be small ripples generated by a passing breeze or enormous, destructive tsunamis generated by earthquakes, which themselves are waves that travel in the Earth's crust. Maxwell's Equations of electromagnetism are wave equations that describe the behavior of light, and of the signals responsible for radio, TV, and the World Wide Web. The probability waves of quantum theory govern the behavior of elementary particles at the smallest spatial scales, and the search for gravitational waves at the largest scales is a major concern of modern cosmology.

Our goal in the 3D-XplorMath Wave Category is to show examples of waves from a fairly limited region of this vast landscape. Namely, the program displays the evolution in time of a one-dimensional “wave-form”, by which we mean a real or complex valued function  $u(x, T)$  of the “time”,  $T$ , and a single “space” variable  $x$ . At a time  $T$ , the wave has a given “shape”, the graph of the function  $x \mapsto u(x, T)$ , and the program displays this graph with  $x$  as abscissa and  $u(x, T)$  as ordinate.

[NOTE: The resolution of this graph is tResolution, and its

---

\* This file is from the 3D-XplorMath project. Please see:

domain runs from tMin to tMax. That is to say, the interval [tMin,tMax] is divided in tResolution points  $x_i, i = 1, \dots, tResolution$  with spacing  $xStep = \frac{(tMax-tMin)}{(tResolution-1)}$ , and the graph is plotted at the points  $(x_i, y_i)$  where  $x_i = tMin + (i - 1) xStep$  and  $y_i = u(x_i, T)$ , and then these plot points are joined into a polygonal graph. Note that the t of tMax tMin and tResolution have nothing to do with the time  $T$ ! Thus to make the graph smoother, you must increase tResolution in the Set Resolution & Scale... dialog, and to change the domain of the graph, you must change tMin and tMax in the Set t,u,v Ranges... dialog.]

The time evolution of the wave-form is shown by the standard flip-book animation technique; i.e., we plot the above graph for

$$T = \text{InitialTime} + k \cdot \text{StepSize}, \quad k = 0, 1, \dots,$$

until the user clicks the mouse. The variables InitialTime and StepSize are set in the dialog brought up by choosing ODE Settings... from the Settings menu. To make the animation slower (but smoother) decrease StepSize, and conversely increase StepSize to make the wave-form evolution proceed more rapidly, but more jerkily.

As usual, formulas defining a wave form  $u(x, T)$  can depend on the parameters aa,bb, ..., ii as well as on  $x$  and  $T$ , and for each of the canned wave-forms these formulas can be checked by choosing About This Object... from the Waves main menu.

In trying to understand features of a wave-form, it helps

to see not only the animated evolution as above, but also to display the graph of the function  $u(x, T)$  as a surface, over the  $(x, T)$ -plane or to show “time-slices” of this graph. Therefore the Waves menu has choices to permit the user to switch between these display methods. (These two alternate formats, being three dimensional objects, can be viewed in stereo.)

There is also a User Wave Form... item in the Wave menu, which brings up a dialog permitting the user to enter a formula for  $u(x, t)$  as a function of  $x, t$ ,  $\alpha, \dots$ ,  $i$ .

Interesting wave-forms generally arise as solutions of so-called “wave equations”. These are partial differential equations of evolution type for a function  $u(x, t)$ . That is, the function  $u(x, t)$  is determined as the unique solution of a PDE satisfying some initial conditions. Perhaps the simplest example is the so-called “linear advection equation”  $u_t + vu_x = 0$  (where  $v$  is some constant “velocity”). This has the general solution  $u(x, t) = f(x - vt)$ . But there are also many interesting non-linear wave equations, in particular the so-called soliton equations, including the Korteweg-DeVries (KDV), Sine-Gordon, and Cubic Schroedinger equations. Many of our examples are pure soliton solutions of these latter examples.

For a fairly detailed account of the elementary theory of wave equations, select *Introduction to Wave Equations* from the Topics submenu of the Documentation menu.

# The Korteweg-de Vries Equation \*

NOTE: For a fuller understanding of the following, you may find it helpful to first read “About This Category” from the Documentation Menu and “Introduction to Wave Equations” from its Topics submenu.

The partial differential equation,

$$u_t(x, t) + u(x, t)u_x(x, t) + u_{xxx}(x, t) = 0$$

for a real-valued function,  $u$ , of two real variables  $x$  and  $t$  (space and time) is known as the Korteweg-de Vries Equation (or simply KdV). It was first derived in 1895 by D.J. Korteweg and G. de Vries to model water waves in a shallow canal. Their goal was to settle a long-standing question; namely whether a solitary wave could persist under those conditions. Based on personal observations of such waves in the 1830’s, the naturalist John Scott Russell insisted that such waves do occur, but several prominent mathematicians, including Stokes, were convinced they were impossible.

Korteweg and de Vries proved Russell was correct by finding explicit, closed-form, traveling-wave solutions to their equation that moreover decay rapidly spatially, and so represent a highly localized moving lump. In fact, they found a one-parameter family of such solutions:

$$u(x, t) = 2a^2 \operatorname{sech}^2(a(x - 4a^2t)), \quad (\text{in 3DXM: } a = cc)$$

---

\* This file is from the 3D-XplorMath project. Please see:

and these are the traveling wave solutions whose evolutions are displayed by 3D-XplorMath, with its parameter  $cc$  playing the rôle of the constant  $a$ . Note that the wave's velocity,  $4a^2$ , is proportional to its amplitude,  $2a^2$ , meaning that the taller waves of this family move faster. Both the fact that such a solution to a non-linear equation could exist and that one could write it in explicit form were later recognized to be highly important, although originally these facts were relatively unnoticed.

The KdV equation did not receive significant further attention until 1965, when N. Zabusky and M. Kruskal published results of their numerical experimentation with the equation. Their computer generated approximate solutions to the KdV equation indicated that any localized initial profile, when allowed to develop according to KdV, asymptotically in time evolved into a finite set of localized traveling waves of the same shape as the original solitary waves discovered in 1895. Furthermore, when two of the localized disturbances collided, they would emerge from the collision as another pair of traveling waves with a shift in phase as the only consequence of their interaction \*. Since the “solitary waves” which made up these solutions seemed to behave like particles, Zabusky and Kruskal coined the name “soliton” to describe them. The formula

$$u(x, t) = \frac{12 \, gg \, (3 + 4 \cosh(2x - 8t) + \cosh(4x - 64t))}{\sqrt{(3 \cosh(x - 28t) + \cosh(3x - 36t))}}$$

---

\* To see this phase shift, choose Display as Graph from the Action Menu.

is one of these solutions, consisting of two lumps and therefore called two-soliton solution of KdV, and it is one of the KdV solutions whose evolution can be displayed using 3D-XplorMath. Shortly after that, another remarkable discovery was made concerning KdV; a paper by C. Gardner, J. Greene, M. Kruskal, and R. Miura demonstrated that it was possible to derive many exact solutions to the equation by using ideas from scattering theory. In particular, the solutions whose evolution are shown by 3D-XplorMath are exact solutions that can be found by this method.

Using modern terminology, we could say that these authors showed that KdV was an *integrable* non-linear partial differential equation. It was the first to be discovered, but since then, many other such equations have been found to be integrable and admit soliton solutions, in particular the Sine-Gordon Equation (SGE) and the Nonlinear Schrödinger Equation (NLS)—solutions to both of which are also shown by 3D-XplorMath. However, KdV is usually considered the canonical example, in part because it was the first equation known to have these properties.

Alex Kasman

Waves TOC

# The Shepard Tones Demo

[Go To Page 1](#)

( Click the Names )

- 1.) [About this Demo](#)
- 2.) [What Are The Shepard Tones?](#)

## The Sound Category \*

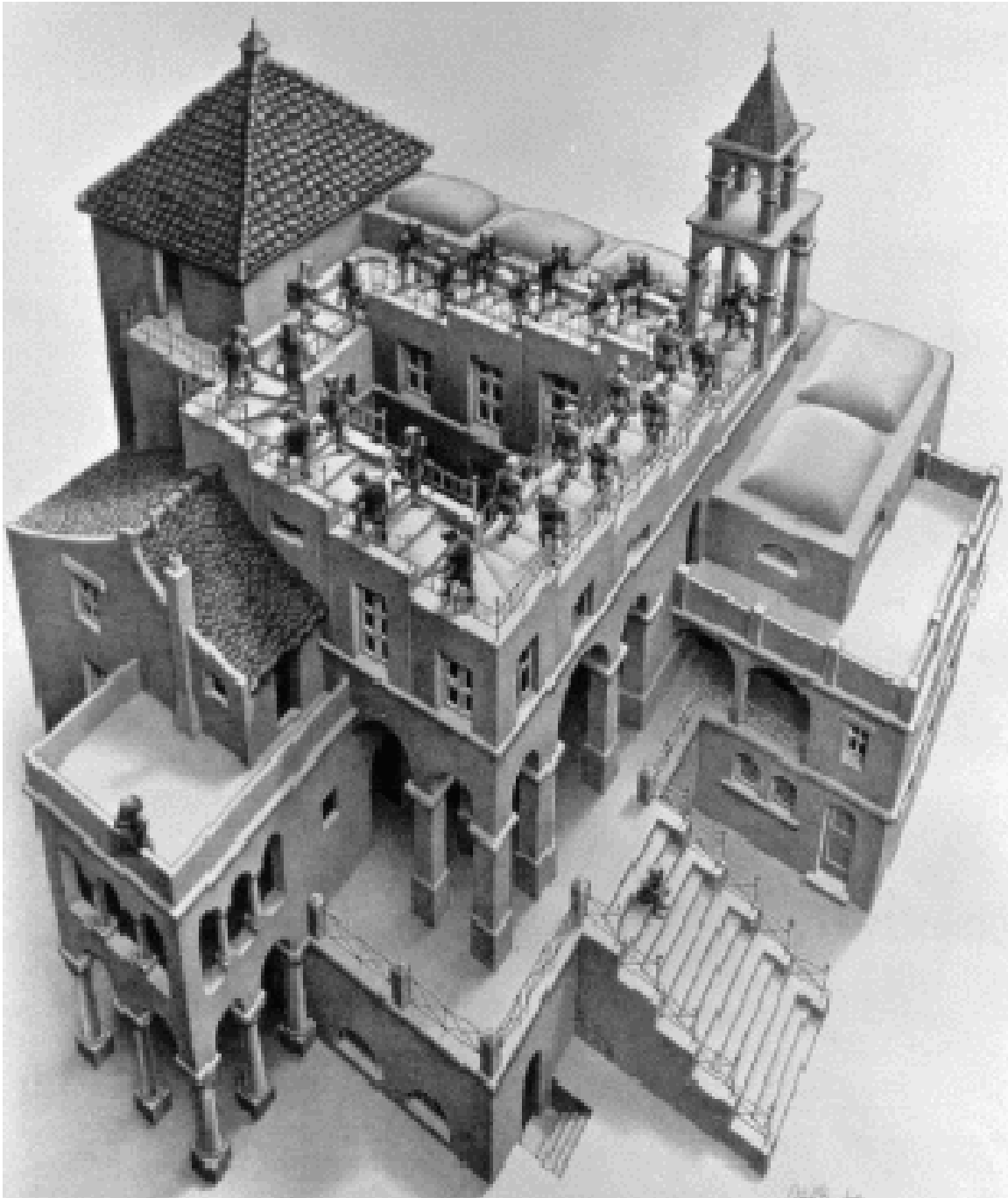
While all the other 3D-XplorMath categories are concerned with the visualization of mathematics—and so make use of your eyes and sense of sight, in this one you will be using your ears and your sense of hearing. For this reason it is important that while using with this category your computer should be attached to a reasonably high fidelity sound system—either headphones or stereo loudspeakers (preferably with a subwoofer).

So far the only exhibit in the Sound Category is the Shepard Tones. For an explanation of this exhibit, select About This Object after selecting Shepard Tones from the Sound menu of 3D-XPlorMath or see the following text.

---

\* This file is from the 3D-XplorMath project. Please see:

## Shepard Tones \*



**Ascending and Descending by M. Escher**

---

\* This file is from the 3D-XplorMath project. Please see:

<http://3D-XplorMath.org/>

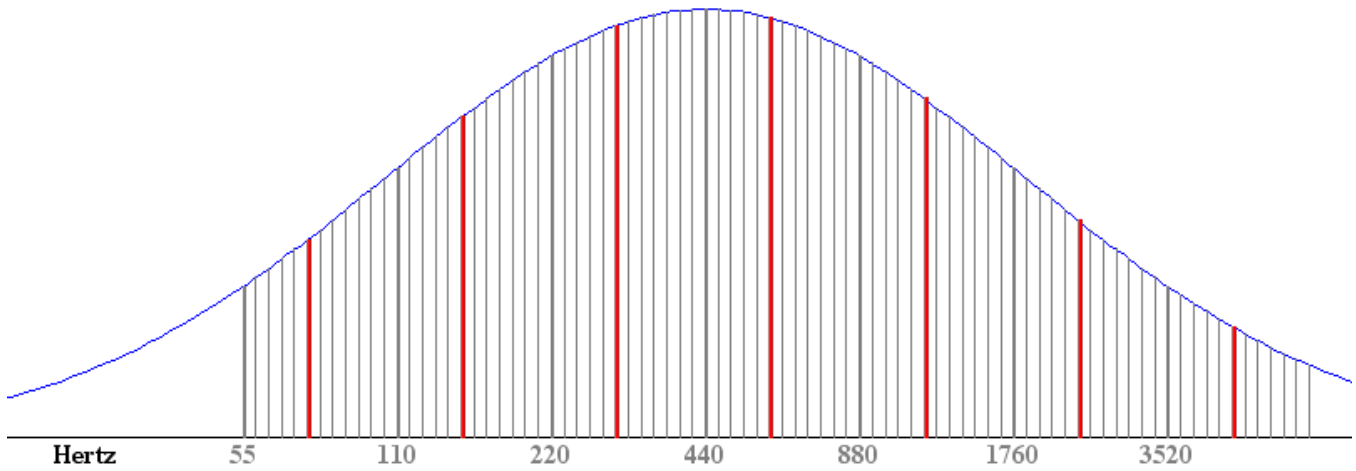
Shepard Tones

If you misread the name of this exhibit, you may have expected to hear some pretty music played on a set of shepherd's pipes. Instead what you heard was a sequence of notes that probably sounded rather unmusical, and may have at first appeared to keep on rising indefinitely, "one note at a time". But soon you must have noticed that it was getting nowhere, and eventually you no-doubt realized that it was even "cyclic", i.e., after a full scale of twelve notes had been played, the sound was right back to where it started from! In some ways this musical paradox is an audible analog of Escher's famous Ascending and Descending drawing.

While this strange "ever-rising note" had precursors, in the form in which it occurs in 3D-XplorMath, it was first described by the psychologist Roger N. Shepard in a paper titled *Circularity in Judgements of Relative Pitch* published in 1964 in the Journal of the Acoustical Society of America.

To understand the basis for this auditory illusion, it helps to look at the sonogram (next page) that is shown while the Shepard Tones are playing. What you are seeing is a graph in which the abscissa represents frequency (in Hertz) and the ordinate represents the intensity at which a sound at a given frequency is played. Note that the Gaussian or bell curve in this diagram shows the intensity envelope at which all sounds of a Shepard tone are played.

## Spectral Sonogram



Parameter	Default	Meaning
aa	4	Lowest Octave ( 4 is minimum)
bb	10	Highest Octave (10 is maximum)
cc	250	Duration of note (msec.)
dd	255	Volume (from 0 to 255)
ee	36	Intensity falls by 1/e every ee notes from center, A above middle C.
ff	25	Pause between notes in 60ths of a second.

A single Shepard tone consists of the same “note” played in seven different octaves—namely the octave containing A above middle C (the center of our bell curve) and three octaves up and three octaves down. Thus the first or “A” Shepard tone consists of simultaneously playing the following frequencies (in Hertz): 55, 110, 220, 440, 880, 1760, 3520, with each frequency being played at the intensity given by the height of the Gaussian at that frequency. Of course, what our ear hears it interprets as the note A of the scale—not the pure tone of A in some particular octave, but rather a rich harmonic mixture of the A notes from seven adjacent octaves of which the central one, A above middle C, sounds most strongly, while the others get less intense as they go up or down from there.

To get the next (or “B”) Shepard tone, each note of the above mixture is increased by a “half-tone”, that is, its

frequency is multiplied by the twelfth root of two. And of course the same bell curve again gives the intensity of each note of the mixture. Now our ear hears the note B (again as a rich harmonic mixture) and by our long experience with the scale, it seems that we have now gone “up” one half-tone from the first note.

Well, you can take it from there. To get the next (third) in the sequence of Shepard Tones, we again multiply every frequency of the B tone by twelfth root of two (i.e., “ascend a half-tone”) and play each tone at the appropriate intensity for that frequency, as given by the bell curve. Again it feels to us that this third Shepard tone is a half-tone “higher” than the second one. And so on for the next nine Shepard tones.

But then as you will see we are right back to where we started!

R.S.P.

Shepard Tones